

From Synthesis to 3D printing: A journey into stereochemistry and its impact on polymer networks

By

Anissa L. Khalfa

A thesis submitted to the University of Birmingham for the degree of

Doctor of Philosophy

School of Chemistry

College of Engineering and Physical Sciences

University of Birmingham

February 2023

UNIVERSITY OF
BIRMINGHAM

University of Birmingham Research Archive

e-theses repository

This unpublished thesis/dissertation is copyright of the author and/or third parties. The intellectual property rights of the author or third parties in respect of this work are as defined by The Copyright Designs and Patents Act 1988 or as modified by any successor legislation.

Any use made of information contained in this thesis/dissertation must be in accordance with that legislation and must be properly acknowledged. Further distribution or reproduction in any format is prohibited without the permission of the copyright holder.

Table of Contents

Table of Contents i
Abstract v
Acknowledgements vii
List of Figures xi
List of Schemes, Tables and Equations xxv
List of Symbols and Abbreviations xxviii
List of publications xxxiv
1 Introduction of stereochemistry in polymers 2
1.1 Origins of stereochemistry 2
1.2 Vocabulary of stereochemistry 5
1.3 The importance of stereochemistry 11
1.3.1 General advances in chemistry 11
1.3.2 In biology 12
1.3.3 In polymers 14
1.4 Stereochemistry of vinylic polymers 15
1.4.1 Tacticity 15
1.4.2 Stereocontrolled synthesis of vinyl polymers 16
1.4.3 Influence of tacticity on bulk polymers 18
1.5 Polymer systems containing *cis/trans* isomerism 19
1.5.1 Natural rubbers and Gutta Percha 19
1.5.2 Challenges of synthesising polymers containing *cis/trans* isomerism 21
1.5.3 Polymer containing *cis/trans* isomerism through post-polymerisation modification 22
1.5.4 Polymer containing *cis/trans* isomerism through in-situ alkene synthesis 23
1.5.5 Polymer containing *cis/trans* isomerism from stereopure monomers 28
1.6 Stereochemistry in Polymer networks 34
1.7 Conclusion 41
1.8 Aim of the project 43
1.9 References 44
2 Di-functional monomers synthesis for thiol-ene step growth polymerisation 55
1.10 Chapter overview 55
1.11 Synthesis of *trans*-2-butene-1,4-diol 56

1.12 Synthesis of Isoidide....58
1.13 Synthesis pathways to 1,4-glucose-derived diol....62
1.13.1 Synthesis of 2,3,6-tri-O-benzyl-D-glucopyranoside (1,4-glucose diol). 64
1.13.2 2.4.3 Deprotection of the anomeric carbon: Hydrolysis....69
1.13.3 2.4.4 Deprotection of the anomeric carbon: Acetolysis....73
1.13.4 Synthesis of 2,3,4-tri-O-benzyl-D-glucopyranoside (1,6-glucose derived diol)....78
1.14 Diacrylate synthesis....82
1.14.1 Synthesis cis/trans diacrylates....84
1.14.2 Synthesis isohexide-derived diacrylates....87
1.14.3 Synthesis of 1,6-glucose diacrylate....88
1.15 Glucose derived dithiol synthesis....89
1.16 Conclusion....96
1.17 References....97
1.18 Appendices....103
1.18.1 Materials and methods....103
1.18.2 Synthetic procedures....107
1.18.3 NMR spectra of monomer diols and intermediates....132
1.18.4 NMR spectra of diacrylate monomers....143
1.18.5 NMR spectra of the 1,6 glucose dithiol (32) and intermediates....149
1.18.6 NMR spectra of selected by-products from studied reaction....152
3 Synthesis of telechelic poly(ester-urethane) oligomers via thiol-Michael step-growth addition....164
3.1 Introduction....164
3.2 Overview of this chapter....167
3.3 Synthesis of the *Cis* and *trans* unsaturated oligomer....169
3.3.1 Control over the molecular weight and termini....170
3.3.2 Experimental molecular weight determination....173
3.3.3 Thermal properties of oligomers....175
3.4 Isohexides oligomers....177
3.4.1 Synthesis....177
3.4.2 Thermal properties of oligomers....181
3.5 Glucose-derived monomers polymerisation....182
3.5.1 Synthesis....182
3.5.2 Thermal properties of oligomers....187
3.6 Conclusion....188
3.7 References....190

3.8 Appendices 195
3.8.1 Materials and methods 195
3.8.2 Synthetic procedures 196
3.8.3 NMR spectra 200
3.8.4 Size exclusion chromatography (SEC) oligomer characterisation 213
4 Effect of the *cis*/*trans* alkene configuration on the thermomechanical properties and degradability of unsaturated poly(ester- urethane) photosets 216
4.1 Introduction 216
4.2 Resin formulation and testing 218
4.3 Study of potential crosslinking or UV triggered isomerisation 223
4.4 Impact of the curing time on *cis* and *trans* materials 227
4.4.1 Mechanical testing 227
4.4.2 Thermal testing 229
4.4.3 Depolymerisation of networks 231
4.5 Impact of the chain length and stereochemistry on the mechanical properties of photoset networks 235
4.5.1 Tensile testing 235
4.5.2 Thermal testing 238
4.5.3 Study of the network's architecture 241
4.6 3D printing of *cis/trans* resin 244
4.6.1 Introduction 244
4.6.2 Resin characterisation 246
4.6.3 Optimising 3D printing parameters 249
4.6.4 Mechanical testing 251
4.6.5 Thermal testing 252
4.6.6 Accelerated degradation study and depolymerisation 253
4.7 Conclusion 256
4.8 References 257
4.9 Appendices 262
4.9.1 Materials and Methods 262
4.9.2 NMR Spectra 268
4.9.3 Uniaxial tensile tests of *cis* and *trans* films 272
4.9.4 Compressive tests of 3D printed scaffolds 274
4.9.5 Differential scanning calorimetry (DSC) characterisation of films and 3D printed scaffolds 275
4.9.6 Thermogravimetric analysis (TGA) characterisation of films and 3D printed scaffolds 279

4.9.7 Appendix references 280
5 Conclusion 282

Abstract

Photo-active polymeric materials are valuable to a myriad of industries from paints and inks to binders in rocket propellers and even in healthcare and 3D printing. Changing the thermomechanical properties relies mostly on changing the functionality of monomer units, which limits the choice of possible candidate owing to restriction resulting from a need for biocompatibility or printability. For this reason, it is of high relevance to manipulate the mechanical properties without a change in the chemical functionality. An emerging technique in the field of thermoplastic polymers is now devoted to tuning the mechanical properties via the rational control of the backbone stereochemistry. More specifically, the thiol-ene step growth addition between a dithiol and a diacrylate proved to be a valuable advance for the implementation of *cis*/*trans* chemistry for high molecular weight thermoplastic. In addition to be mild enough to preclude the occurrence of unwanted crosslinking or isomerisation, the technique revealed itself to be versatile since the diacrylates are prepared from stereopure diols, enabling the preparation of *cis* or *trans* unsaturated or the isohexides ring-based units. In this thesis manuscript, efforts made towards the translation of this unique system to photo-active polymeric materials using 2 kinds of stereopure diacrylate monomers, namely *cis* and *trans* 1,4-but-2-ene diol and isohexides will be described. In parallel, the synthesis of a glucose-derived diacrylate and dithiol will be explored in the aim at synthesising a synthetic polysaccharide via nucleophile catalysed thiol-Michael addition. The first chapter will present the state of the art and impact of stereochemistry in polymers. The second chapter will present the synthesis and further functionalisation of the stereopure diols selected for this study with a commercially available isocyanate-acrylate and

also the synthesis of a glucose derived dithiol. Chapter three will discuss the work made towards controlling the molecular weight and end groups of diacrylate telechelic oligomers *via* Michael step-growth polymerisation of the commercially available 1,6-hexanedithiol and the *cis*/*trans* unsaturated and isohexides-based diacrylate monomer. In addition, the attempt at producing a high molecular weight polysaccharide mimic using the same polymerisation technique will be presented. Finally, the fourth chapter will focus on the formulation of *cis* and *trans* unsaturated prepolymers into photo-active resins to produce films suitable for thermomechanical testing. It was found that for low curing time (< 1 min) the radical initiated crosslinking only occurred at the acrylate end groups and isomerisation of the internal double bonds was mitigated. Furthermore, for films prepared from prepolymers with low molecular weight (4.0 kDa) a significant difference in the thermomechanical properties between *cis* and *trans* films was observed as a consequence of the different degree of crystallinity between the two materials. However, at higher molecular weights (8-10 kDa), the *cis* polymer gains progressive crystallinity and its thermomechanical behaviour becomes comparable to the *trans* polymer network. Finally, the prepolymers were formulated into resins suitable for 3D printing which displayed both thermomechanical and degradation properties dependent on the backbone stereochemistry.

Acknowledgements

First, I would like to thank Etienne Grau and Daniel Taton, without whom I would have never considered applying for a PhD program. Thank you for your trust, humour, and patience but also specifically for teaching me so much, not only about science, but also about becoming a better person. I spend the best 6 months of my life in the LCPO and that is thanks to you but also thanks to Julie “Docteur Tata” Dubois, Boris Bizet, Martin Camus, Dounia Arcens and Sandra Latournerie: we shared moments of exception together which I’ll never forget. Thank you so much for welcoming me with warming heart in your team.

I would like to thank Panos for hosting me in his fumehood and teaching me the basics of ROP during my time at Warwick. Thank you also to Edward Cant and Chiara Arno for your help on this mini-project. Thank also to Chiara for her tremendous help on the 1st year report and her valuable feedback. Thank you for caring in sharing your skills, for your positive reinforcement whilst never thinking yourself as superior than the juniors member of the lab.

During my PhD, I had the opportunity to meet extraordinary people along the austere corridors of the Haworth Building.

I would like to thank specifically, Sètuhn Jimaja for helping me on everything, from drying a solvent the “proper way”, teaching me about the beauty of helixes to always make himself available for a chat. I appreciate your kindness, your great sense of humour and your will to help in solving any issues, scientific or personal.

I would also like to thank Gordon Herwig, thank you for teaching me all I needed to know about formulation, photo-rheology and 3D printing, but also for fixing everything around you, even when nobody asked you for anything.

I also have to thank Kayla Delle Chiaie and Mar Madrigal, you are both scientists and people that I looked up too. Thank you for your amiability but also for your incredible workshop. Kayla, yours almost alleviated my fear for organo-metallic chemistry, *almost*.

Wei Yu, you were more passionate than me about my early PhD work, and I have to thank you for all the extensive chat we had about the 3D printing technology. In addition, I would like to thank you and Yujie Xie for your love for food and for all the Chinese delicacies you introduced to me.

I would also like to express my gratitude to the past and present member of the best lab, namely 7.06. In particular, I would like to thank Josh Worch, Hannah Prydderch, Maher Alraddadi, Daniele Giannantonio, Cinzia Clamor, Ana Cubillo Álvarez, Vivi “Bibi” Chiaradia, and Alexis Perrot, we did share some good laughter together. I would like to particularly thank Maher and Josh for always being available to help out. Thank you both for sharing not only your extensive scientific knowledge with me but also your wisdom, I won’t forget the lessons you taught me. Thank you to Cinzia for your assistance on my “ROP special” and not judging me for not understanding what was so basic to you. Alexis, thank you for not getting mad at my joke about Limoge and being kind enough to proofread chapter 4.

Some gems of people could be found across the corridor too. In particular Natalia Reis, Thiago Ouriques Machado, and Jennifer Frommer. Without you the 7th floor

would be empty, literally as for one of you to be absent, you had to be on your death bed. A very warm thank you to Jenny, who volunteered to proofread chapter 2 of this manuscript. Your comments and insight on sugar chemistry has been very helpful and improved this thesis. I also have to mention Steve Fielden, you are an outstanding chemist, and it is hard to believe how humble you are about it. Thank you for staying true to yourself in all circumstances.

Outside the lab, I would like to warmly thank Tiphaine Labed-Veydert for her constant emotional support. Thank you so much for all the zoom catch ups and your daily messages of encouragement, it did mean the world to me and I won't forget it.

Thank you to my dad, for his support and monthly phone calls. I always love hearing your stories about your gardening, bee keeping and fishing adventures. It always has been a fresh air to me and reminds me what was really of importance in life.

Also, I would like to thank Sara and Barry Stubbs as well as Derek Lake. Thank you so much for making me feel at home around your place and treating me like family. I always appreciate the time spend in your company; you are incredible people. I would like to add a little thought for the "boyz" Sootty and Sweep, which are respectively the most miserable and the most blazé cat I ever meet. Yet, it always been a pleasure to have you around the summer.

I little shout out to Billie the "snowball", Kayla's hamster, which stayed with me for a year and a half. I hope you had as much fun with us than us with you. May you rest in peace.

Lastly, I would like to thank Connor Stubbs, the proud owner of the Connomer trademark, without whom I would have left the group a long time ago. Connor, there is no word to thank you enough for all your support throughout the entire PhD and this is very much thanks to you that this manuscript has been written. Thank you for your patience, constant encouragement, but also for taking the role of “writing police”, asking me every hour “how many words?”. Thanks also for your help on structuring the introduction, for proofreading the entire manuscript at the very last minute and the help in formatting, all with a big smile on your face, as if it was nothing.

List of Figures

Figure 1.1. Enantiomorphous hemihedral crystals of sodium ammonium racemate and the corresponding structure of the tartaric acid which they contain. Figure adapted from reference[5] with permission of John Wiley and Sons. 3

Figure 1.2. Schematic representation of a tetrasubstituted carbon atom in a tetrahedral spatial arrangement and its non-superimposable mirror-image. 4

Figure 1.3. Diagram summarising the most fundamental type of isomerism in chemistry. 6

Figure 1.4. (R,S) diastereoisomer of tartaric acid using different representation to illustrate the assignment of the absolute configuration following the CIP rules. 7

Figure 1.5. Structural aspects of helicene and their stereodescriptors. Reprinted from reference[18] with permission from the Royal Society of Chemistry. 8

Figure 1.6. Illustration of the relationship between anomers, as represented by the α and β anomer of D-glucose, which are epimers on the hemiacetal carbon. If two compounds differ by the absolute configuration of only one carbon, then they are epimers, as it is the case for α-D-glucose and α-D-mannose. 9

Figure 1.7. Tortional surface potential energy diagram for n-butane. Θ represent the dihedral angle between second and third carbon of the molecule. Adapted from reference[19] with permission from Elsevier. 10

Figure 1.8. Structures of the atropoisomer of 4,4',6,6'-dinitrodiphenic acid (DNDA) and 1,1'-bi-2-naphthol (BINOL). 11

Figure 1.9. Representation of the structure of the R and S enantiomers of carvone. 13

Figure 1.10. Schematic representation of the "lock and key" model. The substrate should have a structure complementary to that of the active site of the enzyme for a reaction to proceed. 14

Figure 1.11. Two possible configurations of the propylene stereocenter in the polymer chain. 15

Figure 1.12. Stereochemistry of polypropylene and corresponding properties. ... 16

Figure 1.13. Illustration of the diverse architecture arising from the microphase separation between immiscible polymer blocks occurring within thermoplastic elastomer creating a physical crosslink. In red is represented the crystalline phase or hard phase and the blue represents the amorphous or soft phase. By changing the molecular weight of the blocks, it is possible to obtain a layered, gyroid, or worm-like rod phase separation. Adapted from reference[54] under the Creative Commons Attribution Licence 2020. 19

Figure 1.14. Structure of Gutta Percha and Natural Rubber and their respective crystal structure illustrating the better chain packing abilities of the trans isomer. Adapted from reference[34] with permission from Springer Nature. 20

Figure 1.15. Illustration of the UV triggered isomerisation of trans fumarate to cis maleate with a 30% yield of conversion and random distribution along the polymer chain. This reaction requires the use of 10 mol% Benzophenone as catalyst. The reaction is reversible in the presence of 10 mol% diethylamine. Whilst the 100% trans fumarate polymer is semi-crystalline, isomerising 30% of the unsaturation to cis maleate led to an amorphous material. Reproduced from reference[74] with permission from John Wiley and Sons. 23

Figure 1.16. Scheme representing the addition of thiophenol to ethyl propiolate at room temperature and at concentration of 0.2 M. The table above summarises the impact of the solvent polarity on the yield and stereochemistry of the product.[77] Reproduced from reference[76] under the Creative Commons Attribution Licence 2021. 24

Figure 1.17. Stress-strain curve for thiol-yne elastomer with a cis content of 80% (High cis, in red) and 32% (High %trans, in blue). Reproduced from reference[63] under the Creative Commons Attribution Licence 2016. 25

Figure 1.18. Preparation of unsaturated polymers with a different cis/trans content via ADMET using two ruthenium catalysts.[65] Reproduced from reference[65] with permission from Springer Nature. 28

Figure 1.19. Structure of three common cyclic monomers used to impart cis and trans stereochemistry to polymer. 29

Figure 1.20. Structure of 1,4:3,6-dianhydrohexitols or isohexides. 30

Figure 1.21. Isomannide (IM)-derived poly(ester-urethane) exhibits the mechanical properties of soft elastomers whilst isoidide (II)-derived poly(ester-urethane) are displaying the behaviour of tough thermoplastics. The blending of the two isomorphous polymers yields a fast eroding tough plastic, whereas the copolymerisation of the two isohexides produces an elastomer which degrades slowly.[101] Adapted from reference[101] under the Creative Commons Attribution Licence 2022. 32

Figure 1.22. Structure of fumaric and maleic acid 33

Figure 1.23. Synthesis of poly(ester-urethane) via thiol-Michael step growth addition between an unsaturated cis and trans diacrylate and the commercially available 1,6-hexanedithiol which exhibits different mechanical properties depending on the stereochemistry of the inner double bond.[64] Adapted from reference[64] with permission from the American Chemical Society. 34

Figure 1.24. Illustration of the sol-gel phase transition mechanism occurring via guest-host interaction between a Deoxycholate-β-cyclodextrin derivative and a poly(acrylic acid) copolymer containing pendant azobenzene groups. Reproduced from reference[118] with permission from the American Chemical Society. 36

Figure 1.25. Illustration of the methyl pendant group orientation in a) meso 2,3-butanediol, which favour linear chains and in turn the formation of H-bonding between neighbouring chains or b) (S,S) and c) (R,R) which induce kinks within the chain to minimise steric hindrance. Adapted from reference[126] with permission from the American Chemical Society. 40

Figure 1.26. Figure summarising the work presented in this manuscript. (a) General scheme of the diacrylate monomer synthesis (1) from the reaction of a diol and 2-isocyanatoethylacrylate followed by the polymerisation (2) via nucleophilic thiol-Michael addition with a dithiol in the presence of an excess of diacrylate to obtain telechelic oligomers with reactive acrylate termini. (b) Presentation of the diversity of diol used in this study. (c) Structure of the two dithiols used in this work. (d) Ideal illustration of the network formation from the radical reaction of the acrylate termini in the presence of a photo-initiator and UV light to create a stereopure unsaturated poly(ester-urethane) network. 43

Figure 2.1. Figure summarising the content of this chapter, which focusses on the synthesis of diacrylate monomers starting from of (a) the cis and trans or (b) isohexides or (c) a 1,6-glucose-derived diol. The reactions involve the functionalisation of each diol with a commercially available isocyanate acrylate in the presence of dibutyltin dilaurate (DBTDL) as catalyst (d). (e) Picture of polymers of similar structure containing (solid) or not (liquid) urethane bonds, obtained from the reaction of the same diol with either isocyanatoethylacrylate or acryloyl chloride respectively and polymerised via the nucleophilic thiol-Michael 55

Figure 2.2. ^{1}H NMR (400 MHz, 298 K, d_6-DMSO) spectrum of trans-2-butene-1,4-diol (**1**). 57

Figure 2.3. Structure of the three isohexide isomers. 58

Figure 2.4. Comparison of the ^{1}H NMR (400 MHz, 298 K, d_6-DMSO) spectra of 2.4 Glucose-derived diol 60

Figure 2.5. (a) Structure of α-D-glucopyranose in the most stable chair configuration showing the conventional numbering of the carbons within a pyranose ring. (b) Scheme representing the equilibria existing between the cyclic and linear form of glucose in solution, illustrating that the anomeric oxygen is engaged in a hemiacetal, explaining it electrophilicity leading it to be a good leaving group. On the left, the glucose unit is represented in the clearer stereochemical view. 61

Figure 2.6. (a) Structure of the desired 1,4-glucose-derived diol and (b) Structure of cellulose, where the glucose units are linked through a 1,4-β-glycosidic bond, affording regioregularity to the polymer chain. 62

Figure 2.7. Reaction scheme of the synthesis of a 1,4-glucose-derived diol via (a) benzylation and hydrolysis of β-cyclodextrin, (b) selective acylation of methyl α-D-glucopyranoside followed by hydrolysis of the glycosidic bond, (c) traditional 4 step protection/deprotection strategy starting from methyl α-D-glucopyranoside. 63

Figure 2.8. ^{1}H NMR (400 MHz, 298 K, $CDCl_3$) spectrum of methyl 4,6-O-benzylidene-α-D-glucopyranoside (**6**). 65

Figure 2.9. ^{13}C NMR (101 MHz, 298 K, $CDCl_3$) spectrum of methyl 4,6-O-benzylidene-α-D-glucopyranoside (**6**). 66

Figure 2.10. ^{1}H NMR (400 MHz, 298 K, $CDCl_3$) and ^{13}C NMR (101 MHz, 298 K, $CDCl_3$) spectra of methyl 2,3,6-tri-O-benzyl-α-D-glucopyranoside (**8**). 67

Figure 2.11. Enlargement of the ^{1}H-^{13}C HMBC spectra of methyl 2,3,6-tri-O-benzyl-α-D-glucopyranoside (**8**). 68

Figure 2.12. ^{1}H NMR (400 MHz, 298 K, $CDCl_3$) and ^{13}C NMR (101 MHz, 298 K, $CDCl_3$) spectrum of 2,3,6-tri-O-benzyl-4-acetyl-D-glucopyranose (**10**). 70

Figure 2.13. Enlargement of the ^{1}H-^{13}C HMBC spectrum of 2,3,6-tri-O-benzyl-4-acetyl-D-glucopyranose (**10**)..... 71

Figure 2.14. ^{1}H NMR spectra (400 MHz, 298 K, $CDCl_3$) of (a) 2,3,6-tri-O-benzyl-D-glucopyranoside (**9**) as a racemic mixture of the α and β anomer, in a 65/35 ratio and (b) 2,3,6-tri-O-benzyl-α-D-glucopyranose. Insert (i) shows a picture of the smearing behaviour of the targeted compound on silica gel. Insert (ii) shows the fluffy crystal aspect of the α 1,4-glucose-derived diol (**9**). 72

Figure 2.15. ^{1}H NMR (400 MHz, 298 K, $CDCl_3$) and ^{13}C NMR (101 MHz, 298 K, $CDCl_3$) spectra of acetyl 2,3-di-O-benzyl-4,6-acetyl-α-D-glucopyranoside (**14**). ... 75

Figure 2.16. Enlargement of the ^{1}H-^{13}C HMBC spectra of acetyl 2,3-di-O-benzyl-4,6-acetyl-α-D-glucopyranoside (**14**). 76

Figure 2.17. Schemes representing the synthesis of C4 sulfonates glucose derivatives and the outcome of their subsequent nucleophilic displacement using potassium thio-acetate when the glucose ring is bearing (a) a trityloxy or (b) a benzyloxy on C6. (c) the trifluoromethanesulfonyl is a better leaving group than sulfonyl halides and can be displaced on C4 using potassium acetate. However, its introduction is incompatible with the presence of a trityloxy or tert-butyldimethylsilyloxy group which are labile in acidic conditions. 78

Figure 2.18. Structure of the identified by-products generated during the acetolysis of methyl 2,3,4,6-tetra-O-α-D-glucopyranoside. The structures were coherent with the literature.[54] 80

Figure 2.19. ^{1}H NMR (400 MHz, 298 K, $CDCl_3$) and ^{13}C NMR (101 MHz, 298 K, $CDCl_3$) spectra of 2,3,4-tri-O-benzyl-D-glucopyranoside (1,6-glucose derived diol) (**20**). 81

Figure 2.20. Enlargement of the ^{1}H-^{13}C HMBC spectrum of 2,3,4-tri-O-benzyl-D-glucopyranoside (1,6-glucose-derived diol) (**20**). 82

Figure 2.21. General reaction scheme of the synthesis of diacrylate monomer starting from 2-isocyanatoethyl acrylate and either (a) cis or trans diol, (b) Isohexides or (c) 1,6-glucose derive diol in THF, using dibutyltin (IV) dilaurate (DBTDL) as catalyst. 83

Figure 2.22. a) ^{1}H NMR (400 MHz, $CDCl_3$, 298 K) spectra of cis diacrylate monomer (**24**) (top) and trans diacrylate monomer (**25**) (bottom). b) Table summarising the signal and the integration for each proton of the diacrylate monomer. [a] Signal and integration values were determined via the analysis of the cis and trans diacrylate monomer ^{1}H NMR spectra. 85

Figure 2.23. DSC thermograms for 1st heating cycle of cis and trans monomers. DSC thermal ramp was carried out under N_2 with a heating rate of 10 $°C \cdot min^{-1}$.. 86

Figure 2.24. ^{1}H NMR (400 MHz, $CDCl_3$, 298K) spectrum of the isohexides-derived acrylate monomers. From top to bottom: isosorbide-derived diacryalte (**26**), isomannide-derived diacrylate (**27**) and isoidide-derived diacrylate (**28**). 87

Figure 2.25. ^{1}H NMR (400 MHz, $CDCl_3$, 298 K) spectrum of the 1,6-glucose-derived diacrylate (**29**). 89

Scheme 2.9. Multi-step synthesis of 2,3,4-tri-O-benzyl-1,6-dithio-D-glucopyranose (1,6-glucose-derived dithiol) (**32**). 90

Figure 2.26. (a) Scheme illustrating the expected and obtained product from the reaction of the 1,6-glucose derived diol (**20**) with methanesulfonyl chloride and (b) ^{1}H NMR spectrum of the crude product from the reaction (**30**). (c) After 24h of reaction, the compound is recovered enantiopure as the β anomer. 91

Figure 2.27. Enlargement of the ^{1}H-^{13}C HMBC NMR spectrum of product (**24**). . 93

Figure 2.28. ^{1}H NMR (400 MHz, 298 K, $CDCl_3$) and ^{13}C NMR (101 MHz, 298 K, $CDCl_3$) spectra of acetyl 2,3,4-tri-O-benzyl-1,6-dithio-6- acetyl-D-glucopyranoside (**31**). 95

Figure 2.29. ^{1}H NMR (400 MHz, 298 K, $CDCl_3$) and ^{13}C NMR (101 MHz, 298 K, $CDCl_3$) spectra of 2,3,4-tri-O-benzyl-1,6-dithio-β-D-glucopyranose (**32**). 96

Figure A 2.1. ^{1}H NMR (400 MHz, 298 K, d_6-DMSO) spectrum of the trans-2-butene-1,4-diol (**1**). 132

Figure A 2.2. ^{13}C NMR (101 MHz, 298 K, d_6-DMSO) spectrum of the trans 2-butene-1,4-diol (**1**) 132

Figure A 2.3. ^{1}H NMR (400 MHz, 298 K, $CDCl_3$) spectrum of tosylated isomannide (**2**). 133

Figure A 2.4. ^{13}C NMR (101 MHz, 298 K, $CDCl_3$) spectrum of the tosylated isomannide (**2**). 133

Figure A 2.5. ^{1}H NMR (400 MHz, 298 K, $CDCl_3$) spectrum of acetylated isoidide (**3**). 134

Figure A 2.6. ^{13}C NMR (101 MHz, 298 K, $CDCl_3$) spectrum of the acetylated isoidide (**3**). 134

Figure A 2.7. ^{1}H NMR (400 MHz, 298 K, d_6-DMSO) spectrum of isoidide (**4**). .. 135

Figure A 2.8. ^{13}C NMR (101 MHz, 298 K, d_6-DMSO) spectrum of the isoidide (**4**). 135

Figure A 2.9. ^{1}H NMR (400 MHz, 298 K, $CDCl_3$) spectrum of methyl 4,6-O-benzylidene-α-D-glucopyranoside (**6**). 136

Figure A 2.10. ^{13}C NMR (101 MHz, 298 K, $CDCl_3$) spectrum of methyl 4,6-O-benzylidene-α-D-glucopyranoside (**6**). 136

Figure A 2.12. ^{13}C NMR (101 MHz, 298 K, $CDCl_3$) spectrum of methyl 2,3 di-O-benzyl-4,6-O-benzylidene-α-D-glucopyranoside (**7**). 137

Figure A 2.13. ^{1}H NMR (400 MHz, 298 K, $CDCl_3$) spectrum of methyl 2,3,6-tri-O-benzyl-α-D-glucopyranoside (**8**). 138

Figure A 2.14. ^{13}C NMR (101 MHz, 298 K, $CDCl_3$) spectrum of methyl 2,3,6-tri-O-benzyl-α-D-glucopyranoside (**8**). 138

Figure A 2.15. ^{1}H NMR (400 MHz, 298 K, $CDCl_3$) spectrum of 2,3,6-tri-O-benzyl-α-D-glucopyranose (**9**). 139

Figure A 2.16. ^{13}C NMR (101 MHz, 298 K, $CDCl_3$) spectrum of methyl 2,3,6-tri-O-benzyl-α-D-glucopyranose (**9**). 139

Figure A 2.17. ^{1}H NMR (400 MHz, 298 K, $CDCl_3$) spectrum of methyl 2,3,4,6-tetra-O-benzyl-α-D-glucopyranoside (**18**). 140

Figure A 2.18. ^{13}C NMR (101 MHz, 298 K, $CDCl_3$) spectrum of methyl 2,3,4,6-tetra-O-benzyl-α-D-glucopyranoside (**18**). 140

Figure A 2.19. ^{1}H NMR (400 MHz, 298 K, $CDCl_3$) spectrum of acetyl 2,3,4-tri-O-benzyl-6-acetyl-D-glucopyranoside in a 90/10 α to β anomer ratio (**19**). 141

Figure A 2.20. ^{13}C NMR (101 MHz, 298 K, $CDCl_3$) spectrum of acetyl 2,3,4-tri-O-benzyl-6-acetyl-D-glucopyranoside in a 90/10 α to β anomer ratio (**19**). 141

Figure A 2.21. ^{1}H NMR (400 MHz, 298 K, $CDCl_3$) spectrum of 2,3,4-tri-O-benzyl-D-glucopyranose in a 65/35 ratio of α to β anomer (**20**). 142

Figure A 2.22. ^{13}C NMR (101 MHz, 298 K, $CDCl_3$) spectrum of 2,3,4-tri-O-benzyl-D-glucopyranose in a 65/35 ratio of α to β anomer (**20**). 142

Figure A 2.23. ^{1}H NMR (400 MHz, 298 K, $CDCl_3$) spectrum of the cis diacrylate (**24**). 143

Figure A 2.24. ^{13}C NMR (101 MHz, 298 K, $CDCl_3$) spectrum of the cis diacrylate (**24**). 143

Figure A 2.25. ^{1}H NMR (400 MHz, 298 K, $CDCl_3$) spectrum of the trans diacrylate (**25**). 144

Figure A 2.26. ^{13}C NMR (101 MHz, 298 K, $CDCl_3$) spectrum of the trans diacrylate (**25**). 144

Figure A 2.27. ^{1}H NMR (400 MHz, 298 K, $CDCl_3$) spectrum of the isosorbide-derived diacrylate (**26**). 145

Figure A 2.28. ^{13}C NMR (101 MHz, 298 K, $CDCl_3$) spectrum of the isosorbide-derived diacrylate (**26**). 145

Figure A 2.29. ^{1}H NMR (400 MHz, 298 K, $CDCl_3$) spectrum of the isomannide-derived diacrylate (**27**). 146

Figure A 2.30. ^{13}C NMR (101 MHz, 298 K, $CDCl_3$) spectrum of the isomannide-derived diacrylate (**27**). 146

Figure A 2.31. ^{1}H NMR (400 MHz, 298 K, $CDCl_3$) spectrum of the isoidide-derived diacrylate (**28**). 147

Figure A 2.32. ^{13}C NMR (101 MHz, 298 K, $CDCl_3$) spectrum of the isoidide-derived diacrylate (**28**). 147

Figure A 2.33. ^{1}H NMR (400 MHz, 298 K, $CDCl_3$) spectrum of the 1,6-glucose-derived diacrylate (**29**). 148

Figure A 2.34. ^{13}C NMR (101 MHz, 298 K, $CDCl_3$) spectrum of the 1,6-glucose derived diacrylate (**29**). 148

Figure A 2.35. ^{1}H NMR (400 MHz, 298 K, $CDCl_3$) spectrum of 2,3,4-tri-O-benzyl-6-O-methanesulfonyl-α-D-glucopyranosyl chloride (**30**). 149

Figure A 2.36. ^{13}C NMR (101 MHz, 298 K, $CDCl_3$) spectrum of 2,3,4-tri-O-benzyl-6-O-methanesulfonyl-α-D-glucopyranosyl chloride (**30**). 149

Figure A 2.37. ^{1}H NMR (400 MHz, 298 K, $CDCl_3$) spectrum of acetyl 2,3,4-tri-O-benzyl-1,6-dithio-6- acetyl-β-D-glucopyranoside (**31**)..... 150

Figure A 2.38. ^{13}C NMR (101 MHz, 298 K, $CDCl_3$) spectrum of acetyl 2,3,4-tri-O-benzyl-1,6-dithio-6- acetyl-β-D-glucopyranoside (**31**)..... 150

Figure A 2.39. ^{1}H NMR (400 MHz, 298 K, $CDCl_3$) spectrum of 2,3,4-tri-O-benzyl-1,6-dithio-D-glucopyranose (**32**). 151

Figure A 2.40. ^{13}C NMR (101 MHz, 298 K, $CDCl_3$) spectrum of 2,3,4-tri-O-benzyl-1,6-dithio-D-glucopyranose (**32**). 151

Figure A 2.41. ^{1}H NMR (400 MHz, 298 K, $CDCl_3$) spectrum of 2,3,4-tri-O-benzyl-D-glucopyranose (**9**) in a 65/35 ratio of α to β anomer. 152

Figure A 2.42. ^{13}C NMR (101 MHz, 298 K, $CDCl_3$) spectrum of 2,3,4-tri-O-benzyl-D-glucopyranose (**9**) in a 65/35 ratio of α to β anomer. 152

Figure A 2.43. ^{1}H NMR (400 MHz, 298 K, $CDCl_3$) spectrum of 2,3,6-tri-O-benzyl-4-acetyl-D-glucopyranose (**6**)..... 153

Figure A 2.44. ^{13}C NMR (101 MHz, 298 K, $CDCl_3$) spectrum of 2,3,6-tri-O-benzyl-4-acetyl-D-glucopyranose (**6**). 153

Figure A 2.45. ^{1}H NMR (400 MHz, 298 K, $CDCl_3$) spectrum of benzyl alcohol (**12**), recovered during the acetolysis of methyl 2,3,6-tri-O-benzyl-α -D-glucopyranoside (**8**)..... 154

Figure A 2.46. ^{13}C NMR (101 MHz, 298 K, $CDCl_3$) spectrum of benzyl alcohol (**12**), recovered during the acetolysis of methyl 2,3,6-tri-O-benzyl-α -D-glucopyranoside (**8**)..... 154

Figure A 2.47. ^{1}H NMR (400 MHz, 298 K, $CDCl_3$) spectrum of methyl 2,3,4-tri-O-benzyl-4-acetyl-α-D-glucopyranoside (**13**)..... 155

Figure A 2.48. ^{13}C NMR (101 MHz, 298 K, $CDCl_3$) spectrum of methyl 2,3,4-tri-O-benzyl-4-acetyl-α-D-glucopyranoside (**13**)..... 155

Figure A 2.49. ^{1}H NMR (400 MHz, 298 K, $CDCl_3$) spectrum of acetyl 2,3-di-O-benzyl-4,6-di-acetyl-D-glucopyranoside (**14**). 156

Figure A 2.50. ^{13}C NMR (101 MHz, 298 K, $CDCl_3$) spectrum of acetyl 2,3-di-O-benzyl-4,6-di-acetyl-D-glucopyranoside (**14**). 156

Figure A 2.51. ^{1}H NMR (400 MHz, 298 K, $CDCl_3$) spectrum of methyl 2,3,4,6-tetra-O-benzyl-D-glucopyranoside **(18)** in a 50/50 ratio of α to β anomer..... 157

Figure A 2.52. ^{13}C NMR (101 MHz, 298 K, $CDCl_3$) spectrum of methyl 2,3,4,6-tetra-O-benzyl-D-glucopyranoside **(18)** in a 50/50 ratio of α to β anomer..... 157

Figure A 2.53. ^{1}H NMR (400 MHz, 298 K, $CDCl_3$) spectrum of acetyl 2,4-di-O-benzyl-3,6-di-acetyl-D-glucopyranoside (**22**). 158

Figure A 2.54. ^{13}C NMR (101 MHz, 298 K, $CDCl_3$) spectrum of acetyl 2,4-di-O-benzyl-3,6-di-acetyl-D-glucopyranoside (**22**). 158

Figure A 2.55. ^{1}H NMR (400 MHz, 298 K, $CDCl_3$) spectrum of acetyl 3,4-di-O-benzyl-2,6-di-acetyl-D-glucopyranoside and acetyl 2,3-di-O-benzyl-4,6-di-acetyl-D-glucopyranoside (**21** and **23**). 159

Figure A 2.56. ^{13}C NMR (101 MHz, 298 K, $CDCl_3$) spectrum of acetyl 3,4-di-O-benzyl-2,6-di-acetyl-D-glucopyranoside and acetyl 2,3-di-O-benzyl-4,6-di-acetyl-D-glucopyranoside (**21** and **23**). 159

Figure A 2.57. ^{1}H NMR (400 MHz, 298 K, $CDCl_3$) spectrum of 1,6-anhydro-6-deoxy-6-thio-2,3,4-tri-O-benzyl-β-D-glucopyranose (**33**). By-product of the synthesis of 1,6-dithioacetate (**31**). 160

Figure A 2.58. ^{13}C NMR (101 MHz, 298 K, $CDCl_3$) spectrum of 1,6-anhydro-6-deoxy-6-thio-2,3,4-tri-O-benzyl-β-D-glucopyranose (**33**). By-product of the synthesis of 1,6-dithioacetate (**31**). 160

Figure A 2.59. ^{1}H NMR (400 MHz, 298 K, $CDCl_3$) spectrum of a 1,6-glucose-derived disulfide as an example of intramolecular disulfide formation occurring whilst working with the 1,6-glucose-derived dithiol (**32**). 161

Figure A 2.60. ^{13}C NMR (101 MHz, 298 K, $CDCl_3$) spectrum of a 1,6-glucose-derived disulfide as an example of intramolecular disulfide formation occurring whilst working with the 1,6 dithiol (**26**). 161

Figure 3.1. Overview of this chapter which focusses on (a) the synthesis of acrylate-based telechelic oligomers via thiol-Michael step growth polyaddition were **R** represent either (b) the cis or trans diol, (c) from left to right, isosorbide, isommanide and isoidide or (d) a 1,6-glucose-derived diol. Both unsaturated- and isohexide-derived diacrylate monomer were reacted with 1,6-hexane dithiol whilst the 1,6-glucose-derived diacrylate has been reacted first with a 1,6-glucose-derived dithiol (f,bottom) then with 1,6-hexane dithiol (f, top). 168

Figure 3.2. The dependence of polymer molecular weight on the stoichiometry of the acrylate monomers. Experimental data for both the cis (blue) and trans (red) polymers and theoretical molecular weights (black) are shown. 173

Figure 3.3. ^{1}H NMR spectra (400 MHz, $CDCl_3$, 298 K) of a cis 4.0 kDa oligomer (top) and a trans 4.5 kDa oligomer (bottom). 174

Figure 3.4. DSC thermograms of 1st and 2nd heating cycles for the cis 4.0 kDa oligomer and the trans 4.5 kDa oligomer. 176

Figure 3.5. ^{1}H NMR spectra (400 MHz, $CDCl_3$, 298 K) of (a) a 3.3 kDa isosorbide based oligomer, (b) a 3.9 kDa isomanide derived oligomer and (c) a 3.3 kDa isoidide derived oligomer. The molecular weight has been obtained by end-group analysis, taking the acrylate integration as reference. The integration of the methine protons from the isohexides moieties and the methylene within the thiol spacer were used to determinate the average chain length. 179

Figure 3.6. Picture representing uncontrolled crosslinking encountered during the polymerisation or work up of isohexide derived oligomer. 180

Figure 3.7. 1st heating cycles of the DSC thermograms for the isohexides oligomers. The table presents the key thermal transitions of the oligomers. **[a]**The glass transition temperature (T_g) was taken as the midpoint of the inflection tangent upon the 2nd heating scan. **[b]**The temperature of the first endothermic transition ($T_{m,1}$),

taken at the minimum of the peak on the first heating scan. [c]The temperature of the 2nd endothermic transition ($T_{m,2}$), taken at the minimum of the peak on the 1st heating scan. [d] The total enthalpy of melting (ΔH_m) was calculated from integration and normalisation of all endothermic peaks present on the first heating scan. .. 181

Figure 3.8. (a) Scheme of the polymerisation of the 1,6-glucose-derived diacrylate and dithiol via thiol-Michael addition. The reaction is performed either in DMF or $CHCl_3$ at a diacrylate monomer concentration of 0.25 M and in the presence of DMPP or DBU as catalyst. (b) Table presenting a summary of the results of polymerisation for the glucose derived monomers at the stochiometric balance. M_n, M_w, and $Đ_M$ were determined by SEC (DMF, 0.5% w/w NH_4BH_4). Analysis against poly(methyl methacrylate) (PMMA) standards. 183

Figure 3.9. ^{1}H NMR spectra (400 MHz, $CDCl_3$, 298 K) of an 8.0 kDa glucose-derived polymerisation product. The absence of the resonance peaks characteristic of the acrylate between 5.6 and 6.5 ppm indicates a successful polymerisation..... 185

Figure 3.10. (a) Scheme of the polymerisation of the 1,6-glucose-derived diacrylate and 1,6-hexane dithiol via thiol-Michael addition. The reaction is performed either in DMF or $CHCl_3$ at a diacrylate monomer concentration of 0.25 M and in the presence of DMPP or DBU as catalyst. (b) Table presenting a summary of the results of polymerisation for the glucose derived monomers at the stochiometric balance. M_n, M_w, and $Đ_M$ were determined by SEC (DMF, 0.5% w/w NH_4BH_4). Analysis against poly(methyl methacrylate) (PMMA) standards. 186

Figure 3.11. 1st heating cycles of the DSC thermograms for the polymerisation products of 1,6-glucose-derived diacrylate and 1,6-glucose-derived dithiol “glucose” or 1,6-hexane dithiol “glucose-hexane”. The table present the key thermal properties of the oligomers. [a]The glass transition temperature (T_g) was taken as the midpoint of the inflection tangent upon the 2nd heating scan. [b]The temperature of the first endothermic transition ($T_{m,1}$), taken at the minimum of the peak on the first heating scan. [c]The temperature of the 2nd endothermic transition ($T_{m,2}$), taken at the minimum of the peak on the 1st heating scan. [d] The total enthalpy of melting (ΔH_m) was calculated from integration and normalisation of all endothermic peaks present on the first heating scan. 187

Figure A 3.1. ^{1}H NMR (400 MHz, 298 K, $CDCl_3$) spectrum of a 4.0 kDa cis oligomer. 200

Figure A 3.2. ^{13}C NMR (101 MHz, 298 K, $CDCl_3$) spectrum of a 4.0 kDa cis oligomer. 200

Figure A 3.3. ^{1}H NMR (101 MHz, 298 K, $CDCl_3$) spectrum of a 6.1 kDa cis oligomer. 201

Figure A 3.4. ^{13}C NMR (101 MHz, 298 K, $CDCl_3$) spectrum of a 6.1 kDa cis oligomer. 201

Figure A 3.5. ^{1}H NMR (400 MHz, 298 K, $CDCl_3$) spectrum of a 9.7 kDa cis oligomer. 202

Figure A 3.6. ^{13}C NMR (101 MHz, 298 K, $CDCl_3$) spectrum of a 9.7 kDa cis oligomer. 202

Figure A 3.7. ^{1}H NMR (400 MHz, 298 K, $CDCl_3$) spectrum of a 4.5 kDa trans oligomer. 203

Figure A 3.8. ^{13}C NMR (101 MHz, 298 K, $CDCl_3$) spectrum of a 4.5 kDa trans oligomer. 203

Figure A 3.9. ^{1}H NMR (400 MHz, 298 K, $CDCl_3$) spectrum of a 6.1 kDa trans oligomer. 204

Figure A 3.10. ^{13}C NMR (101 MHz, 298 K, $CDCl_3$) spectrum of a 6.1 kDa trans oligomer. 204

Figure A 3.11. ^{1}H NMR (400 MHz, 298 K, $CDCl_3$) spectrum of a 9.7 kDa trans oligomer. 205

Figure A 3.13. ^{1}H NMR (400 MHz, 298 K, $CDCl_3$) spectrum of a 3.3 kDa isosorbide derived oligomer. 206

Figure A 3.14. ^{13}C NMR (101 MHz, 298 K, $CDCl_3$) spectrum of a 3.3 kDa isosorbide derived oligomer. 206

Figure A 3.15. ^{1}H NMR (400 MHz, 298 K, $CDCl_3$) spectrum of a 3.9 kDa isosorbide derived oligomer. 207

Figure A 3.16. ^{13}C NMR (101 MHz, 298 K, $CDCl_3$) spectrum of a 3.9 kDa isosorbide derived oligomer. 207

Figure A 3.17. ^{1}H NMR (400 MHz, 298 K, $CDCl_3$) spectrum of a 4.5 kDa isosorbide derived oligomer. 208

Figure A 3.18. ^{13}C NMR (101 MHz, 298 K, $CDCl_3$) spectrum of a 4.5 kDa isosorbide derived oligomer. 208

Figure A 3.19. ^{1}H NMR (400 MHz, 298 K, $CDCl_3$) spectrum of a 3.9 kDa isomannide derived oligomer. 209

Figure A 3.20. ^{13}C NMR (101 MHz, 298 K, $CDCl_3$) spectrum of a 3.9 kDa isomannide derived oligomer. 209

Figure A 3.21. ^{1}H NMR (400 MHz, 298 K, $CDCl_3$) spectrum of a 4.5 kDa isomannide derived oligomer. 210

Figure A 3.22. ^{13}C NMR (101 MHz, 298 K, $CDCl_3$) spectrum of a 4.5 kDa isomannide derived oligomer. 210

Figure A 3.23. ^{1}H NMR (400 MHz, 298 K, $CDCl_3$) spectrum of a 3.3 kDa isoidide derived oligomer. 211

Figure A 3.24. ^{13}C NMR (101 MHz, 298 K, $CDCl_3$) spectrum of a 3.3 kDa isoidide derived oligomer. 211

Figure A 3.25. ^{1}H NMR (400 MHz, 298 K, $CDCl_3$) spectrum of an 8.0 kDa glucose-glucose oligomer. 212

Figure A 3.26. Compiled size exclusion chromatogram of trans oligomers (DMF, 0.5% w/w NH_4BH_4). (a) 4.5 kDa trans oligomer, (b) 6.1 kDa trans oligomer, (c) 6.6 kDa trans oligomer, (d) 9.7 kDa trans oligomer. Analysis against poly(methyl methacrylate) (PMMA) standards. 213

Figure A 3.27. Compiled size exclusion chromatogram of cis oligomers (DMF, 0.5% w/w NH_4BH_4). (a) 4.0 kDa cis oligomer, (b) 6.1 kDa cis oligomer, (c) 6.6 kDa cis oligomer, (d) 9.7 kDa cis oligomer. Analysis against poly(methyl methacrylate) (PMMA) standards. 214

Figure 4.1. Chemical structure of stereopure (a) trans and (b) cis oligomers using in this study. 218

Figure 4.2. Photography of (a) an oligomer after synthesis, (b) a photocurable resin prepared from a 50:50:1 % ratio of oligomer, diluent and photoinitiator, (c) a film obtained after exposing the resin to 405 nm UV light and thermal post-curing, (d) dumbbell shaped samples for mechanical testing cut out from a film. 219

Scheme 4.1. Photolysis of phenylbis (2,4,6-trimethylbenzoyl)-phosphine oxide (Omnirad® 819). 219

Figure 4.3. Stress versus strain curves of films prepared using 4.5 kDa trans oligomer in PC. Young's modulus E= 2.18 (±0.16) MPa, stress at break σ_b= 1.80 (±0.24) MPa, strain at break ε_b = 120 (±15) % on average over 3 repeats. 220

Figure 4.4. Stress vs. strain curves of films prepared from 5 kDa cis and trans oligomers. trans: Young's modulus E= 1.59 (±0.32) MPa, stress at break σ_b= 1.52 (±0.12) MPa, strain at break ε_b = 207 (±14)% cis: Young modulus E= 1.67 (±0.11) MPa, stress at break σ_b= 1.57 (±0.073) MPa, strain at break ε_b = 163 (±12.8)% 222

Figure 4.5. ^{1}H NMR (300 MHz, $CDCl_3$, 298 K) spectra of a thiol-end-capped cis oligomer after a) 15 min and b) 20 sec of UV irradiation. 224

Figure 4.6. Top: Scheme of the end-capped cis oligomer submitted to a variable period of UV irradiation. (a) Comparison of ^{1}H NMR (300 MHz, $CDCl_3$, 298K) spectra vinyl region of thiol end-capped cis oligomer resins exposed to UV radiation from 0 s to 15 min. (b) Percentage of isomerisation occurring during UV irradiation of a cis end-capped oligomer on an Otoflash postcuring light pulsing unit (flash box, 300 nm ≤ λ ≤ 700 nm, 11 W) and a Formlab form cure curing station (curing oven, =405 nm, 39 W). No isomerisation occurs if the oligomer is not in the presence of a photoinitiator (**Appendix Figure A5**). 226

Figure 4.7. Stress vs. strain curves of films from cis and trans oligomers cured for a varying amount of time. 228

Figure 4.8. DSC thermograms for films prepared from cis 4.0 kDa and trans 4.5 kDa oligomers and cured for 15 min, 1 min or 20s. 229

Figure 4.9. ^{1}H NMR (300 MHz, 298 K, DMSO-d_6) spectra of a linear cis 4.0 kDa oligomer (top) and its depolymerisation products (bottom). 232

Figure 4.10. ^{1}H NMR (300 MHz, 298 K, DMSO-d_6) spectrum of a linear trans 4.5 kDa oligomer (top) and its depolymerisation products (bottom). 233

Figure 4.11. (a) Representation of the major depolymerisation products of cis and trans films. (b) ^{1}H NMR (300 MHz, d_6-DMSO, 298 K) spectra of cis and trans depolymerised films after a varying UV exposure time. 235

Figure 4.12. Representative stress-strain curves of (a) a 4.5 kDa trans film and a 4.0 kDa cis film, (b) 6.1 kDa trans film and a 6.1 kDa cis film, (c) a 10 kDa trans film

and a 9.7 kDa cis film. The molecular weights have been determined via ^{1}H NMR spectroscopy. 236

Figure 4.13. Idealistic representation of the network formation and final structure at the molecular level: the radical initiate the crosslinking of the acrylate end group; however, the internal unsaturation remains unreactive. 238

Figure 4.14. (a) 1st heating scans of DSC thermograms for (a) trans films of 4.5, 6.1, 7.1 and 10 kDa showing a constant degree of crystallisation and (b) cis films of 4.0, 6.1, 7.1 and 10 kDa showing the dependence of the crystallinity with the oligomer chain length. 239

Figure 4.15. 1st heating scans of DSC thermograms for (a) trans films of 4.5 kDa, (b) cis films of 4.0 kDa, (c) trans films of 6.1 kDa and (d) cis films of 6.6 kDa. ... 240

Figure 4.16. Swelling ratio relative to the initial sample weight after 24h in THF at 25˚C. Each data point was averaged from 4 samples with the standard deviation taken as the uncertainty. 242

Figure 4.17. Structure of N-methyl pyrrolidone and N-vinyl pyrrolidone, used as unreactive and reactive diluent respectively and table summarising the formulation of the original resin containing 0% of NVP and resin which contains either 8 or 25 wt% of NVP. 243

Figure 4.18. Stress-strain curves of both cis and trans films containing (a) 8% NVP and (b) 25% NVP. 244

Figure 4.19. Representation of (a) the slicing process converting a 3D model into a compilation of 2D images or slices and (b) a DLP 3D printer general structure and process. 246

Figure 4.20. 3D printing resin viscosity between a shear rate of 0.1 and 100 s^{-1}. 247

Figure 4.21. UV-Vis absorbance of (a) 4.0 kDa cis oligomer and 4.5 kDa trans oligomer in NMP. (b) cis and trans resin (oligomer, NMP, TPO-L, paprika resin in a 50:50:0.5:0.5 wt% ratio.) The absorbance peak at 377 nm is due to the presence of TPO-L, the absorbance peak at 470 nm is characteristic of the paprika resin, and (c) TPO-L and paprika resin and their maxima of absorbance at 377 nm and 377/470 nm respectively. 248

Figure 4.22. Evolution of the storage (G') and loss (G") moduli with time during UV irradiation of (a) trans resin and (b) cis resin containing 50 wt% oligomer in NMP, 0.5 wt% of photoinitiator and 0.5 wt% photoinhibitor. The lamp is switched on at 50 s. The insets are close-up for the intersections of G' and G" curves. 249

Figure 4.23. Photographs from 3 different angles (top, side and corner view) of 3D printed 4.5 kDa cis cubes from resins containing different amounts of photoinhibitor. On the bottom right corner is presented illustration of the computerised structure (side and corner view). 250

Figure 4.24. Picture of a 3D printed 4.0 kDa trans scaffold next to a standard paperclip for scale. 250

Figure 4.25. Compressive stress-strain curves of 4.5 kDa cis and 4.0 kDa trans scaffolds. 251

Figure 4.26. Stress and strain obtained from the cyclic compression of a 4.5 kDa cis scaffold submitted to stress up to 1 MPa for 10 cycles. 252

Figure 4.27. 1st heating scan of the DSC thermogram for a cis and a trans 3D printed scaffold. ΔH_m = 11.7 and 7.2 $J \cdot g^{-1}$, T_g = – 10.06 °C and – 15.89 °C, T_m = 52.35 °C and T_m = 45.86°C for the 4.0 kDa trans and 4.5 kDa cis scaffold respectively... 253

Figure 4.28. hydrolytic degradation profiles for the 4.5 kDa cis and 4.0 kDa trans photosets in a solution of NaOH 1M at 37 °C. Each data point represents the average weight of 4 samples. 254

Figure 4.29. ^{1}H NMR (300 MHz, 298 K, DMSO-d_6) spectrum of a depolymerised 3D printed 4.5 kDa cis scaffold. 255

Figure 4.30. (a) Representation of the major depolymerisation products of cis printed films. (b) ^{1}H NMR (300 MHz, d_6-DMSO, 298 K) spectra of cis depolymerised printed films after 15 mins of exposure to the 3D printer light source (top) or increasing 6 times the light intensity I (bottom). 256

Figure A 4.1. Pictures of the film cutting before and after depolymerisation..... 266

Figure A 4.2. Pictures of an uncured resin (left), a film obtained after curing (centre) and dumbbell-shaped samples (right). 267

Figure A 4.4. ^{1}H NMR (300 MHz, 298 K, d_6-DMSO) spectra of a depolymerised cis film cured for 15 min (top) and 20 sec (bottom). 269

Figure A 4.5. ^{1}H NMR (300 MHz, 298 K, d_6-DMSO) spectra of a cis resin formulated without the photoinitiator and exposed to UV for 15 mins. No isomerisation reaction occurred. 269

Figure A 4.6. ^{1}H NMR (400 MHz, 298 K, $CDCl_3$) spectra of a 4.0 kDa trans oligomer used in the trans 3D printed resin. 270

Figure A 4.7. ^{13}C NMR (101 MHz, 298 K, $CDCl_3$) spectra of a 4.0 kDa trans oligomer used in the trans 3D printed resin. 270

Figure A 4.8. ^{1}H NMR (400 MHz, 298 K, $CDCl_3$) spectra of a 4.5 kDa cis oligomer used in the cis 3D printed resin. 271

Figure A 4.9. ^{13}C NMR (101 MHz, 298 K, $CDCl_3$) spectra of a 4.5 kDa cis oligomer used in the cis 3D printed resin. 271

Figure A 4.10. Compiled tensile elongation of (a) 4.5 kDa trans films (red) and 4.0 kDa cis films (blue), (d) 6.1 kDa trans films (red) and 6.1 kDa cis films (blue), (c) 6.6 kDa trans films (red) and 6.6 kDa cis films (blue), (d) 9.7 kDa trans films (red) and 9.7 kDa cis films (blue). For each sample, 6 specimens were tested. 272

Figure A 4.11. Compression tests of (a) 3D printed trans scaffolds and (b) 3D printed cis scaffolds and cyclic compression of 3D printed cis scaffolds (c). The maximum compression strength have been set at 50 N. For each sample, a minimum of 6 specimens were tested. 274

Figure A 4.14. DSC thermograms (1st heating scan) of (a) trans films and (b) cis films for increasing molecular weight taken at 2 days of annealing. At all molecular weights, trans films show crystallinity after 2 days of annealing while the cis films only show crystallinity for larger molecular weights. 276

Figure A 4.15. DSC thermograms of (a) a 4.0 kDa trans 3D printed scaffold and (b) a 4.5 kDa cis 3D printed scaffold. The dashed line represents the 1st cooling scan, the middle one, the 2nd heating scan and the bottom line is the 1st heating scan. 277

List of Schemes, Tables and Equations

Scheme 1.1. Representation of the mechanism of the Walden inversion observed in S~~N~~$_2$ nucleophilic substitution. 12

Scheme 1.2. Scheme of the trans to cis isomerisation of azobenzene occurring under UV irradiation. The trans isomer being the thermodynamically stable isomer, hence the cis to trans isomerisation occurs naturally in the absence of irradiation. 22

Scheme 1.3. Synthesis of polyenamines by Cu(I)-catalysed amino-yne polymerisation.[80] Reproduced from reference[80] with permission of the Royal Society of Chemistry. 26

Scheme 1.4. Phenol-yne polymerisation of 100% trans poly(vinylene ether ketone) using DMAP as a catalyst. Reproduced from reference[84] with permission from John Wiley and Sons. 27

Scheme 1.5. Synthesis of renewable polyurethane from hydroxymethyl furfural and isohexide-derived difunctional isocyanates. 31

Scheme 1.6. Synthesis of poly(ester-urethane)s used to study the impact of the isohexide structure on the mechanical properties of the material. 31

Scheme 1.7. Synthesis of unsaturated poly(ester-urethanes) from stereo-defined diacrylates and 1,6-hexanedithiol. 34

Scheme 1.8. Synthesis via thiol-yne click chemistry of either a cis or trans rich hydrogel network from the reaction of an alkyne terminated and a thiol terminated 4-arm poly(ethylene glycol) precursors. The use of a strong base in a polar solvent favours a trans rich network and a cis rich network is obtained by using a weak base in an apolar solvent. Reproduced from reference[123] under the Creative Commons Attribution Licence 2021. 38

Scheme 1.9. Synthesis of a bisbenzoxazine monomer from a isosorbide diamine and cardanol via Mannich-like condensation under microwave irradiation in the absence of solvent. Adapted from reference[124] with permission from the American Chemical Society. 39

Scheme 2.1. Synthesis of trans-2-butene-1,4-diol 57

Scheme 2.2. Synthesis of isoidide (**4**). 59

Scheme 2.3. Reaction scheme of the polycondensation of unprotected α-D-glucose and a representation of the structure of the products obtained: the linkage between glucose units is non regio-specific as the hydroxyl on C1 is able to react with one of the four non anomeric free hydroxyls. 61

Scheme 2.4. Multi-step synthesis of 2,3,6-tri-O-benzyl-D-glucopyranoside (1,4-glucose diol) (**9**). 64

Scheme 2.5. Product obtained from both (a) Hydrolysis of methyl 2,3,6-tri-O-benzyl-α-D-glucopyranoside (**8**) in the presence of aqueous H_2SO_4 or HCl 0.1 M in acetic acid at 110 °C following traditional hydrolysis conditions and (b) hydrolysis of (**8**)

using 0.1 equiv. of strontium chloride as cocatalyst in addition of aqueous HCl 1 M in acetic acid at 70 °C. 69

Scheme 2.6. Schemes of (a) acetolysis of methyl 2,3,6-tri-O-benzyl-α-D-glucopyranoside (8) in the presence of H2SO4 0.1 M in acetic acid at -10 °C and (b) acetolysis of (8) in milder conditions, using H2SO4 0.015 M in a mixture of Ac2O and AcOH (2:3). 73

Scheme 2.7. Potential preparation method of a 1,4-glucose-derived diol by sequential deacetylation and selective protection of the primary alcohol using trityl chloride (TrCl) to give compound (**16**) or tert-butyldimethylsilyl chloride (TBDMSCl) to give compound (**17**). 77

Table 2.1. Comparison of the resonance signals of protons and carbons in C1 and C6 of α 1,6-glucose-derived diol (**20**) and sulfonated product (**30**) prior to its structure determination. 92

Scheme 2.10. Products obtained from reacting compound (**30**) with potassium thioacetate in refluxing acetone: 1,6-glucose-derived dithioacetate (8/92 α to β ratio) (**31**) and 1,6-glucose-derived thio-ether (**33**) in a 80/20 ratio of product to by-product. All ratios were determined from the relative integration of the anomeric proton signal of the distinct compound on the ^{1}H NMR spectrum of the crude. 94

Table 2.2. Comparison of the resonance signals of protons and carbons in C1 and C6 of β-1,6-glucose derived diacetate (**19**) and dithioacetate (**31**). 94

Scheme 3.1. Synthesis of cis and trans stereopure acrylate-terminated telechelic oligomers via thiol-Michael addition. The reaction is performed in DMF at a diacrylate monomer concentration of 0.25 M and in the presence of 0.5 mol% of DMPP as catalyst. 169

Table 3.1. Stoichiometry between an unsaturated acrylate and dithiol monomers for a targeted molecular weight based on the Carother's equation. 171

Table 3.2. Summary of molecular weights obtained by ^{1}H NMR and GPC for cis and trans unsaturated oligomers. **[a]**Determined by ^{1}H NMR spectroscopy (400 MHz, 298 K, $CDCl_3$). **[b]**M_n, M_w, $Đ_M$ were determined by SEC (DMF, 0.5% w/w NH_4BH_4) analysis against poly(methyl methacrylate) (PMMA) standards. 175

Scheme 3.2. Synthesis of isohexides acrylate-terminated telechelic oligomers via thiol-Michael addition. The reaction is performed in DMF at a diacrylate monomer concentration of 0.25 M and in the presence of DMPP as a catalyst. 177

Table 3.3. Stoichiometry between isohexide derived diacrylate and dithiol monomers for a targeted molecular weight based on the Carother's equation... 177

Table 3.4. Summary of molecular weights obtained by ^{1}H NMR and GPC for the isosorbide and isomannide derived oligomers. **[a]**Determined by ^{1}H NMR spectroscopy (400 MHz, 298 K, $CDCl_3$). **[a]**Determined by ^{1}H NMR spectroscopy (400 MHz, 298 K, $CDCl_3$). **[b]**M_n, M_w, $Đ_M$ were determined by SEC (DMF, 0.5% w/w NH_4BH_4) analysis against poly(methyl methacrylate) (PMMA) standards. 178

Table 3.5. Summary of the results of polymerisation for the glucose-derived monomers using an equivalent of diacrylate to dithiol inferior to the unity. M_n, M_w, and $Đ_M$ were determined by SEC (DMF, 0.5% w/w NH_4BH_4). Analysis against poly(methyl methacrylate) (PMMA) standards. 184

Table 3.6. Summary of the results of polymerisation for the glucose-derived monomers using a 1:1 molar ratio of diacrylate to dithiol. M_n, M_w, and $Đ_M$ were determined by SEC (DMF, 0.5% w/w NH_4BH_4). Analysis against poly(methyl methacrylate) (PMMA) standards. 185

Table A3.1. Oligomer characterisation by SEC. 214

Table 4.1. Solubility tests of oligomer in different solvent/oligomer ratio and their stability over time. rt = room temperature. 221

Scheme 4.2. Thiol end-capping of a cis oligomer using 1-hexanethiol. 223

Table A 4.1. Summary of key tensile parameters for the films. 273

Table A 4.2. Summary of key tensile parameters for 3D printed scaffolds. 274

Table A 4.3. Summary of thermal properties for films and 3D printed scaffolds. 278

Table A 4.4. Degradation temperature of selected films, 3D scaffolds and TPO-L. 280

List of Symbols and Abbreviations

3D	3 dimensional
Ac_2O	Acetic anhydride
AcOH	Acetic acid
ADMET	Acyclic diene metathesis
aPP	Atactic polypropylene
BHT	Butylated hydroxytoluene
BINAP	2,2'-bis(dimethylphosphino)-1,1'-binaphtyl
BINOL	1,1'-bi-2-naphtol
BnCl	Benzyl chloride
BzCl	Benzoyl chloride
$CDCl_3$	Deuterated chloroform
CHDA	1,4-cyclohexanedicarboxylic acid
CHDA	1,4-cyclohexanedicarboxylic acid
CHDM	1,4-cyclohexenedimethanol
CIP	Cahn-Ingold-Prelog
CSA	Camphor-10-sulfonic acid
d_6-DMSO	Deuterated dimethyl sulfoxide
Da	Dalton ≡ $g.mol^{-1}$
DACH	1,4-Diaminocyclohexane
DBTDL	Dibutyltin(IV) dilaurate

DBU	1,8-diazabicyclo[5.4.0]undec-7-ene
DLP	Digital Light Processing
$Đ_M$	Dispersity
DMAP	Dimethylaminopyridine
DMF	N,N'-dimethylformamide
DMPP	Dimethylphenylphosphine
DMSO	Dimethyl sulfoxide
DNDA	4,4',6,6'-dinitrodiphenic acid
DP	Degree of polymerisation
DSC	Differential Scanning Calorimetry
E	Young modulus
E_c	Compressive Young modulus
EG	Ethylene glycol
equiv.	Equivalent
Et_2O	Diethyl ether
Et_3N	Triethylamine
EtOAc	Ethyl acetate
EtOH	Ethanol
g	Gram
G'	Storage modulus
G"	Loss modulus
GPC	Gel permeation chromatography

h	Hour
HMBC	Heteronuclear multiple bond correlation
iPP	Isotactic polypropylene
Irgacure® 819	Phenylbis(2,4,6-trimethylbenzoyl)phosphine oxide
J	Joule
kDa	Kilodaltons
KOAc	Potassium acetate
KSAc	Potassium thioacetate
LED	Light-emitting diode
LNR	Liquid natural rubbers
M	Molar ≡ $mol.L^{-1}$
M_c	Molecular weight between crosslinks
MeOH	Methanol
min	Minute
mL	Milliliter
mm	Millimeter
mmol	Millimole
$\bar{M}_n$	Average molecular weight in weight
mol	Mole
MPa	Mega Pascal
MS	Mass spectrometry
$\bar{M}_w$	Average molecular weight in weight

N	Newton
$NaHCO_3$	Sodium bicarbonate
NaOMe	Sodium methoxide
nm	Nanometer
NMP	N-methyl pyrrolidinone
NMR	Nuclear magnetic resonance
NR	Natural rubber
NVP	N-vinyl pyrrolidone
Pa	Pascals
PC	Propylene carbonate
PEG	Poly(ethylene glycol)
pKa	Acid dissociation constant
PMMA	Poly(methyl methacrylate)
ppm	Part per million
PS	Polystyrene
ROMP	Ring opening metathesis polymerisation
rt	Room temperature
s	Seconds
SEC	Size-exclusion chromatography
SLA	Stereolithography
S_N2	Bimolecular nucleophilic substitution
TBAI	Tetrabutylammonium iodide

TBD	Triazabicyclodecene
TBDMS	Tert-butyldimethylsilyl
TBDMSCl	Tert-butyldimethylsilyl chloride
Td 5%	Temperature at 5% weight loss
T_g	Glass transition temperature
THF	Tetrahydrofuran
TLC	Thin layer chromatography
T_m	Melting temperature
TPO-L	Ethyl(2,4,6-Trimethylbenzoyl)-phenyl phosphinate
TrCl	Trityl chloride
TsCl	*p*-Toluenesulfonyl chloride
UV	Ultra-violet
VOC	Volatile organic compounds
W	Watt
wt%	Weight %
$\overline{X}_n$	Average value of the degree of polymerisation
δ	Chemical shift
ΔH_m	Total enthalpy of melting
ε_{1MPa}	Strain at a stress of 1 MPa
ε_b	Strain at break
λ	Wavelength
µL	Microliter

$\sigma_{50\%}$	Stress when the cube is reaching 50% of its original height
σ_b	Stress at break

List of publications

1. **AL Khalfa**, ML Becker, AP Dove, Stereochemistry-Controlled Mechanical Properties and Degradation in 3D-Printable Photosets, *Journal of the American Chemical Society*, (2021), 143, 17510 - 17516
2. CJ Stubbs, **AL Khalfa**, V Chiaradia, JC Worch, AP Dove, Intrinsically Re-curable Photopolymers Containing Dynamic Thiol-Michael Bonds, *Journal of the American Chemical Society*, (2022), 144, 11729-11735.

Chapter 1 – Introduction

1 Introduction of stereochemistry in polymers

1.1 Origins of stereochemistry

The genesis of the study of the spatial arrangement of atoms within molecules, namely stereochemistry, originated in Paris with the pioneering work of Louis Pasteur on the sodium ammonium tartrates.[1, 2] The driving force towards this work was an article from the German chemist Mitscherlich published in 1844 reporting that both sodium ammonium tartrate and racemate (or paratartrate) were identical in every aspect of their composition, crystal structure and physico-chemical properties.[3] However, the former was optically active when the later was not. Pasteur, at that time convinced of a possible relationship existing between hemihedrism and optical activity, conjectured that the paratartrate salt were simply not presenting any hemihedry. In an attempt to corroborate this hypothesis, the scientist found that the crystallisation of both types of tartrates results in similar crystals but indeed noticed that whilst the tartrate salt formed strictly identical hemihedral crystals, the paratartrate salt produced dissymmetric hemihedral crystals which he described as non-superimposable mirror-image of each other.[4] (**Figure 1.1**)

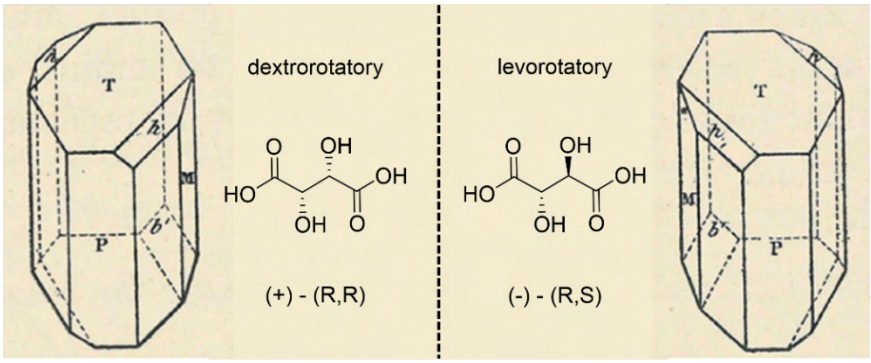


Figure 1.1. *Enantiomorphous hemihedral crystals of sodium ammonium racemate and the corresponding structure of the tartaric acid which they contain. Figure adapted from reference*[5] *with permission of John Wiley and Sons.*

Surprised by this unexpected result, Pasteur decided to manually separate the left-handed hemihedral crystals from the right-handed and study the optical activity of their respective solution. He then also discovered that the left-handed crystals were producing solutions that deviated polarised light to the left and the solution of right-handed crystals was deviating polarised light to the right with both deviations being identical in absolute value. Moreover, a solution made from a mixture of the two types of crystals in equal weight was optically inactive. These observations led Pasteur to propose that the rotary power of an organic solution is derived from molecular asymmetry which consequently produces non-superimposable mirror-imaged structures and in 1860, he postulated that the atoms constituting the right-handed tartaric acid could potentially be in a right-handed spiral arrangement or located at the apices of an irregular tetrahedron without further development. Nonetheless, this early work laid the foundation necessary to reform the prevailing structural theory which could not account for particular cases of isomerism encountered with chemical compound such as lactic acid, maleic/fumaric acid or tartaric acid. [6, 7]

In 1874, both Van't Hoff and Le Bel, independently proposed that the spatial arrangement of atoms should be considered to resolve the limitation of the then prevailing structural theory. [8, 9] As one of Kekulé's former student, Van't Hoff based his suggestions on the theory of a tetravalent carbon and deduced that only a tetrahedral arrangement of the hydrogen around the carbon atom could explain the number of isomers experimentally obtained for a mono-, di, tri and tetra-substituted methane molecule. (**Figure 1.2**)

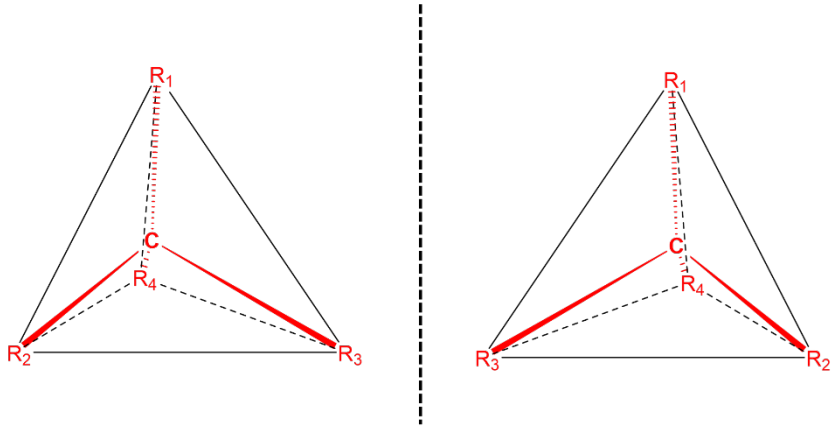


Figure 1.2. *Schematic representation of a tetrasubstituted carbon atom in a tetrahedral spatial arrangement and its non-superimposable mirror-image.*

In the same communication, he further introduced the concept of the asymmetric carbon ("assymmetrisch koolstof-atoom") that refers to a carbon atom bonded with 4 different substituents, since, depending on the relative arrangement of the latter, two distinct tetrahedrons could be obtained which were mirror-images of each other. He also demonstrated, with examples taken from the literature of the time, that all optically active compounds possessed an asymmetric carbon. Finally, he also claimed that a disubstituted ethylenic compound could also give rise to 2 different isomers, supporting his hypothesis with previously reported studies. Le Bel's proposition was published only 2 months after that of Van't Hoff and overall led to

the same conclusion of a spatial tetrahedral arrangement, although he was considering the symmetry of the molecule as a whole instead of that of one single carbon atom. He also considered that the four hydrogens of ethylene were directed towards the corner of a squared-based pyramid, since a double substitution give rise to two isomers.[10]

As strange as it appears today, these two communications on the importance of the spatial arrangement of atoms within molecules was at first received by the scientific community with indifference, if not with defamatory attacks towards the authors themselves.[11] Yet, this revolutionary theory could only be proven correct by following experimental work and, in 1880, Meyer proposed the term stereochemistry to refer to the study of molecules in a three dimensional space.[10, 12]

1.2 Vocabulary of stereochemistry

Stereochemistry is a rich and complex science which necessitated the development of a robust system of nomenclature to avoid confusion, of which the basis will be briefly covered within this section but more thorough analysis can be found in the literature.[13-16] Isomerism was the term originally proposed by Berzelius in 1830 to refer to the study of compound with the same empirical formula whilst having a different structural arrangement.[10] These types of isomers are now called constitutional isomers, as their difference resides in their structure, which could be derived from a divergence in function, position of substituent or connectivity of the backbone. (**Figure 1.3**)

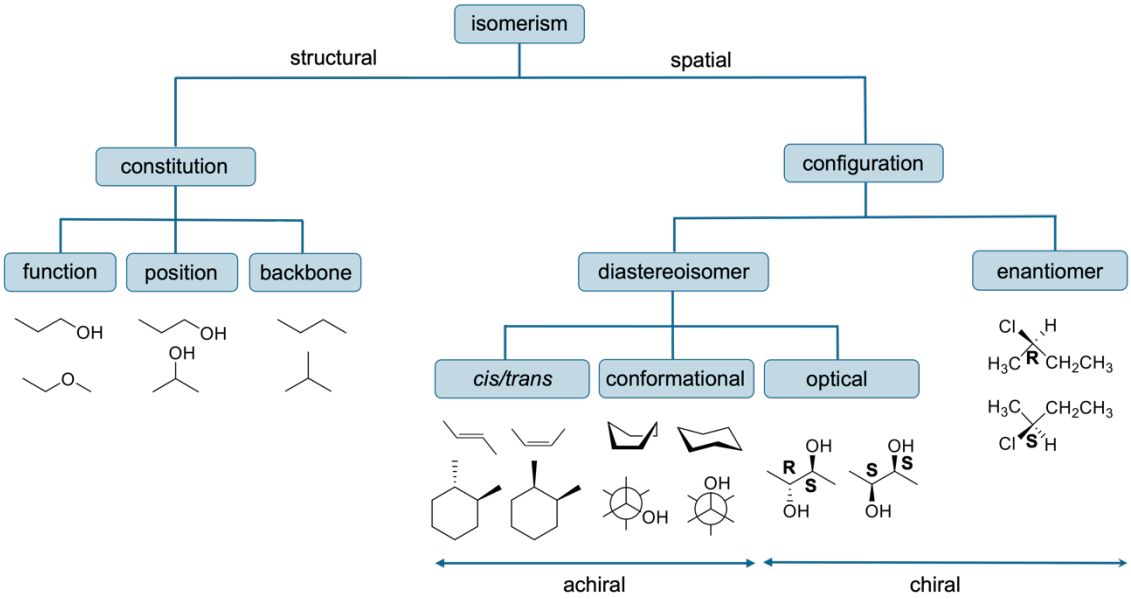


Figure 1.3. *Diagram summarising the most fundamental type of isomerism in chemistry.*

Stereoisomerism, on the other hand, refer to the study of compounds with the same constitution but with a different arrangement of the atoms in the 3 dimensions. Hence, they are called configurational isomers. More specifically, if two molecules are non-superimposable mirror-image of each other, namely chiral, they are called enantiomers. In solution, these types of molecules can deviate the plane of polarised light, either to the right (dextrorotatory) or to the left (levorotatory). This should not be confused with the determination of their absolute configuration using the Cahn, Ingold and Prelog (CIP) rules[17], which is required to assign priority to the 4 substituents of an atom by molecular weight and draw the compound such as the smallest substituent is the furthest from the observer. (**Figure 1.4**) The compound will be assigned with the absolute configuration *R* (for rectus, right) if passing from a substituent to another in a decreasing order of priority requires to turn clockwise. In the opposite case, the absolute configuration is *S* (for sinister, left).

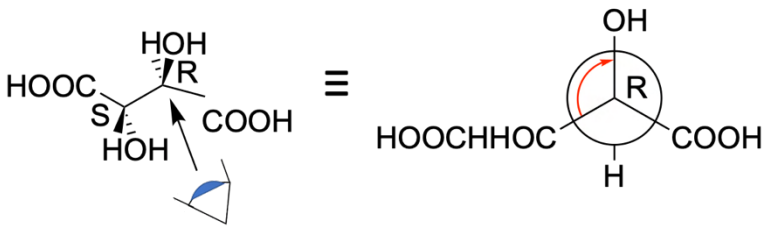


Figure 1.4. *(R,S) diastereoisomer of tartaric acid using different representation to illustrate the assignment of the absolute configuration following the CIP rules.*

However, no correlation exists between the absolute configuration *R* and a dextrorotatory optical activity and not all molecules with an *S* configuration would be levorotatory. Enantiomers possess identical physico-chemical properties in an achiral environment, and their optical activity will be of the same absolute value in the opposite direction. A mixture of two enantiomers in equal proportion is racemic, in tribute to racemic acid, also known as paratartaric acid, which was the first mixture of this kind to be discovered. Finally, it is important to note that not all chiral compounds are bearing an asymmetric carbon since chirality can also arise from the three-dimensional arrangement of the molecule as a whole. This is the case for helical species such as helicenes, which enantiomers are distinguished using the stereodescriptor *P* (for plus). Starting from the observer's closest benzene ring, the helice spiral is clockwise. Conversely, if the helice spiral is anti-clockwise, the enantiomer is referred to as *M* (for minus). (**Figure 1.5**)

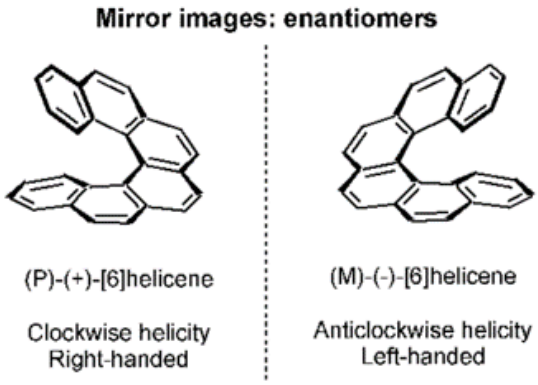


Figure 1.5. *Structural aspects of helicene and their stereodescriptors. Reprinted from reference[18] with permission from the Royal Society of Chemistry.*

Any other stereoisomerism relationship which does not involve chiral compounds are referred to as diastereoisomerism. This category includes, amongst others; the isomerism originating around a double bond, formerly referred to as geometric isomerism and known nowadays as *cis*/*trans* isomerism. Since no rotation can occur around unsaturation, a disubstitution can either lead to the presence of 2 substituents on the same side of the double bond, namely the *cis* isomer, or on opposite sides for the *trans* isomer. *Cis*/*trans* isomerism can also occur in cyclic compound since no rotation is possible around a single carbon bond in this particular case.

The diastereoisomerism also includes any isomeric relationships existing between molecules bearing an asymmetric carbon without being chiral overall. A typical example would be any pair of optical isomers which differ from the absolute configuration of one or more (but not all) asymmetric carbons such as an (*R,R*) and (*R,S*) configuration. In the specific case when two diastereomers have only one asymmetric carbon of opposite absolute configuration, they are referred to as epimers. For instance, β-D-mannose is an epimer of β-D-glucose. A particular kind of epimers, which are specifically involving the hemiacetal carbon of saccharide

rings, are known as anomers. In the specific case of glucopyranose, when the substituent at the C1 position of a carbohydrate is directed in the opposite direction that the substituent on C5, then the molecule is the α anomer, otherwise the molecule is the β anomer. (**Figure 1.6**)

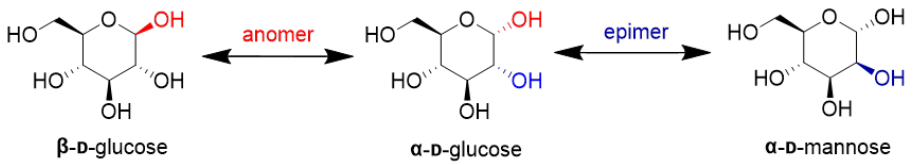


***Figure 1.6**. Illustration of the relationship between anomers, as represented by the α and β anomer of D-glucose, which are epimers on the hemiacetal carbon. If two compounds differ by the absolute configuration of only one carbon, then they are epimers, as it is the case for α-D-glucose and α-D-mannose.*

The term conformation was coined by Haworth in 1929 to refer specifically to the isomers of cyclohexane, known as boat, chair or twist.[10] To date, the conformational isomer or conformer refers generally to any isomer originating from steric hinderance restricting the free rotation around a carbon single bond. This phenomenon is observed for instance with the butane molecule, which can only adopt the rotational conformation corresponding to a local minimum of potential energy. Hence, the eclipsed or *syn* configuration, where both methyls are facing one another has an energy barrier high enough, owing to steric repulsion, that it is highly disfavoured against the two bisecting or in gauche configuration or the most stable *anti* configuration, where both methyl groups are facing an opposite direction. This type of isomers is known as rotational isomers or rotamers when the kinetics of rotation is slow enough to enable experimental observation. (**Figure 1.7**)

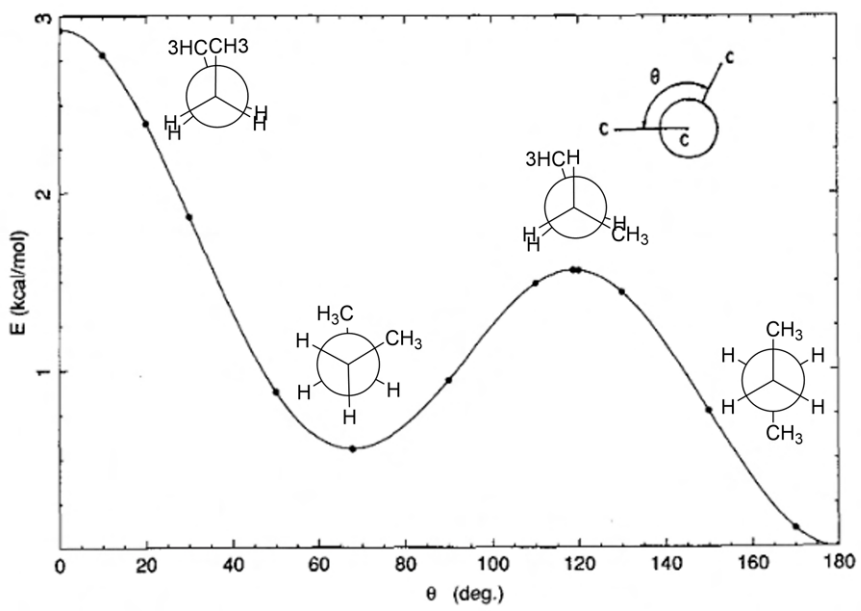


Figure 1.7. *Tortional surface potential energy diagram for n-butane. Θ represent the dihedral angle between second and third carbon of the molecule. Adapted from reference[19] with permission from Elsevier.*

When the rotation around a carbon-carbon single bond is slow enough to permit the individual isolation of isomers, then the specific term of atropoisomer is employed and the stereodescriptors *P* and *M* are most commonly used. This type of isomerism can be observed for instance with tetrasubstituted biaryl compounds, such as 4,6-dinitrodiphenic acid and 4,4',6,6'-dinitrodiphenic acid (DNDA), 1,1'-bi-2-naphthol (BINOL), or 2,2'-bis(dimethylphosphino)-1,1'-binaphthyl (BINAP). If a molecule presents a case of atropoisomerism whilst being chiral, as it is the case for the aforementioned examples, then the two arising isomers are also enantiomer of each other. (**Figure 1.8**)

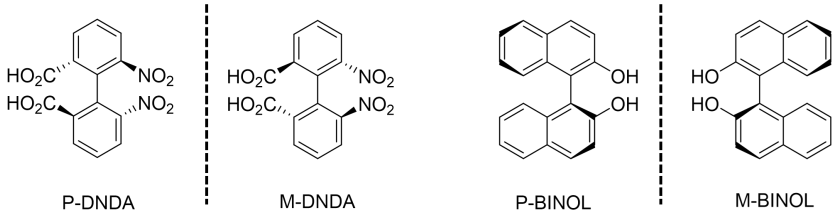
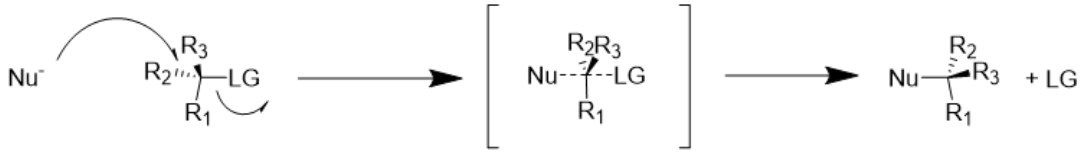


Figure 1.8. *Structures of the atropoisomer of 4,4',6,6'-dinitrodiphenic acid (DNDA) and 1,1'-bi-2-naphthol (BINOL).*

1.3 The importance of stereochemistry

1.3.1 General advances in chemistry

The advent of stereochemistry led to major discoveries which revolutionised the field of chemistry and opened a novel approach for the investigation of organic reaction mechanisms. Amongst others, it is notable to mention the well-known effect of "steric hinderance", theorised by Meyer in the 1890's as the reason for the poor yield obtain during the esterification of mesitylenecarboxylic acid.[20] Another impactful event related to the development of stereochemistry is the observation of "optical cycles" by Walden occurring during the synthesis of (+)-chlorosuccinic acid from (-)-malic acid in the presence of phosphorus pentoxide PCl_5.[21] This phenomenon was coined as "Walden inversion" by Fisher, and was explained in 1935, 40 years after Walden's initial report, when Ingold and Hughes theorised that bimolecular nucleophilic substitution (S_N2) involved a planar transition state with the entrance of the nucleophile and the departure of the leaving group being concerted, which results in the inversion of the absolute configuration of the asymmetric carbon.[22] (**Scheme 1.1**)



Scheme 1.1. *Representation of the mechanism of the Walden inversion observed in S~~N~~$_2$ nucleophilic substitution.*

It is also noteworthy to mention that Fisher was one of the early chemists adopting the theory of Van't Hoff and Le Bel, which led him to determine the configuration of numerous carbohydrates and their stereochemical relationship.[10]

1.3.2 In biology

The enantioselectivity of metabolism in micro-organisms was also discovered by Pasteur.[23, 24] Whilst studying the fermentation processes involved in the production of ethanol from sugar beets, Pasteur discovered that the fermentation of ammonium racemate using yeasts solutions would proceed as long as the solution was containing the dextrorotatory enantiomer (+)-tartaric acid and would reach termination, leaving the levorotatory (-)-tartaric acid unfermented. Following the reaction progression using a light polariser, he observed that the solution exhibited a left-oriented rotary power, which absolute value increased until reaching a plateau for the total consumption of the (+) - enantiomer. This observation led him to the conclusion that an intrinsic relationship existed between physiological mechanism and the absolute configuration of an enantiomer.[6]

In 1886, Piutti, whilst working on the industrial synthesis of asparagine, observed that the newly isolated D-asparagine had a sweet taste that its naturally occurring enantiomeric form L-asparagine did not possess.[25, 26] This was the first observation of the enantioselectivity of the taste sense. This led Ehrlich[27] and Langley[28] to

propose 15 years later the concept of receptors and the inherent enantioselectivity in biology beyond the sole enzymatic activity.[29] As an example, we can cite that the sense of smell, based on olfactive receptors, is also enantioselective. This is illustrated by *R* -carvone smelling like spearmint, whilst the *S* -carvone smells like caraway.[30] (**Figure 1.9**)

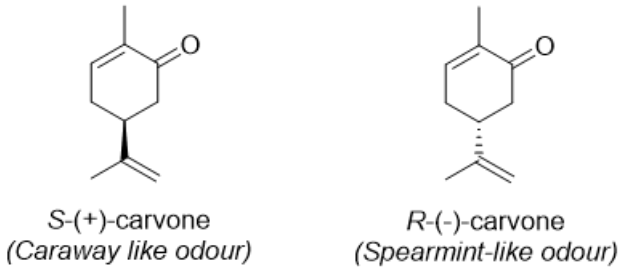


Figure 1.9. *Representation of the structure of the R and S enantiomers of carvone.*

Later, Fisher discovered that enzymatic reactions such as microbial fermentation were both enantio- and diastereospecificity by observing that carbohydrates such as D-glucose, D-galactose and D-fructose could be fermented by beer yeast but not their enantiomeric form and that such yeast could hydrolyse α-methyl-D-glucopyranoside but not its anomeric form β-methyl-D-glucopyranoside. Furthermore, this systematic study led to the conclusion that the fermentation processes were the results of enzymatic activity and theorised as the “lock and key” model to explain the complementary spatial configurations necessary for a reaction to take place.[29, 31] (**Figure 1.10**)

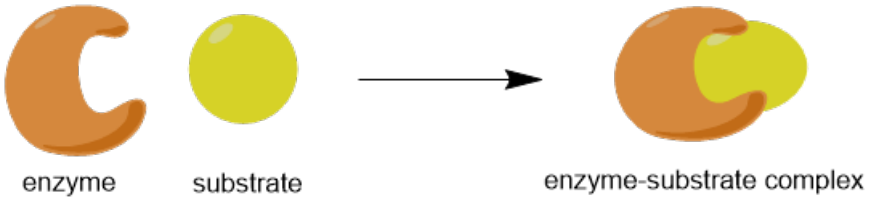


Figure 1.10. *Schematic representation of the "lock and key" model. The substrate should have a structure complementary to that of the active site of the enzyme for a reaction to proceed.*

1.3.3 In polymers

Polymer sciences, since their origin, have closely intertwined with the concept of stereochemistry. This does not come as a surprise since the first polymeric materials industrially produced were extracted from biomass. Biological systems rely heavily on stereospecific processes in molecular recognition, messaging, and signalling. Thus, bio-sourced polymers are intrinsically endowed with a stereo- and regio-regular backbones, as exemplified by natural rubber and cellulose derivatives: two of the earliest industrially relevant polymers. Even during these early days of polymer chemistry, the regularity of polymer chains was identified to be related to the capacity for crystallisation within the produced material. This was suggested by Staudinger in 1929 when he realised that the polymerisation of indene was yielding amorphous polymers, which he conjectured to be caused by a lack of regio-regularity along the chains, as two neighbouring indene rings could be either in *cis* or *trans* configuration.[32] The relationship existing between structural regularity and bulk properties was corroborated long ago, particularly through the historical development of regio- or stereospecific polymerisation process for the production of regular polyolefins.[33] To date, this area of research is still relevant with a focus on a better control over the mechanical properties solely based on leveraging the stereochemistry within polymers with more complex structures than common

polyolefins. In particular, an extraordinarily well written article thoroughly reviewed the topic of the enhancement of polymers through a better control over the stereochemistry.[34]

1.4 Stereochemistry of vinylic polymers

1.4.1 Tacticity

In the case of vinyl polymers, which are prepared from monomers with a general formula CH_2=CXY, where X and Y refer to two different substituents, the repeating units along the chain can exist as two different isomers. (**Figure 1.11**)

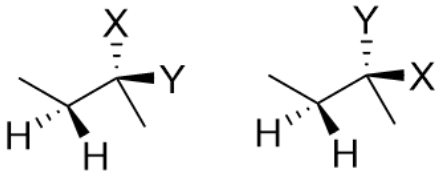


Figure 1.11. *Two possible configurations of the propylene stereocenter in the polymer chain.*

As there is no inversion possible around the axis of the polymer backbone, once added to the chain, the configuration is locked. Hence, the same repeating unit can exist in two different configurations along the polymer backbone. The linear distribution of the stereoisomer and their relative arrangement along the polymer chain is known as tacticity. When, along a polymer chain, the repeating units are in the same configuration (*e.g R-R-R-R*, or *S-S-S-S*) the polymer is isotactic, if they are randomly ordered, the polymer is atactic, and when the polymer has stereocenters perfectly alternating it is referred to as syndiotactic.[35, 36] (**Figure 1.12**)

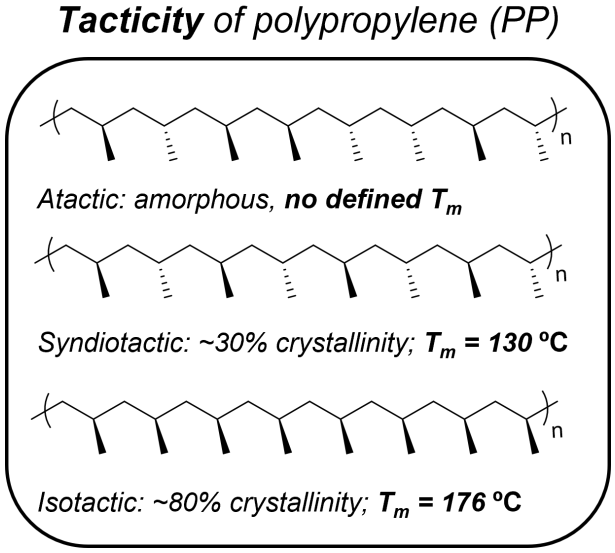


Figure 1.12. *Stereochemistry of polypropylene and corresponding properties.*

The on demand efficient production of a specific type of tacticity has been made possible through constant effort towards the development of stereospecific polymerisation procedures.

1.4.2 Stereocontrolled synthesis of vinyl polymers

Before the synthesis of isotactic polypropylene, olefinic macromolecule containing asymmetric carbons within their backbone were without exception amorphous in nature and it was attributed to the random arrangement of asymmetric carbons differing in their absolute configurations.[37] Moreover, prior to the development of the second generation of Ziegler-Natta catalyst, atactic polypropylene was only obtained as low molecular weight by-product of the polymerisation of isotactic polypropylene (iPP) since the first-generation catalysts would only produce atactic polypropylene (aPP) of low quality. However, the introduction of the Ziegler-Natta metallocene catalyst enabled the production of high-grade aPP by increasing the molecular weight from about 10 to 100 kDa, which

enabled the industrial usage of this type of polymer as a commodity plastic.[38] Soon after the report of an efficient synthesis of crystalline iPP, synthetic method aiming at yielding crystalline polyolefins using different monomers were developed. For instance, 2 years after Natta's original report on the synthesis, the crystalline form of poly(methyl methacrylate) PMMA was obtained *via* free radical and anionic polymerisation. Interestingly, the anionic polymerisation of methyl methacrylate was achieved using 9-fluorenyllithium in 1,2-dimethoxyethane at -60 °C produced the isotactic form of PMMA, and only changing the solvent for toluene produced the syndiotactic PMMA.[39] Although the synthesis of isotactic polystyrene (PS) has been achieved by anionic coordination by Natta in 1955, the synthesis of syndiotactic polystyrene was achieved only in 1986.[40] In the 2000s, the research effort in catalysis for the polymerisation of vinyl polymers focussed on the synthesis of polymers with blocks of controlled stereochemistry and molecular weight.[41-45] To date, research efforts are focussed on polymerisation processes with improved functional group tolerance as illustrated by a recent report of stereoselective cationic polymerisation of vinyl ethers offering a new procedure to obtain isotactic polyvinyl from a polar monomer bearing an oxygen atom outside of common acrylates and methacrylates.[46] Research which focusses on the controlled polymerisation of polar monomers are also extremely relevant to enable the production of sustainable polymers from bio-sourced monomers, which by nature, tend to possess a structure containing heteroatoms.

1.4.3 Influence of tacticity on bulk polymers

To date, in the case of the most common vinyl polymer such as PP, PS, or PMMA, the control over the arrangement of stereocenter is most efficiently achieved by the coordination-insertion polymerisation catalysed by transition metals[47, 48] and led to materials with considerable differences in terms of bulk properties. For example, iPP is a hard thermoplastic with a melting temperature of 160°C whilst aPP is a wax-like, rubbery material.[49] Syndiotactic polypropylene has 4 different crystalline forms depending on the stereoregularity and statistical disorder within the crystals. Its mechanical properties will depend on the crystalline organisation. Highly ordered and oriented fibres bestow the material with elastomeric behaviour whilst un-oriented compressed moulded material will behave as common hard crystalline polymers.[50] Consequently, crystallinity has a major impact on the thermomechanical properties of the bulk material. Hence, tacticity, which directly correlates to the crystallisation abilities of vinyl polymers by providing order to the polymer structure has a tremendous impact on the thermomechanical properties of the bulk material. This relationship between tacticity and crystallinity has been exploited in the development of thermoplastics elastomers by alternating the tacticity of the PP repeating units along the backbone.[44] In those materials, blocks of different tacticity contain crystalline domains, that forms upon cooling, play the role of physical crosslinks (**Figure 1.13**). As this network is reversible, the material is recyclable.[51-53]

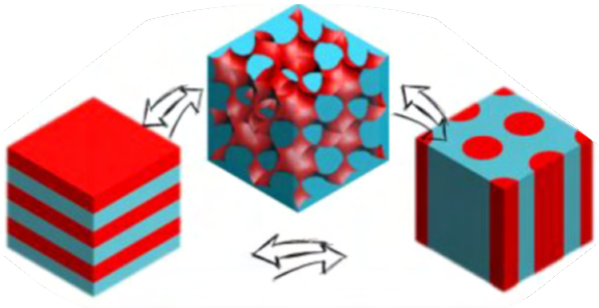


Figure 1.13. *Illustration of the diverse architecture arising from the microphase separation between immiscible polymer blocks occurring within thermoplastic elastomer creating a physical crosslink. In red is represented the crystalline phase or hard phase and the blue represents the amorphous or soft phase. By changing the molecular weight of the blocks, it is possible to obtain a layered, gyroid, or worm-like rod phase separation. Adapted from reference[54] under the Creative Commons Attribution Licence 2020.*

1.5 Polymer systems containing *cis/trans* isomerism

1.5.1 Natural rubbers and Gutta Percha

The divergence thermomechanical properties of materials produced from 100 % *cis* or 100 % *trans* polymer has been well-known for over a century. Both 1,4-*cis*-polyisoprene and 1,4-*trans*-polyisoprene can be extracted from the latex produced by the (sub)-tropical rubber tree (*Hevea brasiliensis*) or ~~the~~ gutta percha tree (*Palaquium oblongifolia)*, respectively.[55] These two bio-sourced polymers found industrially relevant applications as early as the 1770's as pencil rubber for the *cis* isomer and, although the *trans* isomer was known in the western world since 1656, it is only in 1845 that the Gutta Percha Company popularised the material as a commodity thermoplastic for various applications such as filling for dentistry, golf balls, or as insulator for underwater telegraph cables.[56-59] The applications for which natural rubber and gutta percha are used are broadly different as the *cis* isomer, once vulcanised, gives highly elastomeric soft material with a melting temperature T_m of 34 °C whilst its isomeric form would produce hard and brittle thermoplastic

with a T_m of 89 °C.[60] This difference in thermomechanical properties is believed to originate from the higher inclination to crystallise of the *trans* isomer owing to a better chain packing ability.[61] (***Figure* 1.14**)

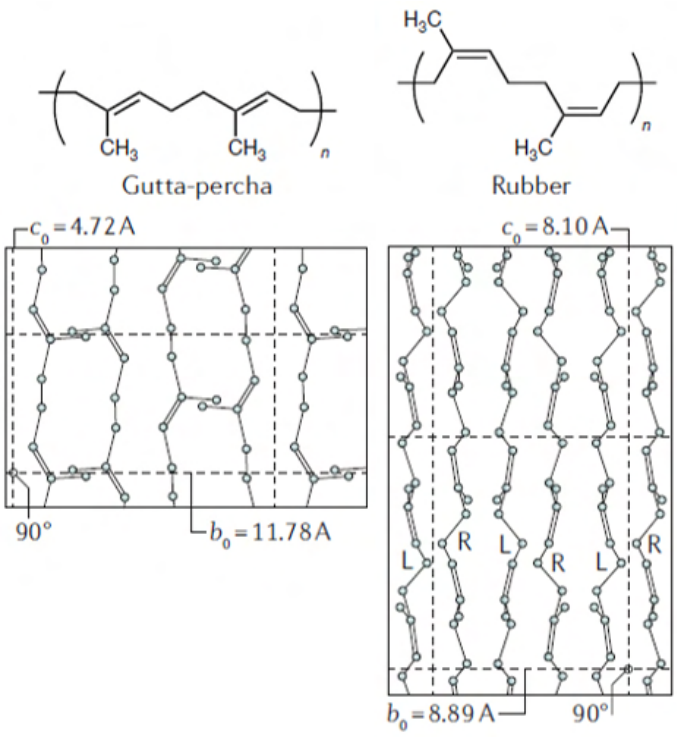


Figure 1.14. *Structure of Gutta Percha and Natural Rubber and their respective crystal structure illustrating the better chain packing abilities of the trans isomer. Adapted from reference[34] with permission from Springer Nature*.

Although synthetic analogues of both of these polymers have been industrially produced for at least 70 years[62], polymerisation processes with strong functionality tolerance is still an challenging research endeavour today. Thus, it is believed that controlling the stereochemistry within synthetic polymers could potentially lead to the control of the mechanical properties as exemplified by the studies carried on vinyl polymers.[63] However recent studies demonstrated that general rules to predict the outcome on the bulk material properties of the presence of one isomer over the other cannot yet be defined with assurance, since it has been observed that

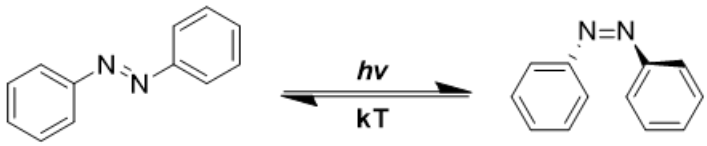
elastomeric properties are not always derived from the *cis* configuration and an all-*trans* polymer is not exhibiting the properties of a hard plastic in every instance.[63-66] For this reason, it would be counterintuitive to segregate the synthesis from the outcome of the stereochemistry on the mechanical properties. Instead, this section will present the important developments towards the rational implementation of *cis*/*trans* unsaturation within heteroatom rich polymer backbones, and where possible, examples of the manipulation of the physical properties in the bulk materials.

1.5.2 Challenges of synthesising polymers containing *cis/trans* isomerism

The introduction of *cis* and *trans* type stereochemistry within synthetic polymers has presented synthetic challenges for decades since unsaturation is prone to isomerisation or crosslinking, which could be especially triggered in harsh polymerisation processes involving high temperature, high pressure, strong acid or base catalysts or the production of free radicals. For this reason, pure *cis* or *trans* chains of the same chemical structure are hard to access and is still a topic of ongoing research. Thus, different strategies were established towards the production of stereospecific *cis*/*trans* polymers, such as post-polymerisation isomerisation starting from isomeric-defined chains, stereoselective in-situ production of *cis* or *trans* unsaturation, or the use of unsaturated or rigid-rings stereopure monomers. These polymerisation techniques and their outcome are presented in the following paragraphs.

1.5.3 Polymer containing *cis/trans* isomerism through post-polymerisation modification

A well-known example of the modulation of polymer chains stereochemistry is *via* the incorporation of diphenyl substituted diazene derivative, namely azobenzene.[67] This type of molecule, are able to isomerise from *trans* to *cis* using UV-light irradiation, and it is possible to control the isomerisation ratio using different wavelengths.[68] Although, increasing the strain can decrease the kinetic of the reaction, owing to the greater thermodynamic stability of about 50 to 55 kJ·mol^{-1} of the *trans* isomer, the polymer slowly reverts back to the *trans* configuration once the irradiation is supressed.[69] (**Scheme 1.2**)



Scheme 1.2. *Scheme of the trans to cis isomerisation of azobenzene occurring under UV irradiation. The trans isomer being the thermodynamically stable isomer, hence the cis to trans isomerisation occurs naturally in the absence of irradiation.*

Examples of less reversible thermal isomerisation can be found in the early literature: one such example where various *cis*/*trans* contents were created from the thermal isomerisation of a *cis* pure polyacetylene material.[70, 71] This isomerisation technique is still used to date and can be triggered *via* thiyl radical-catalysed reaction,[72] diethylamine basic catalysis for isomerising the activated alkenes of poly(propylene maleate) into poly(propylene fumarate),[73] or a combination of both methods to obtain a polyester which could be reversibly switched from a configuration to the other to afford polymers with a *trans* ratio from 0 to 100% and

therefore a wide array of mechanical properties from soft elastomer to hard plastic.[74] (**Figure 1.15**)

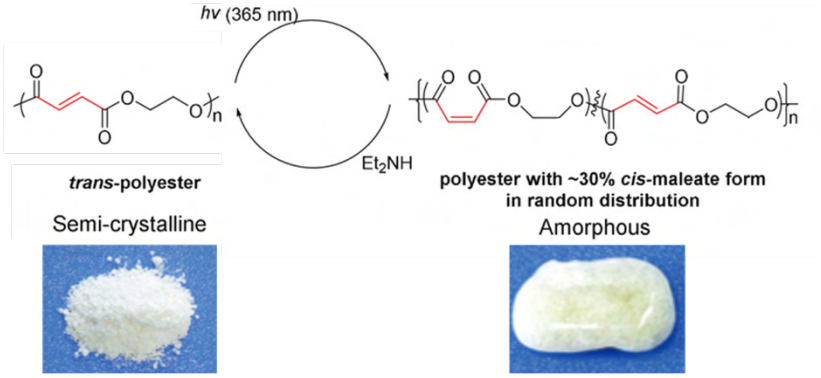
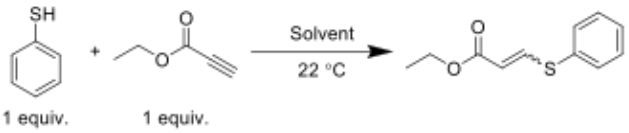


Figure 1.15. *Illustration of the UV triggered isomerisation of trans fumarate to cis maleate with a 30% yield of conversion and random distribution along the polymer chain. This reaction requires the use of 10 mol% Benzophenone as catalyst. The reaction is reversible in the presence of 10 mol% diethylamine. Whilst the 100% trans fumarate polymer is semi-crystalline, isomerising 30% of the unsaturation to cis maleate led to an amorphous material. Reproduced from reference[74] with permission from John Wiley and Sons.*

1.5.4 Polymer containing *cis/trans* isomerism through in-situ alkene synthesis

Research in organic chemistry of small molecules is in constant development and a plethora of reactions have been developed throughout history that can perform stereoselective transformations and couplings. In order to be efficiently translated to polymerisation processes, reactions should be able to reach high conversion of a single product in a timely fashion, which led to the “craze” for exploring “click reactions” towards the development of novel polymerisation techniques ever since the original article highlighting the superiority of a few reaction processes was published in 2001.[75] Specifically, the nucleophilic addition to alkynes activated by the presence of an electron-withdrawing group has long been known as a means to control the stereochemical outcome of the product by altering the

catalyst, thermal conditions, or the solvent in which the reaction is carried out.[76] The thiolation of alkynyl esters can produce an addition product with a ratio of the *cis* and *trans* diastereomer correlated to to the solvent polarity. The best results both in terms of stereopurity and efficiency were achieved using water as solvent, which yielded the *trans* isomer in 97% purity in 5 min of reaction at room temperature. This reaction was not only efficient, but adhered to a majority of green chemistry requirements such as high atom economy and minimal by-product formation.[77] (**Figure 1.16**)



solvent	time (min)	yield (%)	*cis/trans*
H_2O	5	98	97/3
MeCN[a]	15	90	87/13
MeOH	25	85	85/15
DMF[b]	20	80	53/47
CH_2Cl_2	20	44	74/26
THF[c]	30	30	68/32
EtOAc	25	12	83/17
Acetone	20	74	80/20
Toluene	40	18	75/25
n-C_6H_{13}	40	19	67/33

[a]MeCN = acetonitrile; [b]DMF = dimethylformamide; [c]THF = tetrahydrofuran

Figure 1.16. *Scheme representing the addition of thiophenol to ethyl propiolate at room temperature and at concentration of 0.2 M. The table above summarises the impact of the solvent polarity on the yield and stereochemistry of the product.[77] Reproduced from reference[76] under the Creative Commons Attribution Licence 2021.*

This concept was applied to the coupling of commercially available aliphatic thiols with propiolate terminated poly(ethylene glycol) (PEG) oligomers using 10 mol% of triethylamine (Et_3N) as catalyst. The obtained product exhibited a *cis*/*trans* ratio similar to that observed with small molecules, with a *trans* content spanning

from 2% up to 96% whilst working in benzene or water respectively.[78] This method was successfully applied to the step-growth polymerisation of a dialkyne monomer and 1,6-hexanedithiol to yield high molecular weight polymers with a *cis* content which could be tuned between 32 and 80% which exhibited different mechanical properties. Interestingly in this system, the higher the *cis* content, the more crystalline the final material, which is the opposite trend of that observed for the isomers of 1,4-polyisoprene.[63] (**Figure 1.17**) This type of reaction was then exploited for the manipulation of the mechanical properties of polyamides which displayed similar mechanical properties than Nylon 6,6.[79]

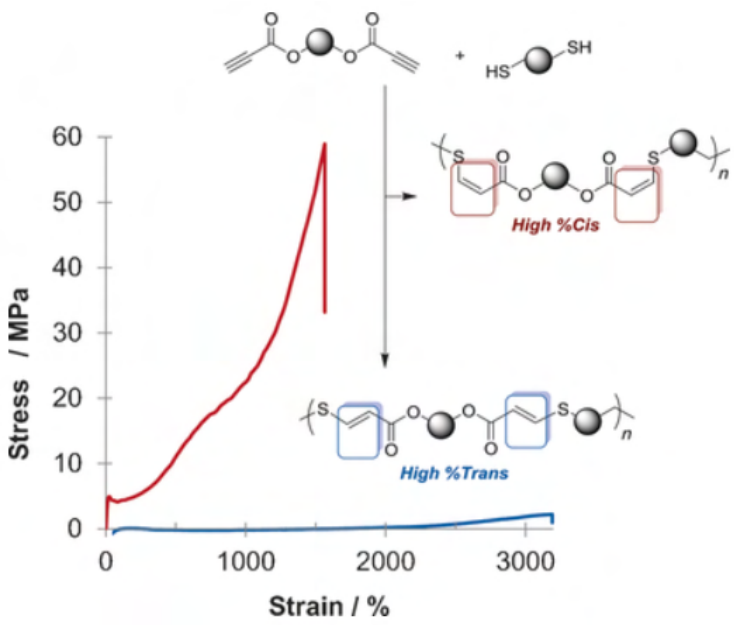
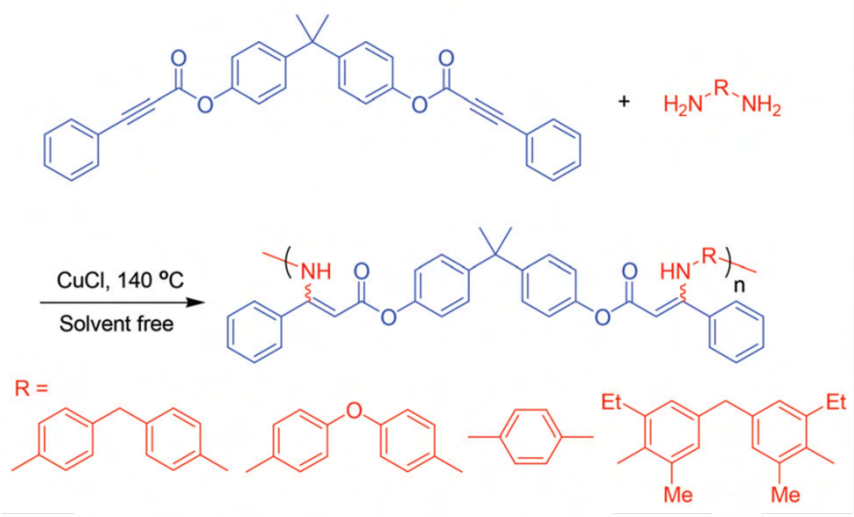


Figure 1.17. *Stress-strain curve for thiol-yne elastomer with a cis content of 80% (High cis, in red) and 32% (High %trans, in blue). Reproduced from reference[63] under the Creative Commons Attribution Licence 2016.*

Although, thiols are the most popular nucleophile for the stereospecific nucleophilic addition to activated alkenes owing to the wide array of isomeric ratios which could potentially be obtained, some previous reports have mentioned the potential to control the stereochemical outcome of the coupling of an alkyne with

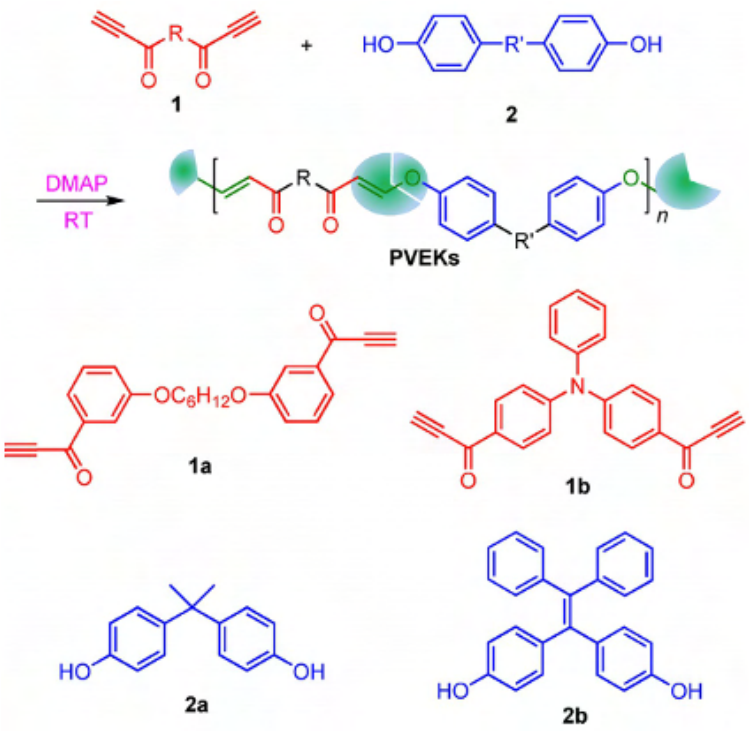
amines. For instance, it was demonstrated that an isomer ratio of either 88% or 39% *cis* high molecular weight poly-enamines could be obtained by exchanging the copper(I) halide salt used as catalyst from CuCl to CuI.[80] (**Scheme 1.3**) Moreover, whilst performed at room temperature without the addition of any catalyst, 100% *trans* poly-enamines could be obtained.[81, 82] However control of the *cis*/*trans* ratio as well as molecular weight were hard to achieve, therefore studies related to their structure-properties relationship were not conducted.



Scheme 1.3. *Synthesis of polyenamines by Cu(I)-catalysed amino-yne polymerisation.[80] Reproduced from reference[80] with permission of the Royal Society of Chemistry.*

Lastly, the emergence of alcohol-yne reactions could also be mentioned for their propensity to be modulated using different trialkyl-phosphine catalysts or solvents.[83] In this particular study, however, the use of triphenyl phosphine as catalyst only provides small deviations, from 75% to 88%, in the *cis*/*trans* ratio of the product of the addition of benzyl alcohol onto methyl propionate. Whereas, using tributylphosphine affords the *trans* isomer in 100% diastereopurity using solvents of a broad range of polarity from benzene to tetrahydrofuran. The limited control of the

stereochemistry (between 75 to 100%) makes hydroxyl-yne far less versatile than the thiol-yne reaction described previously. This is further illustrated by the synthesis of poly(vinylene ether ketone) via DMAP catalysed phenol-yne polymerisation which only yield the *trans* isomer.[84] (**Scheme 1.4**)



Scheme 1.4. *Phenol-yne polymerisation of 100% trans poly(vinylene ether ketone) using DMAP as a catalyst. Reproduced from reference[84] with permission from John Wiley and Sons.*

Outside the nucleophilic addition to alkynes, ring opening metathesis polymerisation (ROMP) of norbornene or tetracyclododecene were also reported to produce good control over the stereochemical outcome of the product. ROMP has been shown to be able to yield 98% of the in-chain unsaturation as the *cis* configuration.[85] More recently, excellent control over the ratio of *cis*/*trans* of poly(*p*-phenylenevinylene) though stereoretentive ROMP. Using different ruthenium-based catalysts, the *cis* content along the polymer chain was varied from 50 to 99%.

Moreover, the photoisomerization of the all-*cis* conjugated polymer could afford the all-*trans* isomer after 30 min of UV light exposure at 365 nm.[86] More recently, the same group developed stereoselective dithiolate ruthenium carbenes catalyst which afforded excellent control of the configuration of the in-chain double bond *via* acyclic diene metathesis (ADMET) polymerisation. This procedure was tolerant towards a variety of functionalities which permitted to yield a wide array of polymers such as polycarbonates, polyesters or even polyethers and polysulfites.[65] (**Figure 1.18**)

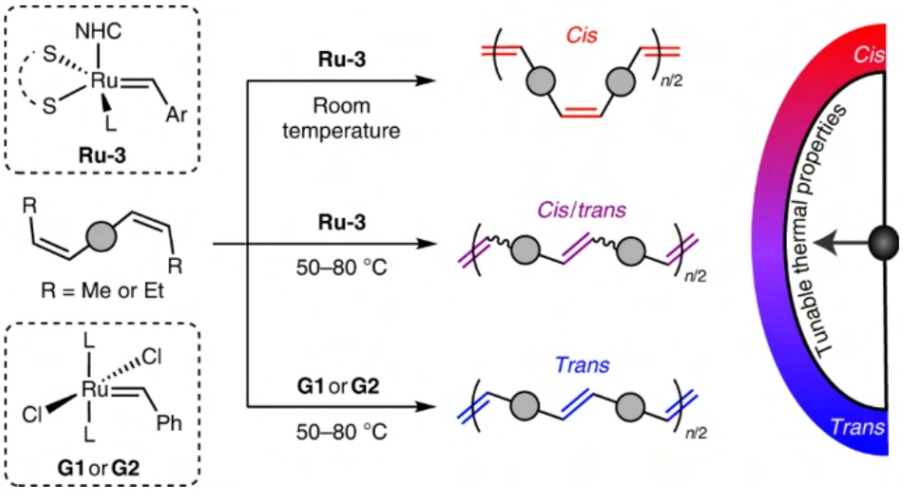


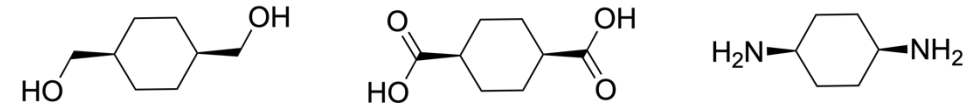
Figure 1.18. *Preparation of unsaturated polymers with a different cis/trans content via ADMET using two ruthenium catalysts.[65] Reproduced from reference[65] with permission from Springer Nature.*

1.5.5 Polymer containing *cis/trans* isomerism from stereopure monomers

The incorporation of stereopure monomers within the polymer backbone can be achieved by step-growth polymerisation techniques such as polycondensation or polyaddition and certainly represent a valuable technique if the selected molecules and its isomeric forms are individually available in high purity.

The addition of cyclic monomers is an ingenious way of incorporating *cis*/*trans* type stereochemistry within a polymer chain as it removes the possibility of

unwanted crosslinking usually encountered with unsaturated polymers under the harsh reaction condition of traditional polycondensation. For example, 1,4-cyclohexenedimethanol (CHDM) has been copolymerised with 2,5-furandicarboxylate and ethylene glycol (EG) by transesterification in the presence of zinc acetate, followed by polycondensation using antimony trioxide as catalysts. (**Figure 1.19**) It has been found that the CHDM configuration was influencing the overall properties of the polymer.



1,4-cyclohexenedimethanol 1,4-cyclohexenedicarboxylic acid 1,4-diaminocyclohexane

Figure 1.19. *Structure of three common cyclic monomers used to impart cis and trans stereochemistry to polymer.*

Besides the crystallinity and the material toughness that increased with the *trans* content of (CHDM), the permeability of O_2 and CO_2 was also correlated to the configuration ratio and decreased with increasing *trans* content.[87] Similarly, cyclic monomers such as 1,4-cyclohexanedicarboxylic acid (CHDA) and 1,4-diaminocyclohexane (DACH), when in their *trans* configuration, were found to positively impact polyamides mechanical properties in a similar way.[88] However, it is noteworthy to mention that CHDA is not an ideal candidate since it has been proved that it can isomerise in the presence of a strong acid catalyst[89] or under a high temperature required during polycondensation.[90] Although one study reported the possibility to control the mechanical properties by changing the *cis*/*trans* ratio present along the polymer backbone from 0.12 to 0.71. [91] The authors describe that increasing the *cis* content, introduces kinks in the chain, which decreases the chain-

packing ability of the polymer. As a results, the chain disorder increased, and the polymer exhibits reduced crystallinity to become totally amorphous at a *cis* content of 71%.

Another kind of ring often used in order to study the effect of stereochemistry on the polymer properties is the sugar-derived 1,4:3,6-dianhydrohexitols or isohexides. (**Figure 1.20**) Besides multitudes of advantages linked to their sugar-based nature such as being relatively cheap to produce, biocompatible and bio-sourced[92, 93], their unique V-shaped bicyclic structures and the relative stereochemistry of their two hydroxyl groups makes them valuable candidates in the study of the relationship between stereochemistry and polymer properties.[94]

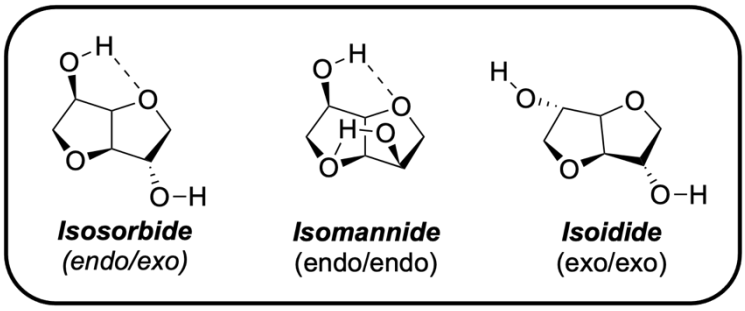
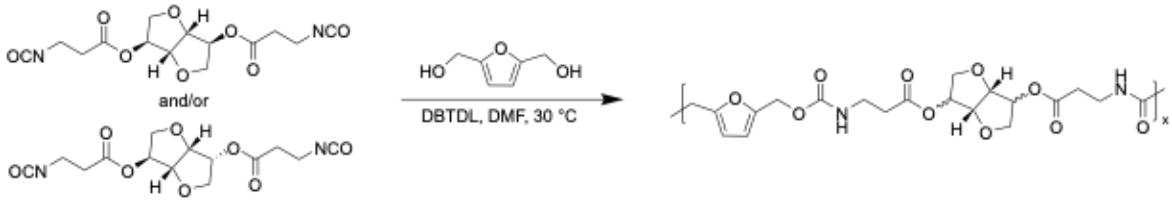


Figure 1.20. *Structure of 1,4:3,6-dianhydrohexitols or isohexides.*

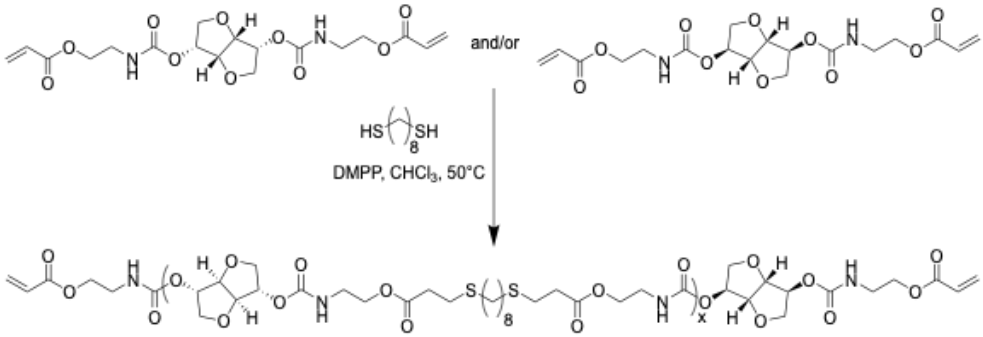
As such, incorporation of isohexides have been exploited in step growth polymerisation of polyamides[95], polyacetals[96], polyesters[97, 98] and polyureas/polyurethanes.[99] In all cases, the T_g was dependant on the stereochemistry in the order: isosorbide<isomannide<isoidide. The main problem shared by those studies on isohexides, is that the mechanical properties - and how they are affected by the stereochemistry - is either marginally or not discussed.[34] This fortunately has been corrected by the publication of 2 recent reports. The first report highlights the possibility of manipulating the value of the T_g, density and

entanglement molar mass by varying the feed in isosorbide and isommanide monomer during the copolymerisation with hydroxymethyl furfural yielding renewable polyurethanes.[100] (**Scheme 1.5**)



Scheme 1.5. *Synthesis of renewable polyurethane from hydroxymethyl furfural and isohexide-derived difunctional isocyanates.*

More recently, Stubbs *et al.* investigated the mechanical properties of poly(ester-urethane) resulting from the copolymerisation of 1,8-octane dithiol with a diacrylate monomer including either a isoidide or isommanide unit. (**Scheme 1.6**)



Scheme 1.6. *Synthesis of poly(ester-urethane)s used to study the impact of the isohexide structure on the mechanical properties of the material.*

The study revealed that whilst the former isohexide generated tough thermoplastics, the later endowed the final material with soft elastomeric properties. Moreover, the hydrolytic degradation of the materials could be controlled individually from the mechanical properties by either the blending of the two kind of polymers or through the copolymerisation of the two isomers.[101] (**Figure 1.21**)

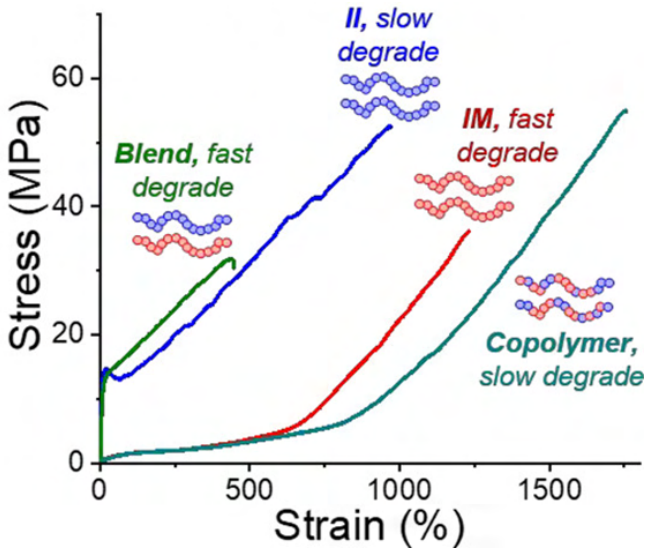


Figure 1.21. *Isomannide (IM)-derived poly(ester-urethane) exhibits the mechanical properties of soft elastomers whilst isoidide (II)-derived poly(ester-urethane) are displaying the behaviour of tough thermoplastics. The blending of the two isomorphous polymers yields a fast eroding tough plastic, whereas the copolymerisation of the two isohexides produces an elastomer which degrades slowly.*[101] *Adapted from reference*[101] *under the Creative Commons Attribution Licence 2022.*

Further work highlighted the dependence between the isohexide stereochemistry and the biodegradation rate of a similar poly(ester-urethane) resulting from the thiol-Michael type copolymerisation of dianydro sugar-based diacrylates with various dithiol.[102] It should also be noted that the same technique was successfully applied to incorporate the cyclopropane rings within a polymer backbone, however the impact of *cis/trans* stereochemistry around the 3-membered ring yielded only a modest difference in the T_g.[103]

Although the structure-property relationships of *cis* and *trans* commodity polymers such as polyisoprene and polybutadiene is well understood and controlled, it is not the case for the numerous other unsaturated polymer systems.[104-106] The polycondensation of maleic and fumaric acid with an alkanediol (**Figure 1.22**) for the preparation of polyesters is another strategy developed for

controlling the stereochemistry of unsaturated polymers. Pure *trans* homopolymers can be easily prepared thanks to the higher energy stability of the *trans* configuration. Hence, a 100% *trans* configuration polymer have already found applications in biomaterials.[107-110] However, the pure *cis* polymer is hard to obtain since the *cis* double bond is prone to isomerisation under the high temperatures required for polycondensation.[110] When the pure *cis* poly(hexamethylene maleate) has been reported, the molecular weight was unfortunately too low (5 kDa) for the polymer to have robust mechanical performance. This is the reason why, most of the attention was focused on the copolymerisation of maleic and fumaric acid at various *cis/trans* ratios.[109, 111] The idea was to prepare biomaterials with tuneable mechanical and degradation properties. However, the precise control upon the *cis/trans* isomer ratio remains a challenge as a consequence of isomerisation reaction affecting the *cis* double bond during the polymerisation process.[110, 112]

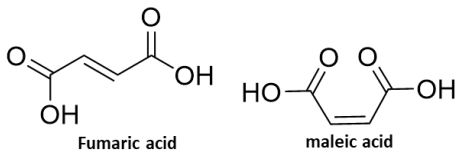
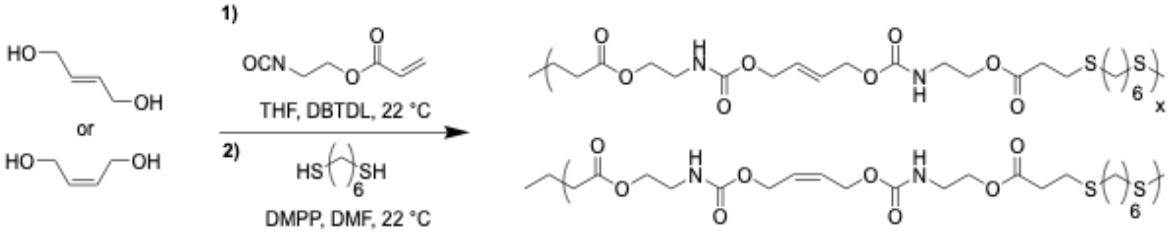


Figure 1.22. *Structure of fumaric and maleic acid*

Emergent techniques based on milder polymerisation method derived from “click” reactions are currently representing a breakthrough in the study of the influence of the stereochemistry present along a polymer backbone on the physical properties of the bulk material. In particular, it has been reported that the Michael addition thiol-ene reaction proved itself as a powerful tool to obtain stereo-controlled unsaturated polymers. One study reporting the successful synthesis of high molecular weight poly(ester-urethane), which displayed different mechanical

behaviour depending on the configuration of the in-chain unsaturation.[64] **(Scheme 1.7)**



Scheme 1.7. *Synthesis of unsaturated poly(ester-urethanes) from stereo-defined diacrylates and 1,6-hexanedithiol.*

In this specific system, both *cis* and *trans* polymers were obtained without unwanted crosslinking and isomerisation and both behaved has hard thermoplastic with the *trans* (*E* = 66 MPa) isomer exhibiting a Young's modulus over two times that of the *cis* isomer (*E* = 25 MPa). (**Figure 1.23**)

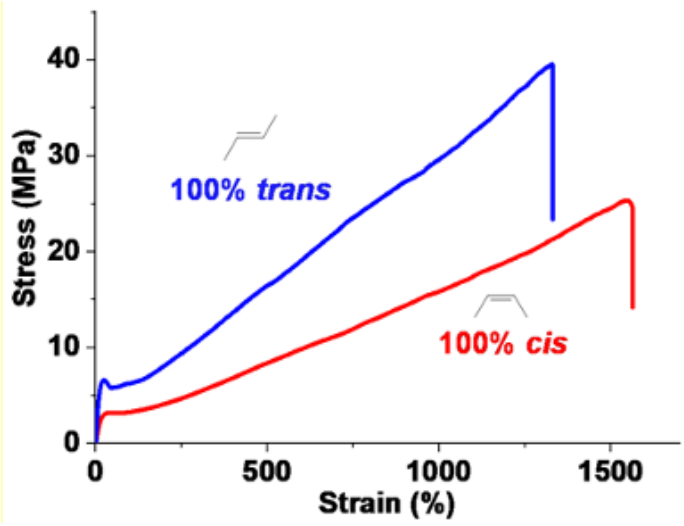


Figure 1.23. *Synthesis of poly(ester-urethane) via thiol-Michael step growth addition between an unsaturated cis and trans diacrylate and the commercially available 1,6-hexanedithiol which exhibits different mechanical properties depending on the stereochemistry of the inner double bond.[64] Adapted from reference[64] with permission from the American Chemical Society.*

1.6 Stereochemistry in Polymer networks

Polymer networks are distinguishable from polymer thermoplastics through the existence of chemical crosslinking which permeate the whole mass of the bulk material and account for 15-20% of the global polymer production accounting for about 22 M tons per annum.[113-115] Their structural particularity endows the material improved resistance to high temperatures and solvent and overall mechanical properties. For instance, it is through the formation of covalent crosslinking between polymer chains via vulcanisation process that the Natural Rubber gains its exemplary elastic behaviour and resistance to fatigue. However, owing to the presence of crosslinking, they are not soluble, thus the exact architecture of this type of material can be harder to analyse thoroughly by common analytical means.[116] Moreover crosslinking reactions are not controlled reactions, often involving the presence of radicals or high temperature. Hence, the content of double-bonds and their stereochemistry, particularly in the case of unsaturated polymer networks, is inherently different from that of the feed since the harsh reaction conditions can induce isomerisation. For this reason studies on the impact of the stereochemistry on the mechanical properties of unsaturated polymer networks could scarcely be found and the very few examples focussing on the stereochemistry within networks are mainly conducted on hydrogels. The first method reported within the literature is the use of azobenzene photoswitches especially with biological application in mind.[117] For example, Yan-Li Zhao and J. Fraser Stoddard reported in 2009 the use of deoxycholate-β-cyclodextrin derivative coupled with poly(acrylic acid) copolymer containing pendant azobenzene group to create a reversible gel through host-guest interaction controlled by light exposure. Thus, the gel-to-sol transition occurred whilst the gel was irradiated at 355 nm and

the azobenzene moiety in the *trans* configuration, however if subjected to a 450 nm wavelength light, the azobenzene is converted into the *cis* configuration, disrupting the host-guest interaction and therefore triggering the gel-to-sol phase transition.[118] (**Figure 1.24**).

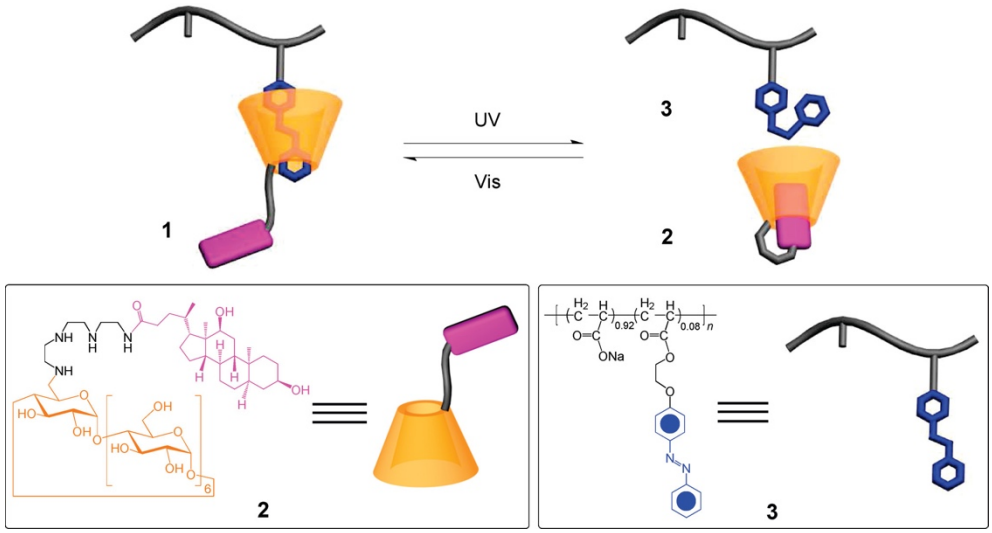
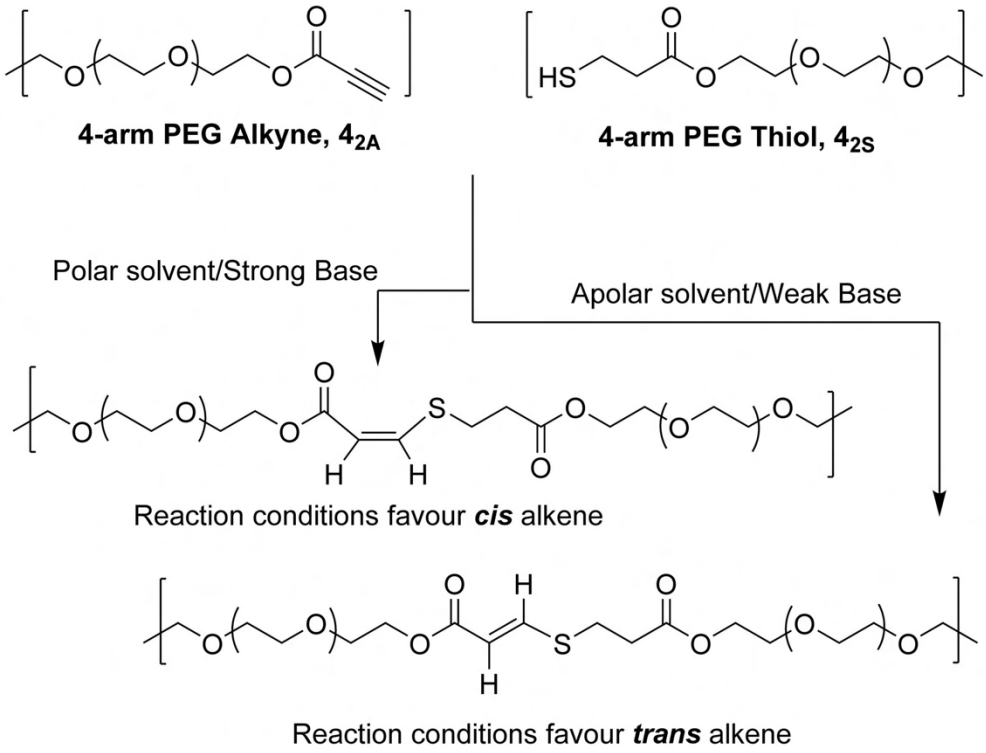


Figure 1.24. *Illustration of the sol-gel phase transition mechanism occurring via guest-host interaction between a Deoxycholate-β-cyclodextrin derivative and a poly(acrylic acid) copolymer containing pendant azobenzene groups. Reproduced from reference[118] with permission from the American Chemical Society.*

This type of reversible complexation between azobenzene and cyclodextrin has also been exploited in another study using poly(*N*-isopropylacrylamine) as the guest polymer which made the system temperature sensitive. Moreover, the cyclodextrin-based dimers were connected by a disulfide bond, thus the crosslinking for the gel could also be triggered by redox reaction. Thus, the novelty of this particular study was the obtention of a multi-stimuli system with a sol-gel phase transition able to be triggered either by light, temperature or redox reaction.[119] However, a study conducted by Tamesue *et al.* cyclodextrin-branched curdlan and either dodecamer of poly(acrylic acid) containing azo pendant group or azobenzene terminated dimers highlighted the difficulty of finding the right condition essential to the gel formation

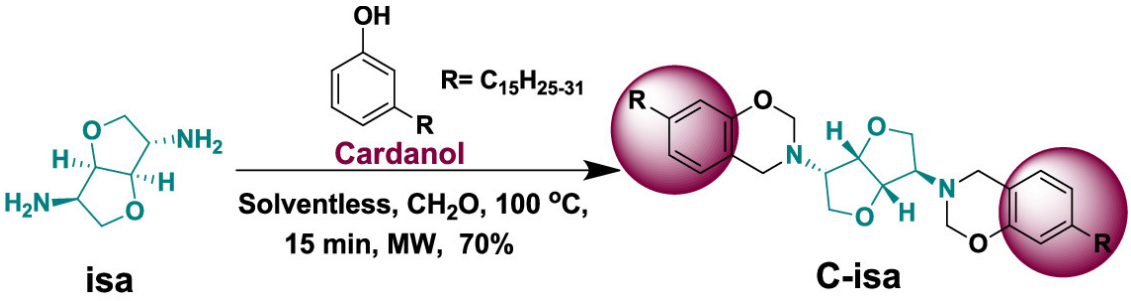
such as the ratio of cyclodextrin units to the azobenzene groups, the morphology of the guest polymer or the small constant of association for the inclusion complex formed from cyclodextrin and azobenzene.[120] Interestingly, azobenzene photoswitches have also been exploited to modify the stiffness of a chemically crosslinked hydrogel formed by the thio-michael addition between a vinylsulfone terminated 6-armed poly(ethylene-glycol) and a azobenzene-functionalised peptide. The resulting hydrogel demonstrated a cytocompatible, light-responsive alteration in elasticity which made it a good candidate for cell culture substrates in mechanobiology studies. However, although occurring slowly within 18h at 37 °C, the *cis* azo group inevitably relaxes to the thermodynamically stable *trans* isomer, moreover the reduction in stiffness imparted from the *trans* to *cis* photoisomerization was only in the 2% range.[121] Building up from this system, I-Ning Lee *et al.* achieved a *cis* rich network stability of about 2 weeks with a 76% range of stiffness between the two isomers using acrylamide as monomer and 4,4'-Di(acrylamido)azobenzene crosslinker.[122]

Another technique which has been employed to tune the mechanical properties of hydrogel relaying on the change of stereoisomer of unsaturated polymer networks was the use of thiol-yne click chemistry. Originally encountered within thermoplastics, this method enables the control over the stereochemistry of the unsaturation formed in situ from the manipulation of the reaction conditions. Hence, the reaction between an alkyne terminated and a thiol terminated 4-arm poly(ethylene glycol) could either give rise to the formation of a *cis* rich or *trans* rich network by using a strong base in a polar solvent or a weak base in an apolar solvent respectively.[123](**Scheme 1.8**)



Scheme 1.8. *Synthesis via thiol-yne click chemistry of either a cis or trans rich hydrogel network from the reaction of an alkyne terminated and a thiol terminated 4-arm poly(ethylene glycol) precursors. The use of a strong base in a polar solvent favours a trans rich network and a cis rich network is obtained by using a weak base in an apolar solvent. Reproduced from reference[123] under the Creative Commons Attribution Licence 2021.*

In the recent literature, only three occurrences of the study of the impact of stereochemistry on the mechanical properties within thermoset could be found. The first example has been carried on isohexide-base polybenzoxazine. In this study, thermoset networks were formed from the modification of isosorbide diol to isosorbide diamine which was further reacted either with biosourced phenols such as cardanol to obtain bisbenzoxazine monomers.[124] (**Scheme 1.9**) This study revealed that the *exo-endo* configuration of the isosorbide unit within the polymer was found to influence the ring opening temperature, the maximum thermal stability, the glass temperature and the adhesive strength compared to the previously studied isomannide-containing polymer of the same structure.[125]



Scheme 1.9. *Synthesis of a bisbenzoxazine monomer from a isosorbide diamine and cardanol via Mannich-like condensation under microwave irradiation in the absence of solvent. Adapted from reference*[124] *with permission from the American Chemical Society.*

Moreover, the storage modulus increased from 68 MPa to 240 MPa by only changing the isomannide (*endo-endo*) to a isosorbide unit (*endo-exo*). This observation was hypothesised to be correlated to the better chain packing enabled by the facilitated hydrogen bonding arising from the special orientation of the isosorbide rigid ring. This postulation has been corroborated by a more recent study on the impact of the stereochemistry of 2,3-butanediol when used as chain extender within polyurethanes. Thus, the orientation of the pendant methyl groups in the meso 2,3-butane diol has been found to favour a more linear polymer chain which in turn supports the formation of large crystalline phases through strong hydrogen bonding interaction between neighbouring polymer chains in the hard segment. However, when the 2,3-butane diol are in (R,R) or (S,S) configuration, the methyl group are oriented to minimize the steric hindrance which introduced kinks within the polymer chain and overall disfavour H-bonding.[126] **(Figure 1.25)**

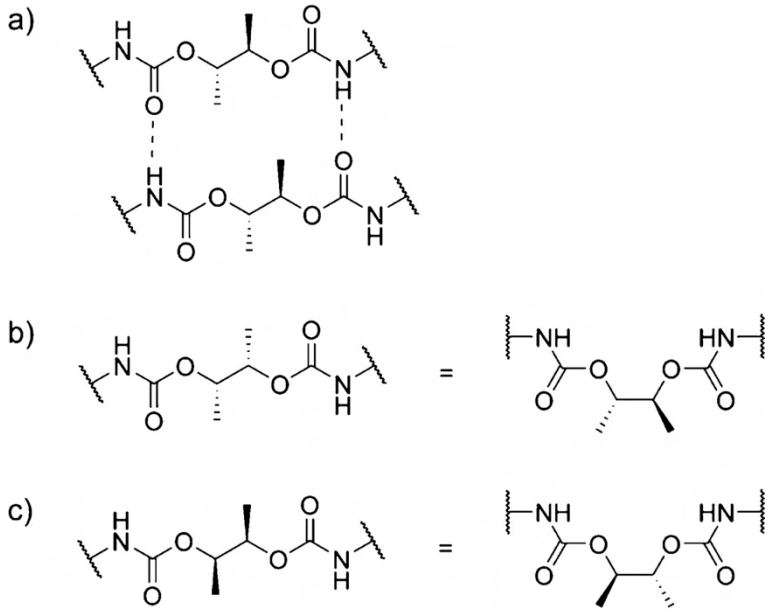


Figure 1.25. *Illustration of the methyl pendant group orientation in a) meso 2,3-butanediol, which favour linear chains and in turn the formation of H-bonding between neighbouring chains or b) (S,S) and c) (R,R) which induce kinks within the chain to minimise steric hindrance. Adapted from reference[126] with permission from the American Chemical Society.*

Finally, the third report attempting at studying the effect of stereochemistry within networks presented thermoset networks arising from the copolymerisation of pure *cis* or *trans* limonene dioxide monomers with glutaric anhydride. A slight difference in reactivity towards copolymerisation with glutaric anhydride could be noticed via DSC analysis, with the *cis* and *trans* limonene dioxide displayed an enthalpy of reaction of 553 and 592 J·s, respectively, indicating the higher reactivity of the *trans* stereoisomer. In addition, the *trans* network presented a glass transition temperature of 27 °C, which was almost 3 times lower than of its *cis* counterpart (80 °C). However, the mechanical properties of the *trans* rich network could not be evaluated since the final network was too brittle to withstand mechanical analysis procedure.[127]

The ability to induce crystallinity through the control of stereoisomerism is to date still in its infancy and will require much more research effort to develop into a powerful tool to tune the mechanical properties of robust polymer networks, especially needed in biomedical applications or 3D printing. Thus, both these applications require varying a multitude of parameters within a narrow window of applicability mostly caused by biocompatibility or printability constraints, which cannot always rely on a change of monomer units.

1.7 Conclusion

Since the early days of polymer chemistry, the stereoregularity of the chains was hinted to be a major parameter influencing the mechanical properties of the final material. More regular backbones lead to better chain packing abilities ultimately resulting in enhanced crystallinity. This realisation led to synthetic investigations aimed towards the production of regio- and stereo-specific polymers. The study of polyvinyl polymers corroborated the early hypothesis that the stereochemistry within the polymer backbones was a parameter as important as the molecular weight on the mechanical properties. Regarding unsaturated polymers, the bio-sourced Natural Rubber and Gutta Percha or *cis*-1,4-polyisoprene and *trans*-1,4-polyisoprene, displayed divergent thermomechanical properties. Thus, the former exhibits the mechanical behaviour of a soft elastomer and a temperature of melting T_m of 34 °C whilst the latter is a hard thermoplastic with a T_m of 89 °C. This remarkable impact of the isomerism on the mechanical properties inspired the development of stereospecific polymerisation techniques and soon, synthetic *trans* and *cis*-1,4-polyisoprene or 1,4-polybutadiene were produced on industrial scale. To date, the growing concern around the deleterious environmental impact of

petroleum-based polymer materials drove the research to focus on renewable resources which are more chemically diverse than the monomers obtained from petroleum which are mainly hydrocarbons. For this reason, the need for finding new synthetic techniques for the implementation of *cis*/*trans* stereochemistry containing oxygen based degradable functionalities is still of high relevance and very recently, various systems have been developed to that aim. However, these studies mainly focused on linear polymers and studies concerning chemically cross-linked polymer networks could scarcely be found with the very few examples focussing on the stereochemistry within networks mainly conducted on hydrogels. With some emerging applications such as 3D printing or biotechnology being restricted within the choices of chemical functionalities. For instance, the former requires the chemical structure to be UV active and displays physical properties in line with the printing conditions and the latter requires the fabricated materials to be biocompatible. For this reason, the development of ways to efficiently implement stereochemistry to tune the mechanical properties of the final product could be beneficial to these research fields.

1.8 Aim of the project

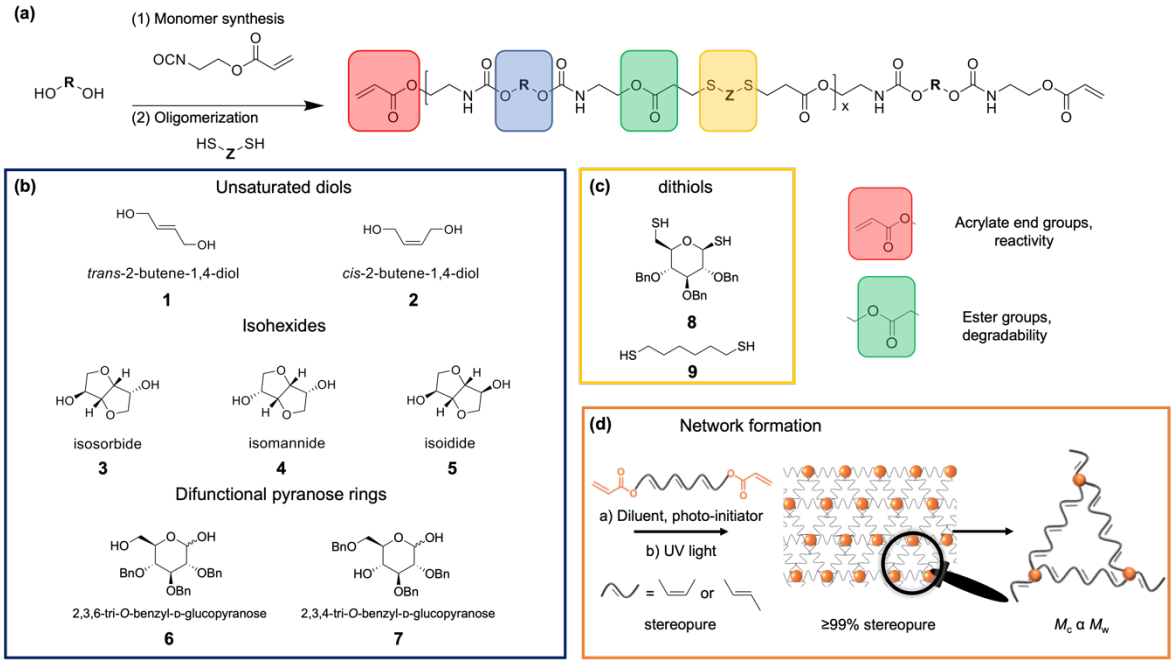


Figure 1.26. *Figure summarising the work presented in this manuscript. (a) General scheme of the diacrylate monomer synthesis (1) from the reaction of a diol and 2-isocyanatoethylacrylate followed by the polymerisation (2) via nucleophilic thiol-Michael addition with a dithiol in the presence of an excess of diacrylate to obtain telechelic oligomers with reactive acrylate termini. (b) Presentation of the diversity of diol used in this study. (c) Structure of the two dithiols used in this work. (d) Ideal illustration of the network formation from the radical reaction of the acrylate termini in the presence of a photo-initiator and UV light to create a stereopure unsaturated poly(ester-urethane) network.*

Within the currently available means to implement *cis*/*trans* stereochemistry within polymeric backbones, the thiol-Michael step growth addition has been highlighted as one of the most efficient and versatile techniques. High molecular weight poly(ester-urethanes) synthesised from the reaction of a dithiol and a diacrylate derived from *cis* and *trans* but-2-ene-1,4-diol or isohexides were obtained without the occurrence of unwanted crosslinking or isomerisation. The aim of this project is to explore the feasibility of synthesising diacrylate telechelic oligomers with good control over the molecular weight using the same monomer units with the

ultimate goal of forming covalently crosslinked networks with divergent mechanical properties. **(Figure 1.26)** It is hypothesised that the network structure would be ideal as the molecular weight between crosslinks is controlled by the molecular weight of the reacted oligomer. **(Figure 1.26 (d))** In parallel, the feasibility of synthesising a synthetic polysaccharide from a glucose-derived diacrylate and dithiol will be explored. The second chapter of this manuscript will describe the synthesis of the diacrylate monomers derived from *cis* and *trans* but-2-ene-1,4-diol, and isohexides in addition of a glucose-based diacrylate and dithiol, with the two later monomers being described for the first time to our knowledge. Chapter three will present the attempt at forming diacrylate telechelic oligomer via nucleophilic thiol-ene addition. Lastly, chapter 4 will explain the efforts towards the formulation of *cis* and *trans* but-2-ene-1,4-diol based diacrylate telechelic oligomers into a photo-active resins and the resulting mechanical behaviour arising from stereopure networks and the translation of the technology to 3D printed materials.

1.9 References

(1) Gal, J. Louis Pasteur, language, and molecular chirality. I. Background and Dissymmetry. *Chirality* **2011**, *23,* 1-16

(2) Pasteur, L. Memoires sur la relation qui peut exister entre la forme crystalline et la composition chimique, et sur la cause de la polarization rotatoire. *C. R. Hebd. Seances Acad. Sci.* **1848**, *26,* 535-538

(3) Flack, H. D. Louis Pasteur's discovery of molecular chirality and spontaneous resolution in 1848, together with a complete review of his crystallographic and chemical work. *Acta Crystallogr., Sect. A: Found. Crystallogr.* **2009**, *65,* 371-389

(4) Mauskopf, S. H. Crystals and compounds: molecular structure and composition in nineteenth-century French science. *Trans. Am. Philos. Soc.* **1976**, *66,* 1-82

(5) Gal, J. Louis Pasteur, Chemist: An Account of His Studies of Cinchona Alkaloids. *Helv. Chim. Acta* **2019**, *102,* e1800226

(6) Drayer, D. E. The early history of stereochemistry: from the discovery of molecular asymmetry and the first resolution of a racemate by Pasteur to the asymmetrical chiral carbon of van't Hoff and Le Bel. In *Drug Stereochemistry*, CRC Press, 2012; pp 11-26.

(7) Pasteur, L. Recherches sur la dissymétrie moléculaire des produits organiques naturels. Deuxième leçon. In *Œuvres de Pasteur*, Masson et Cie, 1922; pp 341-342.

(8) Le Bel, J. A. Sur les relations qui existent entre les formules atomiques des corps organiques et le pouvoir rotatoire de leurs dissolutions. *Bull. Soc. Chim. Fr* **1874**, *22,* 337-347

(9) Van't Hoff, J. H. Sur les formules de structure dans l'espace. *Arch. Neerl. Sci. Exactes Nat.* **1874**, *9,* 445-454

(10) Weyer, J. A Hundred Years of Stereochemistry—The Principal Development Phases in Retrospect. *Angew. Chem., Int. Ed. Engl.* **1974**, *13,* 591-598

(11) Kolbe, H. Vertrauliches Schreiben an Professor Kolbe. *J. Prakt. Chem.* **1877**, *16,* 467-472

(12) Riddell, F. G.; Robinson, M. J. T. J. H. van't Hoff and J. A. Le Bel—their historical context. *Tetrahedron* **1974**, *30,* 2001-2007

(13) Collet, A.; Crassous, J.; Dutasta, J.-P. *Molécules chirales: Stéréochimie et propriétés*; EDP Sciences et CNRS Editions, 2009.

(14) Mislow, K. M. *Introduction to stereochemistry*; Courier Corporation, 2002.

(15) Eliel, E. L.; Wilen, S. H. *Stereochemistry of organic compounds*; John Wiley & Sons, 1994.

(16) Moss, G. P. Basic terminology of stereochemistry (IUPAC Recommendations 1996). *Pure Appl. Chem.* **1996**, *68,* 2193-2222

(17) Cahn, R. S.; Ingold, C.; Prelog, V. Specification of Molecular Chirality. *Angew. Chem., Int. Ed. Engl.* **1966**, *5,* 385-415

(18) Gingras, M.; Félix, G.; Peresutti, R. One hundred years of helicene chemistry. Part 2: stereoselective syntheses and chiral separations of carbohelicenes. *Chem. Soc. Rev.* **2013**, *42,* 1007-1050

(19) Huang, M. B.; Lunell, S. Rotational potential energy surface and hyperfine structure of the n-butane cation. *J. Mol. Struct.: THEOCHEM* **1990**, *205,* 317-325

(20) van Loon, J.; Meyer, V. Das Fluor und die Esterregel. *Ber. Dtsch. Chem. Ges.* **1896**, *29,* 839-845

(21) Walden, P. Ueber die optische Drehung stereoisomerer Verbindungen. *Z. Phys. Chem.* **1896**, *20,* 377-388

(22) Hughes, E. D.; Ingold, C. K. Mechanism of substitution at a saturated carbon atom. Part IV. A discussion of constitutional and solvent effects on the mechanism, kinetics, velocity, and orientation of substitution. *J. Chem. Soc. (Resumed)* **1935**, 244-255

(23) Gal, J. The discovery of biological enantioselectivity: Louis Pasteur and the fermentation of tartaric acid, 1857--a review and analysis 150 yr later. *Chirality* **2008**, *20,* 5-19

(24) Pasteur, L. Mémoire sur la fermentation de l'acide tartrique. *C. R. Hebd. Seances Acad. Sci.* **1858**, *46,* 615-618

(25) Piutti, A. Sintesi e costituzione delle asparagine. *Gazz. Chim. Ital.* **1888**, *18,* 457-472

(26) Gal, J. The discovery of stereoselectivity at biological receptors: Arnaldo Piutti and the taste of the asparagine enantiomers—History and analysis on the 125th anniversary. *Chirality* **2012**, *24,* 959-976

(27) Ehrlich, P.; Morgenroth, J. Über Hämolysine Dritte Mitheilung. *Berl. Klin. Wochenschr.* **1900**, *37,* 453-458

(28) Langley, J. N. On the reaction of cells and of nerve-endings to certain poisons, chiefly as regards the reaction of striated muscle to nicotine and to curari. *J. Physiol.* **1905**, *33,* 374

(29) Gal, J. Molecular Chirality: Language, History, and Significance. In *Differentiation of Enantiomers I*, Springer International Publishing, 2013; pp 1-20.

(30) Barham, P.; Skibsted, L. H.; Bredie, W. L. P.; Bom Frøst, M.; Møller, P.; Risbo, J.; Snitkjær, P.; Mortensen, L. M. Molecular Gastronomy: A New Emerging Scientific Discipline. *Chem. Rev.* **2010**, *110,* 2313-2365

(31) Fischer, E. Einfluss der Configuration auf die Wirkung der Enzyme. *Ber. Dtsch. Chem. Ges.* **1894**, *27,* 2985-2993

(32) Staudinger, H.; Ashdown, A.; Brunner, M.; Bruson, H.; Wehrli, S. Über hochpolymere Verbindungen. 22. Mitteilung. Über die Konstitution des Poly-indens. *Helv. Chim. Acta* **1929**, *12,* 934-957

(33) Flory, P. J. Effects of Molecular Structure on Physical Properties of Butyl Rubber. *Ind. Eng. Chem.* **1946**, *38,* 417-436

(34) Worch, J. C.; Prydderch, H.; Jimaja, S.; Bexis, P.; Becker, M. L.; Dove, A. P. Stereochemical enhancement of polymer properties. *Nat. Rev. Chem.* **2019**, *3,* 514-535

(35) Jenkins, A. D. Stereochemical definitions and notations relating to polymers. *Pure Appl. Chem.* **2006**, *53,* 733-752

(36) Young, R. J.; Lovell, P. A. Stereochemsitry and coordination polymerization. In *Introduction to polymers*, CRC press, 2011; pp 147-167.

(37) Natta, G.; Pino, P.; Corradini, P.; Danusso, F.; Mantica, E.; Mazzanti, G.; Moraglio, G. Crystalline high polymers of α-olefins. *J. Am. Chem. Soc.* **1955**, *77,* 1708-1710

(38) Karger-Kocsis, J. Amorphous or atactic polypropylene. In *Polypropylene: An A-Z reference*, Springer Netherlands, 1999; pp 7-12.

(39) Fox, T.; Garrett, B.; Goode, W.; Gratch, S.; Kincaid, J.; Spell, A.; Stroupe, J. Crystalline polymers of methyl methacrylate. *J. Am. Chem. Soc.* **1958**, *80,* 1768-1769

(40) Ishihara, N.; Seimiya, T.; Kuramoto, M.; Uoi, M. Crystalline syndiotactic polystyrene. *Macromolecules* **1986**, *19,* 2464-2465

(41) Giller, C.; Gururajan, G.; Wei, J.; Zhang, W.; Hwang, W.; Chase, D. B.; Rabolt, J. F.; Sita, L. R. Synthesis, characterization, and electrospinning of architecturally-discrete isotactic− atactic− isotactic triblock stereoblock polypropene elastomers. *Macromolecules* **2011**, *44,* 471-482

(42) Harney, M. B.; Zhang, Y.; Sita, L. R. Discrete, multiblock isotactic–atactic stereoblock polypropene microstructures of differing block architectures through programmable stereomodulated living Ziegler–Natta polymerization. *Angew. Chem. Int. Ed.* **2006**, *45,* 2400-2404

(43) Madkour, T. M.; Mark, J. E. Mesoscopic modeling of the polymerization, morphology, and crystallization of stereoblock and stereoregular polypropylenes. *J. Polym. Sci., Part B: Polym. Phys.* **2002**, *40,* 840-853

(44) Coates, G. W.; Waymouth, R. M. Oscillating Stereocontrol: A Strategy for the Synthesis of Thermoplastic Elastomeric Polypropylene. *Science* **1995**, *267,* 217-219

(45) Mallin, D. T.; Rausch, M. D.; Lin, Y. G.; Dong, S.; Chien, J. C. W. rac-[Ethylidene(1-.eta.5-tetramethylcyclopentadienyl)(1-.eta.5-indenyl)]dichlorotitanium and its homopolymerization of propylene to crystalline-amorphous block thermoplastic elastomers. *J. Am. Chem. Soc.* **1990**, *112,* 2030-2031

(46) Teator, A. J.; Leibfarth, F. A. Catalyst-controlled stereoselective cationic polymerization of vinyl ethers. *Science* **2019**, *363,* 1439-1443

(47) Coates, G. W. Precise Control of Polyolefin Stereochemistry Using Single-Site Metal Catalysts. *Chem. Rev.* **2000**, *100,* 1223-1252

(48) Coates, G. W.; Domski, G. J. Polymerization and oligomerization of olefins. In *Organotransition Metal Chemistry - From Bonding to Catalysis*, University Science Books, 2010; pp 1047-1100.

(49) Natta, G. Properties of isotactic, atactic, and stereoblock homopolymers, random and block copolymers of α-olefins. *J. Polym. Sci.* **1959**, *34,* 531-549

(50) Razavi, A. Syndiotactic Polypropylene: Discovery, Development, and Industrialization via Bridged Metallocene Catalysts. In *Polyolefins: 50 years after Ziegler and Natta II: Polyolefins by Metallocenes and Other Single-Site Catalysts*, Springer 2013; pp 43-116.

(51) Drobny, J. G. *Handbook of thermoplastic elastomers*; Elsevier, 2014.

(52) Holden, G. Thermoplastic elastomers. In *Rubber technology*, Springer, 1987; pp 465-481.

(53) Ruzette, A.-V.; Leibler, L. Block copolymers in tomorrow's plastics. *Nat. Mater.* **2005**, *4,* 19

(54) Kim, J.; Jung, H. Y.; Park, M. J. End-Group Chemistry and Junction Chemistry in Polymer Science: Past, Present, and Future. *Macromolecules* **2020**, *53,* 746-763

(55) Semegen, S. T. In *Encyclopedia of physical science and technology*, 3rd ed.; Academic Press, 2003; pp 381–394.

(56) Baker, I. Gutta Percha. In *Fifty Materials That Make the World*, Springer International Publishing, 2018; pp 89-91.

(57) Khatavkar, R. A.; Hegde, V. S. The Weak Link in Endodontics: Gutta-Percha-A Need for Change. *World J. Dent.* **2010**, *1,* 217-224

(58) Morton, M. *Rubber technology*; Springer Science & Business Media, 2013.

(59) Wagner, H. L.; Flory, P. J. Molecular Dimensions of Natural Rubber and Gutta Percha[1]. *J. Am. Chem. Soc.* **1952**, *74,* 195-200

(60) Mark, J. E. Polymer Data Handbook. 2nd ed.; Oxford University Press: New York, 2009.

(61) Bunn, C. W.; Bragg, W. H. Molecular structure and rubber-like elasticity I. The crystal structures of gutta-percha, rubber and polychloroprene. *Proc. R. Soc. A* **1942**, *180,* 40-66

(62) Horne, S. E.; Kiehl, J. P.; Shipman, J. J.; Folt, V. L.; Gibbs, C. F.; Willson, E. A.; Newton, E. B.; Reinhart, M. A. Ameripol SN—A Cis-,4-Polyisoprene. *Ind. Eng. Chem.* **1956**, *48,* 784-791

(63) Bell, C. A.; Yu, J.; Barker, I. A.; Truong, V. X.; Cao, Z.; Dobrinyin, A. V.; Becker, M. L.; Dove, A. P. Independent control of elastomer properties through stereocontrolled synthesis. *Angew. Chem., Int. Ed.* **2016**, *55,* 13076-13080

(64) Stubbs, C. J.; Worch, J. C.; Prydderch, H.; Becker, M. L.; Dove, A. P. Unsaturated Poly(ester-urethanes) with Stereochemically Dependent Thermomechanical Properties. *Macromolecules* **2020**, *53,* 174-181

(65) Hsu, T.-W.; Kempel, S. J.; Felix Thayne, A. P.; Michaudel, Q. Stereocontrolled acyclic diene metathesis polymerization. *Nat. Chem.* **2023**, *15,* 14-20

(66) McGuire, T. M.; Pérale, C.; Castaing, R.; Kociok-Köhn, G.; Buchard, A. Divergent Catalytic Strategies for the Cis/Trans Stereoselective Ring-Opening Polymerization of a Dual Cyclic Carbonate/Olefin Monomer. *J. Am. Chem. Soc.* **2019**, *141,* 13301-13305

(67) Hartley, G. S. The Cis-form of Azobenzene. *Nature* **1937**, *140,* 281-281

(68) Bandara, H. M. D.; Burdette, S. C. Photoisomerization in different classes of azobenzene. *Chem. Soc. Rev.* **2012**, *41,* 1809-1825

(69) Rau, H. 1 - Photoisomerization of Azobenzenes. In *Photoreactive Organic Thin Films*, Academic Press, 2002; pp 3-47.

(70) Chiang, C. K.; Fincher, C. R.; Park, Y. W.; Heeger, A. J.; Shirakawa, H.; Louis, E. J.; Gau, S. C.; MacDiarmid, A. G. Electrical Conductivity in Doped Polyacetylene. *Phys. Rev. Lett.* **1977**, *39,* 1098-1101

(71) Shirakawa, H.; Ikeda, S. Preparation and morphology of as-prepared and highly stretch-aligned polyacetylene. *Synth. Met.* **1980**, *1,* 175-184

(72) Qi, X.; Zhang, Y.; Zhang, L.; Yue, D. Bioinspired Sustainable Polymer with Stereochemistry-Controllable Thermomechanical Properties. *Macromolecules* **2023**, *56,* 416-425

(73) Wilson, J. A.; Luong, D.; Kleinfehn, A. P.; Sallam, S.; Wesdemiotis, C.; Becker, M. L. Magnesium Catalyzed Polymerization of End Functionalized Poly(propylene maleate) and Poly(propylene fumarate) for 3D Printing of Bioactive Scaffolds. *J. Am. Chem. Soc.* **2018**, *140,* 277-284

(74) Wan, Z.-Q.; Ren, W.-M.; Yang, S.; Li, M.-R.; Gu, G.-G.; Lu, X.-B. Reversible Transformation between Amorphous and Crystalline States of Unsaturated Polyesters by Cis–Trans Isomerization. *Angew. Chem., Int. Ed.* **2019**, *58,* 17636-17640

(75) Kolb, H. C.; Finn, M. G.; Sharpless, K. B. Click Chemistry: Diverse Chemical Function from a Few Good Reactions. *Angew. Chem. Int. Ed.* **2001**, *40,* 2004-2021

(76) Worch, J. C.; Stubbs, C. J.; Price, M. J.; Dove, A. P. Click Nucleophilic Conjugate Additions to Activated Alkynes: Exploring Thiol-yne, Amino-yne, and Hydroxyl-yne Reactions from (Bio)Organic to Polymer Chemistry. *Chem. Rev.* **2021**, *121,* 6744-6776

(77) Randive, N. A.; Kumar, V.; Nair, V. A. A facile approach to substituted acrylates by regioselective and stereoselective addition of thiols and amines to an alkynyl ester in water. *Monatsh. Chem. Chem. Mon.* **2010**, *141,* 1329-1332

(78) Truong, V. X.; Dove, A. P. Organocatalytic, Regioselective Nucleophilic "Click" Addition of Thiols to Propiolic Acid Esters for Polymer–Polymer Coupling. *Angew. Chem.* **2013**, *125,* 4226-4230

(79) Worch, J. C.; Weems, A. C.; Yu, J.; Arno, M. C.; Wilks, T. R.; Huckstepp, R. T. R.; O'Reilly, R. K.; Becker, M. L.; Dove, A. P. Elastomeric polyamide biomaterials with stereochemically tuneable mechanical properties and shape memory. *Nat. Commun.* **2020**, *11,* 3250

(80) He, B.; Zhen, S.; Wu, Y.; Hu, R.; Zhao, Z.; Qin, A.; Tang, B. Z. Cu(i)-Catalyzed amino-yne click polymerization. *Polym. Chem.* **2016**, *7,* 7375-7382

(81) He, B.; Su, H.; Bai, T.; Wu, Y.; Li, S.; Gao, M.; Hu, R.; Zhao, Z.; Qin, A.; Ling, J.; et al. Spontaneous Amino-yne Click Polymerization: A Powerful Tool toward Regio- and Stereospecific Poly(β-aminoacrylate)s. *J. Am. Chem. Soc.* **2017**, *139,* 5437-5443

(82) Zeng, R.; Sheng, H.; Rao, B.; Feng, Y.; Wang, H.; Sun, Y.; Chen, M.; Zhu, M. An efficient and green approach to synthesizing enamines by intermolecular hydroamination of activated alkynes. *Chem. Res. Chin. Univ.* **2015**, *31,* 212-217

(83) Junji, I.; Yoshiyasu, B.; Takeshi, H. Organic Synthesis with Trialkylphosphine Catalysts. Conjugate Addition of Alcohols to α,β-Unsaturated Alkynic Acid Esters. *Chem. Lett.* **1993**, *22,* 241-244

(84) Shi, Y.; Bai, T.; Bai, W.; Wang, Z.; Chen, M.; Yao, B.; Sun, J. Z.; Qin, A.; Ling, J.; Tang, B. Z. Phenol-yne Click Polymerization: An Efficient Technique to Facilely Access Regio- and Stereoregular Poly(vinylene ether ketone)s. *Chem. Eur. J.* **2017**, *23,* 10725-10731

(85) Autenrieth, B.; Schrock, R. R. Stereospecific Ring-Opening Metathesis Polymerization (ROMP) of Norbornene and Tetracyclododecene by Mo and W Initiators. *Macromolecules* **2015**, *48,* 2493-2503

(86) Hsu, T.-W.; Kim, C.; Michaudel, Q. Stereoretentive Ring-Opening Metathesis Polymerization to Access All-cis Poly(p-phenylenevinylene)s with Living Characteristics. *J. Am. Chem. Soc.* **2020**, *142,* 11983-11987

(87) Wang, J.; Liu, X.; Jia, Z.; Sun, L.; Zhang, Y.; Zhu, J. Modification of poly(ethylene 2,5-furandicarboxylate) (PEF) with 1, 4-cyclohexanedimethanol: Influence of stereochemistry of 1,4-cyclohexylene units. *Polymer* **2018**, *137,* 173-185

(88) Vanhaecht, B.; Rimez, B.; Willem, R.; Biesemans, M.; Koning, C. E. Influence of stereochemistry on the thermal properties of partially cycloaliphatic polyamides. *J. Polym. Sci., Part A-1: Polym. Chem.* **2002**, *40,* 1962-1971

(89) Kricheldorf, H. R.; Schwarz, G. New polymer syntheses, 17. Cis/trans isomerism of 1,4-cyclohexanedicarboxylic acid in crystalline, liquid-crystalline and amorphous polyesters. *Makromol. Chem.* **1987**, *188,* 1281-1294

(90) Vanhaecht, B.; Teerenstra, M. N.; Suwier, D. R.; Willem, R.; Biesemans, M.; Koning, C. E. Controlled stereochemistry of polyamides derived from cis/trans-1,4-cyclohexanedicarboxylic acid. *J. Polym. Sci., Part A: Polym. Chem.* **2001**, *39,* 833-840

(91) Liu, F.; Zhang, J.; Wang, J.; Liu, X.; Zhang, R.; Hu, G.; Na, H.; Zhu, J. Soft segment free thermoplastic polyester elastomers with high performance. *J. Mater. Chem. A* **2015**, *3,* 13637-13641

(92) Galbis, J. A.; García-Martín, M. d. G.; de Paz, M. V.; Galbis, E. Synthetic Polymers from Sugar-Based Monomers. *Chem. Rev.* **2016**, *116,* 1600-1636

(93) Rose, M.; Palkovits, R. Isosorbide as a Renewable Platform chemical for Versatile Applications—Quo Vadis? *ChemSusChem* **2012**, *5,* 167-176

(94) Fenouillot, F.; Rousseau, A.; Colomines, G.; Saint-Loup, R.; Pascault, J. P. Polymers from renewable 1,4:3,6-dianhydrohexitols (isosorbide, isomannide and isoidide): A review. *Prog. Polym. Sci.* **2010**, *35,* 578-622

(95) Thiem, J.; Bachmann, F. Synthesis and properties of polyamides derived from anhydro- and dianhydroalditols. *Makromol. Chem.* **1991**, *192,* 2163-2182

(96) Rajput, B. S.; Gaikwad, S. R.; Menon, S. K.; Chikkali, S. H. Sustainable polyacetals from isohexides. *Green Chem.* **2014**, *16,* 3810-3818

(97) Wu, J.; Eduard, P.; Jasinska-Walc, L.; Rozanski, A.; Noordover, B. A. J.; van Es, D. S.; Koning, C. E. Fully Isohexide-Based Polyesters: Synthesis, Characterization, and Structure–Properties Relations. *Macromolecules* **2013**, *46,* 384-394

(98) Storbeck, R.; Rehahn, M.; Ballauff, M. Synthesis and properties of high-molecular-weight polyesters based on 1,4:3,6-dianhydrohexitols and terephthalic acid. *Makromol. Chem.* **1993**, *194,* 53-64

(99) Bachmann, F.; Reimer, J.; Ruppenstein, M.; Thiem, J. Synthesis of Novel Polyurethanes and Polyureas by Polyaddition Reactions of Dianhydrohexitol Configurated Diisocyanates. *Macromol. Chem. Phys.* **2001**, *202,* 3410-3419

(100) Kieber, R. J.; Silver, S. A.; Kennemur, J. G. Stereochemical effects on the mechanical and viscoelastic properties of renewable polyurethanes derived from isohexides and hydroxymethylfurfural. *Polym. Chem.* **2017**, *8,* 4822-4829

(101) Stubbs, C. J.; Worch, J. C.; Prydderch, H.; Wang, Z.; Mathers, R. T.; Dobrynin, A. V.; Becker, M. L.; Dove, A. P. Sugar-Based Polymers with Stereochemistry-Dependent Degradability and Mechanical Properties. *J. Am. Chem. Soc.* **2022**, *144,* 1243-1250

(102) Takeuchi, S.; Takasu, A. Synthesis and Biodegradability of Poly(ester-urethane)s via the Thiol-Michael Polyaddition of Dianhydro Sugar-Based Diacrylates. *ACS Appl. Polym.* **2022**, *4,* 4486-4494

(103) Stubbs, C. J.; Dove, A. P. Understanding structure–property relationships of main chain cyclopropane in linear polyesters. *Polym. Chem.* **2020**, *11,* 6251-6258

(104) Mark, J. E. *Physical properties of polymers handbook*; Springer, 2007.

(105) Kent, E. G.; Swinney, F. B. Properties and applications of trans-1, 4-polyisoprene. *Ind. Eng. Chem. Prod. Res. Dev.* **1966**, *5,* 134-138

(106) Bueche, F. Mechanical properties of natural and synthetic rubbers. *J. Polym. Sci.* **1957**, *25,* 305-324

(107) Timmer, M. D.; Ambrose, C. G.; Mikos, A. G. In vitro degradation of polymeric networks of poly(propylene fumarate) and the crosslinking macromer poly(propylene fumarate)-diacrylate. *Biomaterials* **2003**, *24,* 571-577

(108) Lewandrowski, K.-U.; Gresser, J. D.; Wise, D. L.; White, R. L.; Trantolo, D. J. Osteoconductivity of an injectable and bioresorbable poly(propylene glycol-co-fumaric acid) bone cement. *Biomaterials* **2000**, *21,* 293-298

(109) Walker, J. M.; Bodamer, E.; Krebs, O.; Luo, Y.; Kleinfehn, A.; Becker, M. L.; Dean, D. Effect of Chemical and Physical Properties on the In Vitro Degradation of 3D Printed High Resolution Poly(propylene fumarate) Scaffolds. *Biomacromolecules* **2017**, *18,* 1419-1425

(110) Yu, Y.; Wei, Z.; Leng, X.; Li, Y. Facile preparation of stereochemistry-controllable biobased poly(butylene maleate-co-butylene fumarate) unsaturated copolyesters: a chemoselective polymer platform for versatile functionalization via aza-Michael addition. *Polym. Chem.* **2018**, *9,* 5426-5441

(111) Kricheldorf, H. R.; Yashiro, T.; Weidner, S. Isomerization-Free Polycondensations of Maleic Anhydride with α,ω-Alkanediols. *Macromolecules* **2009**, *42,* 6433-6439

(112) Tran, R. T.; Thevenot, P.; Gyawali, D.; Chiao, J.-C.; Tang, L.; Yang, J. Synthesis and characterization of a biodegradable elastomer featuring a dual crosslinking mechanism. *Soft Matter* **2010**, *6,* 2449-2461

(113) Fortman, D. J.; Brutman, J. P.; De Hoe, G. X.; Snyder, R. L.; Dichtel, W. R.; Hillmyer, M. A. Approaches to Sustainable and Continually Recyclable Cross-Linked Polymers. *ACS Sustainable Chem. Eng.* **2018**, *6,* 11145-11159

(114) Helms, B. A.; Russell, T. P. Reaction: Polymer Chemistries Enabling Cradle-to-Cradle Life Cycles for Plastics. *Chem* **2016**, *1,* 816-818

(115) Bapat, A. P.; Sumerlin, B. S.; Sutti, A. Bulk network polymers with dynamic B–O bonds: healable and reprocessable materials. *Mater. Horiz.* **2020**, *7,* 694-714

(116) Wang, R.; Sing, M. K.; Avery, R. K.; Souza, B. S.; Kim, M.; Olsen, B. D. Classical Challenges in the Physical Chemistry of Polymer Networks and the Design of New Materials. *Acc. Chem. Res.* **2016**, *49,* 2786-2795

(117) Beharry, A. A.; Woolley, G. A. Azobenzene photoswitches for biomolecules. *Chem. Soc. Rev.* **2011**, *40,* 4422-4437

(118) Zhao, Y.-L.; Stoddart, J. F. Azobenzene-Based Light-Responsive Hydrogel System. *Langmuir* **2009**, *25,* 8442-8446

(119) Guan, Y.; Zhao, H.-B.; Yu, L.-X.; Chen, S.-C.; Wang, Y.-Z. Multi-stimuli sensitive supramolecular hydrogel formed by host–guest interaction between PNIPAM-Azo and cyclodextrin dimers. *RSC Advances* **2014**, *4,* 4955-4959

(120) Tamesue, S.; Takashima, Y.; Yamaguchi, H.; Shinkai, S.; Harada, A. Photoswitchable Supramolecular Hydrogels Formed by Cyclodextrins and Azobenzene Polymers. *Angew. Chem. Int. Ed.* **2010**, *49,* 7461-7464

(121) Rosales, A. M.; Mabry, K. M.; Nehls, E. M.; Anseth, K. S. Photoresponsive elastic properties of azobenzene-containing poly (ethylene-glycol)-based hydrogels. *Biomacromolecules* **2015**, *16,* 798-806

(122) Lee, I. N.; Dobre, O.; Richards, D.; Ballestrem, C.; Curran, J. M.; Hunt, J. A.; Richardson, S. M.; Swift, J.; Wong, L. S. Photoresponsive Hydrogels with Photoswitchable Mechanical Properties Allow Time-Resolved Analysis of Cellular Responses to Matrix Stiffening. *ACS Appl. Mater. Interfaces* **2018**, *10,* 7765-7776

(123) Macdougall, L. J.; Pérez-Madrigal, M. M.; Shaw, J. E.; Worch, J. C.; Sammon, C.; Richardson, S. M.; Dove, A. P. Using Stereochemistry to Control Mechanical Properties in Thiol–Yne Click-Hydrogels. *Angew. Chem. Int. Ed.* **2021**, *60,* 25856-25864

(124) Amarnath, N.; Mukherjee, S.; Lochab, B. Understanding the Stereochemical Effect on the Properties of Emerging Thermosets: Sustainable Polybenzoxazines. *ACS Sustainable Chem. Eng.* **2021**, *9,* 7550-7560

(125) Amarnath, N.; Shukla, S.; Lochab, B. Isomannide-Derived Chiral Rigid Fully Biobased Polybenzoxazines. *ACS Sustainable Chem. Eng.* **2019**, *7,* 18700-18710

(126) Duval, A.; Sarbu, A.; Dalmas, F.; Albertini, D.; Avérous, L. 2,3-Butanediol as a Biobased Chain Extender for Thermoplastic Polyurethanes: Influence of Stereochemistry on Macromolecular Architectures and Properties. *Macromolecules* **2022**, *55,* 5371-5381

(127) Louisy, E.; Olivero, S.; Michelet, V.; Mija, A. On the Influence of the cis/trans Stereochemistry of Limonene Oxides toward the Synthesis of Biobased Thermosets by Crosslinking with Anhydrides. *ACS Sustainable Chem. Eng.* **2022**, *10,* 7169-7179

Chapter 2 – Di-functional monomer synthesis for thiol-ene step growth polymerisation

2 Di-functional monomers synthesis for thiol-ene step growth polymerisation

1.10 Chapter overview

The focus of this chapter is to present the synthesis of 6 diacrylates monomers for thiol-ene step growth polymerisation that will be used in subsequent chapters. The general scheme of the synthesis is presented in **Figure 2.1 (d)**.

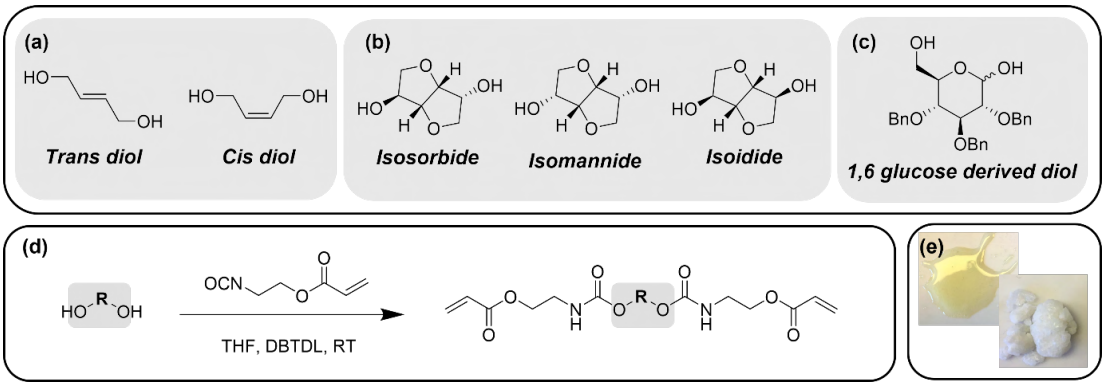


Figure 2.1. *Figure summarising the content of this chapter, which focusses on the synthesis of diacrylate monomers starting from of (a) the cis and trans or (b) isohexides or (c) a 1,6-glucose-derived diol. The reactions involve the functionalisation of each diol with a commercially available isocyanate acrylate in the presence of dibutyltin dilaurate (DBTDL) as catalyst (d). (e) Picture of polymers of similar structure containing (solid) or not (liquid) urethane bonds obtained from the reaction of the same diol with either isocyanatoethylacrylate or acryloyl chloride respectively and polymerised via the nucleophilic thiol-Michael*

By reacting various diol precursors with the commercially available 2-isocyanatoethyl acrylate, it was possible to synthesise 3 distinct sets of diacrylate monomers which would ultimately offer the possibility of studying the effect of both unsaturated *cis/trans* and rigid ring *endo*/*exo* type of stereochemistry within polymer networks. (**Figure 2.1(a) and (b)**). Moreover, to explore the feasibility of producing a synthetic polysaccharide *via* thiol-ene step growth polymerisation, both a glucose-

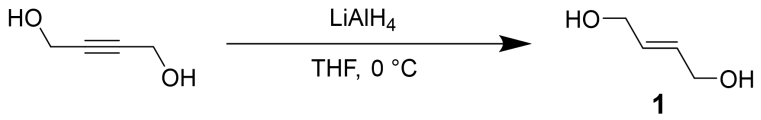
derived diacrylate and dithiol have been synthesised from the corresponding 1,6-glucose-derived diol precursor. (**Figure 2.1(c)**)

Usage of 2-isocyanatoethyl acrylate had the unique advantage to not only giving access to a wide array of diacrylate monomers from a single preparation in near quantitative yields, but also of incorporating urethane groups within the polymer backbones, which proved to be crucial in the obtention of materials possessing robust mechanical properties through the formation of H-bonding. Thus, a preliminary experiment showed that only liquid to tacky solids were obtained if the urethane bonds were removed from the polymer backbone by reacting acryloyl chloride with a diol precursor to synthesise the diacrylate monomer. (**Figure 2.1(e)**)

This chapter will first start by presenting the synthesis of the three non-commercial diol precursors: *trans*-2-butene-1,4-diol, isoidide and the glucose derived diol. The choice of synthesising a 1,6-glucose-derived diol came logically after the synthesis of the originally planned 1,4-glucose diol gave unsatisfactory results both in terms of yield and purity, which would be discussed in detail below. Then, the general synthesis of the diacrylate will be presented and finally, the synthesis of the 1,6-glucose derived dithiol will be developed.

1.11 Synthesis of *trans*-2-butene-1,4-diol

Whilst *cis*-2-butene-1,4-diol is commercially available and inexpensive, the *trans* isomer (**1**) has been prepared by stereoselective reduction of 1,4-butyne diol with lithium aluminium hydride in THF adapted from a previously reported strategy.[1] (**Scheme 2.1)**



Scheme 2.1. *Synthesis of trans-2-butene-1,4-diol*

The resultant product was purified by column chromatography to afford *trans*-2-butene-1,4-diol (**1**) in 44 to 51% yield on a 10 g scale and 35% yield on a 30 g scale. The yield obtained for this synthesis are lower than already reported (98%). Firstly, for safety reasons, the reaction was performed at room temperature overnight instead of at reflux for 3 h as indicated in the original 2 g scale procedure. In addition, the formation of aluminium salts occurs during the work up, in combination with an increased reaction scale causes the washing stage to be more challenging and resulted in a lower yield.

Analysis of the product by ^{1}H NMR spectroscopy in d_6-DMSO confirmed the stereo-purity of the compound, showing only one characteristic resonance peak in the vinylic proton region at δ = 5.67 ppm (*trans*) and none at δ = 5.47 ppm (*cis*).[2] (**Figure 2.2**)

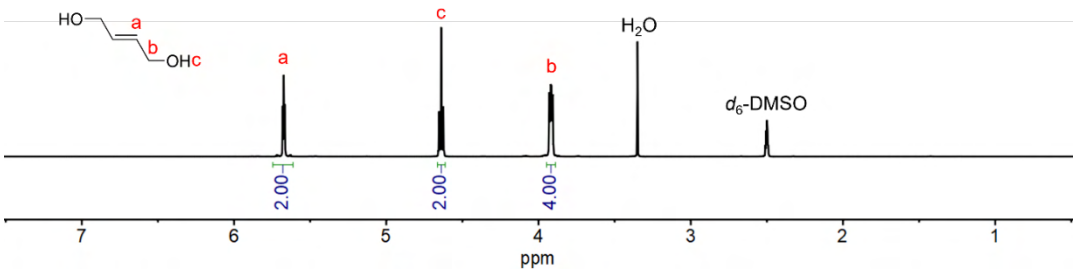


Figure 2.2. *^{1}H NMR (400 MHz, 298 K, d_6-DMSO) spectrum of trans-2-butene-1,4-diol (**1**).*

1.12 Synthesis of Isoidide

Isoidide is one of the three 1,4:3,6-dianhydrohexitol or isohexides isomers along with isosorbide and isomannide. These three diols are particularly interesting owing to their peculiar geometric configuration. The structure is comprised of two *cis*-fused tetrahydrofuran rings that are in a V-shaped configuration, with a 120° angle between the rings. In addition, hydroxyl groups oriented in *endo*, are able to form hydrogen bonding with the ethereal oxygen of the neighbouring ring, providing them with increased nucleophilicity. This particular arrangement is observed on the only *endo* hydroxyl in isosorbide and both hydroxyl groups in isomannide, whilst it is not observed on isoidide since both hydroxyl groups are *exo* oriented.[3] (**Figure 2.3)**. Thus, isohexides, owing to their uncommon V-shape and 2 chiral centers, were interesting candidates to explore the impact of *endo*/*exo* type stereochemistry within our polymer system.

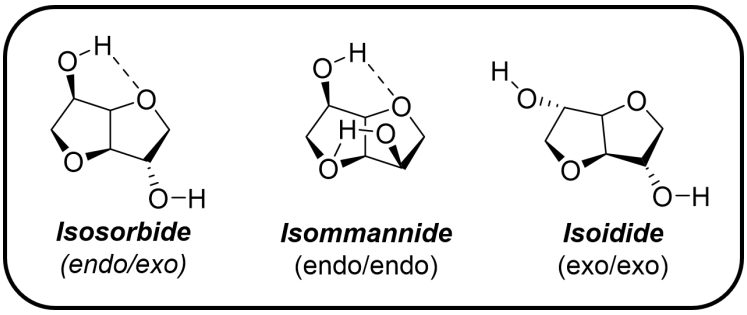
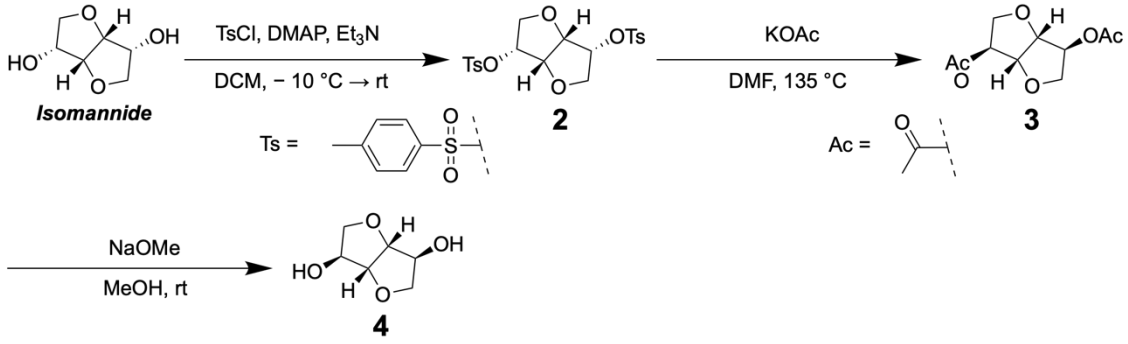


Figure 2.3. *Structure of the three isohexide isomers.*

Isosorbide and isomannide are industrially obtained from the sequential dehydrogenation and double dehydration of their sugar precursor D-glucose and D-mannose respectively and, are both commercially available.[3-5] Isoidide, was obtained from the epimerisation of isomannide in three synthetic steps following a procedure previously optimised within the group.[6] First, the hydroxyl groups are

tosylated using *p*-methanetoluenesulfonyl chloride in dichloromethane, offering a better leaving group for the following nucleophilic substitution using potassium acetate in dimethylformamide. After this reaction, the original *exo*/*exo* stereochemistry of isomannide is inverted to *endo*/*endo*, providing an acetylated isoidide (**3**). The final step consists in deprotecting the hydroxyl groups *via* deacetylation in the presence of sodium methoxide in methanol, otherwise known as the Zemplèn transesterification, to give isoidide (**4**). (**Scheme 2.2**) These reactions have been easily scaled up to 30 g in yield from 78 to 90%.



Scheme 2.2. *Synthesis of isoidide (**4**).*

As the only by-product of the deprotection stage is methyl acetate, isoidide is obtained after acidification of the reaction media using a proton exchange resin and evaporation of the solvent under vacuum without the need for further purification. Comparing the ^{1}H NMR spectra of the product and the starting material confirmed the obtention of isoidide. (**Figure 2.4**) Thus, the resonance signal of hydroxyl protons shifted from δ = 4.76 ppm (isomannide) to δ = 5.11 ppm (isoidide **4**) and the methylene protons displayed a stronger splitting pattern are both evidence of the different spatial environment surrounding the protons.

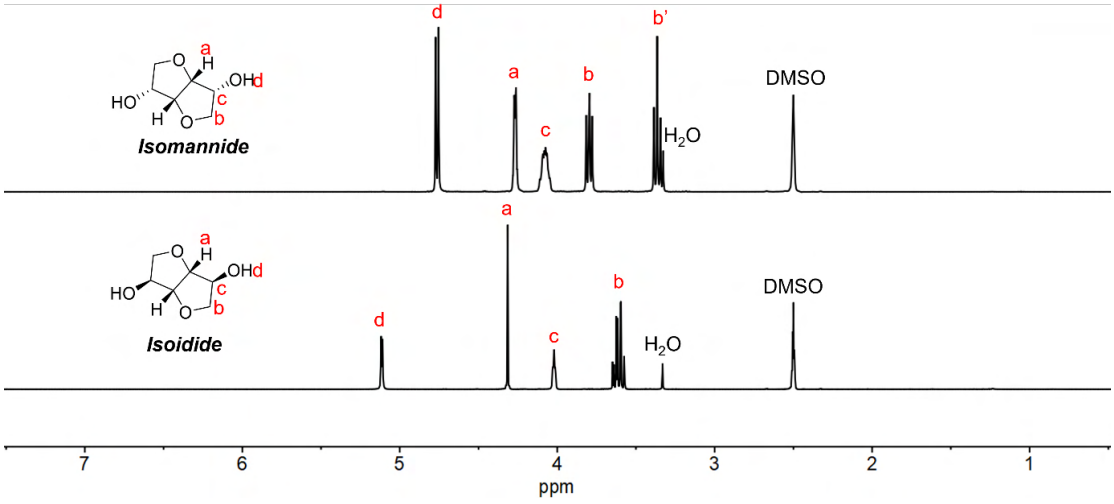


Figure 2.4. *Comparison of the ^{1}H NMR (400 MHz, 298 K, d_6-DMSO) spectra of 2.4 Glucose-derived diol*

Glucose is the most abundant representative of the monosaccharide family and is industrially obtained from the enzymatic hydrolysis of corn starch.[7] Owing to its natural origin, inexpensiveness, innocuousness, and remarkable stereochemical and structural characteristics (**Figure 2.5**), research effort towards its polymerisation started as early as the 1950's [8] and is still relevant to this day.[9-14]

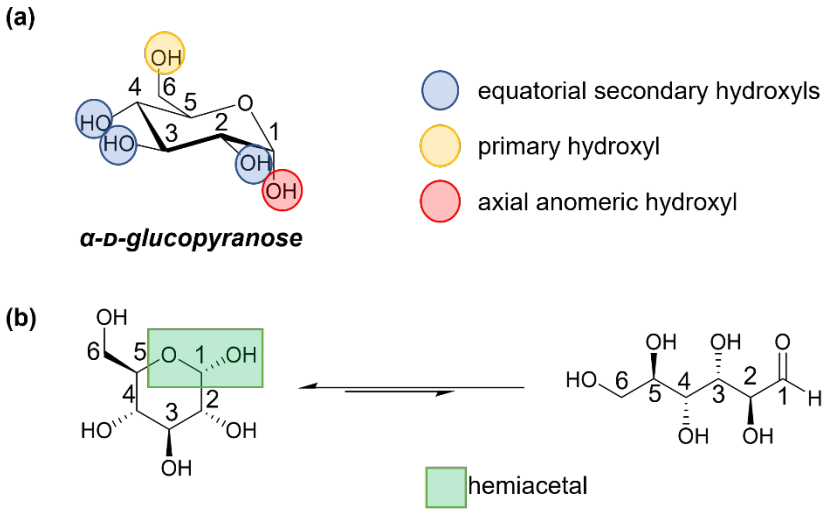
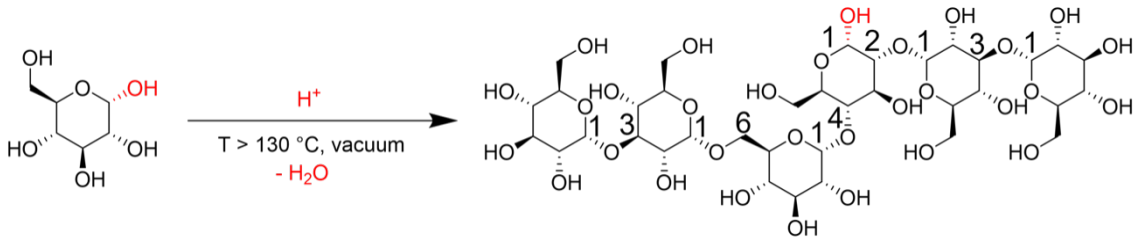


Figure 2.5. *(a) Structure of α-D-glucopyranose in the most stable chair configuration showing the conventional numbering of the carbons within a pyranose ring. (b) Scheme representing the equilibria existing between the cyclic and linear form of glucose in solution, illustrating that the anomeric oxygen is engaged in a hemiacetal, explaining it electrophilicity leading it to be a good leaving group. On the left, the glucose unit is represented in the clearer stereochemical view.*

Although the electrophilic characteristic of the anomeric oxygen has been exploited for the formation of linear polycondensates from unprotected glucose in the presence of an acid catalyst [15] (**Error! Reference source not found.**), the obtention of regio-regular glycoside bonds relies on the appropriate protection/deprotection strategy towards the synthesis of a glucose-based difunctional monomer.[11, 16, 17]



Scheme 2.3. *Reaction scheme of the polycondensation of unprotected α-D-glucose and a representation of the structure of the products obtained: the linkage between glucose units is non regio-specific as the hydroxyl on C1 is able to react with one of the four non anomeric free hydroxyls.*

The incorporation of glucose moieties into our monomer system necessitated the synthesis of a sugar diol and, amongst the variety of diols that could be derived from glucose, attention was focussed at first upon the obtention of a 1,4-glucose-derived diol. This configuration offers, once polymerised, the potential to mimic the backbone connectivity observed in cellulose, known for enhancing the mechanical properties of the polymer through better chain packing.[18, 19] (**Figure 2.6**)

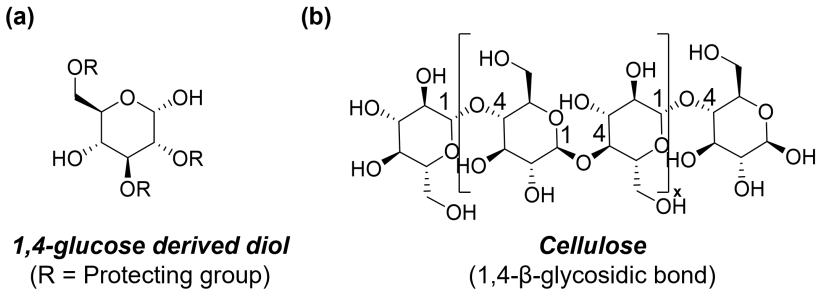


Figure 2.6. *(a) Structure of the desired 1,4-glucose-derived diol and (b) Structure of cellulose, where the glucose units are linked through a 1,4-β-glycosidic bond, affording regioregularity to the polymer chain.*

1.13 Synthesis pathways to 1,4-glucose-derived diol

The synthesis of a synthon bearing free hydroxyl groups on the 1st and 4th position can be potentially achieved by: (i) the sequential benzylation and hydrolysis of β-cyclodextrin[20] (**Figure 2.7 (a)**), (ii) the selective benzoylation of methyl-α-D-glucopyranoside on the 2nd, 3rd, and 6th position[21, 22] followed by the cleavage of the methyl group on the first position (**Figure 2.7 (b)**), or by (iii) following a well-established 4-step synthesis starting from α-D-glucopyranoside.[10] (**Figure 2.7 (c)**)

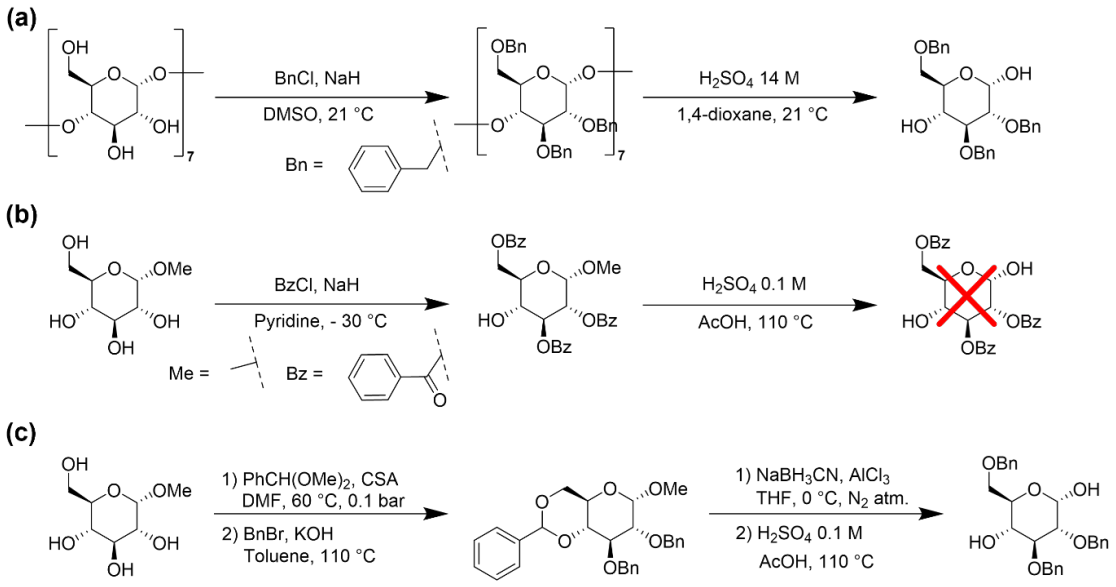
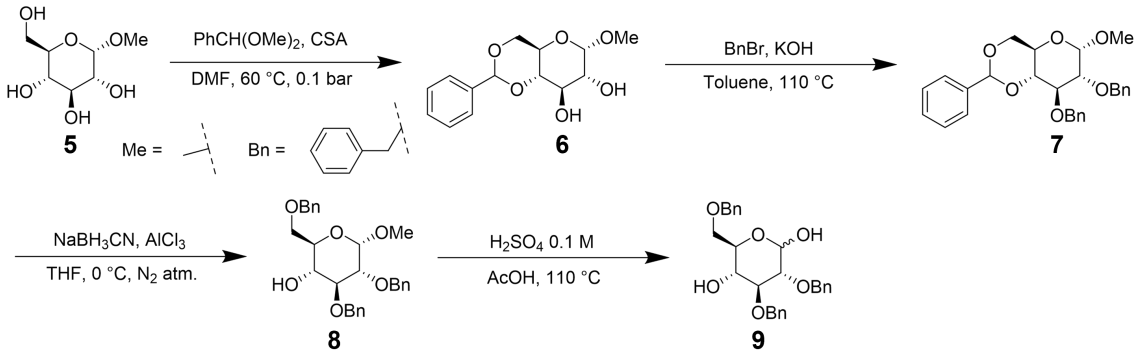


Figure 2.7. *Reaction scheme of the synthesis of a 1,4-glucose-derived diol via (a) benzylation and hydrolysis of β-cyclodextrin, (b) selective acylation of methyl α-D-glucopyranoside followed by hydrolysis of the glycosidic bond, (c) traditional 4 step protection/deprotection strategy starting from methyl α-D-glucopyranoside.*

Although the first option seemed ideal, the purification process involves two columns and a slow recrystallisation, which would be tedious to achieve on a scale required for our application. The second option has been considered, but quickly abandoned because of the inability to cleave the methyl ether protecting the anomeric hydroxyl group in the presence of benzoyl groups decorating the remaining hydroxyls.[23, 24] Hence, the choice has been made to follow the route involving the multi-step synthesis, which offered the crucial advantages of being largely documented and easily scalable. In addition, the incorporation of a benzylated 1,4-diol has already been investigated for the synthesis of polycarbonate materials,[10] thus, using this compound in our polymer system opens the possibility of investigating the monomer behaviour with a different polymerisation as well as comparing the bulk characteristics of the obtained polymers.

1.13.1 Synthesis of 2,3,6-tri-O-benzyl-D-glucopyranoside (1,4-glucose diol).

Starting from the commercially available methyl α-D-glucopyranoside (**5**), the 1,4-glucose diol (**9**) has been obtained in 4 synthetic steps following routine protection/deprotection strategies in carbohydrate chemistry (**Scheme 2.4**).



Scheme 2.4. *Multi-step synthesis of 2,3,6-tri-O-benzyl-D-glucopyranoside (1,4-glucose diol) (**9**).*

First, the 1,3-diol, occupying the 4th (C4) and 6th carbon (C6) of the sugar ring (**5**), is selectively protected by acetalation to give compound (**6**). Introduction of a benzylidene acetal on a glucose ring can be achieved by (i) reaction with benzaldehyde and zinc chloride as originally reported [25, 26] or by (ii) transacetalation using benzaldehyde dimethyl acetal in the presence of a Lewis acid catalyst such as *p*-toluenesulfonic acid, camphor-10-sulfonic acid or boron trifluoride etherate.[27] The main disadvantage of these two methods lies in the requirement of a large excess of benzaldehyde, which is commonly used as the reaction solvent.[28] Being interested in carrying out this reaction on large scale: improving the atom economy of this reaction to reduce waste and allow for easier purification has been a key factor in selecting a synthetic procedure. Hence, the decision was made to follow more recent literature, claiming that the use of iodide[29] or a heterogeneous catalysis such as sulfuric acid immobilised on silica,[30] improves substantially the reaction

efficiency whilst only requiring a stochiometric ratio of the reactants and minimizing the work up. Unfortunately, the first method led to the preparation of the benzylidene acetal glucose derivative (**6**) in only 18% yield after 4 days of reaction. Following the second preparation, the reaction completion has never been reached. Surprisingly, none of these two reports mentioned the need of heating or performing the reaction under vacuum, which constitutes a logical means to remove the methanol produced during the reaction and thereby drive the equilibrium towards the formation of product (**6**). Hence, inspired by a previous report [27, 31] the reaction was performed on a rotary evaporator at 60 °C using only 1.2 equivalents of benzaldehyde dimethyl acetal and 0.003 equivalent of camphor-10-sulfonic acid and allowed the preparation of methyl 4,6-O-benzylidene-α-D-glucopyranoside (**6**) in 89% yield within 4 hours on a scale up to 60 g of the starting material. The successful protection has been confirmed by the apparition of the characteristic resonance signals of both benzyl protons at δ = 7.49 and δ = 7.37 ppm and a methine proton at δ = 5.52 ppm on the ^{1}H NMR spectrum of the product. (**Figure 2.8**)

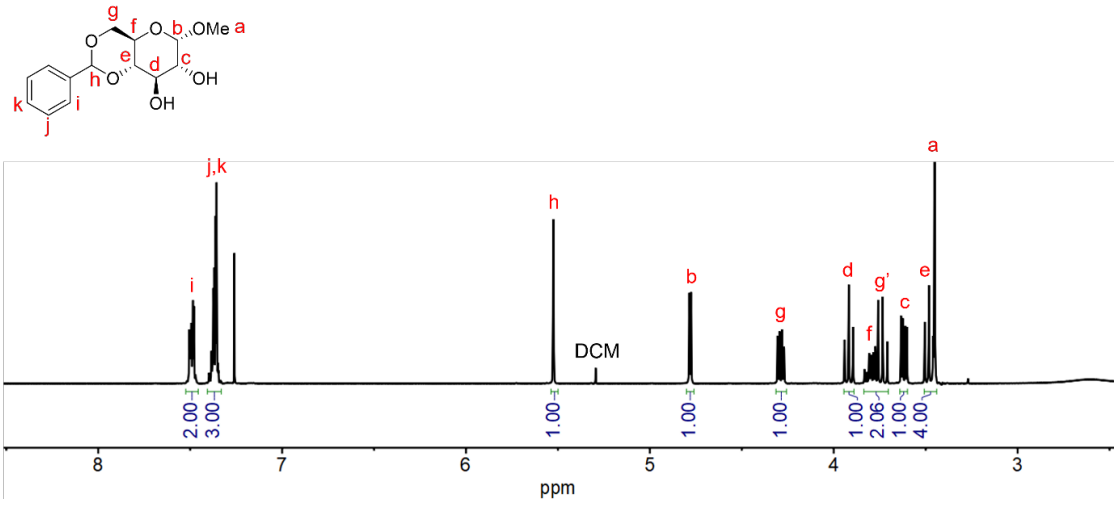


Figure 2.8. *^{1}H NMR (400 MHz, 298 K, $CDCl_3$) spectrum of methyl 4,6-O-benzylidene-α-D-glucopyranoside (**6**).*

Whilst two methine signals could be expected theoretically from the formation of a new stereogenic centre, the reversibility of the transacetalation permit the obtention of a diastereopure compound (**6**) with the phenyl group located in the more thermodynamically stable equatorial position.[32]

In addition, the apparition of 4 signals corresponding to aromatic carbons between δ = 137.2 and δ = 126.5 ppm and a deshielded methine carbon at δ = 102.1 ppm on the ^{13}C NMR spectrum of the product supported the previous conclusion. (Error! Reference source not found.)

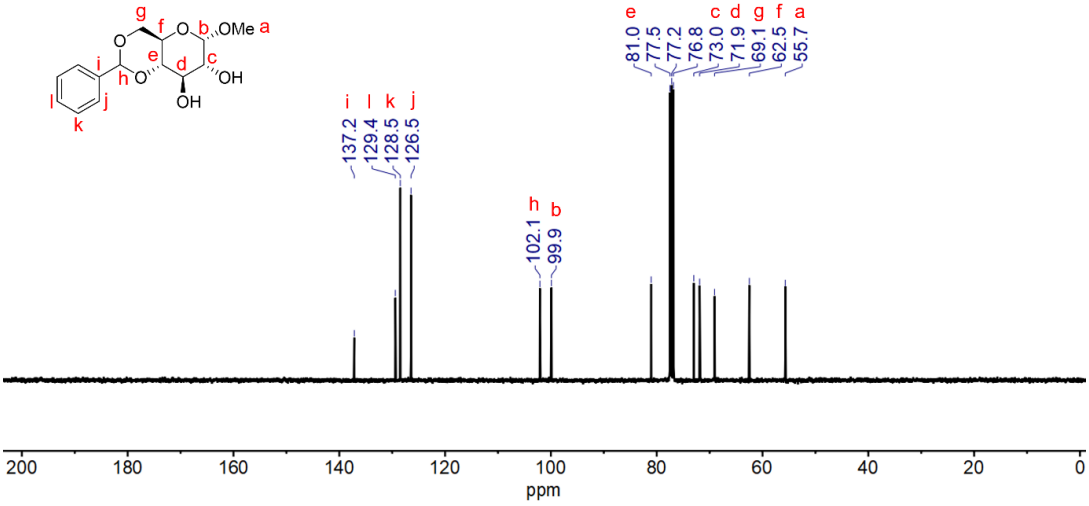


Figure 2.9. *^{13}C NMR (101 MHz, 298 K, $CDCl_3$) spectrum of methyl 4,6-O-benzylidene-α-D-glucopyranoside (**6**).*

Next, the secondary alcohols located on the 2nd (C2) and 3rd (C3) carbon of the sugar rings were benzylated using benzyl bromide in the presence of sodium hydroxide following a previously reported procedure.[10] Modifying the original procedure by decreasing the equivalents of benzyl bromide and sodium hydroxide from 6 to 2.5 and opting for a purification by recrystallisation instead of column chromatography allowed the obtention of the fully protected methyl 2,3-di-O-benzyl-4,6-O-benzylidene-α-D-glucopyranoside (**7**) in 75% yield on a 45 g scale of starting

material. The alcohol on C4 is then deprotected by regioselective cleavage of the benzylidene acetal to a benzyl ether on C6 in the presence of sodium cyanoborohydride and aluminium chloride. This reduction method afforded methyl 2,3,6-tri-O-benzyl-α-D-glucopyranoside (**8**) in 85% yield on a 25 g scale of the benzylidene acetal. The cleavage of the benzylidene acetal has been confirmed by the disappearance of the resonance signal corresponding to the methine at δ = 5.52 ppm and δ = 102.1 ppm on the ^{1}H and ^{13}C NMR spectra of the product, respectively. (**Figure 2.10**)

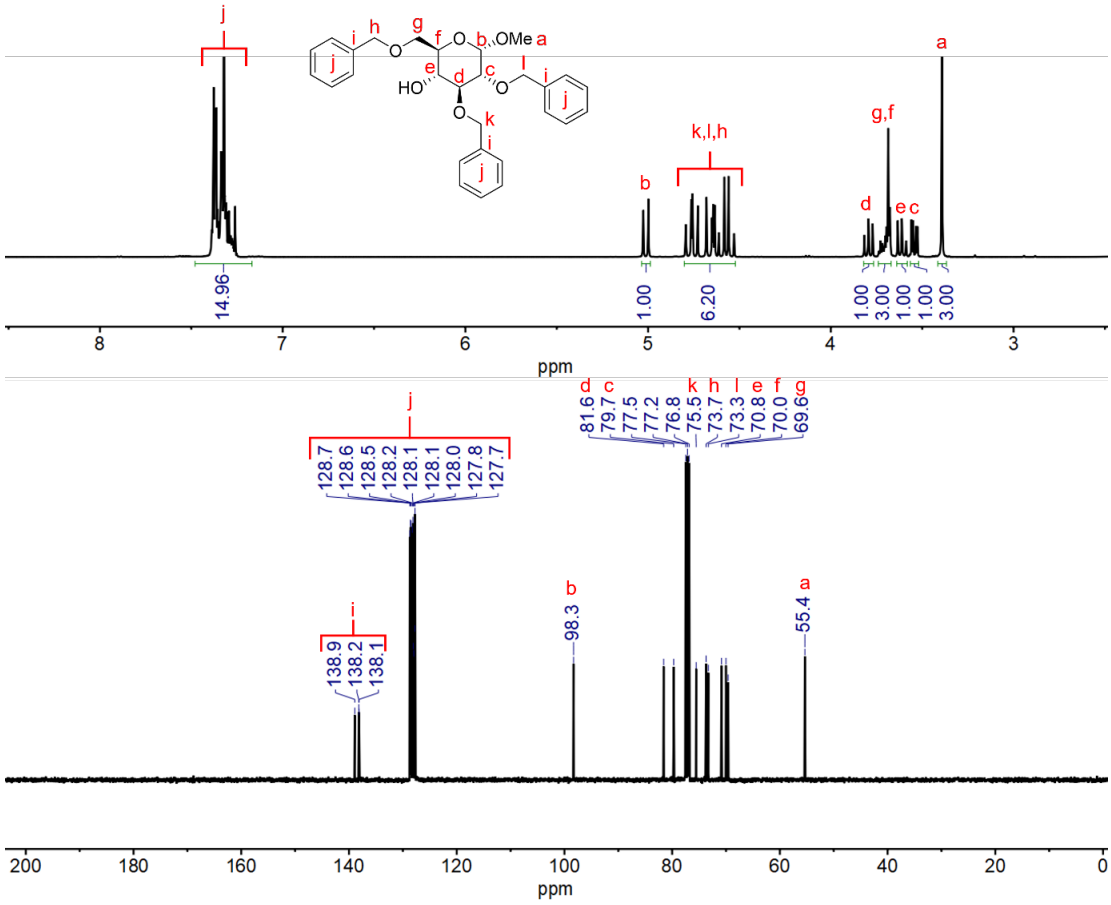


Figure 2.10. *^{1}H NMR (400 MHz, 298 K, $CDCl_3$) and ^{13}C NMR (101 MHz, 298 K, $CDCl_3$) spectra of methyl 2,3,6-tri-O-benzyl-α-D-glucopyranoside (**8**).*

Moreover, analysis of the ^{1}H - ^{13}C Heteronuclear Multiple Bond Correlation (HMBC) NMR spectrum revealed that only the protons on C2, C3 and C6 of the

sugar ring were correlating with the methylene carbons present on the benzyl protecting groups. The absence of this type of correlation for the proton on C4, clearly indicates the presence of a free hydroxyl on this carbon. (**Figure 2.11**)

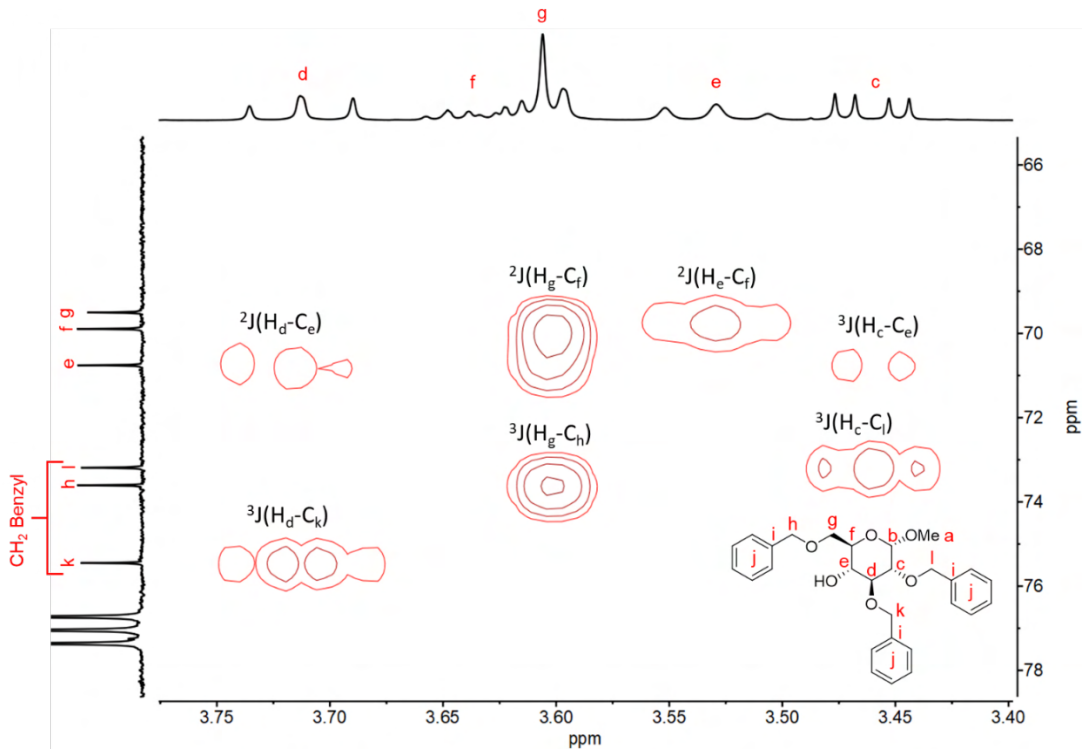


Figure 2.11. *Enlargement of the ^1H-^{13}C HMBC spectra of methyl 2,3,6-tri-O-benzyl-α-D-glucopyranoside (**8**).*

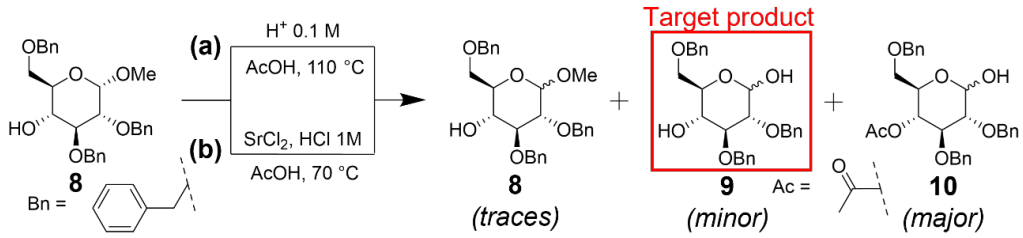
The final synthetic step consists of the cleavage of the *O*-glycosidic bond, resulting in the obtention of a free hydroxyl group on C1. Interestingly, the anomeric carbon is distinguishable from the other carbons within the sugar ring as it is engaged in an asymmetric acetal with an exocyclic oxygen atom being more reactive than the endocyclic. Such structural features confer the unique ability to perform the deprotection of the anomeric hydroxyl whilst leaving the cyclic structure of the saccharide intact, as the endocyclic oxygen remains unreactive.[33] Moreover, it also explains why a methyl group can be cleaved in the presence of the less stable benzyl groups, which cannot be achieved on usual polyols with hydroxyls of

equivalent reactivity.[23] The most popular method to deprotect the anomeric centre is by electrophilic solvolysis, namely hydrolysis and acetolysis.[34, 35]

1.13.2 2.4.3 Deprotection of the anomeric carbon: Hydrolysis

However, against all expectations, attempts at deprotecting methyl 2,3,6-tri-O-benzyl-α-D-glucopyranoside by traditional methods using strong acid catalyst such as hydrogen chloride [36] and sulfuric acid [37] at 100 °C yielded the targeted 1,4-glucose-derived diol (**9**) as minor product. (**Scheme 2.5 (a)**) Using strontium chloride as co-catalyst, which according to a previous study has been found to improve the yield and purification process of glycosides hydrolysis [38], led to the same experimental observation: the targeted compound remains the minor product. (**Scheme 2.5 (b)**).

I - Hydrolysis



Scheme 2.5. *Product obtained from both (a) Hydrolysis of methyl 2,3,6-tri-O-benzyl-α-D-glucopyranoside (**8**) in the presence of aqueous H_2SO_4 or HCl 0.1 M in acetic acid at 110 °C following traditional hydrolysis conditions and (b) hydrolysis of (**8**) using 0.1 equiv. of strontium chloride as cocatalyst in addition of aqueous HCl 1 M in acetic acid at 70 °C.*

The major product obtained from both hydrolysis method has been identified as being a mixture of α and β anomer of 2,3,6-tri-O-benzyl-4-acetyl-D-glucopyranose (**10**) in approximatively a 65:35 ratio as indicated by the presence of two singlets at

δ = 1.76 ppm (α) and δ = 1.75 ppm (β) on the ^{1}H NMR spectrum of this compound, characteristic of the acetate protons. The presence of the resonance signals corresponding to acetate peaks at δ = 21.0 ppm (methyl) and δ = 169.9 ppm (carbonyl) were also identified on the ^{13}C carbon NMR spectrum of the compound. (**Figure 2.12**)

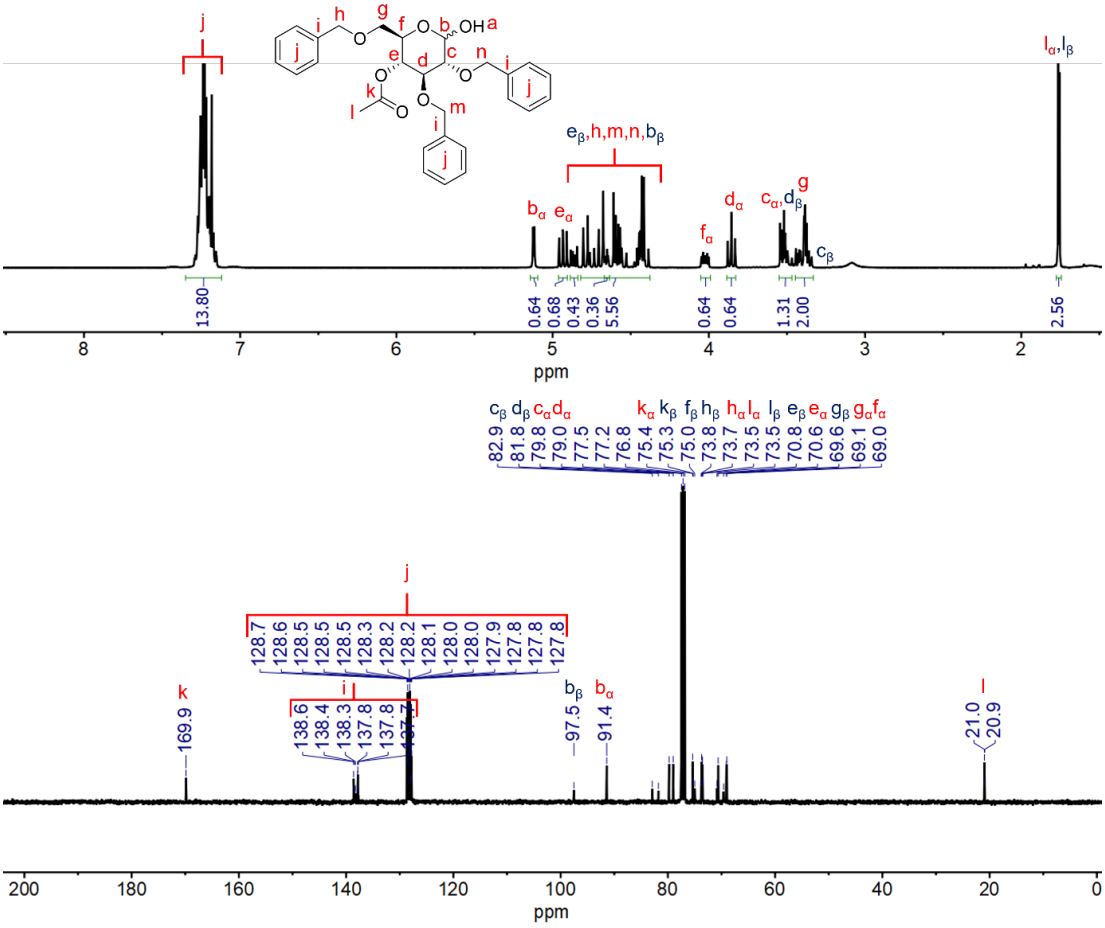


Figure 2.12. *^{1}H NMR (400 MHz, 298 K, $CDCl_3$) and ^{13}C NMR (101 MHz, 298 K, $CDCl_3$) spectrum of 2,3,6-tri-O-benzyl-4-acetyl-D-glucopyranose (**10**).*

In addition, the carbonyl group of the acetate correlates with the proton on C4 as seen on the ^{1}H-^{13}C HMBC NMR spectrum of compound (**10**), which further confirmed the obtention of the aforementioned structure. (**Figure 2.13**)

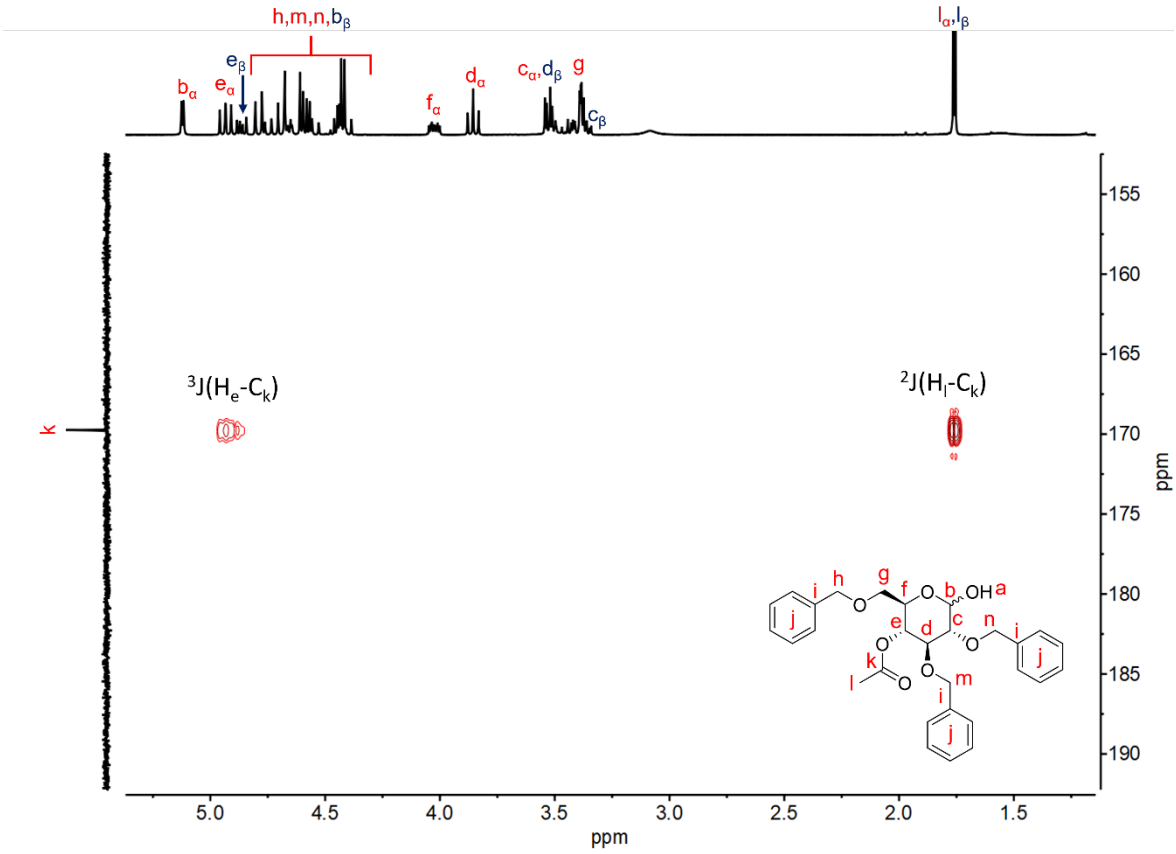


Figure 2.13. *Enlargement of the ^{1}H-^{13}C HMBC spectrum of 2,3,6-tri-O-benzyl-4-acetyl-D-glucopyranose (**10**).*

Moreover, not only the targeted 1,4-glucose-derived diol (**9**) was the minor product of hydrolysis, the separation of the targeted compound from the crude by column chromatography proved to be particularly challenging owing to the presence of at least one free hydroxyl group on all compounds which tended to streak on silica gel. For these reasons, even after optimisation, hydrolysis afforded the targeted 1,4-glucose-derived diol (**9**) as a 65:35 ratio of α and β anomers with a maximum yield of 30% in an 88% purity as determined by ^{1}H NMR spectroscopy. Further purification by two sequential recrystallisations afforded the pure α anomer in a 16% yield. (**Figure 2.14**)

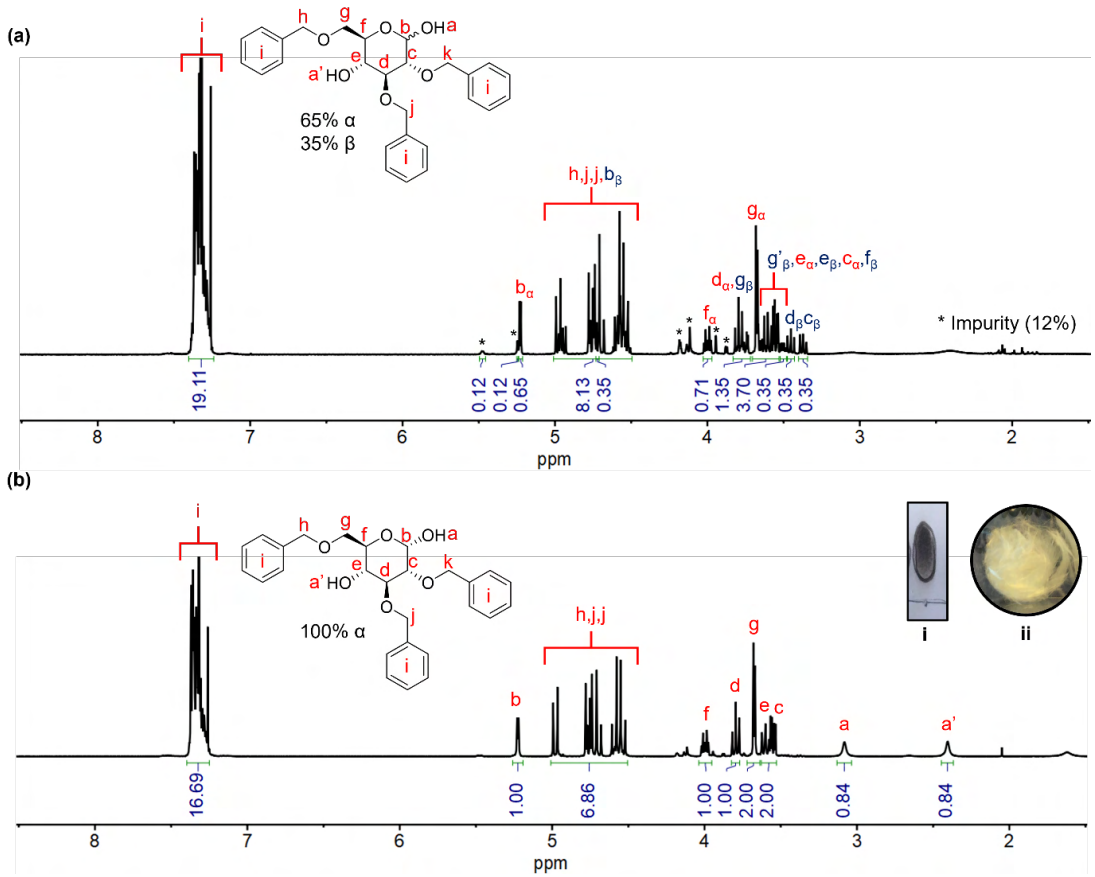
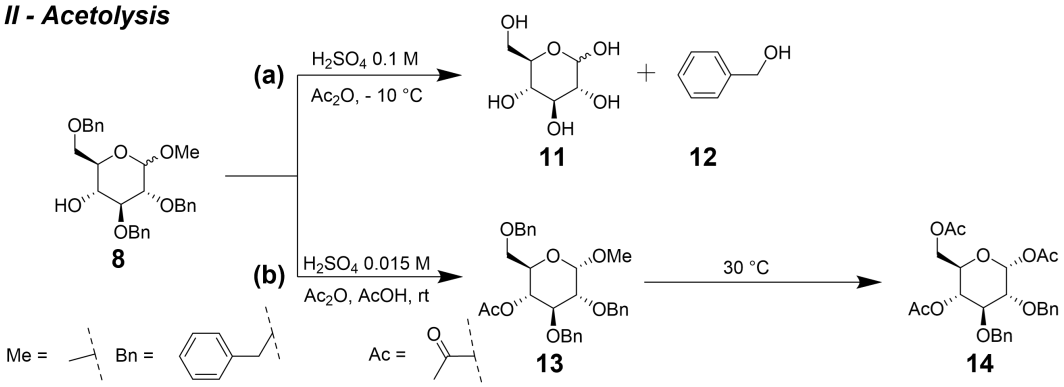


Figure 2.14. *^{1}H NMR spectra (400 MHz, 298 K, $CDCl_3$) of (a) 2,3,6-tri-O-benzyl-D-glucopyranoside (**9**) as a racemic mixture of the α and β anomer, in a 65/35 ratio and (b) 2,3,6-tri-O-benzyl-α-D-glucopyranose. Insert (i) shows a picture of the smearing behaviour of the targeted compound on silica gel. Insert (ii) shows the fluffy crystal aspect of the α 1,4-glucose-derived diol (**9**).*

Unfortunately, the hydrolysis reactions produced unsatisfactory results for the deprotection of methyl 2,3,6-tri-O-benzyl-α-D-glucopyranoside (**8**), both in terms of yield and work up efficiency, which required to be high in order to pursue the synthesis towards the obtention of a 1,4-glucose-derived diol (**9**) on a scale large enough to accommodate material production and analysis. Consequently, whilst looking for avenues to improve the deprotection yield, the removal of the methyl protecting group *via* acetolysis has been explored.

1.13.3 2.4.4 Deprotection of the anomeric carbon: Acetolysis

The principle of acetolysis relies on the exchange of the methyl group for an acetyl group, which is known to be easily cleaved by Zemplén deacetylation in quantitative yields.[39] Unfortunately, carrying out the acetolysis by reacting the glucoside derivative in the presence of a 0.1 M solution of H_2SO_4 in acetic anhydride at -10 °C led to the complete deprotection of the starting material to yield D-glucose and benzyl alcohol. (**Scheme 2.6 (a)**) Overcoming this issue necessitated the finding of milder reaction conditions, and in the next attempt, the reaction was carried out in a mixture of Ac_2O and $CHCl_3$ (1:7) instead of pure Ac_2O. However, this modification experimentally resulted in the same outcome and only glucose and benzyl alcohol were recovered.



Scheme 2.6. *Schemes of (a) acetolysis of methyl 2,3,6-tri-O-benzyl-α-D-glucopyranoside (8) in the presence of H2SO4 0.1 M in acetic acid at -10 °C and (b) acetolysis of (8) in milder conditions, using H2SO4 0.015 M in a mixture of Ac2O and AcOH (2:3).*

Next, the concentration of H_2SO_4 was decreased 7 folds, from 0.1 M to 0.015 M. In these conditions, methyl 2,3,6-tri-O-benzyl-α-D-glucopyranoside (**8**) is acetylated on C4 after 5 mins of reaction at room temperature to give (**13**) in quantitative yield whilst increasing the temperature to 30 °C and leaving the reaction running for 13 h

led to the successful acetolysis at the anomeric carbon. However, this reaction is non regio-selective and occurs simultaneously on both C1 and C6 hydroxyls, [40] affording triacetate (**14**) in a α to β ratio of 80/20 before purification and 95/5 after recrystallisation (**Scheme 2.6 (b)**). The structure of this single reaction product has been confirmed by ^{1}H, ^{13}C and ^{1}H-^{13}C HMBC NMR spectroscopy using the same method exposed earlier for the starting material (**8**). Thus, upon examination of the ^{1}H and ^{13}C NMR spectra of (**5**), the disappearance of the methyl resonance signal at δ = 3.31 ppm and δ = 55.4 ppm has been accompanied by the appearance of resonance signals around δ = 2 ppm and δ = 21 ppm, corresponding respectively to the methyl protons and carbons of 3 acetate groups. (**Figure 2.15**)

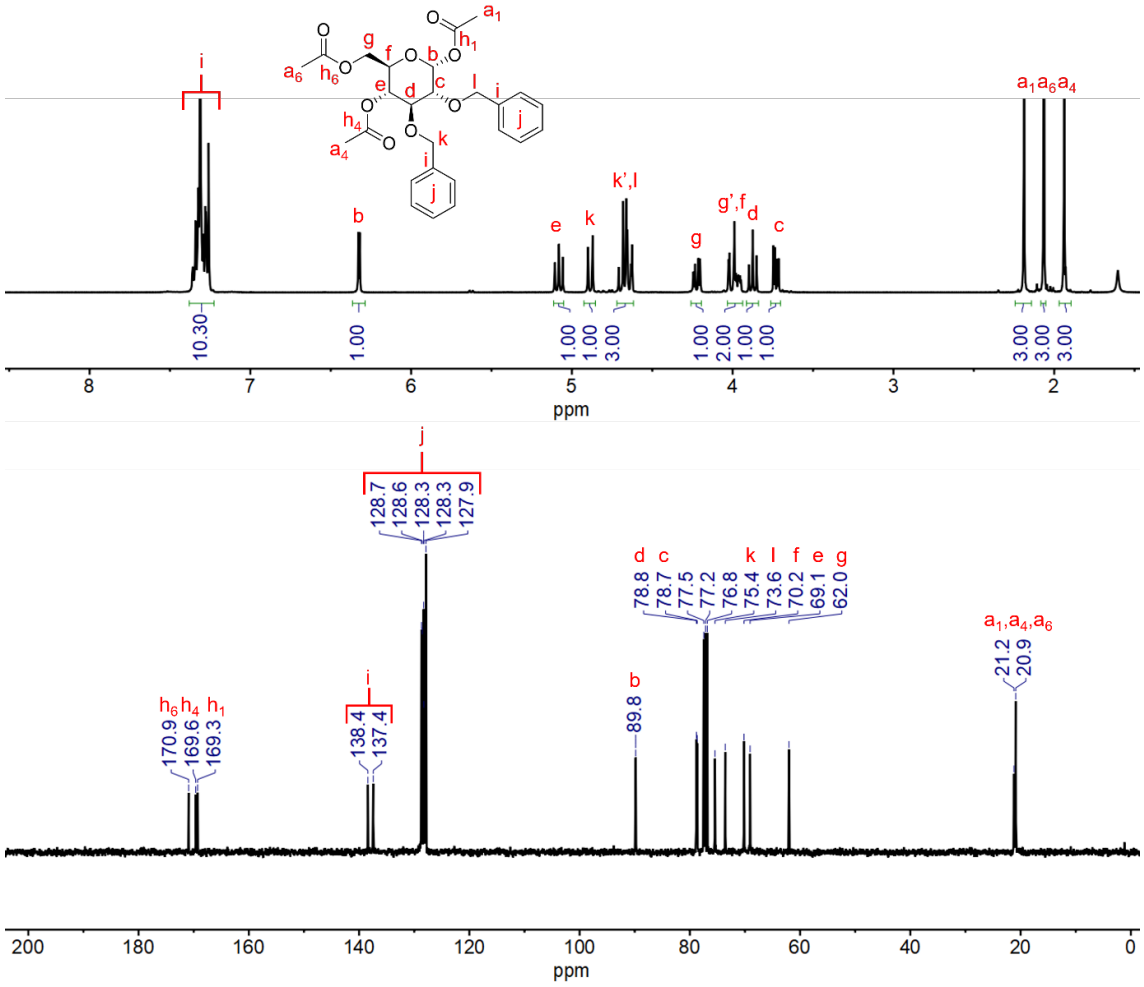


***Figure 2.15**. [1]H NMR (400 MHz, 298 K, $CDCl_3$) and [13]C NMR (101 MHz, 298 K, $CDCl_3$) spectra of acetyl 2,3-di-O-benzyl-4,6-acetyl-α-D-glucopyranoside (**14**).*

In addition, the resonance signals around δ = 170 ppm corresponding to the carbonyls, were identified to be correlating with the protons on C1, C4 and C6 of the sugar ring by analysis of the ^{1}H-^{13}C HMBC NMR spectrum. (**Figure 2.16**)

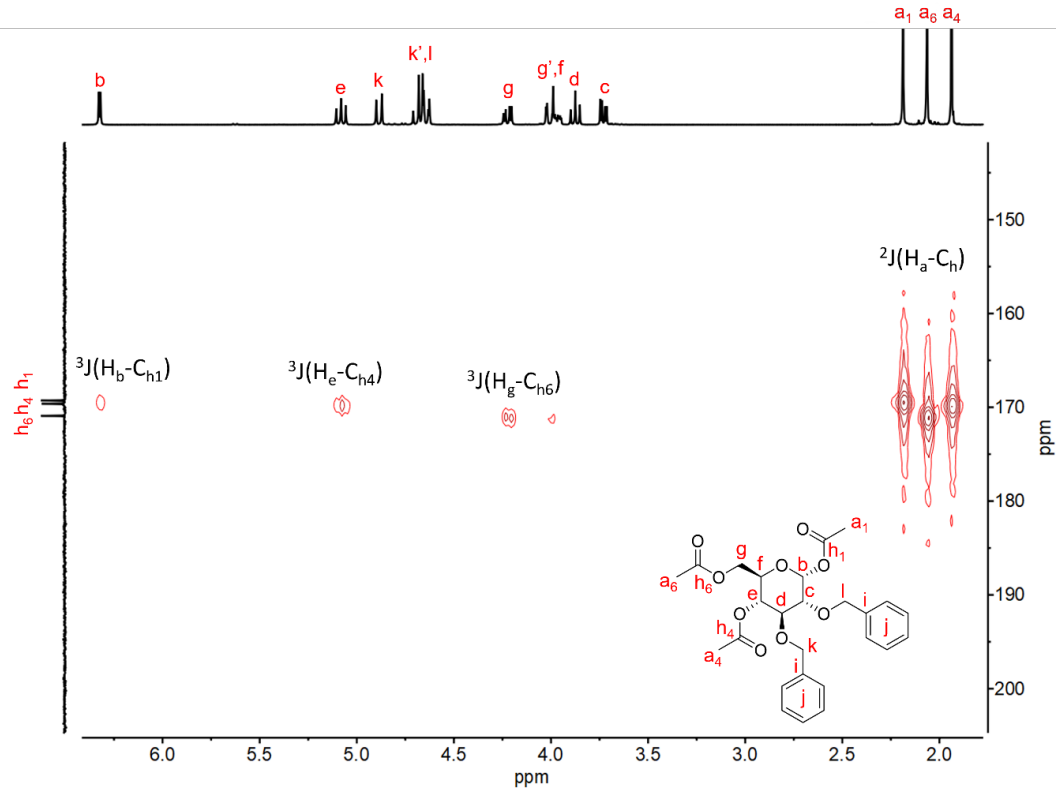
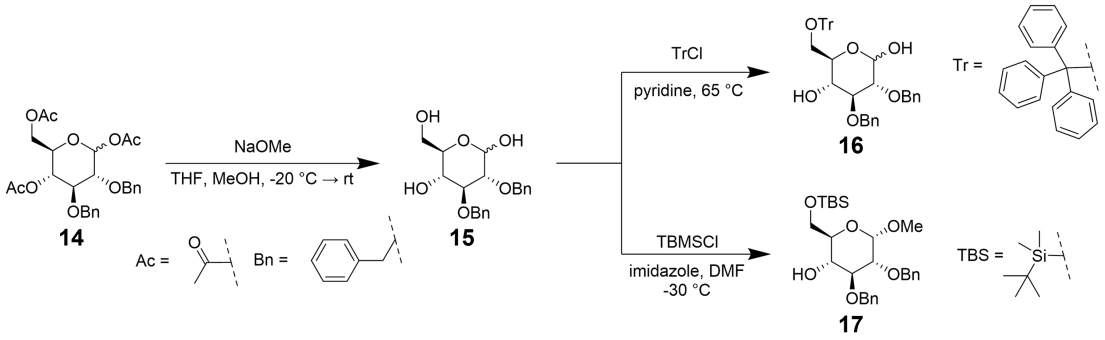


Figure 2.16. *Enlargement of the ^{1}H-^{13}C HMBC spectra of acetyl 2,3-di-O-benzyl-4,6-acetyl-α-D-glucopyranoside (**14**).*

Synthesising a 1,4-glucose-derived diol from triacetate (**14**) could be achieved by sequential deacetylation via methanolysis followed by selective protection of the primary hydroxyl on C6 using a bulky group such as trityl chloride or tert-butyldimethylsilyl chloride (**Figure 2.7**).[40-42] However, the resultant increase of the steric hindrance around the C4 hydroxyl is likely to be incompatible with the ultimate objective of introducing a thiol on this specific position. Indeed, the conventional approach for the synthesis of a thiol derivative of glucose is achieved through the displacement of a sulfonate ester or halo group by a thiol precursor such as potassium thioacetate or potassium thiocyanate which occurs *via* a bimolecular nucleophilic substitution (SN_2) mechanism.[43, 44]



Scheme 2.7. *Potential preparation method of a 1,4-glucose-derived diol by sequential deacetylation and selective protection of the primary alcohol using trityl chloride (TrCl) to give compound (**16**) or tert-butyldimethylsilyl chloride (TBDMSCl) to give compound (**17**).*

For this reason, the displacement of stable C4 sulfonate does not occur when a trityloxy group is present on C6 [45] (**Figure 2.17 (a)**) and are known to be challenging to achieve on the particularly stable C4 sulfonate groups in the presence of benzyloxy protecting groups (**Figure 2.17 (b)**).[46, 47] To overcome this issue, trifluoromethanesulfonic anhydride is commonly used as sulfonating agent (**Figure 2.17 (c)**). [47-49] Yet, the acidic conditions necessary for the introduction of the more reactive triflate would simultaneously lead to the removal of the trityl or *tert*-butyldimethylsilyl (TBDMS) protecting group.[23] Lastly, an alternative synthetic route toward the installation of a thiol on C4 could be envisioned starting from 1,4-glucose-derived diol (**8**) by displacement of an iodine using potassium thioacetate. [50, 51] However, a report of the iodination of C4 in the presence of a TBDMS protecting group on O6 and its further displacement with potassium acetate as presented on **Figure 2.17 (d)** could only be found once in the literature.[52] Moreover, the iodination of C1 required to follow different procedure than for C4.[53] For these reasons, this method was left unexplored to instead work toward the obtention of the less synthetically challenging 1,6-glucose derived diol.

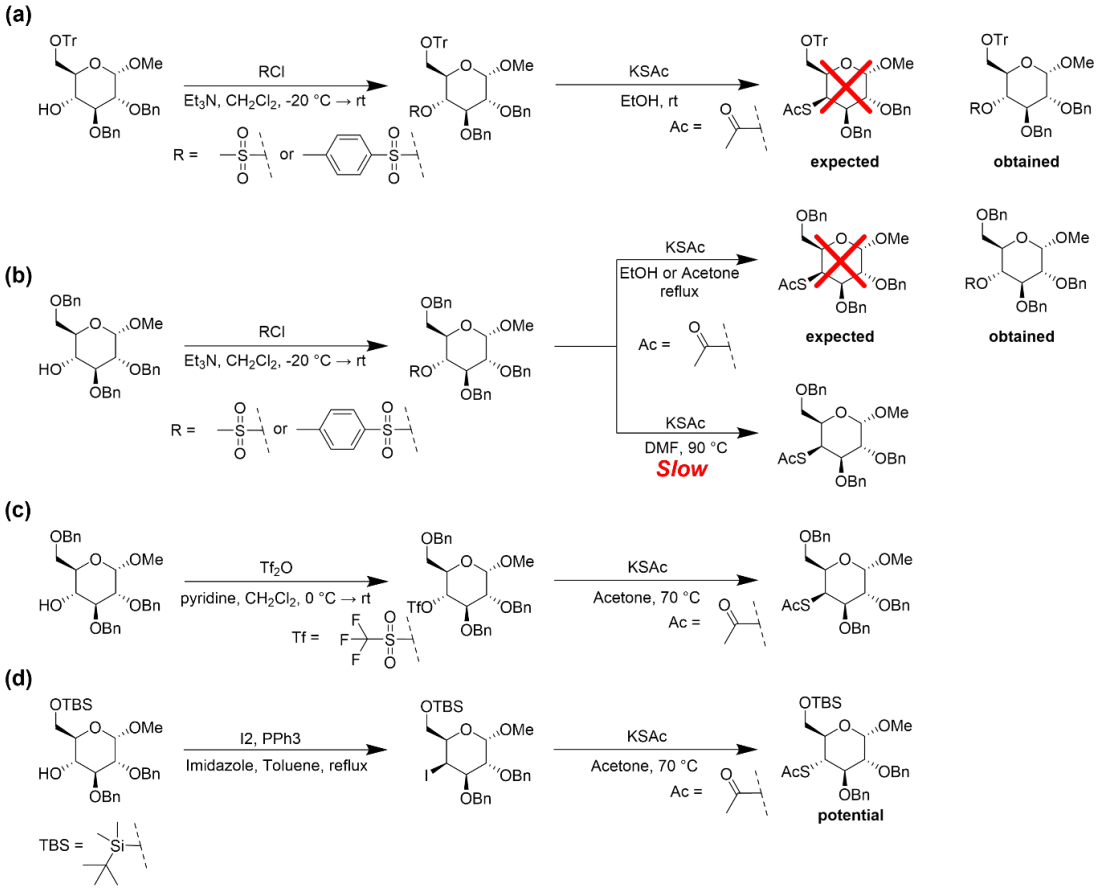
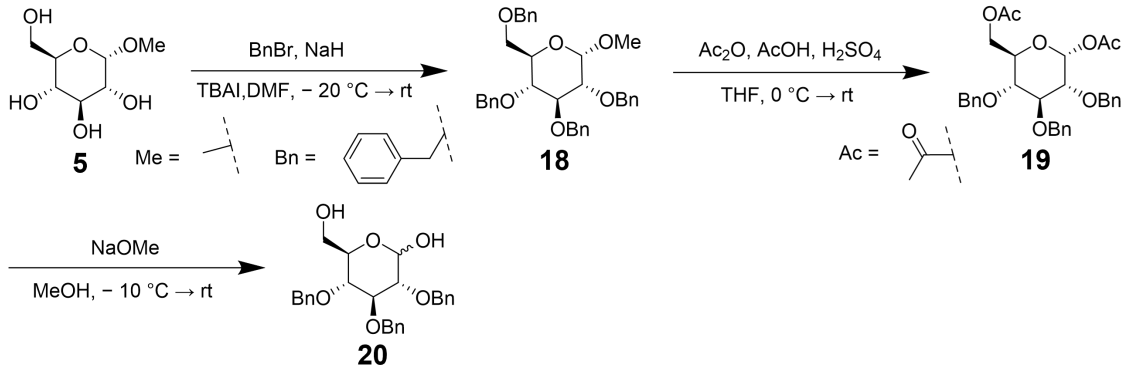


Figure 2.17. *Schemes representing the synthesis of C4 sulfonates glucose derivatives and the outcome of their subsequent nucleophilic displacement using potassium thio-acetate when the glucose ring is bearing (a) a trityloxy or (b) a benzyloxy on C6. (c) the trifluoromethanesulfonyl is a better leaving group than sulfonyl halides and can be displaced on C4 using potassium acetate. However, its introduction is incompatible with the presence of a trityloxy or tert-butyldimethylsilyloxy group which are labile in acidic conditions.*

1.13.4 Synthesis of 2,3,4-tri-O-benzyl-D-glucopyranoside (1,6-glucose derived diol)

As an alternative to the 1,4-glucose-derived diol, the choice was made to work toward the synthesis of 1,6-glucose-derived diol instead, since the C1 and C6 hydroxy exhibit a similar reactivity towards acetolysis. 1,6-glucose-derived diol (**20**) was easily obtained on scale in 3 synthetic steps starting from commercially

available and inexpensive α-D-glucopyranoside (**5**) following well establish carbohydrate chemistry.[10] (**Scheme 2.8**)



Scheme 2.8. *Multi-step synthesis of 2,3,4-tri-O-benzyl-D-glucopyranoside (1,6-glucose derived diol) (**20**).*

Firstly, the 4 unprotected hydroxyls are benzylated using benzyl bromide and sodium hydride in DMF to afford the fully protected derivative (**18**) in 76% yield on scales up to 35 g. The only by-products identified from the analysis of the crude were benzyl alcohol and surprisingly a mixture of α and β methyl tetra-*O*-benzyl-D-glucopyranoside in a 50/50% ratio, which means that against all expectations, the cleavage of the glycosidic bond has occurred appreciably within the conditions of the reaction.(Appendix **Figure A45- A46**) The following acetolysis of compound (**18**), as mentioned during the discussion on the acetolysis of methyl 2,3,6-tri-O-benzyl-α-D-glucopyranoside (**8**), allows to cleave simultaneously the O-glycosidic bonds and the primary benzyl ether to yield the 1,6 glucose derived diacetate (**19**).[40] The yield obtained was highly dependent not only on the reaction scale but also on the temperature at which the reaction and the neutralisation steps are carried out. Performing the reaction at - 10 °C for 16 h and maintaining a negative temperature during quenching with sodium hydrogen carbonate afforded a yield as high as 98% with a ratio of 80/20 α to β anomer on a 20 g scale. Conversely, leaving the reaction

to run at room temperature for 4 h after the addition of H_2SO_4 and allowing the temperature to increase significantly during the neutralisation step causes the formation of various over-acetylated by-products, which leads to a decrease in yield of about 50%. (**Figure 2.18**and **Appendix Figure A53 to A56**). This has been experienced on scales of 35 g and above, whilst maintaining a controlled temperature becomes more challenging owing to a diminished efficiency in heat dissipation.

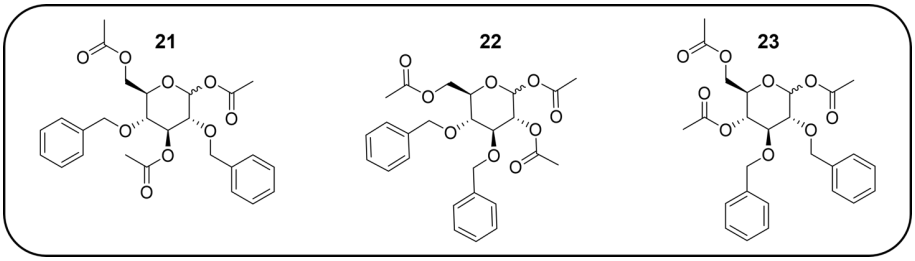


Figure 2.18. *Structure of the identified by-products generated during the acetolysis of methyl 2,3,4,6-tetra-O-α-D-glucopyranoside. The structures were coherent with the literature.*[54]

The installation of temporary acetate groups on C1 and C2 permitted to obtain 1,6-glucose-derived diol (**20**) via selective deprotection of the acetate groups in 98% yield on scale up to 42 g as a 65/35 ratio of α to β anomer. Moreover, the only by-product of the deprotection stage being methyl acetate, which is easily removed under vacuum, hence extensive purification was unnecessary. The success of the deprotection step and the structure of 1,6-glucose diol (**20**) has been corroborated by ^{1}H, ^{13}C and ^{1}H-^{13}C HMBC NMR spectroscopy. Consequently, no resonance signals corresponding to acetate groups could be observed on the ^{1}H NMR spectrum of the products at δ = 2.16 ppm (COC**H**$_3$, αC1), δ = 2.06 ppm (COC**H**$_3$, βC1) and δ = 2.03 ppm (COC**H**$_3$, C6) or on the ^{13}C NMR spectrum at δ = 21.0 ppm (CO**C**H$_3$, C6), δ = 21.2 ppm (CO**C**H$_3$, C1), δ = 169.2 ppm (**C**OCH$_3$, βC1), δ = 169.5

ppm (**C**OCH$_3$, αC1) and δ = 170.8 ppm (**C**OCH$_3$, C6). In addition, the integration of benzyl protons accounted for the presence of 3 benzyl groups within the molecule. (**Figure 2.19**)

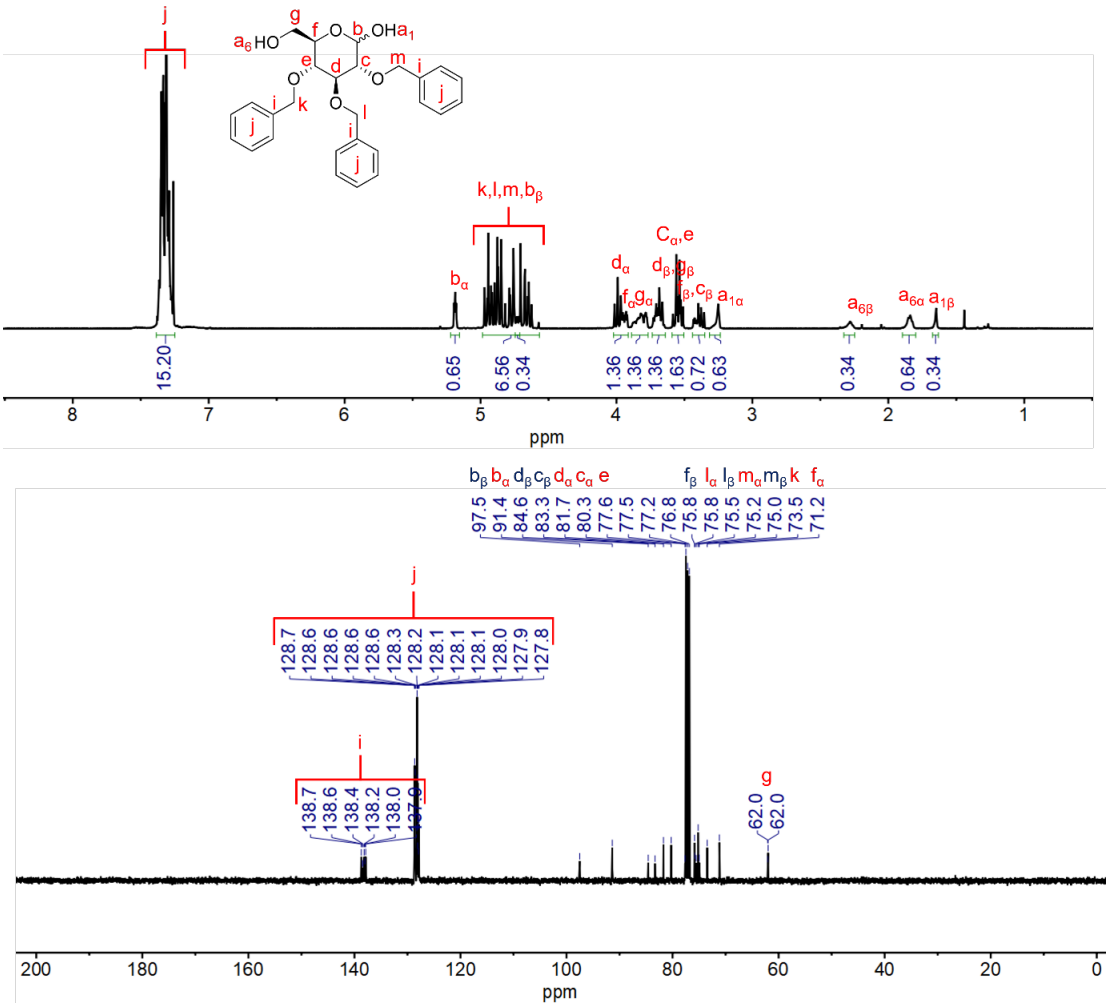


Figure 2.19. *^{1}H NMR (400 MHz, 298 K, $CDCl_3$) and ^{13}C NMR (101 MHz, 298 K, $CDCl_3$) spectra of 2,3,4-tri-O-benzyl-D-glucopyranoside (1,6-glucose derived diol) (**20**).*

Finally, the location of the free alcohol on the sugar ring was verified by ^{1}H-^{13}C HMBC NMR spectroscopy of the compound. Only the protons on C2, C3 and C6 of the sugar ring correlated with the methylene carbon of a benzyl group, which confirmed the presence of free hydroxyl group on C1 and C6. (**Figure 2.20**)

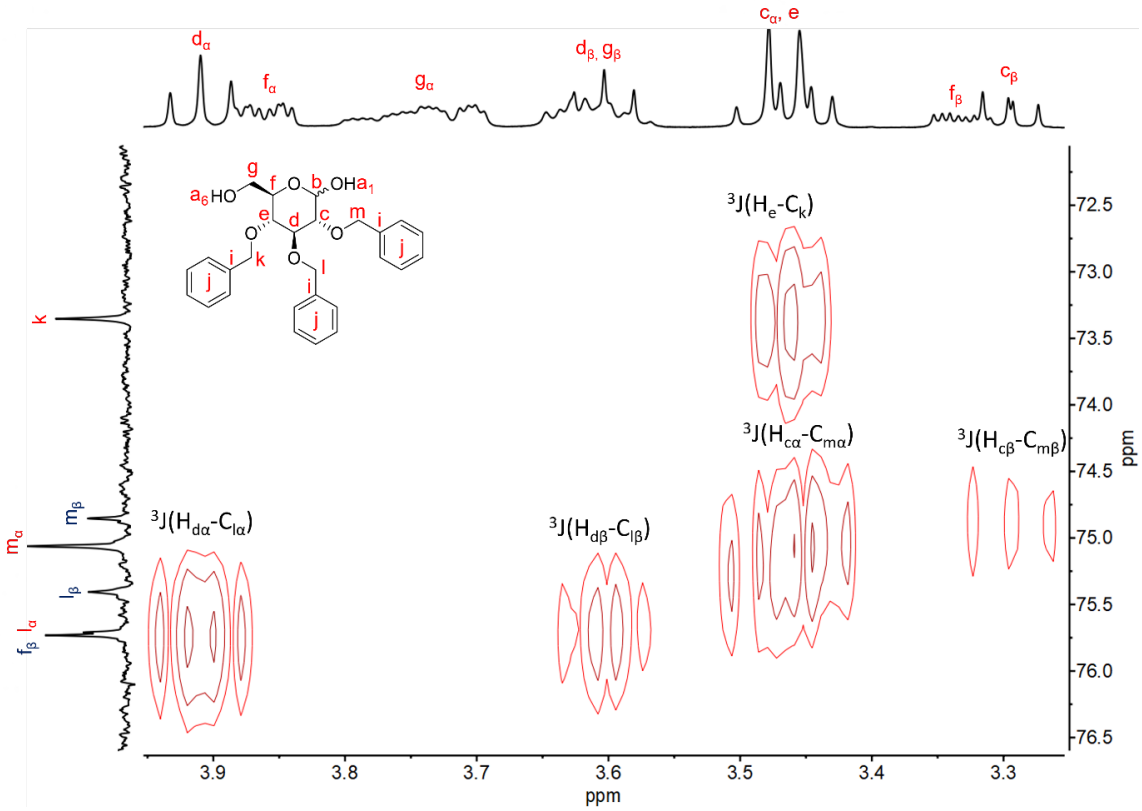


Figure 2.20. *Enlargement of the ^1H-^{13}C HMBC spectrum of 2,3,4-tri-O-benzyl-D-glucopyranoside (1,6-glucose-derived diol) (**20**).*

1.14 Diacrylate synthesis

The diols of interest which synthesis has been discussed in the previous sections of this chapter served the ultimate purpose of providing precursors for the formation of diacrylate monomers suitable for thiol-Michael step-growth polymerisation with the intend to study if the mechanical properties of the final polymer network could be impacted by (i) a change from *cis* to *trans* configuration of unsaturated polymers (Error! Reference source not found. **(a)**) or (ii) the effect of a change in endo/exo type configuration of locked V-shaped isohexides bicyclic rings. (Error! Reference source not found. **(b)**). In addition, a glucose derived diacrylate was designed to explore the ability of integrate a sugar ring within a

polymer using Michael step-growth polymerisation (Error! Reference source not found. **(c)**).

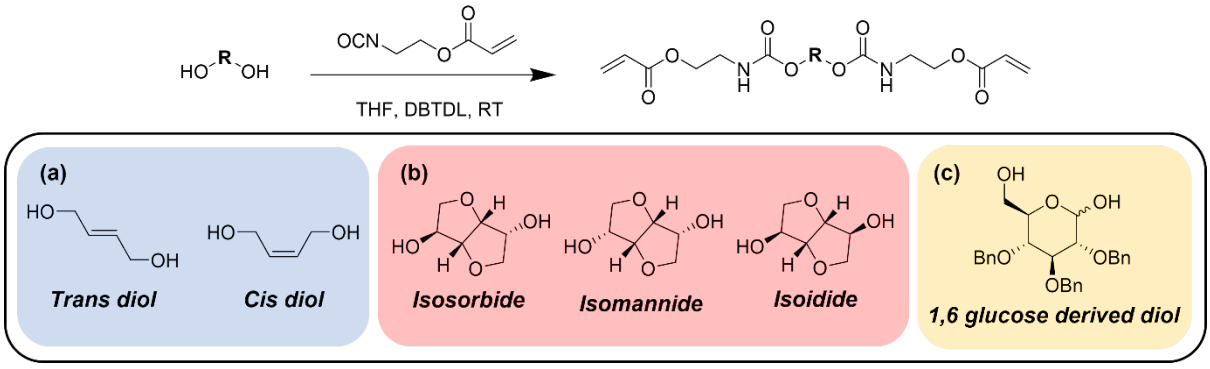


Figure 2.21. *General reaction scheme of the synthesis of diacrylate monomer starting from 2-isocyanatoethyl acrylate and either (a) cis or trans diol, (b) Isohexides or (c) 1,6-glucose derive diol in THF, using dibutyltin (IV) dilaurate (DBTDL) as catalyst.*

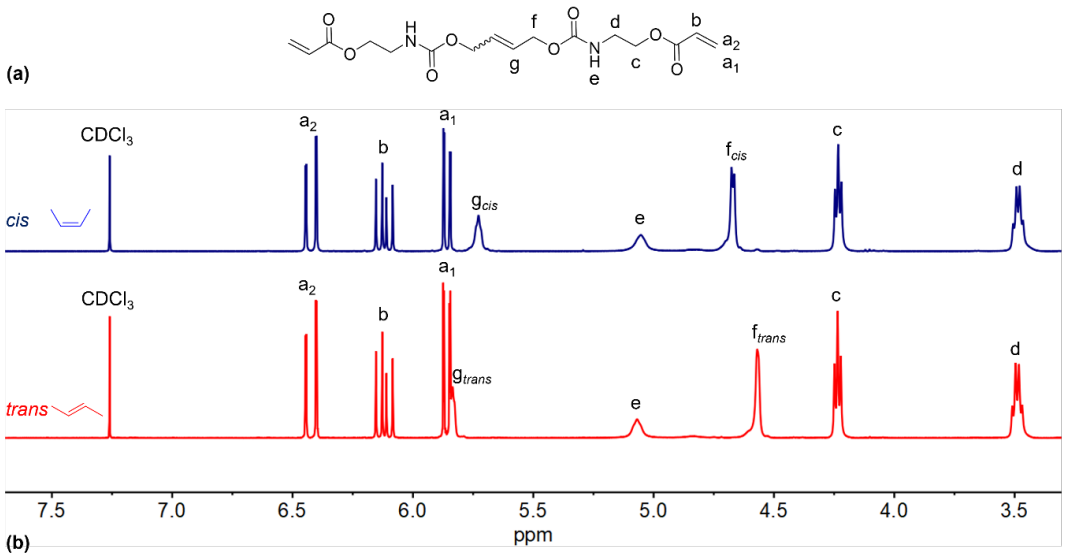
The functionalisation of the diol precursors presented in **Figure 2.21** was carried out by reacting each diol with the commercially available 2-isocyanatoethyl acrylate in THF (0.5 M) to obtain the corresponding diacrylate monomer following a previously reported procedure.[6, 55, 56] The choice of using 2-isocyanatoethyl acrylate instead of the more available acryloyl chloride stemmed from a preliminary study indicating that the presence of urethane bonds were essential to achieve adequate mechanical robustness through H-bonding. The reaction is catalysed by dibutyltin(IV) dilaurate (DBTDL) which is an organotin Lewis acid known to favour the diol/isocyanate reaction over the isocyanate/water side reaction[57] making this procedure easier since tedious moisture-free Schlenk techniques are redundant. Moreover, this procedure allowed the synthesis of a diacrylate monomer, starting from a variety of diol precursors on scales ranging from 7 to 60 g with little to no synthetic adaptations. The only noticeable experimental differences resided in the reaction time and the relative reactivity of the final monomers. For instance, the

unsaturated *cis* and *trans* diacrylates were obtained after 3 hours and were very prone to premature crosslinking and as such, the reaction temperature during the reaction and drying step was kept below 0 °C. On the contrary, the synthesis of both the isohexides and 1,6-glucose-derived diacrylate only reached completion after 12 h minimum, and a negative temperature was not necessary. In addition, no premature crosslinking was observed with either the isohexides or 1,6-glucose-derived diacrylate and qualitatively, the relative sensitivity of monomers was observed to follow the order: unsaturated diacrylate > isohexide derived diacrylate > 1,6-glucose-derived diacrylate. Nevertheless, this reaction was quantitative for all the 6 monomers tested and did not cause substantial issues. Whilst the section on the *cis* and *trans* diacrylate synthesis will be presenting in detail the NMR characterisation and some technical specifics inherent to the presence of a double bond which can isomerise. The section about the isohexides and 1,6-glucose-derived diacrylates will only briefly present the characterised ^{1}H NMR spectrum of the synthesised diacrylates.

1.14.1 Synthesis cis/trans diacrylates

The success of the synthesis has been substantiated by the presence of the 3 resonance signals characteristic of acrylate groups at δ = 6.40 ppm, δ = 6.09 ppm and 5.84 ppm on the ^{1}H NMR spectra of both the *cis* and *trans* diacrylate; the integration were consistent with the presence of two functionalities per in chain-alkene (**Figure 2.22**). These observations were in accordance with a previous report.[55] Moreover, the functionalisation of the unsaturated diols proceeded without side reactions involving the internal alkene. As seen on the ^{1}H NMR spectra of both the *cis* and *trans* diacrylate monomers (**Figure 2.22**), the vinylic and allylic protons

around the unsaturated stereocenter, labelled **g** and **f** respectively, have different signals depending on the isomer. For the *cis* monomer, the vinylic proton appears at δ = 5.73 ppm and the allylic proton at δ = 4.67 ppm, whilst they shift to δ = 5.83-5.84 ppm and δ = 4.57 ppm respectively when the unsaturated isomer is in its *trans* configuration. These signals are crucial in distinguishing the different isomers from one another by ^{1}H NMR spectroscopy, as all other protons within the monomers have a similar signal irrespectively of the stereochemistry of the unsaturation.



Proton label	a_1	a_2	b	c	d	e	f		g	
							cis	*trans*	*cis*	*trans*
Signal[a] (ppm)	5.85	6.42	6.12	4.23	3.49	5.05	4.67	4.57	5.73	5.83
Integration[a]	1	1	1	2	2	1	1	1	1.02	1

Figure 2.22. *a) ^{1}H NMR (400 MHz, $CDCl_3$, 298 K) spectra of cis diacrylate monomer (**24**) (top) and trans diacrylate monomer (**25**) (bottom). b) Table summarising the signal and the integration for each proton of the diacrylate monomer. [a] Signal and integration values were determined via the analysis of the cis and trans diacrylate monomer ^{1}H NMR spectra.*

As there is no overlap in between the signal characteristic of the isomers **g** and ***f***, the presence of any isomerisation and/or loss of double bonds will coincide with the appearance of two different peaks for both **g** and **f** in the former case and with an integration value lesser than the unity in the latter. Thus, by observing the

presence of only one peak for **g** and **f** and that these same protons integrated for 1 on both the *cis* and *trans* diacrylate monomer ^{1}H NMR spectra (**Figure 2.22**), it is possible to conclude that, this reaction allows a conversion of near 100% in less than 3 h without causing either unwanted isomerisation or crosslinking which makes it a highly efficient, mild reaction that allowed the possibility for scale up to 60 g.

Interestingly, performing Differential Scanning Calorimetry (DSC) of the diacrylate (**Figure 2.23**) highlighted that the stereochemistry has also a noticeable impact on the physical properties of the monomers itself. Whilst the *trans* diacrylate monomer crystallises and has a melting point at 77 °C, the *cis* diacrylate monomer is a powder with a melting point of 41 °C. However, the first heating DSC scans of both unsaturated monomer (**Figure 2.23**) also present an exothermic event at 100 °C (*cis*) and 120 °C (*trans*), which is likely related to uncontrolled, thermally promoted radical homopolymerisation of the diacrylate monomers, otherwise known as crosslinking reactions.

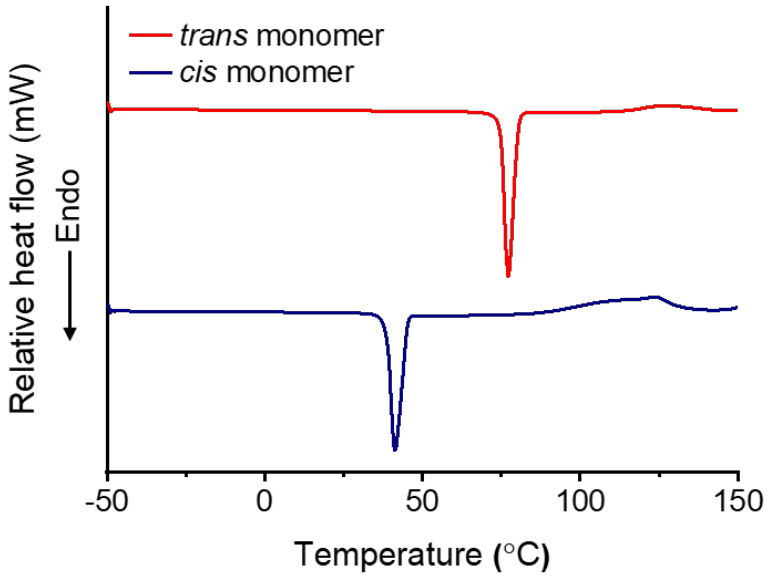


Figure 2.23. *DSC thermograms for 1st heating cycle of cis and trans monomers. DSC thermal ramp was carried out under N_2 with a heating rate of 10 °C·min^{-1}.*

This phenomenon has been experimentally observed since the addition of DBTDL produces an exotherm which could initiate uncontrolled crosslinking; hence it is critical to keep the reaction at temperature below 0 °C during the synthesis and the drying of the monomer.

1.14.2 Synthesis isohexide-derived diacrylates

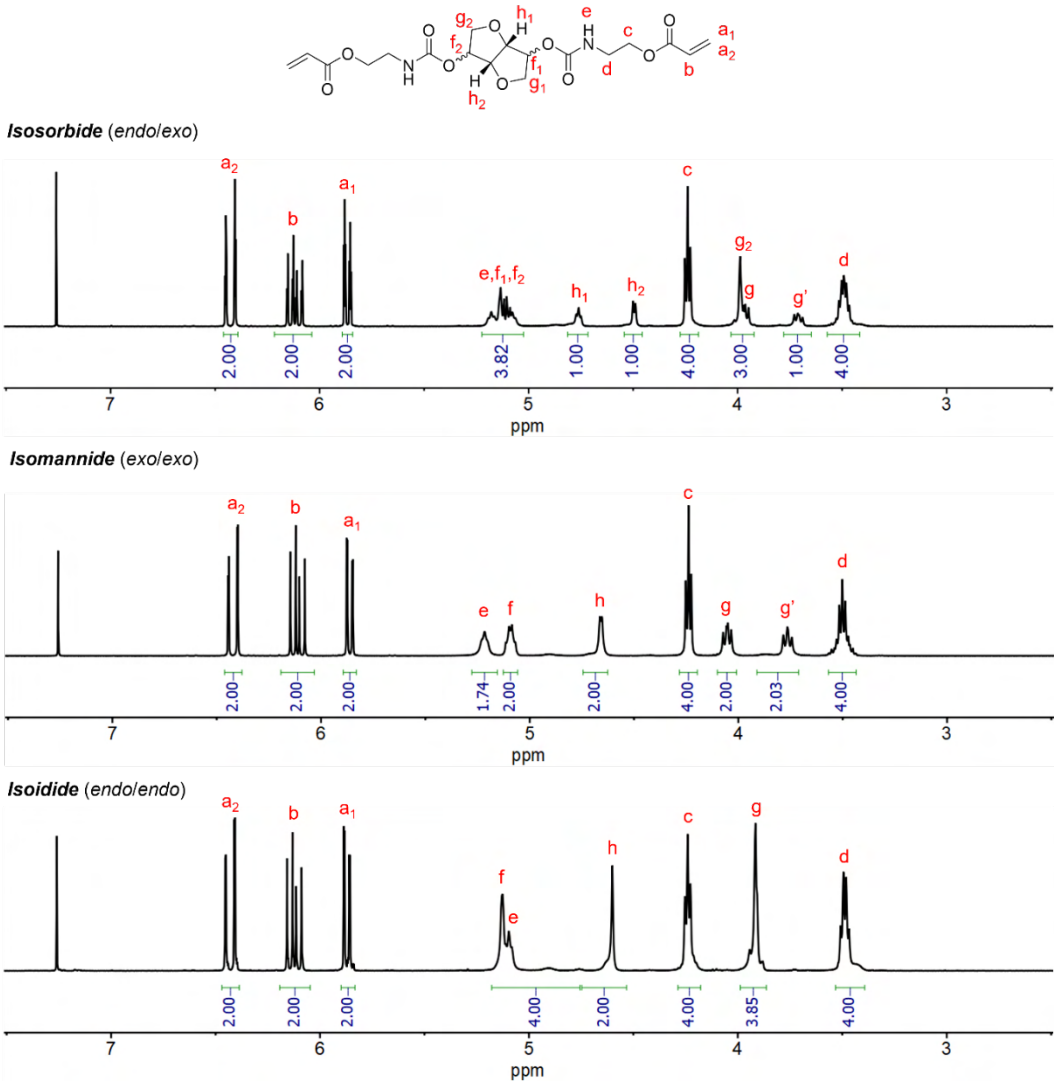


Figure 2.24. *^{1}H NMR (400 MHz, $CDCl_3$, 298K) spectrum of the isohexides-derived acrylate monomers. From top to bottom: isosorbide-derived diacryalte (**26**), isomannide-derived diacrylate (**27**) and isoidide-derived diacrylate (**28**).*

The ^{1}H NMR spectra of isohexides-derived diacrylate were each presenting the 3 resonance signals characteristic of acrylate groups at δ = 6.40 ppm, δ = 6.09 ppm and δ = 5.84 ppm with integrations indicating the presence of two functionalities if compared to the integration of the methine h_1 or h_2. (**Figure 2.24**). Moreover, these results were consistent with the literature.[6, 56] Interestingly, these monomers were challenging to dry. For instance, the ^{1}H NMR spectrum presented were collected

from the analysis of monomers which were left drying over phosphorus pentoxide for 7 days, yet all the water could not be removed in these conditions.

1.14.3 Synthesis of 1,6-glucose diacrylate

The ^{1}H NMR spectrum of the 1,6-glucose-derived diacrylate showed the same resonance signals characteristics for the acrylate end group at δ = 6.40 ppm, δ = 6.09 ppm and δ = 5.84 ppm. In addition, comparing their corresponding integration with the anomeric proton **b**, confirmed the successful functionalisation of both hydroxyl groups (**Figure 2.25**). Interestingly, whilst the starting material was a mixture of α and β anomer in a 65.35 ratio, the 1,6-glucose-derived diacrylate has been obtained as the pure β anomer.

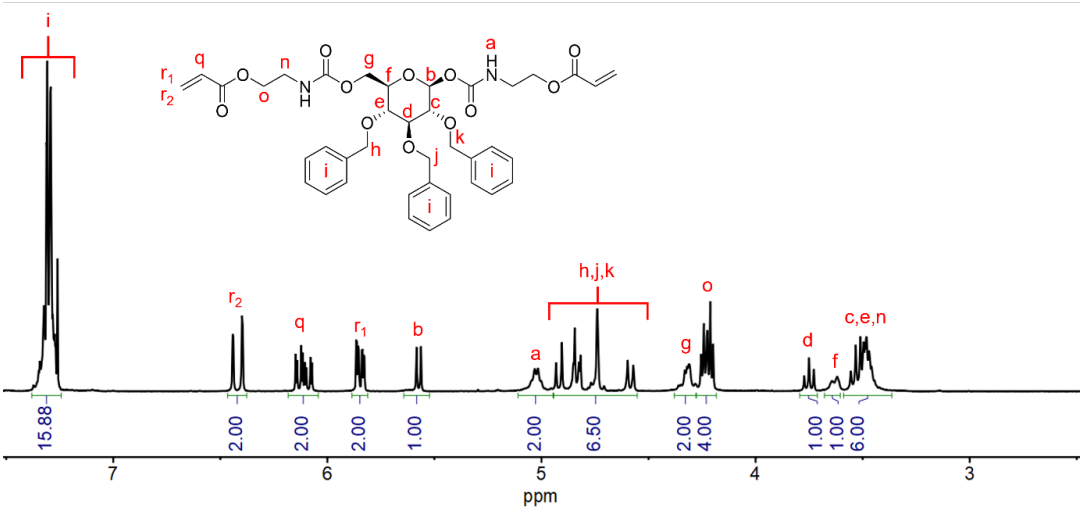
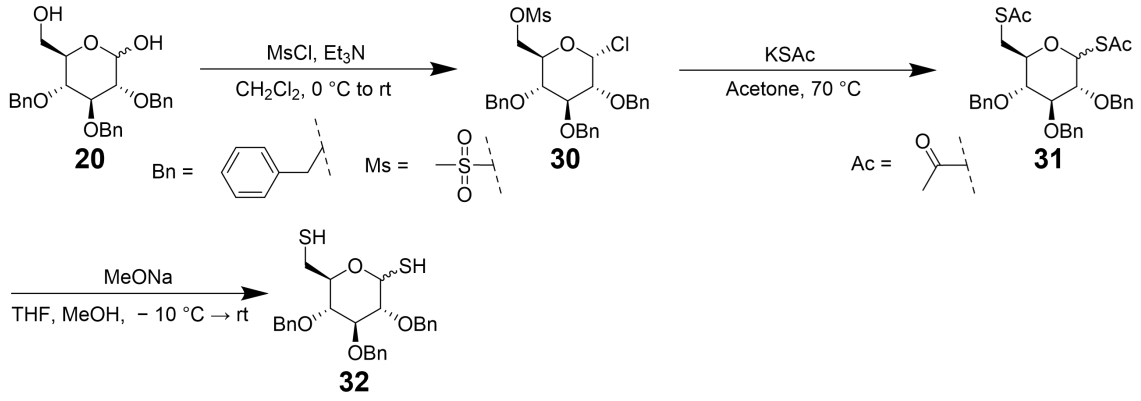


Figure 2.25. *^{1}H NMR (400 MHz, $CDCl_3$, 298 K) spectrum of the 1,6-glucose-derived diacrylate (**29**).*

1.15 Glucose derived dithiol synthesis

Both the C1 and C6 hydroxyls are known to share similarities in terms of reactivity, being both more reactive than the four other hydroxyl groups.[40] This particularity offers the tremendous advantage for potential one pot functionalisation

as both C1 and C6 could be reacted under the same reaction conditions. The preparation of both 1-glucose-derived dithiol and 6-glucose-derived dithiol have precedence in the literature and the procedures are diverse. Thus 1-glucose-derived thiol or 6-glucose-derived thiol are most commonly prepared by Mitsunobu condensation in the presence of diethyl azodicarboxylate and triphenyl phosphine[58, 59] or by the displacement of a sulfonate or halo compound.[60, 61] The latter synthetic method was adopted due to potential challenges removing triphenylphosphine impurities and the explosive nature of diethyl azodicarboxylate (DEAD) used in the Mitsunobu transformation would be hazardous on this scale. The last step only consists in the straightforward deprotection of the thiols via Zemplèn deacetylation **Scheme 2.9**).



Scheme 2.9. *Multi-step synthesis of 2,3,4-tri-O-benzyl-1,6-dithio-D-glucopyranose (1,6-glucose-derived dithiol) (**32**).*

Whilst a 1,6-di-sulfonated glucose derivative was expected as a product from the reaction of diol (**20**) with 4 equivalents of methanesulfonyl chloride and triethylamine in dichloromethane, the combination of both ^{1}H and ^{13}C NMR and mass spectroscopy analysis indicated the presence of only one mesylate group and a chlorine atom within the product obtained after 1h of reaction (**Figure 2.26 (a)**).

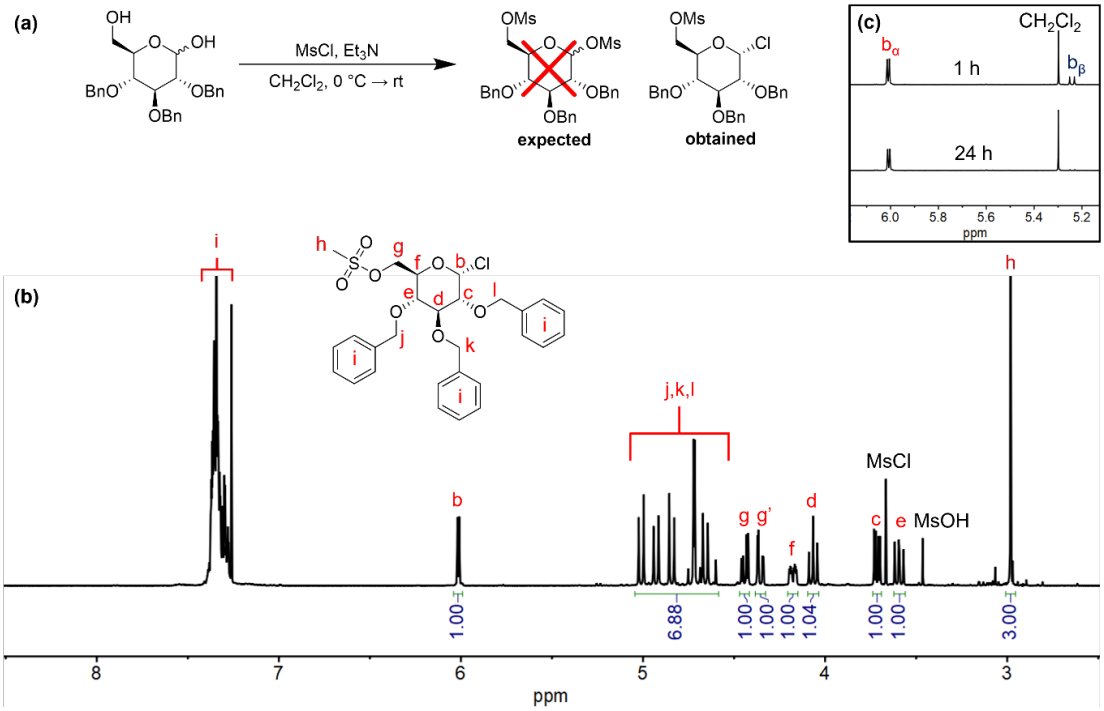


Figure 2.26. *(a) Scheme illustrating the expected and obtained product from the reaction of the 1,6-glucose derived diol (**20**) with methanesulfonyl chloride and (b) ^{1}H NMR spectrum of the crude product from the reaction (**30**). (c) After 24h of reaction, the compound is recovered enantiopure as the β anomer.*

The signal characteristic of a methyl group (**h**, δ = 2.98 ppm) can be observed on the ^{1}H NMR spectrum of product (**30**). Leaving the reaction for 24 hours resulted in the disappearance of the resonance signal corresponding to the β anomeric proton. Thus, increasing the reaction time yielded the improvement of the anomeric purity from 80% to 97%, however the attempt at a second mesylation reaction of product (**30**) remained unsuccessful, as once again, only one signal corresponding to a methyl group could be observed on the ^{1}H NMR spectra (**Figure 2.26 (b)** and **(c)**). As a mono-mesylated compound was not expected and this reaction does not seem to have precedence in the literature, the structure of the reaction product (**30**) required to be determined. First, by comparing the ^{1}H and ^{13}C NMR spectrum of the product (**30**) to that of the starting diol (**20**), significant downfield shifts could be observed for C1 and C6 and related protons, suggesting the presence of electron

withdrawing groups on these two carbons. (**Table 2.1**) As chlorination is a well-known side reaction occurring whilst working with methanesulfonyl chloride [44, 62], the first consideration has been the presence of a chlorine within the product. Mass spectroscopy analysis corroborated this assumption as the mass found was identical to the calculated mass of 545.1414 (m/z) $[M - H]^+$.

Table 2.1. *Comparison of the resonance signals of protons and carbons in C1 and C6 of α 1,6-glucose-derived diol (**20**) and sulfonated product (**30**) prior to its structure determination.*

Compound	**1,6-glucose-derived diol (20)**		**Sulfonated product (30)**	
label	b_a	g	b_α	g
^{1}H NMR signal (ppm)	5.19	3.83	6.01	4.40
^{13}C NMR signal (ppm)	97.5	62.0	92.7	67.6

Finally, the relative position of the sulfonate and chlorine on the sugar ring has been determined by observing the correlation existing between the methyl (**h**) and C6 (**g**) protons on the ^{1}H-^{13}C HMBC of compound (**24**) (**Figure 2.27**). Whilst this exact structure was not expected, it is still theoretically possible to allow simultaneous nucleophilic displacement at C1 and C6 as both chlorine and mesylate are better leaving groups than hydroxyls. The simplicity of this transformation is highlighted by the near quantitative yield (98%), lack of by-products and impressive atom economy, even on scales up to 35g.

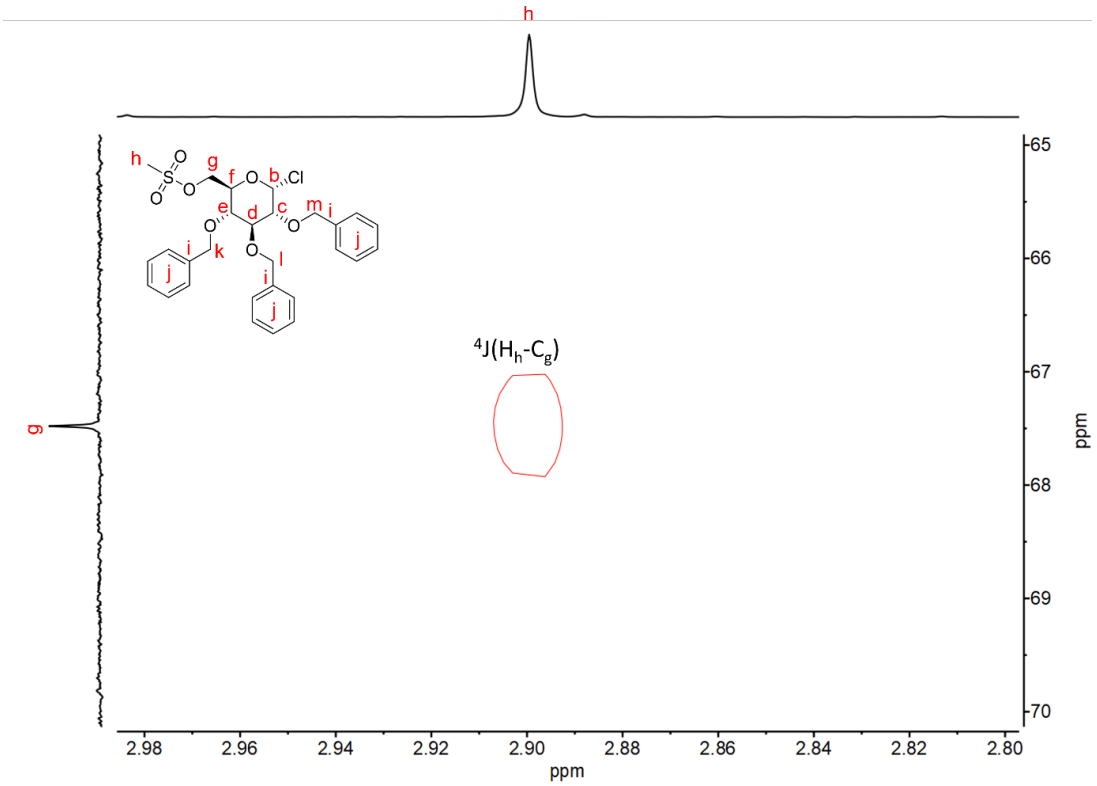
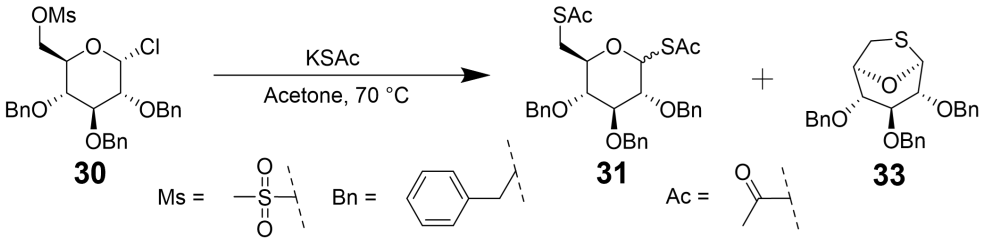


Figure 2.27. *Enlargement of the ^1H-^{13}C HMBC NMR spectrum of product (**24**).*

Mechanistically, the anomeric hydroxyl is known to be by far the best leaving group. For this reason, it has been conjectured that the double mesylation occurs, however, in apolar solvent, the chlorine is nucleophile enough to displace the mesylate leaving group on C1. Furthermore, the reverse reaction does not occur since the nucleophilicity of the mesylate is not high enough to displace a chlorine.

Then, after isolation, compound (**30**) was reacted with potassium thioacetate in either acetone or DMF at reflux temperature gave a 1,6-glucose-derived dithioacetate (**31**) as major product in an 8/92 α to β ratio with 20% of cyclic thio-ether (**27**) as a single by-product. (**Scheme 2.10** and **Appendix Figure A57 to A58**)



Scheme 2.10. *Products obtained from reacting compound (**30**) with potassium thioacetate in refluxing acetone: 1,6-glucose-derived dithioacetate (8/92 α to β ratio) (**31**) and 1,6-glucose-derived thio-ether (**33**) in a 80/20 ratio of product to by-product. All ratios were determined from the relative integration of the anomeric proton signal of the distinct compound on the ^{1}H NMR spectrum of the crude.*

The presence of the two sulfur atoms has first been suggested by observing the substantial shift for both C1 and C6 carbons for the dithioacetate (**31**) compared to the diacetate (**19**). Thus, a shift over δ = 30 ppm upfield could be observed for both C1 and C6 carbon and a shift over δ = 1 ppm could be observed for the corresponding protons whilst comparing compound (**30**) to (**19**) ^{1}H and ^{13}C NMR spectra. (**Table 2.2**) Mass spectrometry analysis corroborated the presence of 2 thiols within compound (**31**) as the mass found was identical to the calculated mass of 589.1707 (m/z) $[M + Na]^{+}$.

Table 2.2. *Comparison of the resonance signals of protons and carbons in C1 and C6 of β-1,6-glucose derived diacetate (**19**) and dithioacetate (**31**).*

Compound	**1,6-diacetate (19)**		**1,6-dithioacetate (31)**	
Atom label	b_{β}	g	b_{β}	g
^{1}H NMR signal (ppm)	5.62	4.26	5.12	3.22
^{13}C NMR signal (ppm)	94.0	62.8	81.7	31.0

This reaction has been scaled up to 42 g of the starting material, unfortunately, the separation of compound (**31**) from compound (**33**) proved to be particularly challenging, causing the yield after purification to range between 30 and 50% only.

Since the α anomer was only representing 6% of the crude, the dithioacetate was obtained as the pure β anomer after purification. (**Figure 2.28**)

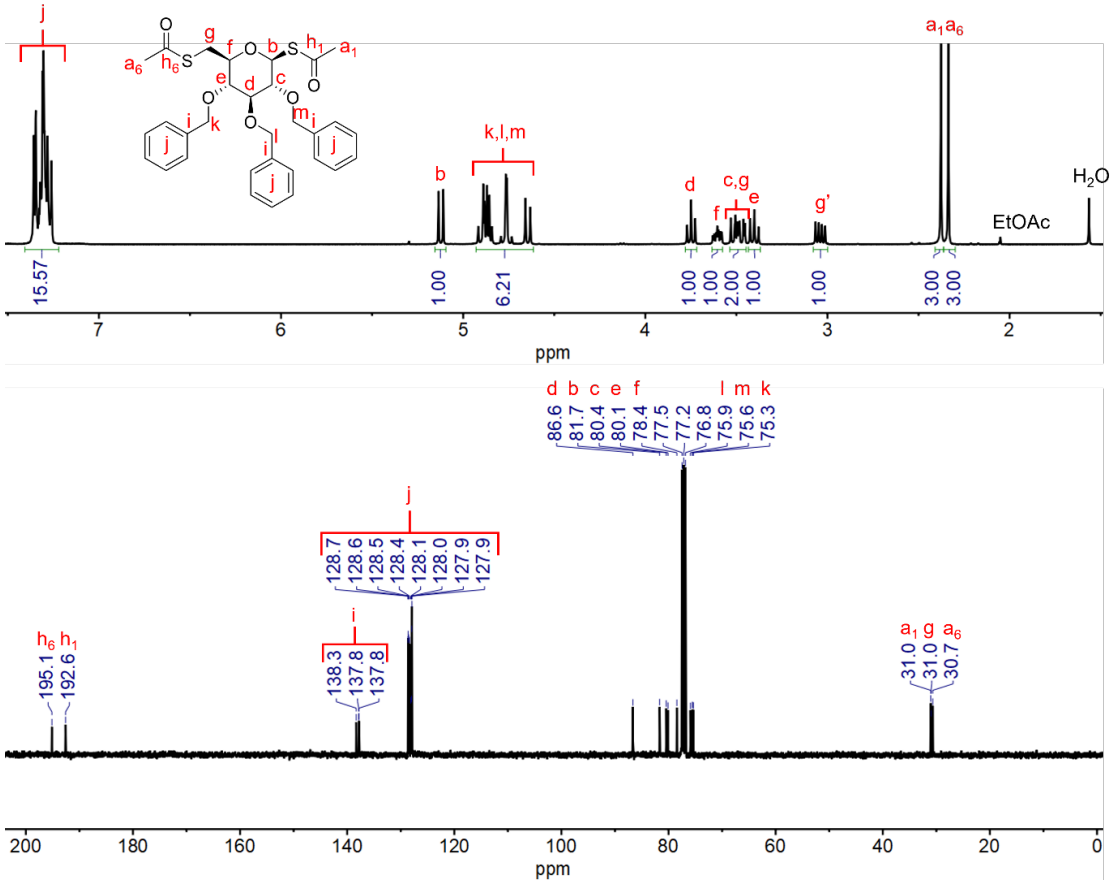


Figure 2.28. *^{1}H NMR (400 MHz, 298 K, $CDCl_3$) and ^{13}C NMR (101 MHz, 298 K, $CDCl_3$) spectra of acetyl 2,3,4-tri-O-benzyl-1,6-dithio-6- acetyl-D-glucopyranoside (**31**).*

Once the 1,6-dithioacetate (**31**) has been obtained pure and after optimisation of the reaction conditions, both thiols were successfully deprotected by Zemplèn deacetylation as determined from observing the disappearance of the resonance signal characteristic of the acetate groups at δ = 2.34 and δ = 2.38 ppm or at δ = 31.0 (methyl), δ = 192.6 (carbonyl, C1) and δ = 195.1 ppm (carbonyl, C6) on respectively the ^{1}H and ^{13}C NMR spectra of the 1,6-dithiol (**32**). (Error! Reference source not found.) The desired 1,6-dithiol (**32**) has been obtained at a 90% yield as

the pure β anomer before purification. Unfortunately, the purity required for step-growth polymerisation needs to meet the highest of standards, thus the purification of this compound has been explored without significant success as the 1,6-dithiol seems to be unstable on silica, and purification by recrystallisation returned a compound of the same purity at a maximum of 50% yield. Moreover, the formation of intra and inter molecular disulfides was also observed. (**Appendix Figures A59-60**)

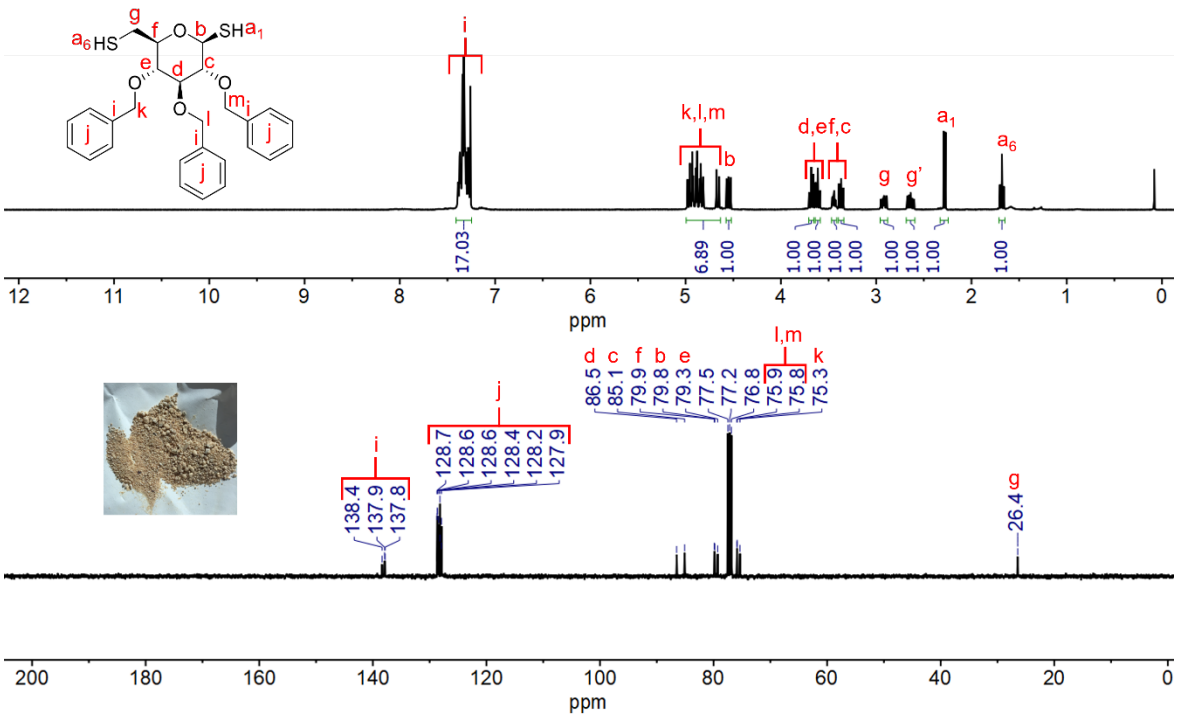


Figure 2.29. *^{1}H NMR (400 MHz, 298 K, $CDCl_3$) and ^{13}C NMR (101 MHz, 298 K, $CDCl_3$) spectra of 2,3,4-tri-O-benzyl-1,6-dithio-β-D-glucopyranose (**32**).*

1.16 Conclusion

In conclusion 6 different diacrylates were successfully synthesised from reacting various diol precursors with 2-isocyanatoethyl acrylate. Whilst the synthesis of the unsaturated *trans* diol and isoidide was straightforward on scale up to 30 g with adjustment of previously reported procedures, the synthesis of a glucose derived

diol proved to be challenging on scales large enough for material synthesis. Furthermore, all hydroxyls have different reactivities which is impacted by its relative position on the sugar, the neighbouring protecting group, and its axial or equatorial configuration. For this specific reason all glucose diols are not equal in accessibility and reactivity, which led to abandoning the synthesis of the 1,4-glucose-derived diol to focus on the synthesis of the more accessible 1,6-glucose-derived diol precursor. During the synthetic journey towards this dithiol, was discovered an unusually high yielding asymmetric functionalisation of a benzyl protected 1,6-glucose-derived diol with mesylate chloride. Further investigation into the limits of this reaction could provide a useful derivative for asymmetric sugar synthesis, and furthermore uncover a previously unreported transformation. Since this was not theme of the thesis, further work was not undertaken within this area.

From these synthetised diacrylate and dithiol monomers, it is expected to carry thiol-ene step-growth polymerisation to study the impact of the two types of stereochemistry, namely *cis/trans* and *endo/exo* and also the feasibility of synthesising a polysaccharide mimic *via* nucleophilic thiol-ene step-growth polymerisation.

1.17 References

(1) Organ, M. G.; Cooper, J. T.; Rogers, L. R.; Soleymanzadeh, F.; Paul, T. Synthesis of Stereodefined Polysubstituted Olefins. 1. Sequential Intermolecular Reactions Involving Selective, Stepwise Insertion of Pd(0) into Allylic and Vinylic Halide Bonds. The Stereoselective Synthesis of Disubstituted Olefins[1]. *J. Org. Chem.* **2000**, *65,* 7959-7970

(2) Rosmarion, K.; Tokhunts, R.; Rothchild, R. Diels-Alder Adducts of 3,6-Dibromophencyclone with Symmetrical 1,4-Disubstituted-Cis-2-Butenes: Comparisons with the Adduct of Phencyclone and N-Benzylmaleimide, and One-Dimensional and Two-Dimensional Nuclear Magnetic Resonance Studies and Ab Initio Structure Calculations. *Appl. Spectrosc.* **2005**, *59,* 366-375

(3) Fenouillot, F.; Rousseau, A.; Colomines, G.; Saint-Loup, R.; Pascault, J. P. Polymers from renewable 1,4:3,6-dianhydrohexitols (isosorbide, isomannide and isoidide): A review. *Prog. Polym. Sci.* **2010**, *35,* 578-622

(4) Zia, K. M.; Noreen, A.; Zuber, M.; Tabasum, S.; Mujahid, M. Recent developments and future prospects on bio-based polyesters derived from renewable resources: A review. *Int. J. Biol. Macromol.* **2016**, *82,* 1028-1040

(5) Saxon, D. J.; Luke, A. M.; Sajjad, H.; Tolman, W. B.; Reineke, T. M. Next-generation polymers: Isosorbide as a renewable alternative. *Prog. Polym. Sci.* **2020**, *101,* 101196

(6) Stubbs, C. J.; Worch, J. C.; Prydderch, H.; Wang, Z.; Mathers, R. T.; Dobrynin, A. V.; Becker, M. L.; Dove, A. P. Sugar-Based Polymers with Stereochemistry-Dependent Degradability and Mechanical Properties. *J. Am. Chem. Soc.* **2022**, *144,* 1243-1250

(7) Corma, A.; Iborra, S.; Velty, A. Chemical Routes for the Transformation of Biomass into Chemicals. *Chem. Rev.* **2007**, *107,* 2411-2502

(8) Pacsu, E.; Mora, P. T. Polycondensation of d-glucose and other simple sugars in presence of acids. *J. Am. Chem. Soc.* **1950**, *72,* 1045-1045

(9) Pati, D.; Chen, Z.; Feng, X.; Hadjichristidis, N.; Gnanou, Y. Synthesis of polyglycocarbonates through polycondensation of glucopyranosides with CO2. *Polym. Chem.* **2017**, *8,* 2640-2646

(10) Lonnecker, A. T.; Lim, Y. H.; Felder, S. E.; Besset, C. J.; Wooley, K. L. Four Different Regioisomeric Polycarbonates Derived from One Natural Product, d-Glucose. *Macromolecules* **2016**, *49,* 7857-7867

(11) Galbis, J. A.; García-Martín, M. d. G.; de Paz, M. V.; Galbis, E. Synthetic Polymers from Sugar-Based Monomers. *Chem. Rev.* **2016**, *116,* 1600-1636

(12) Delbianco, M.; Seeberger, P. H. Materials science based on synthetic polysaccharides. *Mater. Horiz.* **2020**, *7,* 963-969

(13) Li, L.; Xu, Y.; Milligan, I.; Fu, L.; Franckowiak, E. A.; Du, W. Synthesis of Highly pH-Responsive Glucose Poly(orthoester). *Angew. Chem. Int. Ed.* **2013**, *52,* 13699-13702

(14) Azechi, M.; Matsumoto, K.; Endo, T. Anionic ring-opening polymerization of a five-membered cyclic carbonate having a glucopyranoside structure. *J. Polym. Sci., Part A: Polym. Chem.* **2013**, *51,* 1651-1655

(15) Mora, P. T.; Wood, J. W. Synthetic Polysaccharides. I. Polycondensation of Glucose[1]. *J. Am. Chem. Soc.* **1958**, *80,* 685-692

(16) Galbis, J. A.; García-Martín, M. G. Chapter 5 - Sugars as Monomers. In *Monomers, Polymers and Composites from Renewable Resources*, Elsevier, 2008; pp 89-114.

(17) Galbis, J. A.; García-Martín, M. G. Synthetic Polymers from Readily Available Monosaccharides. In *Carbohydrates in Sustainable Development II*, Springer Berlin Heidelberg, 2010; pp 147-176.

(18) Kim, S. H.; Lee, C. M.; Kafle, K. Characterization of crystalline cellulose in biomass: Basic principles, applications, and limitations of XRD, NMR, IR, Raman, and SFG. *Korean J. Chem. Eng.* **2013**, *30,* 2127-2141

(19) Atalla, R. H. The structure of cellulose: recent developments. In *Wood and Agricultural Residues—Research on Use for Feed, Fuels, and Chemicals*, Academic, New York, 1983; pp 59-77.

(20) Sato, T.; Nakamura, H.; Ohno, Y.; Endo, T. Synthesis of 1,4-anhydro-2,3,6-tri-O-benzyl-a-d-glucopyranose by cis-ring-closure of a glycosyl chloride. *Carbohydr. Res.* **1990**, *199,* 31-35

(21) Williams, J. M.; Richardson, A. C. Selective acylation of pyranoside—I.: Benzoylation of methyl α-d-glycopyranosides of mannose, glucose and galactose. *Tetrahedron* **1967**, *23,* 1369-1378

(22) Zhang, Z.; Wong, C.-H. Regioselective benzoylation of sugars mediated by excessive Bu2SnO: observation of temperature promoted migration. *Tetrahedron* **2002**, *58,* 6513-6519

(23) Greene, T. W., Wuts, P.G.M. Protection for the Hydroxyl Group, Including 1,2- and 1,3-Diols. In *Protective Groups in Organic Synthesis*, fourth ed.; 1999; pp 17-245.

(24) Kocienski, P. J. *Protecting groups*; G. Thieme Stuttgart, 1994.

(25) Freudenberg, K.; Toepffer, H.; Andersen, C. C. Zur Kenntnis der Aceton-Zucker, XV.: Versuche zur Synthese von Disacchariden. *Ber. Dtsch. Chem. Ges.* **1928**, *61,* 1750-1760

(26) Van Cleve, J. W. Improved preparation of methyl 4,6-O-benzylidene-α-D-glucopyranoside. *Carbohydr. Res.* **1971**, *17,* 461-464

(27) Calinaud, P.; Gelas, J. Synthesis of Isopropylidene, Benzylidene, and related acetals. In *Preparative Carbohydrate Chemistry*, 1997; pp 3-33.

(28) de Belder, A. N. Cyclic Acetals of the Aldoses and Aldosides. In *Advances in Carbohydrate Chemistry*, Academic Press, 1965; pp 219-302.

(29) Panchadhayee, R.; Kumar Misra, A. Efficient Iodine-Catalyzed Preparation of Benzylidene Acetals of Carbohydrate Derivatives. *J. Carbohydr. Chem.* **2008**, *27,* 148-155

(30) Mukhopadhyay, B. Sulfuric acid immobilized on silica: an efficient promoter for one-pot acetalation–acetylation of sugar derivatives. *Tetrahedron Lett.* **2006**, *47,* 4337-4341

(31) Evans, M. E. Methyl 4,6-O-benzylidene-α- and -β-d-glucosides. *Carbohydr. Res.* **1972**, *21,* 473-475

(32) Demchenko, A. V.; Pornsuriyasak, P.; De Meo, C. Acetal Protecting Groups in the Organic Laboratory: Synthesis of Methyl 4,6-O-Benzylidene-α-D-Glucopyranoside. *J. Chem. Educ.* **2006**, *83,* 782

(33) Bochkov, A. F.; Zaikov, G. E. General Characteristics of the *O*-glycosidic Bond. In *Chemistry of the O-glycosidic bond: formation and cleavage*, Pergamon Press Ltd., 2016; pp 1-4.

(34) Bochkov, A. F.; Zaikov, G. E. Cleavage of O-glycosidic bonds. In *Chemistry of the O-glycosidic bond: formation and cleavage*, Pergamon Press, 2016; pp 177-201.

(35) Boons, G. J. Mono- and Oligosaccharides: Structure, Configuration and Conformation. In *Organic Synthesis with Carbohydrates*, 2002; pp 1-25.

(36) Schmidt, O. T.; Auer, T.; Schmadel, H. 2.3.4.6-Tetrabenzyl-α-D-glucose. *Chem. Ber.* **1960**, *93,* 556-557

(37) Fréchet, J. M. J.; Baer, H. H. Synthesis and methanolysis of 2,3,4-tri-O-benzyl-α-l- rhamnopyranosyl bromide. *Carbohydr. Res.* **1975**, *42,* 369-372

(38) Shi, Y.-H.; Xie, Y.-F.; Liu, Y.-Q.; Wei, Q.-C.; Xu, W.-R.; Tang, L.-D.; Zhao, G.-L. SrCl2 as an efficient cocatalyst for acidic hydrolysis of methyl glycosides. *Chin. Chem. Lett.* **2014**, *25,* 561-566

(39) Wang, Z. Zemplén Deacetylation. In *Comprehensive Organic Name Reactions and Reagents*, 2010; pp 3123-3128.

(40) Lipták, A.; Borbás, A.; Bajza, I. 1.06 - Protecting Group Manipulations in Carbohydrate Synthesis. In *Comprehensive Glycoscience*, Elsevier, 2007; pp 203-259.

(41) Hussain, A.; Yousuf, S. K.; Kumar, D.; Lambu, M.; Singh, B.; Maity, S.; Mukherjee, D. Intramolecular Base-Free Sonogashira Reaction for the Synthesis of Benzannulated Chiral Macrocycles Embedded in Carbohydrate Templates. *Adv. Synth. Catal.* **2012**, *354,* 1933-1940

(42) Klaffke, W.; Warren, C. D.; Jeanloz, R. W. Syntheses of oligosaccharides having the β-d-GlcpNAc-(1 → 4)-d-Glc- structure. *Carbohydr. Res.* **1993**, *244,* 171-179

(43) Horton, D.; Hutson, D. H. Developments in the Chemistry of Thio Sugars. In *Advances in Carbohydrate Chemistry*, Academic Press, 1963; pp 123-199.

(44) Tipson, R. S. Sulfonic Esters of Carbohydrates. In *Advances in Carbohydrate Chemistry*, Academic Press, 1953; pp 107-215.

(45) Owen, L. N.; Ragg, P. L. Thio-sugars. Part II. The thiofuranose ring. *J. Chem. Soc. C* **1966**, 1291-1296

(46) Varela, O.; Cicero, D.; De Lederkremer, R. M. A convenient synthesis of 4-thio-D-galactofuranose. *J. Org. Chem.* **1989**, *54,* 1884-1890

(47) Lipták, A.; Balla, E.; Jánossy, L.; Sajtos, F.; Szilágyi, L. The first synthesis of secondary sugar sulfonic acids by nucleophilic displacement reactions. *Tetrahedron Lett.* **2004**, *45,* 839-842

(48) Elhalabi, J.; Rice, K. G. Thiosugar nucleotide analogues: synthesis of uridine 5′-(2,3,6-tri-O-acetyl-4-S-acetyl-4-thio-α-d-galactopyranosyl diphosphate). *Carbohydr. Res.* **2001**, *335,* 159-165

(49) Pei, Z.; Dong, H.; Ramström, O. Solvent-Dependent, Kinetically Controlled Stereoselective Synthesis of 3- and 4-Thioglycosides. *J. Org. Chem.* **2005**, *70,* 6952-6955

(50) Vauzeilles, B.; Sinaÿ, P. Selective radical synthesis of β-C-disaccharides. *Tetrahedron Lett.* **2001**, *42,* 7269-7272

(51) Garegg, P. J.; Samuelsson, B. Novel reagent system for converting a hydroxy-group into an iodo-group in carbohydrates with inversion of configuration. Part 2. *J. Chem. Soc., Perkin Trans. 1* **1980**, 2866-2869

(52) Wang, L.-X.; Sakairi, N.; Kuzuhara, H. 1,6-Anhydro-β-D-glucopyranose derivatives as glycosyl donors for thioglycosidation reactions. *J. Chem. Soc., Perkin Trans. 1* **1990**, 1677-1682

(53) Meloncelli, P. J.; Martin, A. D.; Lowary, T. L. Glycosyl iodides. History and recent advances. *Carbohydr. Res.* **2009**, *344,* 1110-1122

(54) Cao, Y.; Okada, Y.; Yamada, H. Facile and regioselective preparation of partly O-benzylated d-glucopyranose acetates via acid-mediated simultaneous debenzylation–acetolysis. *Carbohydr. Res.* **2006**, *341,* 2219-2223

(55) Stubbs, C. J.; Worch, J. C.; Prydderch, H.; Becker, M. L.; Dove, A. P. Unsaturated Poly(ester-urethanes) with Stereochemically Dependent Thermomechanical Properties. *Macromolecules* **2020**, *53,* 174-181

(56) Petersen, S. R.; Prydderch, H.; Worch, J. C.; Stubbs, C. J.; Wang, Z.; Yu, J.; Arno, M. C.; Dobrynin, A. V.; Becker, M. L.; Dove, A. P. Ultra-Tough Elastomers from Stereochemistry-Directed Hydrogen Bonding in Isosorbide-Based Polymers. *Angew. Chem. Int. Ed.* **2022**, *61,* e202115904

(57) Damusis, A.; McClellan, J. M.; Wissman, H. G.; Hamilton, C. W.; Frisch, K. C. Polyether Urethane Elastic Sealants. *Ind. Eng. Chem. Prod. Res. Dev.* **1962**, *1,* 269-274

(58) Falconer, R. A.; Jablonkai, I.; Toth, I. Efficient synthesis of thioglycosides via a Mitsunobu condensation. *Tetrahedron Lett.* **1999**, *40,* 8663-8666

(59) Besson, T.; Neirabeyeh, M. A.; Viaud, M.-C.; Rollin, P. Mitsunobu Thiofunctionalization-Part 2.1 an Expedient Synthesis of Aza-Heterocycle/Thiosugar Hybrids. *Synth. Commun.* **1990**, *20,* 1631-1639

(60) Pachamuthu, K.; Schmidt, R. R. Synthetic Routes to Thiooligosaccharides and Thioglycopeptides. *Chem. Rev.* **2006**, *106,* 160-187

(61) Li, P.; Sun, L.; Landry, D. W.; Zhao, K. Synthesis of 1-thioglycosides. *Carbohydr. Res.* **1995**, *275,* 179-184

(62) Ball, D. H.; Parrish, F. W. Sulfonic Esters of Carbohydrates: Part I. In *Advances in Carbohydrate Chemistry*, Academic Press, 1968; pp 233-280.

1.18 Appendices

1.18.1 Materials and methods

Materials

Cis/trans monomer synthesis

Tetrahydrofuran (THF, ≥99.9%), lithium aluminum hydride ($LiAlH_4$, 95%) and dibutyltin (IV) dilaurate (DBTDL, 95%) were purchased from Sigma-Aldrich company. But-2-yne-1,4-diol (99%) and *cis*-2-butene-1,4-diol (97%) were purchased from Acros Organics. 2-isocyanatoethyl acrylate (>99.8%) was purchased from TCI chemicals. Unless stated otherwise, all compounds were used as received.

Isohexides monomer synthesis

Dibutyltin (IV) dilaurate (DBTDL, 95%), dimethylaminopyridine (DMAP, ≥99%), *p*-toluenesulfonyl chloride (TsCl, 99%), potassium acetate (KOAc, ≥99%) and sodium methoxide (MeONa, 25wt% in MeOH) were purchased from Sigma-Aldrich company. Anhydrous methanol (MeOH, 99.9%), dichloromethane (CH_2Cl_2, 99%), N,N'-dimethylformamide (DMF, 99.5%) and tetrahydrofuran (THF, ≥99.5%) were purchased from Fisher Scientific. 2-isocyanatoethyl acrylate (>99.8%) and Isomannide (>98%) were purchased from TCI Chemicals. Triethylamine (Et_3N, 99%) and methanol (MeOH, 99.8%) were purchased from VMR Chemicals. Isosorbide (≥99%) was kindly provided by Roquette (Polysorb®). Isosorbide was recrystallised twice in ethyl acetate/hexanes before use. All other compounds were used as received.

Glucose derived monomer synthesis

Benzylidene acetal (95%), sodium hydride (NaH, 60% in mineral oil), tetrabutylammonium iodide (TBAI, ≥98%), acetic anhydride (Ac_2O, ≥98%), sodium methoxide (MeONa, 25wt% in MeOH), acryloyl chloride (≥98%), potassium thioacetate (KSAc, 98%) and dibutyltin (IV) dilaurate (DBTDL, 95%) were purchased from Sigma-Aldrich. Anhydrous DMF (Extra Pure, SLR), DMF (99.5%), glacial acetic acid (AcOH, Extra Pure, SLR), H_2SO_4 (96% solution in water, Extra Pure), Potassium hydroxide (KOH, ≥86%), toluene (≥99.8%), tetrahydrofuran (THF, ≥99.5%) and dichloromethane (CH_2Cl_2, 99%) were purchased from Fisher Scientific. Benzyl bromide (BnBr, 99%), sodium cyanoborohydride ($NaBH_3CN$, 95%), methanesulfonyl chloride (MsCl, 98%) and camphor-10-sulfonic acid (CSA) were purchased from Alfa Aesar. Methanol (MeOH, ≥99.8%) and triethylamine (Et_3N, 99%) were purchased from VMR Chemicals. Aluminium chloride ($AlCl_3$, ≥99%) was purchased from Honeywell (Fluka®). 2-isocyanatoethyl acrylate (>99.8%) was purchased from TCI Chemicals. Methyl-α-D-glucopyranoside (≥99%) was purchased from Acros Organics. Where specified, both anhydrous tetrahydrofuran and toluene refers were purified and dried by a PureSolv MD 5 purification system. Benzyl Bromide was purified by distillation prior to use. All other compounds were used as received.

Purification

Diethyl ether (Et_2O, ≥99.7%), hydrochloric acid (HCl, 36% solution in water), lithium chloride (LiCl, 95%), dichloromethane (CH_2Cl_2, 99%), absolute ethanol (EtOH, 99.8%), sodium hydroxide (NaOH, ≥97%), sodium Chloride (NaCl, ≥99.5%)

and sodium hydrogen carbonate ($NaHCO_3$, ≥99%) were purchased from Fisher Scientific. Magnesium sulfate ($MgSO_4$, 98%), Dowex® 50WX8 (100-200 mesh), Cyclohexane (99.7%) were purchased from Sigma-Aldrich. Ethyl acetate (EtOAc, ≥99.9%), hexane (≥99.5%) and triethylamine (Et_3N, 99%) were purchased from VMR Chemicals. Silica (SiO_2, 60Å, 40-60 µm) was purchased from Apollo Scientific. Celite S (untreated, dried) was purchased from Scientific Laboratory Supplies.

Characterisation

Deuterated dimethyl sulfoxide (d_6-DMSO, ≥99.9%) was purchased from Sigma-Aldrich Company. Deuterated chloroform ($CDCl_3$, >99.8%) was purchased from Apollo Scientific. TLC plates (Silica gel 60 F254) were purchased from Merck.

TLC stain preparation

The anisaldehyde/H_2SO_4 was prepared by adding H_2SO_4 (10 mL) and glacial AcOH (2 mL) to a solution composed of EtOH (95% solution in water, 180 mL) and anisaldehyde (10 mL).

The potassium permanganate stain was prepared by dissolving $KMnO_4$ (1.5 g), K_2CO_3 (10 g) in a solution of NaOH (10% solution in water, 1.25 mL) and water (200 mL).

Methods

Determination of the anomeric configuration

Regarding the assignment of the anomeric proton as α or β, the method employed throughout this chapter consisted in careful assessment of the ^1H NMR spectra of the targeted compound. Thus, it is generally accepted that the anomeric

protons, in either α or β configuration resonate at a lower field than the other protons present on the sugar ring. This is due to the inductive effect of the internal oxygen atom. Moreover, equatorial protons are known to generally resonate at lower field than their axial counterpart. Consequently, it is possible to resolve the signals corresponding to the different anomers *via* ^{1}H NMR spectroscopy. In addition, it is also possible to tell the two configurations apart by determination of the coupling constant of the doublets corresponding to the anomeric proton resonance signal. Hence, in the β configuration, the adjacent protons will have a dihedral angle of 180 ° and the coupling constant will generally be comprised between 7 to 10 Hz, whilst in the α configuration, the dihedral angle between adjacent proton is equal to 60 ° and therefore, the coupling constant will be of lower values, usually encompassed between 2 to 4 Hz.[1]

Nuclear magnetic resonance spectroscopy (NMR)

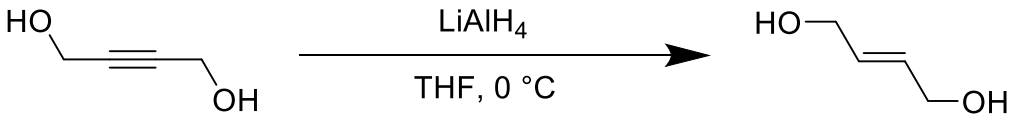
NMR spectroscopy of monomers were recorded at 298 K on a Bruker AVANCE NEO console spectrometer equipped with a 5 mm BBFO smart probe operating at 400 MHz for ^{1}H and 100.57 MHz for ^{13}C, respectively. Chemical shifts of ^{1}H NMR spectra were referenced to the solvent residual proton (δ = 7.26 ppm for $CHCl_3$ in $CDCl_3$, δ= 2.50 ppm for DMSO-d_5 in DMSO-d_6) and ^{13}C NMR spectra were referenced to the solvent resonance signal (δ= 77.16 ppm for $CDCl_3$, δ= 39.52 ppm for DMSO-d_6). The data obtained were processed and analyzed using MestReNova 12.0.3 software. The resonance multiplicities are described as s (singlet), d (doublet), t (triplet), q (quartet) or m (multiplet).

Mass spectrometry analysis

Mass spectrometry was performed by University of Birmingham School of Chemistry Analytical facility.

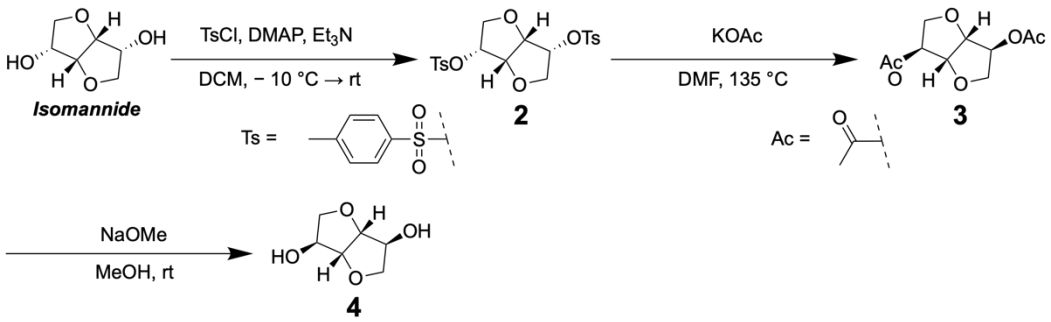
1.18.2 Synthetic procedures

Synthesis of trans-butene-1,4-diol (1)

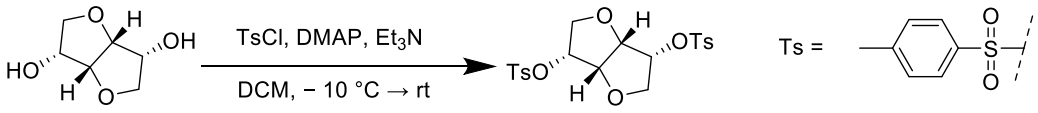


In a 2 L round bottom flask equipped with a magnetic stirrer, 800 mL of tetrahydrofuran (THF) was added, and the flask was cooled down to -10 °C with a brine/ice bath. Lithium aluminum hydride ($LiAlH_4$, 15.9 g, 418 mmol, 1.2 equiv.) is suspended in the THF. In a separate 1 L flask, a solution of but-2-yne-1,4-diol (30 g, 348 mmol, 1 equiv.) in THF (400 mL) is prepared and added to the suspension of $LiAlH_4$ *via* cannula transfer over 1 h. After the addition, the reaction mixture is left stirring for 48 h at 22 °C. The reaction is then cooled to -10 °C and quenched by addition of an aqueous solution of NaOH (3 M) until no gas evolution is observed and subsequently left stirring for 1 h. The reaction mixture is filtered to remove the aluminum salts and washed with warm THF. The filtrate is concentrated *in vacuo* and purified by vacuum distillation at 130 °C to afford a colorless oil (10.4 g, 123 mmol, 35%). Characterizing data is consistent with that reported previously. [2] ^{1}H NMR (400 MHz, 298 K, DMSO-d_6, ppm) δ 5.67 (m, 2H, C***H***=C***H***), 4.64 (t, J = 5.6 Hz, O***H***), 3.92 (m, C***H***$_2$). ^{13}C NMR (101 MHz, 298 K, DMSO-d_6, ppm) δ 129.9, 61.1.

Overview - Synthesis of isoidide



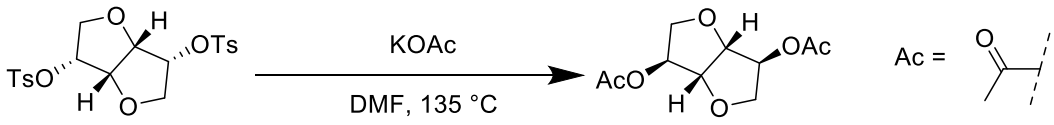
Synthesis of tosylated isomannide (2)



An oven-dried 500 mL 2-neck round bottom flask was charged with CH_2Cl_2 (200 mL), isomannide (30.0 g, 205.4 mmol, 1 equiv.), triethylamine (52.0 g, 513.5 mmol, 2.5 equiv.) and dimethylaminopyridine (2.51 g, 20.54 mmol, 0.1 equiv.). The reaction media is cooled down to -10 °C using a brine/ice bath, and *p*-toluenesulfonyl chloride (82.24 g, 431.4 mmol, 2.1 equiv.) is added dropwise over 1 h using a dropping funnel. The reaction is left stirring overnight (*ca.* 16 h) before being transferred in a separating funnel and washed with 1 M HCl solution (1×150 mL), water (3×150 mL), saturated $NaHCO_3$ solution (1×150 mL) and brine (1×150 mL). The organic phase is dried over $MgSO_4$ and the solvent is removed under vacuum to afford a white solid. The crude solid is ground into a powder using a pestle and mortar and purified by recrystallisation in ethanol (81.9 g, 180.1 mmol, 88% after 2 sequential recrystallisations). Characterisation data is consistent with that reported previously.[3] ^{1}H NMR (400 MHz, 298 K, $CDCl_3$, ppm) δ 7.83 – 7.77 (d, *J* = 8.5, 2.1 Hz, 4H, CC***H***CHCCH$_3$), 7.36 – 7.31 (m, 4H, CCHC***H***CCH$_3$), 4.87 – 4.81 (m, 2H, CHC***H***OCH$_2$), 4.48 – 4.45 (m, 2H, CH$_2$OC***H***COH), 3.91 (dd, *J* = 9.5, 6.7 Hz, 2H,

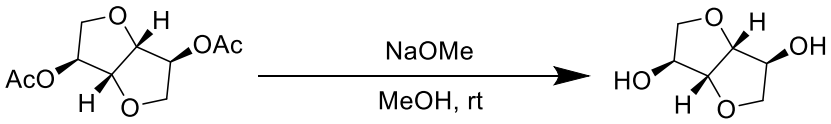
CHOC***H***HO), 3.72 (dd, *J* = 9.5, 7.7 Hz, 2H, CHOCH***H***O), 2.44 (s, broad, 6H, CHC***H***$_3$). ^{13}C NMR (101 MHz, 298 K, $CDCl_3$, ppm) δ 145.4, 133.2, 130.1, 128.1, 80.1, 78.0, 77.5, 77.2, 76.8, 70.2, 21.8.

Synthesis of acetylated isoidide (3)



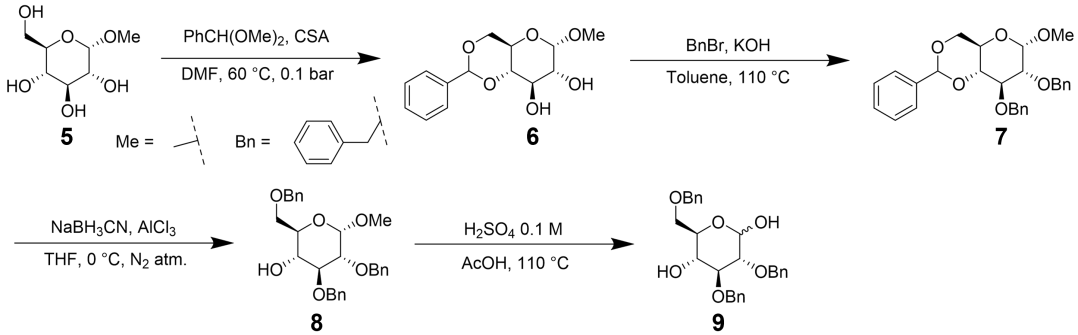
A 500 mL round bottom flask was charged with DMF (270 mL), tosylated isomannide (74.0 g, 163 mmol, 1 equiv.) and potassium acetate (322 g, 977 mmol, 6 equiv.). A waterless condenser (Findenser®) is fitted to the round bottom flask and the reaction is heated at 135 °C and left stirring overnight (*ca.* 16 h). Once the reaction media returned to room temperature, the reaction media is diluted with 250 mL of water, placed in a separating funnel and extracted with EtOAc (3×250 mL). The volume of the organic phase is reduced to approximatively 300 mL under vacuum before being washed with water (3×200 mL), 5 wt% LiCl solution (2×200 mL) and brine (1×200 mL). The organic phase is then dried over $MgSO_4$ and the solvent removed under vacuum to afford a white solid which is used without further purification (29.3 g, 127.4 mmol, 78.2%). Characterisation data is consistent with that reported previously.[3] ^{1}H NMR (400 MHz, 298 K, $CDCl_3$, ppm) δ 5.18 (m, 2H, CHC***H***OCH_2), 4.62 (s, broad, 2H, CH_2OC***H***CHO), 3.92 (m, 4H, CHOC***H***$_2$O), 2.07 (s, 6H, C***H***$_3$). ^{13}C NMR (101 MHz, 298 K, $CDCl_3$, ppm) δ 170.1, 85.5, 77.7, 77.5, 77.2, 76.8, 72.7, 21.0.

Synthesis of isoidide (4)

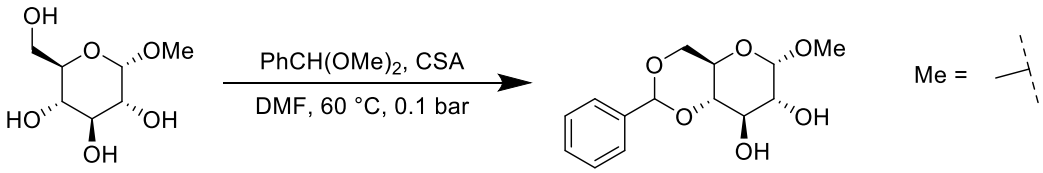


A 500 mL round bottom flask is charged with anhydrous MeOH (400 mL), acetylated isoidide (29.3 g, 127.4 mmol, 1 equiv.) and sodium methoxide (25 wt% in MeOH, 9.5 mL, 34.7 mmol, 0.3 equiv.). The reaction is left stirring at room temperature. After 45 mins, no traces of acetylated isoidide could be seen on a TLC (50/50 EtOAc/Hexane, stained with a potassium permanganate solution), indicating the completion of the reaction. Dowex® 50W X8 resin is added to the reaction media and left stirring for an additional hour. Once the pH reached neutrality, the reaction media is filtered, and the solvent is removed under vacuum to afford a white solid which is used without further purification (16 g, 114.3 mmol, 90%). Characterisation data is consistent with that reported previously.[3] ^{1}H NMR (400 MHz, 298 K, DMSO-d_6, ppm) δ 5.11 (d, J = 3.6 Hz, 2H, O***H***), 4.31 (s, 2H, OC***H***CHOCH$_2$), 4.02 (m, 2H, OCHC***H***OCH$_2$), 3.60 (m, 3.4 Hz, 4H, CHOC***H***$_2$O). ^{13}C NMR (101 MHz, 298 K, DMSO-d_6, ppm) δ 87.2, 74.8, 74.0, 40.2, 39.9, 39.7, 39.5, 39.3, 39.1, 38.9.

Overview - Synthesis of 1,4-glucose-derived diol (9)



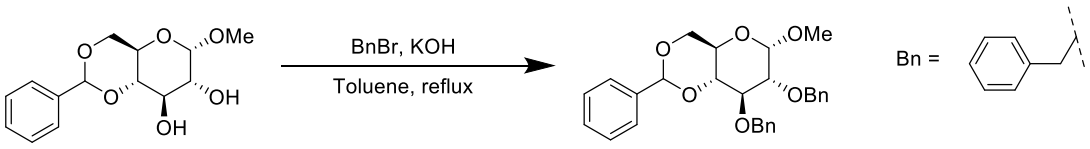
Synthesis of methyl 4,6-O-benzylidene-α-D-glucopyranoside (6)



Methyl-α-D-glucopyranoside (60.9 g, 314.0 mmol, 1 equiv.) and camphor-10-sulfonic acid (250 mg, 1.08 mmol, 0.0034 equiv.) are placed in an oven-dried 1 L round bottom flask and dried at 100 °C under vacuum for 3 h. Then, anhydrous DMF (200 mL) and benzaldehyde dimethyl acetal (48.5 g, 318.7 mmol, 1.01 equiv.) are added to the reaction vessel. The round bottom flask is then fitted to a rotary evaporator equipped with a solvent trap. The water bath is set at 60 °C, the vacuum at 100 mbar and the rotation at medium speed. After 2 h, some methyl-α-D-glucopyranoside could still be seen on TLC (80/20 EtOAc/Hexane, stained with an anisaldehyde/H_2SO_4 solution), therefore benzylidene acetal (4.5 g, 29.6 mmol, 0.094 equiv.) is added to the reaction media. After a total of 4 h, the reaction is stopped, quenched with Et_3N and the solvent removed under vacuum to afford a white solid. The crude solid ~~is~~ purified by recrystallisation in a mixture of EtOAc and Hexane to yield methyl 4,6-O-benzylidene-α-D-glucopyranoside (78 g, 277 mmol, 89% yield). *Note:* Another work up method consisted in the removal of the solvent under vacuum until the formation of a precipitate before the addition of water and a saturated solution of $NaHCO_3$. The crude is stirred in the basic aqueous phase at a temperature of 100 °C until total dissolution of the precipitate is observed. Upon cooling, the targeted compound precipitates, which can be collected by filtration. Further drying afford pure methyl 4,6-O-benzylidene-α-D-glucopyranoside. Recrystallisation of the compound is also possible in water, ethanol 95%, ethanol,

dichloromethane/hexane. Characterisation data is consistent with that reported previously.[4] ^{1}H NMR (400 MHz, 298 K, $CDCl_3$, ppm) δ 7.52 – 7.46 (m, 2H, Ar***H***, *ortho*), 7.41 – 7.33 (m, 3H, Ar***H***, *meta* and *para*), 5.52 (s, 1H, C***H*** acetal bridge), 4.78 (d, *J* = 3.9 Hz, 1H, ***H-1***), 4.31 – 4.26 (m, 1H, ***H-6***), 3.92 (t, *J* = 9.3 Hz, 1H, ***H-3***), 3.84 – 3.70 (m, 2H, ***H-5, H-6***), 3.62 (dd, *J* = 9.2, 3.9 Hz, 1H, ***H-2***), 3.48 (t, *J* = 9.3 Hz, 1H, ***H-4***), 3.45 (s, 3H, C***H***$_3$). ^{13}C NMR (101 MHz, 298 K, $CDCl_3$, ppm) δ 137.2, 129.4, 128.5, 126.5, 102.1, 99.9, 81.1, 77.5, 77.2, 76.8, 73.0, 71.9, 69.1, 62.5, 55.7. HRMS (TOF-MS-ES$^+$) (m/z): $[M^+H]^+$ calculated for $C_{28}H_{30}O_6H$, 463.2121; found, 463.2107.

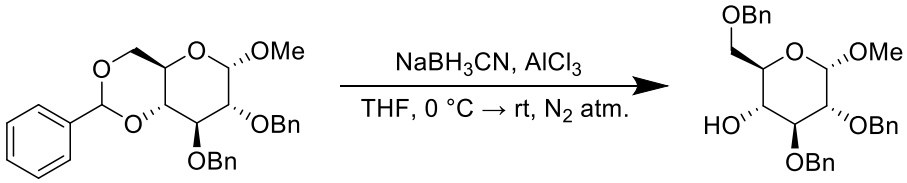
Synthesis of methyl 2,3-di-O-benzyl-4,6-O-benzylidene-α-D-glucopyranoside (7)



Methyl 4,6-O-benzylidene-α-D-glucopyranoside (45.03 g, 159.5 mmol, 1 equiv.), freshly distilled benzyl bromide (68.2 g, 399 mmol, 2.5 equiv.) and potassium hydroxide (22.37 g, 399 mmol, 2.5 equiv.) are suspended in anhydrous toluene (400 mL) in an oven-dried 1 L round bottom flask equipped with a Dean-Stark apparatus and a waterless condenser (Findenser®). Then, the temperature is increased to 110 °C. After *ca.* 16 h of reaction, no traces of 4,6-O-benzylidene-α-D-glucopyranoside could be observed by TLC (20/80 EtOAc/Hexane, stained with an anisaldehyde/H_2SO_4 solution), indicating the completion of the reaction. The reaction media is diluted in dichloromethane (500 mL) and washed with water (3×500mL) and brine (1×500mL). The organic phase is then dried over $MgSO_4$ and the solvent removed under vacuum to afford a white solid. The crude is purified by

recrystallisation in Hexane (600 mL) to yield methyl 2,3-di-O-benzyl-4,6-O-benzylidene-α-D-glucopyranoside (54.2 g, 117 mmol, 73%). Characterisation data is consistent with that reported previously.[5] ^{1}H NMR (400 MHz, 298 K, $CDCl_3$, ppm) δ 7.52 – 7.46 (m, 2H, Ar***H***, ortho), 7.43 – 7.24 (m, 13H, Ar***H***, *meta* and *para*), 5.56 (s, 1H, C***H*** acetal bridge), 4.92 – 4.71 (m,4H, C$\boldsymbol{H}_2$ benzyl), 4.60 (d, *J* = 3.7 Hz, 1H, ***H-1***), 4.27 (dd, *J* = 10.1, 4.7 Hz, 1H, ***H-6***), 4.05 (t, *J* = 9.3 Hz, 1H, ***H-3***), 3.87 – 3.80 (m, 1H, ***H-5***), 3.71 (t, *J* = 10.2 Hz, 1H, ***H-6***), 3.61 (t, *J* = 9.4 Hz, 1H, ***H-4***), 3.57 (dd, *J* = 9.3, 3.7 Hz, 1H, ***H-2***), 3.41 (s, 3H, C$\boldsymbol{H}_3$). ^{13}C NMR (101 MHz, 298 K, $CDCl_3$, ppm) δ 138.9, 138.3, 137.6, 129.1, 128.6, 128.5, 128.4, 128.3, 128.2, 128.1, 127.7, 126.2, 101.4, 99.4, 82.3, 79.3, 78.8, 77.5, 77.2, 76.8, 75.5, 73.9, 69.2, 62.5, 55.5. HRMS (TOF-MS-ES$^+$) (m/z): $[M^+Na]^+$ calculated for $C_{14}H_{18}O_6Na$, 305.1014; found, 305.1010.

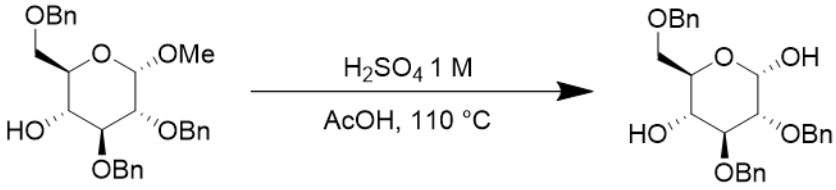
Synthesis of Methyl 2,3,6-tri-O-benzyl-α-D-glucopyranoside (8)



Methyl 2,3-di-O-benzyl-4,6-O-benzylidene-α-D-glucopyranoside (23.5 g, 50.6 mmol, 1 equiv.), sodium cyanoborohydride (28.6 g, 456 mmol, 9 equiv.), anhydrous THF (500 mL) and 3Å molecular sieves (activated, 40 mL) are placed in an oven-dried 1 L round bottom flask and left stirring at room temperature for 45 mins. Then, the reaction is cooled down to 0 °C and aluminium chloride (60.72 g, 455 mmol, 9 equiv.) is added. Then, the reaction is left stirring at room temperature overnight (*ca.* 13 h). TLC analysis (30/70 EtOAc/Hexane, stained with an anisaldehyde/H_2SO_4

solution) indicated the completion of the reaction. The reaction mixture is diluted in dichloromethane, quenched with saturated $NaHCO_3$ solution and filtered on a pad of celite. The organic phase is then washed with saturated $NaHCO_3$ solution, water and brine before being dried over $MgSO_4$ and concentrated under vacuum. The crude yellow oil is purified by chromatography column (7.5 cm width, 20 cm length, 30/70 EtOAc/Hexane) to afford methyl 2,3,6-tri-O-benzyl-α-D-glucopyranoside as a colourless oil (20 g, 43.1 mmol, 84.6%). Characterisation data is consistent with that reported previously.[5] ^{1}H NMR (400 MHz, 298 K, $CDCl_3$, ppm) δ 7.48 – 7.17 (m, 15H, Ar***H***), 5.01 – 4.65 (m, 4H, C***H***$_2$ benzyl), 4.64 (d, *J* = 3.5 Hz, 1H, ***H-1***), 4.63 – 4.52 (m, 2H, C***H***$_2$ benzyl), 3.79 (m, 1H, ***H-3***), 3.74 – 3.67 (m, 3H, ***H-4***, ***H-6***), 3.61 (m, 1H, ***H-5***), 3.54 (dd, *J* = 9.6, 3.6 Hz, 1H, ***H-2***), 3.39 (s, 3H, C***H***$_3$). ^{13}C NMR (101 MHz, 298 K, $CDCl_3$, ppm) δ 138.9, 138.2, 138.1, 128.7, 128.6, 128.5, 128.2, 128.1, 128.1, 128.0, 127.8, 127.7, 98.3, 81.6, 79.7, 77.5, 77.2, 76.8, 75.5, 73.7, 73.3, 70.8, 70.0, 69.6, 55.4. HRMS (TOF-MS-ES$^+$) (m/z): $[M^+NH_4]^+$ calculated for $C_{27}H_{30}O_6NH_4$, 482.2526; found, 482.2526.

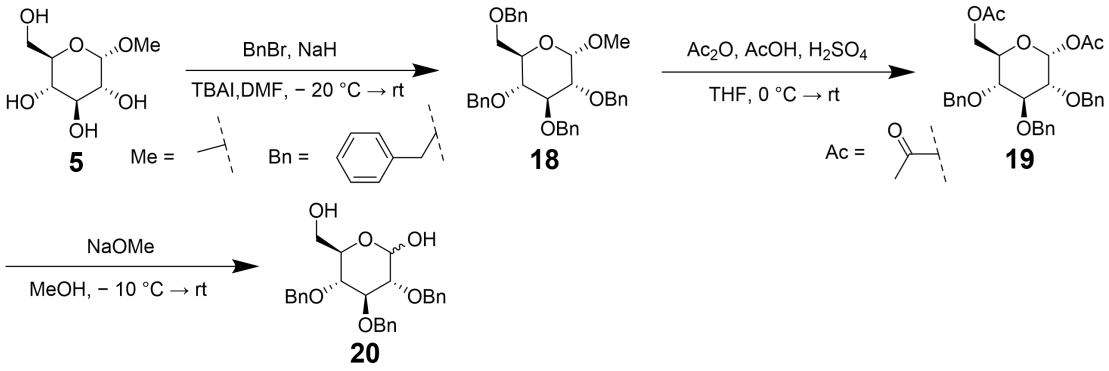
Synthesis of 2,3,6-tri-O-benzyl-D-glucopyranose (9)



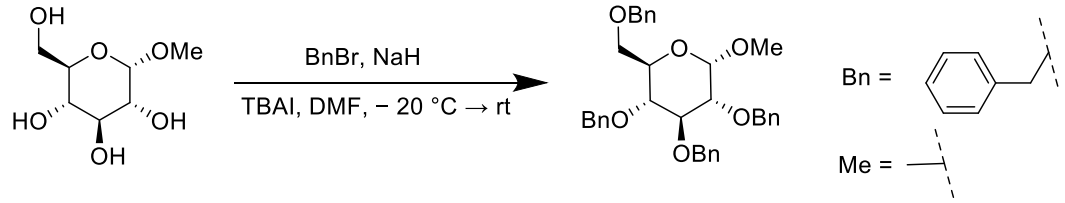
Methyl 2,3,6-tri-O-benzyl-α-D-glucopyranoside (5.0 g, 10.8 mmol, 1 equiv.) is dissolved in glacial acetic acid (25 mL) in an oven-dried 2-neck 100 mL round bottom flask equipped with a waterless condenser (Findenser®) under constant nitrogen flux. The mixture was left stirring at room temperature until the total

dissolution of methyl 2,3,6-tri-O-benzyl-α-D-glucopyranoside, then the temperature is raised to 110 °C and a solution of H_2SO_4 (0.27 mL, 5.07 mmol, 0.5 equiv.) preliminarily diluted in distilled water (5 mL) is added dropwise over the course of 5 mins. The reaction is stopped after 2h30, once only faint traces of the starting material could be observed on TLC (30/70 EtOAc/Hexane, stained with an anisaldehyde/H_2SO_4 solution). The reaction is then quenched with NaOH 1 M solution (60 mL) and extracted with dichloromethane (3×50 mL). The organic phase is washed with brine (3×100 mL) and water (1×100 mL), dried over $MgSO_4$ and concentrated under vacuum to afford a brown oil. The crude is purified by chromatography column (30/70 EtOAc/Hexane, dry loading) and recrystallisation in a mixture of hexane and EtOAc (90:10) to yield 2,3,6-tri-O-benzyl-D-glucopyranose as a mixture of α and β anomers (65% α, 35% β, 1.2 g, 2.7 mmol, 24.7%) Further purification by recrystallisation (Hexane/EtOAc 90/10) affords 2,3,6-tri-O-benzyl-D-glucopyranose as pure α anomer (0.8 g, 1.7 mmol, 16%) . Characterisation data is consistent with that reported previously.[5] α anomer :^{1}H NMR (400 MHz, 298 K, $CDCl_3$, ppm) δ 7.40 – 7.27 (m, 15H, Ar***H***), 5.22 (d, *J* = 3.5 Hz, 1H, ***H-1***), 4.98 (d, *J* = 11.4 Hz, 1H, C***H***$_2$ benzyl, **C-3**), 4.80 – 4.66 (m, 3H, C***H***$_2$ benzyl, ***C-3***, ***C-2***), 4.63 – 4.50 (m, 2H, C***H*** benzyl, ***C-6***), 4.00 (m, 1H, ***H-5***), 3.80 (t, *J* = 9.2 Hz, 1H, ***H-3***), 3.67 (d, *J* = 4.1 Hz, 2H, ***H-6***), 3.60 (m, 1H, ***H-4***), 3.55 (dd, *J* = 9.4, 3.5 Hz, 1H, ***H-2***). ^{13}C NMR (101 MHz, 298 K, $CDCl_3$, ppm) δ 138.8, 138.0, 137.9, 128.7, 128.7, 128.6, 128.6, 128.5, 128.2, 128.1, 128.2, 128.0, 127.9, 127.9, 91.4, 81.2, 79.8, 77.5, 77.2, 76.8, 75.5, 73.8, 73.2, 71.0, 70.2, 69.8. HRMS (TOF-MS-ES+) (m/z): $[M^+NH_4]^+$ calculated for $C_{27}H_{30}O_6NH_4$, 468.2386; found, 468.2390.

Overview - Synthesis of 1,6-glucose diol (20)



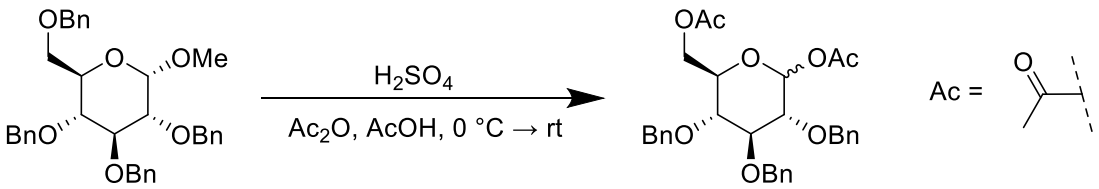
Synthesis of methyl 2,3,4,6-tetra-O-benzyl-α-D-glucopyranoside (18)



NaH (60% in mineral oil, 44.2 g, 1.10 mol, 9 equiv.) is suspended in DMF (600 mL) in an oven-dried 3-neck 1 L round bottom, under a constant nitrogen flux. Then, the reaction media is cooled down to -20 °C using an ice/methanol bath and methyl-α-D-glucopyranoside (23.4 g, 121 mmol, 1 equiv.) is added. The reaction media is left stirring for 30 mins, then TBAI (4.01 g, 14.4 mmol, 0.1 equiv.) and benzyl bromide (85.7 g, 501 mmol, 4 equiv.) are added. The cooling bath is removed, and the temperature is allowed to return to 22 °C. After stirring at room temperature for 3 h, no traces of methyl- methyl-α-D-glucopyranoside could be detected on TLC (30/70 EtOAc/Hexane, stained with an anisaldehyde/H2SO4 solution, R_f product = 0.65), indicating the completion of the reaction. The reaction media is cooled down to -20 °C using an ice/methanol bath and quenched by slowly adding a saturated $NaHCO_3$ solution. The reaction media is then partitioned into 2 fractions, that both

are extracted in diethyl ether (3×500 mL). The organic phases are collected, and the total volume decreased to approximatively 500 mL by removing the solvent under vacuum. The obtained organic phase is then washed with water (3×500 mL) and brine (1×500 mL) before being dried over $MgSO_4$ and concentrated under vacuum. The afforded crude oil is purified by chromatography column (gradient eluant from 90/10 EtOAc/Hexane to 50/50, 8.5 cm width, 20 cm length) to yield methyl 2,3,4,6-tetra-O-benzyl-α-D-glucopyranoside as a yellow oil (54.1 g, 97.5 mmol, 81%). Note: It is possible to perform the reaction on the open atmosphere. However, without Schlenk techniques, the yield decreases to values comprised between 72 to 76%. Characterisation data is consistent with that reported previously.[5] ^{1}H NMR (400 MHz, 298 K, $CDCl_3$, ppm) δ 7.41 – 7.23 (m, 18H, Ar***H***), 7.17 – 7.09 (m, 2H, Ar***H***, ortho, C-3), 5.04 – 4.44 (m, 9H, ***H-1***, C***H***$_2$ benzyl), 3.99 (t, *J* = 9.2 Hz, 1H, ***H-3***), 3.78 – 3.70 (m, 2H, ***H-5***, ***H-6***), 3.68 – 3.60 (m, 2H, ***H-4***, ***H-6***), 3.56 (dd, *J* = 9.6, 3.6 Hz, 1H, ***H-2***), 3.38 (s, 3H, C***H***$_3$). ^{13}C NMR (101 MHz, 298 K, $CDCl_3$, ppm) δ 139.0, 138.4, 138.3, 138.1, 128.7, 128.6, 128.5, 128.5, 128.5, 128.3, 128.1, 128.1, 128.0, 127.8, 127.8, 127.7, 98.4, 82.3, 80.0, 77.8, 77.5, 77.2, 76.8, 75.9, 75.2, 73.6, 73.5, 70.2, 68.6, 55.3. HRMS (TOF-MS-ES+) (m/z): $[M^+Na]^+$ calculated for $C_{35}H_{38}O_6Na$, 577.2566; found, 577.2563.

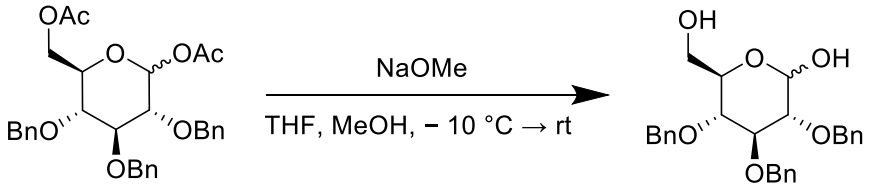
Synthesis of acetyl 2,3,4-tri-O-benzyl-6-acetyl-D-glucopyranoside (19)



Methyl 2,3,4,6-tetra-O-benzyl-α-D-glucopyranoside (54.1 g, 97.5 mmol, 1 equiv.) is dissolved in a mixture of acetic acid (150 mL) and acetic anhydride (150 mL) in a 1 L round bottom flask. The reaction media is cooled down to 0 °C using a water/ice bath and concentrated H_2SO_4 (4 mL, 4.7 mmol, 0.05 equiv.) is added dropwise over the course of 45 mins. The cooling bath is removed, and the temperature is allowed to return to 22 °C. After stirring at room temperature for 4 h, only faint traces of methyl-α-D-glucopyranoside could be detected on TLC (30/70 EtOAc/Hexane, stained with an anisaldehyde/H_2SO_4 solution, R_f product = 0.52). The reaction media is cooled down to -20 °C using a methanol/ice bath and quenched with saturated $NaHCO_3$ (400 mL). The reaction media is then partitioned into 3 fractions, that are each extracted in dichloromethane (3×500 mL). The organic phases are collected, and the total volume decreased to approximatively 500 mL by removing the solvent under vacuum. The obtained organic phase is then washed with water (3×500 mL) and brine (1×500 mL) before being dried over $MgSO_4$ and concentrated under vacuum. The afforded crude oil is purified by chromatography column (30/70 EtOAc/Hexane, 8.5 cm width, 32 cm length) to yield acetyl 2,3,4-tri-O-benzyl-6-acetyl-D-glucopyranoside as a yellow oil (80% α, 20% β, 35.5 g, 66.4 mmol, 68%). Note: The temperature should be carefully monitored during the addition of H_2SO_4 and during the quenching. An increase of temperature above 22 °C will induce the formation of more by-products. Characterisation data is consistent with that reported previously.[5] α anomer: ^{1}H NMR (400 MHz, 298 K, $CDCl_3$, ppm) δ 7.42 – 7.20 (m, 15H, Ar***H***), 6.32 (d, *J* = 3.6 Hz, 1H, ***H-1***), 5.03 – 4.54 (m, 6H, C***H***$_2$ benzyl), 4.32 – 4.22 (m, 2H, ***H-6***), 3.98– 3.90 (m, 2H***, H-3, H-5***), 3.67 (dd, *J* = 9.6, 3.6 Hz, 1H, ***H-2***), 3.57 (m, 1H, ***H-4***), 2.15 (s, 3H, C***H***$_3$, acetate, C-1), 2.03 (s, 3H, C***H***$_3$, acetate, C-6).

^{13}C NMR (101 MHz, 298 K, $CDCl_3$, ppm) δ 170.8, 169.5, 138.6, 137.7, 137.6, 128.7, 128.67, 128.6, 128.3, 128.3, 128.2, 128.2, 128.0, 127.9, 89.8, 81.8, 79.0, 77.5, 77.2, 76.8, 76.7, 75.9, 75.4, 73.4, 71.2, 62.8, 21.2, 21.0. HRMS (TOF-MS-ES$^+$) (m/z): $[M^+Na]^+$ calculated for $C_{31}H_{34}O_8Na$, 557.2151; found, 557.2149.

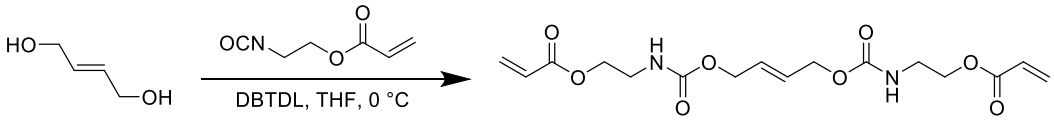
Synthesis of 2,3,4-tri-O-benzyl-D-glucopyranoside (20)



Acetyl 2,3,4-tri-O-benzyl-6-acetyl-D-glucopyranoside (42.9 g, 97.5 mmol, 1 equiv.) is dissolved in a mixture of THF (480 mL) and MeOH (190 mL) in a 1 L round bottom flask. After total dissolution of the starting material, the temperature of the reaction media is decrease to -10 °C, using a methanol/ice bath, and MeONa (25% in MeOH, 18 mL, 65.7 mmol, 0.7 equiv.) is added. Then, the methanol/ice bath is removed, and the reaction is left stirring while the temperature is allowed to increase to 0 °C. After 45 mins, no traces of acetyl 2,3,4-tri-O-benzyl-6-acetyl-D-glucopyranoside could be detected on TLC (30/70 EtOAc/Hexane, stained with an anisaldehyde/H_2SO_4 solution, R_f product = 0.08), indicating the completion of the reaction. The reaction is quenched with saturated $NaHCO_3$ (200 mL) and extracted in EtOAc (1×500 mL). The organic phase is washed with water (3×500 mL) and brine (1×500 mL) before being dried over $MgSO_4$ and concentrated under vacuum. The colourless crude oil is further dried on high vacuum to afford 2,3,4-tri-O-benzyl-D-glucopyranoside as an off-white solid (65% α, 35% β, 35.4 g, 78.7 mmol, 98%). This compound is used without further purification. Note: Another work up method

consist in adding 10 g of Dowex® 50W X8 resin, leave the reaction stirring overnight, filter and concentrate. Purifying the crude by chromatography column does not improve the purity and decrease the yield to 80%. Characterisation data is consistent with that reported previously.[5] α anomer: ^{1}H NMR (400 MHz, 298 K, $CDCl_3$, ppm) δ 7.39 – 7.25 (m, 15H, Ar***H***), 5.19 (t, *J* = 3.1 Hz, 1H, ***H-1***), 4.99 – 4.57 (m, 6H, C***H***$_2$ benzyl), 3.99 – 3.91 (m, 2H, ***H-3, H-5***) 3.83 (m, 2H, ***H-6***), 3.54 (m, 2H, ***H-2***, ***H-4***), 3.25 (d, broad, *J* = 2.8 Hz, 1H, O***H***, C-1), 1.84 (t, broad, *J* = 6.5 Hz, 1H, O***H***, C-1). ^{13}C NMR (101 MHz, 298 K, $CDCl_3$, ppm) δ 138.7, 138.6, 138.4, 138.2, 138.0, 137.9, 128.7, 128.6, 128.6, 128.6, 128.6, 128.3, 128.2, 128.1, 128.1, 128.1, 128.0, 127.9, 127.8, 91.4, 81.7, 80.3, 77.6, 77.5, 77.2, 76.8, 75.8, 75.2, 73.5, 71.2, 62.0. HRMS (TOF-MS-ES$^+$) (m/z): [M$^+$Na]$^+$ calculated for $C_{27}H_{30}O_6Na$, 473.1940; found, 473.1946.

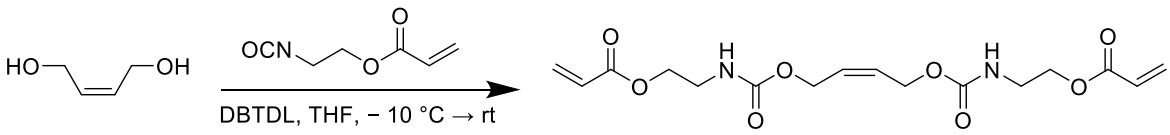
Synthesis of trans diacrylate monomer (25)



An oven-dried 100 mL round bottom flask is charged with THF (25 mL) and freshly distilled *trans* 2-butene-1,4-diol (1) (7.28 g, 82.74 mmol, 1 equiv.). The mixture is degassed under N_2 for 30 min and cooled down to -10 °C using a brine/ice bath. Then, 2-isocyanatoethyl acrylate (24.5 g, 173 mmol, 2.1 equiv.) and dibutyltin(IV) dilaurate (0.104 g, 0.165 mmol, 0.002 equiv.) are added consecutively to the reaction mixture. After the addition, the reaction is left stirring at -10 °C for an additional 30 min before warming to 22 °C. As the reaction progressed, precipitate is often observed, however it could be solubilized by either heating the mixture to

40 °C or by adding additional THF. The reaction completion is monitored using thin layer chromatography (TLC) (90/10 EtOAc/Hexane, stained with potassium permanganate, R_f product = 0.7) and usually complete after 3 h at 22 °C. The solvent is removed *in vacuo* at -8 °C using a Schlenk line and the isolated crude product is purified by recrystallisation in a mixture of EtOAc/Hexane at *ca.* 50 °C followed by a hot filtration step to remove insoluble reaction by-products. Note: heating the acrylate product can induce undesirable crosslinking, hence care should be taken to not heat the compound (or a solution of the compound) over *ca*. 50 °C or for an extended period of time. The target compound is isolated as a white crystalline solid (26.6 g, 71.8 mmol, 88.4%). Characterizing data is consistent with that reported previously.[6] ^{1}H NMR (400 MHz, 298 K, $CDCl_3$, ppm) δ 6.42 (dd, *J* = 17.3, 1.4 Hz, 2H, C***H***H=CHC(O)O), 6.12 (dd, *J* = 17.3, 10.5 Hz, 2H, CHH=C***H***C(O)O), 5.85 (d, *J* = 1.4 Hz, 2H, CH***H***=CHC(O)O), 5.84 – 5.83 (m, 2H, CH_2C***H***=C***H***CH_2), 5.07 (s, 2H, N***H***), 4.57 (s, 4H, CH_2CH=CHC***H***$_2$), 4.24 (t, *J* = 5.3 Hz, 4H, NHCH_2C***H***$_2$O), 3.49 (dt, *J* = 5.4, 5.5 Hz, 4H, NHC***H***$_2$CH_2O). ^{13}C NMR (101 MHz, 298 K, $CDCl_3$, ppm) δ 166.1, 156.2, 131.5, 128.3, 128.0, 64.6, 63.6, 40.3. HRMS (TOF-MS-ES$^+$) (m/z): $[M^+Na]^+$ calculated for $C_{16}H_{22}N_2O_8Na$, 393.1274; found, 393.1282.

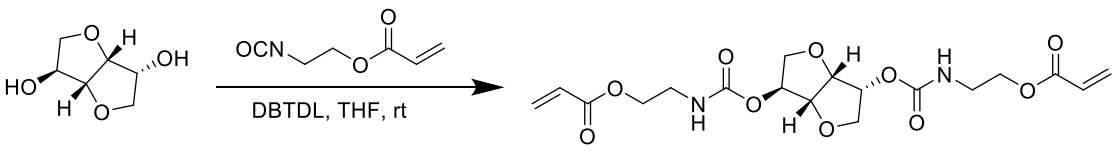
Synthesis of cis diacrylate monomer (24)



An oven-dried 100 mL round bottom flask is charged with THF (25 mL) and *cis*-2-butene-1,4-diol (7.58 g, 86.12 mmol, 1 equiv.). The mixture is degassed under N_2 for 30 min and cooled down to -10 °C using a brine/ice bath. Then, 2-isocyanatoethyl

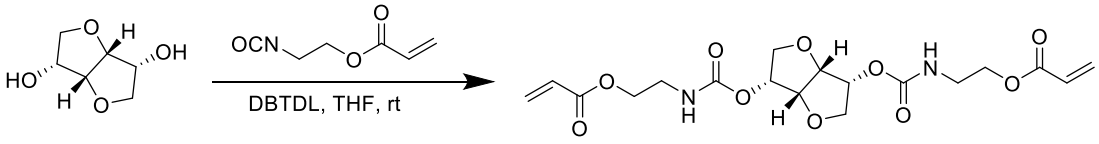
acrylate (25.5 g, 180 mmol, 2.1 equiv.) and dibutyltin(IV) dilaurate (0.108 g, 0.172 mmol, 0.002 equiv.) are added to the reaction mixture. The reaction is stirred at -10 °C for an additional 30 min, then warmed to 22 °C and monitored by TLC (90/10 EtOAc/Hexane, stained with potassium permanganate solution, R_f product = 0.7). The reaction is usually complete after 3 h at 22 °C and the solvent is removed under vacuum at -8 °C using a Schlenk line to afford a white solid. The crude solid is ground into a powder using a pestle and mortar and purified by recrystallisation in a mixture of EtOAc/Hexane at 50 ˚C followed by a hot filtration step. Note: heating the acrylate product can induce undesirable crosslinking, hence care should be taken to not heat the compound or a solution of the compound) over *ca*. 50 °C or for an extended period. The title compound is afforded as a white crystalline solid (28.7 g, 77.6 mmol, 90%). Characterisation data is consistent with that reported previously.[6] ^{1}H NMR (400 MHz, 298 K; $CDCl_3$, ppm) δ 6.42 (dd, *J* = 17.3, 1.4 Hz, 2H, C***H***H=CHC(O)O, 6.12 (dd, *J* = 17.3, 10.4 Hz, 2H, CHH=C***H***C(O)O), 5.86 (dd, *J* = 10.4, 1.4 Hz, 2H CH***H***=CHC(O)O), 5.73 (s, b, 2H, CH2C***H***=C***H***CH2), 5.05 (s, 1H, N***H***), 4.67 (d, *J* = 4.3 Hz, 4H, CH_2CH=CHC***H***$_2$), 4.23 (t, *J* = 5.3 Hz, 4H, $NHCH_2C$***H***$_2O$), 3.49 (dt, *J* = 5.3, 5.5 Hz, 4H, NHC***H***$_2CH_2OC$).^{13}C NMR (101 MHz, 298 K, $CDCl_3$, ppm) δ 166.2, 156.3, 131.6, 128.4, 128.1, 63.7, 60.7, 40.3. HRMS (TOF-MS-ASAP+) (m/z): $[M^+H]^+$ calculated for $C_{16}H_{22}N_2O_8H$, 371.1454; found, 371.1465.

Synthesis of isosorbide- derived diacrylate monomer (26)



An oven-dried 250 ml 2-neck round bottom flask is charged with THF (60 mL), recrystallised isosorbide (17.51 g, 119.8 mmol, 1 equiv.) and 2-isocyanatoethyl acrylate (35.46 g, 251.5 mmol, 2.1 equiv.). Once the isosorbide is fully dissolved, dibutyltin(IV) dilaurate (0.1512 g, 0.24 mmol, 0.002 equiv.) is added to the reaction media. The reaction completion was usually reached after 3 to 4 h, when no traces of isosorbide could be observed by TLC (80/20 EtOAc/Hexane, stained with potassium permanganate solution, R_f product = 0.53). The solvent is removed under vacuum to afford a white solid. The crude solid is ground into a powder using a pestle and mortar and purified by recrystallisation in a mixture of hexane and ethyl acetate (50 mL and 200 mL respectively) at 55 °C. Note: During the reaction, the gelation of the reaction media is often observed. Adding more THF (40 mL) resolves this solubility issue. The title compound is afforded as a white crystalline solid (43.7 g, 102.1 mmol, 85% after 2 sequential recrystallisations). Characterisation data is consistent with that reported previously. [7] ^{1}H NMR (400 MHz, 298 K, $CDCl_3$, ppm) δ 6.43 (dd, overlapping, *J* = 17.3, 1.3 Hz, 2H, C***H***H=CHC(O)O), 6.12 (dd, overlapping, *J* = 17.3, 10.4, Hz, 2H, CHH=C***H***C(O)O), 5.87 (dd, overlapping, *J* = 10.4, 1.5 Hz, 2H, CH***H***=CHC(O)O), 5.23 – 5.03 (m, 4H, C***H***OC(O)N***H***), 4.76 (t, broad, *J* = 4.8 Hz, 1H, CH_2OC***H***CHO), 4.49 (d, *J* = 4.4 Hz, 1H, CHOC***H***OCH_2), 4.24 (t, *J* = 5.5,Hz, 4H, NHCH_2C***H***$_2$O), 4.07 – 3.92 (m, 3H, OC***H***$_2$CHO and CHOC***H***HO), 3.71 (m, 1H, CHOCH***H***O), 3.50 (m, 4H, NHC***H***$_2$$CH_2$O). ^{13}C NMR (101 MHz, 298 K, $CDCl_3$, ppm) δ 166.1, 155.6, 155.3, 131.7, 128.0, 86.0, 81.1, 78.8, 77.5, 77.2, 76.8, 74.6, 73.9, 70.1, 63.5, 40.4.

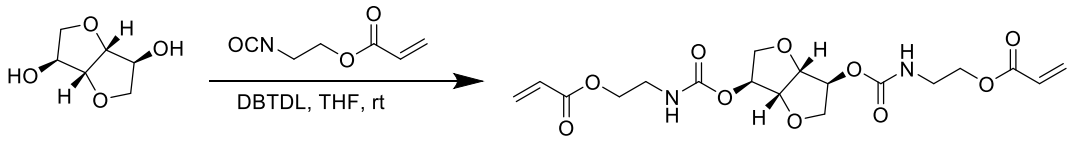
Synthesis of isomannide-derived diacrylate (27)



An oven-dried 250 ml 2-neck round bottom flask is charged with THF (100 mL), isomannide (17.51 g, 119.8 mmol, 1 equiv.) and 2-isocyanatoethyl acrylate (35.48 g, 251.6 mmol, 2.1 equiv.). To achieve total dissolution of isomannide, DMF (30 mL) is added to the reaction media. Then, dibutyltin(IV) dilaurate (0.1512 g, 0.24 mmol, 0.002 equiv.) is diluted in THF (10 mL) and then is added to the reaction media. The reaction completion ~~is~~ usually reached after 24 h, when no traces of isomannide could be observed by TLC (80/20 EtOAc/Hexane, stained with potassium permanganate solution, R_f product = 0.48). The solvent is removed under vacuum to afford a white solid. The crude solid is ground into a powder using a pestle and mortar and purified by recrystallisation in a mixture of hexane and ethyl acetate (150 mL and 350 mL respectively) at 60 °C. Notes: The isomannide will not dissolve in THF at room temperature (22 °C) at the concentration of 1.2 M unless some DMF is added. The title compound is afforded as a white crystalline solid (41.2 g, 96.3 mmol, 80% after 2 sequential recrystallisations). Note: The reaction can still reach completion without the complete solubilisation of isomannide in 24 h.Characterisation data is consistent with that reported previously. [7] ^{1}H NMR (400 MHz, 298 K, $CDCl_3$, ppm) δ 6.42 (dd, *J* = 17.3, 1.4 Hz, 2H, C***H***H=CHC(O)O), 6.11 (dd, *J* = 17.3, 10.4 Hz, 2H, CHH=C***H***C(O)O), 5.86 (dd, *J* = 10.5, 1.4 Hz, 2H, CH***H***=CHCOH), 5.22 (s, broad, 2H, N***H***), 5.13 – 5.06 (m, 2H, CHC***H***OCH_2), 4.66 (d, broad, *J* = 3.8 Hz, 2H, CH_2OC***H***COH), 4.24 (t, *J* = 5.3 Hz, 4H, NHCH_2C***H***$_2$O), 4.05 (dd, *J* = 9.2, 6.5 Hz, 2H, CHOC***H***HO), 3.76 (dd, *J* = 9.2, 6.5 Hz, 2H, CHOCH***H***O),

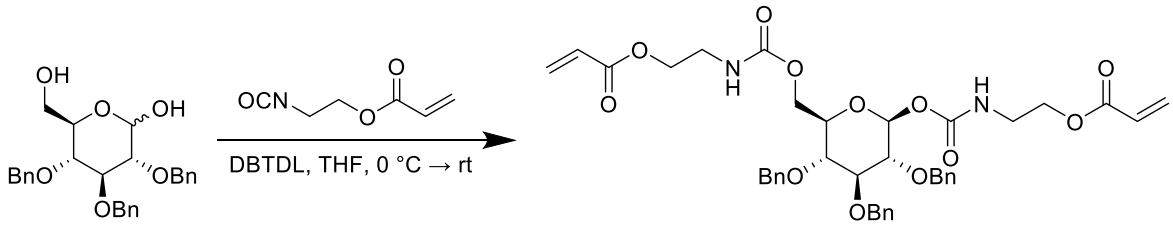
3.50 (m, 4H, NHC***H***$_2$CH$_2$O). ^{13}C NMR (101 MHz, 298 K, $CDCl_3$, ppm) δ 166.1, 155.6, 131.7, 128.0, 81.0, 77.5, 77.2, 76.8, 74.4, 70.6, 63.5, 40.4.

Synthesis of isoidide-derived diacrylate (28)



An oven-dried 100 ml 2-neck round bottom flask is charged with THF (30 mL), isoidide (4.75 g, 33.9 mmol, 1 equiv.) and 2-isocyanatoethyl acrylate (10.04 g, 71.2 mmol, 2.1 equiv.). Once the isoidide is fully dissolved, dibutyltin(IV) dilaurate (0.043 g, 0.00678 mmol, 0.002 equiv.) is added to the reaction media. Then, the reaction is left stirring at room temperature overnight (*ca.* 16 h). Once no traces of isoidide could be observed by TLC, most of the solvent is removed under vacuum and cyclohexane (200 mL) is added to the crude, causing the formation of a white precipitate. The crude is left stirring in cyclohexane before being filtered. The afforded white solid is washed with cyclohexane and purified by recrystallisation in a mixture of hexane and ethyl acetate at 60 °C (11.6 g, 27.11 mmol, 80%). Characterisation data is consistent with that reported previously.[3] ^{1}H NMR (400 MHz, 298 K, $CDCl_3$, ppm) δ 6.37 (dd, *J* = 17.3, 1.4 Hz, 2H, C***H***H=CHC(O)O), 6.06 (dd, *J* = 17.3, 10.5 Hz, 2H, CHH=C***H***C(O)O), 5.81 (dd, *J* = 10.5, 1.4 Hz, 2H, CH***H***=CHC(O)O), 5.23 – 4.73 (m, 4H, C***H***OC(O)N***H***), 4.54 (s, broad, 2H, CH$_2$OC***H***COH), 4.18 (t, broad, *J* = 5.2 Hz, 4H, NHCH$_2$C***H***$_2$O), 3.96 – 3.77 (m, 4H, CHOC***H***$_2$O), 3.43 (q, *J* = 5.5 Hz, 4H, NHC***H***$_2$CH$_2$O). ^{13}C NMR (101 MHz, 298 K, $CDCl_3$, ppm) δ 166.2, 155.2, 131.7, 128.0, 85.5, 78.3, 77.5, 77.2, 76.8, 72.8, 63.5, 40.4.

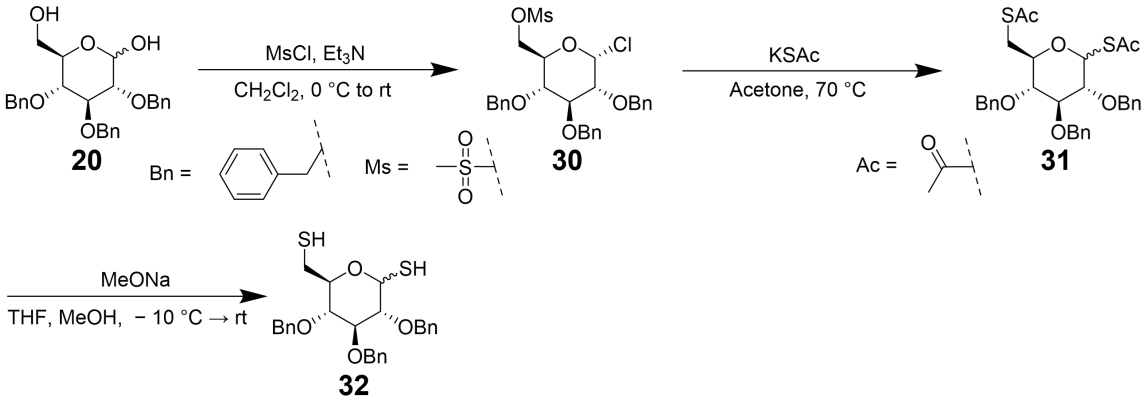
Synthesis of 1,6-glucose diacrylate (29)



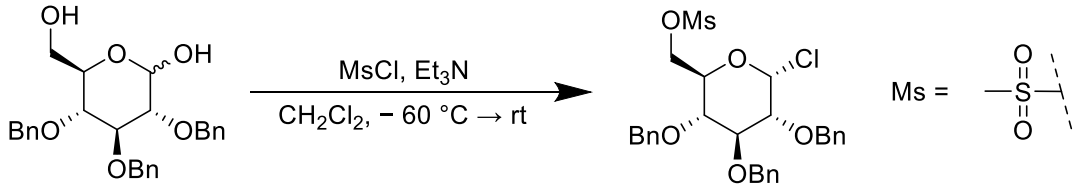
An oven-dried 100 mL round bottom flask is charged with THF (38 mL), 2,3,6-tri-O-benzyl-D-glucopyranoside (7.3 g, 16.2 mmol, 1 equiv.) and 2-isocyanatoethyl acrylate (4.8 g, 34.1 mmol, 2.1 equiv.). The reaction media is cooled down to 0 °C using a water/ice bath and dibutyltin(IV) dilaurate (0.030 g, 0.032 mmol, 0.002 equiv.) is added to the reaction mixture. After 10 mins of stirring at 0 °C, the water/ice bath is removed, allowing the temperature to return to 22 °C. The reaction is left stirring overnight (*ca.* 12 h). TLC analysis indicated the completion of the reaction as no traces of starting material could be detected (80/20 EtOAc/Hexane, stained with a potassium permanganate solution, R_f product = 0.68). The solvent is removed under vacuum to afford a white solid. The crude is purified by chromatography column (80/20 EtOAc/Hexane) and recrystallisation in a mixture of ethyl acetate and hexane to yield the 1,6-glucose diacrylate monomer as a white solid (100% β, 7.1 g, 9.7 mmol, 60%). ^{1}H NMR (400 MHz, 298 K, $CDCl_3$, ppm) δ 7.38 – 7.21 (m, 15H, Ar***H***), 6.42 (d, *J* = 17.3, 0.9 Hz, 2H, C***H***H=CHC(O)O), 6.11 (dd, overlapping, *J* = 10.4, 2.9 Hz, 2H, CHH=C***H***C(O)O), 5.85 (dd, overlapping, *J* = 3.5, 1.4 Hz, 2H, CH***H***=CHC(O)O), 5.57 (d, *J* = 8.2 Hz, 1H, ***H-1***), 5.02 (m, 2H, N***H***), 4.92 – 4.58 (6H, C$\boldsymbol{H}_2$ benzyl), 4.38 – 4.27 (m, 2H, ***H-6***), 4.23 (dt, *J* = 12.0, 5.3 Hz, 4H, NHCH$_2$C$\boldsymbol{H}_2$O), 3.75 (t, *J* = 9.0 Hz, 1H, ***H-3***), 3.63 (m, 1H, ***H-5***), 3.59 – 3.38 (m, 6H, ***H-2***, ***H-4***, NHC$\boldsymbol{H}_2$CH$_2$O). ^{13}C NMR (101 MHz, 298 K, $CDCl_3$, ppm) δ 166.1, 154.2, 138.3,

138.2, 137.7, 131.8, 131.6, 128.7, 128.6, 128.5, 128.4, 128.2, 128.1, 128.0, 127.9, 95.2, 84.8, 81.2, 77.5, 77.2, 76.8, 76.0, 75.2, 75.2, 74.1, 63.7, 63.4, 40.4, 40.3. HRMS (TOF-MS-ES$^+$) (m/z): $[M^+Na]^+$ calculated for $C_{39}H_{44}N_2O_{12}Na$, 755.2792; found, 755.2802.

Overview - Synthesis of 1,6-glucose dithiol (32)



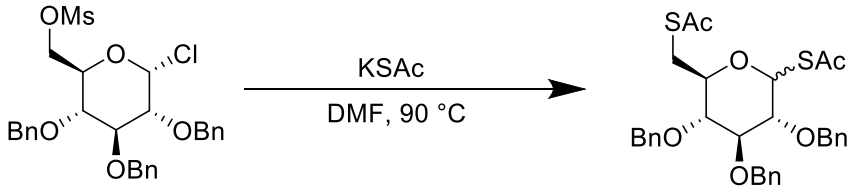
Synthesis of 2,3,4-tri-O-benzyl-6-O-methanesulfonyl-α-D-glucopyranosyl chloride (30)



2,3,4-tri-O-benzyl-D-glucopyranoside (37.8 g, 84 mmol, 1 equiv.) is dissolved in dichloromethane (200 mL) in a 500 mL round bottom flask. After total dissolution of the starting material, the temperature of the reaction media is decrease to -60 °C, using an acetone/dry ice bath and Et_3N (47 mL, 336 mmol, 4 equiv.) is added to the reaction vessel. Then, methanesulfonyl chloride (26 mL, 336 mmol, 4 equiv.) is

added dropwise over the course of 1 h. The cooling bath is removed, allowing the temperature to return to 22 °C. After 24 h, no traces of 2,3,4-tri-O-benzyl-D-glucopyranoside could be seen on TLC (30/70 EtOAc/Hexane, stained with an anisaldehyde/H_2SO_4 solution, R_f product = 0.37), indicating the completion of the reaction. The temperature of the reaction media is decreased to -10 °C using a brine/ice bath. The reaction is quenched with saturated $NaHCO_3$ (200 mL). The organic phase is collected and washed with water (1×200 mL) and brine (1×200 mL) before being dried over $MgSO_4$ and concentrated under vacuum to afford 2,3,4-tri-O-benzyl-6-O-methanesulfonyl-α-D-glucopyranosyl chloride as a yellow oil (100% α, 45 g, 83.1 mmol, 99%). This compound is used without further purification. Note: Purifying the crude by chromatography column (30/70 EtOAc/Hexane) does not improve the purity and decrease the yield to 98%. The reaction reaches completion after 2-3 h, however, leaving the reaction stirring for 24 h, afford 100% of the α anomer. ^{1}H NMR (400 MHz, 298 K, $CDCl_3$, ppm) δ 7.91 – 6.82 (m, 15H, Ar***H***), 6.01 (d, *J* = 3.8 Hz, 1H, ***H-1***), 5.05 – 4.58 (m, 6H, C***H***$_2$ benzyl), 4.44 (dd, *J* = 11.3, 3.8 Hz, 1H, ***H-6***), 4.35 (dd, *J* = 11.4, 2.0 Hz, 1H, ***H-6***), 4.21 – 4.15 (m, 1H, ***H-5***), 4.07 (t, *J* = 9.2 Hz, 1H, ***H-3***), 3.71 (dd, *J* = 9.4, 3.8 Hz, 1H, ***H-2***), 3.59 (dd, *J* = 10.2, 8.9 Hz, 1H, ***H-4***), 2.98 (s, 3H, C***H***$_3$ mesylate). ^{13}C NMR (101 MHz, 298 K, $CDCl_3$, ppm) δ 138.3, 137.6, 137.3, 128.9, 128.8, 128.7, 128.6, 128.4, 128.3, 128.3, 128.2, 128.1, 128.0, 92.7, 81.2, 79.8, 77.5, 77.2, 76.8, 76.0, 75.7, 75.5, 73.2, 71.8, 67.6, 37.8. HRMS (TOF-MS-ES-) (m/z): $[M - H]^+$ calculated for $C_{28}H_{30}{}^{35}ClO_7S$, 545.1414; found, 545.1414.

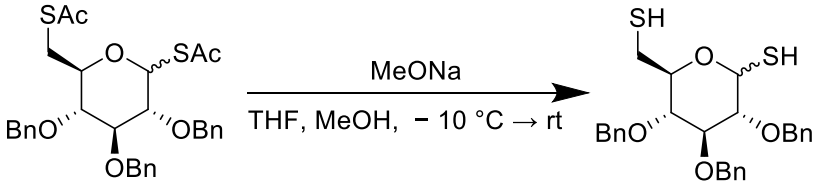
Synthesis of acetyl 2,3,4-tri-O-benzyl-1,6-dithio-6- acetyl-D-glucopyranoside (31)



2,3,4-tri-O-benzyl-6-O-methanesulfonyl-α-D-glucopyranosyl chloride (42 g, 74.2 mmol, 1 equiv.) is dissolved in DMF (400 mL) in a 1 L round bottom flask. Then, potassium thioacetate (51 g, 447 mmol, 6 equiv.) is added to the reaction vessel. A waterless condenser (Findenser®) is fitted to the round bottom flask and the temperature of the reaction increased to 90 °C. After 1 h 45, no starting material could be detected on TLC (30/70 Et_2O/Hexane, stained with an anisaldehyde/H_2SO_4 solution, R_f product = 0.16), indicating the completion of the reaction). The reaction media is cooled down to 0 °C using a water/ice bath and quenched with saturated $NaHCO_3$ (400 mL). The reaction media is then partitioned into 3 fractions, that are each extracted in Et_2O (3×500 mL). The organic phases are collected, and the total volume decreased to approximatively 500 mL by removing the solvent under vacuum. The obtained organic phase is then washed with water (2×500 mL) and brine (1×500 mL) before being dried over $MgSO_4$ and concentrated under vacuum to afford a burgundy oil. The crude is purified by chromatography column (30/70 Et_2O/Hexane) and recrystallisation in a mixture of EtOAc (80 mL) and Hexane (400 mL) to yield acetyl 2,3,4-tri-O-benzyl-1,6-dithio-6- acetyl-D-glucopyranoside as brown-red crystals (100% β, 18.0 g, 31.8 mmol, 43%). It is possible to purify the crude by recrystallisation only, however, the yield decrease to 35% and the product recovered as a mixture of α and β anomer in a 35:65 ratio. α anomer: ^1H NMR (400

MHz, 298 K, $CDCl_3$, ppm) δ 7.41 – 7.22 (m, 15H, Ar***H***), 5.12 (d, *J* = 10.2 Hz, 1H, ***H-1***), 4.93 – 4.61 (m, 6H, C***H***$_2$ benzyl), 3.75 (t, *J* = 8.9 Hz, 1H, ***H-3***), 3.60 (ddd, *J* = 9.8, 7.0, 3.0 Hz, 1H, ***H-5***), 3.54 – 3.45 (m, 2H, ***H-2***, ***H-6***), 3.40 (t, *J* = 9.2 Hz, 1H, ***H-4***), 3.04 (dd, *J* = 13.8, 7.0 Hz, 1H, ***H-6***), 2.38 (s, 3H, C***H***$_3$, thioacetate, C-1), 2.34 (s, 3H, C***H***$_3$, thioacetate, C-6). ^{13}C NMR (101 MHz, 298 K, $CDCl_3$, ppm) δ 195.13, 192.59, 138.31, 137.83, 137.80, 128.65, 128.62, 128.52, 128.36, 128.12, 127.99, 127.95, 127.92, 86.65, 81.66, 80.44, 80.11, 78.45, 77.48, 77.16, 76.84, 75.92, 75.56, 75.35, 31.04, 30.98, 30.67. HRMS (TOF-MS-ES$^+$) (m/z): $[M^+Na]^+$ calculated for $C_{31}H_{34}O_6S_2Na$, 589.1708; found, 589.1707.

Synthesis of 2,3,4-tri-O-benzyl-1,6-dithio-D-glucopyranose (32)



Acetyl 2,3,4-tri-O-benzyl-1,6-dithio-6-acetyl-D-glucopyranoside (10 g, 17.7 mmol, equiv.) is dissolved in a mixture of THF (150 mL) and MeOH (50 mL) in a 500 mL round bottom flask. After total dissolution of the starting material, the temperature of the reaction media is decrease to -10 °C, using a methanol/ice bath, and MeONa (25% in MeOH, 5 mL, 18.3 mmol, 1 equiv.) is added dropwise over 5 mins. Then, the methanol/ice bath is removed, and the reaction is left stirring while the temperature is allowed to return to room temperature. After 1h15, no traces of Acetyl 2,3,4-tri-O-benzyl-1,6-dithio-6- acetyl-D-glucopyranoside could be detected on TLC (30/70 EtOAc/Hexane, stained with an anisaldehyde/H_2SO_4 solution, R_f product = 0.8), indicating the completion of the reaction. The reaction is quenched

with saturated $NaHCO_3$ (100 mL) and extracted in EtOAc (3×150 mL). The organic phase is washed with water (3×150 mL) and brine (1 $NH_4$150 mL) before being dried over $MgSO_4$ and concentrated under vacuum to afford a brown oil. The crude is purified by chromatography column (30/70 EtOAc/Hexane) and recrystallised (EtOAc/Hexane) to afford 2,3,4-tri-O-benzyl-1,6-dithio-ɒ-glucopyranoside as a white crystalline solid (100% β, 2.75 g, 5.7 mmol, 32%). Note: Monitoring the reaction by ^{1}H NMR proved to be more convenient than by thin layer chromatography as the product and the starting materials have the same R_f in (30/70 EtOAc/Hexane). ^{1}H NMR (400 MHz, 298 K, $CDCl_3$, ppm) δ 7.41 – 7.25 (m, 15H, Ar***H***), 4.99 – 4.63 (m, 6H, C***H***$_2$ benzyl), 4.55 (dd, *J* = 9.5, 8.0 Hz, 1H, ***H-1***), 3.68 (t, *J* = 8.8 Hz, 1H, ***H-3***), 3.61 (t, *J* = 9.1 Hz, 1H, ***H-4***), 3.44 (ddd, *J* = 9.2, 6.3, 2.8 Hz, 1H, ***H-5***), 3.37 (dd, *J* = 9.5, 8.7 Hz, 1H, ***H-2***), 2.92 (ddd, *J* = 14.1, 8.5, 2.8 Hz, 1H, ***H-6***), 2.64 (ddd, *J* = 14.1, 8.4, 6.3 Hz, 1H, ***H-6***), 2.28 (d, *J* = 8.0 Hz, 1H, S***H***, C-1), 1.68 (t, *J* = 8.4 Hz, 1H, S***H***, C-6). ^{13}C NMR (101 MHz, 298 K, $CDCl_3$, ppm) δ 138.37, 137.94, 137.83, 128.70, 128.64, 128.62, 128.41, 128.17, 128.15, 127.93, 127.88, 86.49, 85.09, 79.86, 79.79, 79.27, 77.48, 77.16, 76.84, 75.86, 75.84, 75.33, 26.45. HRMS (TOF-MS-ES$^+$) (m/z): $[M^+NH_4]^+$ calculated for $C_{27}H_{30}O_4S_2NH_4$, 500.1943; found, 500.1938.

1.18.3 NMR spectra of monomer diols and intermediates

^{1}H and ^{13}C NMR spectra of trans butene-1,4-diol (1)

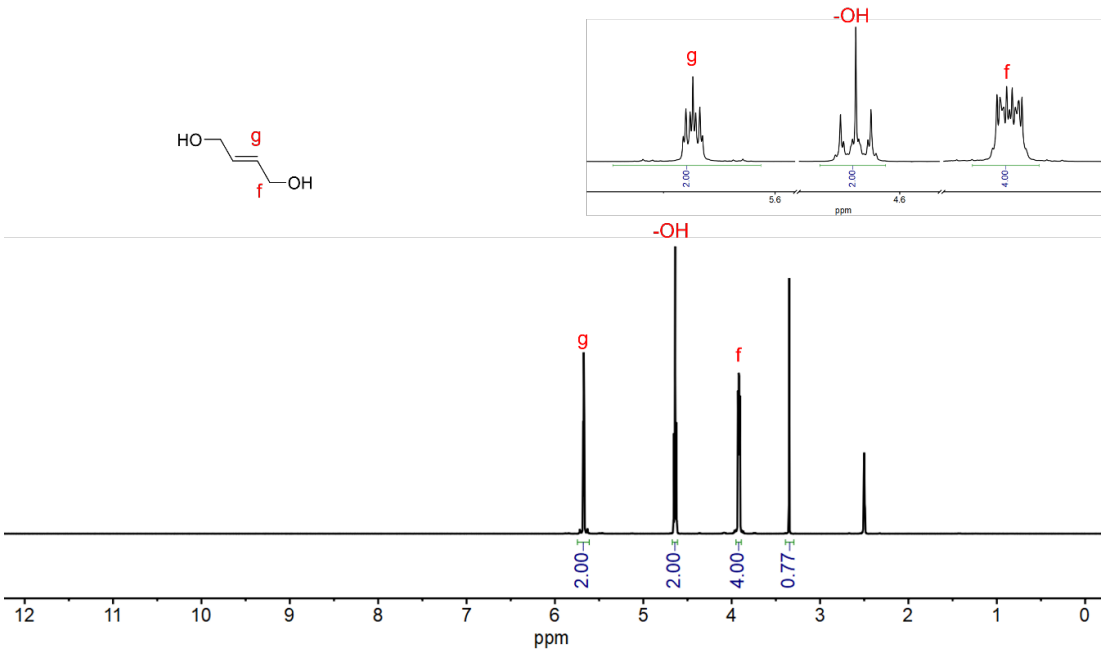


Figure A 2.1. *^{1}H NMR (400 MHz, 298 K, d_6-DMSO) spectrum of the trans-2-butene-1,4-diol (**1**).*

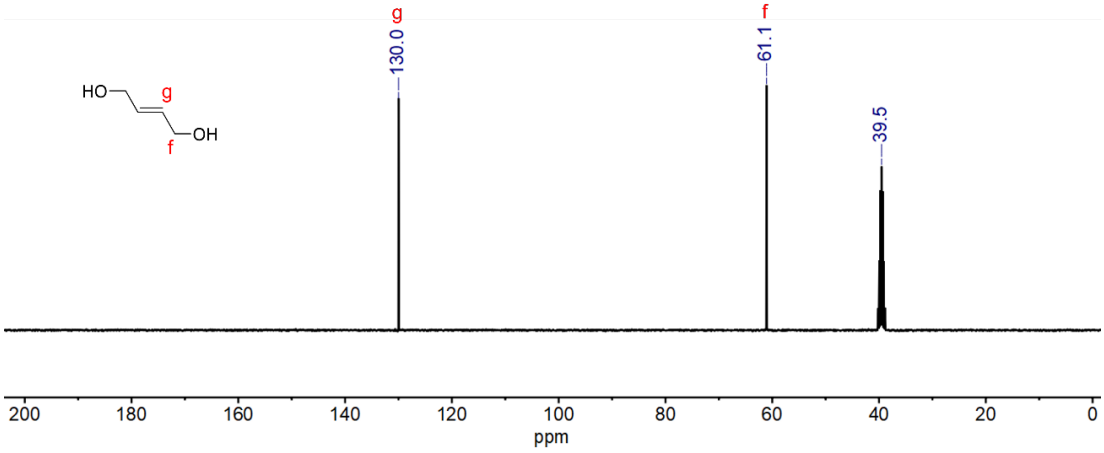


Figure A 2.2. *^{13}C NMR (101 MHz, 298 K, d_6-DMSO) spectrum of the trans 2-butene-1,4-diol (**1**)*

^{1}H and ^{13}C NMR spectra of tosylated isomannide (2)

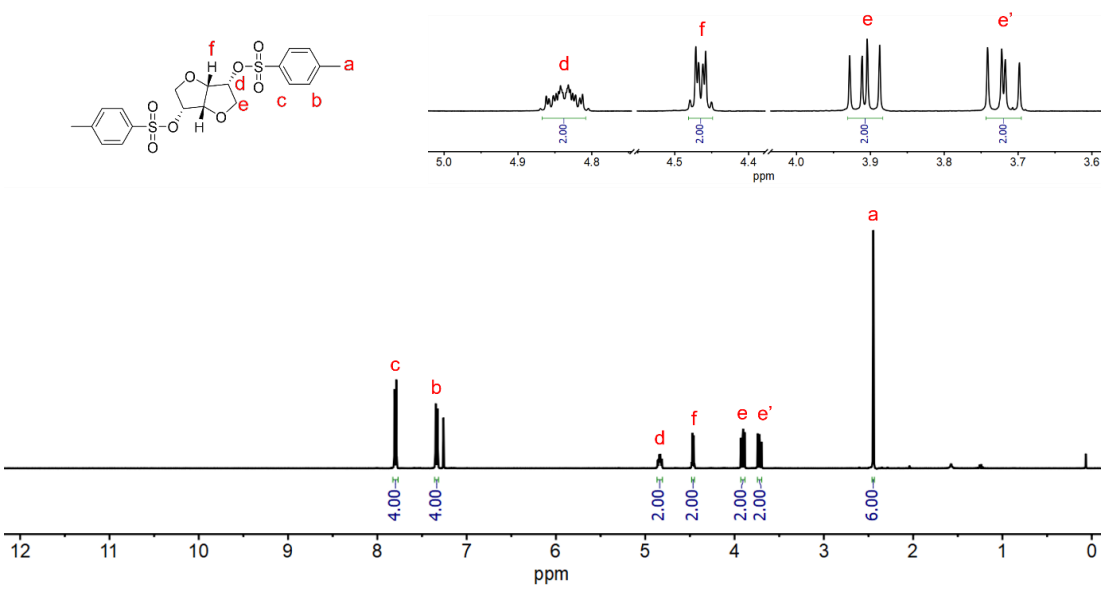


Figure A 2.3. *^{1}H NMR (400 MHz, 298 K, $CDCl_3$) spectrum of tosylated isomannide (**2**).*

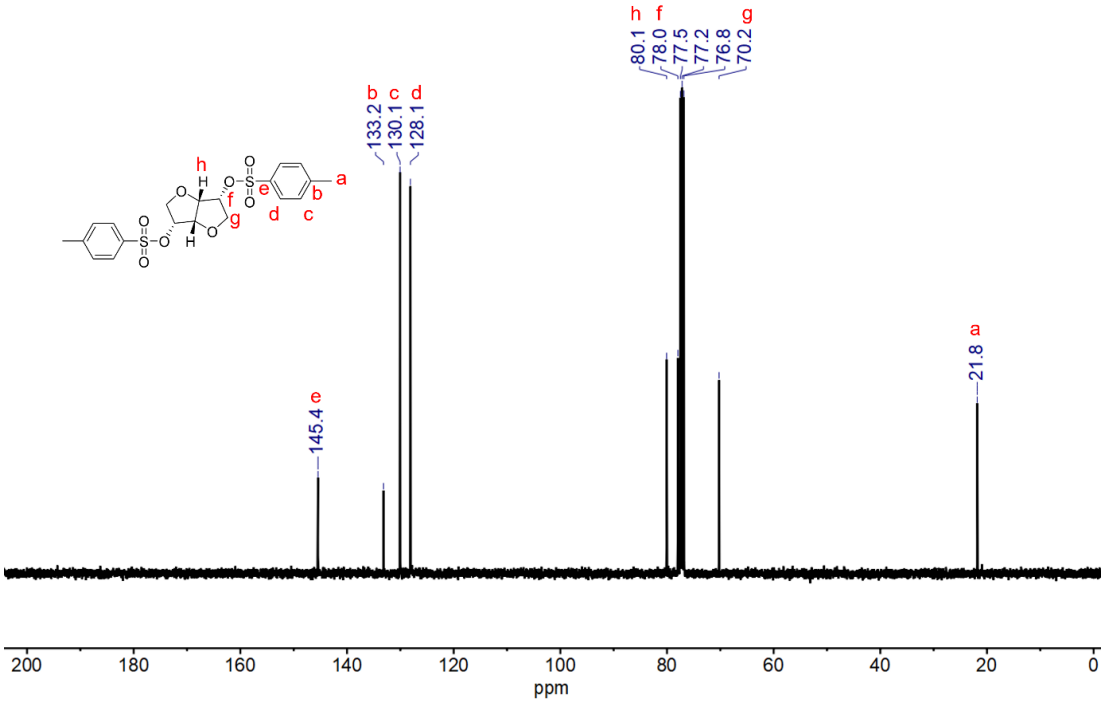


Figure A 2.4. *^{13}C NMR (101 MHz, 298 K, $CDCl_3$) spectrum of the tosylated isomannide (**2**).*

^{1}H and ^{13}C NMR spectra of acetylated isoidide (3)

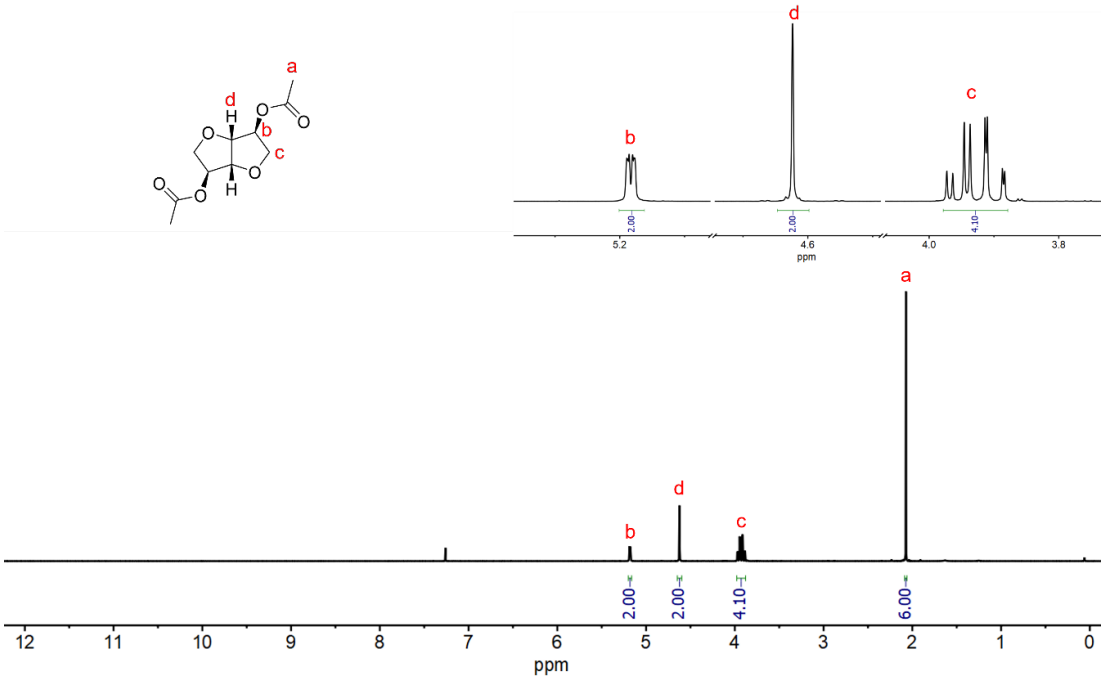


Figure A 2.5. *^{1}H NMR (400 MHz, 298 K, $CDCl_3$) spectrum of acetylated isoidide (**3**).*

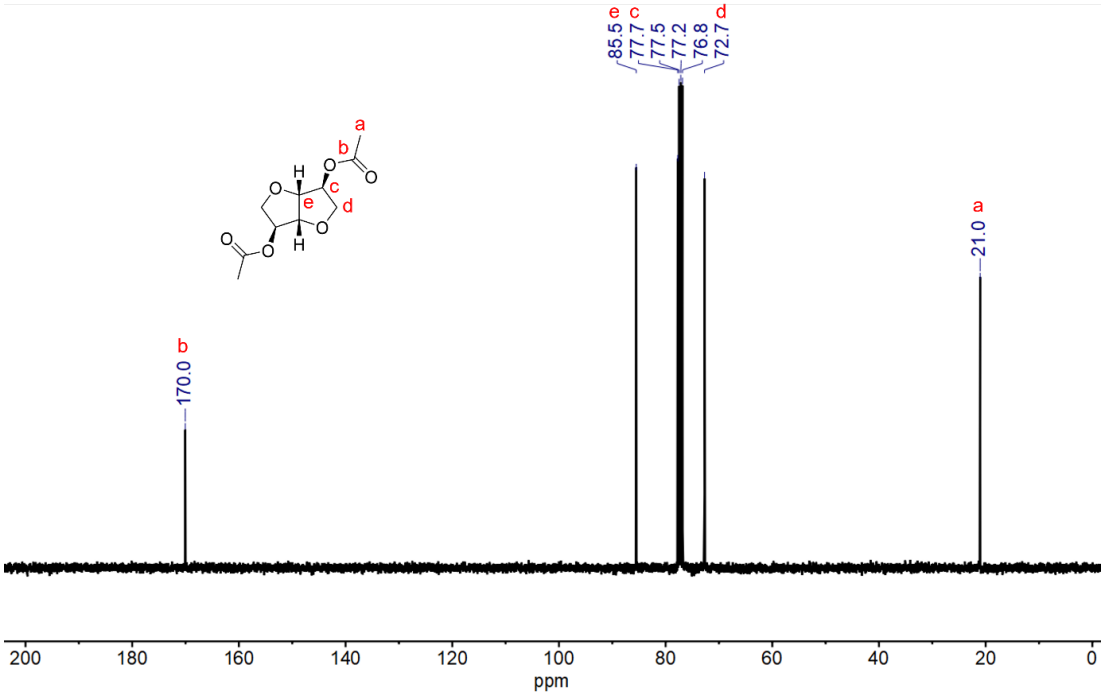


Figure A 2.6. *^{13}C NMR (101 MHz, 298 K, $CDCl_3$) spectrum of the acetylated isoidide (**3**).*

^{1}H and ^{13}C NMR spectra of isoidide (4)

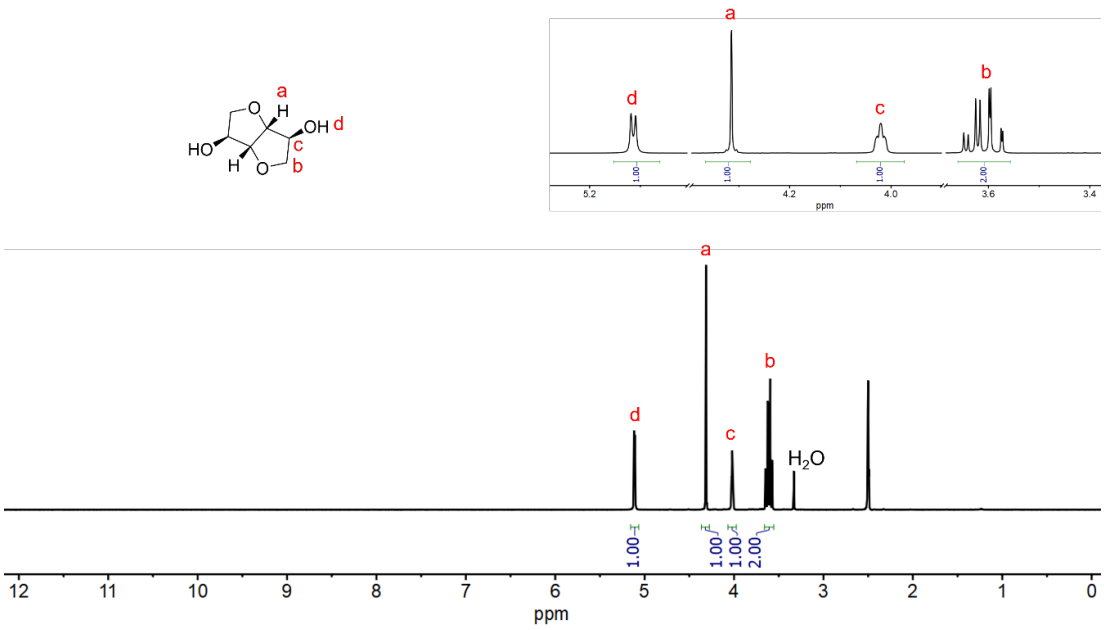


Figure A 2.7. *^{1}H NMR (400 MHz, 298 K, d_6-DMSO) spectrum of isoidide (**4**).*

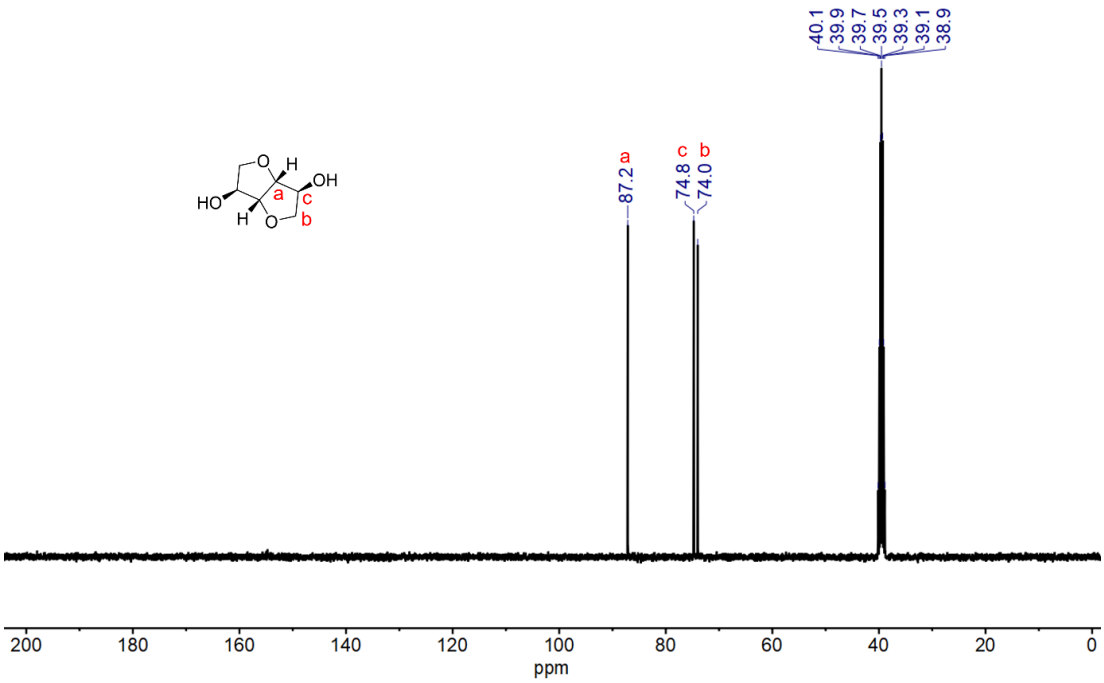


Figure A 2.8. *^{13}C NMR (101 MHz, 298 K, d_6-DMSO) spectrum of the isoidide (**4**).*

^{1}H, ^{13}C and 2D NMR spectra of methyl 4,6-O-benzylidene-α-D-glucopyranoside (6)

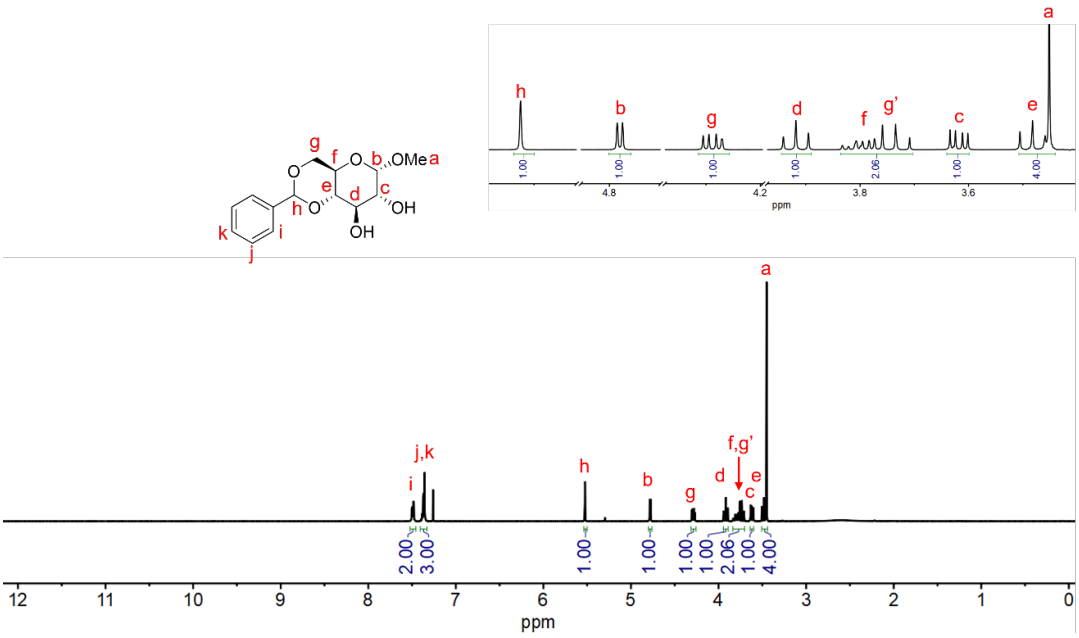


Figure A 2.9. *^{1}H NMR (400 MHz, 298 K, $CDCl_3$) spectrum of methyl 4,6-O-benzylidene-α-D-glucopyranoside (**6**).*

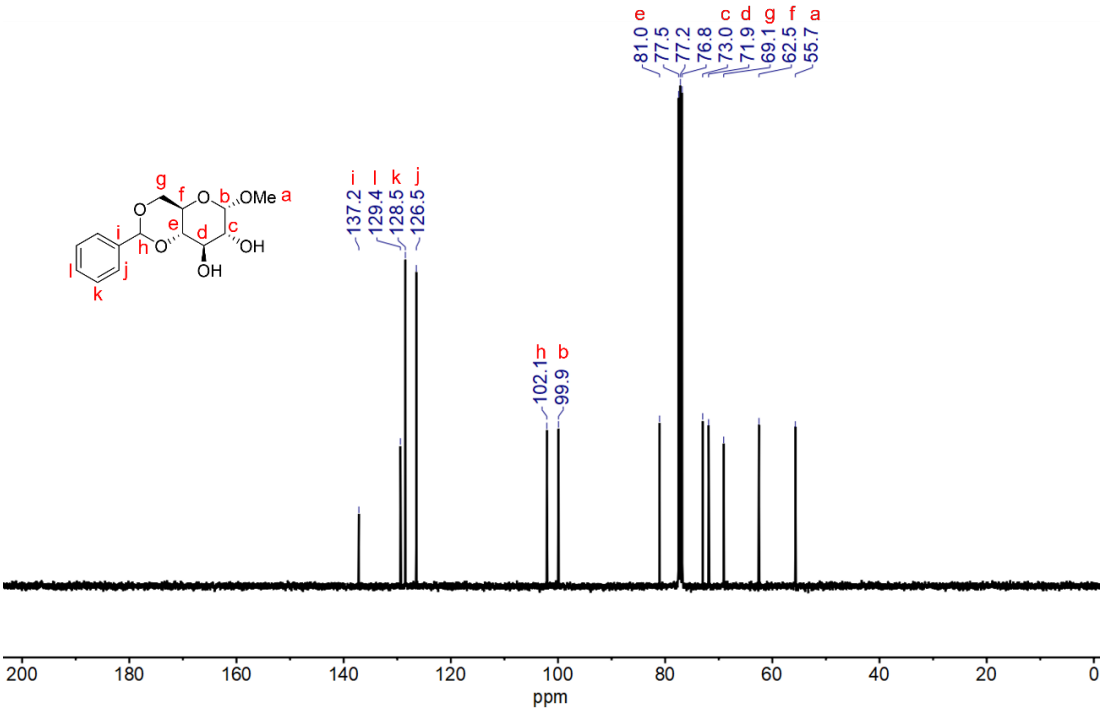


Figure A 2.10. *^{13}C NMR (101 MHz, 298 K, $CDCl_3$) spectrum of methyl 4,6-O-benzylidene-α-D-glucopyranoside (**6**).*

^{1}H, ^{13}C and 2D NMR spectra of methyl 2,3-di-O-benzyl-4,6-O-benzylidene-α-D-glucopyranoside (7)

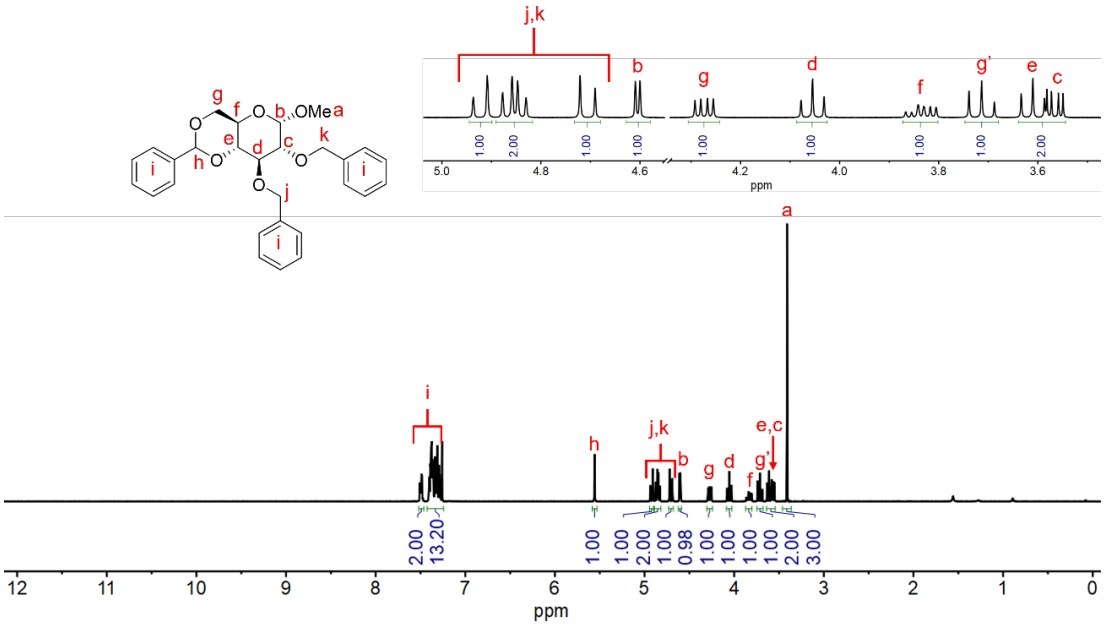


Figure A 2.11. *1H NMR (400 MHz, 298 K, $CDCl_3$) spectrum of methyl 2,3 di-O-benzyl-4,6-O-benzylidene-α-D-glucopyranoside (**7**).*

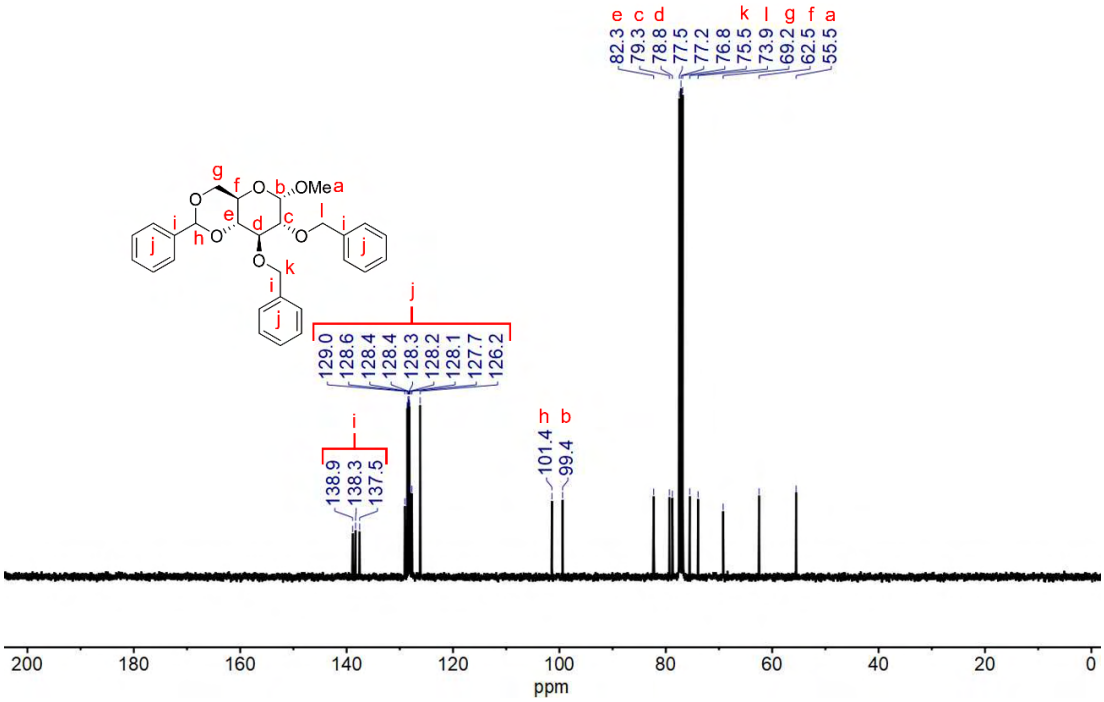


Figure A 2.12. *^{13}C NMR (101 MHz, 298 K, $CDCl_3$) spectrum of methyl 2,3 di-O-benzyl-4,6-O-benzylidene-α-D-glucopyranoside (**7**).*

^{1}H, ^{13}C and 2D NMR spectra of methyl 2,3,6-tri-O-benzyl-α-D-glucopyranoside (8)

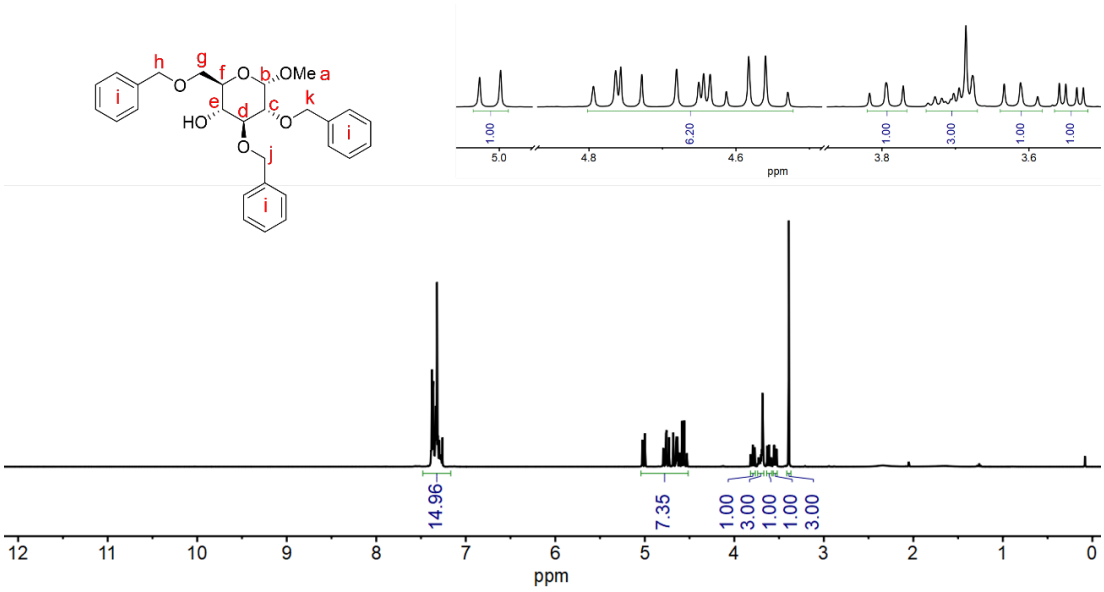


Figure A 2.13. *^{1}H NMR (400 MHz, 298 K, $CDCl_3$) spectrum of methyl 2,3,6-tri-O-benzyl-α-D-glucopyranoside (**8**).*

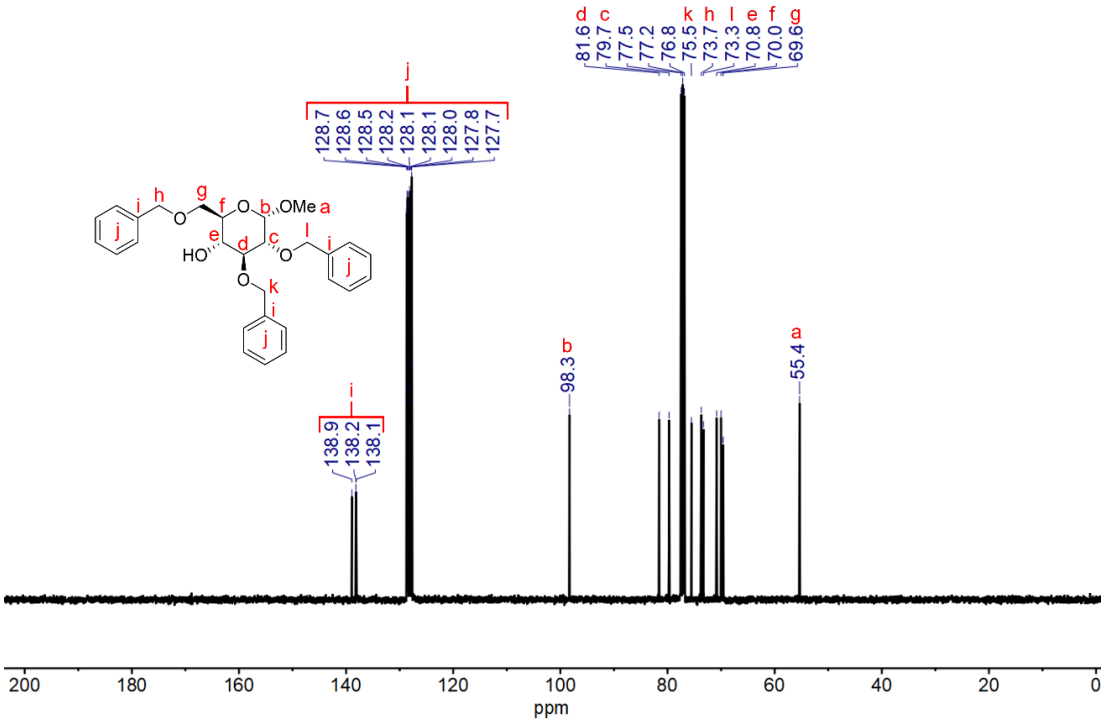


Figure A 2.14. *^{13}C NMR (101 MHz, 298 K, $CDCl_3$) spectrum of methyl 2,3,6-tri-O-benzyl-α-D-glucopyranoside (**8**).*

^{1}H, ^{13}C and 2D NMR spectra of 2,3,6-tri-O-benzyl-α-D-glucopyranose (9)

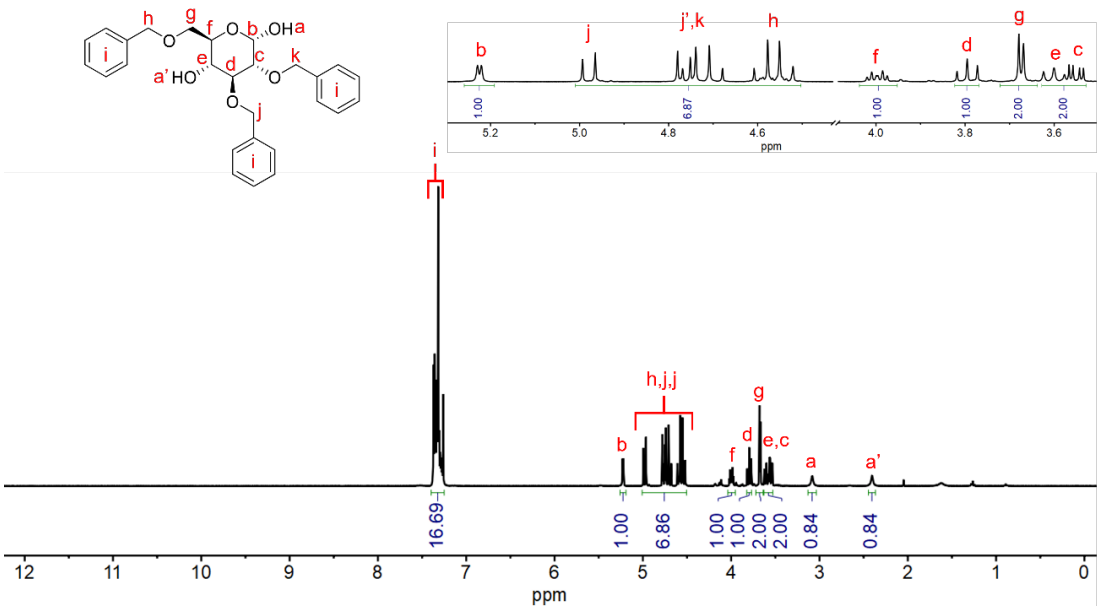


Figure A 2.15. *^{1}H NMR (400 MHz, 298 K, $CDCl_3$) spectrum of 2,3,6-tri-O-benzyl-α-D-glucopyranose (**9**).*

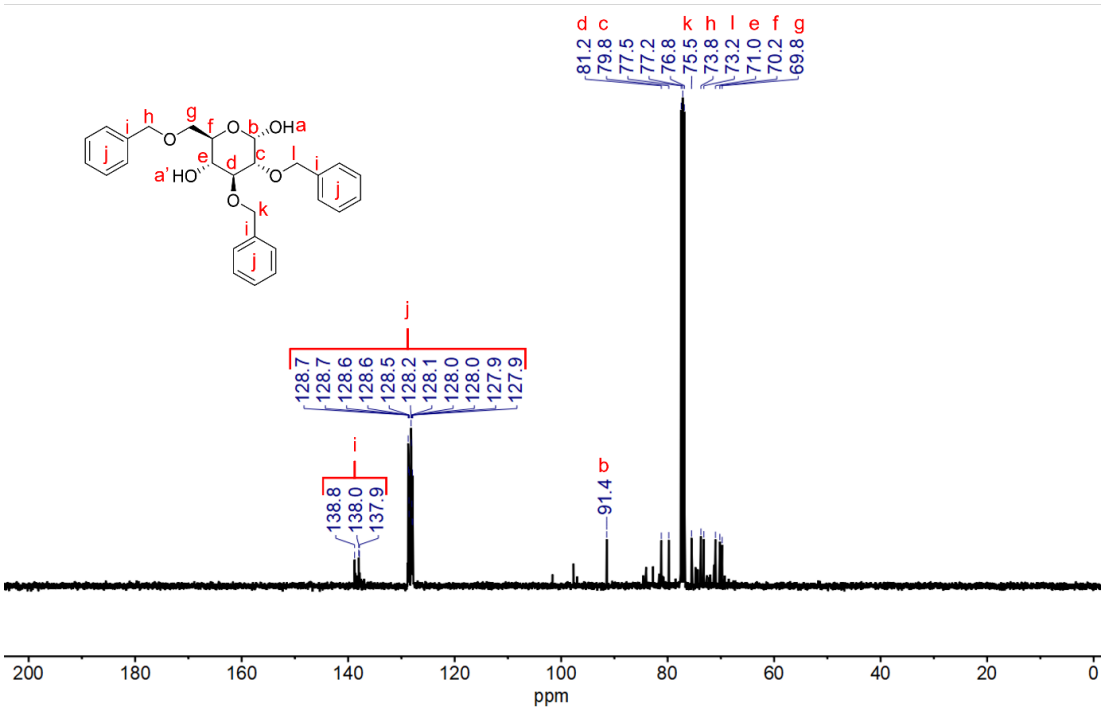


Figure A 2.16. *^{13}C NMR (101 MHz, 298 K, $CDCl_3$) spectrum of methyl 2,3,6-tri-O-benzyl-α-D-glucopyranose (**9**).*

^{1}H, ^{13}C and 2D NMR spectra of methyl 2,3,4,6-tetra-O-benzyl-α-D-glucopyranoside (18)

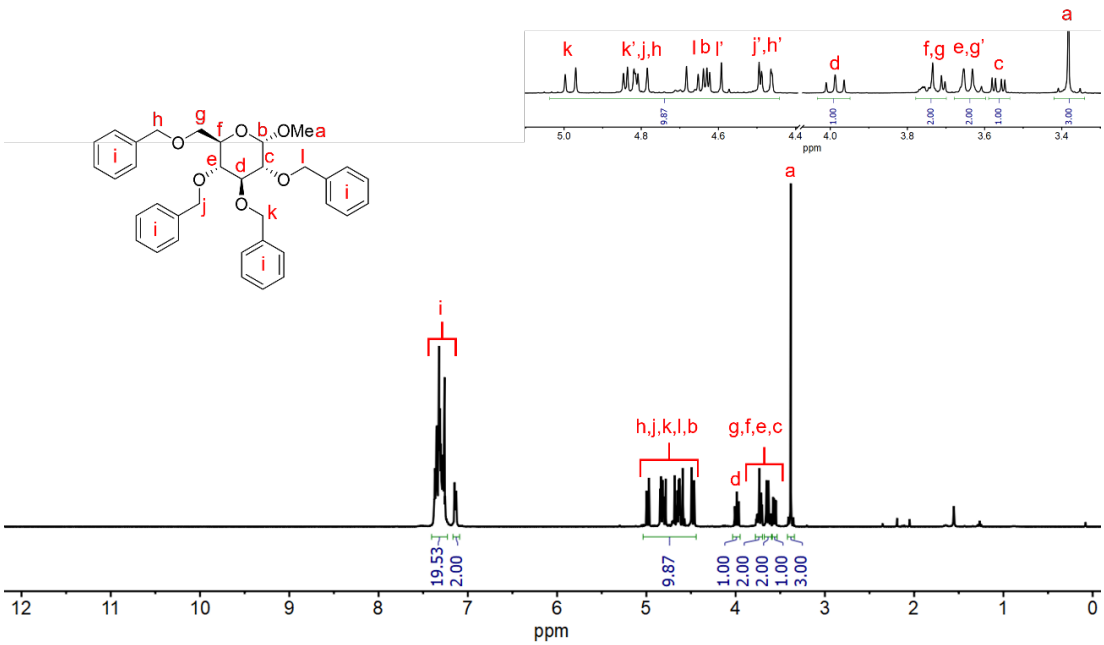


Figure A 2.17. *^{1}H NMR (400 MHz, 298 K, $CDCl_3$) spectrum of methyl 2,3,4,6-tetra-O-benzyl-α-D-glucopyranoside (**18**).*

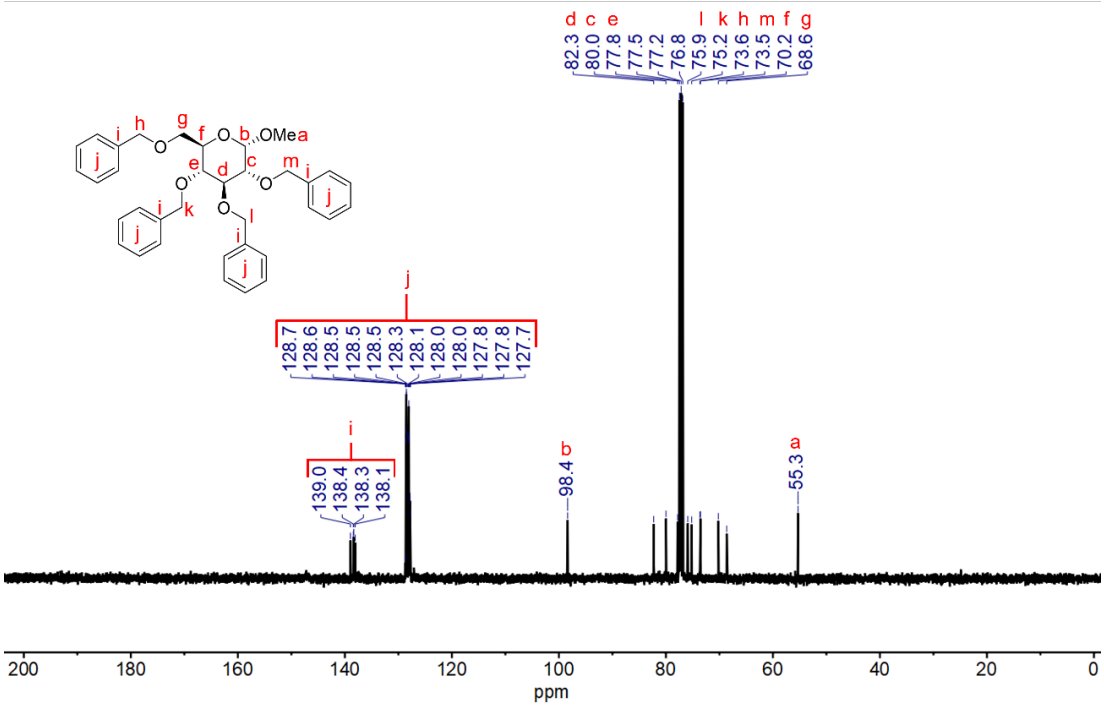


Figure A 2.18. *^{13}C NMR (101 MHz, 298 K, $CDCl_3$) spectrum of methyl 2,3,4,6-tetra-O-benzyl-α-D-glucopyranoside (**18**).*

^{1}H, ^{13}C and 2D NMR spectra of acetyl 2,3,4-tri-O-benzyl-6-acetyl-D-glucopyranoside (19)

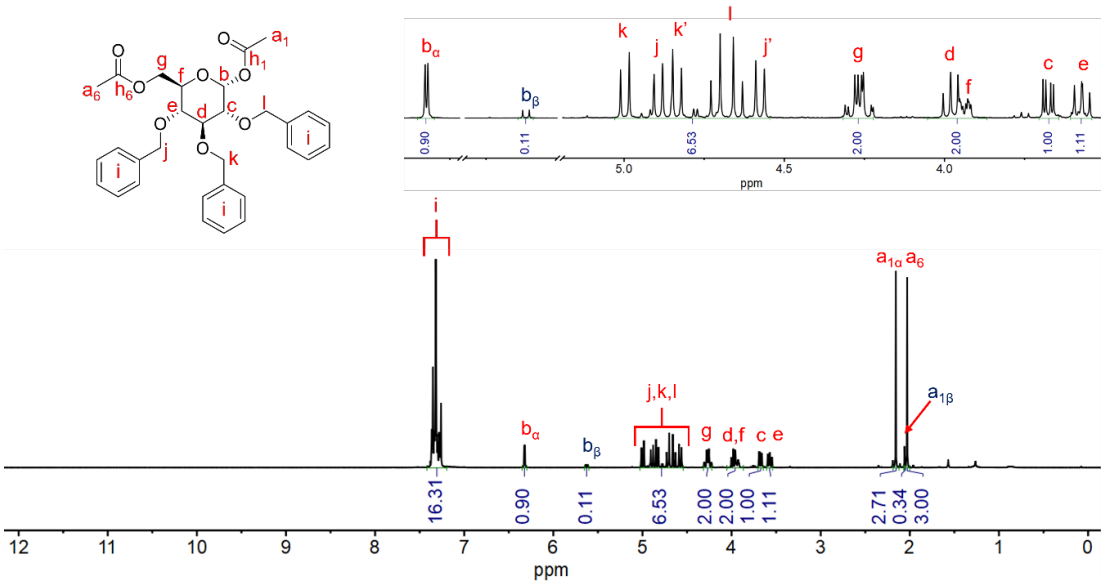


Figure A 2.19. *^{1}H NMR (400 MHz, 298 K, $CDCl_3$) spectrum of acetyl 2,3,4-tri-O-benzyl-6-acetyl-D-glucopyranoside in a 90/10 α to β anomer ratio (**19**).*

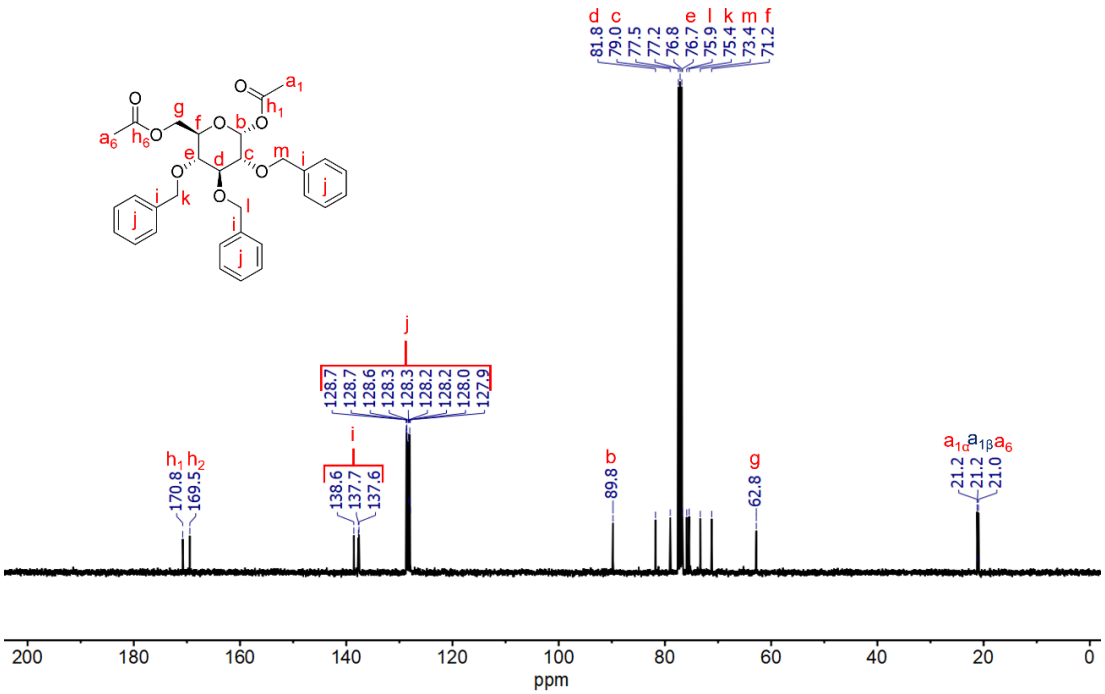


Figure A 2.20. *^{13}C NMR (101 MHz, 298 K, $CDCl_3$) spectrum of acetyl 2,3,4-tri-O-benzyl-6-acetyl-D-glucopyranoside in a 90/10 α to β anomer ratio (**19**).*

^{1}H, ^{13}C and 2D NMR spectra of 2,3,4-tri-O-benzyl-D-glucopyranoside (20)

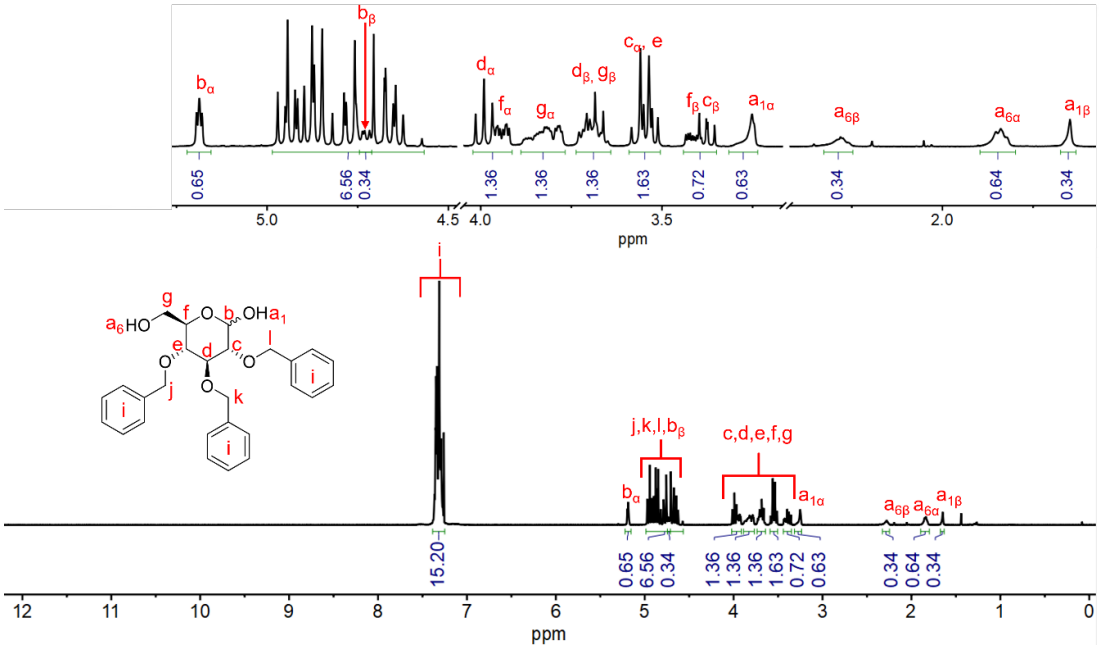


Figure A 2.21. *^{1}H NMR (400 MHz, 298 K, $CDCl_3$) spectrum of 2,3,4-tri-O-benzyl-D-glucopyranose in a 65/35 ratio of α to β anomer (**20**).*

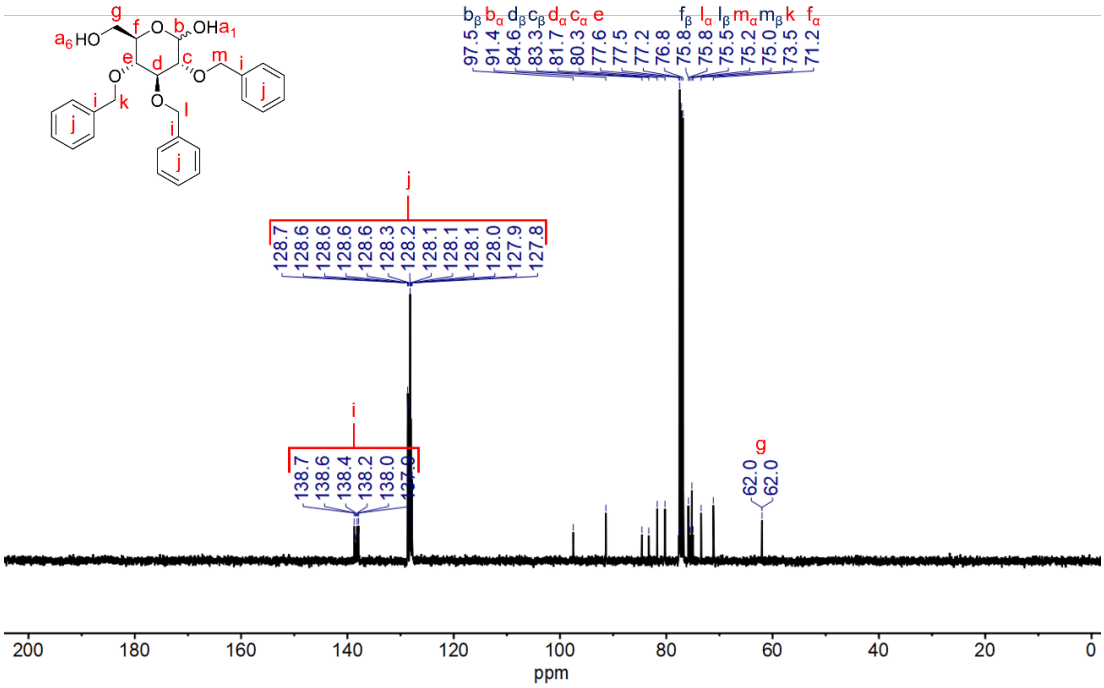


Figure A 2.22. *^{13}C NMR (101 MHz, 298 K, $CDCl_3$) spectrum of 2,3,4-tri-O-benzyl-D-glucopyranose in a 65/35 ratio of α to β anomer (**20**).*

1.18.4 NMR spectra of diacrylate monomers

^{1}H and ^{13}C NMR spectra of the cis diacrylate (24)

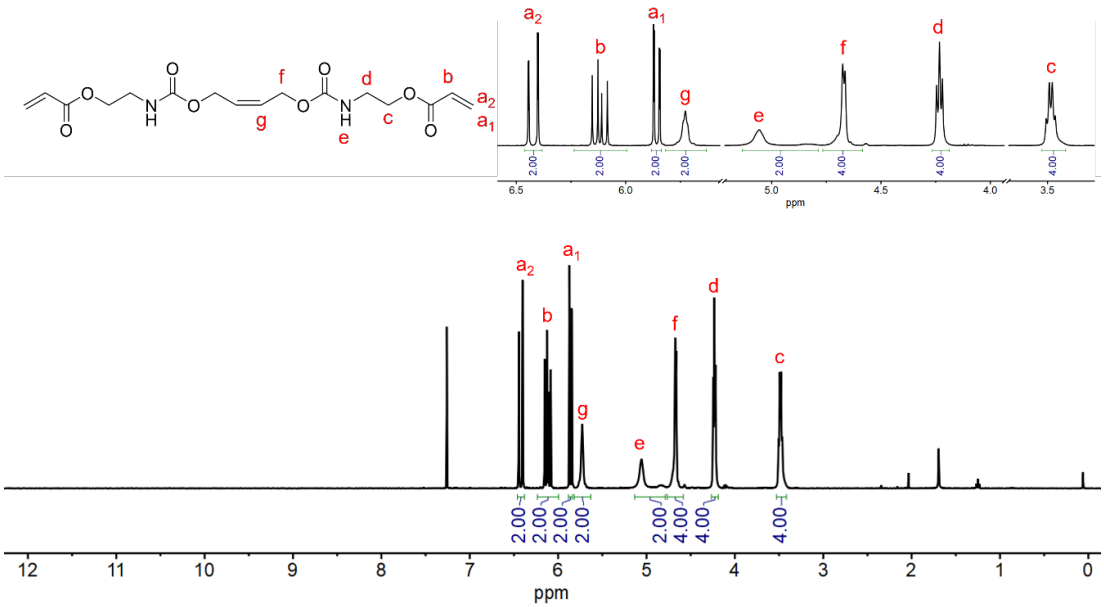


Figure A 2.23. *^{1}H NMR (400 MHz, 298 K, $CDCl_3$) spectrum of the cis diacrylate (**24**).*

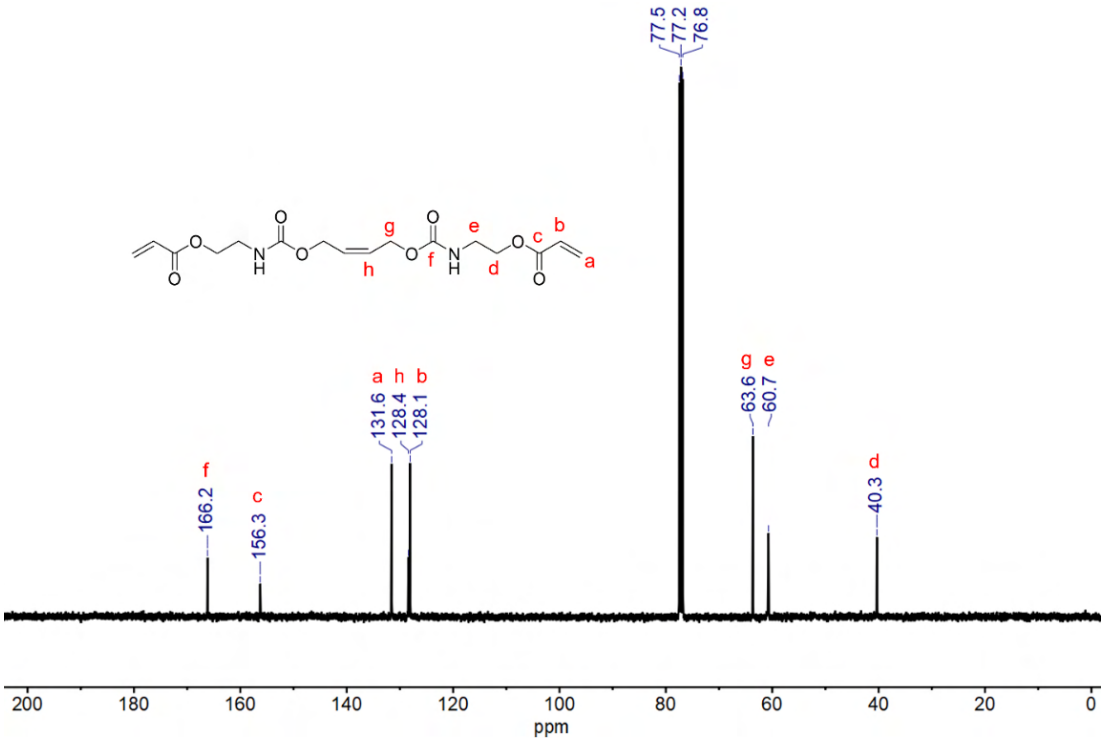


Figure A 2.24. *^{13}C NMR (101 MHz, 298 K, $CDCl_3$) spectrum of the cis diacrylate (**24**).*

^{1}H and ^{13}C NMR spectra of the trans diacrylate (25)

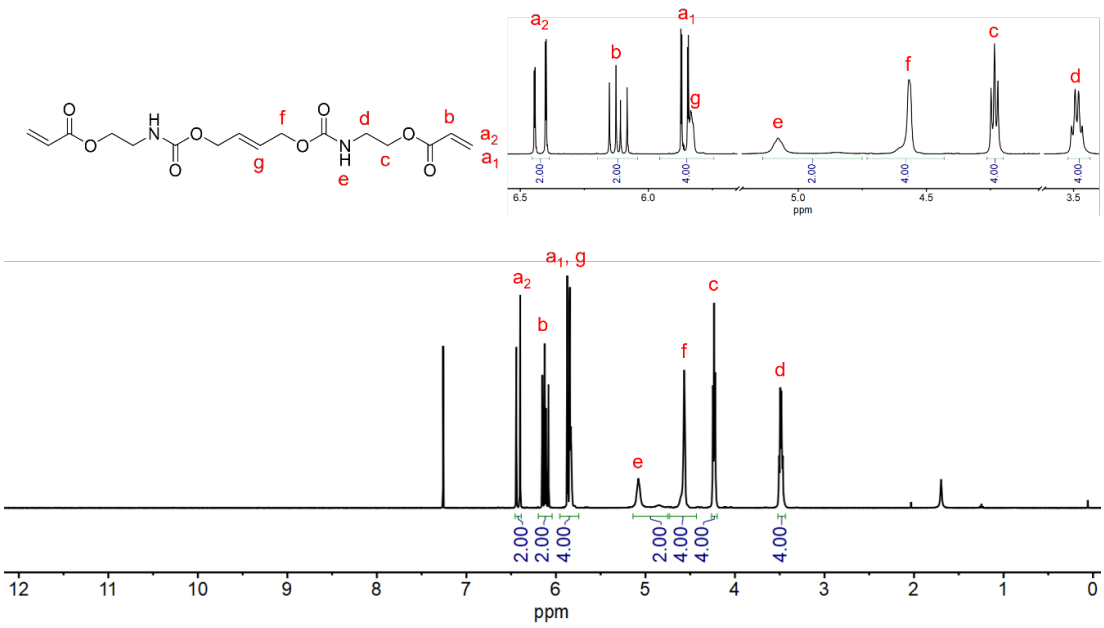


Figure A 2.25. *^{1}H NMR (400 MHz, 298 K, $CDCl_3$) spectrum of the trans diacrylate (**25**).*

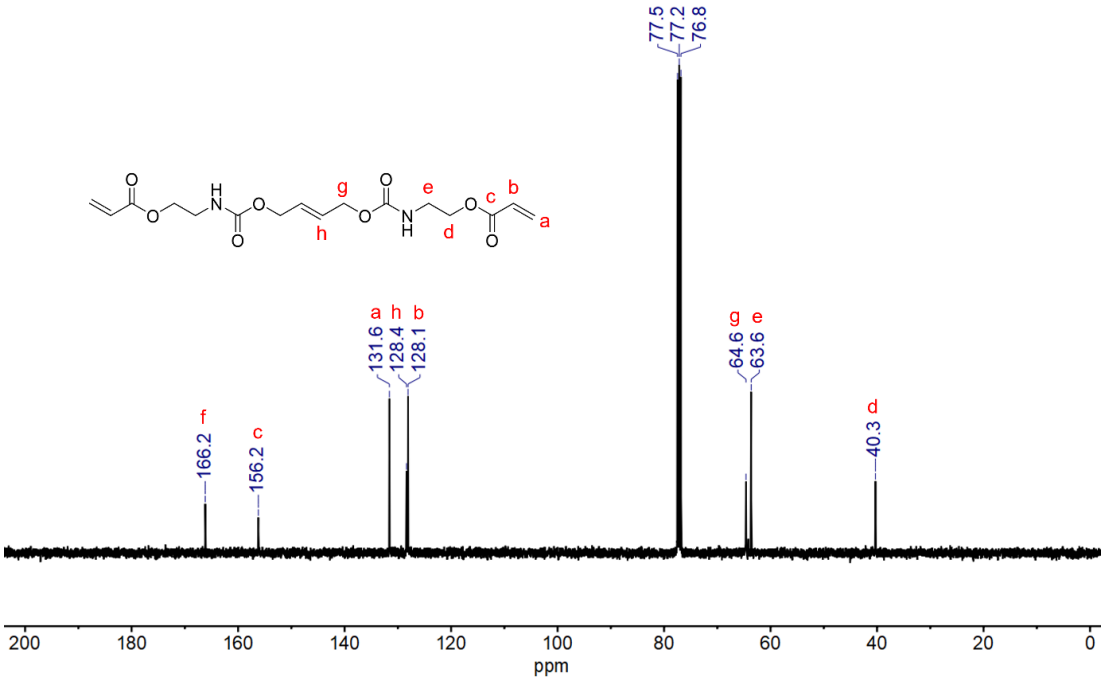


Figure A 2.26. *^{13}C NMR (101 MHz, 298 K, $CDCl_3$) spectrum of the trans diacrylate (**25**).*

^{1}H and ^{13}C NMR spectra of the isosorbide diacrylate (26)

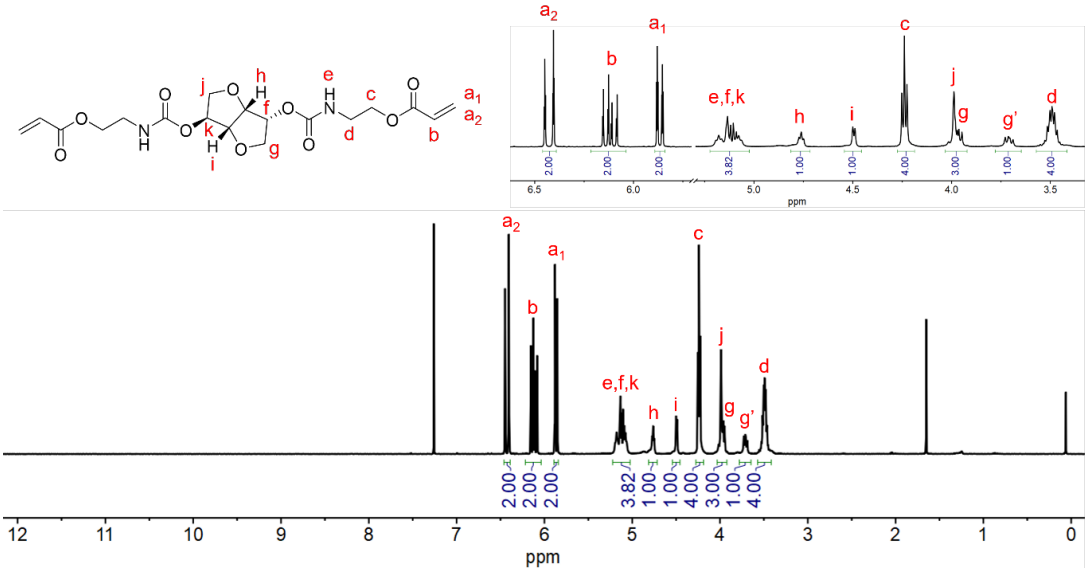


Figure A 2.27. *^{1}H NMR (400 MHz, 298 K, $CDCl_3$) spectrum of the isosorbide-derived diacrylate (**26**).*

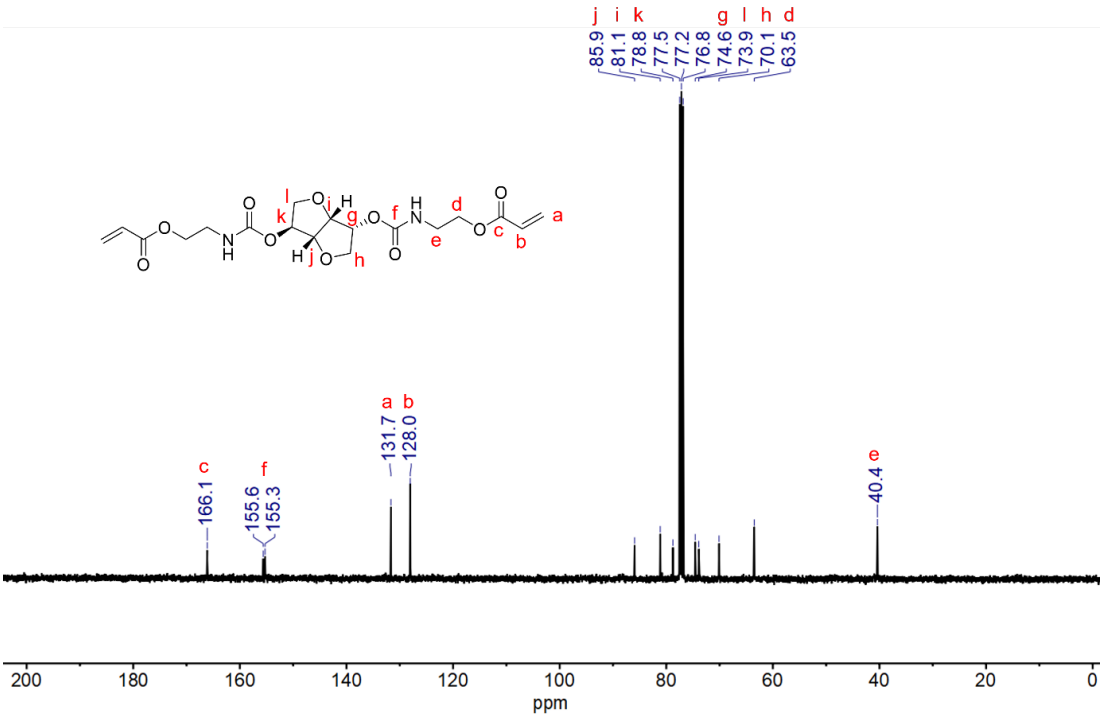


Figure A 2.28. *^{13}C NMR (101 MHz, 298 K, $CDCl_3$) spectrum of the isosorbide-derived diacrylate (**26**).*

^{1}H and ^{13}C NMR spectra of the isomannide diacrylate (27)

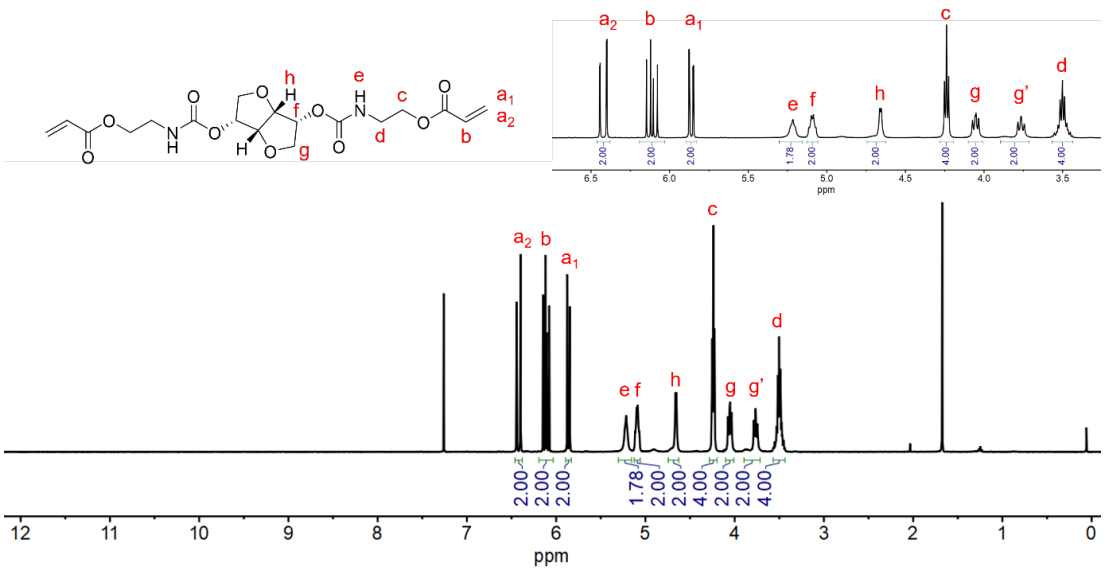


Figure A 2.29. *^{1}H NMR (400 MHz, 298 K, $CDCl_3$) spectrum of the isomannide-derived diacrylate (**27**).*

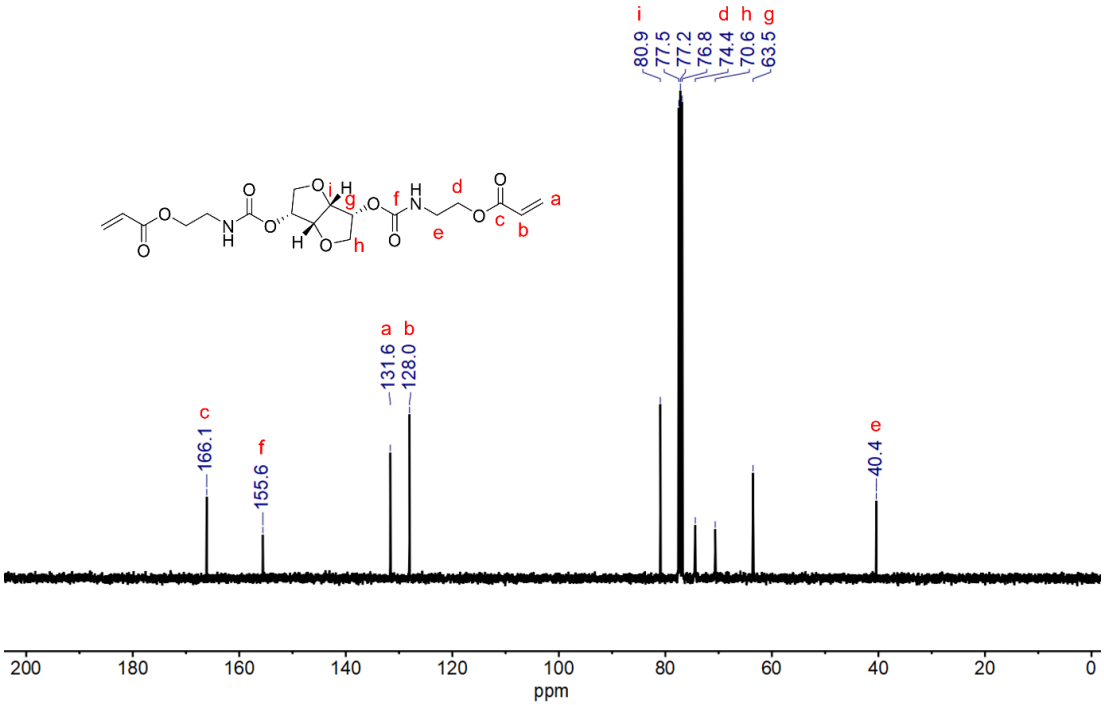


Figure A 2.30. *^{13}C NMR (101 MHz, 298 K, $CDCl_3$) spectrum of the isomannide-derived diacrylate (**27**).*

^{1}H and ^{13}C NMR spectrum of the isoidide diacrylate monomer (28)

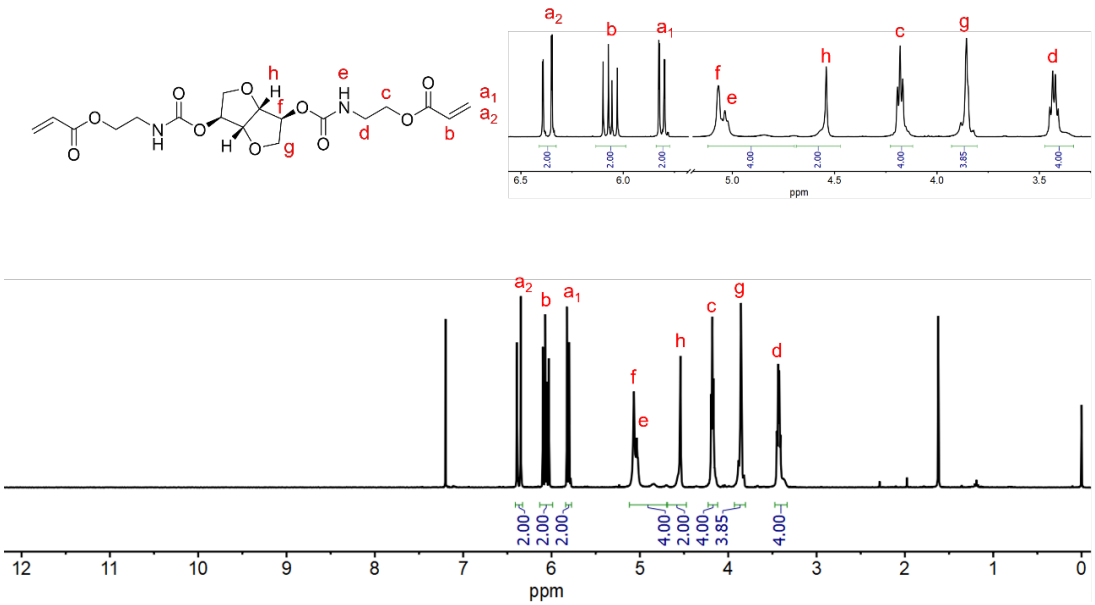


Figure A 2.31. *^{1}H NMR (400 MHz, 298 K, $CDCl_3$) spectrum of the isoidide-derived diacrylate (**28**).*

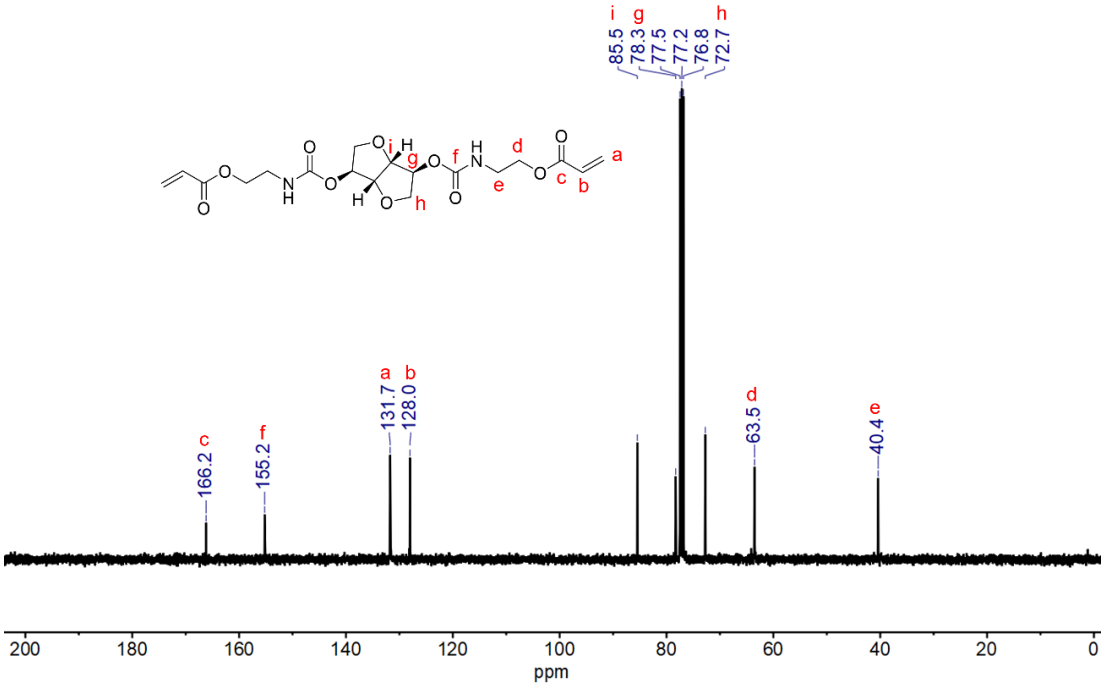


Figure A 2.32. *^{13}C NMR (101 MHz, 298 K, $CDCl_3$) spectrum of the isoidide-derived diacrylate (**28**).*

^{1}H, ^{13}C and 2D NMR spectra of 1,6-glucose-derived diacrylate monomer (29)

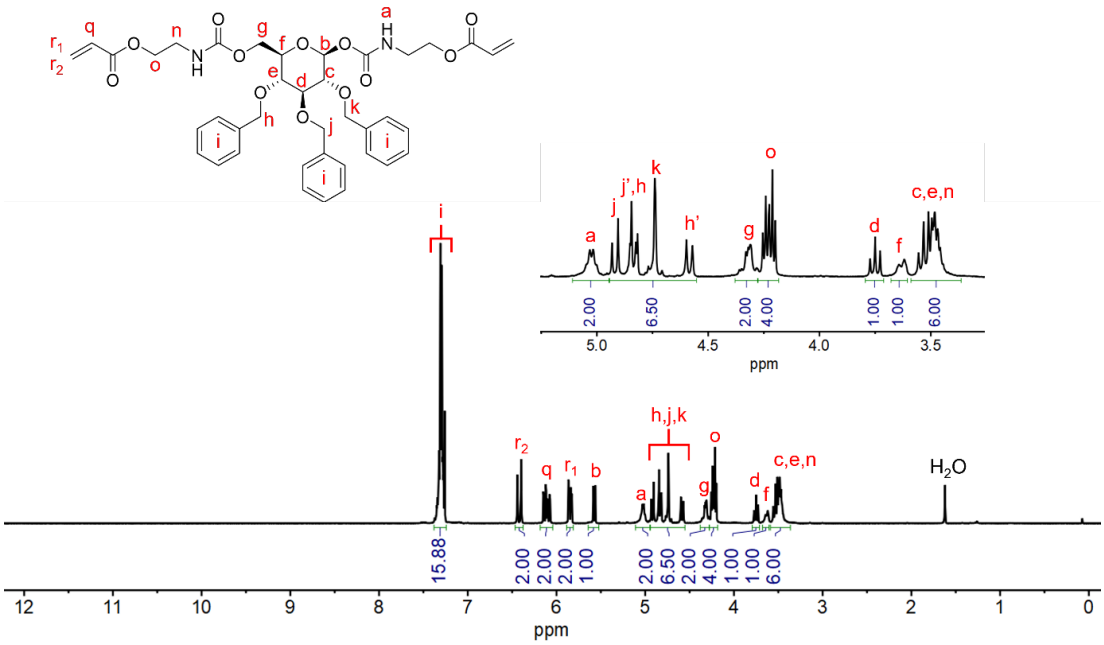


Figure A 2.33. *^{1}H NMR (400 MHz, 298 K, $CDCl_3$) spectrum of the 1,6-glucose-derived diacrylate (**29**).*

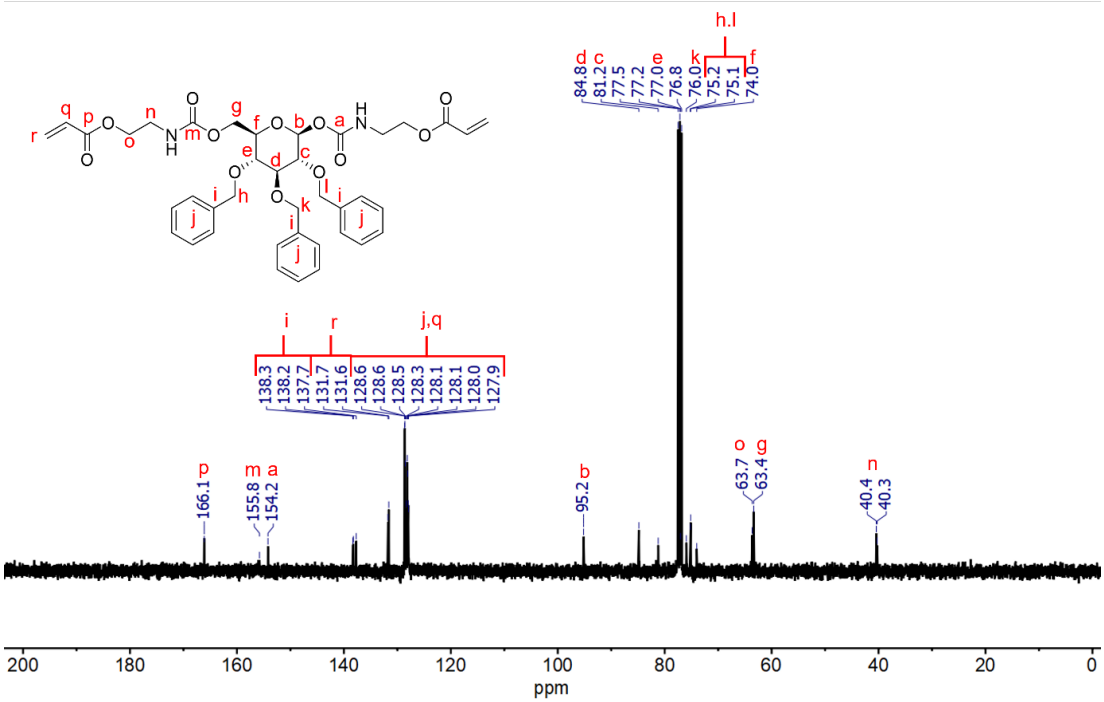


Figure A 2.34. *^{13}C NMR (101 MHz, 298 K, $CDCl_3$) spectrum of the 1,6-glucose derived diacrylate (**29**).*

1.18.5 NMR spectra of the 1,6 glucose dithiol (32) and intermediates

^{1}H, ^{13}C and 2D NMR spectra of 2,3,4-tri-O-benzyl-6-O-methanesulfonyl-α-D-glucopyranosyl chloride (30)

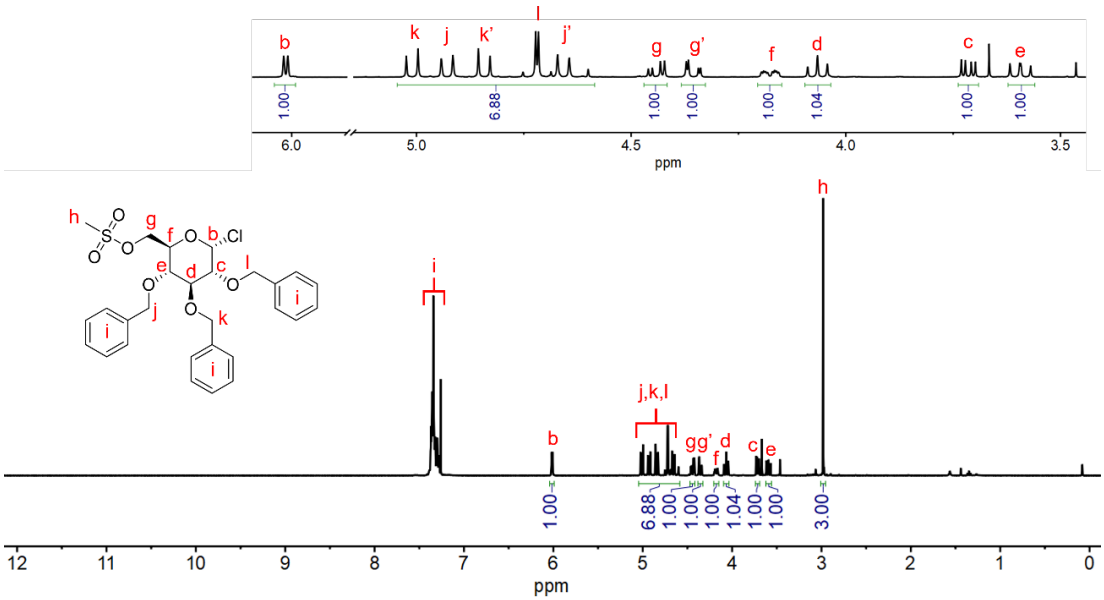


Figure A 2.35. *^{1}H NMR (400 MHz, 298 K, $CDCl_3$) spectrum of 2,3,4-tri-O-benzyl-6-O-methanesulfonyl-α-D-glucopyranosyl chloride (**30**).*

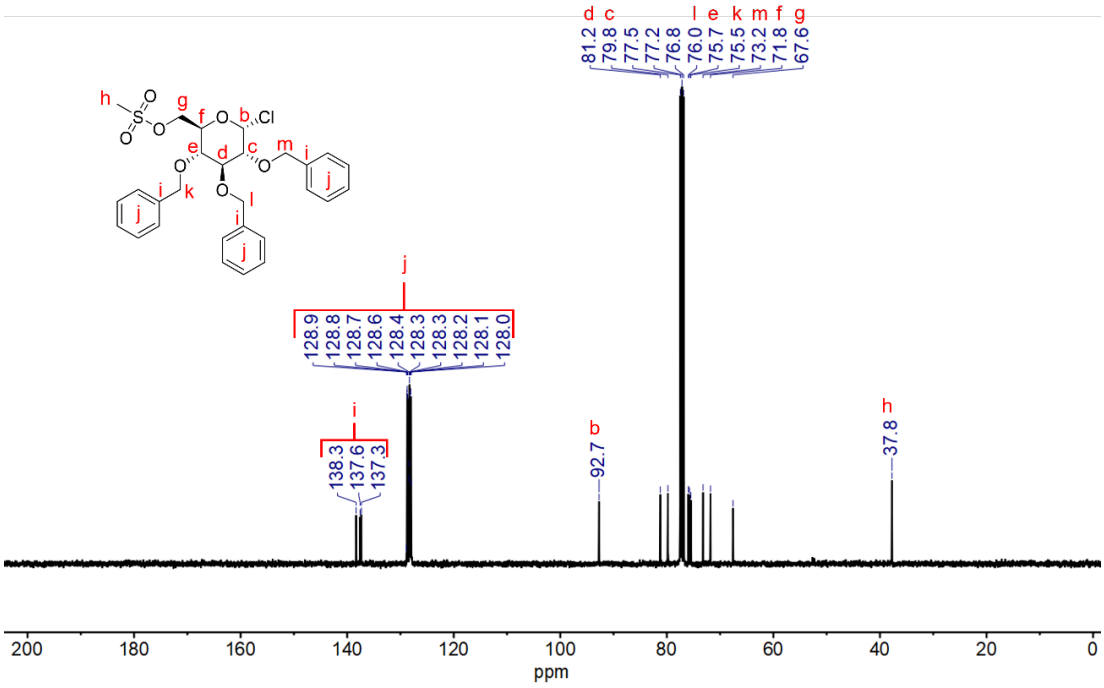


Figure A 2.36. *^{13}C NMR (101 MHz, 298 K, $CDCl_3$) spectrum of 2,3,4-tri-O-benzyl-6-O-methanesulfonyl-α-D-glucopyranosyl chloride (**30**).*

^{1}H, ^{13}C and 2D NMR spectra of acetyl 2,3,4-tri-O-benzyl-1,6-dithio-6- acetyl-β-D-glucopyranoside (31)

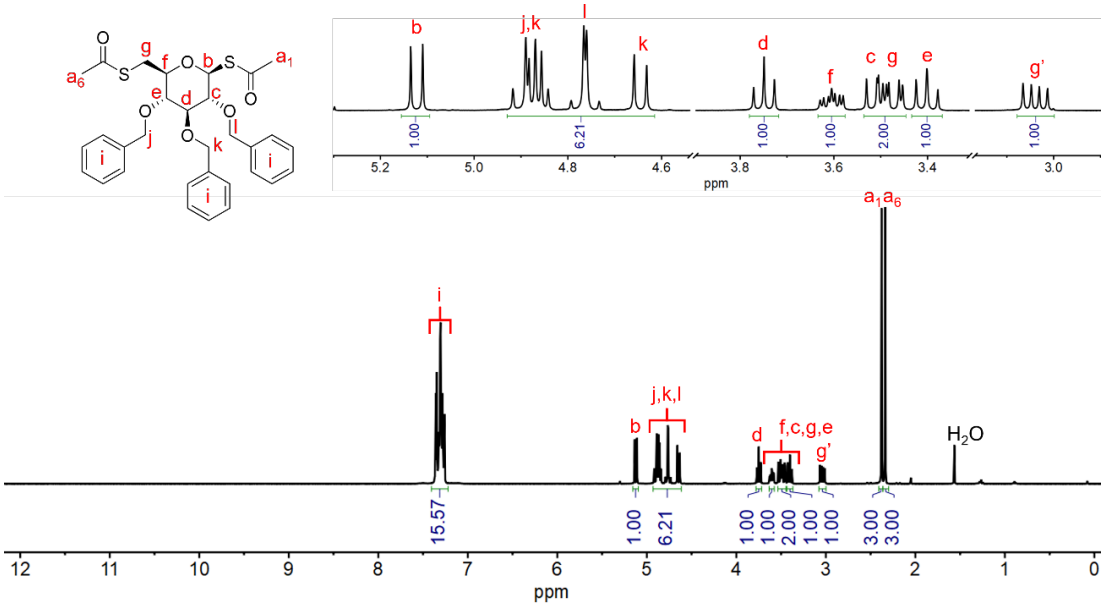


Figure A 2.37. *^{1}H NMR (400 MHz, 298 K, $CDCl_3$) spectrum of acetyl 2,3,4-tri-O-benzyl-1,6-dithio-6- acetyl-β-D-glucopyranoside (**31**).*

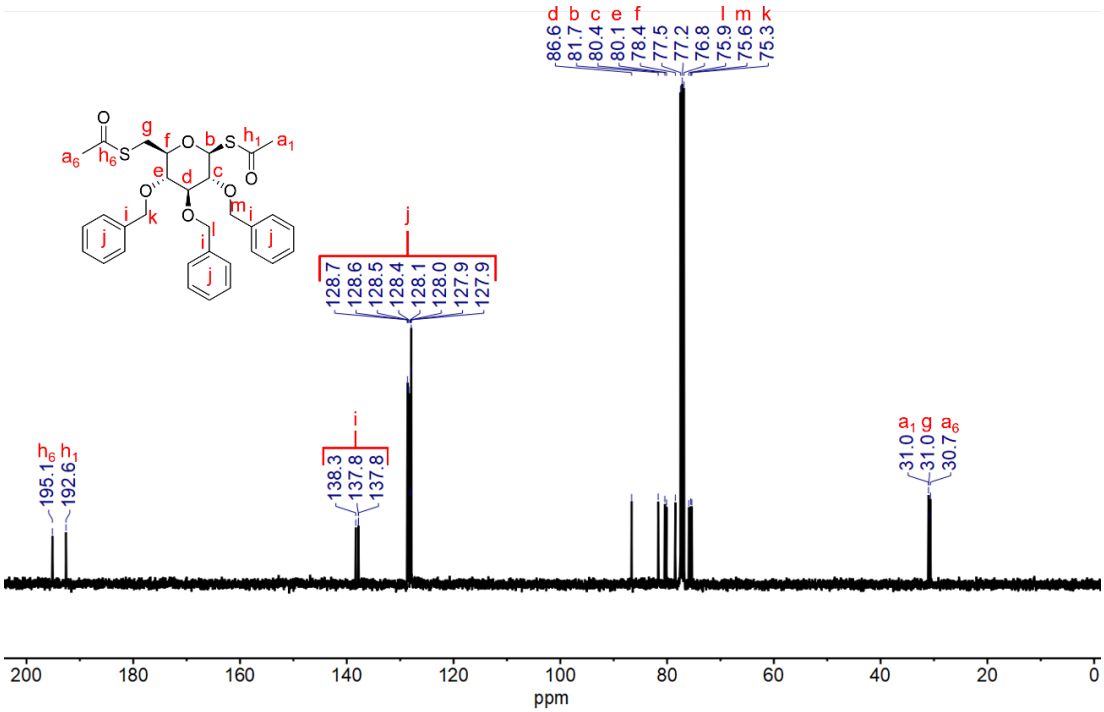


Figure A 2.38. *^{13}C NMR (101 MHz, 298 K, $CDCl_3$) spectrum of acetyl 2,3,4-tri-O-benzyl-1,6-dithio-6- acetyl-β-D-glucopyranoside (**31**).*

^{1}H, ^{13}C and 2D NMR spectra of 2,3,4-tri-O-benzyl-1,6-dithio-D-glucopyranose (32)

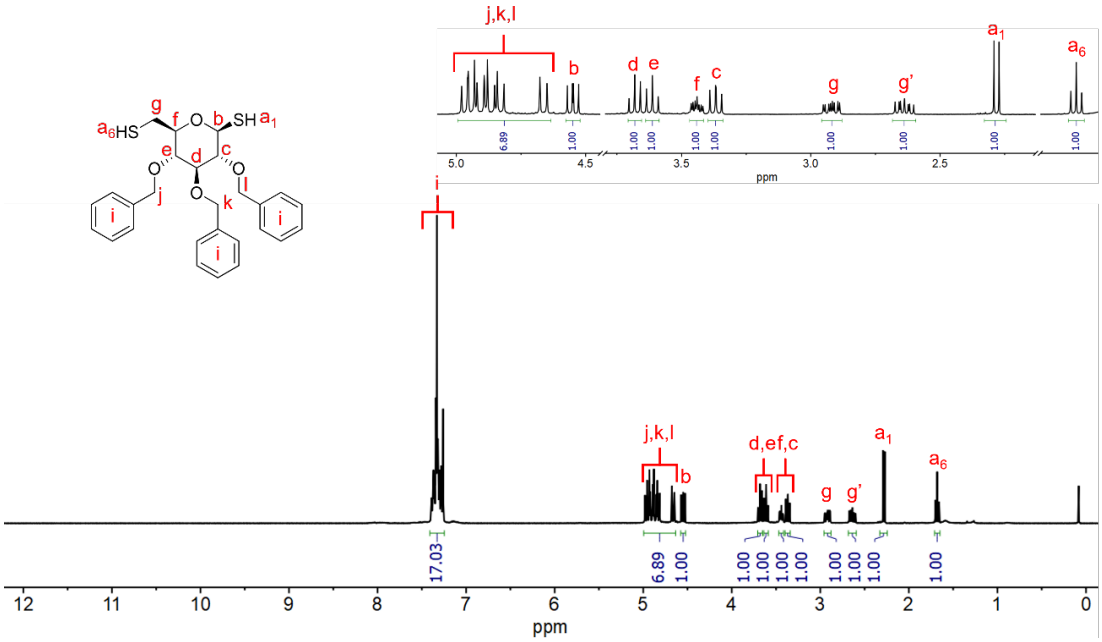


Figure A 2.39. *^{1}H NMR (400 MHz, 298 K, $CDCl_3$) spectrum of 2,3,4-tri-O-benzyl-1,6-dithio-D-glucopyranose (**32**).*

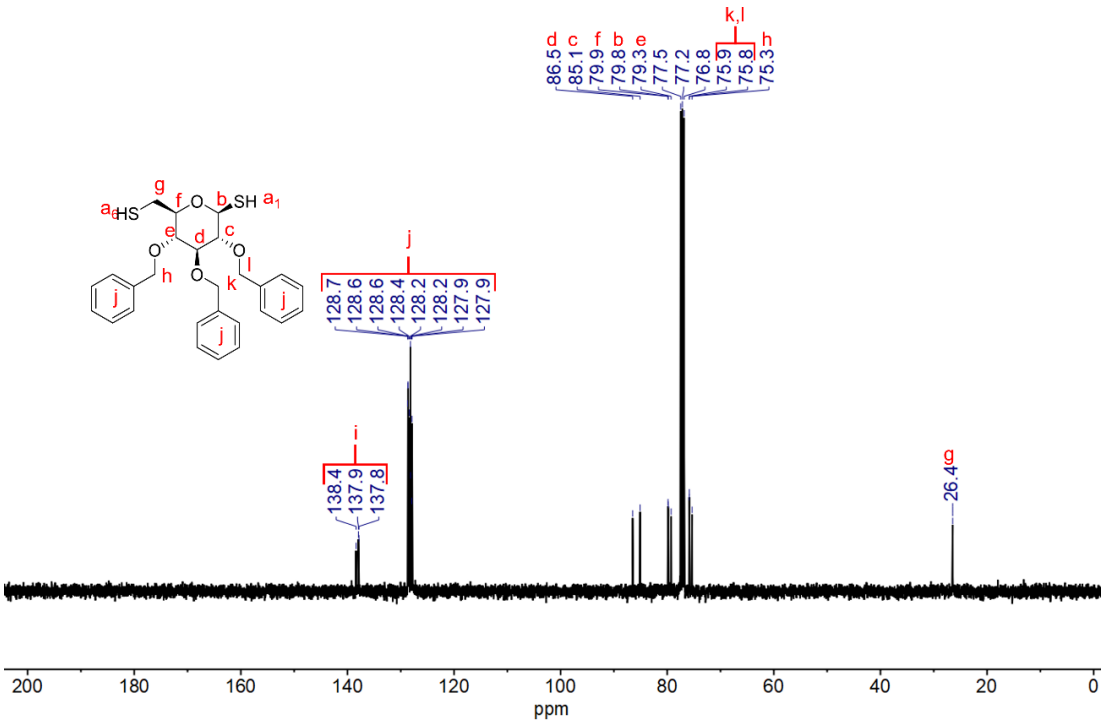


Figure A 2.40. *^{13}C NMR (101 MHz, 298 K, $CDCl_3$) spectrum of 2,3,4-tri-O-benzyl-1,6-dithio-D-glucopyranose (**32**).*

1.18.6 NMR spectra of selected by-products from studied reaction

^{1}H, ^{13}C and 2D NMR spectra of spectrum of 2,3,6-tri-O-benzyl-D-glucopyranose (9) (racemic 65/35 α to β)

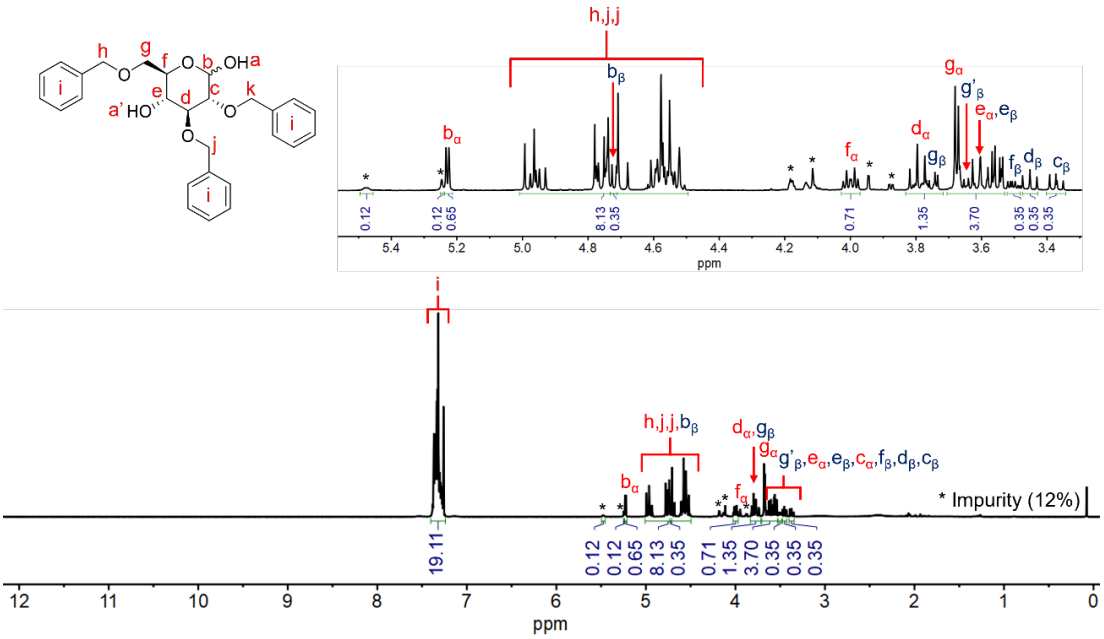


Figure A 2.41. *^{1}H NMR (400 MHz, 298 K, $CDCl_3$) spectrum of 2,3,4-tri-O-benzyl-D-glucopyranose (**9**) in a 65/35 ratio of α to β anomer.*

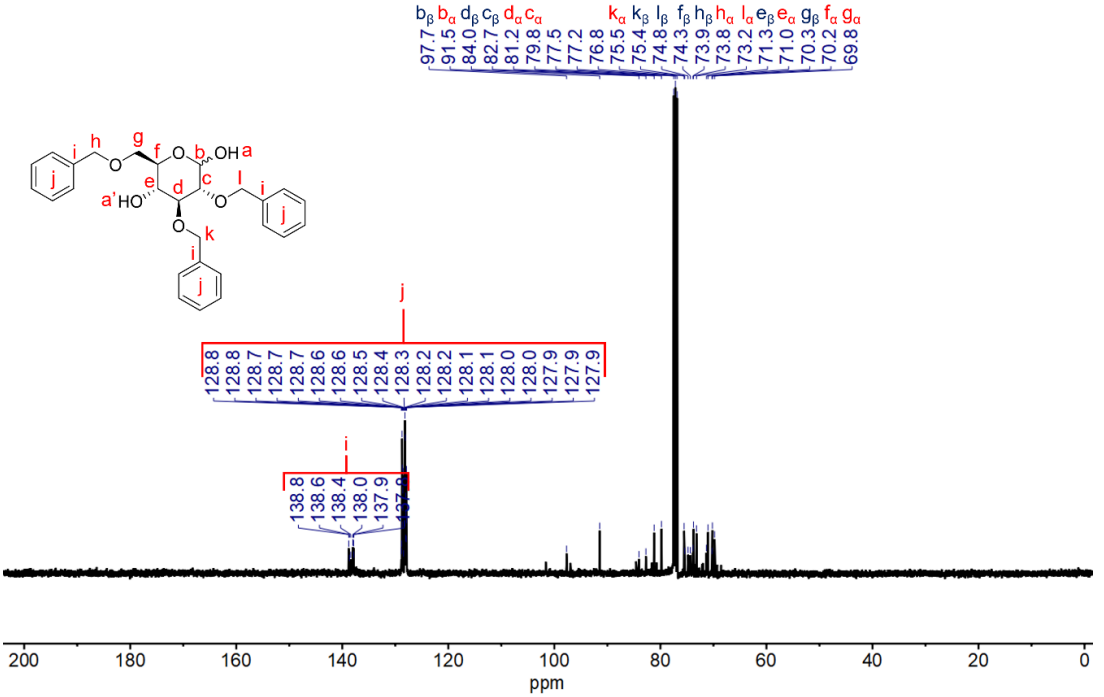


Figure A 2.42. *^{13}C NMR (101 MHz, 298 K, $CDCl_3$) spectrum of 2,3,4-tri-O-benzyl-D-glucopyranose (**9**) in a 65/35 ratio of α to β anomer.*

^{1}H, ^{13}C and 2D NMR spectra of 2,3,6-tri-O-benzyl-4-acetyl-D-glucopyranose (6)

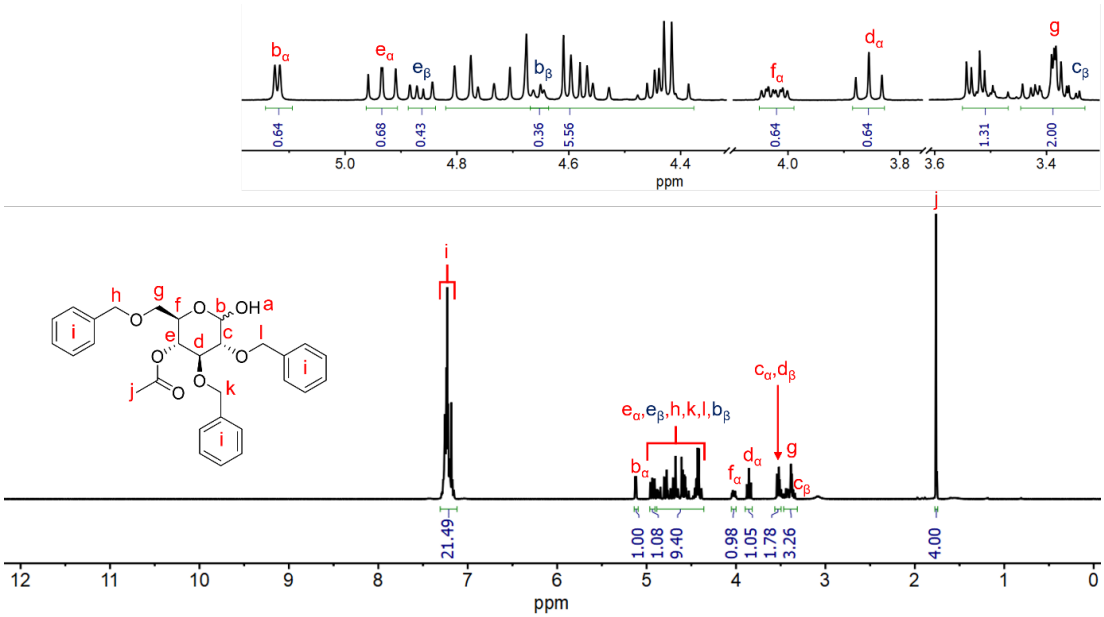


Figure A 2.43. *^{1}H NMR (400 MHz, 298 K, $CDCl_3$) spectrum of 2,3,6-tri-O-benzyl-4-acetyl-D-glucopyranose (**6**).*

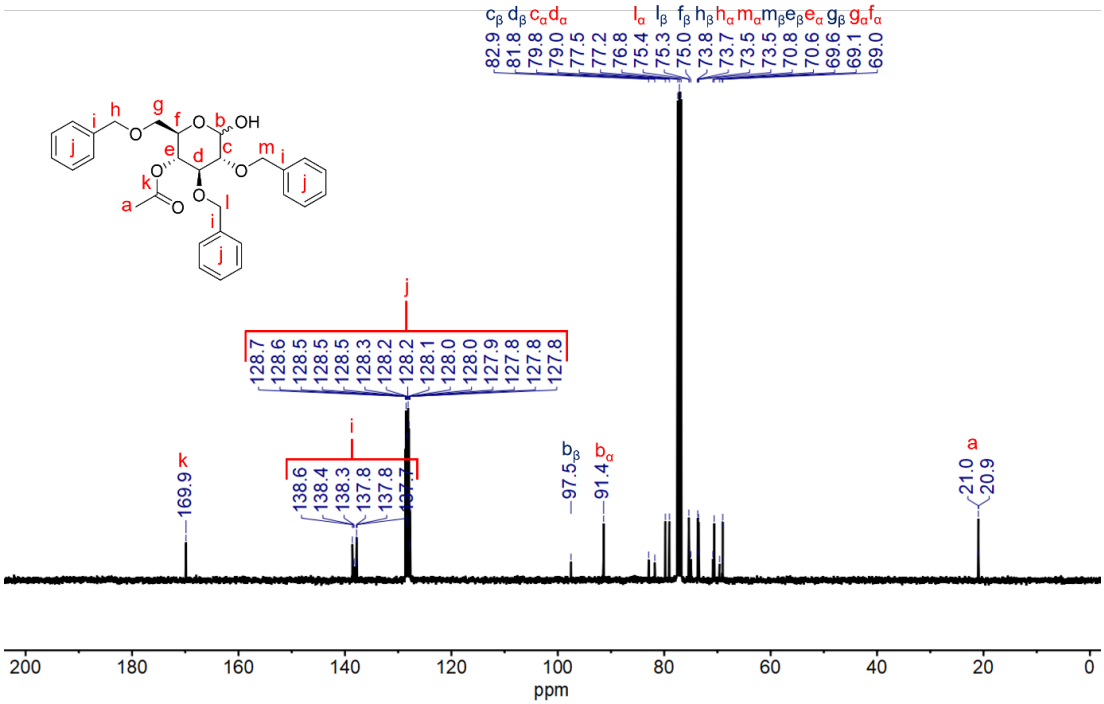


Figure A 2.44. *^{13}C NMR (101 MHz, 298 K, $CDCl_3$) spectrum of 2,3,6-tri-O-benzyl-4-acetyl-D-glucopyranose (**6**).*

^{1}H and ^{13}C spectra of benzyl alcohol (12)

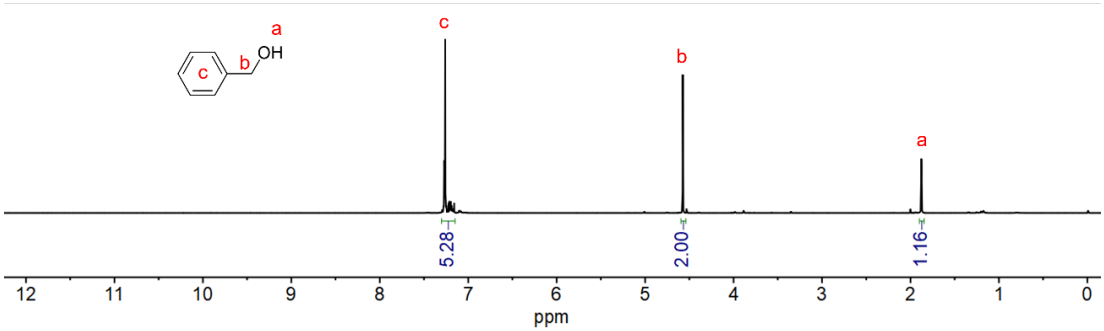


Figure A 2.45. *^{1}H NMR (400 MHz, 298 K, $CDCl_3$) spectrum of benzyl alcohol (**12**), recovered during the acetolysis of methyl 2,3,6-tri-O-benzyl-α -D-glucopyranoside (**8**).*

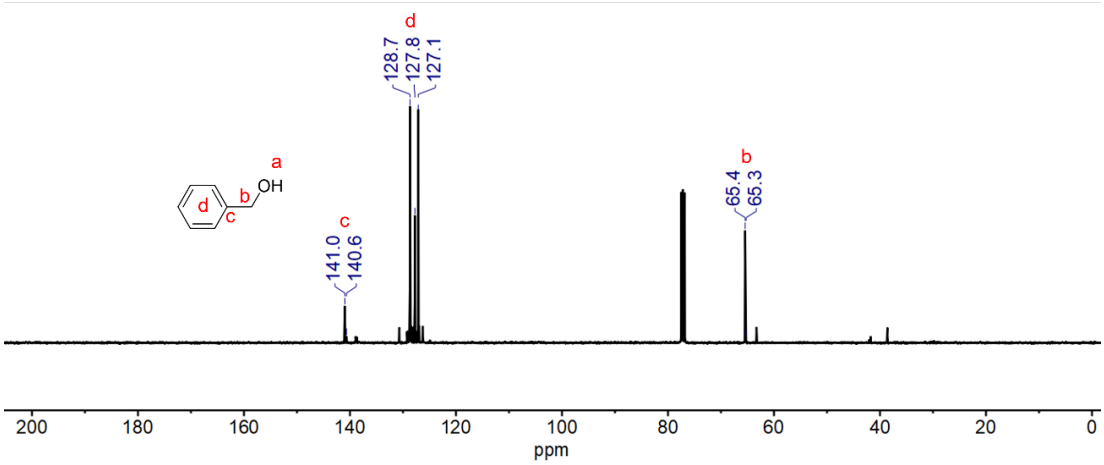


Figure A 2.46. *^{13}C NMR (101 MHz, 298 K, $CDCl_3$) spectrum of benzyl alcohol (**12**), recovered during the acetolysis of methyl 2,3,6-tri-O-benzyl-α -D-glucopyranoside (**8**).*

^{1}H, ^{13}C and 2D NMR spectra of methyl 2,3,4-tri-O-benzyl-4-acetyl-α-D-glucopyranoside (13).

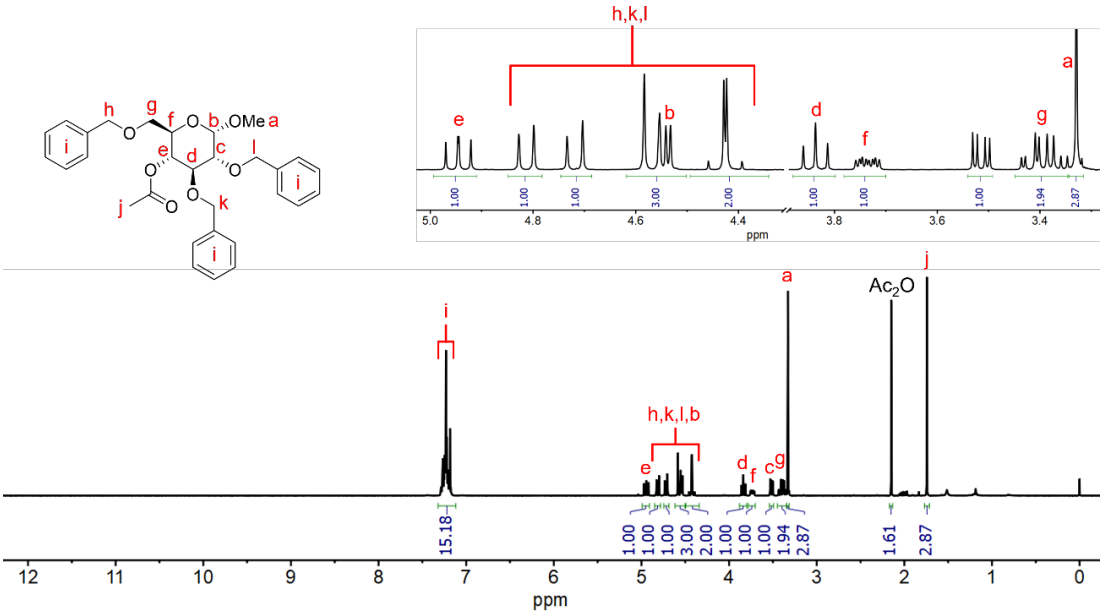


Figure A 2.47. *^{1}H NMR (400 MHz, 298 K, $CDCl_3$) spectrum of methyl 2,3,4-tri-O-benzyl-4-acetyl-α-D-glucopyranoside (**13**).*

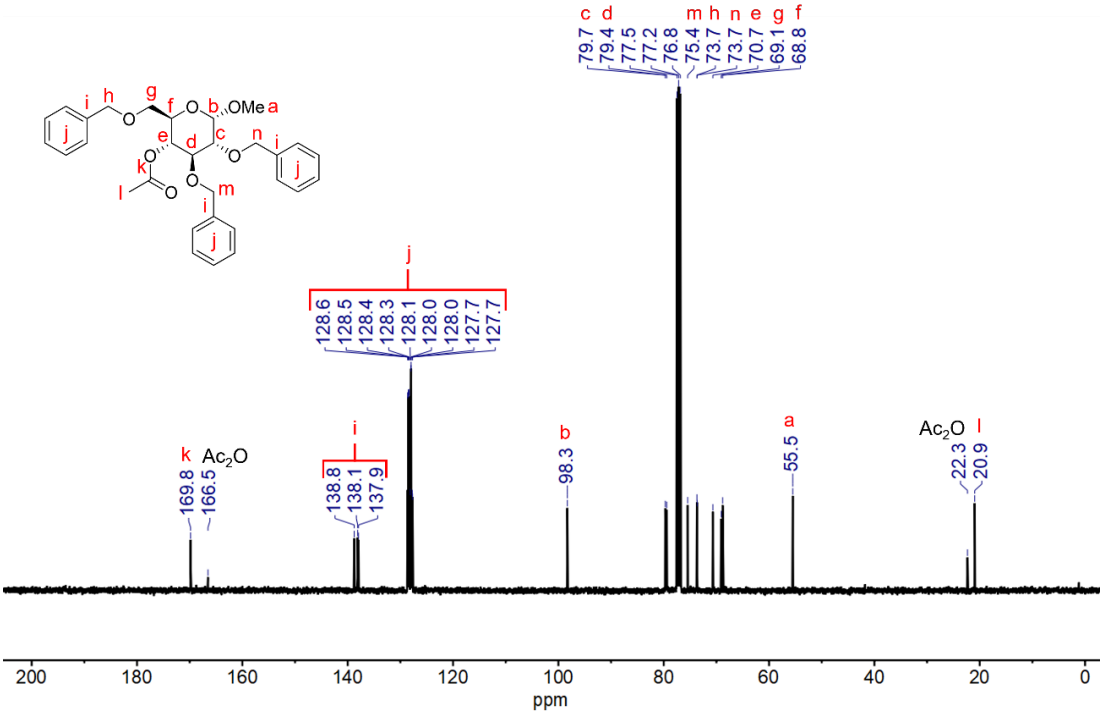


Figure A 2.48. *^{13}C NMR (101 MHz, 298 K, $CDCl_3$) spectrum of methyl 2,3,4-tri-O-benzyl-4-acetyl-α-D-glucopyranoside (**13**).*

^{1}H, ^{13}C and 2D NMR spectra of acetyl 2,3-di-O-benzyl-4,6-di-acetyl-D-glucopyranoside (14)

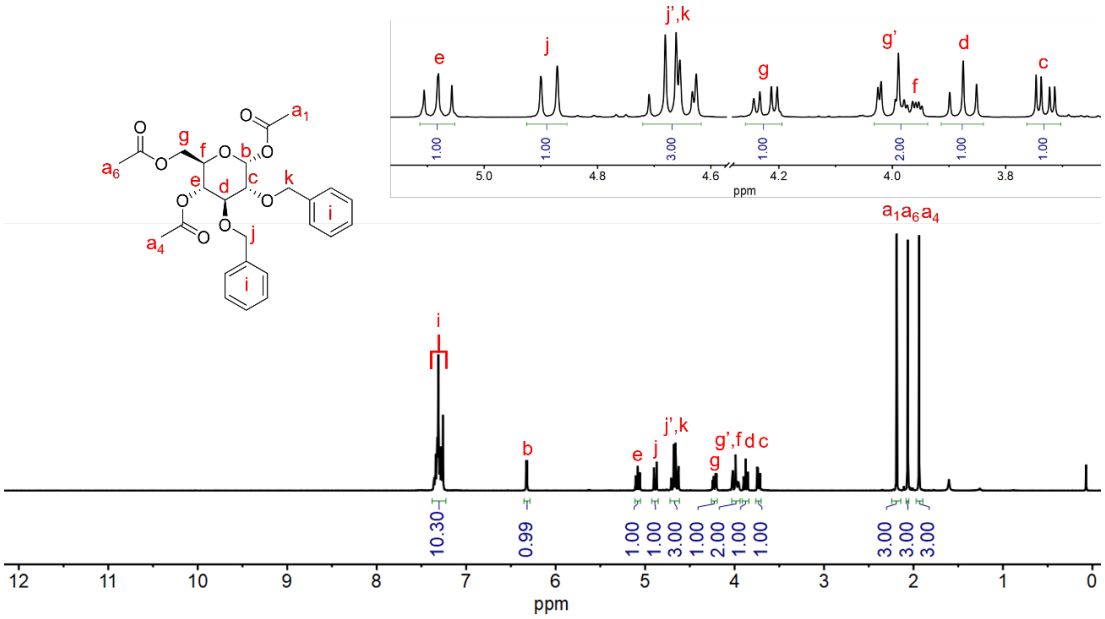


Figure A 2.49. *^{1}H NMR (400 MHz, 298 K, $CDCl_3$) spectrum of acetyl 2,3-di-O-benzyl-4,6-di-acetyl-D-glucopyranoside (**14**).*

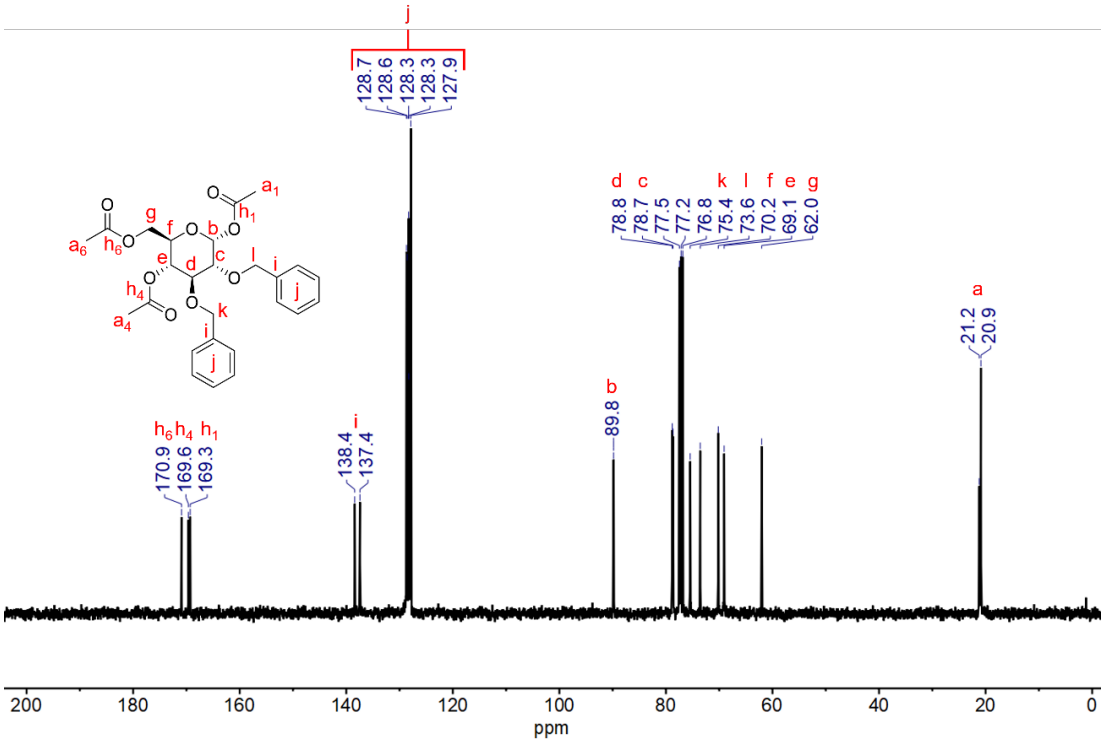


Figure A 2.50. *^{13}C NMR (101 MHz, 298 K, $CDCl_3$) spectrum of acetyl 2,3-di-O-benzyl-4,6-di-acetyl-D-glucopyranoside (**14**).*

^{1}H, ^{13}C and 2D NMR spectra of methyl 2,3,4,6-tetra-O-benzyl-D-glucopyranoside (18) (racemic 50/50 α to β)

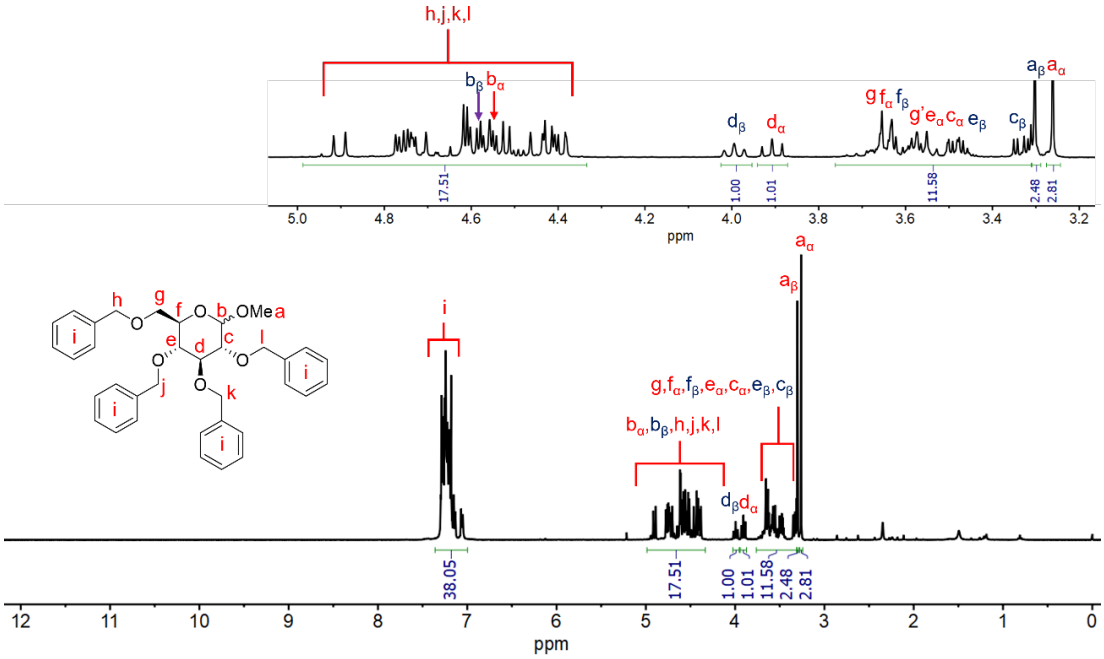


Figure A 2.51. *^{1}H NMR (400 MHz, 298 K, $CDCl_3$) spectrum of methyl 2,3,4,6-tetra-O-benzyl-D-glucopyranoside* ***(18)*** *in a 50/50 ratio of α to β anomer.*

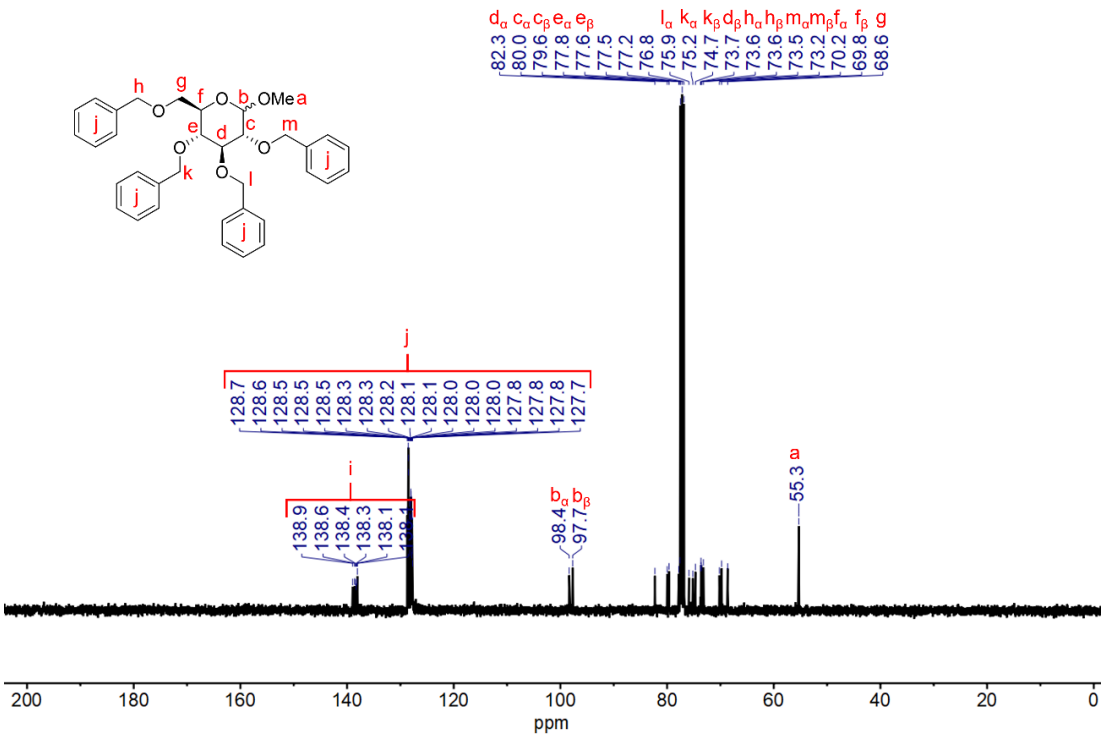


Figure A 2.52. *^{13}C NMR (101 MHz, 298 K, $CDCl_3$) spectrum of methyl 2,3,4,6-tetra-O-benzyl-D-glucopyranoside* ***(18)*** *in a 50/50 ratio of α to β anomer.*

^{1}H, ^{13}C and 2D NMR spectra of acetyl 2,4-di-O-benzyl-3,6-di-acetyl-D-glucopyranoside (22)

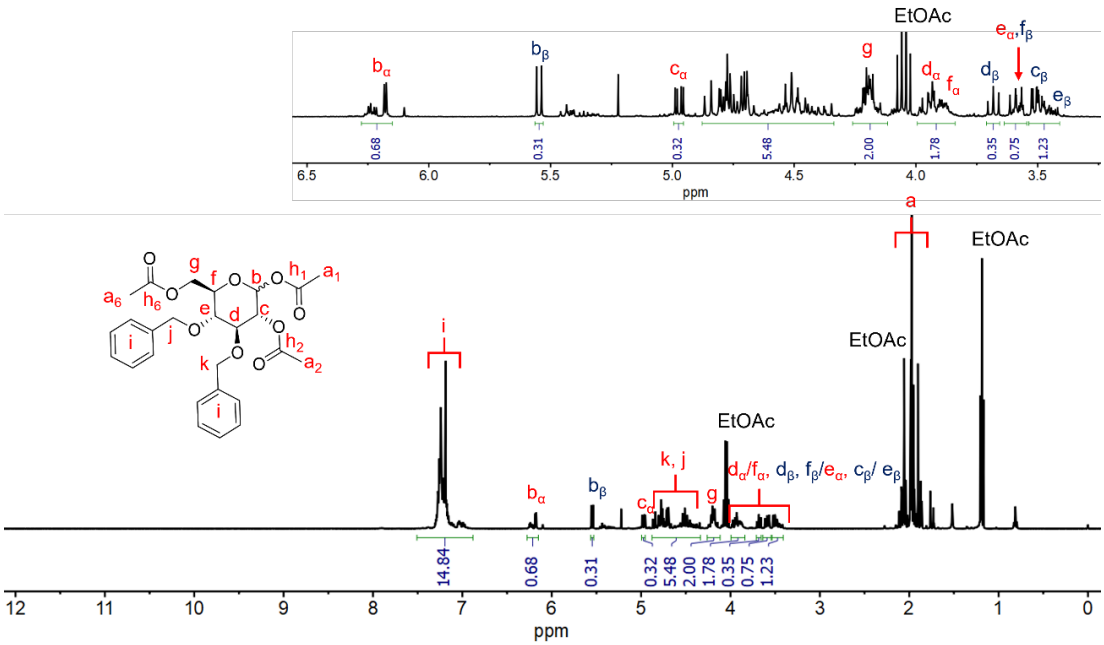


Figure A 2.53. *^{1}H NMR (400 MHz, 298 K, $CDCl_3$) spectrum of acetyl 2,4-di-O-benzyl-3,6-di-acetyl-D-glucopyranoside (**22**).*

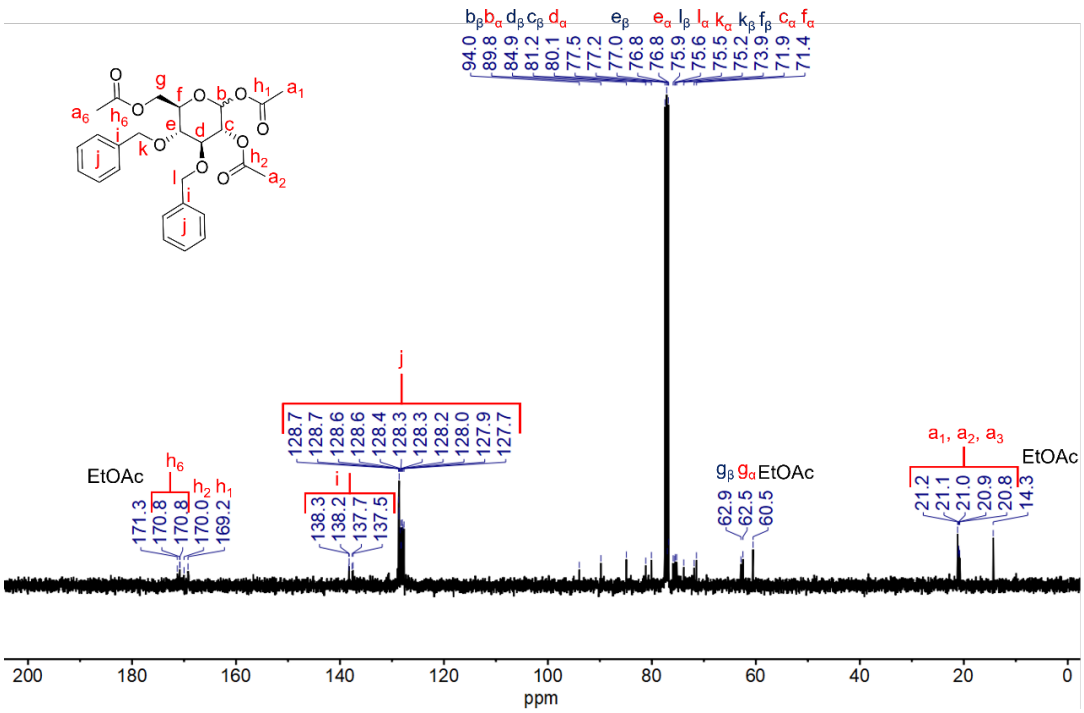


Figure A 2.54. *^{13}C NMR (101 MHz, 298 K, $CDCl_3$) spectrum of acetyl 2,4-di-O-benzyl-3,6-di-acetyl-D-glucopyranoside (**22**).*

^{1}H, ^{13}C and 2D NMR spectra of acetyl 3,4-di-O-benzyl-2,6-di-acetyl-D-glucopyranoside and acetyl 2,3-di-O-benzyl-4,6-di-acetyl-D-glucopyranoside (21 and 23)

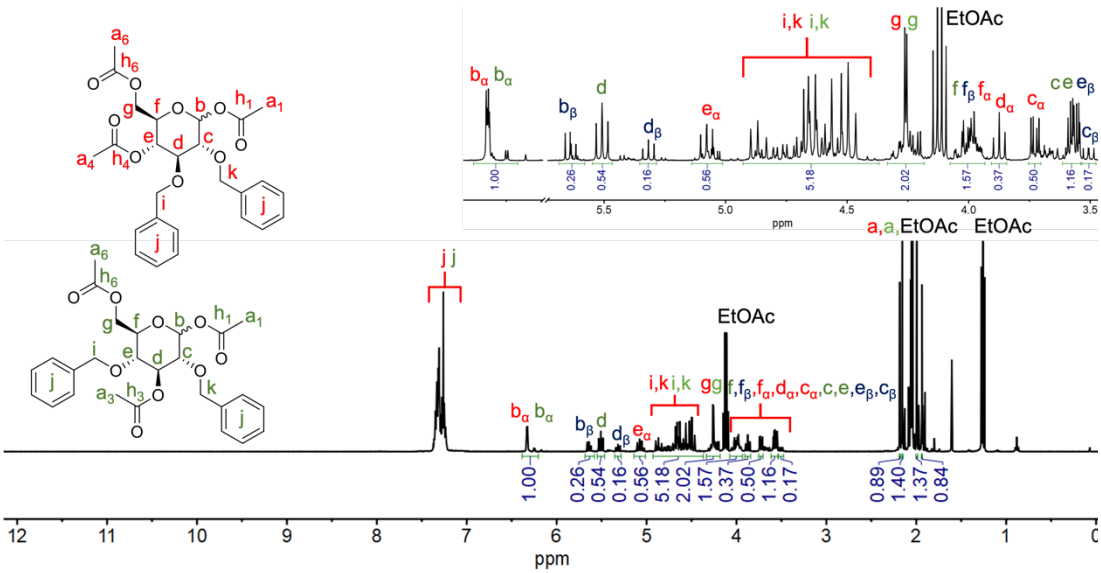


Figure A 2.55. *^{1}H NMR (400 MHz, 298 K, $CDCl_3$) spectrum of acetyl 3,4-di-O-benzyl-2,6-di-acetyl-D-glucopyranoside and acetyl 2,3-di-O-benzyl-4,6-di-acetyl-D-glucopyranoside (**21** and **23**).*

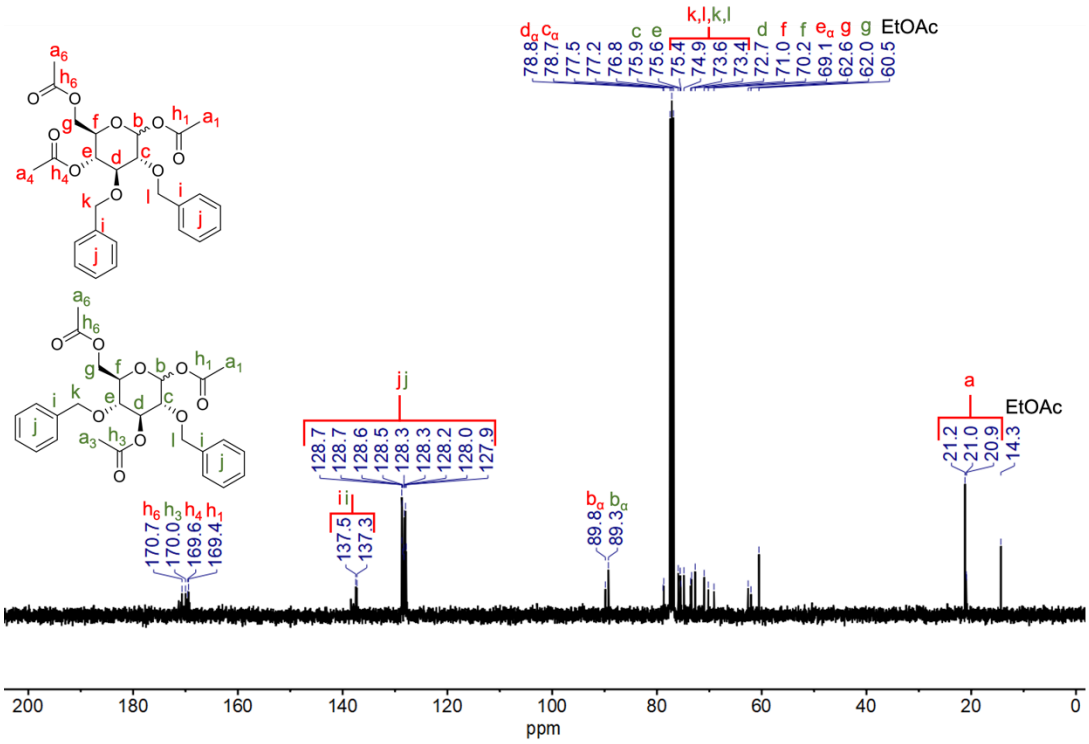


Figure A 2.56. *^{13}C NMR (101 MHz, 298 K, $CDCl_3$) spectrum of acetyl 3,4-di-O-benzyl-2,6-di-acetyl-D-glucopyranoside and acetyl 2,3-di-O-benzyl-4,6-di-acetyl-D-glucopyranoside (**21** and **23**).*

^{1}H, ^{13}C and 2D NMR spectra of 1,6-anhydro-6-deoxy-6-thio-2,3,4-tri-O-benzyl-β-D-glucopyranose (33)

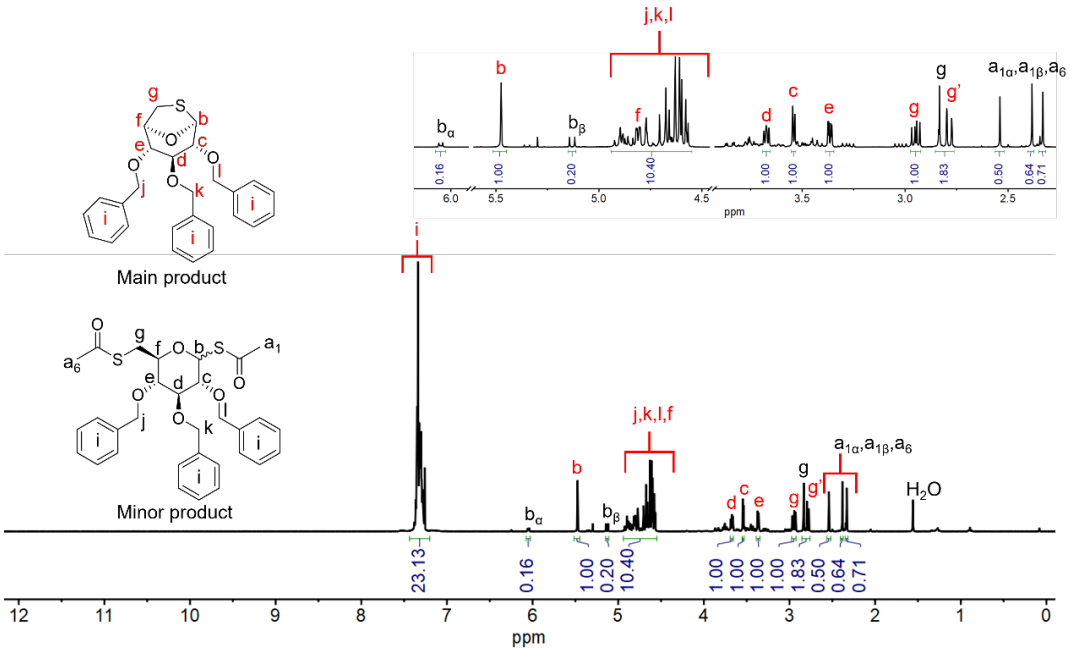


Figure A 2.57. *^{1}H NMR (400 MHz, 298 K, $CDCl_3$) spectrum of 1,6-anhydro-6-deoxy-6-thio-2,3,4-tri-O-benzyl-β-D-glucopyranose (**33**). By-product of the synthesis of 1,6-dithioacetate (**31**).*

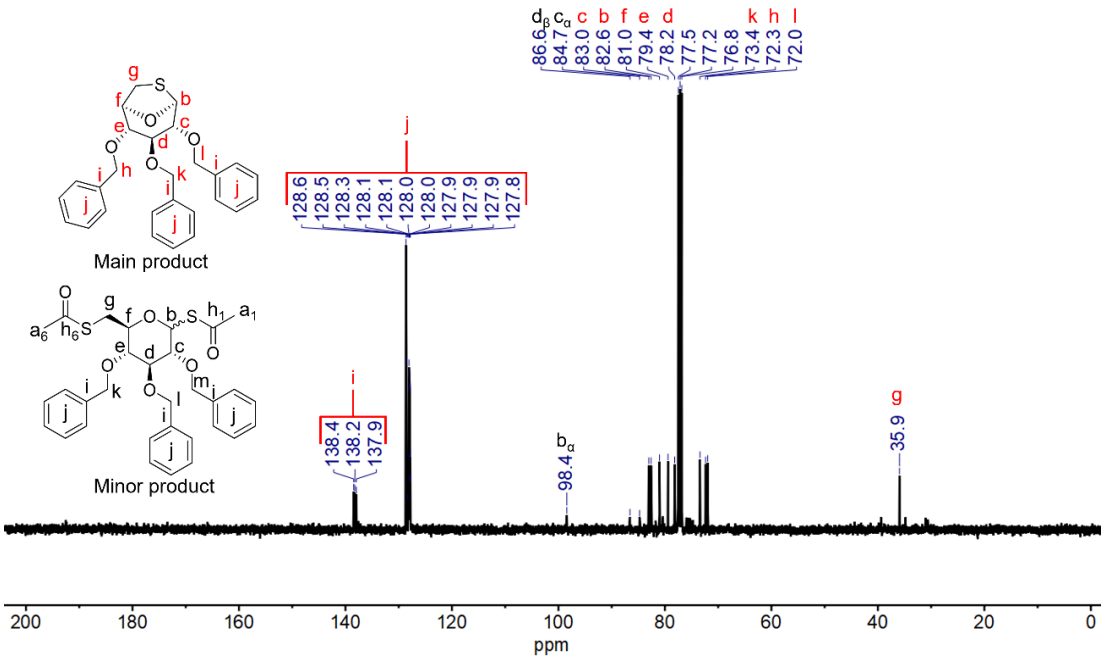


Figure A 2.58. *^{13}C NMR (101 MHz, 298 K, $CDCl_3$) spectrum of 1,6-anhydro-6-deoxy-6-thio-2,3,4-tri-O-benzyl-β-D-glucopyranose (**33**). By-product of the synthesis of 1,6-dithioacetate (**31**).*

^{1}H, ^{13}C and 2D NMR spectrum of a 1,6 glucose derived disulfide

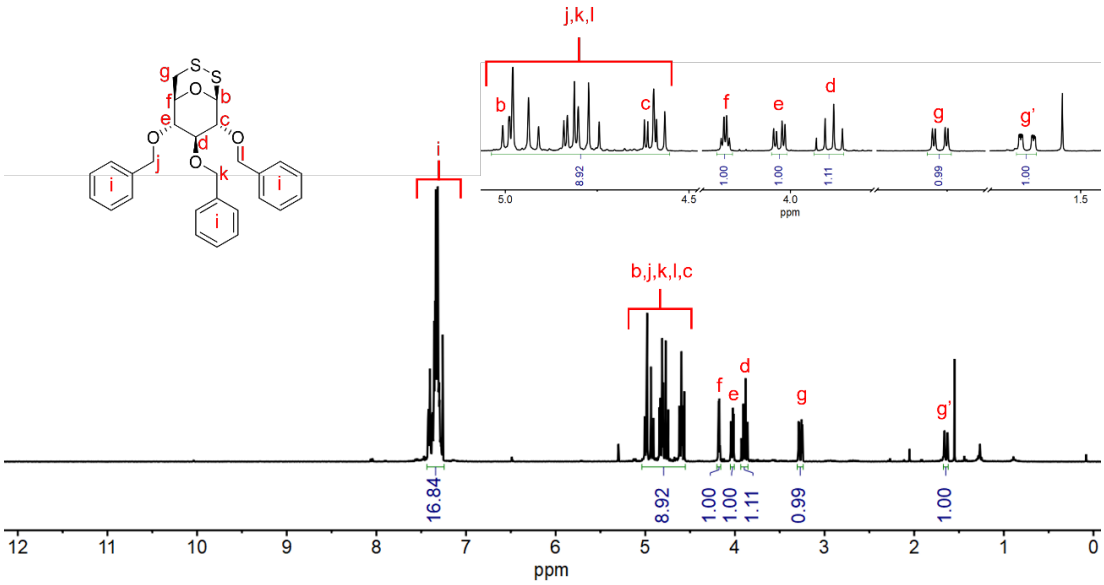


Figure A 2.59. *^{1}H NMR (400 MHz, 298 K, $CDCl_3$) spectrum of a 1,6-glucose-derived disulfide as an example of intramolecular disulfide formation occurring whilst working with the 1,6-glucose-derived dithiol (**32**).*

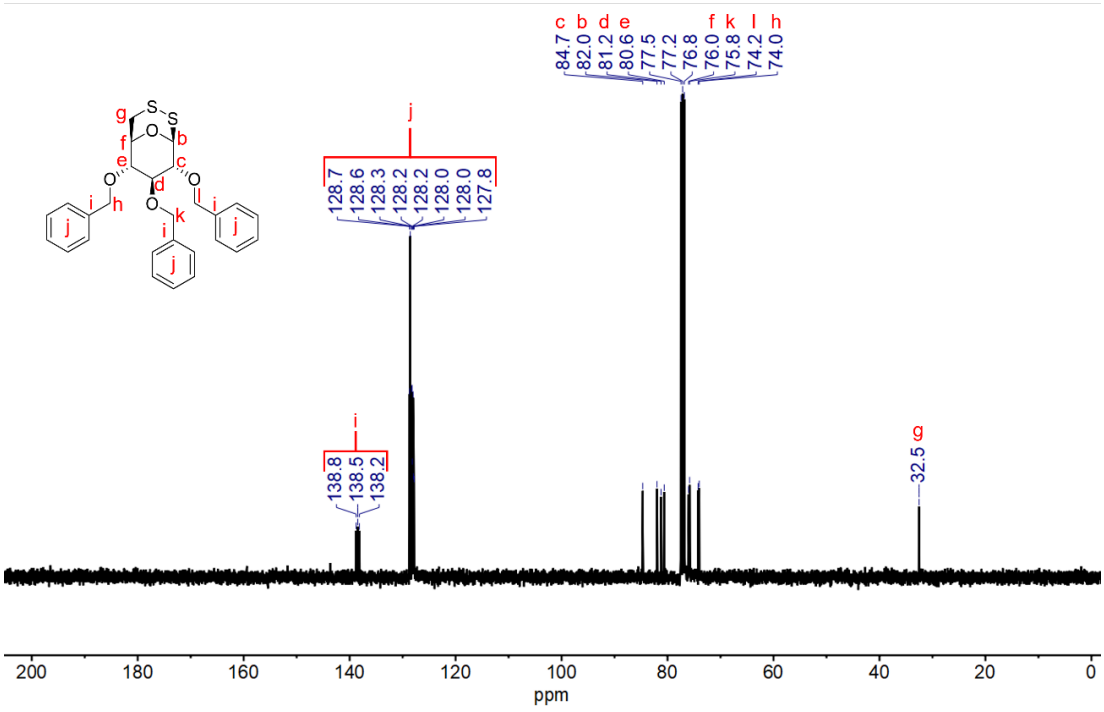


Figure A 2.60. *^{13}C NMR (101 MHz, 298 K, $CDCl_3$) spectrum of a 1,6-glucose-derived disulfide as an example of intramolecular disulfide formation occurring whilst working with the 1,6 dithiol (**26**).*

Appendices References

(1) Drake, E. N.; Brown, C. E. Application of nmr to biochemical kinetics. A laboratory experiment in physical biochemistry. *J. Chem. Educ.* **1977**, *54,* 124

(2) Organ, M. G.; Cooper, J. T.; Rogers, L. R.; Soleymanzadeh, F.; Paul, T. Synthesis of Stereodefined Polysubstituted Olefins. 1. Sequential Intermolecular Reactions Involving Selective, Stepwise Insertion of Pd(0) into Allylic and Vinylic Halide Bonds. The Stereoselective Synthesis of Disubstituted Olefins[1]. *J. Org. Chem.* **2000**, *65,* 7959-7970

(3) Stubbs, C. J.; Worch, J. C.; Prydderch, H.; Wang, Z.; Mathers, R. T.; Dobrynin, A. V.; Becker, M. L.; Dove, A. P. Sugar-Based Polymers with Stereochemistry-Dependent Degradability and Mechanical Properties. *J. Am. Chem. Soc.* **2022**, *144,* 1243-1250

(4) Evans, M. E. Methyl 4,6-O-benzylidene-α- and -β-d-glucosides. *Carbohydr. Res.* **1972**, *21,* 473-475

(5) Lonnecker, A. T.; Lim, Y. H.; Felder, S. E.; Besset, C. J.; Wooley, K. L. Four Different Regioisomeric Polycarbonates Derived from One Natural Product, d-Glucose. *Macromolecules* **2016**, *49,* 7857-7867

(6) Stubbs, C. J.; Worch, J. C.; Prydderch, H.; Becker, M. L.; Dove, A. P. Unsaturated Poly(ester-urethanes) with Stereochemically Dependent Thermomechanical Properties. *Macromolecules* **2020**, *53,* 174-181

(7) Petersen, S. R.; Prydderch, H.; Worch, J. C.; Stubbs, C. J.; Wang, Z.; Yu, J.; Arno, M. C.; Dobrynin, A. V.; Becker, M. L.; Dove, A. P. Ultra-Tough Elastomers from Stereochemistry-Directed Hydrogen Bonding in Isosorbide-Based Polymers. *Angew. Chem. Int. Ed.* **2022**, *61,* e202115904

Chapter 3 – Synthesis of telechelic poly(ester-urethane) oligomers via thiol-Michael step-growth addition

3 Synthesis of telechelic poly(ester-urethane) oligomers via thiol-Michael step-growth addition

3.1 Introduction

For decades, oligomers were merely deemed as undesirable by-products of polymerisation reactions.[1] Although, the concept of reacting an end-functionalised oligomer with another bifunctional molecule was exploited in 1937[2], when Otto Bayer reported for the first time the possibility of synthesising polyurethanes by reacting hydroxyl terminated polyols prepolymers with diisocyanates[3], this type of polyaddition relies on polyethers synthesised from epoxides, which are naturally bearing terminal hydroxyl groups, the research towards purposely functionalising oligomers with reactive groups at both chain ends flourished only in the 1960's. At this period of time, Uraneck *et al.* reported synthetic methods of yielding hydroxyl or carboxyl terminated polybutadiene oligomers and proposed the name "telechelic" - from the Greek "*telos*" (far) and "*chelos*" (claws) - as an adjective to describe this novel type of polymers, which have been specifically devised to bear reactive group at both extremities.[4]

Most interestingly, the primary goal of this pioneering work was to propose a solution to eliminate the formation of dangling chains, which are present in industrially-produced rubber vulcanisates and has been theorised to be detrimental to the strength of the resultant elastomer by Flory 14 years earlier.[5] And 9 years later, the same authors demonstrated that networks originating from the curing for telechelic poly(butadiene-co-styrene) in the presence of peroxides or sulfur-

containing accelerators where indeed showing enhanced strength and elongation at break compared to traditional rubbers of the same chemical composition.[6]

Soon after, this new technology has been exploited by the rubber industry to formulate telechelic liquid natural rubbers (LNR) to produce crosslinked materials for mechanically-demanding applications such as tyres, V-belts or footwear in a more time and cost effective manner since the compounding step of highly viscous natural rubber (NR) was no longer required.[7] Telechelic oligomers have also contributed to other significant advances in materials science. For instance, the possibility to obtain telechelic oligomers of controlled chain length *via* living polymerisation was exploited to synthesise ideal networks, *i.e* with a known molecular weight between crosslinks (M_c) and crosslinking density, which led to a better understanding of structure/property relationships within elastomeric networks.[8-13] Another major interest for telechelics oligomers is the production of multiphase materials of controlled morphologies by a combination of non-miscible oligomers with different backbone chemistries, which lead to the further development of thermoplastic elastomers.[14-19] In this specific application, the telechelic oligomers are usually referred to as “macromonomers” which is still a pertinent research topic to date.[20] The coating industry has also adopted the use of telechelic oligomers instead of high molecular weight polymer in response of regulations limiting the amount of volatile organic compounds (VOC) emissions, as their low viscosity allow for the formulation requiring only 30% of solvent as opposed to 70%.[21-23]

Since radiative chemistry took off in the same era with the ground-breaking work of Chapiro and Charlesby, this is without surprise that telechelic oligomers found

industrially relevant applications in the field of photo-curable resins,[24-26] which received a particular interest from the research community both for environmental and economic grounds.[27] Thus, in addition to being solvent-free, photo-initiated curing processes are endowed with being ultra-fast and proceed at room temperature, which offers the tremendous advantage of time and energy saving compared to more traditional thermal curing systems.[28]

The most abundant functionalities formulated within UV reactive resins are the cationic-initiated epoxides or vinyl ethers and the radical-initiated acrylates, with the latter being largely preferred for their greater reactivity.[29] Whilst early aliphatic acrylic resins presented some major disadvantages such as brittleness and shrinkage of the produced material cause by the inhomogeneity of the formed network, or low curing depths restricting its usage to thin films applications (protective coating, inks, varnishes, and paint), constant research efforts towards the development of more reactive initiators or the introduction of a variety of chemical structures within the polymeric backbone led to the overall improvement of the mechanical properties of the cured material.[30] As a result, UV-curable acrylate-based resins soon penetrated the market of engineering plastics such as dental composites as early as 1986[31] and, owing to advantageous viscosity and rapid curing time, were the basis which contributed to the advent of additive manufacturing. Thus, such resins are mentioned as ideal in the 1984 Charles Hull's patent on stereolithography-based 3D printing[32], and the commercialisation of the first stereolithography (SLA) printer by 3D systems® only followed 2 years later.[33, 34] Since then, acrylate-based resin systems have been the topic of the ever-growing research effort and are nowadays ubiquitous in our everyday life. As such, they are

to be found in a broad variety of industries such as coatings[35] for heat sensitive substrates (paper or wood[36]) but also metal or plastic surfaces[37, 38], dentistry[39], adhesives[40-42], ink-jet printing inks[43, 44] or stereolithography-based 3D printing[45, 46], to only name a few.

Acrylate-based resins are still the topic of intensive research, with the main challenge currently being to improve the sustainability of the curing process by either developing photoinitiators sensitive to sunlight[47-49] or incorporating bio-sourced polymer precursors.[50-56] Yet, monomers derived from the biomass are more often than not bearing temperature sensitive reactive groups such as acetals or unsaturation prone to isomerisation, which makes their handling and incorporation within polymers more challenging than the current monomers originating from petroleum feedstock.[57] Thus, this is still relevant to explore new ways of producing telechelic oligomers with a controlled molecular weight but also allowing the orthogonal introduction of sensitive functions within the polymer backbone. And the exploitation of click reactions such as thiol-ene Michael addition has long ago revealed itself as a promising mean to fulfil these specifications.[58-60]

3.2 Overview of this chapter

This chapter presents the oligomerisation *via* thiol-ene step-growth polyaddition of the 6 diacrylates which synthesis is detailed in chapter 2. The general principle of the study is illustrated in **Figure 3.1**. The diacrylates are copolymerised via thiol-Michael step-growth polymerisation with a dithiol in the presence of a base catalyst such as 1,8-Diazabicyclo[5.4.0]undec-7-ene (DBU) or dimethylphenylphosphine (DMPP) at ambient temperature (**Figure 3.1 (a)** and **(e)**).

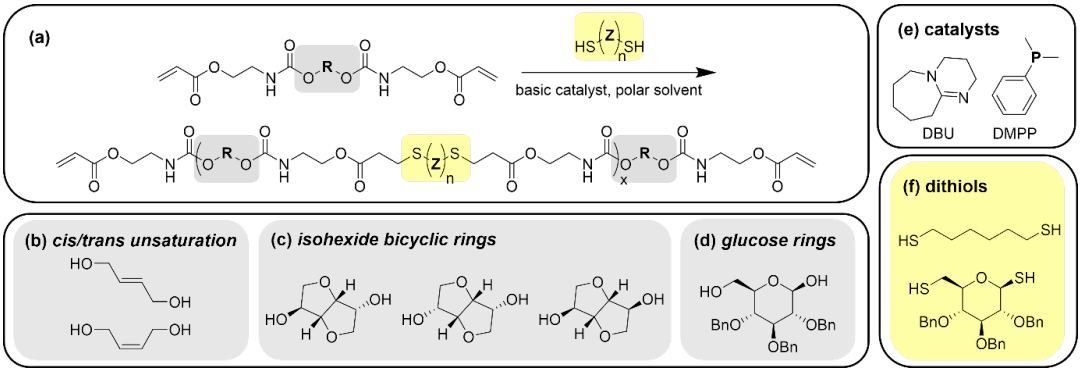


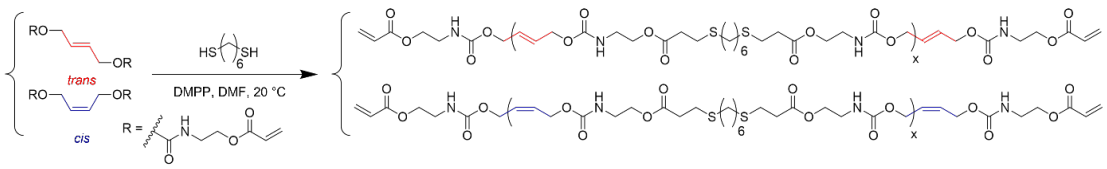
Figure 3.1. *Overview of this chapter which focusses on (a) the synthesis of acrylate-based telechelic oligomers via thiol-Michael step growth polyaddition were* ***R*** *represent either (b) the cis or trans diol, (c) from left to right, isosorbide, isommanide and isoidide or (d) a 1,6-glucose-derived diol. Both unsaturated- and isohexide-derived diacrylate monomer were reacted with 1,6-hexane dithiol whilst the 1,6-glucose-derived diacrylate has been reacted first with a 1,6-glucose-derived dithiol (f,bottom) then with 1,6-hexane dithiol (f, top).*

This exact procedure has been proven adequate for the implementation of sensitive *cis* and *trans* alkene functionality into high molecular weight linear thermoplastic without the occurrence of isomerisation or crosslinking.[61] In addition, isohexides have also been successfully incorporated into long chain linear polymers using this method.[62, 63] Thus, it was judicious to study the feasibility of producing low molecular weight acrylate-terminated telechelic oligomers via nucleophilic catalysed thiol-ene addition to later form photoset networks. Ultimately, the effect of either *cis*/*trans* or rigid ring endo/exo stereochemistry within chemical crosslinked networks could potentially be studied. (**Figure 3.1 (b)** and **(c)**) In parallel, the likelihood of synthesising a polysaccharide mimic by reacting the 1,6-glucose-derived diacrylate (**Figure 3.1 (d)**) with at first the 1,6-glucose dithiol and later with 1,6-hexane dithiol (**Figure 3.1 (f)**) has been investigated. The unique adaptability of this synthetic method is highlighted by the extremely diverse polymer backbones that could potentially be obtained, since the central group of the diacrylate (**R**) or the dithiol (**Z**) could virtually represent an infinite possibility of structures. Moreover, this

reaction can be performed under an ambient atmosphere, *e.g* in the presence of air and moisture even though thiols should be kept under nitrogen both for storage stability and purity concerns. The chapter will first start with the polymerisation of the *cis*/*trans* diacrylates, which will be taken as an opportunity to present the method used to experimentally control the molecular weight of the oligomers as well as ensuring the presence of acrylate termini. In addition, the choice of determining the average molecular weight by number (M_n) by ^{1}H NMR spectroscopy will then be discussed, and the general method presented. Then, the specifics of the polymerisation of isohexides derived diacrylate with the commercial 1,6-hexane dithiol will be discussed. Finally, the attempt at obtaining synthetic polysaccharides by reacting the 1,6-glucose derived diacrylate with the 1,6-glucose-derived dithiol or 1,6-hexane dithiol will be presented.

3.3 Synthesis of the *Cis* and *trans* unsaturated oligomer

Cis and *trans* acrylate-terminated poly(ester-urethane) oligomers were synthesised *via* thiol-Michael step-growth addition in DMF (0.25 M) using dimethylphenylphosphine (DMPP) as catalyst. (**Scheme 3.1**)



Scheme 3.1. *Synthesis of cis and trans stereopure acrylate-terminated telechelic oligomers via thiol-Michael addition. The reaction is performed in DMF at a diacrylate monomer concentration of 0.25 M and in the presence of 0.5 mol% of DMPP as catalyst.*

The control over the molecular weight and termini was achieved by carrying out the reaction in nonstoichiometric conditions[64, 65] and the number average molecular

weight M_n was determined by ^1H NMR spectroscopy over gel permeation chromatography (GPC) analysis. The methods and reasoning will be detailed in the paragraphs below. In addition, only minor changes to the literature procedure[61] such as working at -20 °C during the addition of the catalyst and maintaining the temperature under 0 °C throughout the reaction. Excessive heating was also avoided during the work up and drying stages to reduce the probability for uncontrolled crosslinking. After implementing this adjustment, stereopure *cis* or *trans* oligomer could be obtained on scales up to 60 g of monomer after precipitation into methanol.

3.3.1 Control over the molecular weight and termini

As the polymerisation follows a step-growth process, the diacrylate monomer needs to be introduced in excess, following Carother's equation[66] for a linear copolymer with A-A, B-B monomers:

$$\bar{X}_n = \frac{1 + r}{1 + r - 2rp} \quad (1)$$

Where $\overline{X}_n$ is the average value of the degree of polymerisation (DP), r the ratio of diacrylate and p the conversion. Assuming a quantitative reaction - which is fair assumption for thiol-ene step growth addition, due to the high efficiency and minimal side reactions that are reported - $p = 1$ and therefore equation (1) becomes:

$$\lim_{p \to 1} \bar{X}_n = \frac{1 + r}{1 - r} \quad (2)$$

r is now extracted, equation (2) becomes:

$$r_{>1} = \frac{\bar{X}_{\mathrm{n}} + 1}{\bar{X}_{\mathrm{n}} - 1} \quad (3)$$

Then, by setting $\bar{X}_{\mathrm{n}}$ as an integer > 1 and calculating the theoretical molecular weight of a chain of $\overline{\mathrm{X}}_{\mathrm{n}}$, setting that $\mathrm{n}_{\mathrm{diacrylate}} = \mathrm{n}_{\mathrm{dithiol}} + 1$, it is possible to access the ratio, and therefore the molar equivalent of diacrylate, to target one specific molecular weight. (**Table 3.1**) In practice, the $\bar{M}_{\mathrm{n}}$ obtained was consistently higher than the theoretical one, which could be both explained by experimental error and monomer purity, but also because this equation was developed for polycondensation-type polymerisation, which is reversible, and therefore in an equilibrium.

Table 3.1. *Stoichiometry between an unsaturated acrylate and dithiol monomers for a targeted molecular weight based on the Carother's equation.*

Degree of polymerisation	Number of dithiol unit	Equivalent of diacrylate	Theoretical *MW* (Da)
1	0	-	370
3	1	2	890
5	2	1.5	1410
7	3	1.33333333	1930
9	4	1.25	2450
11	5	1.2	2970
13	6	1.16666667	3490
15	7	1.14285714	4010
17	8	1.125	4530
19	9	1.11111111	5050

In practice, some factors, such as monomer purity and dryness or the balance accuracy, will define how close or how far the obtained molecular weight will be from the theoretical value targeted. In the first experiments, the molecular weights obtained were far higher than the ones targeted, reaching up to 40 kDa when a

3kDa oligomer was expected. The main cause of such discrepancies was that the diacrylate monomer used contained impurities and consequently the equivalence of the diacrylate added was smaller than the one targeted and so longer chains were obtained.

This gap between experimental and theoretical molecular weight was reduced by improving the purity and dryness of the diacrylate monomers and once the optimal procedure for the synthesis and work up of the diacrylate monomers were reached, it was possible to confidently target a molecular weight by using an experimental step-growth curve obtained after changing the equivalence of monomers on small scale experiments. (**Figure 3.2**) Interestingly, there is still a discrepancy between the experimental step-growth curves of both *cis* and *trans* diacrylate monomers and the theoretical one, derived from Carother's equation. This difference could be caused by remaining experimental errors, especially on small scale reactions of 0.2 g or most likely by the fact that Carother's equation is supposed to describe polycondensation reactions and hence could simply be an imperfect model for a phosphine catalysed thiol-Michael addition.

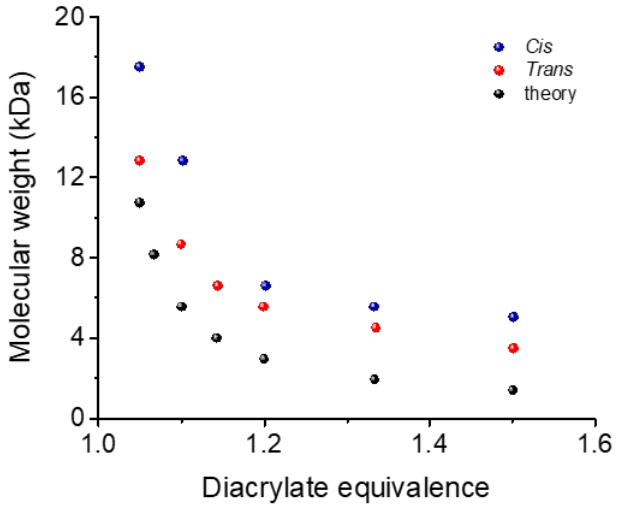


Figure 3.2. *The dependence of polymer molecular weight on the stoichiometry of the acrylate monomers. Experimental data for both the cis (blue) and trans (red) polymers and theoretical molecular weights (black) are shown.*

Regarding the discrepancy in the molecular weight at a given diacrylate equivalence observed between the *cis* and *trans* diacrylate monomer, this could be caused by a variation in reactivity, with the *cis* being more reactive than the *trans* diacrylate.

3.3.2 Experimental molecular weight determination

The molecular weight of the oligomers has been calculated using ^{1}H NMR spectroscopy. Under the assumption that all chains are bearing acrylate termini and that the formation of cyclic oligomers is negligible, this was achieved by taking the peaks from the acrylate end group as reference $\mathbf{a_2}$, $\mathbf{a_1}$ and **b** (2H; dd; δ= 6.45-6.40 ppm) (**Figure 3.3**).

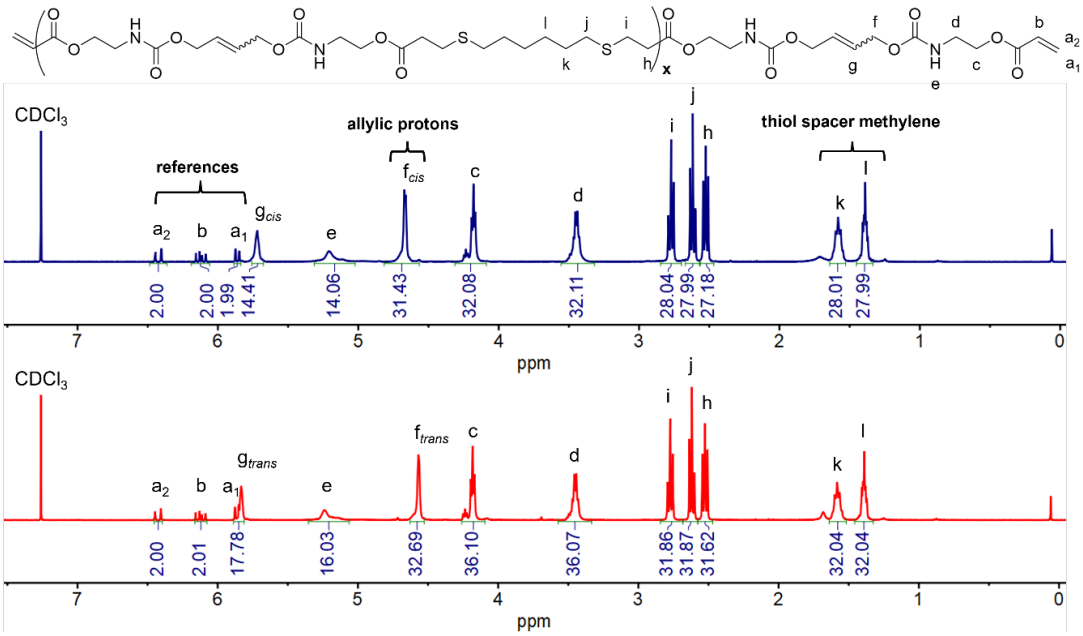


Figure 3.3. *^{1}H NMR spectra (400 MHz, $CDCl_3$, 298 K) of a cis 4.0 kDa oligomer (top) and a trans 4.5 kDa oligomer (bottom).*

When integrated for 2, the methylene within the thiol spacer **l** (4H; m, δ= 1.39 ppm (*trans*), δ= 1.36 ppm (*cis*)) and allylic protons of the unsaturation within the diacrylate moity **f** (4H, δ= 4.57 ppm (*trans*), δ= 4,64ppm (*cis*)) were integrated and divided by four to access the degree of polymerisation DP. This value must be multiplied by the molecular weight of the monomers to access the average molecular weight of the oligomer:

$$\bar{M}_{\mathrm{n}\,(NMR)} = \left(\frac{I_{\mathrm{thiol}}}{2} \times M_{\mathrm{thiol}}\right) + \left(\frac{I_{\mathrm{diacrylate}}}{2} \times M_{\mathrm{diacrylate}}\right) \quad (4)$$

Where $\mathrm{I}_{\mathrm{thiol}}$ represents the integration of the methylene within the thiol linker **l** resonance signal, $\mathrm{I}_{\mathrm{diacrylate}}$ the integration of the allylic protons of the unsaturation within the diacrylate moiety **f**, $\mathrm{M}_{\mathrm{thiol}}$ and $\mathrm{M}_{\mathrm{thiol}}$ the molecular weight of the dithiol and diacrylate monomer, respectively.

This method has been chosen over a size-exclusion chromatography (SEC) analysis because below 10 kDa SEC analysis was giving inconsistent results, which might be a consequence of the resolution being poor at smaller molecular weights (< 10 kDa) because of the broad range of molecular weights covered by the installed SEC columns on the available equipment (**Appendix section 3.8.1**). This was verified on samples with a M_w from 4.5 to 18 kDa (**Table 3.2**): For most entries the SEC gives a M_w smaller than the one expected, which is inconsistent, as the reaction is near quantitative.

Table 3.2. *Summary of molecular weights obtained by ^{1}H NMR and GPC for cis and trans unsaturated oligomers. [a]Determined by ^{1}H NMR spectroscopy (400 MHz, 298 K, $CDCl_3$). [b]M_n, M_w, $Đ_M$ were determined by SEC (DMF, 0.5% w/w NH_4BH_4) analysis against poly(methyl methacrylate) (PMMA) standards.*

Entry	Stereochemistry	*MW* targeted (kDa)	$M_{n\,(NMR)}$[a] (kDa)	$M_{w\,(GPC)}$[b] (kDa)	$Đ_m$[b] (GPC, M_w/M_n)
1	*trans*	4.5	6.6	2.7	2.5
2	*trans*	6.6	7.1	3.4	2.0
3	*trans*	7.1	9.2	3.7	4.2
4	*trans*	20	28	5.4	3.8
5	*cis*	4.5	8.7	2.7	2.2
6	*cis*	4.5	6.6	2.6	2.1
7	*cis*	13	11	5.2	3.8
8	*cis*	18	26	4.2	3.0

Regarding the dispersity $Đ_M$, it is within the range of 2 to 6, which is expected for step growth polymerisation.

3.3.3 Thermal properties of oligomers

The thermal properties of *cis* and *trans* oligomers were analysed using differential scanning calorimetry (DSC) (**Figure 3.4**). Both oligomers experienced a glass transition temperature (T_g) far below room temperature at around -20 °C. The *trans* monomer shows multiple melting transitions during the first heating cycle,

which corresponds to different crystalline domains and some degree of rearrangement from a crystal form to another.[67] In the second heating cycle, a second melting transition is present, meaning that the *trans* oligomer can still crystallise at a temperature ramp of 10 °C min^{-1}.

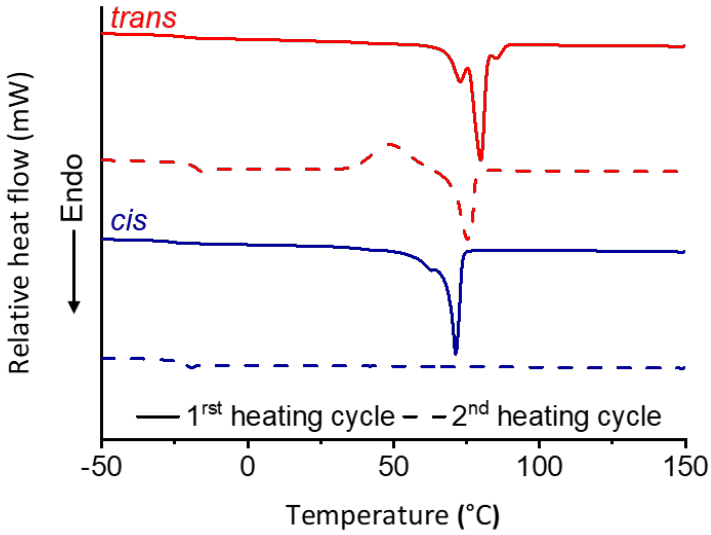


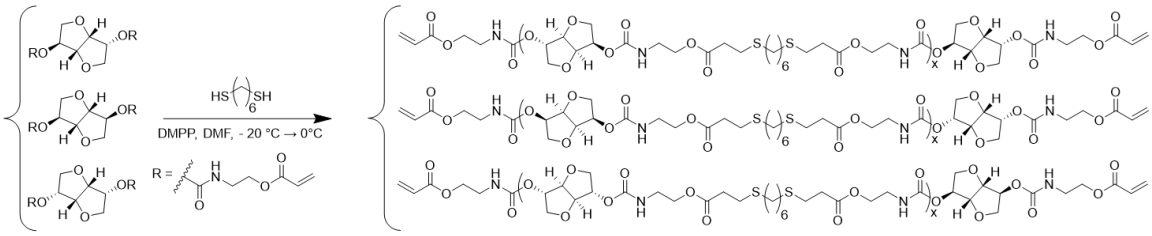
Figure 3.4. *DSC thermograms of 1st and 2nd heating cycles for the cis 4.0 kDa oligomer and the trans 4.5 kDa oligomer.*

On the other hand, the *cis* oligomer presents a melting transition only in the first heating cycle and not in the second one. Therefore, the *cis* oligomer shows some crystalline properties, but it crystallises slower than the *trans* oligomer. This observation is very promising as a difference in crystallinity could potentially translate to divergent mechanical properties.

3.4 Isohexides oligomers

3.4.1 Synthesis

Isohexides derived oligomers were also obtained *via* thiol-Michael step growth addition of a diacrylate monomer and 1,6-hexanedithiol in DMF (0.25 M) using dimethylphenylphosphine (DMPP) as a catalyst. (**Scheme 3.2**)



Scheme 3.2. *Synthesis of isohexides acrylate-terminated telechelic oligomers via thiol-Michael addition. The reaction is performed in DMF at a diacrylate monomer concentration of 0.25 M and in the presence of DMPP as a catalyst.*

The same methodology to target and determine the molecular weight that presented for the synthesis of unsaturated oligomers was exploited. (**Table 3.3**)

Table 3.3. *Stoichiometry between isohexide derived diacrylate and dithiol monomers for a targeted molecular weight based on the Carother's equation.*

Degree of polymerisation	Number of dithiol unit	Equivalent of diacrylate	Theoretical *MW* (Da)
1	0	-	428.39
3	1	2	1006.78
5	2	1.5	1585.17
7	3	1.33333333	2163.56
9	4	1.25	2741.95
11	5	1.2	3320.34
13	6	1.16666667	3898.73
15	7	1.14285714	4477.12
17	8	1.125	5055.51
19	9	1.11111111	5633.9

Using a stochiometric imbalance in the case of the isohexides diacrylate monomers also gave a very good control over the final molecular weight of the obtained oligomers. (**Table 3.4**)

Table 3.4. *Summary of molecular weights obtained by ^{1}H NMR and GPC for the isosorbide and isomannide derived oligomers. [a]Determined by ^{1}H NMR spectroscopy (400 MHz, 298 K, $CDCl_3$). [a]Determined by ^{1}H NMR spectroscopy (400 MHz, 298 K, $CDCl_3$). [b]M_n, M_w, $Đ_M$ were determined by SEC (DMF, 0.5% w/w NH_4BH_4) analysis against poly(methyl methacrylate) (PMMA) standards.*

entry	stereochemistry	MW targeted (kDa)	$M_{n\,(NMR)}$[a] (kDa)	$M_{w\,(GPC)}$[b] (kDa)	$Đ_m$[b] (GPC, M_w/M_n)
1	*endo/exo*	2.2	3.0	5.0	3.3
2	*endo/exo*	2.7	4.0	8	2.8
3	*endo/exo*	3.3	5	10	2.8
4	*endo/endo*	2.2	3.9	8.8	1.4
5	*endo/endo*	2.7	4.5	10	2.0
6	*endo/endo*	3.3	5.3	8.7	1.7

Interestingly, the molecular weights obtained by GPC analysis seemed more consistent than the obtained values for the unsaturated oligomers, however, the choice was made to determinate the molecular weight by ^{1}H NMR analysis for comparison with the prior oligomer system. The original procedure developed in the laboratory for the polyaddition of isohexides diacrylate monomer with a commercial dithiol to obtained high molecular weight required a temperature of 50 °C and also required the use of chloroform as solvent at a concentration of 0.5 M. Unfortunately, this preparation led to uncontrolled crosslinking upon the addition of the catalyst but decreasing the temperature to 0 °C allowed to successfully obtain oligomers with a molecular weight ranging from 3.3 to 3.9 kDa with the 3 different isohexide-derived diacrylate monomers. (**Figure 3.5**)

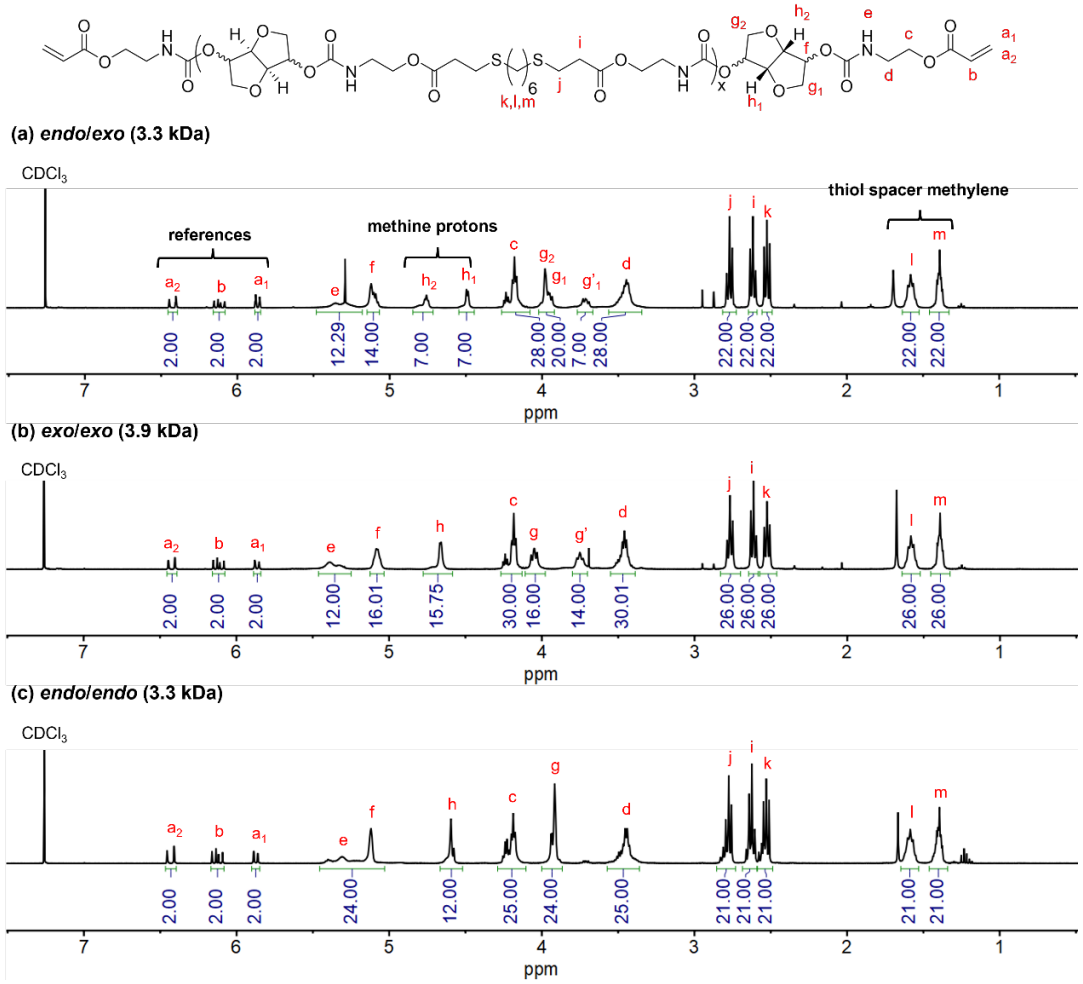


Figure 3.5. *^{1}H NMR spectra (400 MHz, $CDCl_3$, 298 K) of (a) a 3.3 kDa isosorbide based oligomer, (b) a 3.9 kDa isomanide derived oligomer and (c) a 3.3 kDa isoidide derived oligomer. The molecular weight has been obtained by end-group analysis, taking the acrylate integration as reference. The integration of the methine protons from the isohexides moieties and the methylene within the thiol spacer were used to determinate the average chain length.*

Yet, the scale up of this reaction from 1 g to 5 g consistently led to uncontrolled crosslinking even after decreasing the temperature to -20 °C and adding 3 mol% of butylated hydroxyltoluene (BHT) as radical scavenger (**Figure 3.6**). And working at -50 °C hindered the progress of the reaction completely. For this reason, chloroform was replaced by dimethylformamide which does not promote the formation of radical species.

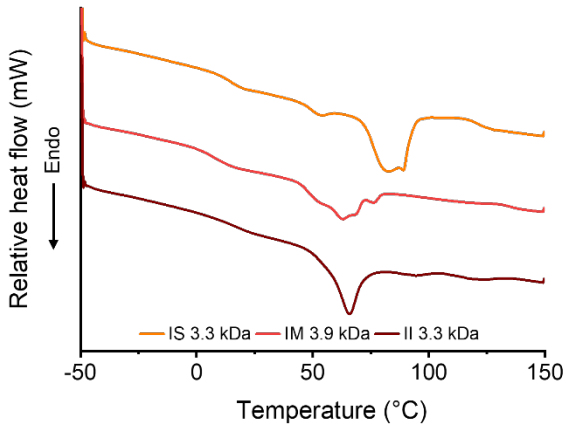


Figure 3.6. *Picture representing uncontrolled crosslinking encountered during the polymerisation or work up of isohexide derived oligomer.*

Although working with dimethylformamide produced the same results in term of molecular weight control, precipitating the oligomer from the crude was unsuccessful even in a volume of methanol 20-fold larger than the reaction media maintained at -78 °C. As an alternative, the DMF was removed *in vacuo*, the crude oligomer dissolved in the minimal amount of chloroform and then precipitated in methanol. Despite the tediousness of this method, the oligomer could still be recovered in good yield ranging from 80 to 85% on a 1 g scale. Nevertheless, it also led to crosslinking during the drying process.

3.4.2 Thermal properties of oligomers

The thermal properties of the isosorbide, isomannide and isoidide derived oligomers were determined by differential scanning calorimetry (DSC). (**Figure 3.7**) Each of the three kinds of oligomer displayed at least one thermal event corresponding to the melting of a crystalline phase. The enthalpy of melting for the isosorbide-derived oligomer was about twice as high (10.8 $J.g^{-1}$) as that of the isomannide (6.3 $J.g^{-1}$) and isoidide (6.8 $J.g^{-1}$) derived oligomers.



sample	T_g[a] (°C)	$T_{m,1}$[b] (°C)	$T_{m,2}$[c] (°C)	ΔH_m[d] ($J \cdot g^{-1}$)
3.3 kDa isosorbide	21.9	54.2	82.9	10.8
3.9 kDa isomannide	17.1	63.0	N/A	6.3
6.1 kDa isoidide	21.4	65.9	N/A	6.8

Figure 3.7. *1st heating cycles of the DSC thermograms for the isohexides oligomers. The table presents the key thermal transitions of the oligomers.* **[a]** *The glass transition temperature (T_g) was taken as the midpoint of the inflection tangent upon the 2nd heating scan.* **[b]** *The temperature of the first endothermic transition ($T_{m,1}$), taken at the minimum of the peak on the first heating scan.* **[c]** *The temperature of the 2nd endothermic transition ($T_{m,2}$), taken at the minimum of the peak on the 1st heating scan.* **[d]** *The total enthalpy of melting (ΔH_m) was calculated from integration and normalisation of all endothermic peaks present on the first heating scan.*

Moreover, no melt transition could be observed on any of the 2nd heating scans. Regarding the T_g of the oligomers, the value ranged from 17.1 °C to 21.9 °C. Despite

having a T_g around room temperature which is highly desirable to produce elastomeric materials, the inability to scale up the reaction above 1 g and the high probability of uncontrolled crosslinking led to the decision to not take this project further.

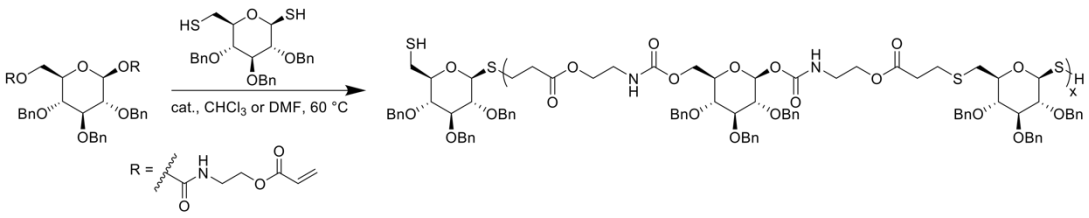
3.5 Glucose-derived monomers polymerisation

Both unsaturated and isohexide derived diacrylates were already reported for the synthesis of high molecular weight thermoplastics via thiol-Michael step growth addition.[61-63] For this reason, the focus of this chapter was to study the potential of synthesising oligomers. Regarding the glucose derived diacrylate and dithiol, which were synthesised in chapter 2, the logical first step was to study the results obtained at a stochiometric balance of both monomers to target high molecular weight polymers.

3.5.1 Synthesis

The first attempts at polymerising the 1,6-glucose-derived diacrylate and dithiol was performed in both DMF and $CHCl_3$ at a concentration of 0.25 M, in the presence of DMPP or DBU as the catalyst. (**Figure 3.8**)

(a)



(b)

entry	solvent	conc. (M)	stoichiometry	catalyst	M_n (kDa)	M_w (kDa)	$Đ_m$ (M_w/M_n)
1	$CHCl_3$	0.25	1	DMPP	4	11	2.5
2	$CHCl_3$	0.25	1	DMPP	3.6	8.1	2.3
3	$CHCl_3$	0.25	1	DBU	3.3	7.6	2.3
4	$CHCl_3$	0.25	1	DBU	3.6	7.7	2.1
5	DMF	0.25	1	DMPP	6.7	19	2.8
6	DMF	0.25	1	DMPP	6.8	18	2.7
7	DMF	0.25	1	DBU	3.8	8.0	2.1
8	DMF	0.25	1	DBU	4.1	9.0	2.2

Figure 3.8. *(a) Scheme of the polymerisation of the 1,6-glucose-derived diacrylate and dithiol via thiol-Michael addition. The reaction is performed either in DMF or $CHCl_3$ at a diacrylate monomer concentration of 0.25 M and in the presence of DMPP or DBU as catalyst. (b) Table presenting a summary of the results of polymerisation for the glucose derived monomers at the stochiometric balance. M_n, M_w, and $Đ_M$ were determined by SEC (DMF, 0.5% w/w NH_4BH_4). Analysis against poly(methyl methacrylate) (PMMA) standards.*

Surprisingly, the reaction did not reach completion at room temperature even after 48 h. For this reason, the subsequent reactions were carried out at 60 °C, which resulted in the reaction completion within 12 h. However, the M_w obtained for a 1 to 1 ratio of monomers were ranging from 7 to 19 kDa, at a fixed concentration of diacrylate of 0.5 M. These results were lower than expected and as such, it was hypothesised that the 1,6-glucose-derived dithiol purity could be causing this issue, therefore the diacrylate to dithiol ratio was decreased, in order to find the stoichiometric balance. (**Table 3.5**) Working with an equivalent of diacrylate of 0.95 and 0.925, whilst using DBU as a catalyst led to an increase of M_w from 7.7 to 18 kDa in chloroform and from 8.0 to 24 kDa in DMF.

Table 3.5. *Summary of the results of polymerisation for the glucose-derived monomers using an equivalent of diacrylate to dithiol inferior to the unity. M_n, M_w, and $Đ_M$ were determined by SEC (DMF, 0.5% w/w NH_4BH_4). Analysis against poly(methyl methacrylate) (PMMA) standards.*

entry	solvent	conc. (M)	stoichiometry	catalyst	M_n (kDa)	M_w (kDa)	$Đ_m$ (M_w/M_n)
1	$CHCl_3$	0.25	0.95	DBU	5.3	18	3.4
2	$CHCl_3$	0.25	0.925	DBU	6.3	18	2.9
3	$CHCl_3$	0.25	0.9	DBU	4.9	14	2.8
4	$CHCl_3$	0.25	0.875	DBU	5.3	13	2.4
5	$CHCl_3$	0.25	0.850	DBU	3.4	7.0	2.1
6	$CHCl_3$	0.25	0.825	DBU	3.9	9.0	2.3
7	$CHCl_3$	0.25	0.850	DBU	3.4	6.9	2.0
8	DMF	0.25	0.95	DBU	7.5	23	3.1
9	DMF	0.25	0.925	DBU	7.8	24	3.1
10	DMF	0.25	0.9	DBU	7.2	23	3.1
11	DMF	0.25	0.875	DBU	7.4	24	3.2

However, no correlation between the stoichiometry and the resulting molecular weight could be observed, highlighting the lack of control over the molecular weight using this technique, this is especially prevalent when DMF is used as solvent. Hence, varying the equivalence of diacrylate from 0.95 to 0.875, the M_w remained stable at 23-24 kDa. **(entry 8-11 Table 3.5)** Unfortunately, in the case of the glucose derived polymerisation products, the GPC was the only available method for the determination of the molecular weight since the ^{1}H NMR spectra was not defined enough to be exploited for this purpose. **(Figure 3.9)** The only information that could be obtained from the ^{1}H NMR spectroscopy is the consumption of the diacrylate termini characteristic peaks around δ = 6 ppm, indicating the success of the polymerisation.

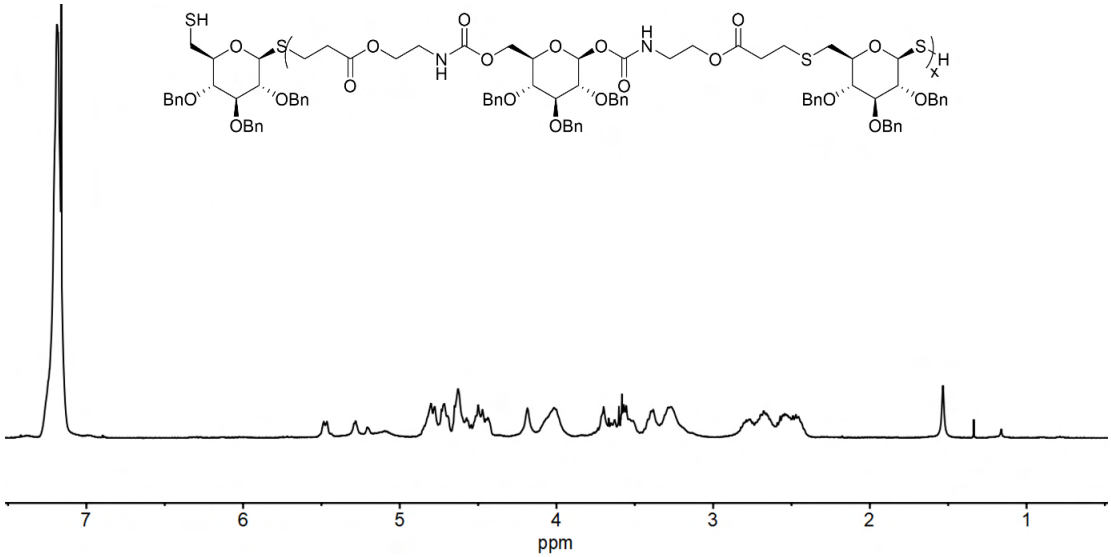


Figure 3.9. *^{1}H NMR spectra (400 MHz, $CDCl_3$, 298 K) of an 8.0 kDa glucose-derived polymerisation product. The absence of the resonance peaks characteristic of the acrylate between 5.6 and 6.5 ppm indicates a successful polymerisation.*

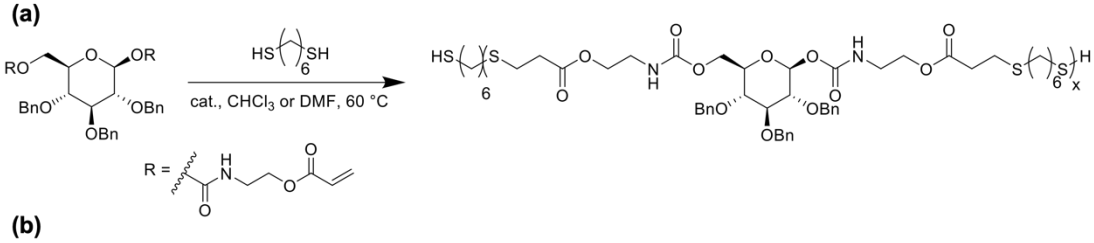
Lastly, the concentration of the diacrylate was modified in an attempt to yield higher molecular weight, however, this parameter did not result in any improvement. **(Table 3.6)**. Increasing the concentration from 0.25 to 0.5 M resulted in the same M_w of about 7.9 kDa whilst increasing the concentration to 1 M resulted in a M_w of 5 kDa. Decreasing the concentration to 0.1 M yielded a 4.5 kDa oligomer.

Table 3.6. *Summary of the results of polymerisation for the glucose-derived monomers using a 1:1 molar ratio of diacrylate to dithiol. M_n, M_w, and $Đ_M$ were determined by SEC (DMF, 0.5% w/w NH_4BH_4). Analysis against poly(methyl methacrylate) (PMMA) standards.*

entry	solvent	conc. (M)	stoichiometry	catalyst	M_n (kDa)	M_w (kDa)	$Đ_m$ (M_w/M_n)
1	$CHCl_3$	0.5	1	DBU	3.5	7.9	2.3
2	$CHCl_3$	1	1	DBU	2.7	5.0	1.9
3	$CHCl_3$	0.1	1	DBU	2.1	4.5	2.2

Since all possible reaction parameters were exploited in an attempt at obtaining a high M_w without success, it has been hypothesised that the difference in reactivity between the thiol on the first position and that of the 6th position of the sugar ring could be the cause. Or this issue could be stemming from the steric hinderance of the benzyl protecting groups at least partially. Hence, if the 1,6-glucose-derived dithiol is replaced by 1,6-hexanedithiol, then the M_w increase from about 18 to 30 kDa using the same reaction conditions. **(Figure 3.10(a))**

(a)



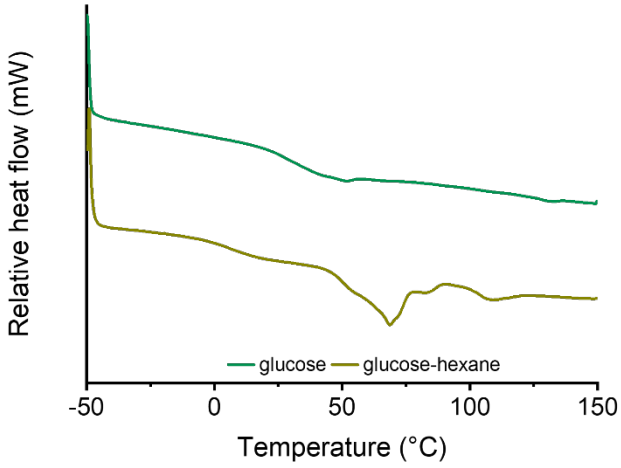
(b)

entry	solvent	conc. (M)	stoichiometry	catalyst	M_n (kDa)	M_w (kDa)	$Đ_m$ (M_w/M_n)
1	DMF	0.25	1	DMPP	6.4	34	5.3
2	$CHCl_3$	0.25	1	DBU	5.9	30	5.0

Figure 3.10. *(a) Scheme of the polymerisation of the 1,6-glucose-derived diacrylate and 1,6-hexane dithiol via thiol-Michael addition. The reaction is performed either in DMF or $CHCl_3$ at a diacrylate monomer concentration of 0.25 M and in the presence of DMPP or DBU as catalyst. (b) Table presenting a summary of the results of polymerisation for the glucose derived monomers at the stochiometric balance. M_n, M_w, and $Đ_M$ were determined by SEC (DMF, 0.5% w/w NH_4BH_4). Analysis against poly(methyl methacrylate) (PMMA) standards.*

3.5.2 Thermal properties of oligomers

The thermal properties of the glucose derived oligomers were determined by differential scanning calorimetry (DSC). (**Figure 3.11**)



sample	T_g[a] (°C)	$T_{m,1}$[b] (°C)	$T_{m,2}$[c] (°C)	ΔH_m[d] (J·g^{-1})
glucose	32.9	51	N/A	0.41
glucose-hexane	11.9	68.8	109	14.7

Figure 3.11. *1st heating cycles of the DSC thermograms for the polymerisation products of 1,6-glucose-derived diacrylate and 1,6-glucose-derived dithiol "glucose" or 1,6-hexane dithiol "glucose-hexane". The table present the key thermal properties of the oligomers.* **[a]** *The glass transition temperature (T_g) was taken as the midpoint of the inflection tangent upon the 2nd heating scan.* **[b]** *The temperature of the first endothermic transition ($T_{m,1}$), taken at the minimum of the peak on the first heating scan.* **[c]** *The temperature of the 2nd endothermic transition ($T_{m,2}$), taken at the minimum of the peak on the 1st heating scan.* **[d]** *The total enthalpy of melting (ΔH_m) was calculated from integration and normalisation of all endothermic peaks present on the first heating scan.*

Interestingly, the glucose-derived oligomer containing the aliphatic 1,6-hexane dithiol present a thermal event at 68.8 °C corresponding to the melting of crystalline phases whilst the oligomer containing only glucose derived monomers is amorphous. This difference is certainly caused by the inability for the latter to form crystalline phase owing to the rigidity of the repeating units in the chain. Unsurprisingly, the addition of an aliphatic spacer increased the free movement

available to the polymers chains which translates to a decrease in the T_g from 32.9 to 11.9 °C. Although it would have been interesting to study their mechanical properties within network, the inability to control the molecular weight using thiol-Michael addition was problematic and therefore led to the decision to not continuing this project further.

3.6 Conclusion

The diacrylate monomers which were presented in chapter 2 were polymerised via thiol-Michael addition. The *cis*/*trans* unsaturated diacrylate successfully polymerised with 1,6-hexane dithiol to produce acrylate-telechelic oligomers from 3 to 10 kDa with excellent control over the molecular weight using the stoichiometric imbalance method. Moreover, once the conditions of reaction were optimised to prevent uncontrolled crosslinking, it was possible to scale this polymerisation up to 60 g. Surprisingly, this control could not be achieved with the isohexide-derived diacrylate since their polymerisation with 1,6-hexanedithiol consistently led to uncontrolled crosslinking. In addition, attempts at producing a synthetic polysaccharide by polymerising the 1,6-glucose-derive diacrylate with the 1,6-glucose dithiol at a 1 to 1 ratio led to molecular weight of a maximum of about 20 kDa. This inability to obtain higher molecular weight was rationalised by the existence of considerable steric hinderance stemming from the presence of bulky benzyl protecting groups since replacing the glucose derived dithiol by 1,6-hexane dithiol led to a noticeable increase in the molecular weight obtained. Moreover, no control over the molecular weight could be achieved. Thus, only the *cis*/*trans* unsaturated oligomer were selected as the candidate to study the impact of stereochemistry within a polymer network, which will be presented in chapter 4.

3.7 References

(1) Tezuka, Y. Telechelic polymers. *Prog. Polym. Sci.* **1992**, *17,* 471-514

(2) Bayer, O. Das di-isocyanat-polyadditionsverfahren (polyurethane). *Angew. Chem.* **1947**, *59,* 257-272

(3) Goethals, E. J. Introductory Remarks. In *Telechelic polymers: synthesis and applications*, CRC press, 2018; pp 1-4.

(4) Uraneck, C. A.; Hsieh, H. L.; Buck, O. G. Telechelic polymers. *J. Polym. Sci.* **1960**, *46,* 535-539

(5) Flory, P. J. Effects of Molecular Structure on Physical Properties of Butyl Rubber. *Ind. Eng. Chem.* **1946**, *38,* 417-436

(6) Uraneck, C. A.; Hsieh, H. L.; Sonnenfeld, R. J. Telechelic elastomers. *J. Appl. Polym. Sci.* **1969**, *13,* 149-168

(7) Nor, H. M.; Ebdon, J. R. Telechelic liquid natural rubber: A review. *Prog. Polym. Sci.* **1998**, *23,* 143-177

(8) Rempp, P.; Herz, J. E. Model networks—synthesis and structure. *Angew. Makromol. Chem.* **1979**, *76,* 373-391

(9) Mark, J. E.; Sullivan, J. L. Model networks of end-linked polydimethylsiloxane chains. I. Comparisons between experimental and theoretical values of the elastic modulus and the equilibrium degree of swelling. *J. Chem. Phys.* **1977**, *66,* 1006-1011

(10) Edwards, D. Network Formation and Reinforcement Studies with Terminally Brominated Polybutadiene. *Rubber Chem. Technol.* **1975**, *48,* 202-217

(11) Gottlieb, M.; Macosko, C.; Benjamin, G.; Meyers, K.; Merrill, E. Equilibrium modulus of model poly (dimethylsiloxane) networks. *Macromolecules* **1981**, *14,* 1039-1046

(12) Dossin, L. M.; Graessley, W. W. Rubber elasticity of well-characterized polybutadiene networks. *Macromolecules* **1979**, *12,* 123-130

(13) Mark, J. The use of model polymer networks to elucidate molecular aspects of rubberlike elasticity. *Polymer Networks* **2005**, 1-26

(14) Charlier, P.; Jerome, R.; Teyssie, P.; Utracki, L. A. Viscoelastic properties of immiscible telechelic polymer blends: effect of acid-base interactions. *Macromolecules* **1992**, *25,* 2651-2656

(15) Tong, J.-D.; Jerôme, R. Dependence of the Ultimate Tensile Strength of Thermoplastic Elastomers of the Triblock Type on the Molecular Weight between Chain Entanglements of the Central Block. *Macromolecules* **2000**, *33,* 1479-1481

(16) Xu, B.; Lin, Y. G.; Chien, J. C. W. Energetic ABA and (AB)n thermoplastic elastomers. *J. Appl. Polym. Sci.* **1992**, *46,* 1603-1611

(17) Weber, M.; Stadler, R. Hydrophilic-hydrophobic two-component polymer networks: 2. Synthesis and characterization of poly(ethylene oxide)-linked-polybutadiene. *Polymer* **1988**, *29,* 1071-1078

(18) Kennedy, J. P. New Sequential Copolymers and Networks by a Combination of Techniques. *Polym. J.* **1985**, *17,* 29-35

(19) Jerome, R.; Henrioulle-Granville, M.; Boutevin, B.; Robin, J. J. Telechelic polymers: Synthesis, characterization and applications. *Prog. Polym. Sci.* **1991**, *16,* 837-906

(20) Kim, J.; Jung, H. Y.; Park, M. J. End-Group Chemistry and Junction Chemistry in Polymer Science: Past, Present, and Future. *Macromolecules* **2020**, *53,* 746-763

(21) Adamsons, K.; Blackman, G.; Gregorovich, B.; Lin, L.; Matheson, R. Oligomers in the evolution of automotive clearcoats: mechanical performance testing as a function of exposure. *Prog. Org. Coat.* **1998**, *34,* 64-74

(22) Athey, R. D. Telechelic polymers — precursors to high solids coatings. *Prog. Org. Coat.* **1979**, *7,* 289-329

(23) Pirman, T.; Ocepek, M.; Likozar, B. Radical Polymerization of Acrylates, Methacrylates, and Styrene: Biobased Approaches, Mechanism, Kinetics, Secondary Reactions, and Modeling. *Ind. Eng. Chem. Res.* **2021**, *60,* 9347-9367

(24) Bhattacharya, A. Radiation and industrial polymers. *Prog. Polym. Sci.* **2000**, *25,* 371-401

(25) Chapiro, A. *Radiation chemistry of polymeric systems, High Polymers.*; Interscience Publishers, 1962.

(26) Charlesby, A. *Atomic radiation and polymers: international series of monographs on radiation effects in materials*; Pergamon press, 1960.

(27) Roose, P.; Fallais, I.; Vandermiers, C.; Olivier, M. G.; Poelman, M. Radiation curing technology: An attractive technology for metal coating. *Prog. Org. Coat.* **2009**, *64,* 163-170

(28) Schroeter, S. H. Radiation Curing of Coatings. *Annu. Rev. Mater. Sci.* **1975**, *5,* 115-133

(29) Decker, C. Photoinitiated crosslinking polymerisation. *Prog. Polym. Sci.* **1996**, *21,* 593-650

(30) Ligon-Auer, S. C.; Schwentenwein, M.; Gorsche, C.; Stampfl, J.; Liska, R. Toughening of photo-curable polymer networks: a review. *Polym. Chem.* **2016**, *7,* 257-286

(31) Craig, R. G.; Welker, D.; Rothaut, J.; Krumbholz, K. G.; Stefan, K.-P.; Dermann, K.; Rehberg, H.-J.; Franz, G.; Lehmann, K. M.; Borchert, M. Dental Materials. In *Ullmann's Encyclopedia of Industrial Chemistry*.

(32) Hull, C. W. Apparatus for production of three-dimensional objects by stereolithography. *United States Patent, Appl., No. 638905, Filed* **1984**,

(33) Su, A.; Al'Aref, S. J. Chapter 1 - History of 3D Printing. In *3D Printing Applications in Cardiovascular Medicine*, Academic Press, 2018; pp 1-10.

(34) Wohlers, T.; Gornet, T. History of additive manufacturing. *Wohlers report* **2014**, *24,* 118

(35) Schwalm, R. 5. Acrylate resins for radiation curable coatings. In *Acrylic Resins*, Vincentz Network, 2014; pp 279-374.

(36) Rawat, R. S.; Chouhan, N.; Talwar, M.; Diwan, R. K.; Tyagi, A. K. UV coatings for wooden surfaces. *Prog. Org. Coat.* **2019**, *135,* 490-495

(37) Javadi, A.; Mehr, H. S.; Sobani, M.; Soucek, M. D. Cure-on-command technology: A review of the current state of the art. *Prog. Org. Coat.* **2016**, *100,* 2-31

(38) Fouassier, J.-P.; Rabek, J. F. *Radiation curing in polymer science and technology: Fundamentals and methods*; Springer Science & Business Media, 1993.

(39) Raszewski, Z.; Nowakowska-Toporowska, A.; Nowakowska, D.; Więckiewicz, W. Update on acrylic resins used in dentistry. *Mini-Rev. Med. Chem.* **2021**, *21,* 2130-2137

(40) Aronovich, D. A.; Boinovich, L. B. Structural Acrylic Adhesives: A Critical Review. In *Progress in Adhesion and Adhesives*, 2021; pp 651-708.

(41) Pitia, E.; Hill, J. Reactive acrylic adhesives. In *Handbook of Adhesive Technology*, CRC Press, 2017; pp 349-365.

(42) Droesbeke, M. A.; Aksakal, R.; Simula, A.; Asua, J. M.; Du Prez, F. E. Biobased acrylic pressure-sensitive adhesives. *Prog. Polym. Sci.* **2021**, *117,* 101396

(43) Graindourze, M. UV-Curable Inkjet Inks and Their Applications in Industrial Inkjet Printing, Including Low-Migration Inks for Food Packaging. In *Handbook of Industrial Inkjet Printing*, 2017; pp 129-150.

(44) Sharma, B.; Sauraj, S.; Kumar, B.; Pandey, A.; Dutt, D.; Negi, Y. S.; Maji, P. K.; Kulshreshtha, A. Synthesis of waterborne acrylic copolymer resin as a binding agent for the development of water-based inks in the printing application. *Polym. Eng. Sci.* **2021**, *61,* 1569-1580

(45) Taormina, G.; Sciancalepore, C.; Messori, M.; Bondioli, F. 3D printing processes for photocurable polymeric materials: technologies, materials, and future trends. *J. Appl. Biomater. Funct. Mater.* **2018**, *16,* 151-160

(46) Al Rashid, A.; Ahmed, W.; Khalid, M. Y.; Koç, M. Vat photopolymerization of polymers and polymer composites: Processes and applications. *Addit. Manuf.* **2021**, *47,* 102279

(47) Tehfe, M. A.; Louradour, F.; Lalevée, J.; Fouassier, J.-P. Photopolymerization Reactions: On the Way to a Green and Sustainable Chemistry. *Appl. Sci.* **2013**, *3,* 490-514

(48) Steyrer, B.; Neubauer, P.; Liska, R.; Stampfl, J. Visible light photoinitiator for 3D-printing of tough methacrylate resins. *Materials* **2017**, *10,* 1445

(49) Dumur, F. Recent advances on visible light photoinitiators of polymerization based on Indane-1, 3-dione and related derivatives. *Eur. Polym. J.* **2021**, *143,* 110178

(50) Droesbeke, M. A.; Simula, A.; Asua, J. M.; Du Prez, F. E. Biosourced terpenoids for the development of sustainable acrylic pressure-sensitive adhesives via emulsion polymerisation. *Green Chem.* **2020**, *22,* 4561-4569

(51) Wu, Q.; Hu, Y.; Tang, J.; Zhang, J.; Wang, C.; Shang, Q.; Feng, G.; Liu, C.; Zhou, Y.; Lei, W. High-performance soybean-oil-based epoxy acrylate resins:“Green” synthesis and application in UV-curable coatings. *ACS Sustainable Chem. Eng.* **2018**, *6,* 8340-8349

(52) Paul, R.; John, B.; Sahoo, S. K. UV-Curable Bio-Based Pressure-Sensitive Adhesives: Tuning the Properties by Incorporating Liquid-Phase Alkali Lignin-Acrylates. *Biomacromolecules* **2022**, *23,* 816-828

(53) Briede, S.; Barkane, A.; Jurinovs, M.; Thakur, V. K.; Gaidukovs, S. Acrylation of biomass: a review of synthesis process–know how and future application directions. *Curr. Opin. Green Sustainable Chem.* **2022**, 100626

(54) Fertier, L.; Koleilat, H.; Stemmelen, M.; Giani, O.; Joly-Duhamel, C.; Lapinte, V.; Robin, J.-J. The use of renewable feedstock in UV-curable materials – A new age for polymers and green chemistry. *Prog. Polym. Sci.* **2013**, *38,* 932-962

(55) Patil, D. M.; Phalak, G. A.; Mhaske, S. T. Design and synthesis of bio-based UV curable PU acrylate resin from itaconic acid for coating applications. *Des. Monomers Polym.* **2017**, *20,* 269-282

(56) Friebel, S.; Sydow, S. Bio-Sourced Artificial Leather for Interior Automotive Applications. In *Technologies for economic and functional lightweight design*, Berlin, Heidelberg, 2021, 2021; Dröder, K., Vietor, T., Eds.; Springer Berlin Heidelberg: pp 189-198.

(57) Williams, C. K.; Hillmyer, M. A. Polymers from Renewable Resources: A Perspective for a Special Issue of Polymer Reviews. *Polym. Rev.* **2008**, *48,* 1-10

(58) Hoyle, C. E.; Bowman, C. N. Thiol–Ene Click Chemistry. *Angew. Chem. Int. Ed.* **2010**, *49,* 1540-1573

(59) Hoyle, C. E.; Lowe, A. B.; Bowman, C. N. Thiol-click chemistry: a multifaceted toolbox for small molecule and polymer synthesis. *Chem. Soc. Rev.* **2010**, *39,* 1355-1387

(60) Nair, D. P.; Podgórski, M.; Chatani, S.; Gong, T.; Xi, W.; Fenoli, C. R.; Bowman, C. N. The Thiol-Michael Addition Click Reaction: A Powerful and Widely Used Tool in Materials Chemistry. *Chem. Mater.* **2014**, *26,* 724-744

(61) Stubbs, C. J.; Worch, J. C.; Prydderch, H.; Becker, M. L.; Dove, A. P. Unsaturated Poly(ester-urethanes) with Stereochemically Dependent Thermomechanical Properties. *Macromolecules* **2020**, *53,* 174-181

(62) Stubbs, C. J.; Worch, J. C.; Prydderch, H.; Wang, Z.; Mathers, R. T.; Dobrynin, A. V.; Becker, M. L.; Dove, A. P. Sugar-Based Polymers with Stereochemistry-Dependent Degradability and Mechanical Properties. *J. Am. Chem. Soc.* **2022**, *144,* 1243-1250

(63) Petersen, S. R.; Prydderch, H.; Worch, J. C.; Stubbs, C. J.; Wang, Z.; Yu, J.; Arno, M. C.; Dobrynin, A. V.; Becker, M. L.; Dove, A. P. Ultra-Tough Elastomers from Stereochemistry-Directed Hydrogen Bonding in Isosorbide-Based Polymers. *Angew. Chem. Int. Ed.* **2022**, *61,* e202115904

(64) Marechal, E. Reactive Oligomers by Step-Growth Polymerization. In *Telechelic polymers: synthesis and applications*, CRC press, 2018; pp 5-32.

(65) Nguyen, H. A.; Maréchal, E. Synthesis of Reactive Oligomers and Their use in Block Polycondensation. *J. Macromol. Sci., Polym. Rev.* **1988**, *28,* 187-291

(66) Carothers, W. H. Polymers and polyfunctionality. *Trans. Faraday Soc.* **1936**, *32,* 39-49

(67) Passingham, C.; Hendra, P. J.; Cudby, M. E. A.; Zichy, V.; Weller, M. The re-evaluation of multiple peaks in the DSC melting endotherm of isotactic polypropylene. *Eur. Polym. J.* **1990**, *26,* 631-638

3.8 Appendices

3.8.1 Materials and methods

Dimethylphenylphosphine (DMPP, 99%), 1,8-Diazabicyclo[5.4.0]undec-7-ene (DBU, 98%) and 1,6-hexanedithiol (97%) were purchased from Sigma-Aldrich Company. N,N'-dimethylformamide (DMF, 99.5%) and dichloromethane (CH_2Cl_2, 99%) were purchased from Fisher scientific. Methanol (MeOH, ≥99.8%) was purchased from VMR Chemicals. Deuterated chloroform ($CDCl_3$, >99.8%) was purchased from Apollo Scientific. Both DBU and 1,6-hexanedithiol were purified by distillation prior to use and the later was kept in an ampule under nitrogen for storage. All other chemicals were used as received unless stated otherwise.

Nuclear magnetic resonance spectroscopy (NMR)

^1H and ^{13}C NMR spectra of monomers and oligomers were recorded at 298 K on an Ascend Bruker 400 spectrometer equipped with a 5 mm BBFO smart probe operating at 400 MHz and 100 MHz, respectively. Chemical shifts of ^1H NMR spectra were referenced to the solvent residual proton resonance signals: δ= 7.26 ppm for $CDCl_3$. Chemical shifts for ^{13}C NMR spectra were referenced to the solvent resonance signal: δ= 77.16 ppm for $CDCl_3$. The data obtained were processed and analysed using MestReNova 12.0.3 software. The resonance multiplicities are described as s (singlet), d (doublet), t(triplet), q(quartet) or m(multiplet).

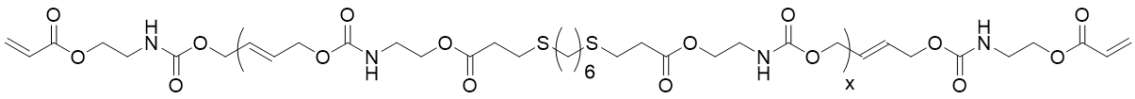
Size exclusion chromatography (SEC)

Size exclusion chromatography (SEC) was performed on an Agilent 1260 Infinity II LC system equipped with a Wyatt DAWN HELEOS II multi-angle laser light

scattering (MALLS) detector, a Wyatt Optilab T-rEX differential refractive index detector, an Agilent 1260 Infinity II WR diode array detector, an Agilent guard column (PLGel 5 µm, 50 × 7.5 mm) and two Agilent Mixed-C columns (PLGel 5 µm, 300 × 7.5 mm). The mobile phase was DMF (HPLC grade) containing 5 mM of ammonium tetrafluoroborate (NH_4BF_4) at 50 °C with a flow rate of 1.0 mL·min^{-1}. Number average molecular weights (M_n), weight average molecular weights (M_w) and dispersities ($Đ_M = M_w/M_n$) were determined using Wyatt ASTRA v7.1.3 software against poly(methyl methacrylate) (PMMA) standards.

3.8.2 Synthetic procedures

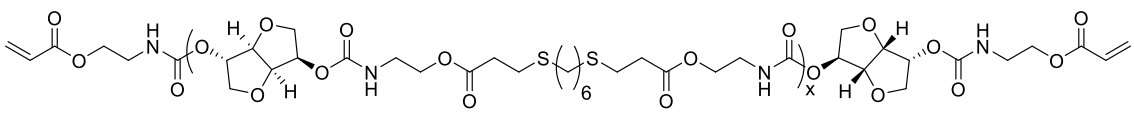
General procedure of unsaturated oligomer synthesis: example for a trans oligomer of 6.1 kDa



Freshly distilled 1,6-hexanedithiol (3.37 g, 22.46 mmol, 1 eq) and the *trans* diacrylate (9.35 g, 25.27 mmol, 1.125 eq) is weighed in two separate 20 mL sintered vial. In a pre-dried 250 mL round bottom flask (left in the oven at 150 °C for 24h) equipped with a stirrer, 1,6-hexanedithiol is added and the vial is washed with DMF that is also added in the round bottom flask. Then the acrylate is added in the same manner. The rest of DMF (0.25 M, 90 mL in total) is added to the vessel and the reaction media is placed in a methanol/dry ice bath. Once the temperature dropped to -15 ˚C, the dimethylphenylphosphine (DMPP, 16 µL, 0.112 mmol, 0.5 mol%) is added to the reaction media. The reaction is left stirring while the temperature increased to room temperature until the disappearance of dithiol is observed by TLC

(80/20 EtOAc/Hexane, stained with potassium permanganate) which usually occurs after 30-45 min. Upon completion, the reaction media is poured into 300 mL of MeOH left stirring for 10 min and stored in the fridge overnight. The precipitated oligomer is then filtered and dried under vacuo. SEC analysis (DMF, 0.5% w/w NH_4BF_4) M_w= 16 kDa, M_n= 9.3 kDa, M_z= 24 kDa, $Đ_M$= 1.71. ^{1}H NMR (400 MHz; 298 K; $CDCl_3$, ppm) δ 6.43 (dd, *J* = 17.3, 1.4 Hz, 2H, C**H**H=CHC(O)O), 6.12 (dd, *J* = 17.3, 10.4 Hz, 2H, CHH=C**H**C(O)O), 5.86 (dd, *J* = 10.5, 1.4 Hz, 2H, CH**H**=CHC(O)O), 5.83 (s, 24H, CH_2C**H**=C**H**CH_2), 5.24 (s, 24H, N**H**), 4.57 (s, 52H, CH_2CH=CHC**H**$_2$), 4.24 (t, *J* = 5.3 Hz, 4H, NHCH_2C**H**$_2$OC(O)O end group), 4.18 (t, *J* = 5.3 Hz, 48H, NHCH_2C**H**$_2$OC(O)O), 3.45 (q, *J* = 5.5 Hz, 52H, NHC**H**$_2$CH_2OC(O)O), 2.77 (t, *J* = 7.2 Hz, 48H, O(O)CCH_2C**H**$_2$S), 2.62 (t, *J* = 7.0 Hz, 48H, CH_2CH_2SC**H**$_2$CH_2), 2.53 (t, *J* = 7.3 Hz, 48H, O(O)CC**H**$_2$CH_2S), 1.58 (dt, *J* = 14.5, 7.1 Hz, 48H, $CH_2CH_2SCH_2$C**H**$_2$), 1.45 – 1.33 (m, 48H, $CH_2SCH_2CH_2$C**H**$_2$).^{13}C NMR (101 MHz, 298 K, $CDCl_3$, ppm) δ 172.0, 156.2, 131.5, 128.3, 64.6, 63.8, 63.7, 40.2, 34.8, 32.17, 29.4, 28.4, 27.1. GPC M_w = 16 kDa, M_n = 9.3 kDa, M_z = 24 kDa, Đ = 1.5. DSC $T_{g,\,(midpoint)}$= −15 °C, $T_{m,1}$= 46 °C, $T_{M,2}$= 66.5 °C, ΔH_m= 26.44 J·g^{-1}. TGA in N_2 $T_{d,5\%}$= 268 °C, $T_{d,\,50\%}$= 308 °C.

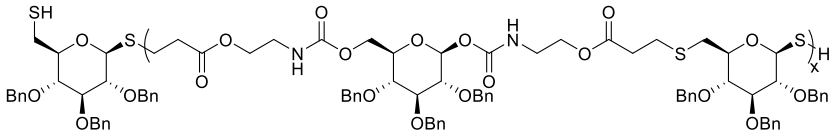
General procedure of isohexide derived oligomer synthesis: example for a isosorbide derived oligomer of 3.3 kDa



Freshly distilled 1,6-hexanedithiol (0.1280 g, 0.853 mmol, 1 eq) and isosorbide derived diacrylate (0.4875 g, 1.137 mmol, 1.333 eq) is weighed in two separate 20 mL sintered vial. Then, the isosorbide monomer is dissolved in 2 ml of DMF prior to

the addition of 1,6-hexanedithiol. The vial which contained 1,6-hexanedithiol is washed with DMF that is also added in the vial containing the diacrylate monomer. The rest of the DMF (0.25 M, 4.5 mL in total) is added to the vial. Dimethylphenylphosphine (DMPP, 2.4 µL, 0.0169 mmol, 2mol%) is added to the reaction media. The reaction is left stirring until the disappearance of dithiol is observed by TLC (80/20 EtOAc/Hexane, stained with potassium permanganate) which usually occurs after 12 h. Upon completion, the reaction media is poured into 60 mL of MeOH left stirring for 10 min and stored in the fridge overnight. The precipitated oligomer is then filtered and dried under vacuo. SEC analysis (DMF, 0.5% w/w NH_4BF_4) M_w= 5.1 kDa, M_n= 1.6 kDa, M_z= 13.3 kDa, $Đ_M$= 3.29. ^{1}H NMR (400 MHz; 298 K; $CDCl_3$, ppm) ^{1}H NMR (400 MHz, Chloroform-*d*) δ 6.43 (dt, *J* = 17.3, 1.2 Hz, 2H, C**H**H=CHC(O)O), 6.12 (ddd, *J* = 17.3, 10.4, 1.3 Hz, 2H, CHH=C**H**C(O)O), 5.87 (dt, *J* = 10.5, 1.4 Hz, 2H, CH**H**=CHC(O)O), 5.29 (s, 12H, N***H***), 5.11 (dd, *J* = 10.2, 4.2 Hz, 14H, C***H***OC(O)NH), 4.76 (t, *J* = 4.8 Hz, 7H, CH_2OC***H***CHO), 4.49 (d, *J* = 4.4 Hz, 7H, CH_2OC***H***CHO), 4.27 – 4.08 (m, 28H, $NHCH_2C$***H***$_2$O), 4.02 – 3.92 (m, 20H, OC***H***$_2$CHO and CHOC***H***HO), 3.77 – 3.67 (m, 7H, CHOCH***H***O), 3.45 (dq, *J* = 11.8, 5.5 Hz, 28H, NHC***H***$_2CH_2$O), 2.77 (t, *J* = 7.4 Hz, 22H, O(O)CCH_2C**H**$_2$S), 2.62 (tt, *J* = 7.2, 1.0 Hz, 22H, O(O)CC**H**$_2CH_2$S), 2.52 (t, *J* = 7.3 Hz, 22H, CH_2CH_2SC**H**$_2CH_2$), 1.58 (d, *J* = 14.4 Hz, 22H, $CH_2CH_2SCH_2C$**H**$_2$), 1.39 (dq, *J* = 7.4, 3.6 Hz, 22H, $CH_2SCH_2CH_2C$**H**$_2$). ^{13}C NMR (101 MHz, 298 K, $CDCl_3$, ppm) δ 171.97, 155.68, 155.35, 131.65, 128.04, 85.99, 81.14, 78.73, 74.55, 73.85, 70.20, 63.66, 40.27, 34.80, 32.15, 29.46, 28.46, 27.12. GPC M_w = 5.1 kDa, M_n = 1.6 kDa, M_z = 13.3 kDa, Đ = 3.3. DSC $T_{g,\,(midpoint)}$= 21.9 °C, $T_{m,1}$= 54.2 °C, $T_{M,2}$= 82.9 °C, ΔH_m= 10.8 J·g^{-1}.

General procedure of glucose derived oligomer synthesis: example for an oligomer of 8.0 kDa



1,6-glucose derived dithiol (0.1010 g, 0.2095 mmol, 1 eq) and diacrylate (0.1534 g, 0.2095 mmol, 1 eq) is weighed in a 20 mL sintered vial. Then, 0.5 ml of DMF is added to the vial. Once the monomers are fully dissolved, freshly distilled 1,8-Diazabicyclo[5.4.0]undec-7-ene (DBU, 0.63 µL, 0.00419 mmol, 2mol%) is added to the reaction media. The reaction is left stirring at 60 °C until of the disappearance of dithiol is observed by TLC (80/20 EtOAc/Hexane, stained with potassium permanganate) which usually occurs after 1.5 h. Upon completion, the reaction media is poured into 20 mL of MeOH left stirring for 10 min and stored in the fridge overnight. The precipitated oligomer is then filtered and dried under vacuo. ^{1}H NMR (400 MHz, Chloroform-*d*) ^{1}H NMR (400 MHz, Chloroform-*d*) ^{1}H NMR (400 MHz, Chloroform-*d*) δ 7.33 – 7.02 (m, *J* = 11.9, 7.7 Hz, 131H), 5.54 – 5.42 (m, *J* = 8.3, 3.4 Hz, 4H), 5.35 – 5.23 (m, 3H), 5.23 – 5.18 (m, *J* = 4.5 Hz, 1H), 4.91 – 4.30 (m, 47H), 4.28 – 4.13 (m, 7H), 4.12 – 3.88 (m, 19H), 3.84 – 3.46 (m, 11H), 3.45 – 3.07 (m, 29H), 2.98 – 2.28 (m, 41H). GPC M_w = 7.9 kDa, M_n = 3.5 kDa, M_z = 18 kDa, Đ = 2.3. DSC $T_{g,\,(midpoint)}$= 32.9 °C, T_m= 51 °C, ΔH_m= 0.41 J·g^{-1}.

3.8.3 NMR spectra

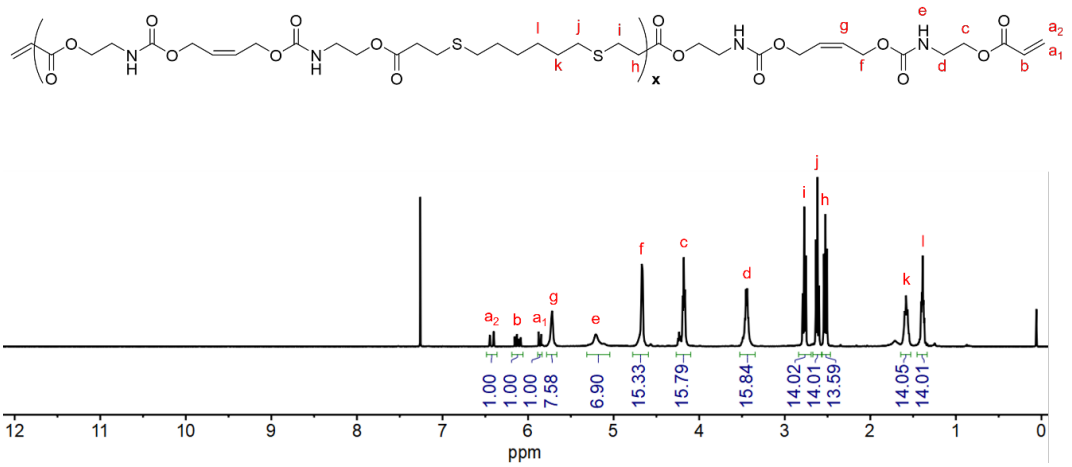


***Figure A 3.1**. [1]H NMR (400 MHz, 298 K, $CDCl_3$) spectrum of a 4.0 kDa cis oligomer.*

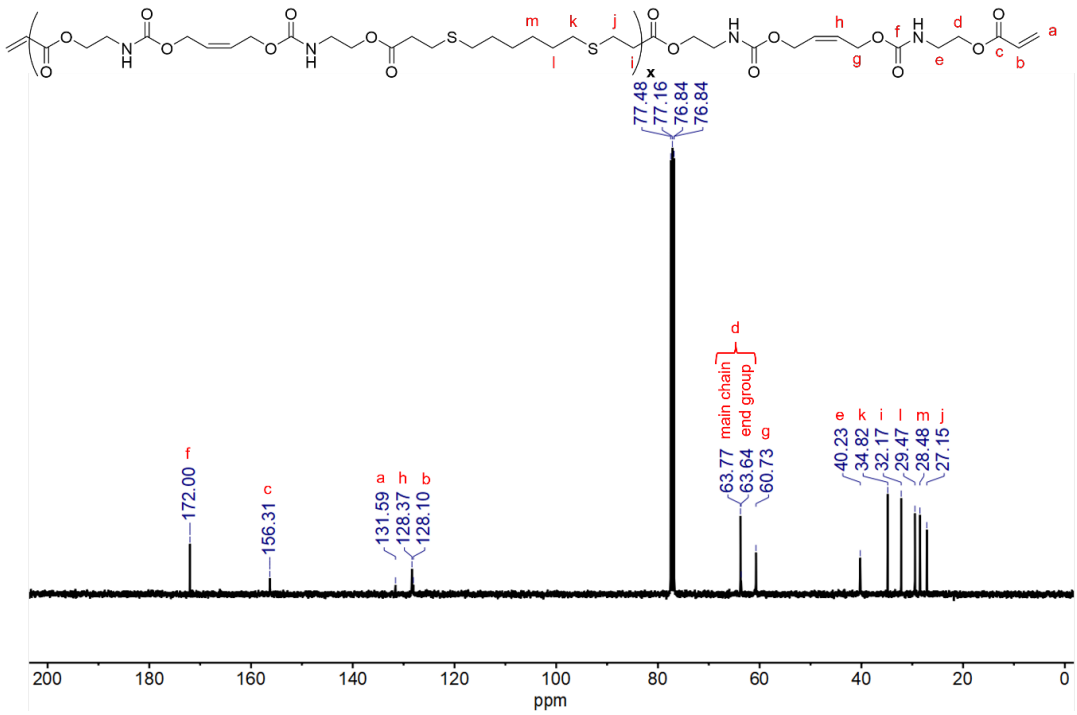


***Figure A 3.2.** [13]C NMR (101 MHz, 298 K, $CDCl_3$) spectrum of a 4.0 kDa cis oligomer.*

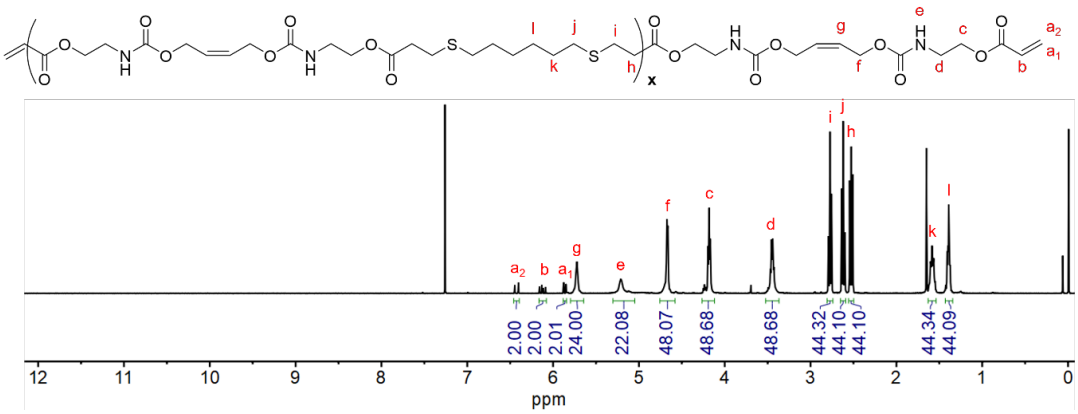


Figure A 3.3. *^{1}H NMR (101 MHz, 298 K, $CDCl_3$) spectrum of a 6.1 kDa cis oligomer.*

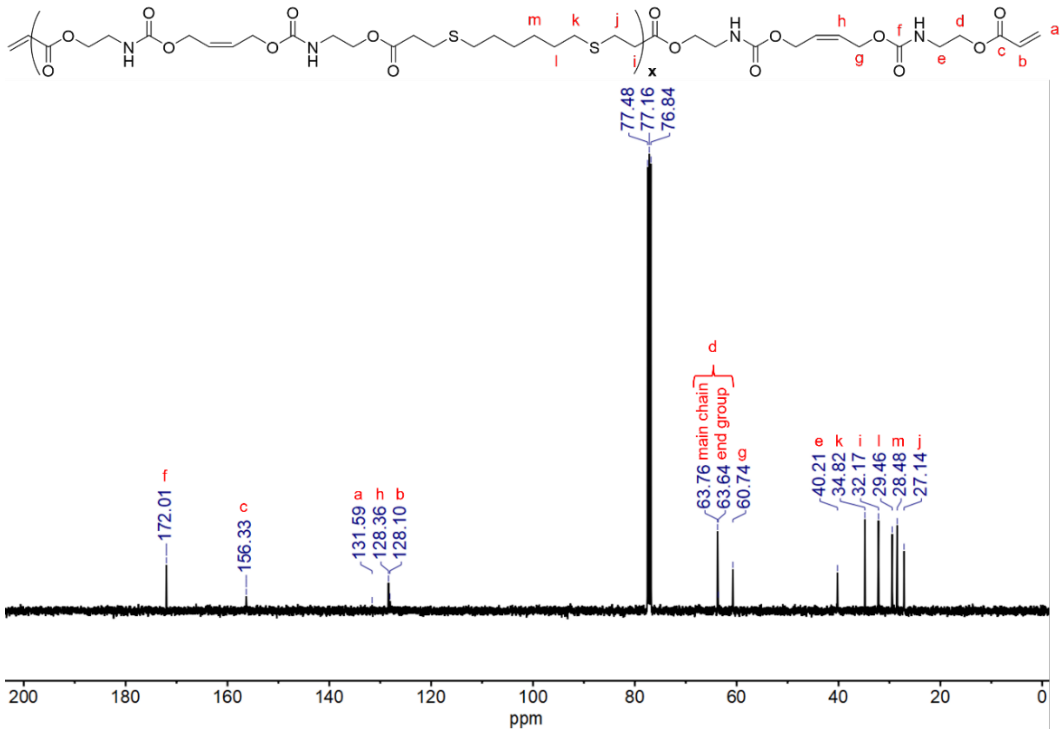


Figure A 3.4. *^{13}C NMR (101 MHz, 298 K, $CDCl_3$) spectrum of a 6.1 kDa cis oligomer.*

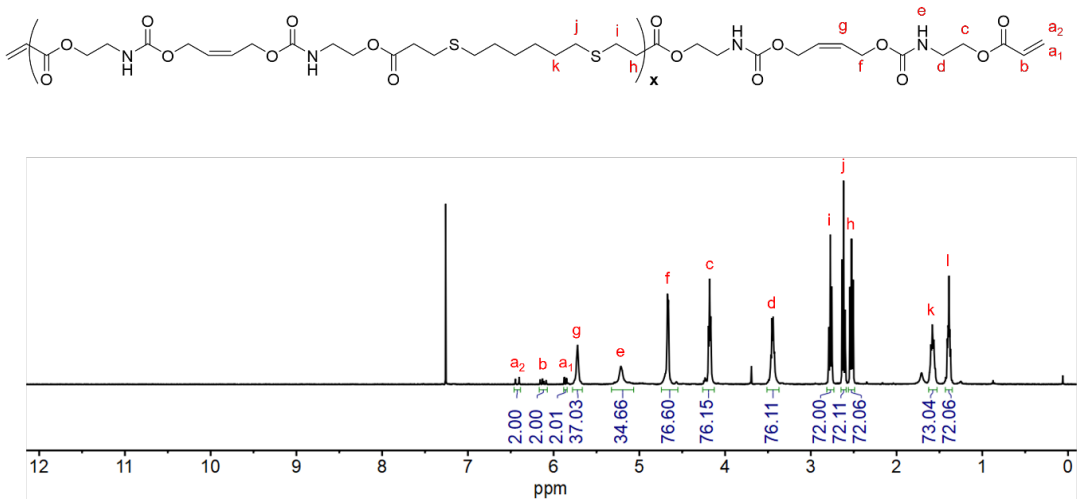


Figure A 3.5. *^{1}H NMR (400 MHz, 298 K, $CDCl_3$) spectrum of a 9.7 kDa cis oligomer.*

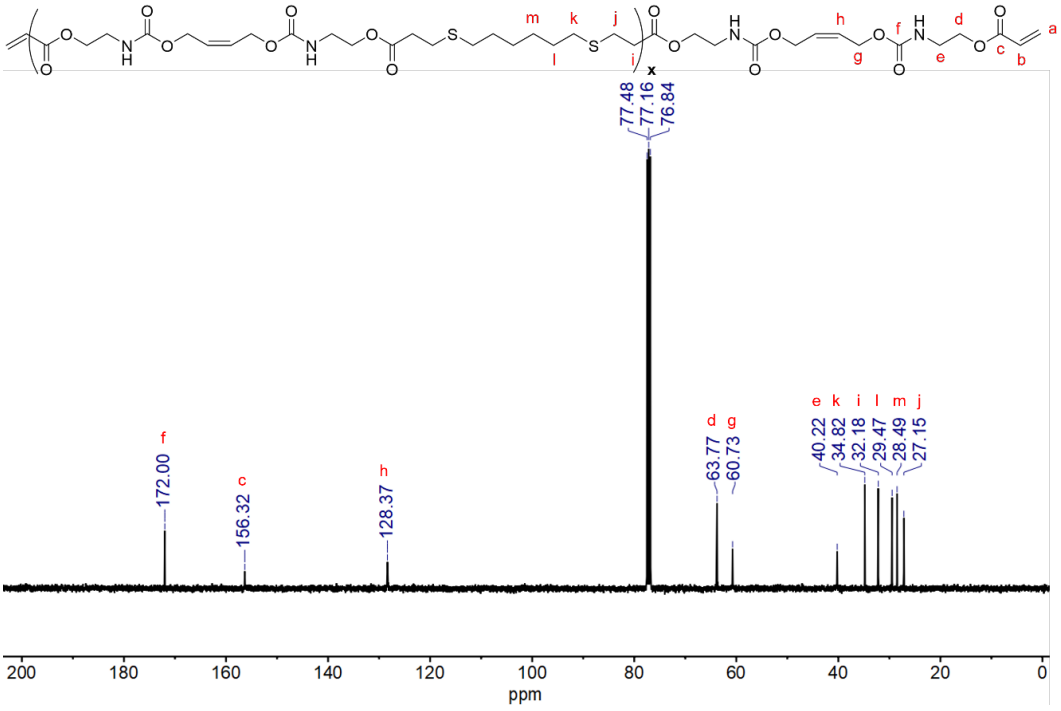


Figure A 3.6. *^{13}C NMR (101 MHz, 298 K, $CDCl_3$) spectrum of a 9.7 kDa cis oligomer.*

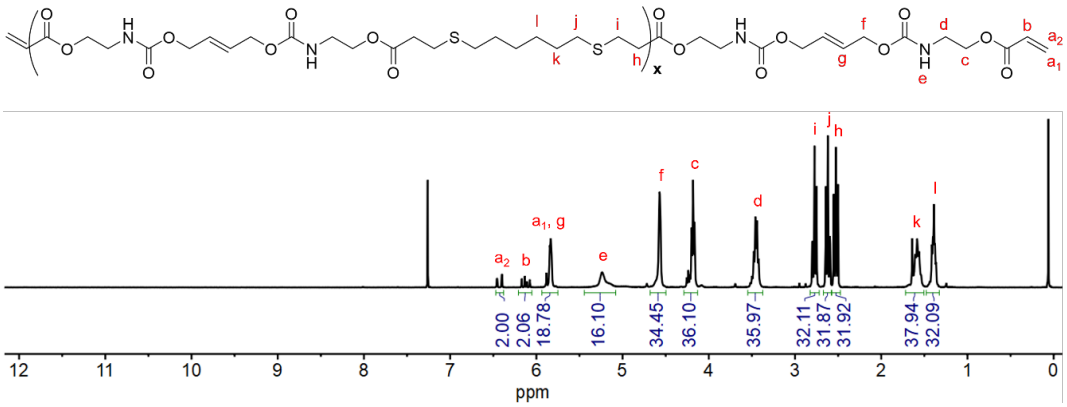


Figure A 3.7. *^{1}H NMR (400 MHz, 298 K, $CDCl_3$) spectrum of a 4.5 kDa trans oligomer.*

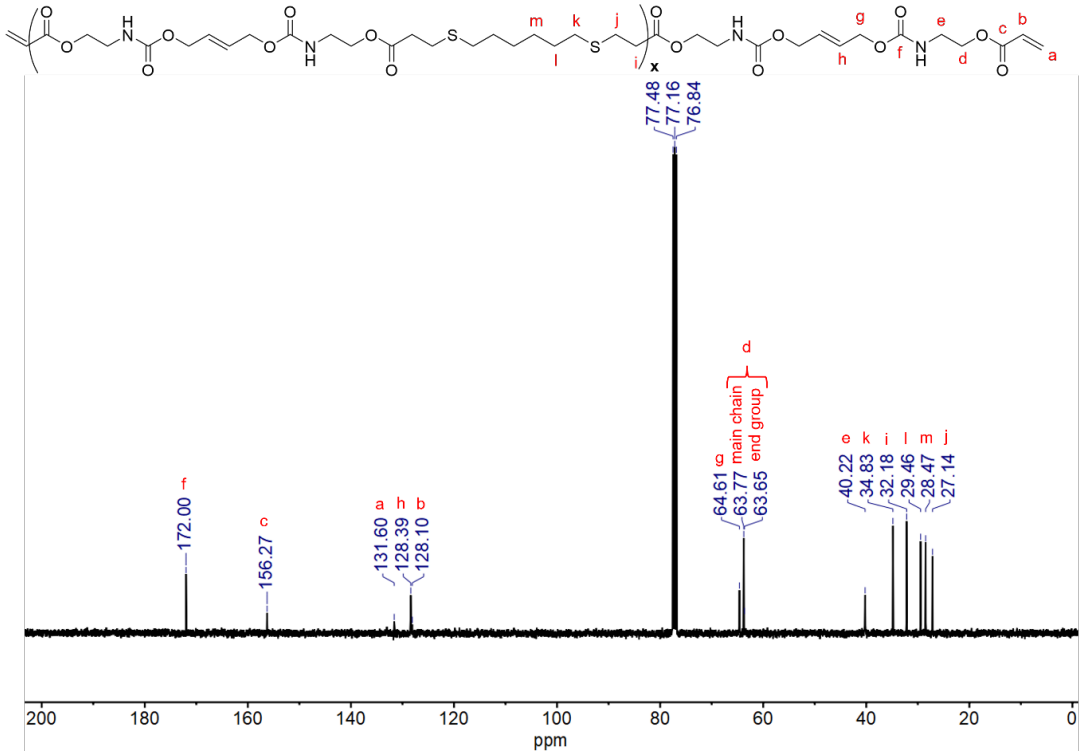


Figure A 3.8. *^{13}C NMR (101 MHz, 298 K, $CDCl_3$) spectrum of a 4.5 kDa trans oligomer.*

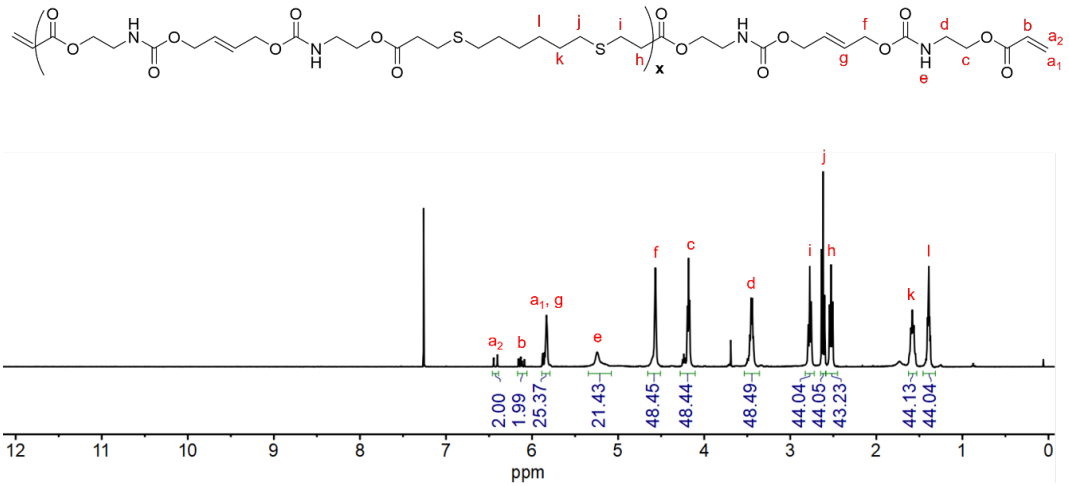


Figure A 3.9. *^{1}H NMR (400 MHz, 298 K, $CDCl_3$) spectrum of a 6.1 kDa trans oligomer.*

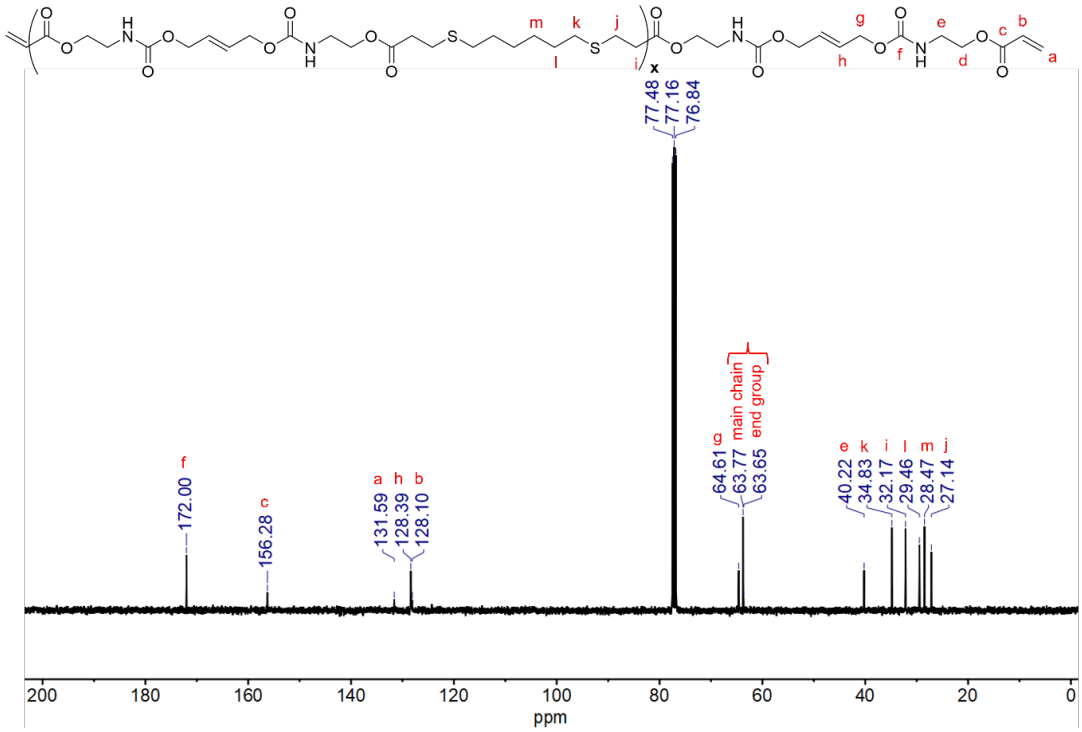


Figure A 3.10. *^{13}C NMR (101 MHz, 298 K, $CDCl_3$) spectrum of a 6.1 kDa trans oligomer.*

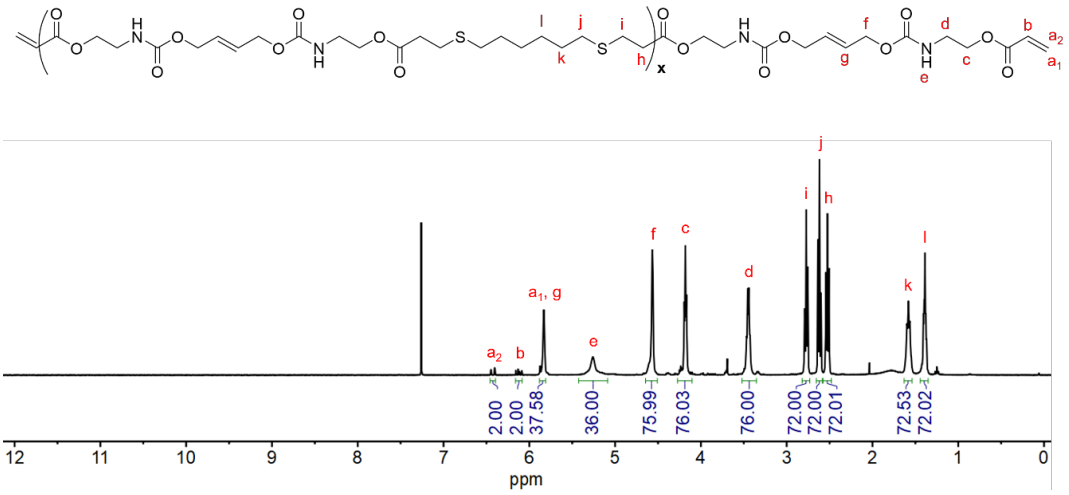


Figure A 3.11. *^{1}H NMR (400 MHz, 298 K, $CDCl_3$) spectrum of a 9.7 kDa trans oligomer.*

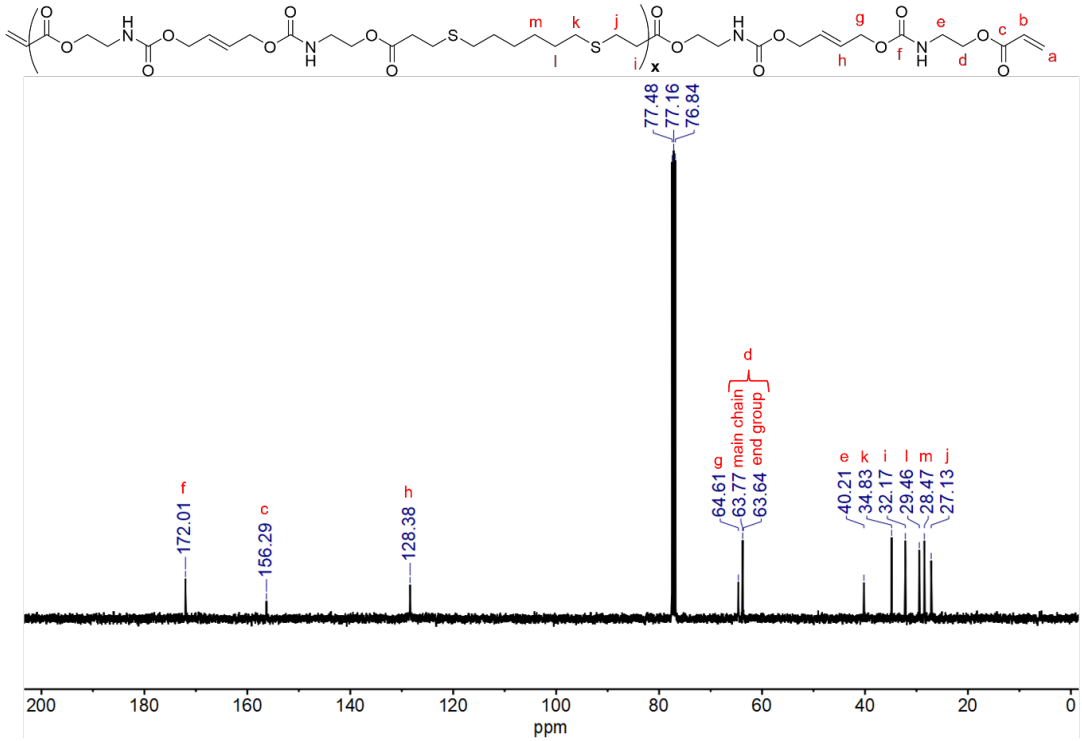


Figure A 3.12. *^{13}C NMR (101 MHz, 298 K, $CDCl_3$) spectrum of a 9.7 kDa trans oligomer.*

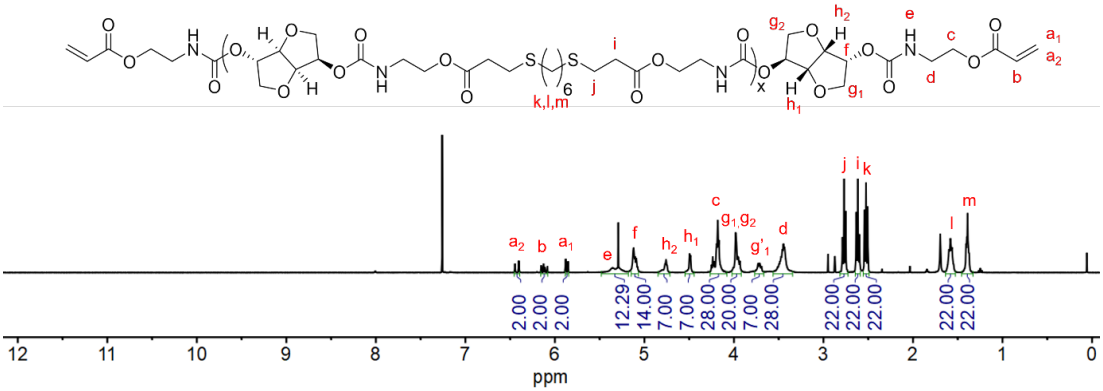


Figure A 3.13. *^{1}H NMR (400 MHz, 298 K, $CDCl_3$) spectrum of a 3.3 kDa isosorbide derived oligomer.*

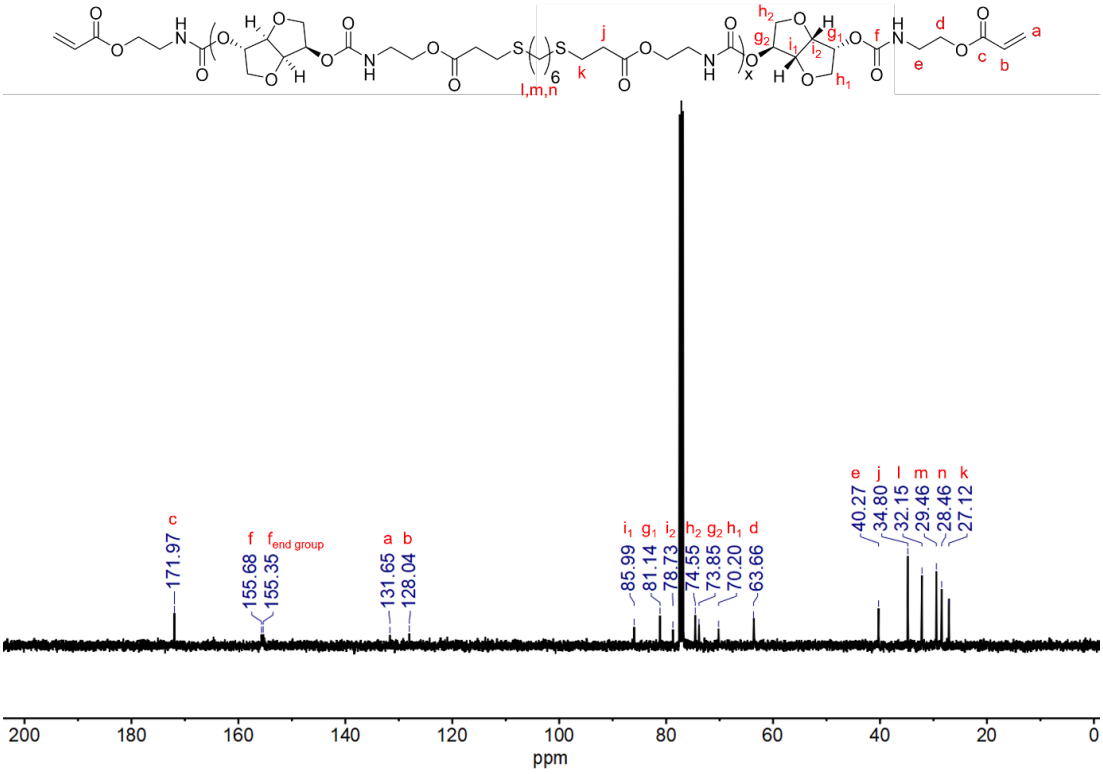


Figure A 3.14. *^{13}C NMR (101 MHz, 298 K, $CDCl_3$) spectrum of a 3.3 kDa isosorbide derived oligomer.*

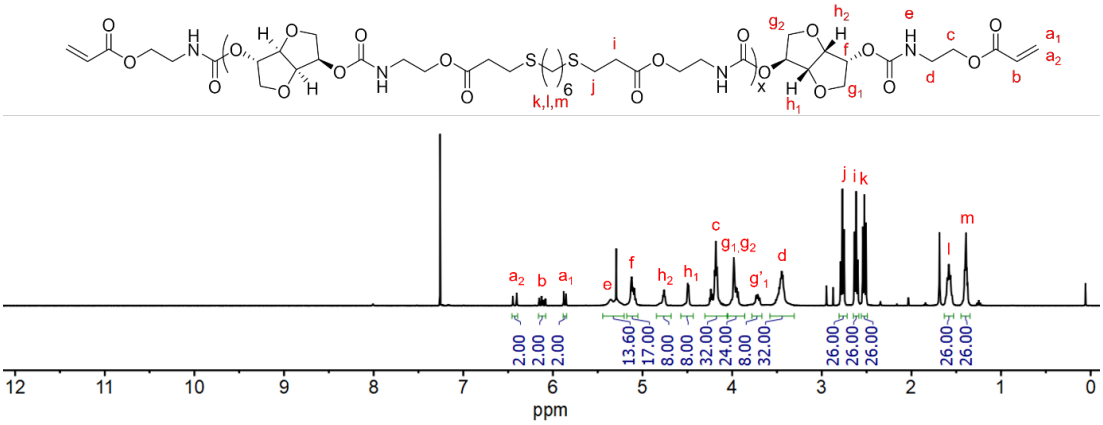


Figure A 3.15. *^{1}H NMR (400 MHz, 298 K, $CDCl_3$) spectrum of a 3.9 kDa isosorbide derived oligomer.*

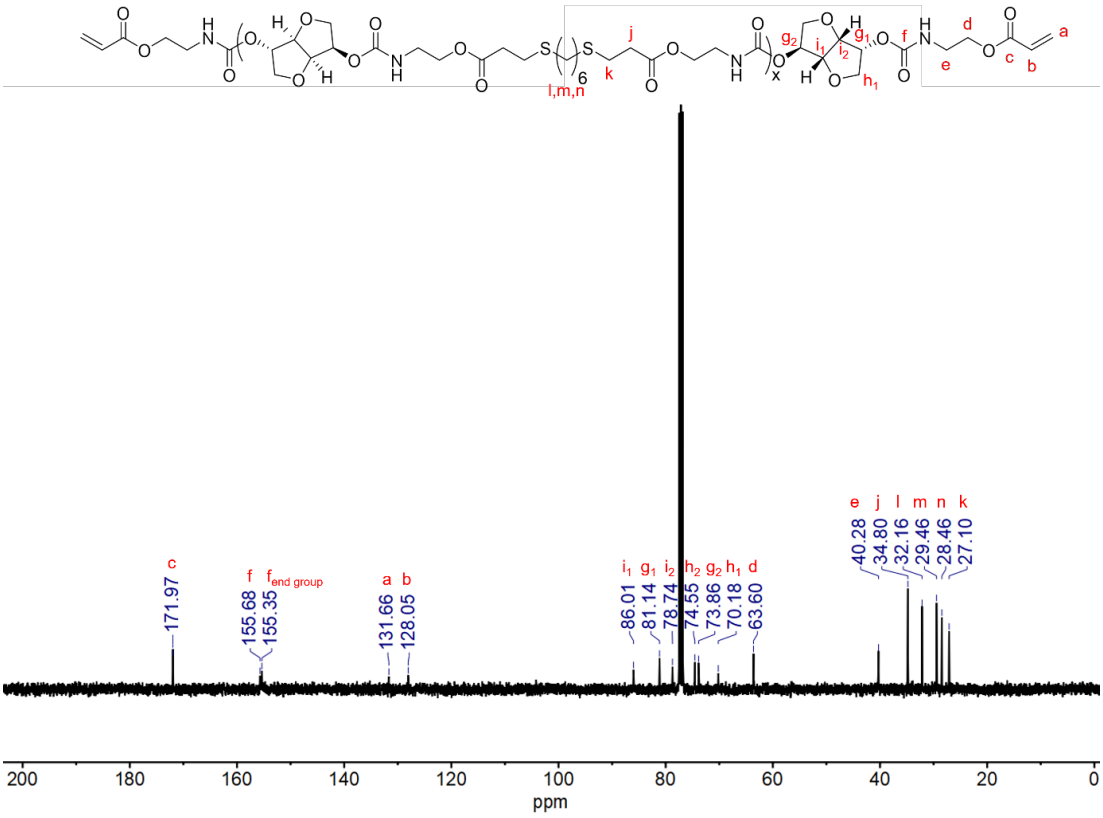


Figure A 3.16. *^{13}C NMR (101 MHz, 298 K, $CDCl_3$) spectrum of a 3.9 kDa isosorbide derived oligomer.*

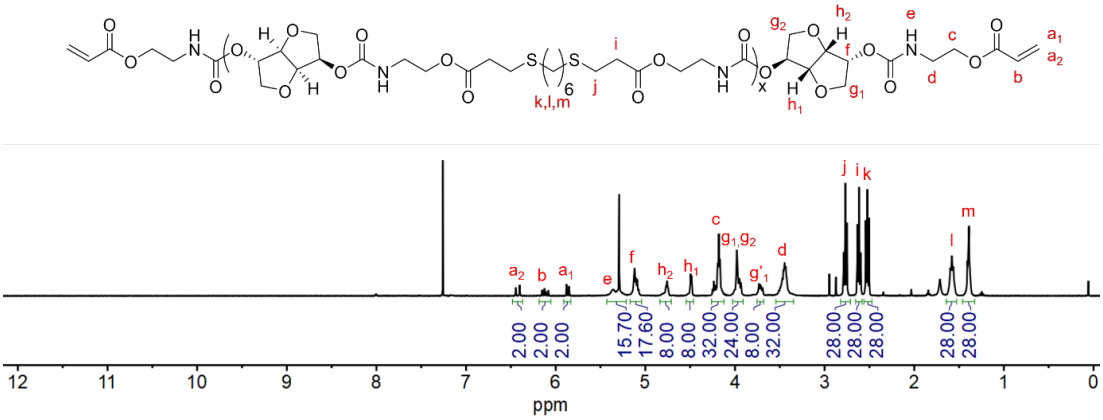


Figure A 3.17. *^{1}H NMR (400 MHz, 298 K, $CDCl_3$) spectrum of a 4.5 kDa isosorbide derived oligomer.*

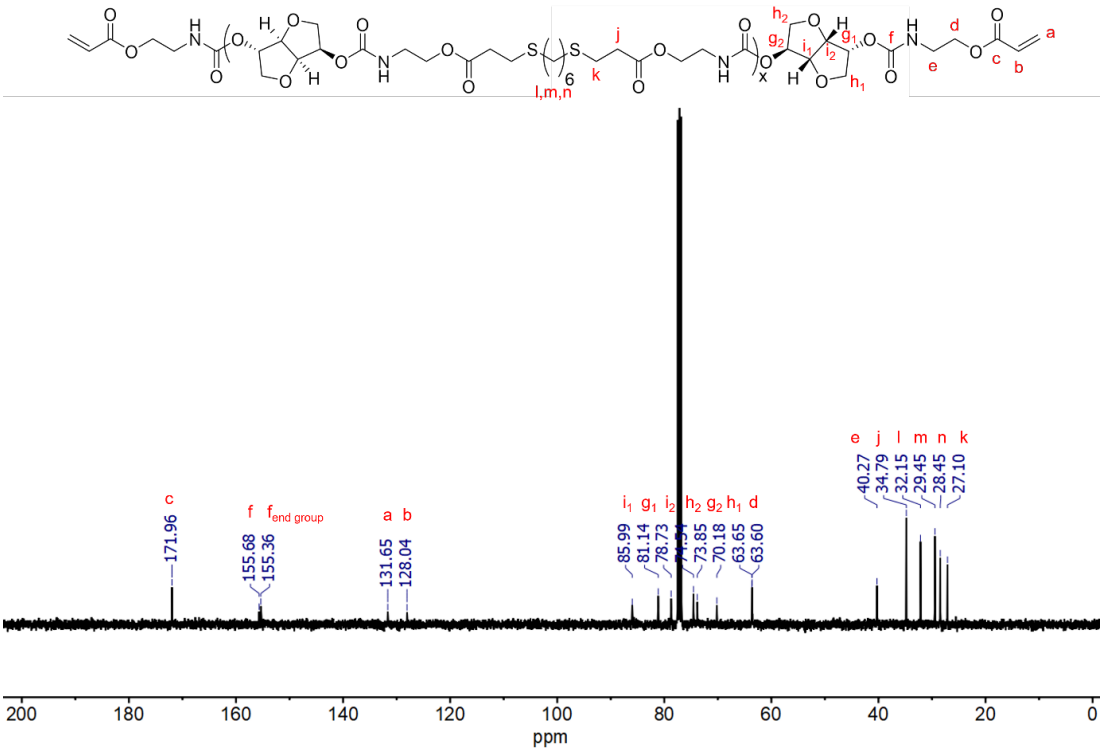


Figure A 3.18. *^{13}C NMR (101 MHz, 298 K, $CDCl_3$) spectrum of a 4.5 kDa isosorbide derived oligomer.*

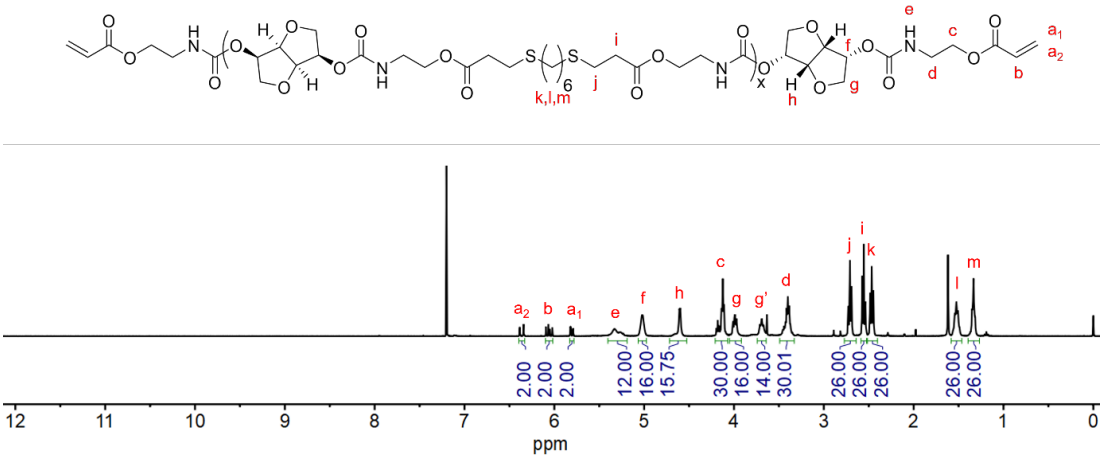


Figure A 3.19. *^{1}H NMR (400 MHz, 298 K, $CDCl_3$) spectrum of a 3.9 kDa isomannide derived oligomer.*

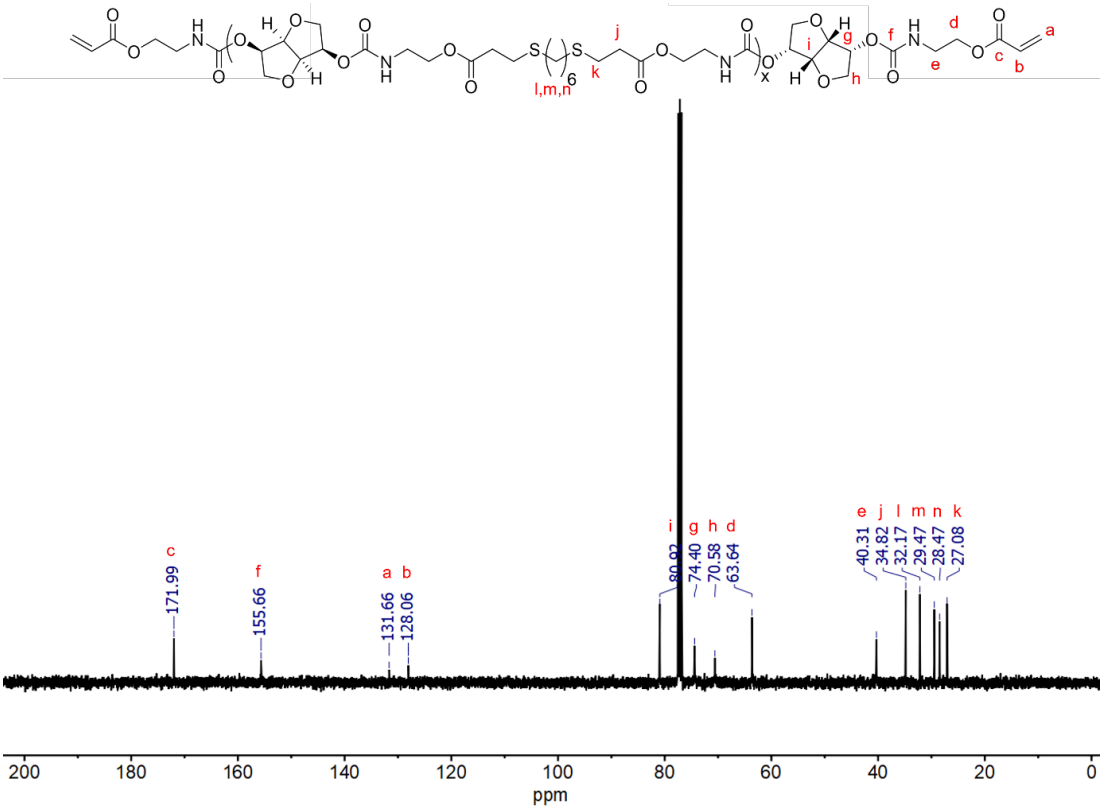


Figure A 3.20. *^{13}C NMR (101 MHz, 298 K, $CDCl_3$) spectrum of a 3.9 kDa isomannide derived oligomer.*

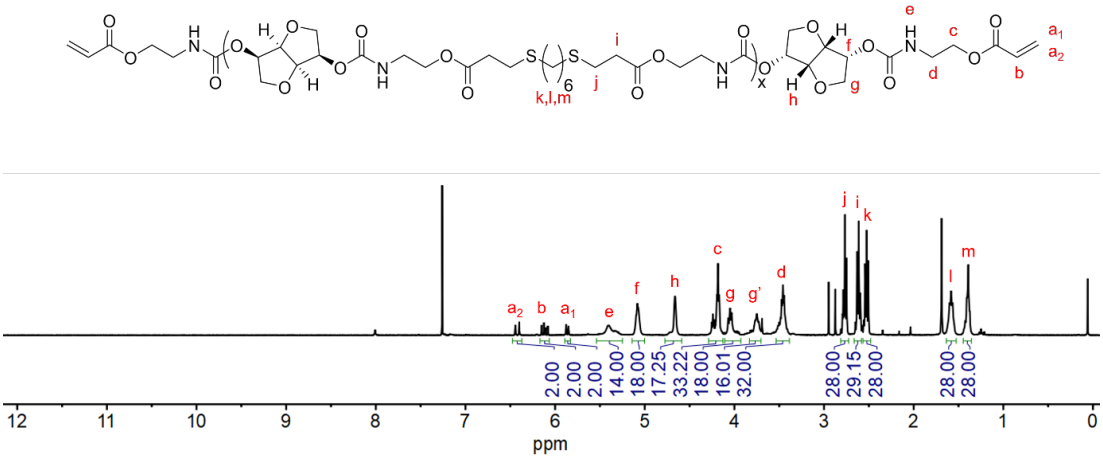


Figure A 3.21. *^{1}H NMR (400 MHz, 298 K, $CDCl_3$) spectrum of a 4.5 kDa isomannide derived oligomer.*

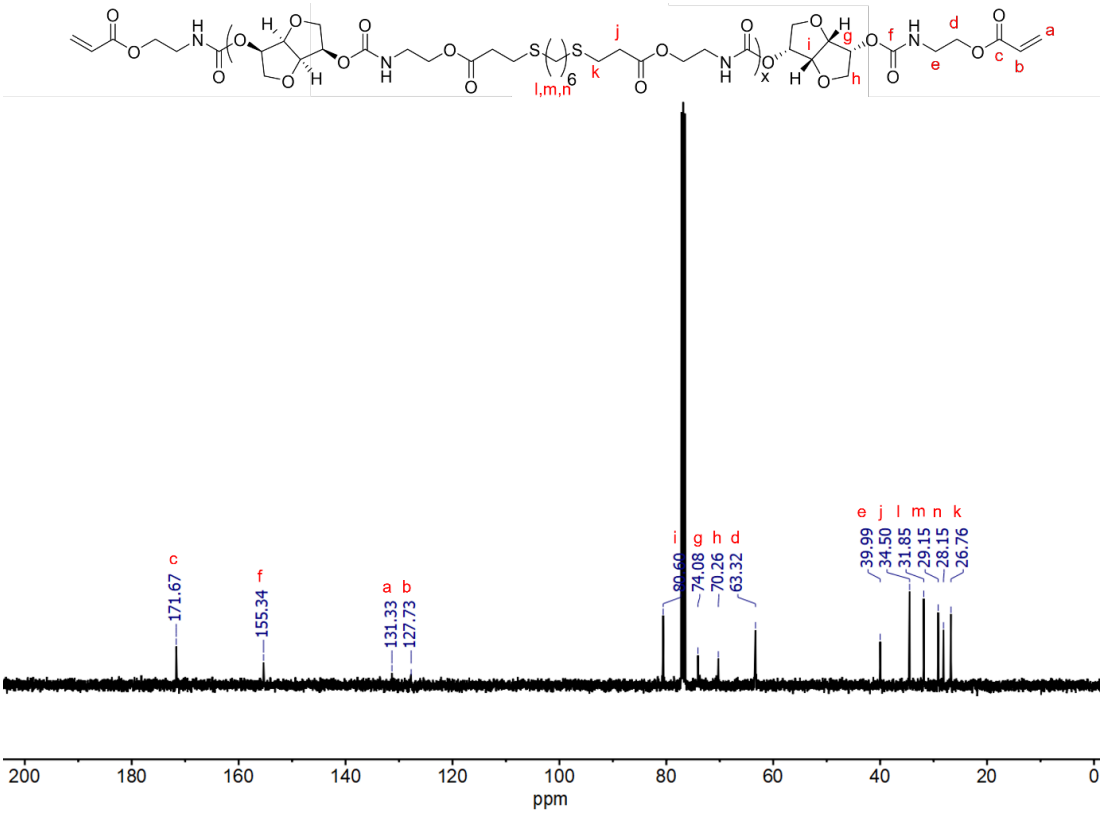


Figure A 3.22. *^{13}C NMR (101 MHz, 298 K, $CDCl_3$) spectrum of a 4.5 kDa isomannide derived oligomer.*

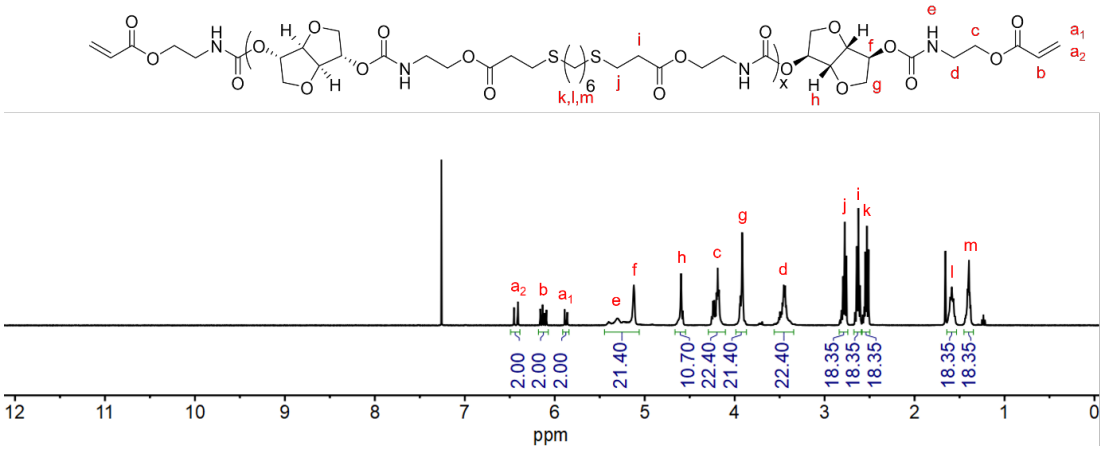


Figure A 3.23. *^{1}H NMR (400 MHz, 298 K, $CDCl_3$) spectrum of a 3.3 kDa isoidide derived oligomer.*

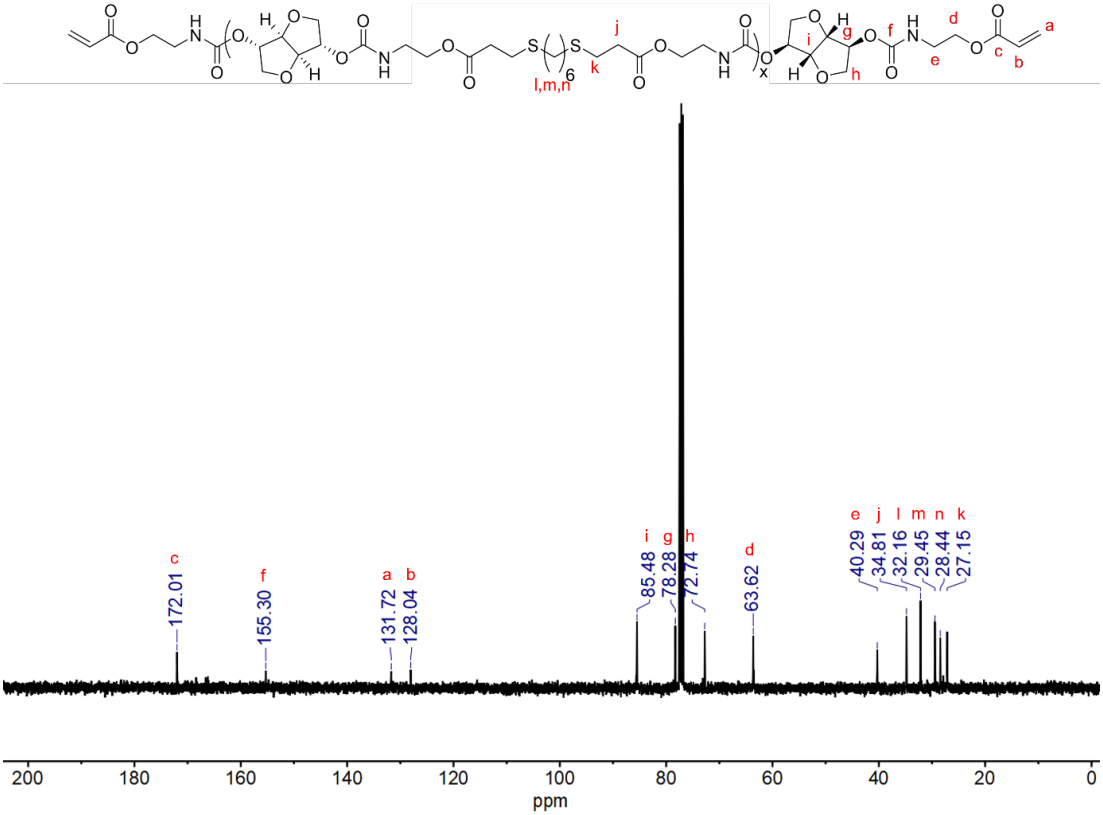


Figure A 3.24. *^{13}C NMR (101 MHz, 298 K, $CDCl_3$) spectrum of a 3.3 kDa isoidide derived oligomer.*

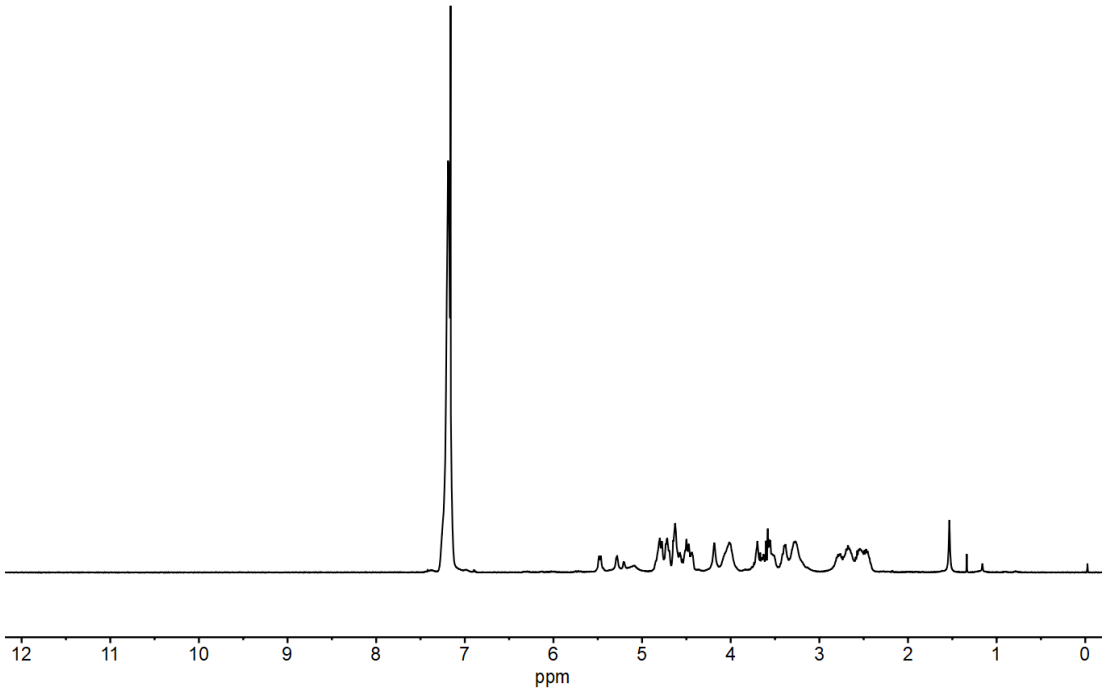


Figure A 3.25. *^{1}H NMR (400 MHz, 298 K, $CDCl_3$) spectrum of an 8.0 kDa glucose-glucose oligomer.*

3.8.4 Size exclusion chromatography (SEC) oligomer characterisation

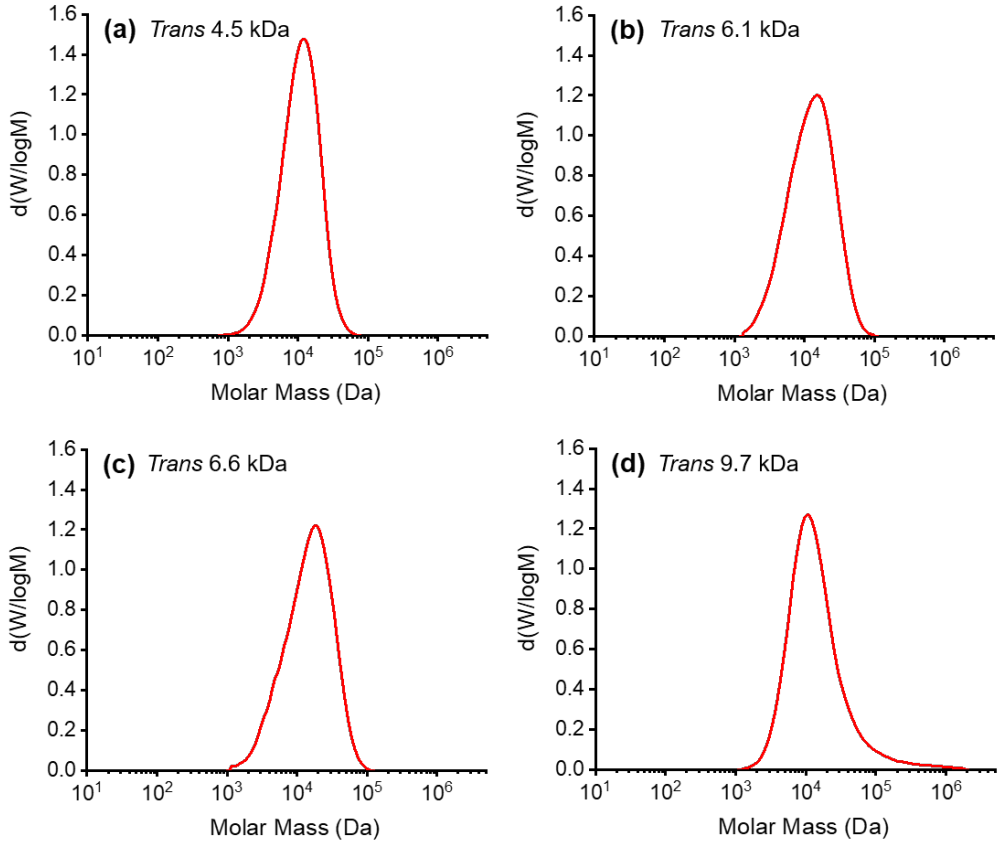


Figure A 3.26. *Compiled size exclusion chromatogram of trans oligomers (DMF, 0.5% w/w NH_4BH_4). (a) 4.5 kDa trans oligomer, (b) 6.1 kDa trans oligomer, (c) 6.6 kDa trans oligomer, (d) 9.7 kDa trans oligomer. Analysis against poly(methyl methacrylate) (PMMA) standards.*

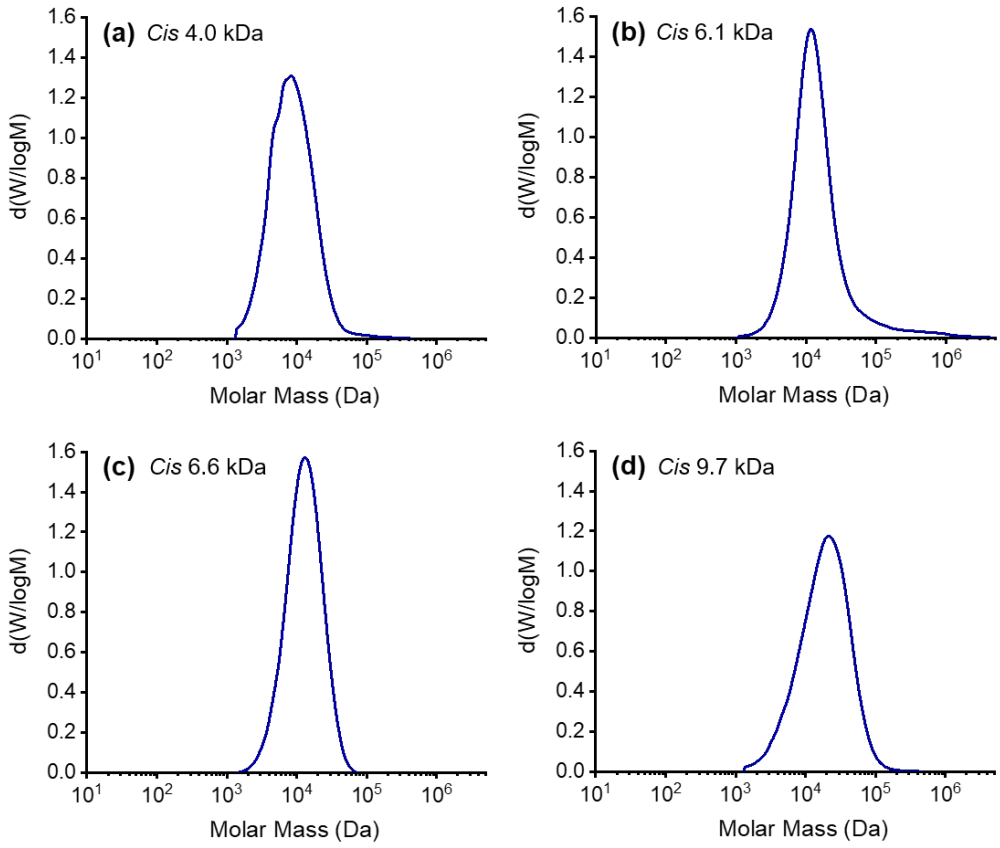


Figure A 3.27. *Compiled size exclusion chromatogram of cis oligomers (DMF, 0.5% w/w NH_4BH_4). (a) 4.0 kDa cis oligomer, (b) 6.1 kDa cis oligomer, (c) 6.6 kDa cis oligomer, (d) 9.7 kDa cis oligomer. Analysis against poly(methyl methacrylate) (PMMA) standards.*

Table A3.1. *Oligomer characterisation by SEC.*

Oligomer[a]	$\bar{M}_n$[b] (kDa)	$\bar{M}_w$[b] (kDa)	$\bar{M}_z$[b] (kDa)	$Đ_M$[b]
trans 4.5 kDa	8.7	13	18	1.47
trans 6.1 kDa	9.3	16	24	1.71
trans 6.6 kDa	10	19	29	1.80
trans 9.7 kDa	10	29	32	2.94
cis 4.0 kDa	6.8	11	31	1.69
cis 6.1 kDa	11	34	570	3.17
cis 6.6 kDa	11	15	20	1.40
cis 9.7 kDa	13	25	45	1.92

[a]M_n determined by ^{1}H NMR spectroscopy. [b]M_n, M_w, M_z, $Đ_M$ were determined by SEC (DMF, 0.5% w/w NH_4BH_4). Analysis against poly(methyl methacrylate) (PMMA) standards.

Chapter 4 – Effect of the *cis*/*trans* alkene configuration on the thermomechanical properties and degradability of unsaturated poly(ester-urethane) photosets

4 Effect of the *cis*/*trans* alkene configuration on the thermomechanical properties and degradability of unsaturated poly(ester-urethane) photosets

4.1 Introduction

Allowing the production of highly intricate designs, while remaining low cost and sustainable; 3D printing constitutes as an appealing alternative to more traditional material processing, and finds applications ranging from consumer products to medical devices.[1] While there is, to date, an ever-increasing variety of techniques available, Digital Light Processing based 3D printing (DLP) stands apart in performance by offering a micron scale resolution as well as unprecedented accuracy and rapidity.[2, 3] Until recently, photocurable resins suitable for DLP were known to be scarce and only produced brittle materials, relegating this technique to industrial prototyping.[4, 5] However, advances in photochemistry methods (thiol-ene[6, 7], addition fragmentation chain transfer,[8, 9] dual cure network[10]) and the enhancement of formulations with additives (siloxanes[11], aliphatic chains[12], and inorganic fillers[13]) contributed to the development of resins yielding materials with improved toughness and ductility.[14, 15] Yet, modifying the mechanical properties within photosets commonly revolves around changing the chemical structure of the network (*e.g* monomer/oligomer substitution), or its crosslinking density. This inevitably results in altering the printability of the resin and therefore further adjustment of either the formulation, the printing parameters or the equipment are

required in the majority of cases.[11, 16] Hence, adaptative UV curable resins allowing the production of mechanically diverse materials while retaining the same chemical structure is highly pertinent as it can potentially bring DLP out of niche market.[12, 17]

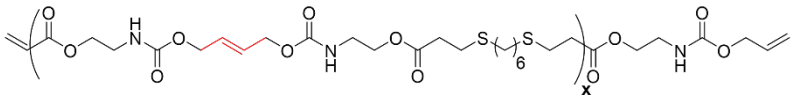
Stereochemistry, in the realm of elastomers, has been successfully used as a tool to access a broad spectrum of mechanical properties using a single polymeric species through the control of the material's crystallinity. For instance, *cis*-1,4-polyisoprene is amorphous and therefore demonstrates soft and elastomeric properties whilst, *trans*-1,4-polyisoprene is comparably closer to a stiff plastic because of its semi-crystalline nature.[18-21] The development towards rational incorporation of *cis/trans* stereochemistry within the polymer backbones to leverage the bulk material properties has been hampered for decades by the synthetic challenges of isomerisation and unwanted crosslinking.[22-25] Nevertheless it is now gaining a growing interest since advances in polymerisation methods allow for milder reaction conditions.[26] For instance, it has been first reported that, via the adjustment of solvent polarity and catalyst basicity, nucleophilic thiol-yne addition of a dialkyne with a dithiol yielded stereo-controlled high molecular weight polymers with a *cis* ratio ranging from 32% up to 80%.[27, 28] More recently, a polymerisation method based on nucleophilic thiol-ene addition between a *cis* or *trans* stereopure diacrylate and a dithiol was proven to be mild enough to preclude the occurrence of isomerisation and allowed the obtention of fully stereopure polymer.[29] Translating this unique strategy to crosslinked systems should greatly benefit the expansion of DLP as tuning the mechanical properties could be achieved by modulating the network stereochemistry instead of its chemical structure, offering a noticeable gain of time and labour in resin design. As such, DLP has been selected as one

application to highlight the leveraging of stereochemistry towards the control of the bulk mechanical properties of the end use polymers as a particularly powerful tool.

Herein, we present the development of photosets and 3D printed scaffolds with stereo-dependant mechanical properties and degradability using the *cis* and *trans* stereopure oligomer which synthesis has been presented in chapter 3. After assessing the optimal conditions, the UV curing and post-processing of the materials occurred without major isomerisation or crosslinking of the in-chain alkenes as proven by ^{1}H NMR analysis of the depolymerised photosets. Leveraging the *cis*/*trans* stereochemistry within the network offered excellent control over the mechanical and degradation properties of the 3D structures.

4.2 Resin formulation and testing

(a) *trans* oligomer



(b) *cis* oligomer

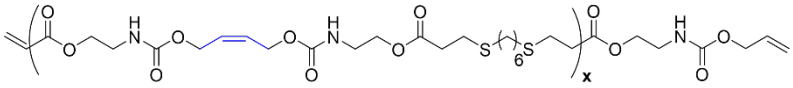


Figure 4.1. *Chemical structure of stereopure (a) trans and (b) cis oligomers using in this study.*

To prepare a moulded film suitable for mechanical testing, the oligomers (*cis* or *trans,* **Figure 4.1**) are first formulated into a resin by mixing them with a diluent and a photoinitiator before being exposed to UV light. (**Figure 4.2**)

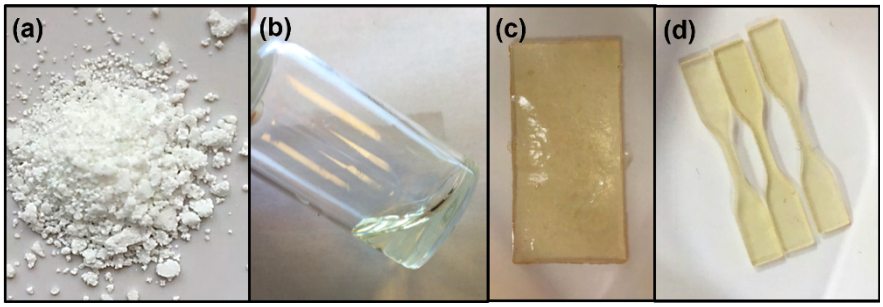
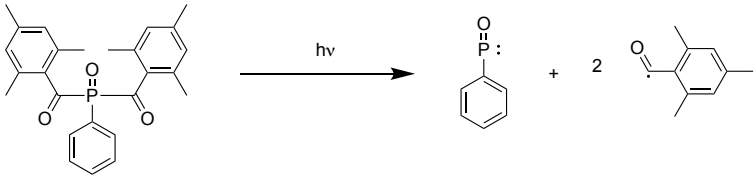


Figure 4.2. *Photography of (a) an oligomer after synthesis, (b) a photocurable resin prepared from a 50:50:1 % ratio of oligomer, diluent and photoinitiator, (c) a film obtained after exposing the resin to 405 nm UV light and thermal post-curing, (d) dumbbell shaped samples for mechanical testing cut out from a film.*

The diluent is essential as both oligomers are solids at room temperature under atmospheric pressure. However, it must be an "unreactive" diluent, a solvent that is inert to UV light or radicals, that will not be taking any part in the network architecture and finally could be removed after the curing process. As for the photoinitiator, it is a molecular species that once exposed to UV light of adequate wavelength will generate a pair of radicals (**Scheme 4.1**), which will then initiate the homopolymerisation by attacking the acrylate end groups of the oligomers present in the resin. The network is formed when sufficient acrylate end groups crosslink with each other.[30]



Scheme 4.1. *Photolysis of phenylbis (2,4,6-trimethylbenzoyl)-phosphine oxide (Omnirad® 819).*

The first films obtained were made from a 3 kDa *trans* oligomers mixed with propylene carbonate (PC) as the diluent and Irgacure® 819 as the photoinitiator in a 60/40/1 wt% ratio and exposed to UV light (405 nm) for 15 min. Propylene carbonate was chosen because of its high boiling point and its biocompatibility.[31] Such obtained films showed encouraging mechanical properties (**Figure 4.3)**, however the resin had to be heated up to 70 °C to allow the oligomers to solubilise in PC.

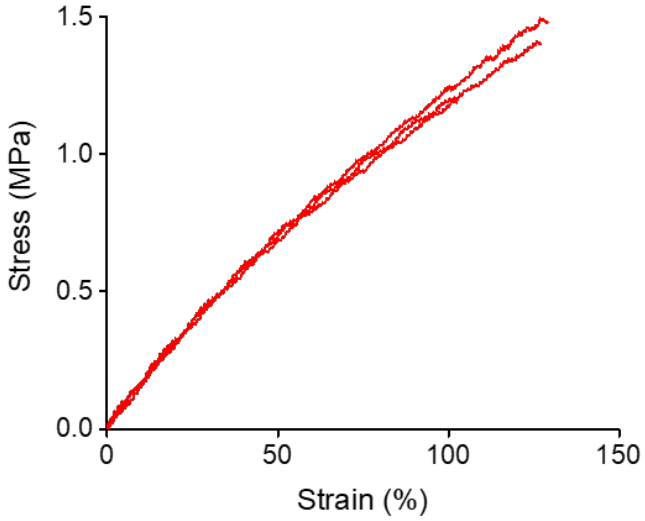


Figure 4.3. *Stress versus strain curves of films prepared using 4.5 kDa trans oligomer in PC. Young's modulus E= 2.18 (±0.16) MPa, stress at break σ_b= 1.80 (±0.24) MPa, strain at break ε_b = 120 (±15) % on average over 3 repeats.*

This technique is not ideal for two reasons: Firstly, because the *cis* oligomer was found to be prone to crosslinking if exposed to temperature above 50 °C for long periods of time or repeatedly. Secondly, manipulating hot resins can be challenging for many applications. Therefore, the resin formulation was re-evaluated.

To achieve this, several compounds have been considered as solvent candidates (**Table 4.1**) N-methyl pyrolidinone (NMP) was selected because it was the only one which can be handled at room temperature with an oligomer content up to 60 wt% and keeps the oligomer stable in solution for days.

Table 4.1. *Solubility tests of oligomer in different solvent/oligomer ratio and their stability over time. rt = room temperature.*

oligomer loading	30 wt%	50 wt%	60 wt%	stability
tetrahydrofuran	rt	50°C	no	minutes
chloroform	rt	50°C	no	minutes
benzyl alcohol	rt	rt	50°C	hours
1,2,4 trimethoxybenzene	rt	rt	50°C	hours
dioxane	rt	50°C	50°C	hours
N-methyl pyrrolidinone	rt	rt	rt	days

Once an appropriate solvent has been found, the choice of the photoinitiator was readapted. Omnirad 819 (solid) was replaced with TPO-L (liquid) to allow for an easier solubilisation in NMP and an increased stability in day light. For this same reason, the concentration of photoinitiator was decreased from 1 wt% to 0.5 wt%. Films were then obtained by curing the resin formulation for 15 min in a UV curing oven, prior to being post-cured at 120 °C in a vacuum oven and finally, the mechanical properties of the *cis* and *trans* samples were tested.

Although the strain at break was twice as high as the one reported for the previous formulation, no significant difference was observed between *cis* and *trans* films in term of Young's modulus (1.6 MPa and 1.5 MPa for *cis* and *trans* respectively) or strain at break (173% and 206% for *cis* and *trans* respectively) (**Figure 4.4**). This similitude in behaviour has been hypothesised to be rooted in either crosslinking or isomerisation of the internal unsaturation, therefore these factors have been investigated further.

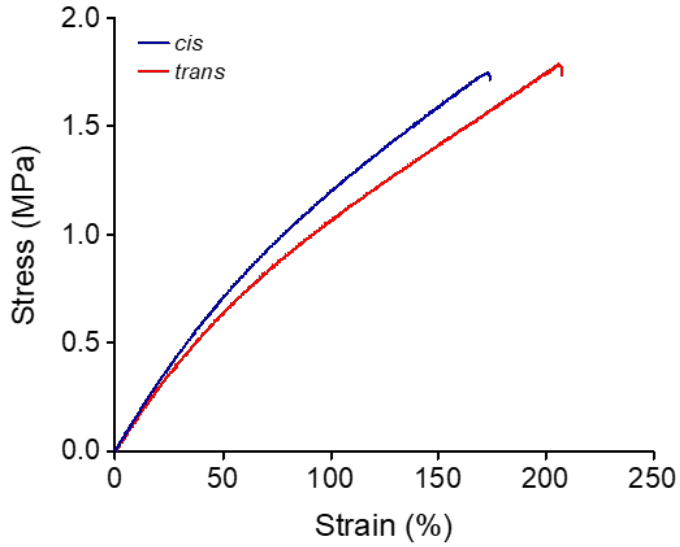
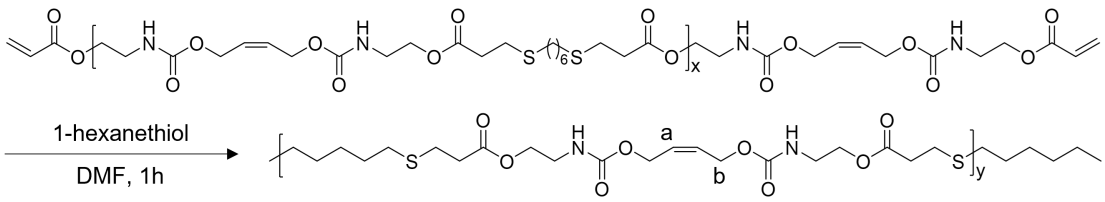


Figure 4.4. *Stress vs. strain curves of films prepared from 5 kDa cis and trans oligomers. trans: Young's modulus E= 1.59 (±0.32) MPa, stress at break σ_b= 1.52 (±0.12) MPa, strain at break ε_b = 207 (±14)% cis: Young modulus E= 1.67 (±0.11) MPa, stress at break σ_b= 1.57 (±0.073) MPa, strain at break ε_b = 163 (±12.8)%*

4.3 Study of potential crosslinking or UV triggered isomerisation

The factor responsible for the similar mechanical behaviour of the *cis* and *trans* materials were primarily ascribed to a loss of the internal unsaturation within the polymer. This could have been caused by a crosslinking reaction of the internal double bond during the UV curing process. In order to assess the stability of the internal double bond, a model study was devised to investigate the effect of the curing process on a thiol end-capped oligomer.

A model experiment was performed where a 4 kDa *cis* oligomer was reacted with 2 equiv. of 1-hexanethiol to prevent the network formation (**Scheme 4.2**).



Scheme 4.2. *Thiol end-capping of a cis oligomer using 1-hexanethiol.*

This model compound was designed to have the same characteristics of an oligomer with a similar molecular weight (4.3 kDa) but without the ability to crosslink as it will not have acrylate end groups. Therefore, if no crosslinking of the internal double bond occurs, the compound would stay soluble in deuterated chloroform ($CDCl_3$) for ^1H NMR spectroscopy even after UV exposure. To recreate an environment identical to the original curing experiment, the obtained thiol-terminated oligomer was formulated into a resin (50 wt% oligomer, 50 wt% NMP, 0.5 wt% TPO-L) prior to be exposed to UV light for a period varying between 10 seconds and 15 minutes. After UV exposure, the mixture was diluted in deuterated chloroform

($CDCl_3$) and analysed by ^1H NMR spectroscopy in order to study the occurrence of potential crosslinking and/or isomerisation. Firstly, the solubilisation of the resin in $CDCl_3$ clearly indicated that no major crosslinking occurred and the analysis of the vinyl area of the ^1H NMR spectra of the resin confirmed this qualitative assumption as it clearly showed that the integration of the allylic **a** and vinylic **b** protons were respectively equal and half the value of the integration of the methylene within the thiol spacer (**Figure 4.5**). This observation led to the conclusion that no crosslinking of the internal double bond occurred during UV exposure. However, the appearance of two signals for both the allylic **a** and vinylic **b** protons of the *cis* double bond indicate that the occurrence of isomerisation during UV exposure (**Figure 4.5**).

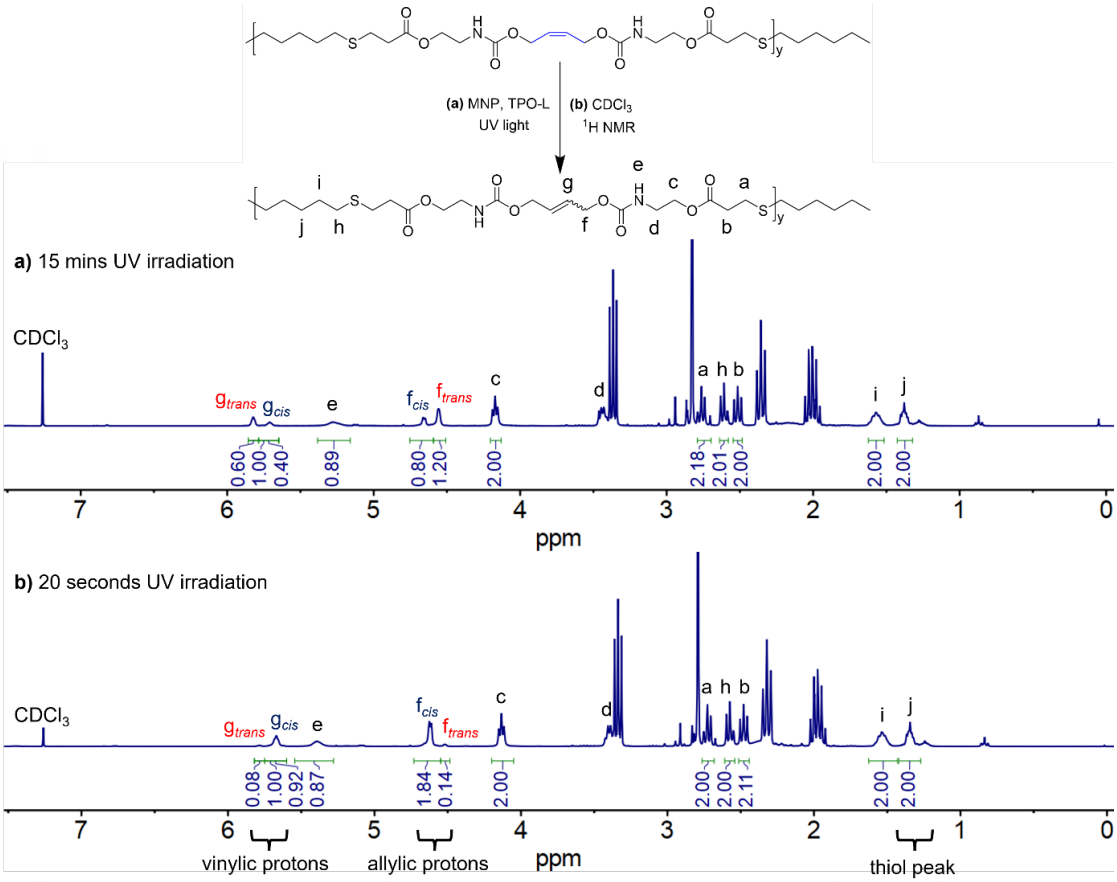


Figure 4.5. *^1H NMR (300 MHz, $CDCl_3$, 298 K) spectra of a thiol-end-capped cis oligomer after a) 15 min and b) 20 sec of UV irradiation.*

As discussed in chapter 3, for the *cis* oligomer, the signal from the vinylic proton is shown at δ = 5.69 ppm, and the 2 allylic protons signals at δ = 4.64 ppm. In the case of the *trans* oligomer, those two peaks shift to δ = 5.83 ppm and δ = 4.57 ppm respectively (**Figure 3.3**). Or here, in the case of the UV exposed end-capped *cis* oligomers, the vinylic proton is showing two signals: one at δ = 5.69 ppm and the other one at δ = 5.83 ppm, and the two allylic protons signals now at δ = 4.64 and δ = 4.57 ppm (**Figure 4.5**). By comparing the integration of the peak characteristic of the vinylic proton of one stereocentre to the integration of all vinylic protons, it is possible to determine the isomerisation percentage of the *cis* double bond and therefore find the ideal condition to minimise isomerisation during the curing process. Using this method on the *cis* end-capped oligomer which was exposed to UV for a varying period of time proved that in the presence of NMP and a photoinitiator, the isomerisation ratio of the *cis* unsaturation raises with the duration of the UV exposure before reaching a plateau after 10 mins (**Figure 4.6 (b)**). Interestingly, the maximum value for the isomerisation is also dependant on the power of the light used. Hence, the maximum value of isomerisation reached with a 11 W flash box was 49 % but switching to a 39 W led bulb curing station yielded 60 % isomerisation at the highest.

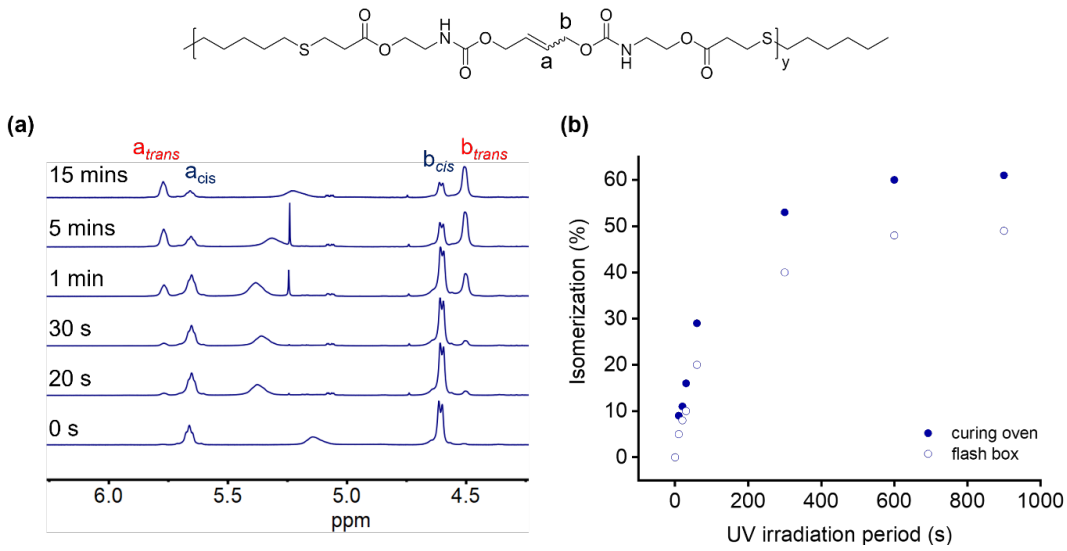


Figure 4.6. *Top: Scheme of the end-capped cis oligomer submitted to a variable period of UV irradiation. (a) Comparison of ^{1}H NMR (300 MHz, $CDCl_3$, 298K) spectra vinyl region of thiol end-capped cis oligomer resins exposed to UV radiation from 0 s to 15 min. (b) Percentage of isomerisation occurring during UV irradiation of a cis end-capped oligomer on an Otoflash postcuring light pulsing unit (flash box, 300 nm ≤ λ ≤ 700 nm, 11 W) and a Formlab form cure curing station (curing oven, =405 nm, 39 W). No isomerisation occurs if the oligomer is not in the presence of a photoinitiator (**Appendix Figure A5**).*

This isomerisation could explain why the *cis* and *trans* films were behaving similarly. In order to confirm this hypothesis, films cured for different amount of time were prepared and their thermomechanical properties have been tested. This experiment will give some insight on the relationship between curing time and mechanical properties.

4.4 Impact of the curing time on *cis* and *trans* materials

4.4.1 Mechanical testing

To study the impact of the curing time on the mechanical properties of the UV cured materials, three sets of resins were prepared and cured for either 15 min, 1 min or 20 s, which was found to be the lowest limit of curing time to obtain a free-standing film. When cured for 15 min, *cis* and *trans* films showed similar mechanical properties but when cured for 1 min or under, the difference between *cis* and *trans* started to appear more prominent (**Figure 4.7**). When cured for 15 min, both *cis* and *trans* films showed a Young's modulus of about 1.5 MPa and a strain at break of 200% approximatively. However, when cured for 1 min and 20s, the *trans* material displays a Young's modulus of 6 MPa and 13.8 MPa along with a strain at break of 227% and 124% respectively. When cured for 1 min and 20 s, the *cis* material displays a Young's modulus of 1.27 MPa and 1 MPa along with a strain at break of 138% and 158% respectively. Therefore, decreasing the curing time from 15 min to 20 s induced a tenfold increase in the stiffness of the *trans* material whilst the stiffness of the *cis* material decreased by a third of its original value.

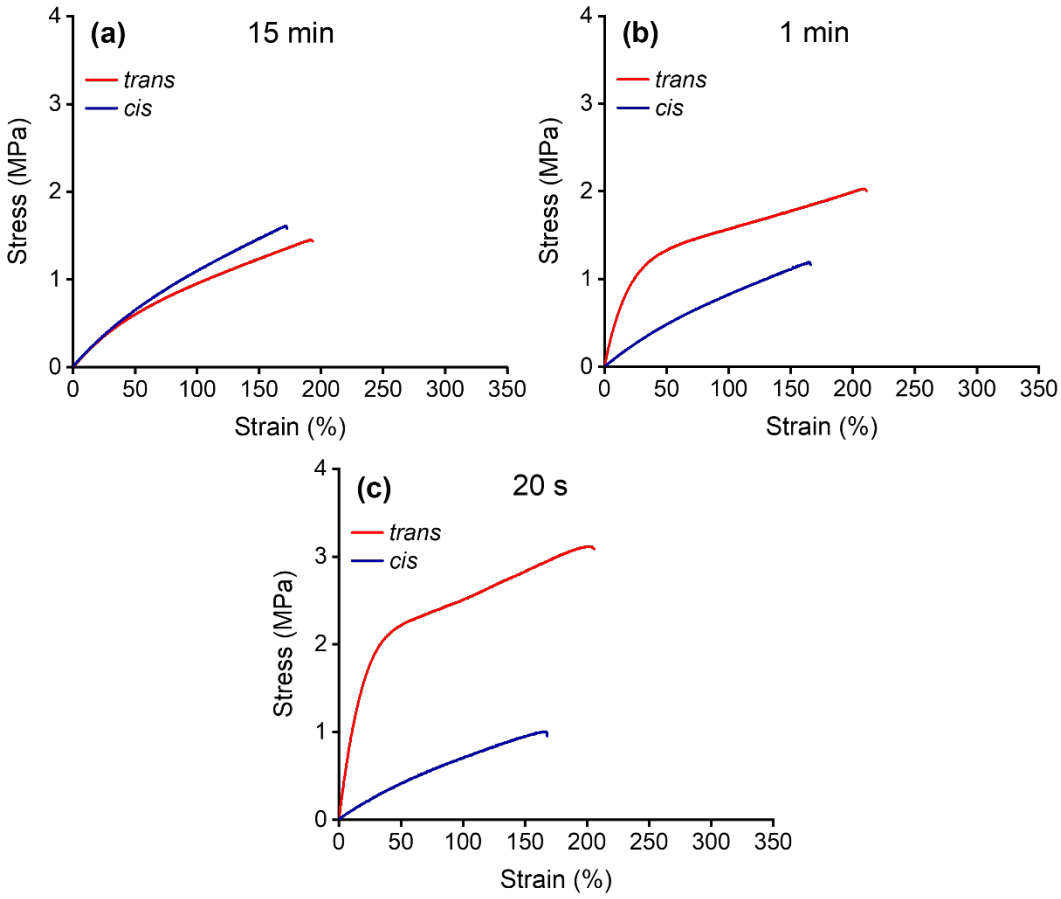


Figure 4.7. *Stress vs. strain curves of films from cis and trans oligomers cured for a varying amount of time.*

It should also be noted that the strain at break decreased when the UV exposure time was decreased. However, this could be the result of swelling the polymer films in methanol at room temperature for 24 h prior to thermal curing to remove the diluent which could plasticise the material and thereby modify the overall mechanical properties of the studied films. At first, this step was redeemed to be necessary to guaranty that the effect seen in the mechanical properties were solely reflected by the impact of the stereochemistry by reducing the number of experimental variables. However, this swelling step yields *trans* materials displaying inferior overall mechanical properties compared to non-swelled films. To overcome this issue, the

swelling step has been later removed from the processing stage as TGA analysis indicated that no NMP was left in the films after thermal post-curing in a vacuum oven at 120 °C. (**Appendix Figure A16**) As a result, the Young's modulus of the *trans* material increased from around 14 to 64 MPa. (**Figure 4.7** and **Appendix Table A1**).

4.4.2 Thermal testing

Secondly, the impact of curing time on the thermal properties of these materials, has been investigated *via* DSC analysis. The aim was to determine if the curing time will also affect the glass transition temperature (T_g) of the materials. Between the T_g of a film cured for 1 min and film cured for 20 s, the differences in the values of T_g observed were under 1 °C for both *cis* and *trans* films, which is negligible (**Figure 4.8**).

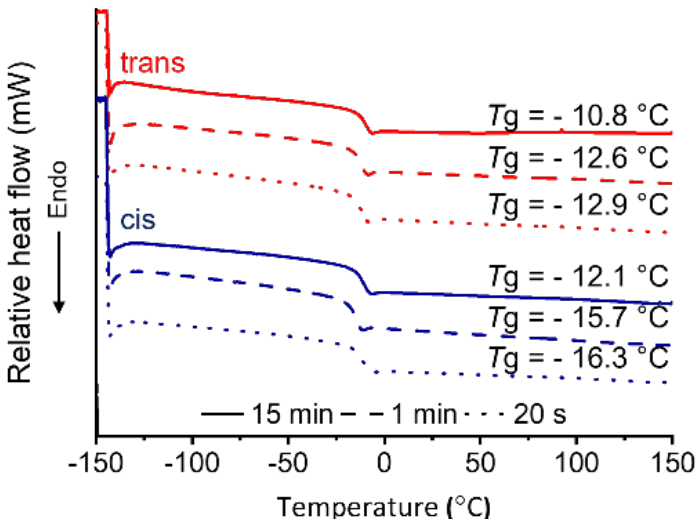


Figure 4.8. *DSC thermograms for films prepared from cis 4.0 kDa and trans 4.5 kDa oligomers and cured for 15 min, 1 min or 20s.*

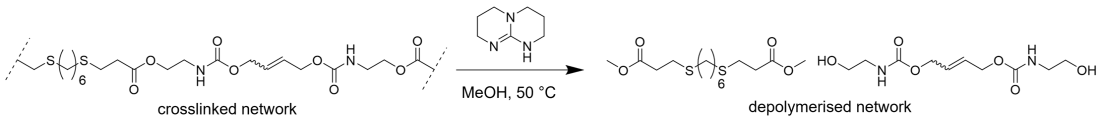
However, a noticeable difference in the values of the T_g has been observed when the curing time has been lowered down from 15 mins and to 20 s, with the *cis* material experiencing a decrease of 4.2 °C, or twice as much as the *trans* material (1.9 °C).

Since the UV exposure time does not trigger the occurrence of isomerisation in the *trans* material, this 2 °C decrease of the T_g value can potentially be ascribed to more free movement available to the polymer chains caused by a decrease in the crosslinking density. It is possible to conclude that after only 20 s of the UV exposure, the radical crosslinking reaction did not reach 100% conversion which allows the network to rearrange and therefore enable a higher ratio of crystallinity later within the material. This hypothesis is also supported by the increase observed in the Young's modulus of the *trans* material when the UV exposure has been decreased to 20 s (**Figure 4.7**). In the case of the *cis* material, the decrease in the T_g is twice as much as that observed for the *trans* material. Additionally, a decrease in the crosslinking density, and the absence of isomerisation of the internal unsaturation also contributed to a lower T_g. Indeed, isomerisation occurring within the *cis* material will result in the appearance of *trans* moieties within the network which inherently hinder the polymer chain flexibility and consequently, increases the value of the T_g. In parallel, a high ratio of *trans* double bonds will also enable a better chain packing and therefore a higher crystallinity ratio that translates to a stiffer material. This was observed during the mechanical testing since the Young's modulus of the *cis* material decreases from 1.5 MPa to 1.0 MPa when exposed to UV light for 15 min or 20 s respectively (**Figure 4.7**). To validate this hypothesis, the films used for the mechanical testing were depolymerised via methanolysis and the

reaction mixture analysed by ^{1}H NMR spectroscopy to evaluate potential isomerisation.

4.4.3 Depolymerisation of networks

Quantifying functionality within networks is challenging owing to their inherent insolubility. Taking advantage of the presence of degradable ester groups within the polymer backbone led us to devise a depolymerisation technique to study the network composition without impacting the internal double bond. Each film was depolymerised by transesterification using triazabicyclodecene (TBD) in methanol to quantitatively assess the composition of the unsaturation and any potential occurrence of isomerisation. TBD, which is a strong base (pKa (TBD conjugate acid) = 21 in THF[32]) activates both the alcohol from the methanol and the ester bond from the oligomer backbone and catalyses an acyl transfer between the two. As a result, the resin is completely depolymerised into smaller units and the mixture is soluble in DMSO, which in return, allows the analysis of the internal double bonds content and stereochemistry within the tested films by ^{1}H NMR spectroscopy (**Scheme 4.3**).



Scheme 4.3. *Depolymerisation method used to quantify double bond stereochemistry in the photoset networks using 2.6 wt% of TBD.*

As a control experiment, both *cis* and *trans* oligomers were depolymerised without being exposed to UV light to verify that the depolymerisation procedure was not impacting the stereochemistry of the unsaturation. The ^{1}H NMR spectra of the crude after depolymerisation via methanolysis, in both the case of *cis* and *trans* oligomers, shows clearly that the stereochemistry of the double bond was not

affected by the depolymerisation conditions, as we can see only one peak for protons **a** at δ = 5.83 ppm (*trans*, H vinylic) and δ = 5.69 ppm (*cis*, H vinylic) and the integration of the allylic protons **b** (δ = 5.83 ppm (trans) and δ = 5.83 ppm (cis)) is equal to the integration of the thiol peaks at δ = 1.49 and δ = 1.33 ppm for both *cis* and *trans* (**Figure 4.9** and **Figure 4.10**).

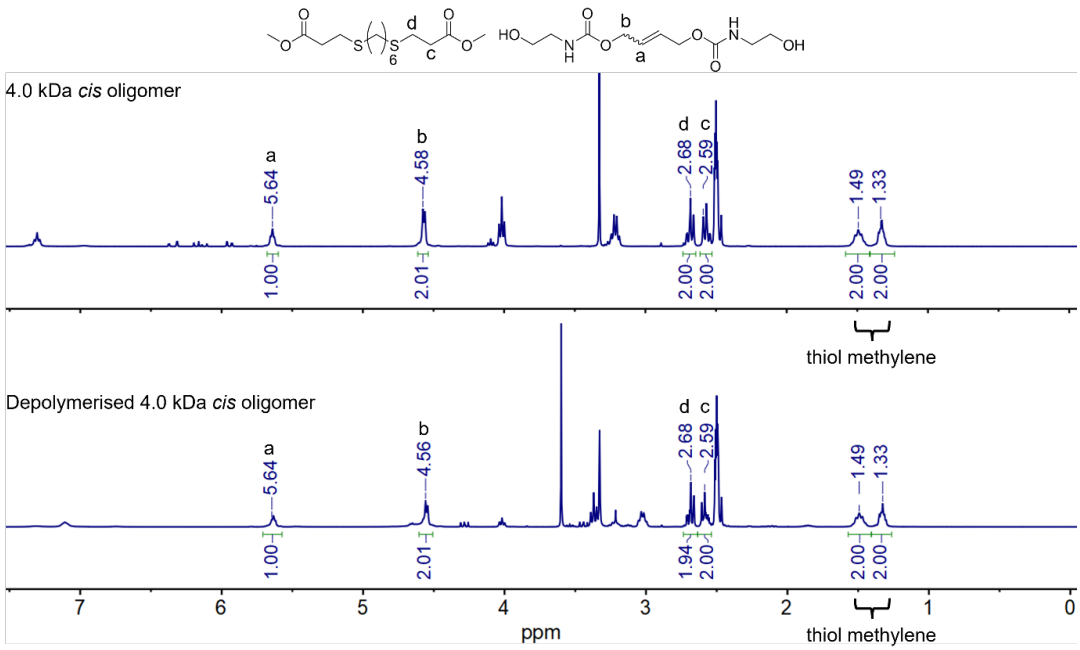


Figure 4.9. *^{1}H NMR (300 MHz, 298 K, DMSO-d_6) spectra of a linear cis 4.0 kDa oligomer (top) and its depolymerisation products (bottom).*

This means that after depolymerisation, the ratio between the methylenes within the thiol spacer and the unsaturation within the diacrylate moieties remained the same, and consequently no double bonds have been lost during the depolymerisation process. In conclusion, this method is adequate to analyse the effect of curing time on unsaturation contained in the network material.

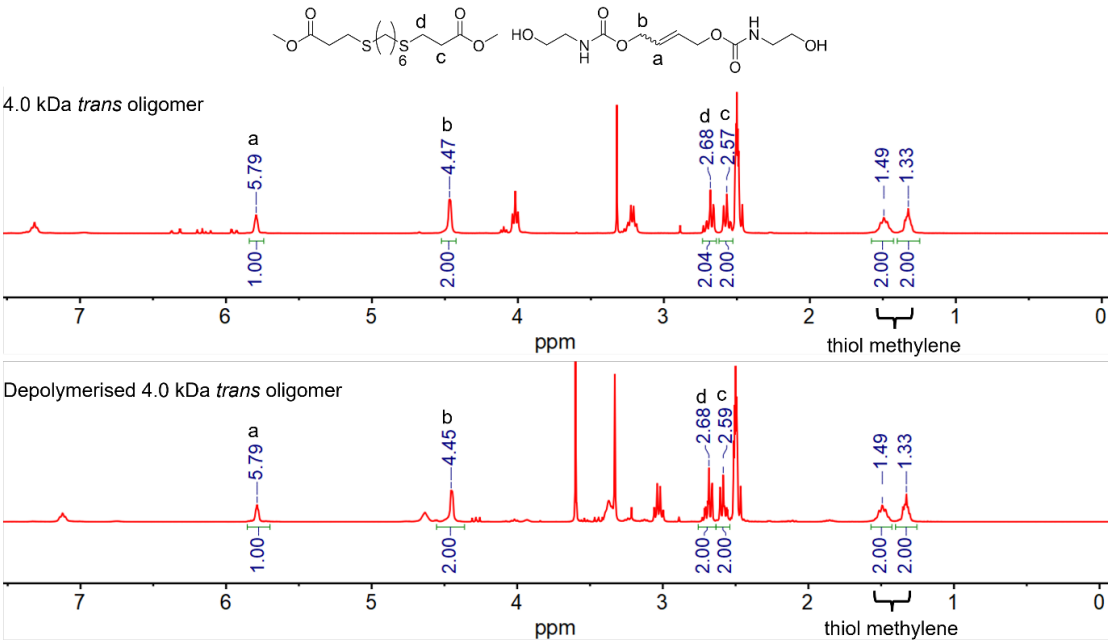


Figure 4.10. *^{1}H NMR (300 MHz, 298 K, DMSO-d_6) spectrum of a linear trans 4.5 kDa oligomer (top) and its depolymerisation products (bottom).*

Hence, the films cured for 15 min, 1 min and 20 sec previously tested (**Figure 4.7**) were depolymerised under the same conditions and the subsequently obtained crude was dissolved in d_6-DMSO for ^{1}H NMR spectroscopy. For the *trans* material, independently of the UV exposure time, neither loss of internal double bonds nor isomerisation could be deduced from analysing the ^{1}H NMR spectra. Hence, the ratio between the signal from the allylic proton within the diacrylate moieties (**b**) and the signal from the methylene within the thiol spacer remained equal to 1, as seen for the oligomer prior to any UV exposure. Also, the presence of only one peak for the signal of the vinylic protons (**a**) indicate that the *trans* stereocentre is stable and does not isomerise at any UV exposure time tested. For the *cis* stereocentre, however, if only one peak (δ = 5.69 ppm) can be observed for the vinylic proton (**a**) on the spectrum of the crude originating from materials cured for 1 min and 20 s, two peaks were observed for the vinylic proton (**a**) (δ = 5.83 and δ = 5.69 ppm) on

the spectra corresponding to the material exposed to UV light for 15 min (**Figure 4.11**). Moreover, the ratio between the methylene within the thiol moieties and unsaturation shows a discrepancy of 15%. This clearly indicates that *cis* in-chain unsaturation, when the material is cured for 15 min, undergo isomerisation in addition to probable crosslinking (**Appendix Figure A4**). These results confirmed the hypothesis stated after the analysis of the mechanical performance of the *cis* and *trans* materials exposed to UV for a variable amount of time: the isomerisation of the *cis* stereocentre is contributing to the increase in Young's modulus observed between a material exposed to UV for 20 s or 15 min. However, this issue could be resolved by shortening the curing time to 1 min or below, since the isomerisation in this case remains under 1%. This result has two significant implications: (i) comparison of the mechanical properties of *cis* and *trans* materials will give reliable information about the influence of stereochemistry on bulk properties as the networks are 99% stereopure when the resin is cured for a short period of time and (ii) because the internal alkenes are not reactive, crosslinks are solely formed at the acrylate end groups. As a result, increasing the molecular weight of the oligomers composing the resin should also impact the mechanical properties.

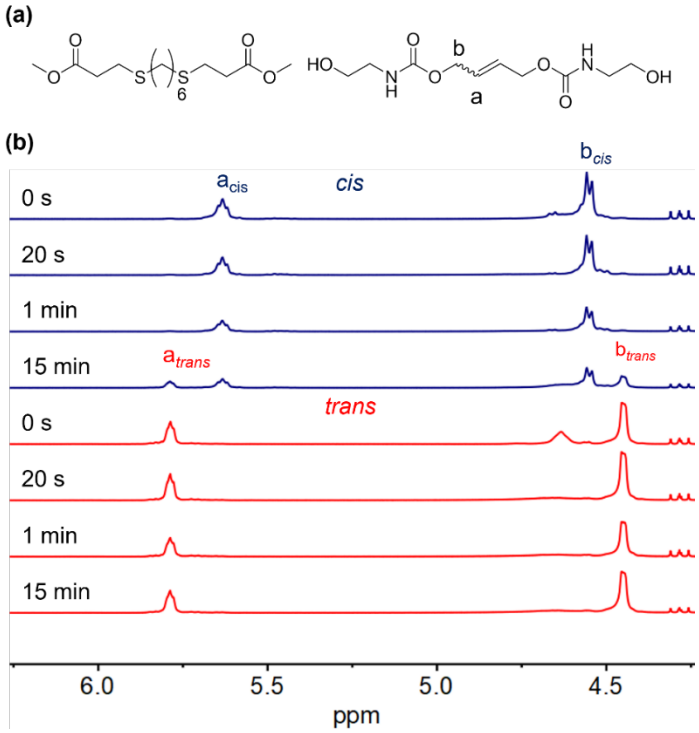


Figure 4.11. *(a) Representation of the major depolymerisation products of cis and trans films. (b) ^{1}H NMR (300 MHz, d_6-DMSO, 298 K) spectra of cis and trans depolymerised films after a varying UV exposure time.*

4.5 Impact of the chain length and stereochemistry on the mechanical properties of photoset networks

4.5.1 Tensile testing

To elucidate both the impact of the stereochemistry and the oligomer length on the mechanical properties of the resultant network, both *cis* and *trans* films were prepared from resins based on stereochemically pure oligomers with a molecular weight of either *ca*. 4, 6 or 10 kDa as determined by ^{1}H NMR analysis. After 20 s of UV exposure and 24 h of thermal curing at 120 °C, the mechanical properties of each film were tested (**Figure 4.12**).

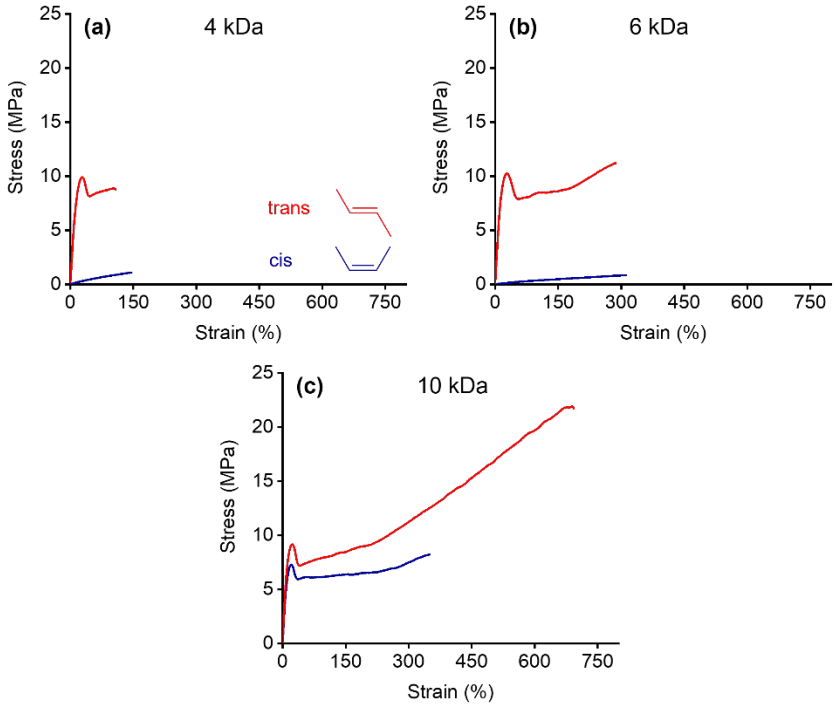


Figure 4.12. *Representative stress-strain curves of (a) a 4.5 kDa trans film and a 4.0 kDa cis film, (b) 6.1 kDa trans film and a 6.1 kDa cis film, (c) a 10 kDa trans film and a 9.7 kDa cis film. The molecular weights have been determined via ^{1}H NMR spectroscopy.*

For resins comprised of shorter oligomers, a striking difference existed between the tensile profiles of the *cis* and *trans* photoset films. The UV cured material that contained *trans* oligomers of around 4 kDa exhibited a Young's modulus (E) of 64 MPa, a yield point (σ_y) of about 10 MPa at 30% elongation and a strain at break (ε_b) of 98% (**Figure 4.12 (a)**). This behaviour is typical of a stiff and moderately ductile plastic.[33] Conversely, with a Young's modulus 50 times smaller than the *trans* material, the absence of yielding and hardly any resistance to deformation until failure (140%), the stress-strain response of the *cis* film is indicative of an elastomeric material. Increasing the oligomer molecular weight within the resins from *ca*. 4 kDa to *ca.* 6 kDa led to films that displayed the same response to tensile stress but in which the strain at break increased to reach 300% (**Figure 4.12 (b)**).

Further increasing the molecular weight of the oligomer to *ca*. 10 kDa resulted in a resin that, when photocured, exhibited improved ductility and strain at break (647%) for the *trans* material, however, the *cis* material unexpectedly behaved similarly. Thus, the *cis* film only shows a 40% improvement of its strain at break while diverging from the elastomeric behaviour, to display plastic deformation (**Figure 4.12 (c)**). While still noticeable, the difference between *cis* and *trans* materials becomes less prominent at relatively longer chains. Since the stereochemistry is the only variable between the *cis* and *trans* films at a given molecular weight, it is possible to state that it constitutes the basis of the mechanical divergence displayed by the photosets. As previously observed in polyisoprene [34, 35] and polybutadiene [36], internal *trans* alkenes tend to result in linear backbones capable of chain packing which promotes a higher degree of crystallinity within the polymeric structure. Hence, the *trans* unsaturated materials presented in this study, because of their semi-crystalline nature, are stiff and tough. Conversely, *cis* alkenes impede the linearity of the backbone resulting in a less ordered structure, reducing the crystallisation probability, which leads to more amorphous materials with soft, elastic properties. As for the increase in elongation with the oligomer molecular weight, it could be proposed that as the crosslinking is selective towards the acrylate end group, an increase of the chain length is equivalent to an increase of the average molecular weight between crosslinks (M_c) inducing a gain in ductility (**Figure 4.13**). The same argument could also explain the unexpected stiffness of the 9.7 kDa *cis* film, as with a higher M_c, the chains gain in free movement and therefore the probability to crystallise is higher. To study the crystallinity properties of both *cis* and

trans films at different molecular weights and validate this hypothesis, thermal analysis of these materials was carried out.

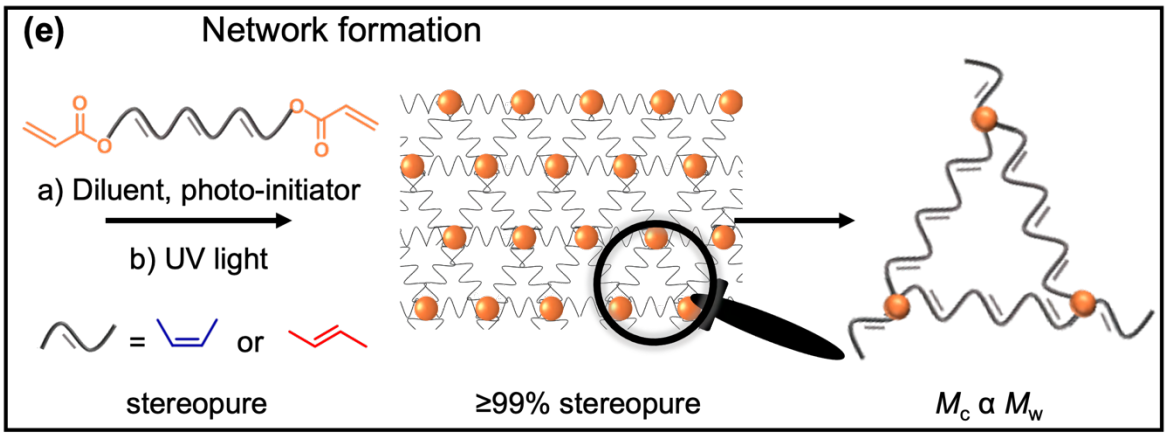


Figure 4.13. *Idealistic representation of the network formation and final structure at the molecular level: the radical initiate the crosslinking of the acrylate end group; however, the internal unsaturation remains unreactive.*

4.5.2 Thermal testing

Conducting DSC analysis on these 6 films highlighted the expected correlation between mechanical properties and crystallinity within the network (**Figure 4.14**). After 2 days of annealing, all *trans* films on their first heating scan displayed two melt transitions around 45 °C and 65 °C, with a total melting enthalpy (ΔH_m) ranging between 26 and 28 $J \cdot s^{-1}$. This suggests that regardless of the oligomer chain length, *trans* films are semi-crystalline.

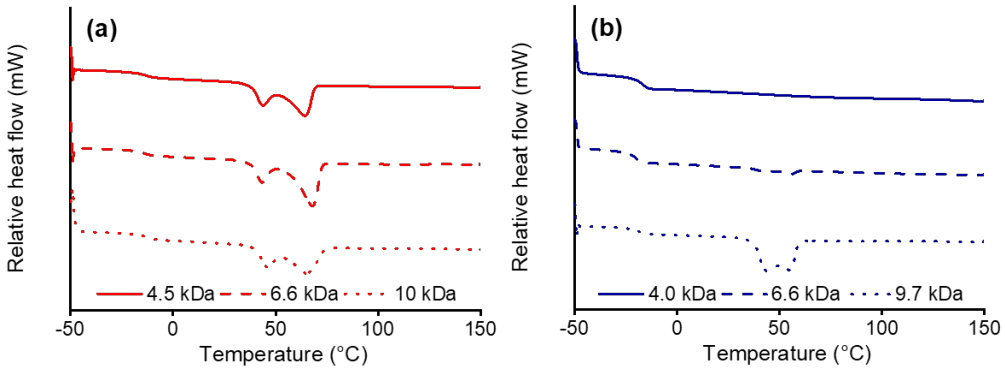


Figure 4.14. *(a) 1st heating scans of DSC thermograms for (a) trans films of 4.5, 6.1, 7.1 and 10 kDa showing a constant degree of crystallisation and (b) cis films of 4.0, 6.1, 7.1 and 10 kDa showing the dependence of the crystallinity with the oligomer chain length.*

The presence of two melting peaks, typically seen in isotactic polypropylene could be ascribed to different crystalline domains within the bulk material. [37, 38] Conversely, the *cis* films appear to present a crystallinity ratio proportional to the oligomer molecular weight. At 4 kDa, no melting transition is observed on the first heating scan of the *cis* film and a melting peak can scarcely be detected with a ΔH_m of 2.6 $J \cdot s^{-1}$ on the first heating scan of a 6 kDa *cis* film. However, the 9.7 kDa *cis* film shows a noticeable melting transition at about 43 °C and 56 °C related to a ΔH_m of 25 $J \cdot s^{-1}$. Reanalysis of the thermal properties of the materials by DSC on the same films after 2 weeks, 10 months and 2 years of annealing showed a discernible evolution in crystallisation for the 6 kDa *cis* film, for which ΔH_m goes from 2.6 $J \cdot s^{-1}$ at two days to 20 $J \cdot s^{-1}$ after 2 weeks of annealing. Interestingly, no significant change in the crystallinity ratio could be observed between the samples annealed for 2 weeks or 10 months. However, after 2 years, all samples DSC scans present a similar melting peak, which indicate a similar crystallinity ratio (**Figure 4.15**).

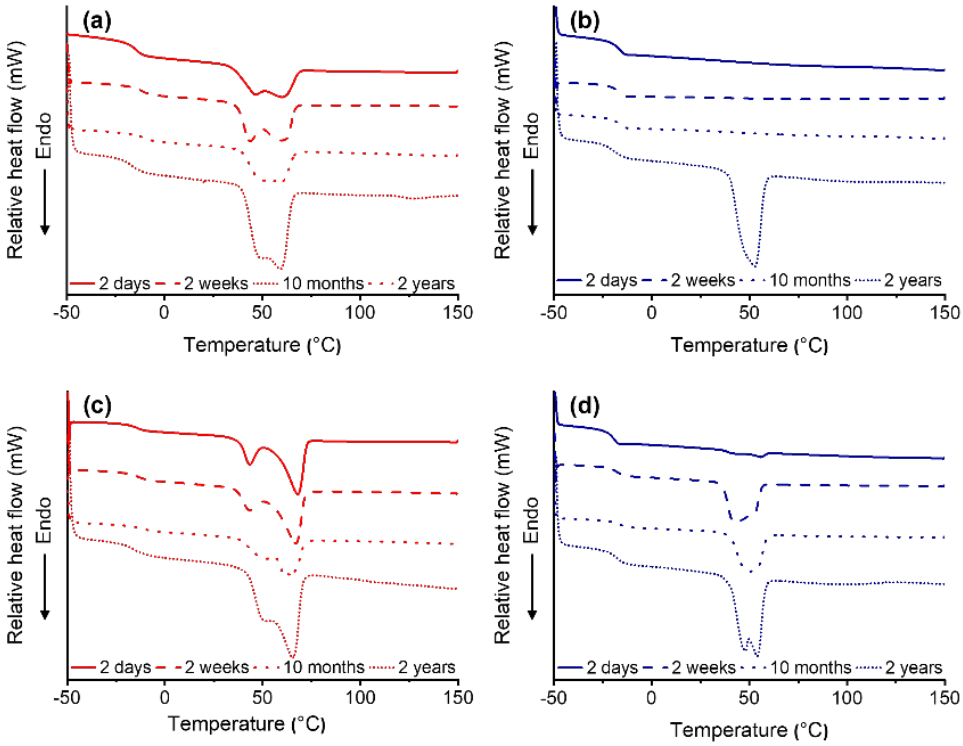


Figure 4.15. *1st heating scans of DSC thermograms for (a) trans films of 4.5 kDa, (b) cis films of 4.0 kDa, (c) trans films of 6.1 kDa and (d) cis films of 6.6 kDa.*

Consequently, it is possible to draw the conclusion that after 2 days, the *trans* materials are semi-crystalline networks independently of their molecular weight and this explains their stiff and tough plastic behaviour during tensile testing. In the case of *cis* films annealed for 2 days, however, the degree of crystallinity is correlated to the molecular chain length of the oligomer present within the resin as the 4 kDa *cis* film is amorphous, whereas both the 6.1 kDa and 9.7 kDa film are semi-crystalline. This highlights that the core difference between the impact of the stereochemistry on the network is mostly driven by their kinetics of crystallisation rather than an inherent ability or inability to crystallise. Moreover, the molecular weight within the network also impacts the rate of crystallisation as none is observed within the 4 kDa material before 2 years annealing time, the 6 kDa film crystallises slowly over two

weeks and the 10 kDa film only takes two days to reach its final degree of crystallinity. This highlights why the former still behaves as a soft elastomer after 2 days of annealing when the latter acts as a stiff plastic. And finally, it is possible to assume that *cis* and *trans* networks will remain as different from each other after 10 months as they did after 2 weeks, however, after 2 years, all samples have had the time to reach a similar ratio of crystallisation and therefore all materials could be expected to have the same mechanical performances.

4.5.3 Study of the network's architecture

Most claims made so far holds on the presumed lattice architecture of the network (**Figure 4.13**). It has already been corroborated by the tensile tests of networks with varying molecular weights that an increase in the molecular weight of the oligomer results in an increase in the strain at break. In addition, the depolymerisation study showed that the internal unsaturation remains unreactive under the curing conditions. However, in order to further validate this hypothesis, the networks were swelled in THF over 24 hours to access the swelling degree or how much the network can expand in a good solvent, which indirectly offers information on the chain length between two crosslink M_c (**Figure 4.16**). The results have shown that the swelling degree was increasing linearly with the molecular weight, which is in accordance with the lattice model used in this study, since the average molecular weight between crosslinks (M_c) is proportional to the average molecular weight of the oligomer constituting the original resin.

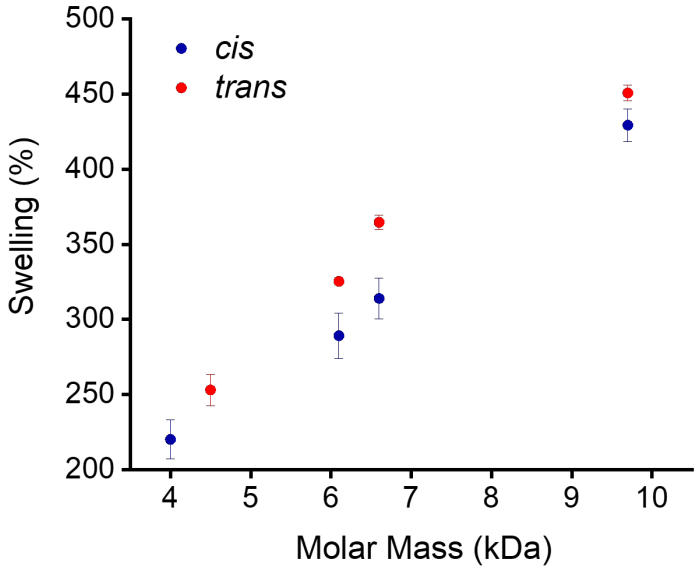
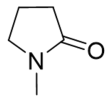
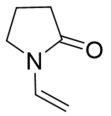


Figure 4.16. *Swelling ratio relative to the initial sample weight after 24h in THF at 25˚C. Each data point was averaged from 4 samples with the standard deviation taken as the uncertainty.*

Lastly, to find out if the difference between *cis* and *trans* will be maintained whilst allowing the internal unsaturation to crosslink, N-vinyl pyrrolidone (NVP) was incorporated into the resin formulation in a ratio of 8 wt% of 25 wt% of the total weight of the resin. This reactive diluent has a similar structure to NMP; however, an allylic functionality is decorating the nitrogen atom (**Figure 4.17**). This unsaturation can undergo radical reactions and should therefore increase the radicals generated during UV exposure of the resin. Consequently, the probability for crosslinking the *cis* or *trans* unsaturation present within the oligomer backbones is significantly increased.



N-methyl pyrrolidone (NMP)



N-vinyl pyrrolidone (NVP)

Resin's constituents	oligomer (wt%)	NMP (wt%)	NVP (wt%)	TPO-L (wt%)
original formulation	50	50	0	0.5
8% NVP	50	42	8	0.5
25% NVP	50	25	25	0.5

Figure 4.17. *Structure of N-methyl pyrrolidone and N-vinyl pyrrolidone, used as unreactive and reactive diluent respectively and table summarising the formulation of the original resin containing 0% of NVP and resin which contains either 8 or 25 wt% of NVP.*

The mechanical properties of *cis* and *trans* versions of the NVP-based resins displayed no measurable difference between the two stereoisomers at any given NVP loading (**Figure 4.18**). The addition of 8% of the reactive diluent to the formulation led to the obtention of an elastomeric material for both isomers, whilst increasing the content of NVP to 25% resulted in the formation of stiff plastics. These results are expected: if the internal unsaturation crosslinks, then the networks are virtually the same since the stereochemistry is lost, and an increase in the reactive diluent results in an increase of the crosslinking density. Or, for lower crosslinking density, an elastomer is obtained and increasing the crosslinking density will causes the formation of a stronger, stiff plastic.

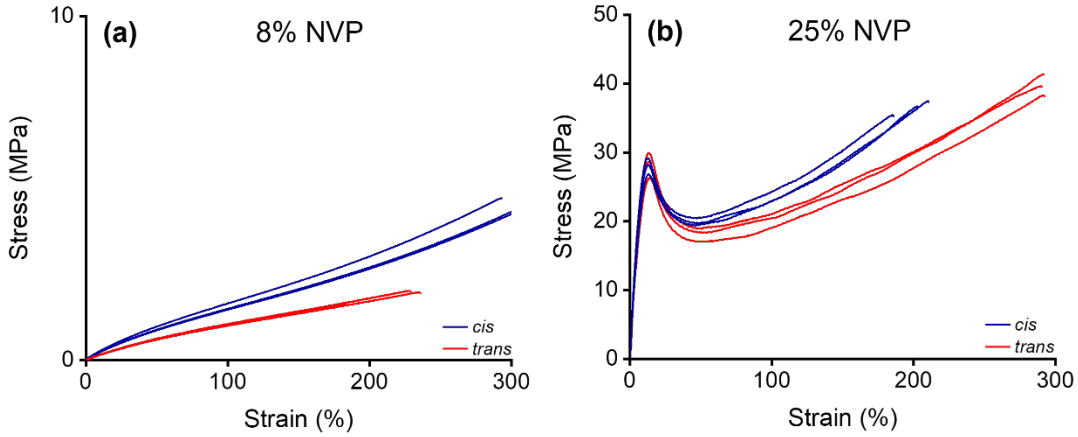


Figure 4.18. *Stress-strain curves of both cis and trans films containing (a) 8% NVP and (b) 25% NVP.*

The depolymerisation of such films was unsuccessful, which suggests that the crosslinking of the internal double bond occurred. Hence, this experiment also supports the idea of a lattice architecture. In conclusion, the difference in behaviour between stereoisomers observed in this study was allowed owing to the orthogonality of the acrylate radical crosslinking reaction which permitted the formation of a lattice specifically crosslinked at the acrylate end groups and so at regular intervals.

4.6 3D printing of *cis/trans* resin

4.6.1 Introduction

Since the *cis* and *trans* materials used in the study about stereochemistry within networks were originating from photocurable resins, it was considered to identify for translation to Digital light processing (DLP) 3D printing. DLP 3D printing is a subcategory of stereolitography (SLA) 3D printing, which uses photocurable resins which formulation include but are not limited to a liquid cross-linkable monomer(s)

and or oligomer(s), a photoinitiator, and a diluent if necessary. After the computer-assisted 3D design of a desired object and its conversion into a compilation of 2D images, the general concept of DLP relies on projecting these images one after the other onto a building plate through a resin bath. After the projection of an image, the UV-light will activate the photoinitiator which leads to the radical crosslinking of the monomer(s)/oligomer(s) within the resin. As a result, the resin hardens and the first layer is built, then the building plate moves up and the cycle repeats until the last layer has been cured (**Figure 4.19**). One advantage that is often associated with DLP is its capacity to rapidly obtain high-resolution printed parts thanks to the use of a Digital Micromirror Device (DMD) as a special light modulator.[39] However, the best results in precision and accuracy can only by achieved with the use of a resin containing adequate chemical and physical properties. Hence, parameters such as viscosity, gelation rate, light absorbance profile and curing depth are critical parameters that require measurement and optimisation where possible prior to 3D printing. Usually, the ideal resin should have a viscosity as low as possible to enable the lowest UV-exposure time per layer possible. However, the formulation of a fast-curing resin resulting in mechanically robust printed part is an ongoing challenge since curing low viscosity monomers will give rise to highly crosslinked networks, which are brittle by nature, and the use of viscosity modifiers in oligomer-containing resin will inevitably impact not only the mechanical properties of the final material but decrease the printing accuracy since a longer exposure time will be required to cure a layer. (Zhu 2020) This general trend shows how intrinsic experimental work is needed for optimisation in the development of a photoreactive resin for 3D printing

since the fundamental parameters cited above are correlated to each other and unique to a resin system/3D printer/curing conditions combination.

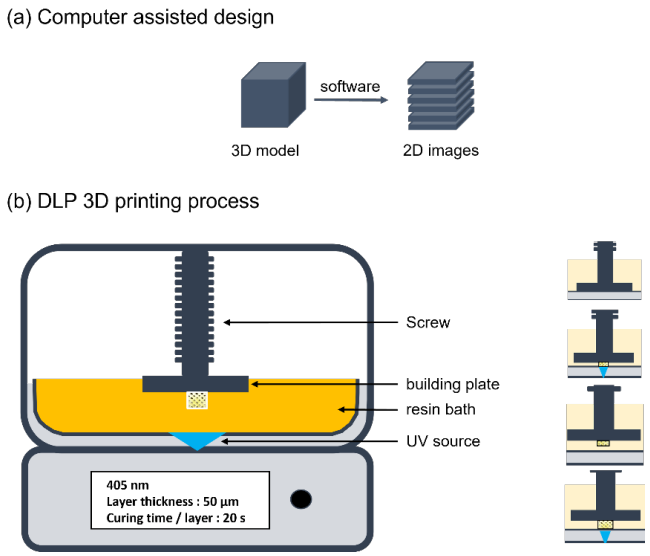


Figure 4.19. *Representation of (a) the slicing process converting a 3D model into a compilation of 2D images or slices and (b) a DLP 3D printer general structure and process.*

4.6.2 Resin characterisation

In regard to the viscosity, since the *cis* and *trans* oligomers are both solids and require a 50% dilution in NMP to form a thick resin, the degree of improvement remained small on this parameter. A higher ratio of diluent would have only resulted in the formation of a gel upon UV irradiation, and, consequently, weaker materials would have been obtained in comparison to the previous study. Fortunately, the viscosity values obtained for both *cis* and *trans* resins were found to be at 0.75 Pa·s and 0.83 Pa·s respectively, as measured at a shear rate of 0.631 s^{-1}(**Figure 4.20**).

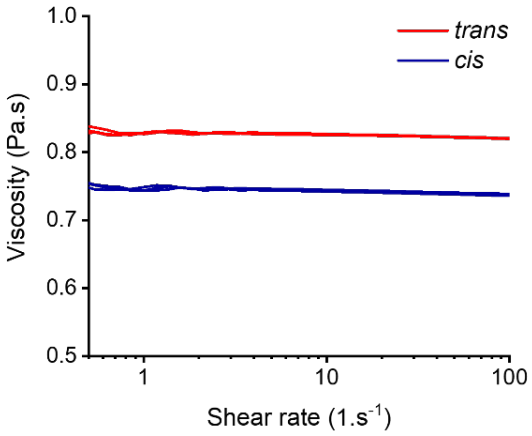


Figure 4.20. *3D printing resin viscosity between a shear rate of 0.1 and 100 s^{-1}.*

These values are high for DLP 3D printing, which usually require the viscosity of the resin to be comprised within 0.5 to 0.8 Pa·s[40] but the inability of changing the diluent - because of the solubility issues with the oligomers - and the incapacity of increasing the ratio of diluent within the resin without affecting the general mechanical properties[41] of the *cis* and *trans* material, this parameter was left at 50 wt%. Instead, to alleviate the loss of resolution resulting from a high viscosity resin, a photo-inhibitor has been added to the original formulation with the aim to reduce the curing depth as much as possible without impacting the curing rate. UV-visible analysis showed that Paprika extract (Kalsec Durabrite®) was an ideal candidate to that purpose as one of its two maximum absorption peaks (377 nm) aligned with the maximum absorption peak of the photo-initiator present in the resin (**Figure 4.21**).

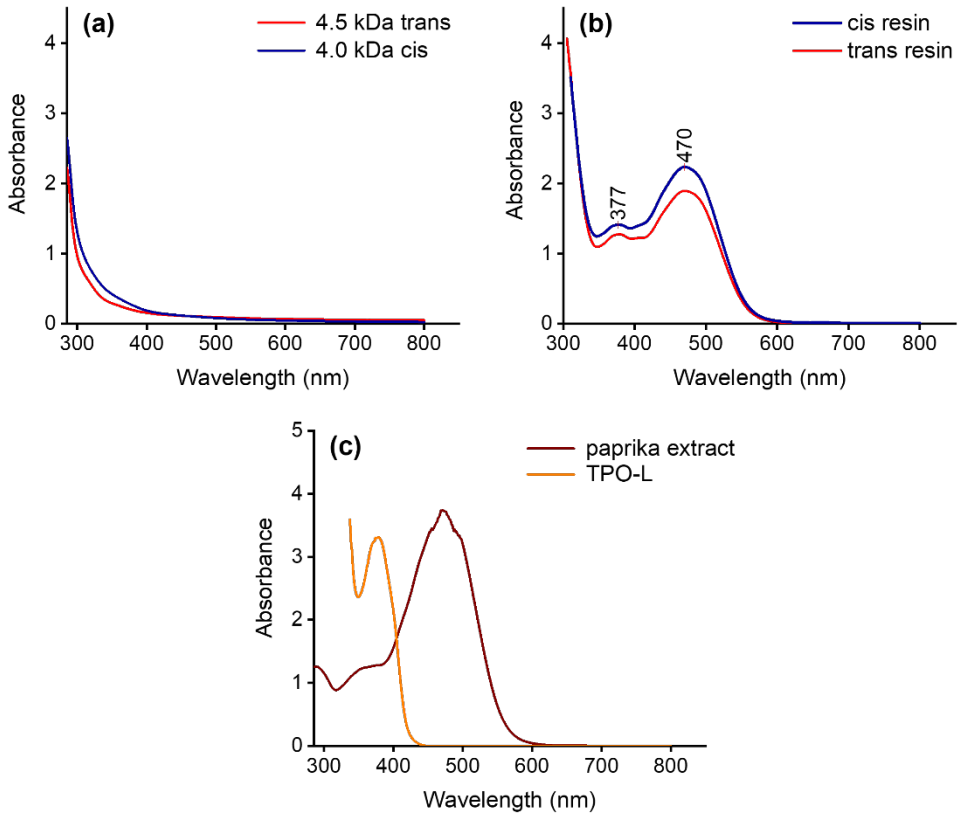


Figure 4.21. *UV-Vis absorbance of (a) 4.0 kDa cis oligomer and 4.5 kDa trans oligomer in NMP. (b) cis and trans resin (oligomer, NMP, TPO-L, paprika resin in a 50:50:0.5:0.5 wt% ratio.) The absorbance peak at 377 nm is due to the presence of TPO-L, the absorbance peak at 470 nm is characteristic of the paprika resin, and (c) TPO-L and paprika resin and their maxima of absorbance at 377 nm and 377/470 nm respectively.*

Next, photorheological analysis were performed to determine the appropriate amount of paprika resin necessary for reducing the curing depth without affecting the curing rate and it has been found that a ratio within the range of 0.25 and 1 wt% still yielded an effective curing time of 3.3 and 5.2 sec for the *cis* and *trans* resin respectively (**Figure 4.22**).

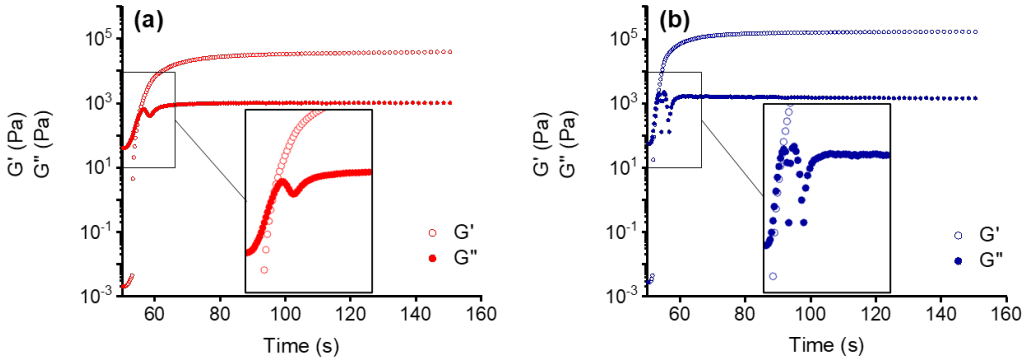


Figure 4.22. *Evolution of the storage (G') and loss (G") moduli with time during UV irradiation of (a) trans resin and (b) cis resin containing 50 wt% oligomer in NMP, 0.5 wt% of photoinitiator and 0.5 wt% photoinhibitor. The lamp is switched on at 50 s. The insets are close-up for the intersections of G' and G" curves.*

4.6.3 Optimising 3D printing parameters

These preliminary results were encouraging and therefore the resins were tested for suitability on the 3D printer. Owing to differences in the light intensity existing between the optical equipment used during the photorheology study and the light source of the 3D printer, the optimised resin was unable to cure when exposed to the light source within the 3D printer. After successfully curing the original resin (e.g without photoinhibitor) using the same light source, the ratio of photoinhibitor was adjusted by visually assessing the prints resolution (**Figure 4.23**). At concentrations ≤ 0.5 wt% of photoinhibitor, the printing parts present no or little resolution due to the lack of control over light scattering and penetration depth in both x,y and z direction (**Figure 4.23**, left). At 0.5 wt%, the best result in terms of accuracy of detail were obtained (**Figure 4.23**, center). At amounts ≥ 0.75%, the printing failed after the burn layer (**Figure 4.23**, right).

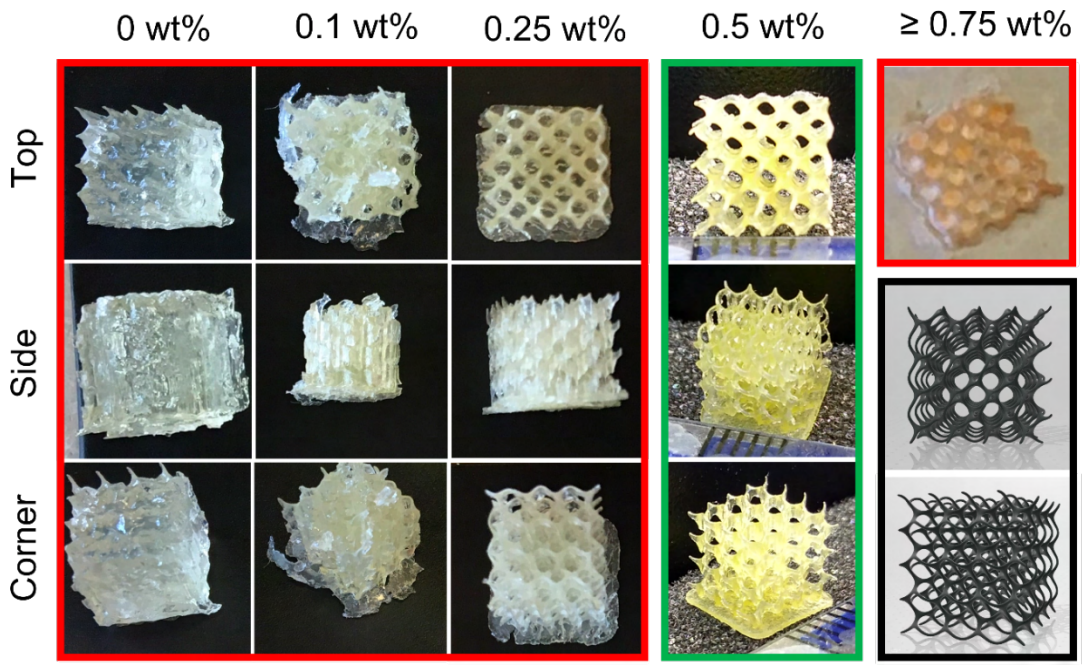


Figure 4.23. *Photographs from 3 different angles (top, side and corner view) of 3D printed 4.5 kDa cis cubes from resins containing different amounts of photoinhibitor. On the bottom right corner is presented illustration of the computerised structure (side and corner view).*

Individual adjustment of the printing parameters demonstrated that irradiating 50 µm thick layers for 25 s were giving the best results in term of printing precision for both *cis* and *trans* resins and high-resolution scaffolds of a 6 mm height were obtained using these settings (**Figure 4.24**).

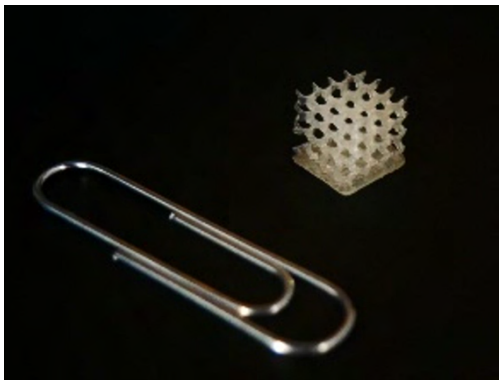


Figure 4.24. *Picture of a 3D printed 4.0 kDa trans scaffold next to a standard paperclip for scale.*

4.6.4 Mechanical testing

Uniaxial compressive tests were conducted on these scaffolds to determine if the *cis* and *trans* stereochemistry could influence the mechanical properties of 3D printed structures (**Figure 4.25**). Compression of polymeric materials are usually not resulting in clear fracture [42], therefore, the compression tests were conducted up to a 50 N force (1 MPa stress), as it was determined to be the maximum limit of loading before causing irreversible damage to the scaffolds.

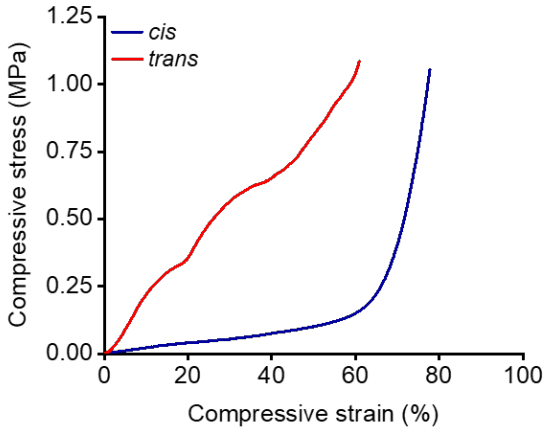


Figure 4.25. *Compressive stress-strain curves of 4.5 kDa cis and 4.0 kDa trans scaffolds.*

Similar to the previously observed performances of photoset films, the stereochemistry within the 3D printed scaffolds has a strong impact on their mechanical properties. Indeed, the *trans* scaffold demonstrates a plastic deformation along with a compressive Young's modulus (E_c) of about 2.4 MPa, whereas the deformation of the *cis* scaffold corresponds to an elastic material with an E_c 13 times smaller (0.18 MPa). The elastic properties of the *cis* scaffold have been further investigated by running cyclic compressive tests. As typically observed in elastomeric materials, softening occurs after the first loading-unloading cycle and

the stabilisation of the stress-strain curve occurred after 3 or 4 cycles. [43-46] The unloading paths shows a hysteresis of 28 kJ·m^{-3} and an average residual strain of 4.5% evidencing a good recovery capacity of the *cis* material after deformation (**Figure 4.26**).

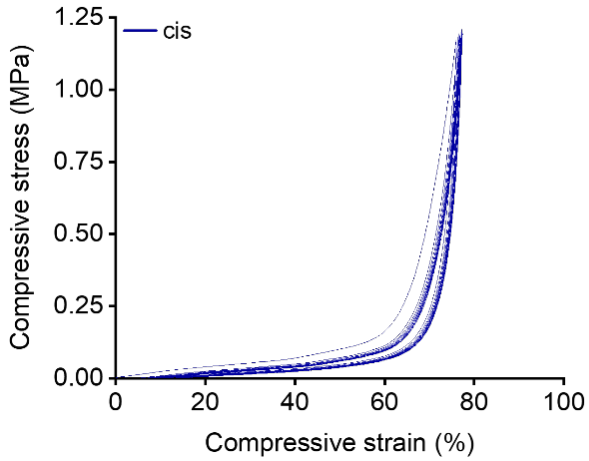


Figure 4.26. *Stress and strain obtained from the cyclic compression of a 4.5 kDa cis scaffold submitted to stress up to 1 MPa for 10 cycles.*

4.6.5 Thermal testing

DSC analysis of both scaffolds supports that their mechanical behaviour is in direct correlation to their crystallinity ratio. However, unlike the case of the 4.0 kDa *cis* film, the 4.0 kDa *cis* printed scaffold DSC thermogram presented a melting peak, indicative of the presence of some degree of crystallinity (**Figure 4.27**). One possibility is that this behaviour could stem from the necessity of washing the printed scaffolds with DCM to remove the excess resin since this procedure could also wash out short polymer chains within the network. However a similar treatment on a 4.0 kDa *cis* film still yielded an amorphous film. A further possibility could be that the addition of paprika resin, which is a red oleoresin, consists mainly of aromatic unsaturated hydrocarbon in the *trans* configuration that could potentialy enhance

the crystallisation of the overall material but it is present in only 0.5 wt% of the total formulation and most of it should be removed after the washing of the printed part.

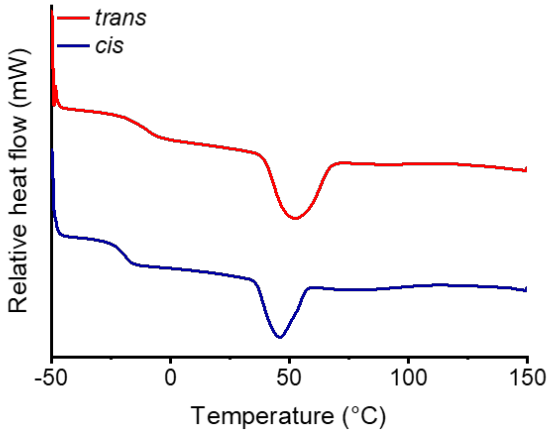


Figure 4.27. *1st heating scan of the DSC thermogram for a cis and a trans 3D printed scaffold. ΔH_m = 11.7 and 7.2 J·g^{-1}, T_g = – 10.06 °C and – 15.89 °C, T_m = 52.35 °C and T_m = 45.86 °C for the 4.0 kDa trans and 4.5 kDa cis scaffold respectively.*

Finally, a more likely argument for this sudden apparition of crystallinity within a 4.0 kDa *cis* network could be that, during the 3D printing process, the gravity aligns the polymer chains and consequently promotes crystallisation within the network.

4.6.6 Accelerated degradation study and depolymerisation

As crystallinity is known to affect the degradation properties of materials, the hydrolytic degradation of *cis* and *trans* materials has also been carried out. Small cylinders, fabricated from the *cis* and *trans* 3D printing resins, were degraded in a solution of NaOH 1M at 37 °C (**Figure 4.28**). The *trans* material fully degrades after 77 days while it only takes 54 days for the *cis* to do so. Furthermore, both materials seem to undergo a linear degradation, which could be ascribed to a surface erosion mechanism. [47]

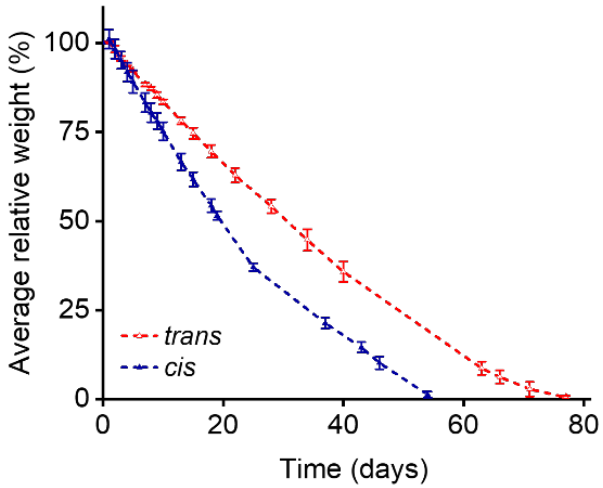


Figure 4.28. *hydrolytic degradation profiles for the 4.5 kDa cis and 4.0 kDa trans photosets in a solution of NaOH 1M at 37 °C. Each data point represents the average weight of 4 samples.*

After mechanical testing, some *cis* scaffold samples were depolymerised and analysed by ^{1}H NMR spectroscopy. The examination of the obtained spectrum led to the conclusion that only 2% isomerisation had occurred during 3D printing (**Figure 4.29**). This result suggested that the presence of crystallinity within the *cis* 3D printed material was not cause by isomerisation. Nevertheless, this study proves that it is possible to control the mechanical or degradation properties of 3D printed designs by leveraging the stereochemistry of the oligomer initially present within the resin without further adaptation of the resin formulation.

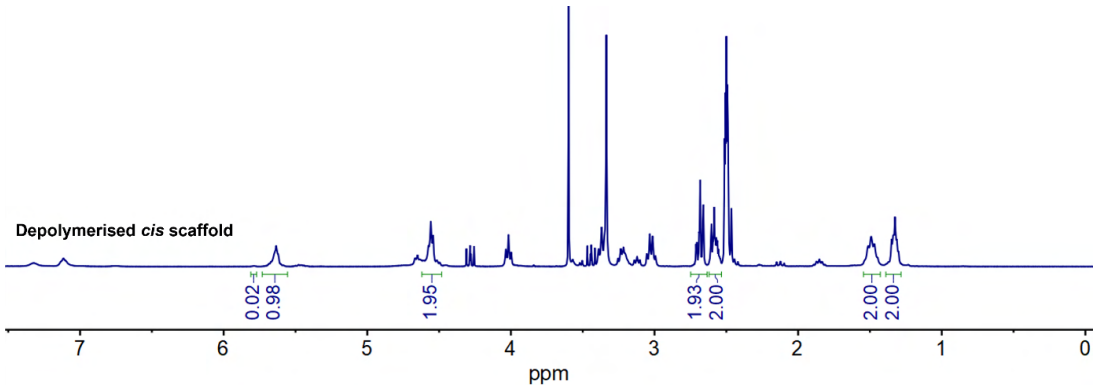


Figure 4.29. *^{1}H NMR (300 MHz, 298 K, DMSO-d_6) spectrum of a depolymerised 3D printed 4.5 kDa cis scaffold.*

Lastly, it was considered whether the isomerisation ability of the *cis* stereocentres could be harnessed to obtain a multi-material. In theory, it should be possible to isomerise the *cis* unsaturation into *trans* by either increasing the curing time per layer or increasing the light intensity. Adjusting these two parameters during the printing of an object could result in a material with regions of a printed part having different mechanical properties, which is desirable as printing multi-materials is still an ongoing challenge.[1] In addition, by controlling the curing time, it is possible to induce a predetermined ratio of *cis* to *trans* unsaturation and consequently this technique could potentially give discrete access to the array of mechanical properties expected from material containing a ratio of *trans* unsaturation anywhere from 0% to 100%. However, this experiment was unsuccessful. Exposing the resin to the 3D printer light source for 15 min, or increasing up to 6 times the light intensity did not yield more than 2 % of isomerisation, as evidenced by the ^{1}H NMR spectra of the depolymerisation products of these parts (**Figure 4.30**).

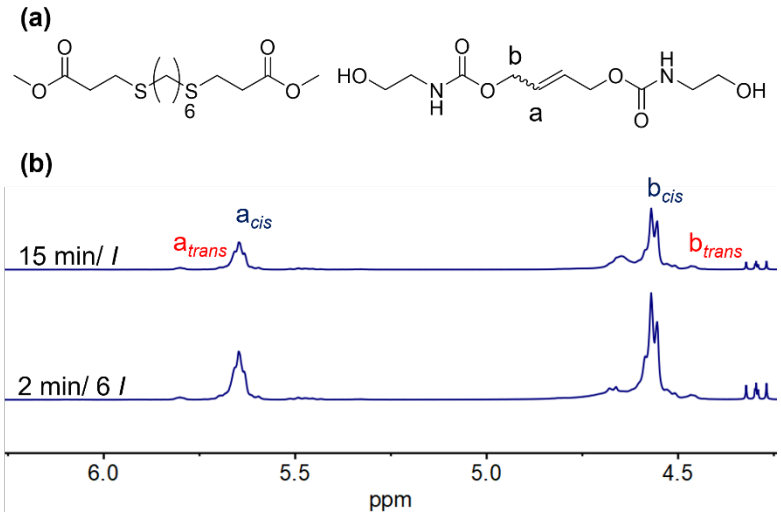


Figure 4.30. *(a) Representation of the major depolymerisation products of cis printed films. (b) ^{1}H NMR (300 MHz, d_6-DMSO, 298 K) spectra of cis depolymerised printed films after 15 mins of exposure to the 3D printer light source (top) or increasing 6 times the light intensity I (bottom).*

4.7 Conclusion

By incorporating acrylate terminated stereopure prepolymers into UV active resins, stereo-defined (*cis* and *trans*) poly(ester-urethane) photosets were obtained. Keeping the internal alkenes in the prepolymer unreacted during radical photo-crosslinking was also achieved when the UV exposure tile was keep at a minimum. As such, the retention of stereochemistry within the photosets was close to 100% within the optimised curing conditions. This has been confirmed by ^{1}H NMR spectroscopy of materials depolymerised by methanolysis. Uniaxial tensile tests revealed that both the alkene stereochemistry of the prepolymer and its average molecular weight had an influence on its final mechanical behaviour. For ~4 and ~6 kDa oligomers, the presence of *trans* alkenes yielded considerably stiffer and tougher materials than their *cis* counterparts, which were found to induce softness and elasticity in the materials. This 2 kDa increase in the chain length, resulted in an improvement of the strain at break for both the *cis* and *trans* materials. Further

increasing the oligomer chain length to about 10 kDa, provoked a substantial increase in stiffness and toughness of the *cis* material. According to DSC data, this striking dissimilarity could be rooted in the degree of crystallinity of the sample, which was further linked to the stereochemistry as well as the chain length of the oligomer composing the network. If it is already well established that chain length and elongation are correlated, the presented stereochemical control of bulk properties is unmatched for existing crosslinked systems. Finally, the addition of a photoinhibitor to the formulation, rendered the resins suitable for 3D printing and allowed the preparation of high-resolution 3D scaffolds with stereo-tuneable mechanical and degradable properties. In the future, this novel method of controlling the bulk properties of crosslinked networks via the means of controlling the stereochemistry could be envisioned as a straightforward technique to access a diversity of materials using a single formulation.

4.8 References

(1) Ligon, S. C.; Liska, R.; Stampfl, J.; Gurr, M.; Mülhaupt, R. Polymers for 3D Printing and Customized Additive Manufacturing. *Chem. Rev.* **2017**, *117,* 10212-10290

(2) Yao, L.; Hu, P.; Wu, Z.; Liu, W.; Lv, Q.; Nie, Z.; Zhengdi, H. Comparison of accuracy and precision of various types of photo-curing printing technology. *J. Phys.: Conf. Ser.* **2020**, *1549,* 032151

(3) Zhang, J.; Hu, Q.; Wang, S.; Tao, J.; Gou, M. Digital Light Processing Based Three-dimensional Printing for Medical Applications. *Int J Bioprint* **2019**, *6,* 242-242

(4) Bagheri, A.; Jin, J. Photopolymerization in 3D Printing. *ACS Appl. Polym. Mater.* **2019**, *1,* 593-611

(5) Zhang, J.; Xiao, P. 3D printing of photopolymers. *Polym. Chem.* **2018**, *9,* 1530-1540

(6) Chen, L.; Wu, Q.; Wei, G.; Liu, R.; Li, Z. Highly stable thiol–ene systems: from their structure–property relationship to DLP 3D printing. *J. Mater. Chem. C* **2018**, *6,* 11561-11568

(7) Sycks, D. G.; Wu, T.; Park, H. S.; Gall, K. Tough, stable spiroacetal thiol-ene resin for 3D printing. *J. Appl. Polym. Sci.* **2018**, *135,* 46259

(8) Gorsche, C.; Seidler, K.; Knaack, P.; Dorfinger, P.; Koch, T.; Stampfl, J.; Moszner, N.; Liska, R. Rapid formation of regulated methacrylate networks yielding tough materials for lithography-based 3D printing. *Polym. Chem.* **2016**, *7,* 2009-2014

(9) Zhang, Z.; Corrigan, N.; Bagheri, A.; Jin, J.; Boyer, C. A Versatile 3D and 4D Printing System through Photocontrolled RAFT Polymerization. *Angew. Chem. Int. Ed.* **2019**, *58,* 17954-17963

(10) Xiao, P.; Dumur, F.; Frigoli, M.; Tehfe, M.-A.; Graff, B.; Fouassier, J. P.; Gigmes, D.; Lalevée, J. Naphthalimide based methacrylated photoinitiators in radical and cationic photopolymerization under visible light. *Polym. Chem.* **2013**, *4,* 5440-5448

(11) Palaganas, J.; de Leon, A. C.; Mangadlao, J.; Palaganas, N.; Mael, A.; Lee, Y. J.; Lai, H. Y.; Advincula, R. Facile Preparation of Photocurable Siloxane Composite for 3D Printing. *Macromol. Mater. Eng.* **2017**, *302,* 1600477

(12) Patel, D. K.; Sakhaei, A. H.; Layani, M.; Zhang, B.; Ge, Q.; Magdassi, S. Highly Stretchable and UV Curable Elastomers for Digital Light Processing Based 3D Printing. *Adv. Mater.* **2017**, *29,* 1606000

(13) Liu, Y.; Lin, Y.; Jiao, T.; Lu, G.; Liu, J. Photocurable modification of inorganic fillers and their application in photopolymers for 3D printing. *Polym. Chem.* **2019**, *10,* 6350-6359

(14) Truby, R. L.; Lewis, J. A. Printing soft matter in three dimensions. *Nature* **2016**, *540,* 371-378

(15) Zhou, L.-Y.; Fu, J.; He, Y. A Review of 3D Printing Technologies for Soft Polymer Materials. *Adv. Funct. Mater.* **2020**, *30,* 2000187

(16) Thrasher, C. J.; Schwartz, J. J.; Boydston, A. J. Modular Elastomer Photoresins for Digital Light Processing Additive Manufacturing. *ACS Appl. Mater. Interfaces* **2017**, *9,* 39708-39716

(17) Borrello, J.; Nasser, P.; Iatridis, J. C.; Costa, K. D. 3D printing a mechanically-tunable acrylate resin on a commercial DLP-SLA printer. *Addit. Manuf.* **2018**, *23,* 374-380

(18) Morton, M. *Rubber technology*; Springer Science & Business Media, 2013.

(19) Kent, E. G.; Swinney, F. B. Properties and applications of trans-1, 4-polyisoprene. *Ind. Eng. Chem. Prod. Res. Dev.* **1966**, *5,* 134-138

(20) Bueche, F. Mechanical properties of natural and synthetic rubbers. *J. Polym. Sci.* **1957**, *25,* 305-324

(21) Wagner, H. L.; Flory, P. J. Molecular Dimensions of Natural Rubber and Gutta Percha[1]. *J. Am. Chem. Soc.* **1952**, *74,* 195-200

(22) Yu, Y.; Wei, Z.; Leng, X.; Li, Y. Facile preparation of stereochemistry-controllable biobased poly(butylene maleate-co-butylene fumarate) unsaturated copolyesters: a chemoselective polymer platform for versatile functionalization via aza-Michael addition. *Polym. Chem.* **2018**, *9,* 5426-5441

(23) Timmer, M. D.; Ambrose, C. G.; Mikos, A. G. In vitro degradation of polymeric networks of poly(propylene fumarate) and the crosslinking macromer poly(propylene fumarate)-diacrylate. *Biomaterials* **2003**, *24,* 571-577

(24) Walker, J. M.; Bodamer, E.; Krebs, O.; Luo, Y.; Kleinfehn, A.; Becker, M. L.; Dean, D. Effect of Chemical and Physical Properties on the In Vitro Degradation of 3D Printed High Resolution Poly(propylene fumarate) Scaffolds. *Biomacromolecules* **2017**, *18,* 1419-1425

(25) Lewandrowski, K.-U.; Gresser, J. D.; Wise, D. L.; White, R. L.; Trantolo, D. J. Osteoconductivity of an injectable and bioresorbable poly(propylene glycol-co-fumaric acid) bone cement. *Biomaterials* **2000**, *21,* 293-298

(26) Worch, J. C.; Prydderch, H.; Jimaja, S.; Bexis, P.; Becker, M. L.; Dove, A. P. Stereochemical enhancement of polymer properties. *Nat. Rev. Chem.* **2019**, *3,* 514-535

(27) Bell, C. A.; Yu, J.; Barker, I. A.; Truong, V. X.; Cao, Z.; Dobrinyin, A. V.; Becker, M. L.; Dove, A. P. Independent control of elastomer properties through stereocontrolled synthesis. *Angew. Chem., Int. Ed.* **2016**, *55,* 13076-13080

(28) Worch, J. C.; Weems, A. C.; Yu, J.; Arno, M. C.; Wilks, T. R.; Huckstepp, R. T. R.; O'Reilly, R. K.; Becker, M. L.; Dove, A. P. Elastomeric polyamide biomaterials with stereochemically tuneable mechanical properties and shape memory. *Nat. Commun.* **2020**, *11,* 3250

(29) Stubbs, C. J.; Worch, J. C.; Prydderch, H.; Becker, M. L.; Dove, A. P. Unsaturated Poly(ester-urethanes) with Stereochemically Dependent Thermomechanical Properties. *Macromolecules* **2020**, *53,* 174-181

(30) Decker, C. Photoinitiated crosslinking polymerisation. *Prog. Polym. Sci.* **1996**, *21,* 593-650

(31) Kim, G.; Ree, M.; Kim, H.; Kim, I. J.; Kim, J. R.; Lee, J. I. Biological affinity and biodegradability of poly(propylene carbonate) prepared from copolymerization of carbon dioxide with propylene oxide. *Macromol. Res.* **2008**, *16,* 473-480

(32) Kiesewetter, M. K.; Scholten, M. D.; Kirn, N.; Weber, R. L.; Hedrick, J. L.; Waymouth, R. M. Cyclic Guanidine Organic Catalysts: What Is Magic About Triazabicyclodecene? *J. Org. Chem.* **2009**, *74,* 9490-9496

(33) Lovo, J. F. P.; Camargo, I. L. d.; Erbereli, R.; Morais, M. M.; Fortulan, C. A. Vat Photopolymerization Additive Manufacturing Resins: Analysis and Case Study. *Mat. Res.* **2020**, *23,*

(34) Baboo, M.; Dixit, M.; Sharma, K.; Saxena, N. S. Mechanical and thermal characterization of cis-polyisoprene and trans-polyisoprene blends. *Polym. Bull.* **2011**, *66,* 661-672

(35) Bhowmick, A. K.; Kuo, C. C.; Manzur, A.; Mac Arthur, A.; Mc Intyre, D. Properties of cis-and trans-polyisoprene blends. *J. Macromol. Sci., Part B: Phys.* **1986**, *25,* 283-306

(36) Short, J. N.; Thornton, V.; Kraus, G. Effect of Cis-Trans Ratio on the Physical Properties of 1,4 Polybutadienes. *Rubber Chem. Technol.* **1957**, *30,* 1118-1141

(37) Passingham, C.; Hendra, P. J.; Cudby, M. E. A.; Zichy, V.; Weller, M. The re-evaluation of multiple peaks in the DSC melting endotherm of isotactic polypropylene. *Eur. Polym. J.* **1990**, *26,* 631-638

(38) Cooper, W.; Vaughan, G. Crystallization of gutta percha and synthetic trans-1,4-Polyisoprenes. *Polymer* **1963**, *4,* 329-340

(39) Hadipoespito, G.; Yang, Y.; Choi, H.; Ning, G.; Li, X. Digital micromirror device based microstereolithography for micro structures of transparent photopolymer and nanocomposites. *Solid Freeform Fabr. Symp. Proc.* **2003**, 13-24

(40) Lebedevaite, M.; Talacka, V.; Ostrauskaite, J. High biorenewable content acrylate photocurable resins for DLP 3D printing. *J. Appl. Polym. Sci.* **2021**, *138,* 50233

(41) Ronca, A.; Ambrosio, L.; Grijpma, D. W. Preparation of designed poly(d,l-lactide)/nanosized hydroxyapatite composite structures by stereolithography. *Acta Biomater.* **2013**, *9,* 5989-5996

(42) *Standard Test Method for Compressive Properties of Rigid Plastics*; ASTM D695-15; West Conshohocken, PA, 2015. DOI: 10.1520/D0695-15.

(43) Diani, J.; Fayolle, B.; Gilormini, P. A review on the Mullins effect. *Eur. Polym. J.* **2009**, *45,* 601-612

(44) Bergström, J. S.; Boyce, M. C. Constitutive modeling of the large strain time-dependent behavior of elastomers. *J. Mech. Phys. Solids* **1998**, *46,* 931-954

(45) Mullins, L. Softening of rubber by deformation. *Rubber Chem. Technol.* **1969**, *42,* 339-362

(46) Drozdov, A. D.; Dorfmann, A. Stress–strain relations in finite viscoelastoplasticity of rigid-rod networks: applications to the Mullins effect. *Continuum Mech. Thermodyn.* **2001**, *13,* 183-205

(47) Laycock, B.; Nikolić, M.; Colwell, J. M.; Gauthier, E.; Halley, P.; Bottle, S.; George, G. Lifetime prediction of biodegradable polymers. *Prog. Polym. Sci.* **2017**, *71,* 144-189

4.9 Appendices

4.9.1 Materials and Methods

Deuterated dimethyl sulfoxide (d_6-DMSO, ≥99.9%), 1-methyl-2-pyrrolidinone (NMP, ≥99%),Triazabicyclodecene (TBD, 98%) and N-vinyl pyrrolidone (NVP, ≥99%) were purchased from Sigma-Aldrich Company. Deuterated chloroform ($CDCl_3$, >99.8%) was purchased from Apollo Scientific. Methanol (MeOH, ≥99.8%) was purchased from VMR Chemicals. Paprika resin (Durabrite©) was purchased from Kalsec and Ethyl(2,4,6-Trimethylbenzoyl)-phenyl phosphinate (Omnirad TPO-L) was purchase from IGM Resins Ltd. Unless stated otherwise, all chemicals and compounds were used as received.

Nuclear magnetic resonance spectroscopy (NMR)

^{1}H and ^{13}C NMR spectra of monomers and oligomers were recorded at 298 K on an Ascend Bruker 400 spectrometer equipped with a 5 mm BBFO smart probe operating at 400 MHz and 100 MHz, respectively. Chemical shifts of ^{1}H NMR spectra were referenced to the solvent residual proton resonance signals: δ = 7.26 ppm for $CDCl_3$. Chemical shifts for ^{13}C NMR spectra were referenced to the solvent resonance signal: δ = 77.16 ppm for $CDCl_3$. The data obtained were processed and analysed using MestReNova 12.0.3 software. The resonance multiplicities are described as s (singlet), d (doublet), t(triplet), q(quartet) or m(multiplet).

Differential scanning calorimetry (DSC)

Glass transition temperature (T_g) and total enthalpy of melting (ΔH_m) were measured on a STARe system DSC3 with auto-sampler (Mettler Toledo,

Switzerland) under N_2 with a heating rate of 10 °C·min^{-1}. Samples weighing between 6 to 8 mg were cut from 2 days annealed polymer films and 3 weeks annealed 3D printed scaffolds. Sample were positioned in 40 µL aluminum pans (Mettler Toledo). Thermograms were recorded from −50 to 150 °C with a 10 °C·min^{-1} heating and cooling rate over three cycles. The glass transition temperature (T_g) was taken as the midpoint of the inflection tangent upon the second heating scan. Total enthalpy of melting (ΔH_m) was calculated from integration and normalisation of all endothermic peaks present on the first heating scan.

Tensile testing

All uniaxial tensile tests were performed on a Testometric M350-5CT universal mechanical testing instrument fitted with a load cell of 10 kgF. Measurements were performed at room temperature on film cut into dumbbell-shaped samples using a custom ASTM Die D-638 Type V with a dye cutter. The gauge length was set at 6.30 mm and the crosshead speed at 10 mm·min^{-1}. The sample width (ca. 1.8 mm) and thickness (ca. 1 mm) were measured 3 times for each individual sample and the average value was recorded before mechanical analysis were conducted. Each specimen was clamped into the tensile holders and subjected to an elongation rate of 10 mm·min^{-1} until failure. For each sample, a minimum of 6 specimens were tested with the mean average values of the ultimate tensile stress and strain, the stress and strain at yield point and the toughness reported herein. WinTest™ Analysis software (v.5.0.34) was used to analyse the data.

All uniaxial compressive tests were performed on a Testometric M350-5CT universal mechanical testing instrument fitted with a load cell of 100 kgF. 3D printed

scaffolds of ca. 6 mm height were annealed for 3 weeks before testing. A preload force of 0.1 N was set and each test was carried out at a compression velocity of 1 mm·min^{-1}. Each specimen was subjected to a maximum force of 50 N. All compression tests were repeated at least 6 times, and an average of the data was taken to find the Compressive Young modulus (E_c), the strain at a stress of 1 MPa (ε_{1MPa}), and the stress when the cube is reaching 50% of its original height ($\sigma_{50\%}$). For cyclic compressive tests of the 3D printed cis hart cubes, the samples were subjected to loading/unloading cycle with a constant strain rate of 1 mm·min^{-1} for 10 cycles. Data were analysed using winTest™ Analysis software (v.5.0.34). The raw data give the force (N) over the depletion (mm). To draw a strain stress curves, the stress (MPa) has been calculated by dividing the force (N) by the sectional area of the sample (ca. 6.8 mm × 6.3 mm) in meter square, the strain (%) has been calculated by subtracting the depletion (mm) to the sample height (ca. 6.0 mm) and then multiplied by 100.

Thermo-gravimetric analysis (TGA)

TGA data was obtained using a Q50-Thermogravimetric Analyzer (TA instruments). Thermograms were recorded under an N_2 atmosphere at a heating rate of 10 °C·min^{-1}, from 25 °C to 600 °C, with an isotherm of 90 min at 202 °C to evaluate the potential presence of residual solvent within the network. Sample weight is of ca. 7 mg.

UV-Vis spectroscopy

UV-Vis spectroscopy was performed on an Evolution 350 UV-Vis spectrophotometer equipped with Xenon Flash Lamp light source and Dual Matched

Silicon Photodiodes detector. Quartz cells (170 - 2000 nm) from Hellma with two polished sides were used for examining the absorption spectra between 275 to 800 nm. Thermo INSIGHT-2 v.10.0.30319.1 software was used for data acquisition.

Otoflash postcuring light pulsing unit (flash box)

Resins were cured into films using the Otoflash postcuring light pulsing unit from Envisiontech equipped with two lamp bulbs of 100 W operating at a frequency of 10 flashes per second. The light emitted by the bulbs is comprised in a spectrum between 300 and 700 nm. Each film was cured for 200 flashes (20 s).

Rheology

Rheology was performed on an Anton Paar MCR 302 equipped with a PP25 geometry plates at room temperature. Resins were loaded directly on the plate and the gap width set at 1 mm. Shear rate sweeps were performed from 0.1 to 100 s^{-1} at 5 s per shear rate in order to determine the resins viscosity.

Photorheology

The crosslinking kinetic of the resins was examined as a function of gelation time by photorheology using an Anton Paar MCR-302 rheometer fitted with a detachable photoillumination system (Exfo OmniCure S1500 UV light source, broadband Hg-lamp, glass plate). Resin samples were sheared between two parallel plates (0.2 mm gap width) at 10 Hz with an amplitude of 1% for 50 s without irradiation. After this time, the light source was switched on and measurements were taken every 0.2 s over the course of 2 min. The intersection point of the storage moduli and loss moduli plots was used to determine the time of gelation of the resin.

3D printing

Porous scaffolds based on George Hart's design[1] were 3D printed using a Miicraft ultra 50 3D printer with a 365 nm LED light source. Resins formulated with 50 wt% of oligomer, 50 wt% of NMP, 0.5 wt% of photo-initiator (TPO-L) and 0.5 wt% of photo-inhibitor (paprika resin). Once homogeneous, resins were added in ca. 40 mL quantities to the resin tray, allowing for coverage of the optical window. After optimising individually the printing parameters (irradiance, irradiation period, qualitative x,y resolution) in the printing vat, the irradiance was set at 70%, the irradiation period at 25 s and the thickness layer at 50 µm. The final materials were washed with dichloromethane to remove residual resin and photo-inhibitor, and postcured in a vacuum oven for 24 h at 120 °C.

General procedure for resin depolymerisation

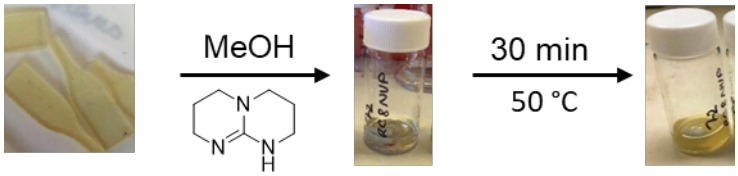


Figure A 4.1. *Pictures of the film cutting before and after depolymerisation.*

In a 20 mL sintered vial, film cuttings (ca. 300 mg) are placed, along with methanol (3 mL) and triazabicyclodecene (TDB) (ca. 8 mg, 2.6 wt%). The vial is capped, and the solution is left stirring at 50 °C until no solid is left, which usually happened after 30 min. Then the methanol is removed using a rotary evaporator and the crude is further dried under vacuum before being dissolved in d_6-DMSO and analysed by ^{1}H NMR spectroscopy.

Film curing

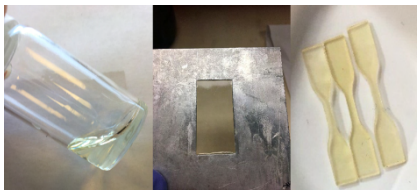


Figure A 4.2. *Pictures of an uncured resin (left), a film obtained after curing (centre) and dumbbell-shaped samples (right).*

In a 20 mL sintered vial, an oligomer (0.75 g, 50 wt%) is dissolved in its weight of NMP (0.75 g, 50 wt%) and left on a shaker overnight. The photo-initiator is then added (TPO-L, 6-8 mg, 0.5 wt%) and stirred into the resin with a spatula until homogeneous. The resin is then subjected to further mixing on an orbital shaker and finally pipetted onto a metallic mold with one side covered by tape. The film is inspected, and the air bubbles are removed with a needle. The film is then subjected to UV light in a flash box for 200 flashes (20 s) then it is placed in a vacuum oven at 120 °C for 24 h, the sample is then annealed for two days at 37 °C and cut into dumbbell-shaped samples using a custom ASTM Die D-638 Type V with a dye cutter.

4.9.2 NMR Spectra

^{1}H NMR spectra depolymerised trans films

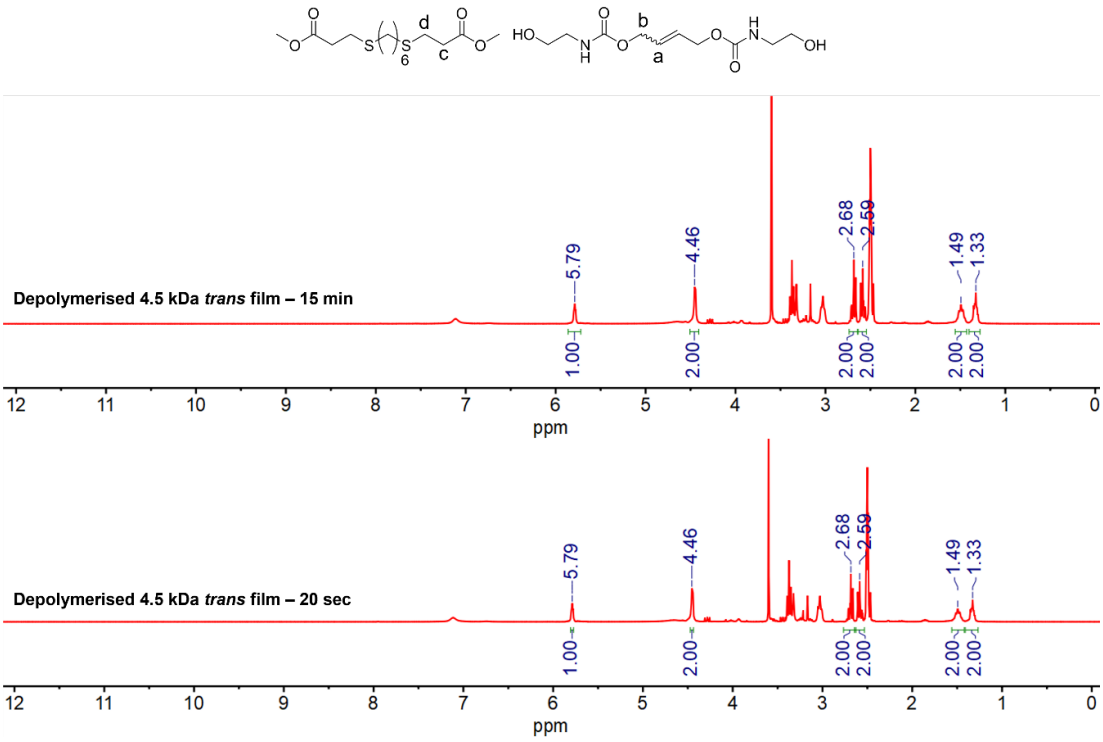


Figure A 4.3. *^{1}H NMR (300 MHz, 298 K, d_6-DMSO) spectra of a depolymerised trans film cured for 15 min (top) and 20 sec (bottom).*

^{1}H NMR spectra depolymerised cis films

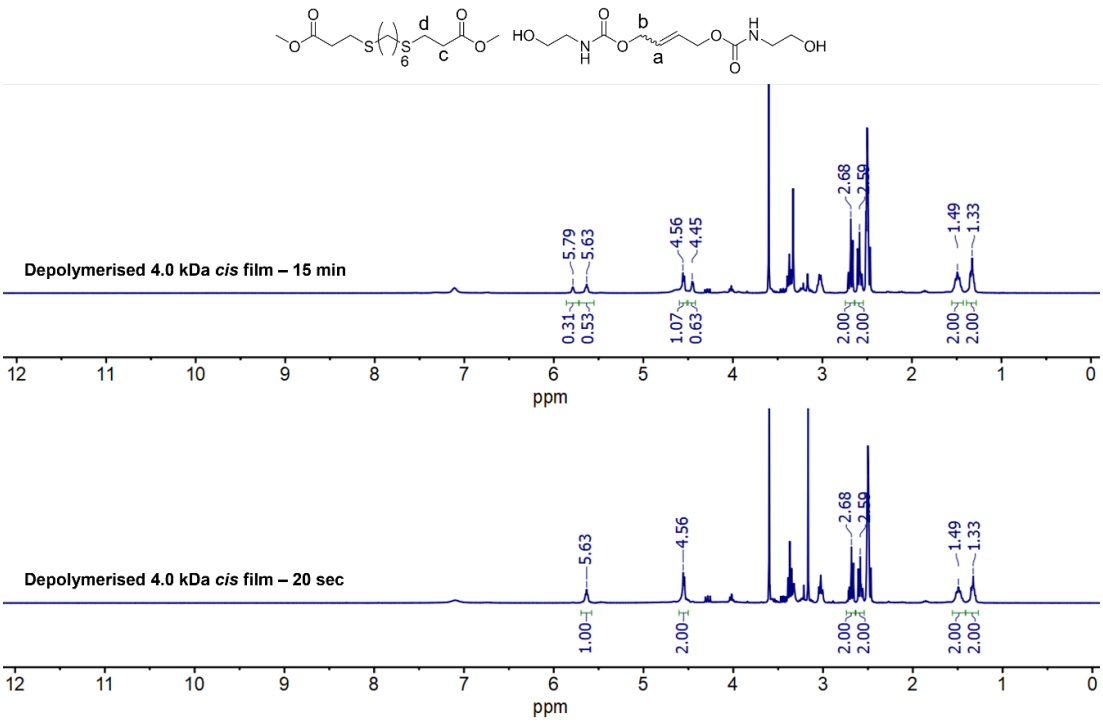


Figure A 4.4. *^{1}H NMR (300 MHz, 298 K, d_6-DMSO) spectra of a depolymerised cis film cured for 15 min (top) and 20 sec (bottom).*

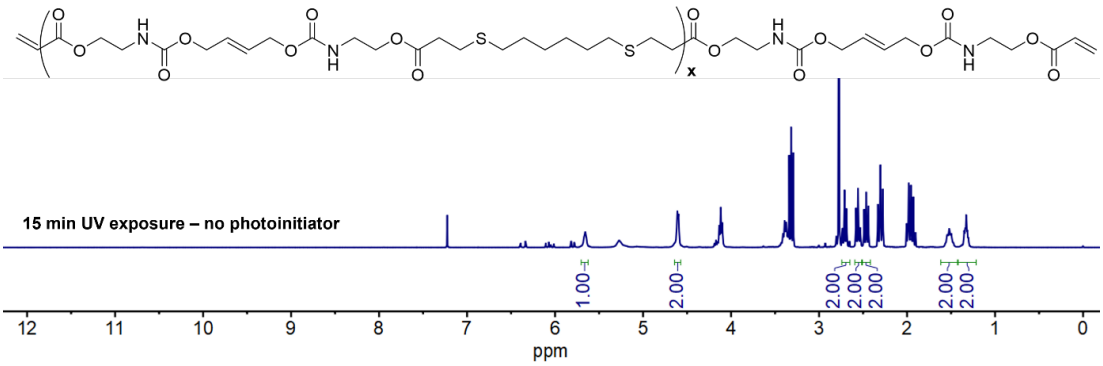


Figure A 4.5. *^{1}H NMR (300 MHz, 298 K, d_6-DMSO) spectra of a cis resin formulated without the photoinitiator and exposed to UV for 15 mins. No isomerisation reaction occurred.*

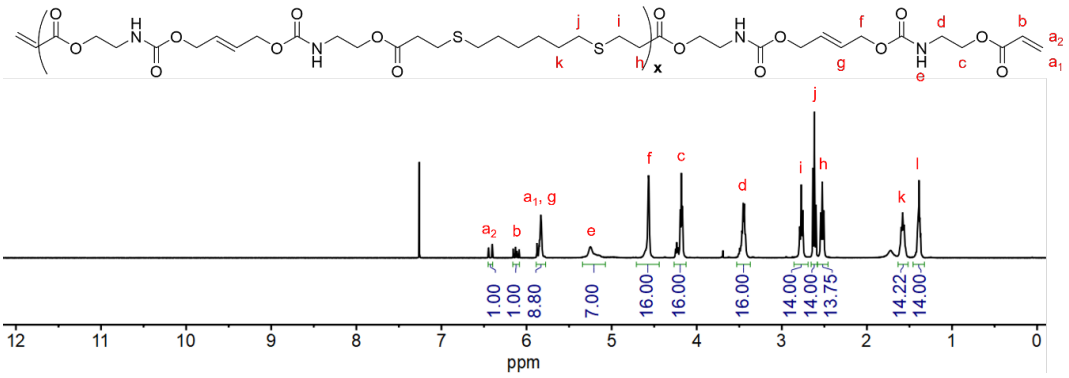


Figure A 4.6. *^{1}H NMR (400 MHz, 298 K, $CDCl_3$) spectra of a 4.0 kDa trans oligomer used in the trans 3D printed resin.*

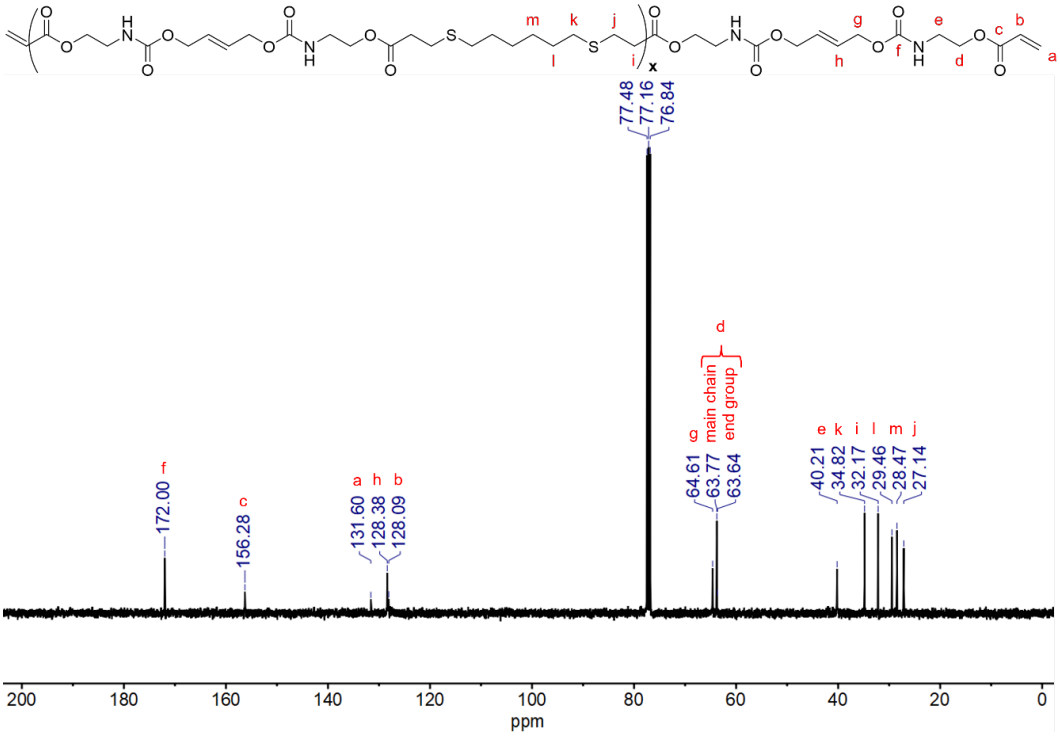


Figure A 4.7. *^{13}C NMR (101 MHz, 298 K, $CDCl_3$) spectra of a 4.0 kDa trans oligomer used in the trans 3D printed resin.*

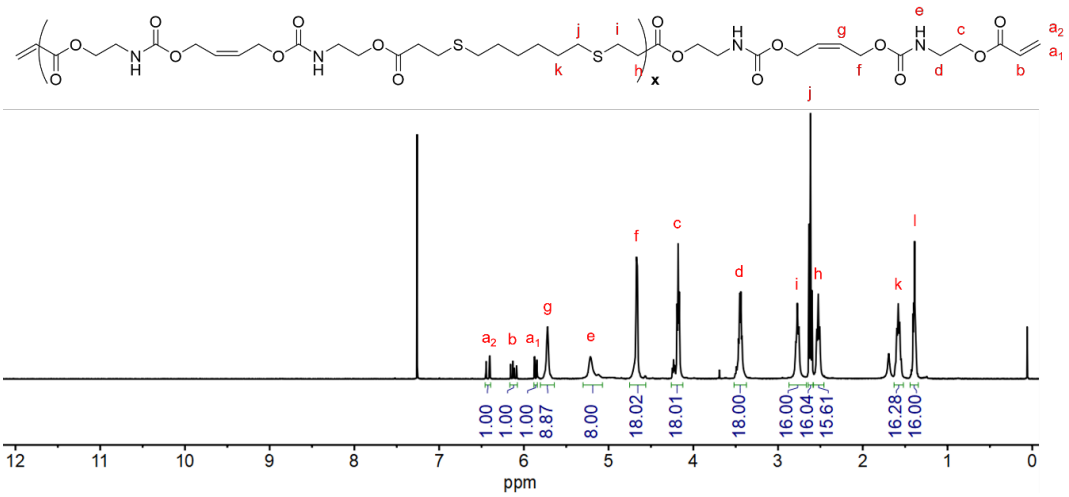


Figure A 4.8. *^{1}H NMR (400 MHz, 298 K, $CDCl_3$) spectra of a 4.5 kDa cis oligomer used in the cis 3D printed resin.*

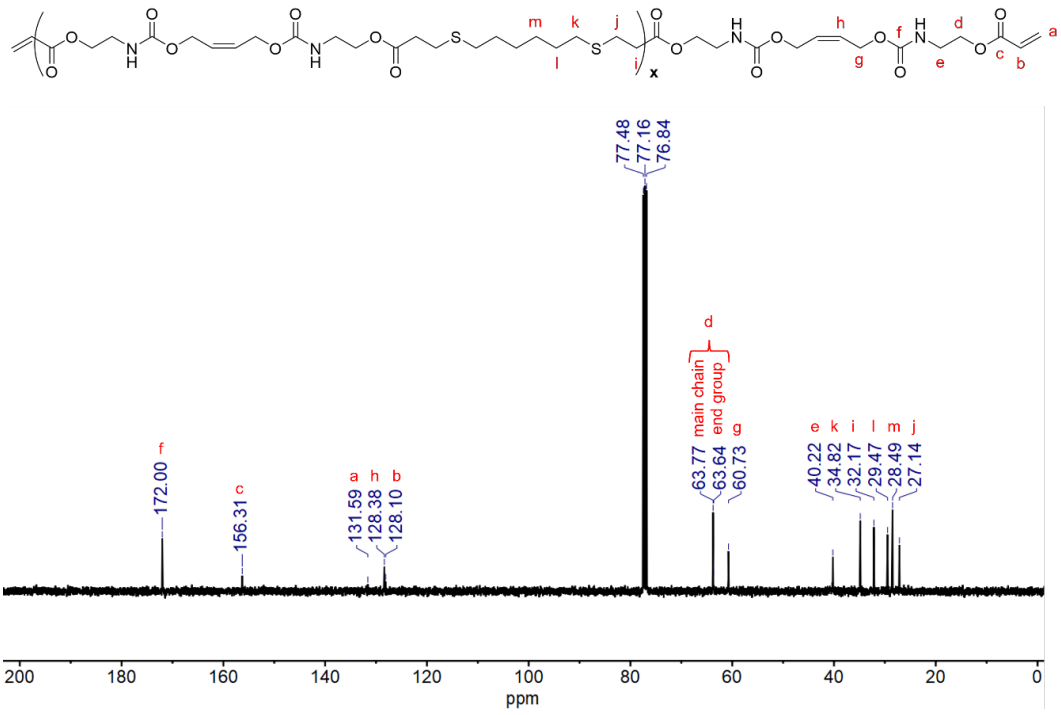


Figure A 4.9. *^{13}C NMR (101 MHz, 298 K, $CDCl_3$) spectra of a 4.5 kDa cis oligomer used in the cis 3D printed resin.*

4.9.3 Uniaxial tensile tests of *cis* and *trans* films

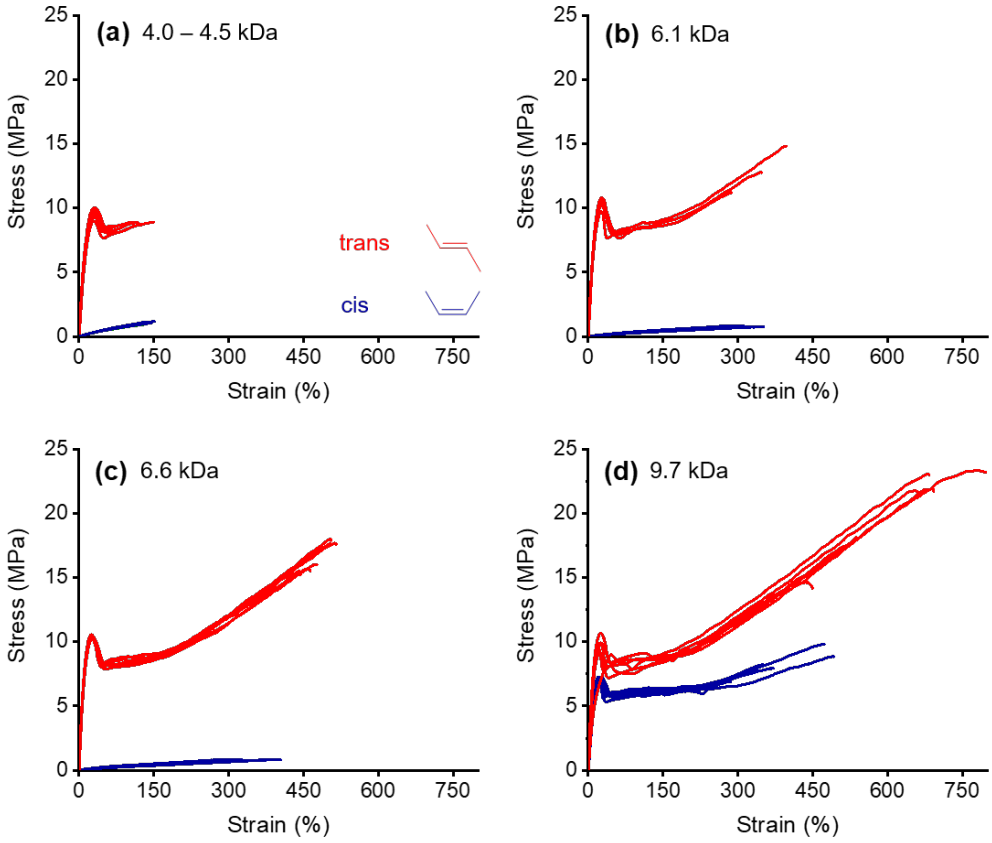


Figure A 4.10. *Compiled tensile elongation of (a) 4.5 kDa trans films (red) and 4.0 kDa cis films (blue), (d) 6.1 kDa trans films (red) and 6.1 kDa cis films (blue), (c) 6.6 kDa trans films (red) and 6.6 kDa cis films (blue), (d) 9.7 kDa trans films (red) and 9.7 kDa cis films (blue). For each sample, 6 specimens were tested.*

Table A 4.1. *Summary of key tensile parameters for the films.*

Film[a]	E[b] (MPa)	σ_b[c] (MPa)	ε_b[d] (%)	U_T[e] (MJ·m^{-3})	ε_y[f] (%)	σ_y[g] (MPa)
4.5 kDa *trans* film	64 (±5.9)	8.6 (±0.36)	98 (±32)	7.9 (±2.7)	30 (±1.6)	9.6 (±0.41)
4.0 kDa *cis* film	1.2 (±0.14)	1.1 (±0.07)	141 (±7.4)	0.87 (±.0085)	N/A	N/A
6.1 kDa *trans* film	82 (±4.2)	11 (±2.8)	208 (±153)	20 (±16)	27 (±0.93)	10 (±0.38)
6.1 kDa *cis* film	0.39 (±0.11)	0.79 (±0.06)	312 (±26)	1.4 (±0.14)	N/A	N/A
6.6 kDa *trans* film	85 (±4.0)	17 (±1.1)	483 (±29)	54 (±5.6)	25 (±0.81)	10 (±0.12)
6.6 kDa *cis* film	0.49 (±0.17)	0.80 (±0.063)	343 (±38)	1.6 (±0.22)	N/A	N/A
10 kDa *trans* film	85 (±16)	21 (±3.6)	647 (±146)	82 (±22)	24 (±1.44)	9.8 (±0.52)
9.7 kDa *cis* film	58 (±13)	8.3 (±0.99)	384 (±81)	0.083 (±0.010)	23 (±2.4)	7.1 (±0.23)

[a]M_n determined by ^{1}H NMR spectroscopy (300 MHz, 298 K, $CDCl_3$). [b]Young modulus, [c]stress at break, [d]Elongation at break, [e]Toughness, [f]Elongation at yield, [g]Stress at yield. The data presented are averaged values with n = 6. Uncertainty presented as the standard deviation of samples.

4.9.4 Compressive tests of 3D printed scaffolds

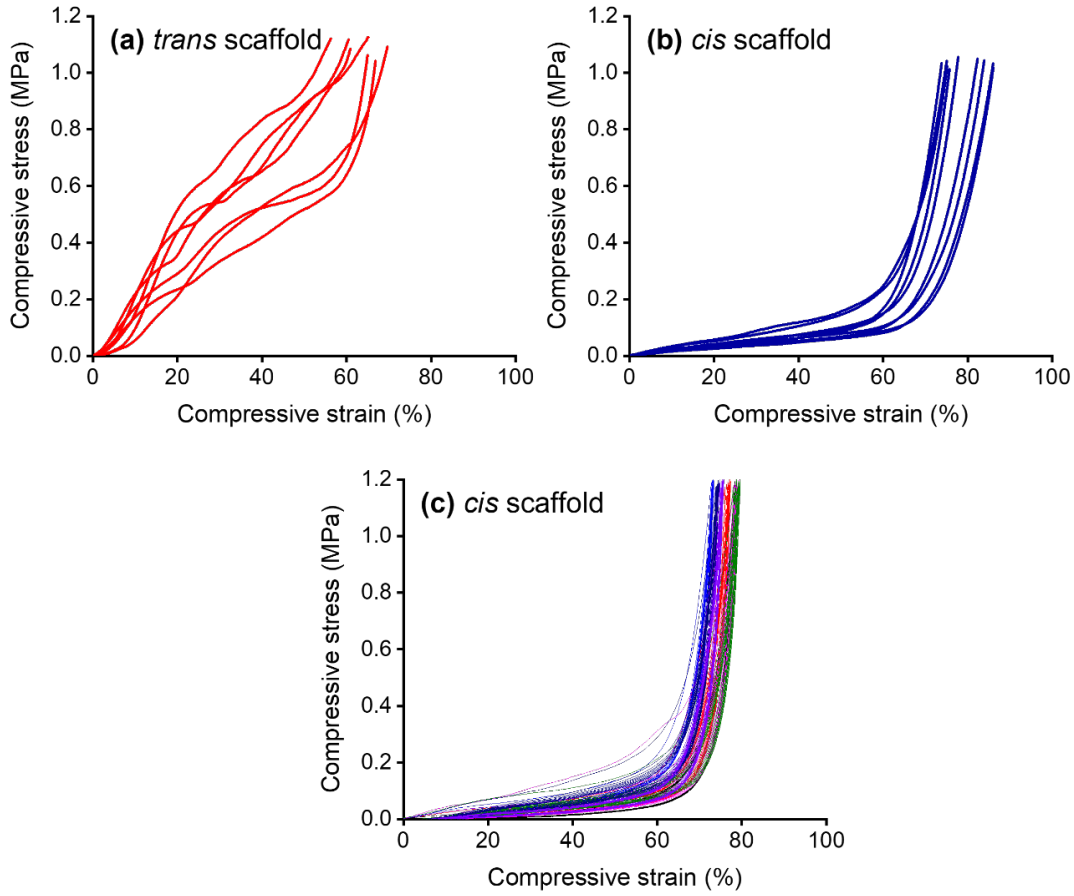


Figure A 4.11. *Compression tests of (a) 3D printed trans scaffolds and (b) 3D printed cis scaffolds and cyclic compression of 3D printed cis scaffolds (c). The maximum compression strength have been set at 50 N. For each sample, a minimum of 6 specimens were tested.*

Table A 4.2. *Summary of key tensile parameters for 3D printed scaffolds.*

3D scaffold	E_c[a] (MPa)	$\sigma_{50\%}$[b] (MPa)	ε_{1MPa}[c] (%)	Relative height at σ=1 MPa (%)	energy loss[d] (kJ·m^{-3})	residual strain[d] (%)
trans scaffold	2.37 (±0.97)	0.74 (±0.17)	63 (±4.5)	37 (±4.5)	N/A	N/A
cis scaffold	0.18 (±0.055)	0.096 (±0.036)	80 (±5.0)	21 (±5.0)	28 (±2.5)	4.5 (±0.64)

[a]Compressive Young's modulus. [b]Stress at 50% of strain. [c]Strain for a stress of 1 MPa. The data presented are averaged values with n ≥ 6. Uncertainty presented as the standard deviation of samples. [d]Estimated by taking the average value from cycle 2 to cycle 10 on 1 representative sample.

4.9.5 Differential scanning calorimetry (DSC) characterisation of films and 3D printed scaffolds

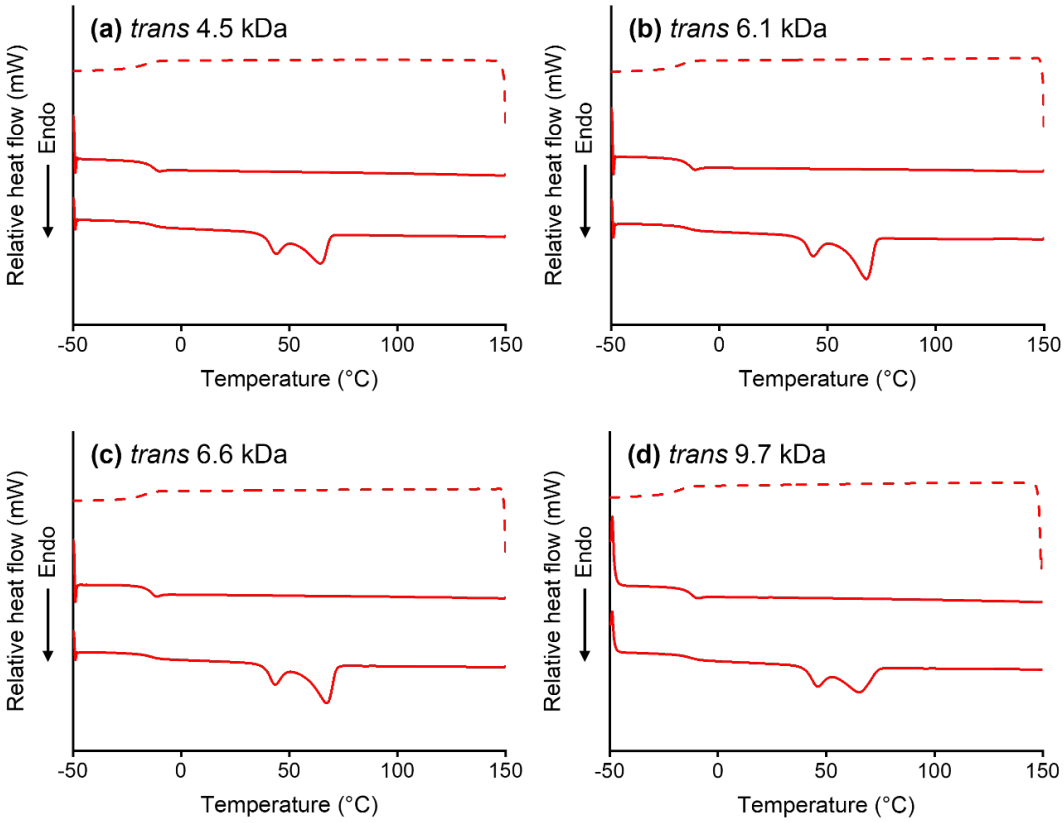


Figure A 4.12. *DSC thermograms of (a) a 4.5 kDa trans film, (b) a 6.1 kDa trans film, (c) a 6.6 kDa trans film and (d) a 10 kDa trans film after two days of annealing. The dashed line corresponds to the 1st cooling scan, the middle line, to the 2nd heating scan and the bottom line represents the 1st heating scan.*

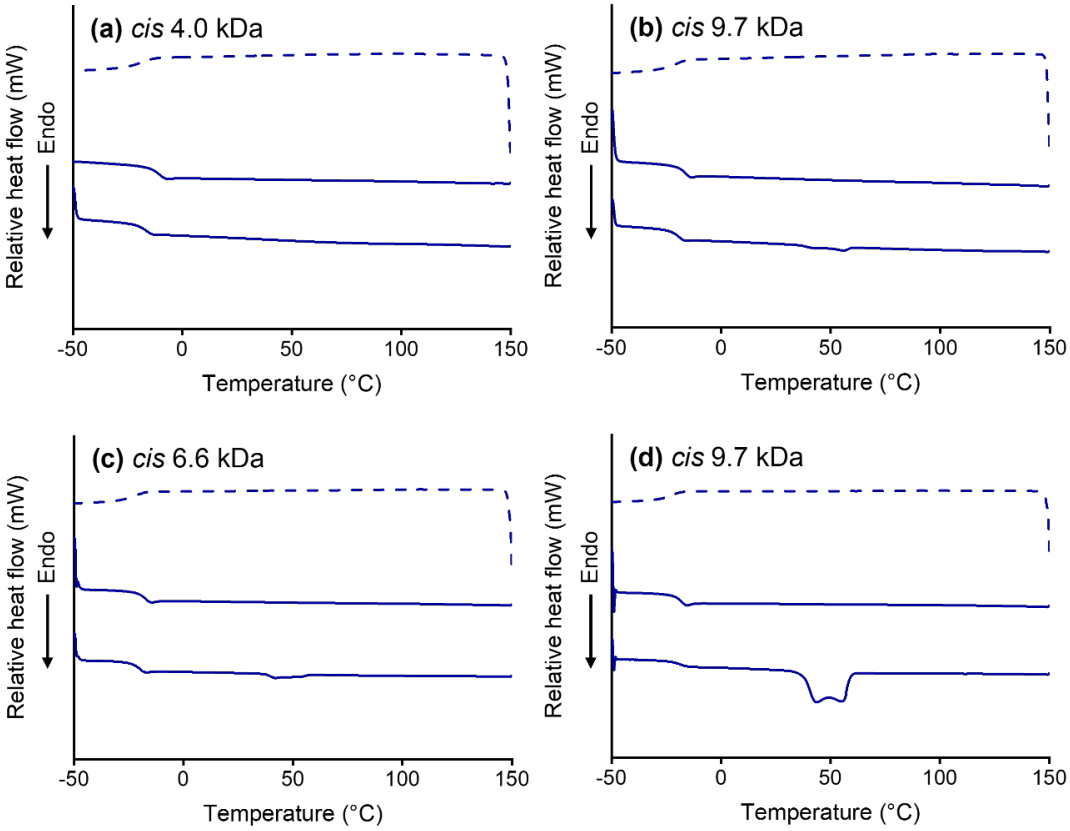


Figure A 4.13. *DSC thermograms of (a) a 4.0 kDa cis film, (b) a 6.1 kDa cis film, (c) a 6.6 kDa cis film and (d) a 9.7 kDa cis film after 2 days of annealing. The dashed line corresponds to the 1st cooling scan, the middle line, to the 2nd heating scan and the bottom line represents the 1st heating scan.*

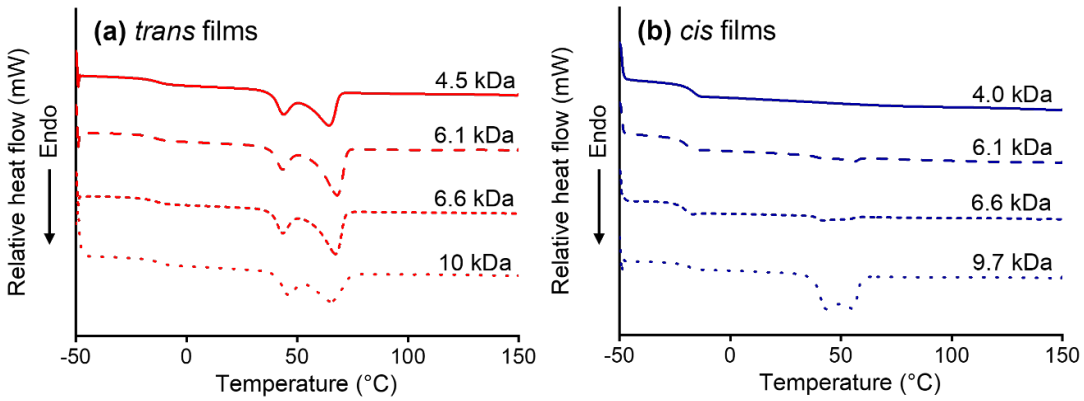


Figure A 4.14. *DSC thermograms (1st heating scan) of (a) trans films and (b) cis films for increasing molecular weight taken at 2 days of annealing. At all molecular weights, trans films show crystallinity after 2 days of annealing while the cis films only show crystallinity for larger molecular weights.*

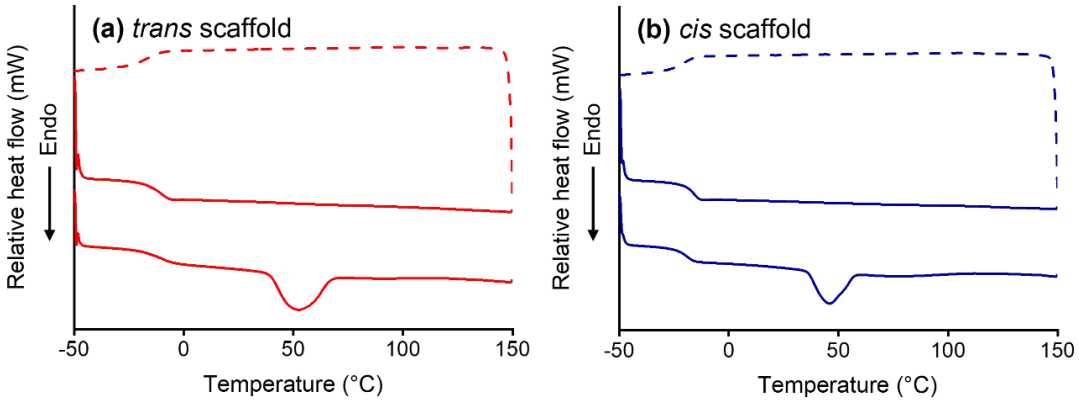


Figure A 4.15. *DSC thermograms of (a) a 4.0 kDa trans 3D printed scaffold and (b) a 4.5 kDa cis 3D printed scaffold. The dashed line represents the 1st cooling scan, the middle one, the 2nd heating scan and the bottom line is the 1st heating scan.*

Table A 4.3. *Summary of thermal properties for films and 3D printed scaffolds.*

sample	*annealing time*	T_g[a] (°C)	$T_{m,1}$[b] (°C)	$T_{m,2}$[c] (°C)	ΔH_m[d] (J·g^{-1})
4.0 kDa *cis* film	2 days	-13.54	N/A	N/A	0.18
4.5 kDa *trans* film	2 days	-12.7	43.91	64.38	26.64
6.1 kDa *cis* film	2 days	-16.04	43.76	55.75	2.44
6.1 kDa *trans* film	2 days	-14.87	45.9	66.52	26.44
6.6 kDa *cis* film	2 days	-17.37	42.1	53.43	2.56
6.6 kDa *trans* film	2 days	-13.53	43.25	67.54	28.06
9.7 kDa *trans* film	2 days	-13.03	45.91	65.22	27.99
9.7 kDa *cis* film	2 days	-17.87	42.73	55.9	24.74
4.5 kDa *trans* film	2 weeks	-11.7	43.41	62.9	25.12
4.5 kDa *trans* film	10 months	-11.06	47.69	60.84	15.42
6.1 kDa *trans* film	2 weeks	-13.37	42.91	67.52	28.85
6.1 kDa *trans* film	6 months	-12.72	49.53	63.65	18.62
4.0 kDa *cis* film	2 weeks	-13.53	N/A	N/A	N/A
4.0 kDa *cis* film	6 months	-13.55	N/A	N/A	0.14
6.1 kDa *cis* film	2 weeks	-16.2	42.56	52.9	20.13
6.1 kDa *cis* film	6 months	-15.38	49.67	54.51	14
trans 3D printed scaffold	3 weeks	-10.06	52.35	N/A	11.69
cis 3D printed scaffold	3 weeks	-15.89	45.86	N/A	7.24

[a]The glass transition temperature (T_g) was taken as the midpoint of the inflection tangent upon the 2nd heating scan. [b]The temperature of the first endothermic transition ($T_{m,1}$), taken at the minimum of the peak on the first heating scan. [c]The temperature of the 2nd endothermic transition ($T_{m,2}$), taken at the minimum of the peak on the 1st heating scan. [d]The total enthalpy of melting (ΔH_m) was calculated from integration and normalisation of all endothermic peaks present on the first heating scan.

4.9.6 Thermogravimetric analysis (TGA) characterisation of films and 3D printed scaffolds

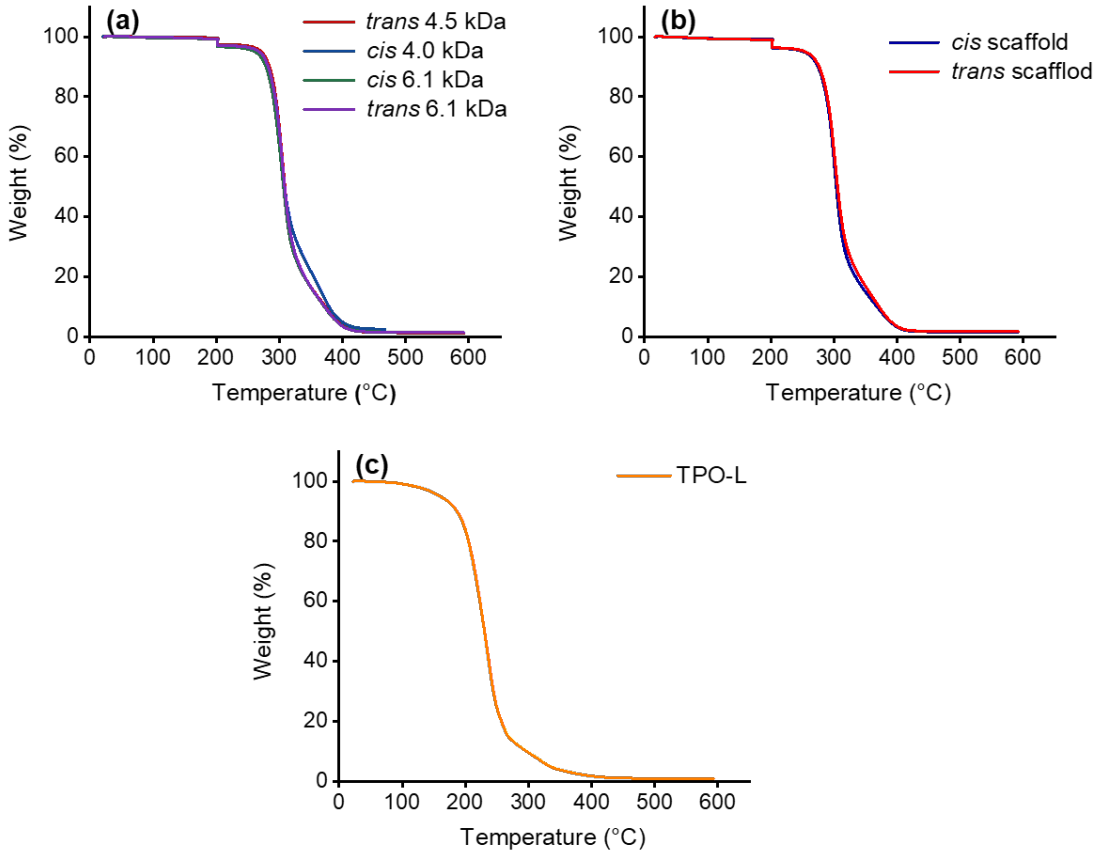


Figure A 4.16. *TGA thermograms of (a) cis and trans selected films, (b) cis and trans 3D printed scaffolds and (c) the formulated photo-initiator (TPO-L). The temperature ramp from room temperature to 600 °C was including an isotherm at 202 °C. The weight loss observed at 202 °C is predominately due to the thermal degradation of TPO-L and its degradation products.*

Table A 4.4. *Degradation temperature of selected films, 3D scaffolds and TPO-L.*

Sample	Weight loss at 202 °C[a] (%)	$T_{d,\ 5\%}$[b] (°C)	$T_{d,50\%}$ [c](°C)
4.5 kDa *trans* film	2.1	272	309
4.0 kDa *cis* film	2.5	262	3081
6.1 kDa *cis* film	2.6	261	306
6.1 kDa *trans* film	1.4	268	308
trans scaffold	1.5	255	306
cis scaffold	1.7	252	304
TPO-L	N/A	160	230

[a]Weight loss occurring during the 90 minutes isotherm at 202 °C. [b]Temperature when 5% of weight is lost. [c] Temperature when 50% of weight is lost.

4.9.7 Appendix references

1 G. W. Hart, "George W. Hart's Rapid Prototyping Web Page", can be found under, http://www.georgehart.com/rp/rp.html,

Chapter 5 – Conclusion

5 Conclusion

The main focus of this thesis were to study the impact of the *cis*/*trans* and *endo*/*exo* stereochemistry on the mechanical properties of polymer networks but also to study the feasibility of synthesising a polysaccharide mimic. To this aim, the nucleophilic thiol-Michael step-growth addition, which has been highlighted in the recent literature as a means to incorporate *cis*/*trans* and *endo*/*exo* stereochemistry within high molecular weight polymers, was selected for this study. The main advantage offered by this polymerisation technique is not only the extreme versatility, but also its mild reaction conditions precluding unwanted isomerisation or other side reactions, which still constitutes a major drawback within this field.

The first step, described in chapter 2, consisted in the synthesis of 6 diacrylate monomers derived from *cis* or *trans* 1,4-but-2-ene diol, each of the three isohexides and a 1,6-glucose-derived diol. Whilst the synthesis of a glucose derived diol was challenging, the functionalisation of all diols with a commercially available isocyanate-acrylate was straightforward and near quantitative. Interestingly, a difference in qualitative sensitivity was noticed with the unsaturated diacrylate being more prone to unwanted crosslinking in the presence of heat whilst both isohexides and glucose derived diacrylate were not. This observation is interesting, since the acrylate termini are placed 7 carbons further than the diol hydroxyls. Yet, a change in the structure of the diol, impacts the sensitivity of the acrylate. A study on the origin of the impact of the diol structure onto the diacrylate reactive site could be very interesting to further the knowledge of the thiol-ene systemused in this study. The last section of chapter 1 describes the synthesis of a 1,6-glucose-derived dithiol

which could further be polymerised with the 1,6-glucose-derived diacrylate in an attempt at obtaining a synthetic polysaccharide. Interestingly, reaction of the 1,6-glucose-derived diol with mesylate chloride in the presence of triethylamine yielded a protected glucose functionalised with a mesylate on the 6th carbon of the sugar ring and a chlorine on the 1st carbon in 98% yield. Further investigation into the limits of this asymmetric reaction could provide a useful derivative for asymmetric sugar synthesis, and furthermore uncover a previously unreported transformation.

In Chapter 3, the diacrylate monomers which were presented in chapter 2 were polymerised via thiol-Michael addition. The effort towards the production of stereopure unsaturated acrylate telechelic oligomers by reacting the *cis* and *trans* diacrylate with 1,6-hexane dithiol yielded excellent control over the molecular weight by stoichiometric imbalances on scales up to 60 g. This control was not achieved with the isohexides-derived diacrylate on scales higher than 1 g, and the oligomers were very sensitive towards crosslinking. This was a surprising result since this sensitivity was not expressed during the synthesis of isohexides-derived diacrylate monomer, which were qualitatively more stable than the *cis*/*trans* diacrylate monomers. This observation highlights once again the need for a better understanding of the impact of the diol structure onto the reactivity of the final diacrylate monomers during both their synthesis and their polymerisation. Regarding the polymerisation of the 1,6-glucose-derived diacrylate and dithiol, the outcomes were underwhelming, as only 20 kDa oligomers were able to be produced at the stochiometric balance and no control over the molecular weight could be achieved in stochiometric imbalance. It has been hypothesised that the steric hindrance deriving from the presence of three benzyl protecting group in addition to

an inherent variation of reactivity between the anomeric and primary hydroxyl in the case of the dithiol. Thus, this work highlighted the limitation of the versatility exhibited by the nucleophile catalysed Michael step-growth polymerisation in addition of the need to find more sustainable and intuitive methods to incorporate sugar moieties within polymers.

Finally, Chapter 4, presents the formulation of the *cis*/*trans* oligomers into a photo-active resins. The *cis* and *trans* networks obtained after UV irradiation of these resins were showing different mechanical properties directly linked to the crystallinity of the final material, with the *cis* material exhibiting the behaviour of a soft elastomer whereas the *trans* network was behaving similarly to a stiff plastic. Conducting thermal analysis *via* DSC after 2 days, 2 weeks, 10 months and 2 years of annealing highlighted that the kinetic of crystallisation was slow for the *cis* pure network, which is the reason for the soft elastomeric nature of the material exhibited up to 10 months after annealing. However, after 2 years, both *cis* and *trans* network displayed similar crystallinity. Finally, the addition of a photoinhibitor to the formulation, rendered the resins suitable for 3D printing and allowed the preparation of high-resolution 3D scaffolds with stereo-tuneable mechanical and degradable properties. If the unsaturated system used in this last study could potentially be considered similar to the historical example of 1,4-polyisoprene, it would be a gross misconception in comparing the two. Thus, although the former system displayed amorphous morphology and elasticity whilst containing *cis* unsaturation but improved stiffness and toughness with the unsaturation in the *trans* configuration, 1,4-polyispoprene requires lightly crosslinked polymer chain of moderate to high molecular weight. Or, in the system presented within this manuscript, the divergence

in mechanical properties was lost after the molecular weight was increased to 6 kda, a relatively low molecular weight. In addition, the creation of *cis* and *trans* polymers identical in every way but for the presence of urethane bonds, results in tacky liquid materials with no difference in mechanical properties. Finally, it is possible to find in the recent literature at least two other occurrences of polymers containing stereodefined unsaturation within their backbone which exhibit the opposite behaviour, with the *trans* rich polymer performing as an amorphous and elastomeric material, whilst the presence of *cis* unsaturation provide the material with a semi-crystalline structure and a stiffer and tougher mechanical behaviour. This incongruity should highlight that the impact of stereochemistry within polymer is not to be confused with the phenomenon observed in small molecules, since no general trend could be drawn without taking into consideration the molecular weight, the distance between stereochemistry-bearing unit along the chain, and first and foremost, the presence and type of other functional groups which will impact the overall behaviour of the polymer. With this in mind, a logical continuation of the work presented within this manuscript would be the study of the synergy between diverse functionality and a chosen stereodefine unit, unsaturation or else, to start to understand how different functionality would compose with stereochemistry in shaping the bulk mechanical properties of the polymer.